ACS SYMPOSIUM SERIES [illegible]

# Ionic Liquids:
## From Knowledge to Application

IQ → $

EDITED BY
Natalia V. Plechkova, Robin D. Rogers,
and Kenneth R. Seddon

Downloaded by 89.163.35.42 on June 28, 2012 | http://pubs.acs.org
Publication Date (Web): December 18, 2009 | doi: 10.1021/bk-2009-1030.fw001

# Ionic Liquids: From Knowledge to Application

Downloaded by 89.163.35.42 on June 28, 2012 | http://pubs.acs.org
Publication Date (Web): December 18, 2009 | doi: 10.1021/bk-2009-1030.fw001

Downloaded by 89.163.35.42 on June 28, 2012 | http://pubs.acs.org
Publication Date (Web): December 18, 2009 | doi: 10.1021/bk-2009-1030.fw001

ACS SYMPOSIUM SERIES **1030**

# Ionic Liquids: From Knowledge to Application

Natalia V. Plechkova, Editor
*The Queen's University of Belfast*

Robin D. Rogers, Editor
*The University of Alabama*

Kenneth R. Seddon, Editor
*The Queen's University of Belfast*

**Sponsored by the**
**ACS Division of Industrial and Engineering Chemistry**

American Chemical Society, Washington DC

In Ionic Liquids: From Knowledge to Application; Plechkova, N., et al.;
ACS Symposium Series; American Chemical Society: Washington, DC, 2010.

Library of Congress Cataloging-in-Publication Data

Ionic liquids : from knowledge to application / [edited by] Natalia V. Plechkova, Robin D. Rogers, Kenneth R. Seddon ; sponsored by the ACS Division of Industrial and Engineering Chemistry.
p. cm. -- (ACS symposium series ; 1030)
Includes bibliographical references and index.
ISBN 978-0-8412-6997-2 (alk. paper)
1. Ionic solutions--Congresses. 2. Electrolyte solutions--Congresses. I. Plechkova, Natalia V. II. Rogers, Robin D. III. Seddon, Kenneth R., 1950- IV. American Chemical Society. Division of Industrial and Engineering Chemistry.
QD565.I587 2009
541'.372--dc22
2009042750

Downloaded by 89.163.35.42 on June 28, 2012 | http://pubs.acs.org
Publication Date (Web): December 18, 2009 | doi: 10.1021/bk-2009-1030.fw001

The paper used in this publication meets the minimum requirements of American National Standard for Information Sciences—Permanence of Paper for Printed Library Materials, ANSI Z39.48−1984.

Copyright © 2009 American Chemical Society

Distributed by Oxford University Press

All Rights Reserved. Reprographic copying beyond that permitted by Sections 107 or 108 of the U.S. Copyright Act is allowed for internal use only, provided that a per-chapter fee of $40.25 plus $0.75 per page is paid to the Copyright Clearance Center, Inc., 222 Rosewood Drive, Danvers, MA 01923, USA. Republication or reproduction for sale of pages in this book is permitted only under license from ACS. Direct these and other permission requests to ACS Copyright Office, Publications Division, 1155 16th Street, N.W., Washington, DC 20036.

The citation of trade names and/or names of manufacturers in this publication is not to be construed as an endorsement or as approval by ACS of the commercial products or services referenced herein; nor should the mere reference herein to any drawing, specification, chemical process, or other data be regarded as a license or as a conveyance of any right or permission to the holder, reader, or any other person or corporation, to manufacture, reproduce, use, or sell any patented invention or copyrighted work that may in any way be related thereto. Registered names, trademarks, etc., used in this publication, even without specific indication thereof, are not to be considered unprotected by law.

PRINTED IN THE UNITED STATES OF AMERICA

# Foreword

The ACS Symposium Series was first published in 1974 to provide a mechanism for publishing symposia quickly in book form. The purpose of the series is to publish timely, comprehensive books developed from the ACS sponsored symposia based on current scientific research. Occasionally, books are developed from symposia sponsored by other organizations when the topic is of keen interest to the chemistry audience.

Before agreeing to publish a book, the proposed table of contents is reviewed for appropriate and comprehensive coverage and for interest to the audience. Some papers may be excluded to better focus the book; others may be added to provide comprehensiveness. When appropriate, overview or introductory chapters are added. Drafts of chapters are peer-reviewed prior to final acceptance or rejection, and manuscripts are prepared in camera-ready format.

As a rule, only original research papers and original review papers are included in the volumes. Verbatim reproductions of previous published papers are not accepted.

**ACS Books Department**

Downloaded by 89.163.35.42 on June 28, 2012 | http://pubs.acs.org
Publication Date (Web): December 18, 2009 | doi: 10.1021/bk-2009-1030.fw001

In Ionic Liquids: From Knowledge to Application; Plechkova, N., et al.;
ACS Symposium Series; American Chemical Society: Washington, DC, 2010.

Downloaded by 89.163.35.42 on June 28, 2012 | http://pubs.acs.org
Publication Date (Web): December 18, 2009 | doi: 10.1021/bk-2009-1030.pr001

# Preface

### Natalia V. Plechkova, Robin D. Rogers, and Kenneth R. Seddon

When the series of Ionic Liquid symposia began with *Green Industrial Applications of Ionic Liquids* at the 221st ACS National Meeting in San Diego (April 2001), we truly had no idea how many different aspects and applications for ionic liquids would appear, nor how the worldwide interest in the topic would endure. However, when we met last August in Philadelphia (the 236th ACS National Meeting) for the fifth symposium in this series, *Ionic Liquids: From Knowledge to Application,* it was clear that ionic liquids are steaming ahead into new and uncharted territory with amazing adaptability.

This book, based primarily on late breaking work discussed at the symposium, provides an interesting snapshot at some of the main lines of current and new research within the field, such as investigation of the novel properties of ionic liquids and their uses in separations (*e.g.*, gases, organics, and metal ions), biochemistry, medicine, and nanochemistry. The chapters also reflect the growing theoretical and computational work within the field leading to new predictive capability.

The breadth and depth of the field of ionic liquids was represented in Philadelphia by top authors and discussion leaders (see URL http://bama.ua.edu/~rdrogers/Philadelphia2008/) presenting their latest work. It was present in the engaging audience discussion, and it was evident from the high level of industrial participation. Although, the room assigned to the symposium was likely the worst we have ever encountered (a topic of much discussion among attendees and a lively debate with ACS), even the poor venue could not detract from the overall enthusiasm in the field.

While the chapter authors herein deserve the credit for the high quality of this volume, we would be remiss without noting those responsible for the high quality of the symposium on which it was based. As at past symposia, the format included ten half-day sessions organised and chaired by leaders in the field. We would like to heartily thank Joan F. Brennecke (Notre Dame) for her role in the overall symposium organisation, and the following session organisers for all of their efforts: Margarida Costa Gomes (Blaise Pascal), Mark B. Shiflett (DuPont), Jared Anderson (Toledo), Phil Jessop (Queen's Canada), Steve Baldelli (Houston), Alessandro Podesta (Milan), Gary Baker (Oak Ridge), Xiangqun Zeng (Oakland University), Jennifer Anthony (Kansas State), Anja Mudring (Bochum), Joe Magee (NIST), Luis Rebelo (ITQB Lisbon), Pietro Ballone (QUILL, Belfast), Ed Maginn (Notre Dame), Doug MacFarlane (Monash), Peter Schwab (Evonik), Megan B. Turner (BASF), James H. Davis, Jr. (South Alabama), and Peter Wasserscheid (Erlangen).

We are also very grateful to our sponsors, including the contributions of our own institutions. Our industrial sponsors were a major contributor to the success of this symposium. We acknowledge the contributions from Nippon Chemical Industrial, Agilent Technologies, and 525Solutions.

The ACS Division of Industrial & Engineering Chemistry and its subdivisions Green Chemistry & Engineering, Separation Science & Technology, and Novel Chemistry with Industrial Applications Subdivision once again proved to be wonderful hosts and we look forward to continuing to program in this division. We would like to note that the Philadelphia ACS meeting was also designated as the 100th anniversary of I&EC and we were proud to be able to take part in this momentous event. Happy Birthday I&EC!

And finally a note to all of our participants who suffered through some trying room assignments; based on our experiences, the ACS has instituted a policy where every room must be inspected in person before it will be used for a technical session. Apparently this had not happened in Philadelphia because of a last minute problem at the Convention Center which forced many sessions to area hotels. Willem Leenstra, Chair of the ACS Meetings and Expositions, provided a detailed explanation and apology for the inconveniences. We all hope you will continue to consider ACS and I&EC for future exciting ionic liquid programming.

Downloaded by 89.163.35.42 on June 28, 2012 | http://pubs.acs.org
Publication Date (Web): December 18, 2009 | doi: 10.1021/bk-2009-1030.pr001

Downloaded by 89.163.35.42 on June 28, 2012 | http://pubs.acs.org
Publication Date (Web): December 18, 2009 | doi: 10.1021/bk-2009-1030.ch001

## Chapter 1

# Gas Solubility (and Related High-Pressure Phenomena) in Systems with Ionic Liquids

**Gerd Maurer and Dirk Tuma**

**Department of Mechanical and Process Engineering
University of Kaiserslautern, Kaiserslautern, Germany**

A review is presented on the solubility of single gases in pure ionic liquids and on the volume expansion of the liquid phase induced by a dissolved gas. Furthermore, the phenomenon of "salting-out" by a near-critical gas (SONG) is discussed. The SONG phenomenon describes the liquid-liquid phase split that might be observed when a binary liquid solvent mixture – here with an ionic liquid component – is pressurised by a gas at a temperature close to the critical temperature of that gas. Due to the large scope of literature on gas solubility in ionic liquids, this review is mainly restricted to work by the authors' research group.

## Introduction

Gas solubility in ionic liquids is of interest in many areas, for example, in chemical reaction engineering when dissolved gases react with other solutes (such as in biphasic hydrogenation and hydroformylation), or for the storage of hazardous gases. The design of processes/equipment requires reliable data on gas solubility as well as on the phenomena that possibly occur in such processes. Two of the most important phenomena are the volume expansion of the liquid

In Ionic Liquids: From Knowledge to Application; Plechkova, N., et al.;
ACS Symposium Series; American Chemical Society: Washington, DC, 2010.

phase and the appearance of a liquid-liquid phase split. In previous (and ongoing) laboratory research, we have investigated the solubility of various non-reacting (single) gases in some pure ionic liquids and the volume expansion of the liquid phase caused by a dissolved gas. In theoretical work, the solubility of single gases in ionic liquids has been predicted by Gibbs Ensemble Monte Carlo simulations. In many applications, gases are dissolved in mixtures that contain an ionic liquid. Thus, experimental work has been extended into that field, in particular to the liquid-liquid phase split that might occur when a completely miscible solvent mixture is pressurised by a gas close to its critical temperature. Here, we review the progress that has been achieved in these research areas

Downloaded by 89.163.35.42 on June 28, 2012 | http://pubs.acs.org
Publication Date (Web): December 18, 2009 | doi: 10.1021/bk-2009-1030.ch001

## Experimental Arrangement for Measuring the Solubility of a Gas in an Ionic Liquid

The most important experimental techniques used to determine the solubility of a gas in a liquid are the gravimetric, the volumetric, the NMR-spectroscopic, and the synthetic methods *(1,2)*. In the gravimetric method, a high-resolution balance is applied to determine the increase of mass when a gas is dissolved in a liquid at preset temperature and pressure. This method needs only small amounts of the solvent, and it can provide data of excellent quality, in particular when the gas solubility is sufficiently high and the volume expansion of the liquid remains small. The volumetric method generally requires more solvent, and the amount of dissolved gas is determined volumetrically either during absorption or desorption. There are a lot of high-precision gas solubility studies known where this method was applied. The NMR-spectroscopic method is a very fast, but less accurate technique. It is mostly used to screen solvents for gases. In the synthetic method, the pressure is determined that is required to dissolve a known amount of gas in a known amount of solvent at a preset temperature. This technique is capable of delivering high-precision data for scarcely, as well as for very, soluble gases. It requires approximately the same amount of solvent as the volumetric method. We have a long-standing expertise in applying the synthetic method for measuring the solubility of single gases in pure solvents and solvent mixtures at temperatures from below room temperature up to about 200 °C *(3)*. Figure 1 shows a scheme of such an apparatus as it was used to determine the solubility of a single gas in a pure ionic liquid *(3)*. The heart of this apparatus is a thermostatted, cylindrical high-pressure view cell (with a cell volume of about 30 $cm^3$) with a sapphire window on each side. In an experiment, the evacuated view cell is charged with an exactly known amount of gas (determined either volumetrically or gravimetrically) before the solvent (here, the ionic liquid) is added *via* a calibrated high-pressure spindle press. The amount of solvent added is sufficiently large to generate a single liquid phase in the view cell. This phase is equilibrated and, afterwards, very small amounts of the mixture are withdrawn *via* the spindle press until the first stable gas bubbles appear. After each withdrawal (*i.e.*, each small pressure drop), the liquid mixture is equilibrated again. When the pressure drop in the last step (*i.e.*, the step that induces a two-phase system in the cell) is sufficiently small, the solubility pressure is reliably determined as the arithmetic mean of the pressure before and after that last step.

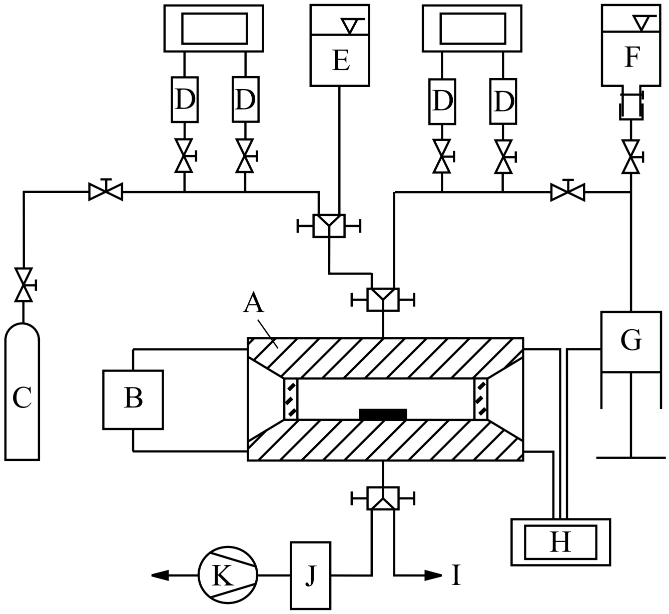

*Figure 1. Scheme of the apparatus for measuring the solubility of a single gas in a solvent at elevated pressures: (A) cylindrical high-pressure equilibrium view cell with two sapphire windows and a magnetic stirrer, (B) thermostat, (C) container for the gas, (D) pressure transducers, (E) tank for rinsing water, (F) tank for the solvent, (G) high-pressure spindle press, (H) AC-bridge with three platinum resistance thermometers, (I) solution outlet, (J) cooling trap, and (K) vacuum pump.*

As both the volume of the cell (from a calibration experiment with pure gas or by filling the cell with pure liquid water) and the amounts of solvent (through the volume displacement of the calibrated spindle press and the density of the solvent) and solute are exactly known, a gas solubility experiment also provides volumetric data that can be used to determine the volume expansion of the ionic liquid by the dissolved gas.

Downloaded by 89.163.35.42 on June 28, 2012 | http://pubs.acs.org
Publication Date (Web): December 18, 2009 | doi: 10.1021/bk-2009-1030.ch001

Table 1 provides an overview of the (gas + ionic liquid) systems that were investigated so far in our group. For a comparison with literature data, the reader is referred to the review article by Anderson *et al. (2)* and the references cited therein.

**Table 1. References for Experimental Work on Gas Solubility in Ionic Liquids in the Authors' Group**

| | $[C_4mim][PF_6]$[a] | $[C_6mim][NTf_2]$[b] | $[C_4mim][CH_3SO_4]$[c] | $[C_4mpyr][NTf_2]$[d] |
|---|---|---|---|---|
| $CO_2$ | (*4*, *10*) | (*8*) | (*10*) | (*16*) |
| CO | (*5*) | (*15*) | (*11*) | — |
| $H_2$ | (*7*) | (*9*) | (*11*) | (*16*) |
| $O_2$ | (*6*) | (*15*) | — | — |
| $CH_4$ | — | (*13*) | (*12*) | — |
| $CF_4$ | — | (*14*) | — | — |
| Xe | — | (*13*) | (*12*) | — |

[a] $[C_4mim][PF_6]$ = 1-butyl-3-methylimidazolium hexafluorophosphate

[b] $[C_6mim][NTf_2]$ = 1-hexyl-3-methylimidazolium bis(trifluoromethylsulfonyl)amide

[c] $[C_4mim][CH_3SO_4]$ = 1-butyl-3-methylimidazolium methylsulfate

[d] $[C_4mpyr][NTf_2]$ = 1-butyl-1-methylpyrrolidinium bis(trifluoromethylsulfonyl)amide

Downloaded by 89.163.35.42 on June 28, 2012 | http://pubs.acs.org
Publication Date (Web): December 18, 2009 | doi: 10.1021/bk-2009-1030.ch001

As a typical example, Figure 2 shows the experimental gas solubility data for the solubility of $CO_2$ (left) and $H_2$ (right) in the ionic liquid $[C_4mpyr][NTf_2]$ as a plot in which for temperatures between 293 K and 413 K the solubility pressure is shown *versus* the gas molality (*i.e.*, the number of moles of dissolved gas per kilogram of ionic liquid). At constant temperature, the solubility pressure increases nearly linearly with increasing gas molality – a behaviour typically observed for "physical gas solubility". Although – at first glance – both parts of Figure 2 look rather similar, there are large differences in the solubility of $CO_2$ and $H_2$ in $[C_4mpyr][NTf_2]$. For example, at the same temperature and pressure, the gas molality differs by a factor of about ten, hydrogen being the less soluble gas. Furthermore, the influence of temperature is substantially different for both gases in that ionic liquid. The solubility of $CO_2$ in $[C_4mpyr][NTf_2]$ decreases with increasing temperature, whereas that of $H_2$ increases.

The experimental results are correlated by an extended version of Henry's law on the molality scale.

$$k_{H,G,IL}(T,p)\,a_G(T,m_G)=f_G(T,p) \tag{1}$$

$k_{H,G,IL}(T, p)$ is Henry's constant on the molality scale of a gas (G) in the ionic liquid (IL) at temperature $T$ and pressure $p$. $a_G(T, m_G)$ is the activity of the gas in the liquid that is related to the gas molality ($m_G$) and the activity coefficient coefficient ($\gamma_G$) through:

$$a_G = \frac{m_G}{m^\circ}\gamma_G\,, \qquad (2)$$

where $m^\circ = 1$ mol kg$^{-1}$. $f_G(T, p)$ is the fugacity of the (pure) gas in the vapour phase.

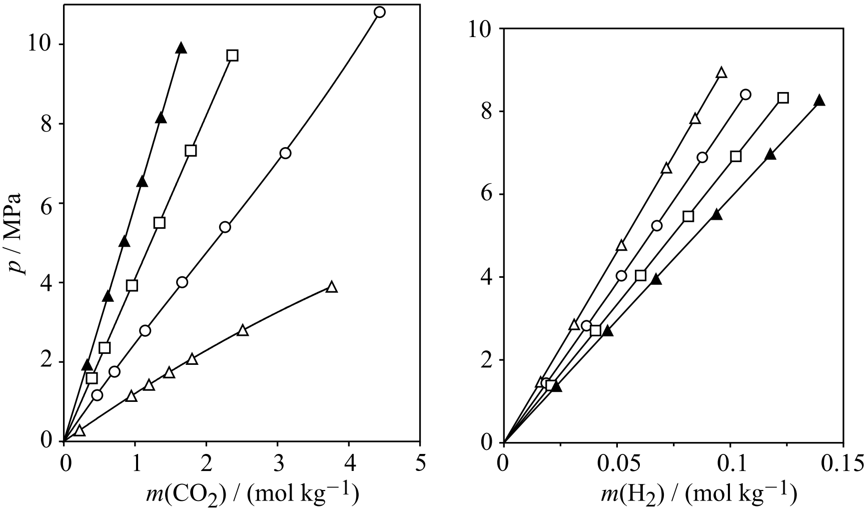

*Figure 2. Total pressure above solutions of ($CO_2$ + [$C_4$mpyr][NTf$_2$]) and ($H_2$ + [$C_4$mpyr][NTf$_2$]): (▲, 293.1 K ($CO_2$), 293.2 K ($H_2$); □, 333.1 K ($CO_2$, $H_2$); ○, 373.2 K ($CO_2$), 373.1 K ($H_2$); Δ, 413.2 K ($CO_2$, $H_2$)) experimental results; (———) correlation.*

Henry's constant of the gas (G) in an ionic liquid (IL) is expressed as:

$$k_{H,G,IL}(T, p) = k^{(0)}_{H,G,IL}(T)\exp\left(\frac{V^{\infty}_{m,G,IL}\;p}{R\,T}\right) \qquad (3)$$

Downloaded by 89.163.35.42 on June 28, 2012 | http://pubs.acs.org
Publication Date (Web): December 18, 2009 | doi: 10.1021/bk-2009-1030.ch001

In Equation (3), $k_{\mathrm{H,G,IL}}^{(0)}(T)$ is Henry's constant at zero pressure, $V_{\mathrm{m,G,IL}}^{\infty}$ stands for the partial molar volume of gas G at infinite dilution in the ionic liquid (IL), and $R$ is the universal gas constant. Henry's constant at zero pressure $k_{\mathrm{H,G,IL}}^{(0)}(T)$ is determined by an extrapolation (at fixed temperature):

$$k_{\mathrm{H,G,IL}}^{(0)}(T) = \lim_{p \to 0}\left[\frac{f_{\mathrm{G}}(T,p)}{\left(m_{\mathrm{G}}/m^{\circ}\right)}\right] \tag{4}$$

The fugacity is calculated from the solubility pressure $p$ and the fugacity coefficient $\varphi_{\mathrm{G}}$ (which is calculated from an equation of state for the pure gas):

$$f_{\mathrm{G}}(T,p) = p\,\varphi_{\mathrm{G}} \tag{5}$$

Figure 3 shows the results from these evaluations for seven gases in the ionic liquid [$C_6$mim][$NTf_2$] together with Henry's constant (transformed to the molality scale) from the literature *(17–22)*.

According to Henry's law

$$\frac{m_{\mathrm{G}}}{m^{\circ}} = \frac{p}{k_{\mathrm{H,G,IL}}^{(0)}} \tag{6}$$

at low pressures (*i.e.*, at low gas molalities), the solubility of a gas in a solvent is proportional to the reciprocal value of Henry's constant. Figure 3 reveals the large differences in the solubility of gases in a particular ionic liquid as well as the differing influence of temperature on gas solubility.

Downloaded by 89.163.35.42 on June 28, 2012 | http://pubs.acs.org
Publication Date (Web): December 18, 2009 | doi: 10.1021/bk-2009-1030.ch001

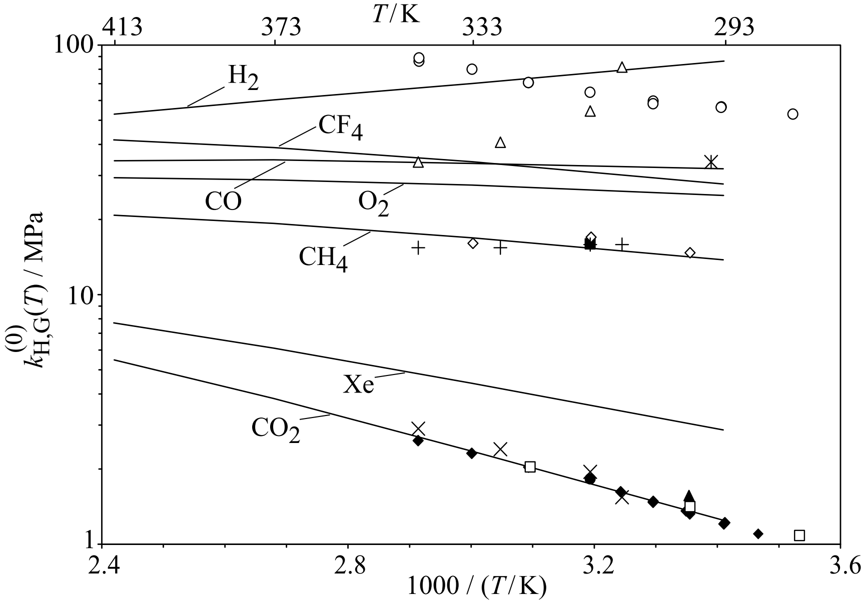

*Figure 3. Henry's constant of some gases in [$C_6$mim][$NTf_2$]. Solid lines: own data (cf. Table I). Other literature data: $CO_2$: ◆, (17); □, (18); ▲, (19); ●, (20); **x**, (21); $CH_4$: ◊, (18); ■, (20); +, (21); CO: ✳, (22); $H_2$: ○, (17), Δ, (21).*

There is sound agreement between the Henry's constants evaluated from our experimental data for [$C_6$mim][$NTf_2$] and the corresponding literature data for the gases $CO_2$, $CH_4$, and CO. The average relative deviation between our values and a corresponding series of reported values for Henry's constant amounts to between 1.9 % *(17)* and 14.9 % *(19)* for $CO_2$, 3.4 % *(20)* and 6.9 % *(21)* for $CH_4$, and to 6.3 % for CO *(22)*, respectively. For $H_2$, however, the data from Costa Gomes *(17)* display an opposite temperature dependence, which is contrary to our results *(7,9,11,16)*. The corresponding average relative deviation assigned to that data amounts to 24 %.

At higher pressures, the influence of pressure on Henry's constant has to be taken into account *via* the partial molar volume of the gas in the ionic liquid, *cf.* Equation (3). For very soluble gases (*e.g.*, $CO_2$ in [$C_6$mim][$NTf_2$] or [$C_4$mpyr][$NTf_2$], respectively), their partial molar volume was determined from the volumetric data that were obtained from the gas solubility measurements *(23)*.

Downloaded by 89.163.35.42 on June 28, 2012 | http://pubs.acs.org
Publication Date (Web): December 18, 2009 | doi: 10.1021/bk-2009-1030.ch001

## Volume Expansion

The volume $V$ of the liquid mixture in the equilibrated view cell (*i.e.*, the volume of that view cell) is

$$V = n_{\mathrm{IL}}\, V_{\mathrm{m,IL}} + n_{\mathrm{G}}\, V_{\mathrm{m,G}}\ , \tag{7}$$

where $n_{\mathrm{IL}}$ and $n_{\mathrm{G}}$ are the amounts of mass (number of moles) of the solvent and the gas in the cell, respectively, and $V_{\mathrm{m,IL}}$ and $V_{\mathrm{m,G}}$ are the partial molar volumes of the solvent and the gas, respectively. Dividing Equation (7) by the mass of the solvent $\widetilde{m}_{\mathrm{IL}}$ results in:

$$1000\,\frac{V\,/\,\mathrm{cm}^3}{\widetilde{m}_{\mathrm{IL}}\,/\,\mathrm{g}} = 1000\,\frac{V_{\mathrm{m,IL}}/\,(\mathrm{cm}^3\ \mathrm{mol}^{-1})}{M_{\mathrm{IL}}} + \frac{m_{\mathrm{G}}}{m^\circ}\,V_{\mathrm{m,G}}\,/\,(\mathrm{cm}^3\ \mathrm{mol}^{-1})\,, \tag{8}$$

where $M_{\mathrm{IL}}$ is the relative molar mass of the ionic liquid. Generally, $V_{\mathrm{m,IL}}$ and $V_{\mathrm{m,G}}$ depend on temperature and composition of the mixture. Therefore, the partial molar volume of the gas (G) at infinite dilution has to be determined by an extrapolation to zero gas molality:

$$\lim_{(m_{\mathrm{G}}/m^\circ)\to 0}\left[\partial\left(\frac{1000\ V\,/\,\mathrm{cm}^3}{\widetilde{m}_{\mathrm{IL}}/\mathrm{g}}\right)\Big/\,\partial\left(\frac{m_{\mathrm{G}}}{m^\circ}\right)\right]_T = V^{\infty}_{\mathrm{m,G,\,IL}}/\,(\mathrm{cm}^3\ \mathrm{mol}^{-1}) \tag{9}$$

At low gas molalities, the partial molar volumes of the solvent and the solute can be approximated by the molar volume of the pure ionic liquid $V^{(0)}_{\mathrm{m,IL}}$ and the partial molar volume of the gas in that solvent at infinite dilution $V^{\infty}_{\mathrm{m,G,\,IL}}$, respectively. In the concentration range where these approximations are valid, Equation (8) results in a linear relationship:

$$1000\,\frac{V\,/\,\mathrm{cm}^3}{\widetilde{m}_{\mathrm{IL}}\,/\,\mathrm{g}} = 1000\,\frac{V^{(0)}_{\mathrm{m,IL}}\,/\,(\mathrm{cm}^3\ \mathrm{mol}^{-1})}{M_{\mathrm{IL}}} + \frac{m_{\mathrm{G}}}{m^\circ}\,V^{\infty}_{\mathrm{m,G,IL}}\,/\,(\mathrm{cm}^3\ \mathrm{mol}^{-1}) \tag{8a}$$

Downloaded by 89.163.35.42 on June 28, 2012 | http://pubs.acs.org
Publication Date (Web): December 18, 2009 | doi: 10.1021/bk-2009-1030.ch001

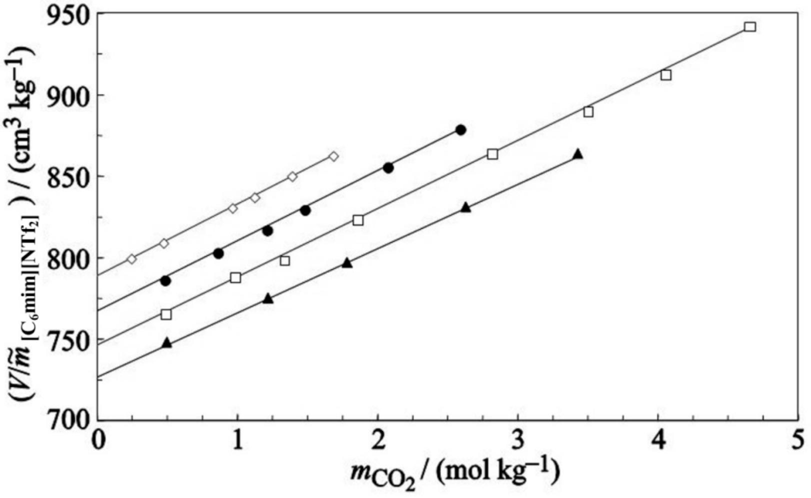

*Figure 4. The volume to solvent mass ratio versus the solute molality for $CO_2$ in $[C_6mim][NTf_2]$: (▲, 293.15 K; □, 333.15 K; ●, 373.2 K; ◊, 413.2 K) experimental results; (——) linear fit.*

The slope of the line is $V^{\infty}_{\mathrm{m,G,IL}}$. Equation (8a) was employed to evaluate the volumetric data. Figure 4 shows, as a typical example, the evaluation of the volumetric data for the system ($CO_2$ + $[C_6mim][NTf_2]$).

For sparsely soluble gases, where the gas molality is much smaller than shown in Figure 4, a reliable evaluation of the volumetric data for the determination of the partial molar volume of the gas in the ionic liquid is not possible. However, it can then be determined in a different procedure from the gas solubility data *(17)*. Figure 5 shows the partial molar volumes of four gases in $[C_6mim][NTf_2]$: two very soluble gases ($CO_2$ and $CH_4$) and two sparsely soluble ones (CO and $H_2$). The values of the partial molar volume for the four gases G range from about 10 to 45 cm$^3$ mol$^{-1}$. For a rough estimate, $V^{\infty}_{\mathrm{m,G,IL}}$ can be replaced by the molar volume of the gas G in its liquid state at the triple point. The partial molar volumes can – together with the molar volumes of the ionic liquids – be used to determine the volume expansion which accompanies the dissolution of the gas. This volume expansion depends on the solubility (*i.e.*, to a first estimate on Henry's constant), on the partial molar volume of the dissolved gas at infinite dilution, and on the molar volume of the solvent. Table 2 shows some typical examples for the relative volume expansion, when a gas is dissolved at 373 K in $[C_6mim][NTf_2]$ to reach a pressure of 10 MPa. Notably, there are large differences in the volume expansion. In those particular examples, the relative volume expansion stretches from only 0.4 % (for the least soluble gas $H_2$ that also has the smallest partial molar volume) to 16 % for $CO_2$

Downloaded by 89.163.35.42 on June 28, 2012 | http://pubs.acs.org
Publication Date (Web): December 18, 2009 | doi: 10.1021/bk-2009-1030.ch001

(which is one of the most soluble gases and also has the largest partial molar volume). The volume expansion is not a particular phenomenon for (gas + ionic liquid) systems, but is also common in other (gas + solvent) systems. The extent of those volume expansions is also within the commonly observed ranges, *cf.* Jessop and Subramaniam *(24)*.

**Table 2. Volume Expansion Caused by the Pressurisation of the Ionic Liquid [$C_6$mim][$NTf_2$] with a Gas to 10 MPa at 373 K** ***(23)***

| Gas G | $\frac{V^{\infty}_{\mathrm{m,G,IL}}}{(\mathrm{cm^3 mol^{-1}})}$ | $\frac{k^{(0)}_{\mathrm{H,G,IL}}}{\mathrm{MPa}}$ | Relative Volume Expansion (100 $\Delta V/V$)/% |
|---|---|---|---|
| $CO_2$ | 44 | 3.81 | 16 |
| Xe | 52 | 6.08 | 11 |
| $CH_4$ | 36 | 19.2 | 2.3 |
| $CF_4$ | 39 | 38.8 | 1.1 |
| $H_2$ | 18 | 60.1 | 0.4 |

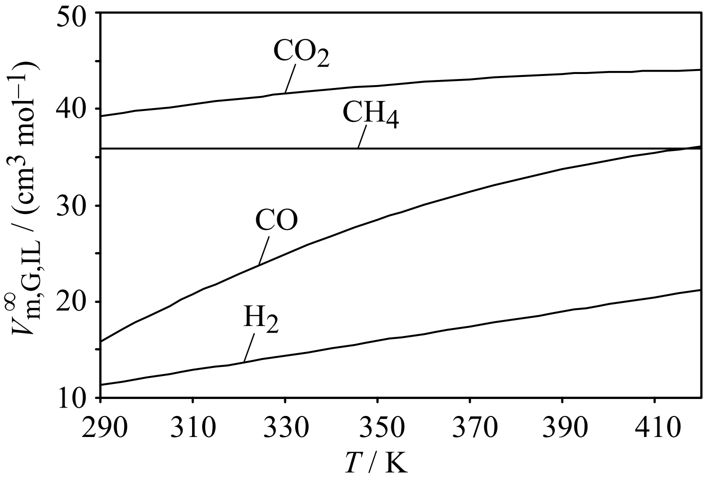

*Figure 5. Influence of temperature on the partial molar volume of some gases in the ionic liquid [$C_6$mim][$NTf_2$].*

## Prediction of Gas Solubility by Molecular Simulation

Experimental data for the solubility of gases in ionic liquids are not only important from an application-oriented point of view, but they also provide a

Downloaded by 89.163.35.42 on June 28, 2012 | http://pubs.acs.org
Publication Date (Web): December 18, 2009 | doi: 10.1021/bk-2009-1030.ch001

data base for the development of correlation methods and predictive tools. Molecular simulation is such a tool, and it has attracted a steadily increasing attention in recent years. It allows for predicting thermodynamic properties from information on intermolecular pair potentials between the components of a mixture *(25–30)*. Figure 6 shows – as typical examples – predictions from Gibbs Ensemble Monte Carlo simulations for the solubility of $CO_2$ in $[C_4mim][CH_3SO_4]$ – upper diagram (Urukova and Maurer *(31)*) – and CO in $[C_4mim][PF_6]$ – lower diagram (Urukova *et al. (32)*). For the simulations, the pair potentials of the gases were taken from the literature (CO: Straub and Karplus *(33)*; $CO_2$: Harris and Yung *(34)*). Both pair potentials are the sum of Coulombic interactions and Lennard-Jones contributions. The pair potentials of both ionic liquids were similarly approximated by multicentre electrical point charges in combination with multicentre Lennard-Jones contributions.

For $[C_4mim][PF_6]$, the pair potential was taken from Shah *et al. (35)*; for $[C_4mim][CH_3SO_4]$, it was estimated from quantum chemical calculations (for the geometry and the electrical point charges) and the United Atoms approach for the Lennard-Jones contributions (Urukova and Maurer *(31)*). Classical mixing rules without adjustable parameters were used to describe interactions between different Lennard-Jones sites. As shown in Figure 6, the prediction results for the solubility of $CO_2$ in $[C_4mim][CH_3SO_4]$ at 333 K almost perfectly agree with the experimental data. However, there are large deviations between the predictions results and the experimental data for the solubility of CO in $[C_4mim][PF_6]$, where the molecular simulation results overestimate the gas solubility by a factor of about three. Thus, dependent on the input, the results from molecular simulation vary from merely capturing trends to an almost quantitative agreement. According to Maginn *(27)*, an upgrade of the performance is to be expected from not only force field refinement, but also from more sophisticated sampling procedures.

Downloaded by 89.163.35.42 on June 28, 2012 | http://pubs.acs.org
Publication Date (Web): December 18, 2009 | doi: 10.1021/bk-2009-1030.ch001

Downloaded by 89.163.35.42 on June 28, 2012 | http://pubs.acs.org
Publication Date (Web): December 18, 2009 | doi: 10.1021/bk-2009-1030.ch001

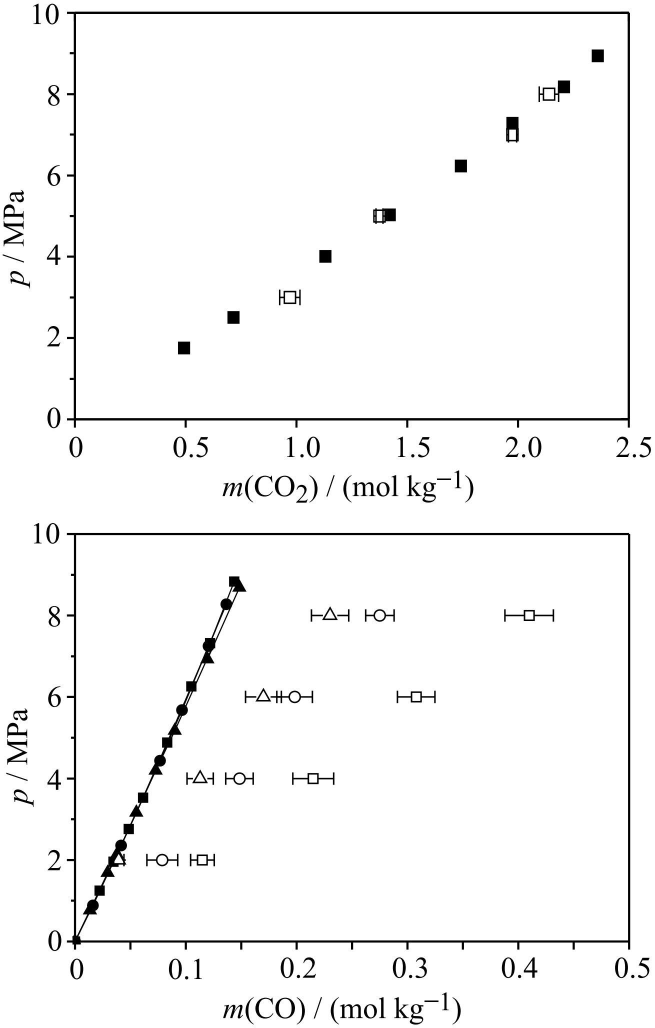

*Figure 6. Gas solubility in ionic liquids. Comparison between experimental data (full symbols) and data from molecular simulation (open symbols). Top: Solubility of $CO_2$ in $[C_4mim][CH_3SO_4]$; ■, 333.1 K; Bottom: Solubility of CO in $[C_4mim][PF_6]$; ■, 293 K; ●, 334 K; ▲, 373 K.*

## Salting-Out by a Near-critical Gas in Systems with Ionic Liquids

When a gas is dissolved under pressure in a solvent mixture (for example, an aqueous solution of a low molecular-weight alcohol) at a temperature near its critical temperature, a liquid-liquid phase split might be induced *(36)*. Then, both liquid phases ($L_1$ and $L_2$) coexist with a vapour phase V. This phenomenon is called "Salting-Out by a Near-critical Gas" (SONG), and that particular term directly dates from the paper by Elgin and Weinstock, who were the first to report this, in 1959 *(37)*. An example is shown in Figure 7.

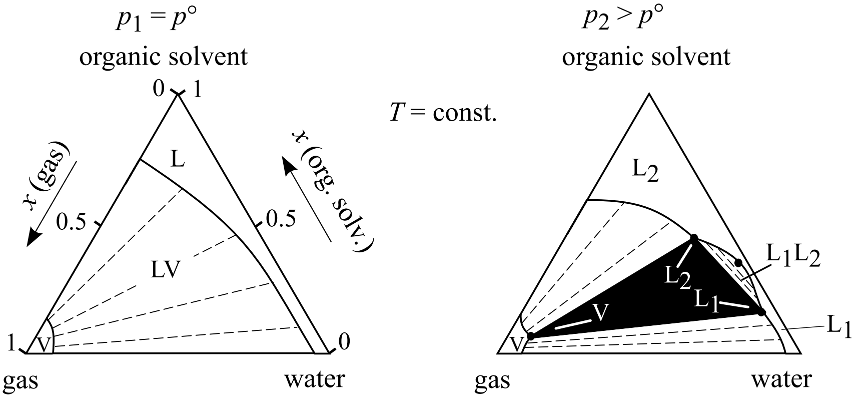

$p_1 = p°$
organic solvent
0
1
x (gas)
0.5
L
LV
V
1
gas
water
0
0.5
x (org. solv.)
T = const.
$p_2 > p°$
organic solvent
$L_2$
$L_1L_2$
$L_2$
$L_1$
V
V
$L_1$
gas
water

*Figure 7. Typical phase behaviour in a system ("near-critical" gas + water + organic solvent). Here, p° = 0.1 MPa.*

Downloaded by 89.163.35.42 on June 28, 2012 | http://pubs.acs.org
Publication Date (Web): December 18, 2009 | doi: 10.1021/bk-2009-1030.ch001

Downloaded by 89.163.35.42 on June 28, 2012 | http://pubs.acs.org
Publication Date (Web): December 18, 2009 | doi: 10.1021/bk-2009-1030.ch001

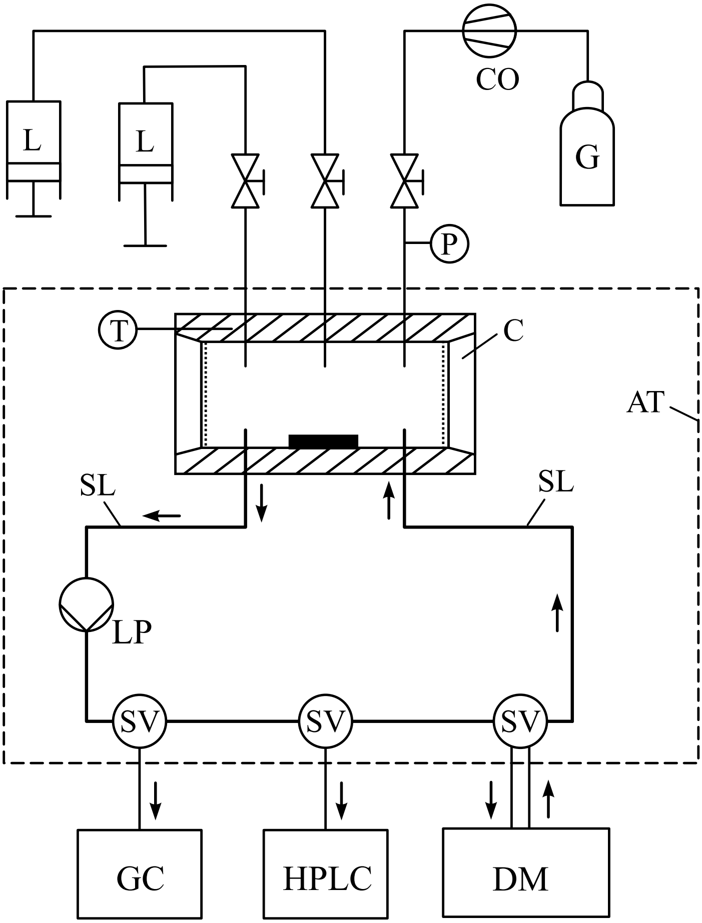

*Figure 8. Scheme of the apparatus for measuring phase equilibria at elevated pressures: (AT) air thermostat; (C) pivot-mounted cylindrical high-pressure view cell with two sapphire windows and a magnetic stirrer; (CO) compressor; (DM) densimeter; (G) gas container; (GC) gas chromatograph; (HPLC) high-pressure liquid chromatograph; (L) high-pressure spindle press containing liquid solvents; (LP) liquid pump; (P) pressure transducer; (SL) one of two sampling loops; (SV) sampling valve; (T) platinum resistance thermometer.*

Downloaded by 89.163.35.42 on June 28, 2012 | http://pubs.acs.org
Publication Date (Web): December 18, 2009 | doi: 10.1021/bk-2009-1030.ch001

Such liquid-liquid phase splits are also observed when a completely miscible binary mixture of an ionic liquid (*e.g.*, [$C_4$mim][$PF_6$]) and an organic solvent (*e.g.*, methanol) is pressurised by $CO_2$ at temperatures below, as well as above, the critical temperature of $CO_2$ ($T_c = 304.13$ K) *(38–41)*.

A scheme of the apparatus to investigate the SONG phenomenon is given in Figure 8 *(42)*. The equipment is similar to that employed for measuring gas solubilities (*cf.* Figure 1), but it operates according to a static analytical method, and is thus equipped with two sampling loops. When the mixture to be analysed is equilibrated, samples of the coexisting (liquid) phases are taken and analysed by gas chromatography (the volatile compounds, *e.g.*, $CO_2$ and methanol) and by high-pressure liquid chromatography (the ionic liquid), respectively. Two phases can be analysed simultaneously, and the density is also recorded.

Figure 9 shows a scheme of such phase equilibria at a temperature above the critical temperature of $CO_2$, for example, at 313 K. On the left-hand side of Figure 9, triangular diagrams – like those shown in Figure 7 – are arranged into a prism, where the pressure increases from bottom to top. The SONG phenomenon exists only in a limited pressure range, *i.e.*, at pressures between the "lower critical endpoint" (LCEP) line and the "upper critical endpoint" (UCEP) line. On the LCEP line, both liquid phases are critical and coexist with a noncritical vapour phase. At the UCEP line, one liquid phase is critical with the vapour phase, and both critical phases coexist with another (noncritical) liquid phase. The right-hand side of Figure 9 shows a pressure *versus* temperature diagram with both critical endpoint lines, as determined by Aki *et al. (39)*, Zhang *et al. (40)*, and Chobanov *(43)*. The UCEP line lies slightly above the critical line for the vapour-liquid equilibrium of the binary system ($CO_2$ + methanol). This was expected, as the solubility of [$C_4$mim][$PF_6$] in the vapour phase is extremely small (for a better understanding, that solubility is largely out of scale on the left-hand side of Figure 9). The liquid-liquid phase split extends over about 2 MPa at low temperatures, and over about 1 MPa at high temperatures. That pressure range contracts with rising temperature, as both critical endpoint lines converge and end in a tricritical point. There, the three phases ($L_1$, $L_2$, and V) all become critical. For the ($CO_2$ + methanol + [$C_4$mim][$PF_6$]) system, the temperature at that tricritical point seems to lie far beyond the experimentally investigated temperature region, presumably at a temperature where the ionic liquid is no longer stable.

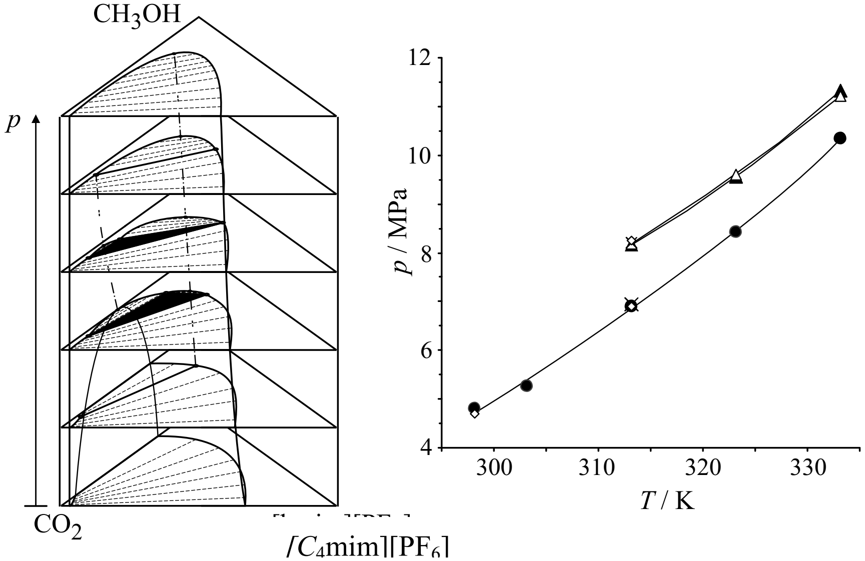

*Figure 9. Phase behaviour of the system ($CO_2$ + methanol + $[C_4mim][PF_6]$). Left-hand side: qualitative phase prism at $T > T_c$ (e.g., 313.15 K). Right-hand side: ▲, UCEP; ●, LCEP; Δ, VLE ($CO_2$ + methanol) (43); ◊, UCEP and LCEP (39);* **x**, *UCEP and LCEP (40).*

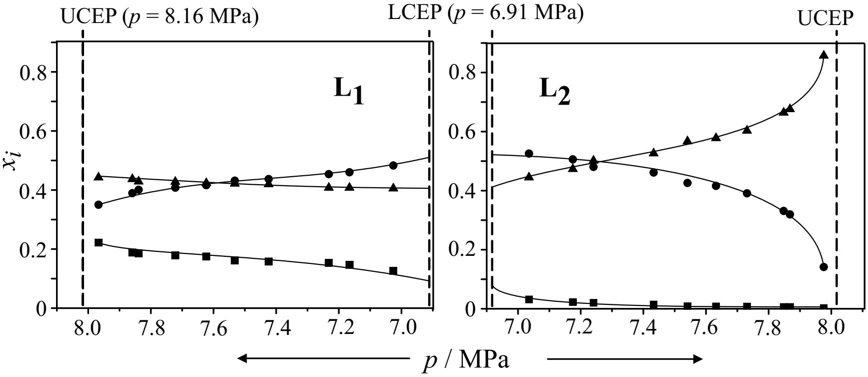

*Figure 10. Three-phase liquid-liquid-vapour equilibrium in the system ($CO_2$ + methanol + $[C_4mim][PF_6]$) at 313.15 K: Compositions of the coexisting liquid phases $L_1$ and $L_2$ (■, $[C_4mim][PF_6]$; ●, methanol; ▲, $CO_2$).*

Downloaded by 89.163.35.42 on June 28, 2012 | http://pubs.acs.org
Publication Date (Web): December 18, 2009 | doi: 10.1021/bk-2009-1030.ch001

Figure 10 shows the compositions of the coexisting liquid phases in the ternary system ($CO_2$ + methanol + [$C_4$mim][$PF_6$]) at 313.15 K *(43)*.

The left-hand side of Figure 10 shows the composition of the ionic liquid-rich phase ($L_1$) plotted *versus* pressure. In that diagram, the pressure increases from right to left. The right-hand side of Figure 10 shows the composition of the liquid phase $L_2$, which is depleted of the ionic liquid – also plotted *versus* pressure. But in this diagram, the pressure increases from left to right. The three-phase region extends between 6.91 MPa and 8.16 MPa. At the lower critical endpoint, the liquid phase contains approximately 0.08 $mol\,mol^{-1}$ [$C_4$mim][$PF_6$] and 0.41 $mol\,mol^{-1}$ $CO_2$. With increasing pressure, the mole fraction of [$C_4$mim][$PF_6$] in the phase $L_1$ increases to about 0.25 at the upper critical endpoint. *Vice versa*, the concentration of [$C_4$mim][$PF_6$] in the liquid phase $L_2$ decreases rapidly with increasing pressure, as at the upper critical endpoint that liquid phase becomes critical with the vapour phase V (which has nearly no solvent power for an ionic liquid). At the upper critical endpoint, the liquid phase $L_2$ contains also very little methanol as the temperature is close to the critical temperature of $CO_2$, and the upper critical endpoint line nearly coincides with the critical line for vapour-liquid equilibrium in the binary system ($CO_2$ + methanol).

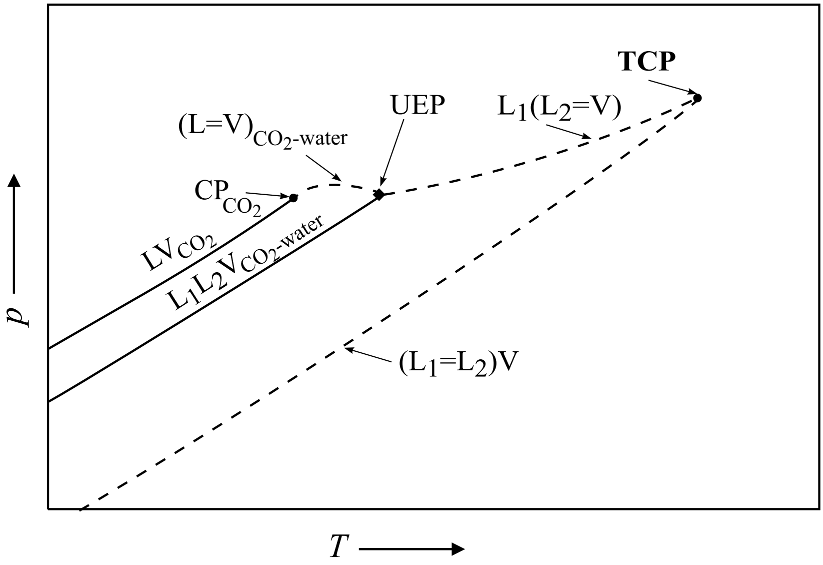

*Figure 11. Qualitative phase behaviour of the system ($CO_2$ + water + hydrophilic ionic liquid): (– – – –) ternary critical endpoint line; UEP, upper endpoint; TCP, tricritical point ($L_1 = L_2 = V$).*

Downloaded by 89.163.35.42 on June 28, 2012 | http://pubs.acs.org
Publication Date (Web): December 18, 2009 | doi: 10.1021/bk-2009-1030.ch001

A liquid-liquid phase split is always observed when a completely miscible mixture of (water + hydrophilic ionic liquid) is pressurised by $CO_2$, as at temperatures below the critical temperature of $CO_2$, the three-phase ($L_1L_2V$) line of the binary system (water + $CO_2$) is the upper critical endpoint line of the ternary system (*cf.* Figure 11). However, for all such systems for which experimental data on this phenomenon are currently available {*cf.* Ventura *et al.* *(44)* and Chobanov *(43)*}, the SONG phenomenon exists only in a very small pressure range (less than about 0.1 MPa).

## Acknowledgements

G. M. gratefully acknowledges financial support by Deutsche Forschungsgemeinschaft (DFG), Bonn, Germany, grant no. Ma 713/40 and grant no. Ma 713/45 (within the priority programme DFG-SPP 1191 "Ionic Liquids").

## References

1. Letcher, T. M., Ed. *Developments and Applications in Solubility*; The Royal Society of Chemistry: Cambridge, 2007.
2. Anderson, J. L.; Anthony, J. L.; Brennecke, J. F.; Maginn, E. In *Ionic Liquids in Synthesis*; Wasserscheid, P.; Welton, T., Eds.; Wiley-VCH: Weinheim, 2008; Second Edition, Vol. 1, pp 103–129.
3. Maurer, G.; Pérez-Salado Kamps, Á. In *Developments and Applications in Solubility*; Letcher, T. M., Ed.; The Royal Society of Chemistry: Cambridge, 2007; pp 41–58.
4. Pérez-Salado Kamps, Á.; Tuma, D.; Xia, J.; Maurer, G. *J. Chem. Eng. Data* **2003**, *48*, 746–749.
5. Kumełan, J.; Pérez-Salado Kamps, Á.; Tuma, D.; Maurer, G. *Fluid Phase Equilib.* **2005**, *228–229*, 207–211.
6. Kumełan, J.; Pérez-Salado Kamps, Á.; Urukova, I.; Tuma, D.; Maurer, G. *J. Chem. Thermodynamics* **2005**, *37,* 595–602; *J. Chem. Thermodynamics* 2**007**, *39*, 335.
7. Kumełan, J.; Pérez-Salado Kamps, Á.; Tuma, D.; Maurer, G. *J. Chem. Eng. Data* **2006**, *51*, 11–14.
8. Kumełan, J.; Pérez-Salado Kamps, Á.; Tuma, D.; Maurer, G. *J. Chem. Thermodynamics* **2006**, *38*, 1396–1401.
9. Kumełan, J.; Pérez-Salado Kamps, Á.; Tuma, D.; Maurer, G. *J. Chem. Eng. Data* **2006**, *51*, 1364–1367.
10. Kumełan, J.; Pérez-Salado Kamps, Á.; Tuma, D.; Maurer, G. *J. Chem. Eng. Data* **2006**, *51*, 1802–1807.

Downloaded by 89.163.35.42 on June 28, 2012 | http://pubs.acs.org
Publication Date (Web): December 18, 2009 | doi: 10.1021/bk-2009-1030.ch001

Downloaded by 89.163.35.42 on June 28, 2012 | http://pubs.acs.org
Publication Date (Web): December 18, 2009 | doi: 10.1021/bk-2009-1030.ch001

11. Kumełan, J.; Pérez-Salado Kamps, Á.; Tuma, D.; Maurer, G. *Fluid Phase Equilib.* **2007**, *260*, 3–8.
12. Kumełan, J.; Pérez-Salado Kamps, Á.; Tuma, D.; Maurer, G. *J. Chem. Eng. Data* **2007**, *52*, 2319–2324.
13. Kumełan, J.; Pérez-Salado Kamps, Á.; Tuma, D.; Maurer, G. *Ind. Eng. Chem. Res.* **2007**, *46*, 8236–8240.
14. Kumełan, J.; Pérez-Salado Kamps, Á.; Tuma, D.; Yokozeki, A.; Shiflett, M. B.; Maurer, G. *J. Phys. Chem. B* **2008**, *112*, 3040–3047.
15. Kumełan, J.; Pérez-Salado Kamps, Á.; Tuma, D.; Maurer, G. *J. Chem. Eng. Data*, DOI.10.1021/je8007556.
16. Kumełan, J. Doctoral thesis, University of Kaiserslautern, Germany, in preparation.
17. Costa Gomes, M. F. *J. Chem. Eng. Data* **2007**, *52*, 472–475.
18. Anderson, J. L.; Dixon, J. K.; Brennecke, J. F. *Acc. Chem. Res.* **2007**, *40*, 1208–1216.
19. Baltus, R. E.; Culbertson, B. H.; Dai, S.; Luo, H.; DePaoli, D. W. *J. Phys. Chem. B* **2004**, *108*, 721–727.
20. Camper, D.; Bara, J.; Koval, C.; Noble, R. *Ind. Eng. Chem. Res.* **2006**, *45*, 6279–6283.
21. Finotello, A.; Bara, J. E.; Camper, D.; Noble, R. D. *Ind. Eng. Chem. Res.* **2008**, *47*, 3453–3459.
22. Ohlin, C. A.; Dyson, P. J.; Laurenczy, G. *Chem. Commun.* **2004**, 1070–1071.
23. Kumełan, J.; Tuma, D.; Maurer, G. *Fluid Phase Equilib.* **2009**, *275*, 132–144.
24. Jessop, P. G.; Subramaniam, B. *Chem. Rev.* **2007**, *107*, 2666–2694.
25. Costa Gomes, M.; Pádua, A. A. H. In *Developments and Applications in Solubility*; Letcher, T. M., Ed.; The Royal Society of Chemistry: Cambridge, 2007; pp 153–170.
26. Hunt, P. A.; Maginn, E. J.; Lynden-Bell, R. M.; Del Pópolo, M. G. In *Ionic Liquids in Synthesis*; Wasserscheid, P.; Welton, T., Eds.; Wiley-VCH: Weinheim, 2008; Second Edition, Vol. 1, pp 206–249.
27. Maginn, E. J. *Acc. Chem. Res.* **2007**, *40*, 1200–1207.
28. Rebelo, L. P. N.; Canongia Lopes, J. N.; Esperança, J. M. S. S.; Guedes, H. J. R.; Łachwa, J.; Najdanovic-Visak, V.; Visak, Z. *Acc. Chem. Res.* **2007**, *40*, 1114–1121.
29. Pádua, A. A. H.; Costa Gomes, M. F.; Canongia Lopes, J. N. A. *Acc. Chem. Res.* **2007**, *40*, 1087–1096.
30. Lynden-Bell, R. M.; Del Pópolo, M. G.; Youngs, T. G. A.; Kohanoff, J.; Hanke, C. G.; Harper, J. B.; Pinilla, C. C. *Acc. Chem. Res.* **2007**, *40*, 1138–1145.
31. Urukova, I.; Maurer, G. University of Kaiserslautern, unpublished results.

32. Urukova, I.; Vorholz, J.; Maurer, G. *J. Phys. Chem. B* **2005**, *109*, 12154–12159; *J. Phys. Chem. B* **2006**, *110*, 18072.
33. Straub, J. E.; Karplus, M. *Chem. Phys.* **1991**, *158*, 221–248.
34. Harris, J. G.; Yung, K. H. *J. Phys. Chem.* **1995**, *99*, 12021–12024.
35. Shah, J. K.; Brennecke, J. F.; Maginn, E. J. *Green Chem.* **2002**, *4*, 112–118.
36. Adrian, T.; Wendland, M.; Hasse, H.; Maurer, G. J. *Supercrit. Fluids* **1998**, *12*, 185–221.
37. Elgin, J. C.; Weinstock, J. J. *J. Chem. Eng. Data* **1959**, *4*, 3–12.
38. Nunes da Ponte, M.; Rebelo, L. P. N. In *Developments and Applications in Solubility*; Letcher, T. M., Ed.; The Royal Society of Chemistry: Cambridge, 2007; pp 59–65.
39. Aki, S. N. V. K.; Brennecke, J. F. *Ind. Eng. Chem. Res.* **2006**, *45*, 5574–5585.
40. Zhang, Z.; Wu, W.; Liu, Z.; Han, B.; Gao, H.; Jiang, T. *Phys. Chem. Chem. Phys.* **2004**, *6*, 2352–2357.
41. Lim, H.-H.; Kim, J.-W.; Paek, S.-M.; Son, B.-K.; Lee, C.-S.; Lee, H.; Ra, C.-S.; Shim, J.-J. *Clean Technol.* **2006**, *12*, 128–137.
42. Freitag, J.; Sanz Díez, M. T.; Tuma, D.; Ulanova, T. V.; Maurer, G. *J. Supercrit. Fluids* **2004**, *32*, 1–13.
43. Chobanov, K. Doctoral thesis, University of Kaiserslautern, Germany, in preparation.
44. Ventura, S. P. M.; Pauly, J.; Daridon, J. L.; Lopes da Silva, J. A.; Marrucho, I. M.; Dias, A. M. A.; Coutinho, J. A. P.; *J. Chem. Thermodynamics* **2008**, *40*, 1187–1192.

Downloaded by 89.163.35.42 on June 28, 2012 | http://pubs.acs.org
Publication Date (Web): December 18, 2009 | doi: 10.1021/bk-2009-1030.ch001

Downloaded by DUKE UNIV on June 28, 2012 | http://pubs.acs.org
Publication Date (Web): December 18, 2009 | doi: 10.1021/bk-2009-1030.ch002

## Chapter 2

# Solubility of Fluorocarbons in Room Temperature Ionic Liquids

**Mark B. Shiflett[1] and A. Yokozeki[2]**

[1] **DuPont Central Research and Development, Experimental Station 304, Wilmington, Delaware 19880-0304**
[2] **DuPont Fluoroproducts Laboratory, Chestnut Run Plaza 711, Wilmington, Delaware 19880-0711**

In this article, we summarise our investigation of the unique phase behaviour of fluorocarbons in room temperature ionic liquids. Gaseous absorption measurements (vapour-liquid equilibria, VLE) were performed using a gravimetric microbalance at various isothermal conditions (temperature between 283.15 and 348.15 K) and at pressures < 2 MPa. Experimental gas solubility data have been successfully correlated using both well-known solution models and a generic Redlich-Kwong (RK) type of cubic equation of state (EOS). Henry's law constants ($k_H$) have been calculated, and a linear correlation has been discovered between $k_H$ and fluorocarbon (methane and ethane series) critical temperature. The equation of state has been used to predict the global phase behaviour, which indicates that many of these systems belong to either type III or type V according to the Scott-van Konynenburg classification scheme. Vapour liquid-liquid equilibria (VLLE) measurements were conducted using simple mass-volume and cloud-point methods to verify the equation

In Ionic Liquids: From Knowledge to Application; Plechkova, N., et al.;
ACS Symposium Series; American Chemical Society: Washington, DC, 2010.

of state predictions. The unique lower critical solution temperature (LCST) behaviour for type-V systems, the large negative excess molar volumes in ionic liquid-rich side solutions, and the strong hydrogen-bonding capability are discussed. The large differences in the solubilities which exist among fluorocarbons have led us to consider using room temperature ionic liquids as extractants for separation and purification.

Downloaded by DUKE UNIV on June 28, 2012 | http://pubs.acs.org
Publication Date (Web): December 18, 2009 | doi: 10.1021/bk-2009-1030.ch002

# Introduction

Fluorocarbons are important industrial compounds typically composed of a few carbon atoms and one or more fluorine atoms *(1)*. Fluorocarbons may also contain other atoms such as hydrogen, oxygen and chlorine which lead to the following classifications: perfluorocarbons (PFCs), chlorofluorocarbons (CFCs), hydrochlorofluorocarbons (HCFCs), hydrofluorocarbons (HFCs) and hydrofluoroethers (HFEs). One of the most important applications of fluorocarbons in modern society has been their use as refrigerants in vapour compression systems (*i.e.* refrigerators, air-conditioners, chillers and heat pumps). Other applications include precision cleaning, foam blowing, and plasma etching, to name a few. Many of these applications require high purity such as refrigerants (>99.9%) and plasma etchants (>99.99995%). The processes for manufacturing fluorocarbons often result in co-products and undesired side-products which can require expensive, energy-intensive cryogenic distillation for separation. In some cases, these mixtures form homogeneous or heterogeneous azeotropes and methods such as extractive distillation are required to achieve separation.

We have conducted the first comprehensive study of the phase behaviour of room temperature ionic liquids with a variety of fluorocarbons to develop a fundamental knowledge about their mixture properties and to assess new applications for separation and purification. Table 1 provides a list of common methane and ethane-series fluorocarbons which were studied, and includes the refrigerant abbreviation, chemical formula, CAS registry number, normal boiling point and critical point temperatures. Ionic liquids belong to a new class of compounds, which are molten salts with low melting points (< 373 K) *(2)*. A unique feature of ionic liquids is a practical lack of vapour pressure which makes them useful as new solvents for extractive distillation. This article is a summary of our published works on the global phase behaviour of fluorocarbons in room-temperature ionic liquids *(3-16)*.

Downloaded by DUKE UNIV on June 28, 2012 | http://pubs.acs.org
Publication Date (Web): December 18, 2009 | doi: 10.1021/bk-2009-1030.ch002

# Experimental

## Materials

High-quality measurements begin with an analysis of the starting materials. In particular, the effect of impurities can have a large effect on thermophysical property measurements. For this reason, we have carefully analysed the purity of the fluorocarbons and ionic liquids used in our work *(3-16)*.

The majority of the fluorocarbons tested were obtained from DuPont Fluoroproducts (Wilmington, Delaware). The purities of the fluorocarbons were measured using a gas chromatography (GC) method (Agilent 6890N, Restek Rtx-200 column, 105 m x 0.25 mm). The purity for each fluorocarbon was reported in our previous works *(3-16)* and most fluorocarbons had a minimum purity of 99 mole percent. The fluorocarbons were used without additional purification; however, a molecular sieve trap was installed to remove trace amounts of moisture from the gases prior to entering the microbalance.

Several commercially available ionic liquids were studied, as well as ten new ionic liquids with fluorinated anions which were synthesised *(4,5)*. Two of the most common ionic liquids studied in our work were 1-butyl-3-methylimidazolium hexafluorophosphate ($[C_4mim][PF_6]$, CAS registry no. 174501-64-5) and 1-ethyl-3-methylimidazolium bis{(trifluoromethyl)sulfonyl}-amide ($[C_2mim][NTf_2]$, CAS registry no. 174899-82-2). $[C_4mim][PF_6]$ and $[C_2mim][NTf_2]$ were obtained from Fluka, Sigma-Aldrich Chemie GmbH (Buchs, Switzerland) and Covalent Associates Inc. (Corvallis, OR), respectively. The stated purity of the $[C_4mim][PF_6]$ and $[C_2mim][NTf_2]$ were >97% and >99.5%, respectively. The ionic liquid samples were carefully analysed to verify the purity using a variety of analytical methods.

The initial as-received mass fraction of water was measured by Karl Fischer titration (Aqua-Star C3000). The extractable ions (fluorine, chlorine, bromine) were measured by ion chromatography (column DIONEX AS17). The total chlorine ion content was measured using a Wickbold torch and ion chromatography method. Elemental analysis was performed by Schwarzkopf Microanalytical Laboratory, Inc. (Woodside, NY). Table 2 provides an example of the chemical analysis of the $[C_2mim][NTf_2]$ ionic liquid *(13)*.

## Table 1. Properties of Fluorocarbon Compounds

| *Refrigerant Abbreviation* | *Chemical Formula* | *CAS Number* | $T_b$ */ K* | $T_c$ */ K* |
|---|---|---|---|---|
| PFC-14 | $CF_4$ | 75-73-0 | 145.10 [b] | 227.51 [b] |
| CFC-11 | $CFCl_3$ | 75-69-4 | 296.86 [b] | 471.11 [b] |
| CFC-113 | $CFCl_2$-$CF_2Cl$ | 76-13-1 | 320.74 [a,b] | 487.21 [b] |
| CFC-113a | $CCl_3$-$CF_3$ | 354-58-5 | 319.31 [c] | 483.42 [c] |
| CFC-114 | $CF_2Cl$-$CF_2Cl$ | 76-14-2 | 276.74 [b] | 418.86 [d] |
| CFC-114a | $CFCl_2$-$CF_3$ | 374-07-2 | 276.59 [a] | 418.60 [d] |
| HCFC-123 | $CHCl_2$-$CF_3$ | 306-83-2 | 300.97 [b] | 456.83 [b] |
| HCFC-123a | $CHClF$-$CF_2Cl$ | 354-23-4 | 301.35 [f] | 461.60 [e] |
| HCFC-124 | $CHFCl$-$CF_3$ | 2837-89-0 | 261.19 [a,b] | 395.43 [b] |
| HCFC-124a | $CHF_2$-$CF_2Cl$ | 354-25-6 | 261.38 [a] | 399.90 [d] |
| HFC-23 | $CHF_3$ | 75-46-7 | 191.13 [b] | 299.29 [b] |
| HFC-32 | $CH_2F_2$ | 75-10-5 | 221.50 [b] | 351.26 [b] |
| HFC-41 | $CH_3F$ | 593-53-3 | 195.03 [b] | 317.28 [b] |
| HFC-125 | $CHF_2$-$CF_3$ | 354-33-6 | 225.06 [b] | 339.17 [b] |
| HFC-134 | $CHF_2$-$CHF_2$ | 359-35-3 | 253.10 [a] | 391.74 [a] |
| HFC-134a | $CH_2F$-$CF_3$ | 811-97-2 | 247.08 [b] | 374.21 [b] |
| HFC-143a | $CH_3$-$CF_3$ | 420-46-2 | 225.91 [b] | 345.86 [b] |
| HFC-152a | $CHF_2$-$CH_3$ | 75-37-6 | 249.13 [b] | 386.41 [b] |
| HFC-161 | $CH_2F$-$CH_3$ | 353-36-6 | 235.60 [b] | 375.30 [b] |
| HFE-125 | $CHF_2$-O-$CF_3$ | 3822-68-2 | 238.09 [b] | 354.62 [b] |
| HFE-143a | $CH_3$-O-$CF_3$ | 421-14-7 | 249.24 [b] | 377.98 [b] |

Downloaded by DUKE UNIV on June 28, 2012 | http://pubs.acs.org
Publication Date (Web): December 18, 2009 | doi: 10.1021/bk-2009-1030.ch002

[a] *(17)*; [b] *(18)*; [c] *(19)*; [d] *(20)*; [e] *(21)*; [f] *(22)*

**Table 2. Chemical Analysis of [$C_2$mim][$NTf_2$] Ionic Liquid**

| | *Units* | *Calculated/ Reported* | *Measured* |
|---|---|---|---|
| *Assay* | | ≥ 99.5 [a] | ≥ 99.4 |
| *Elemental* | | | |
| C | % | 24.55 | 24.60 |
| H | % | 2.83 | 3.02 |
| F | % | 29.13 | 29.70 |
| N | % | 10.74 | 10.75 |
| S | % | 16.39 | 17.05 |
| O | % | 16.35 | NR [b] |
| *$H_2O$* [c] | x $10^{-6}$ | <50 | 413 ± 40 |
| *Halogens* | | | |
| F, Br, Cl [e] | x $10^{-6}$ | | BDL [d] |
| Cl [f] | x $10^{-6}$ | | 460 ± 20 |

[a] *(23)*, [b] Not Reported, [c] Karl Fischer titration (mass fraction)
[d] Below Detection Limit (< 5 $\mu$g $cm^{-3}$)
[e] Ion Chromatography (extractable or soluble F, Br, Cl; mass fraction)
[f] Wickbold torch (total Cl; mass fraction)

The ionic liquids were dried and degassed before use by filling a borosilicate glass tube with about 10 g of material and initially pulling a course vacuum with a diaphragm pump (Pfeiffer model MVP055-3, Nashua, NH) for about 3 h. To ensure that the ionic liquids were as dry as possible, the samples were evacuated further using a turbopump (Pfeiffer, model TSH-071) to a pressure of about 5 x $10^{-7}$ kPa while simultaneously heating and stirring the ionic liquid at a temperature of about 348 K for 5 d. This technique was found to reduce the mass fraction of water in most cases to less than 200 x $10^{-6}$ for the [$C_2$mim][$NTf_2$] and [$C_4$mim][$PF_6$] ionic liquids.

## Gas solubility (vapour-liquid equilibria) measurements

The gas solubility measurements were made using a gravimetric microbalance (Hiden Isochema Ltd, IGA 003). Initially, ionic liquid (60 to

Downloaded by DUKE UNIV on June 28, 2012 | http://pubs.acs.org
Publication Date (Web): December 18, 2009 | doi: 10.1021/bk-2009-1030.ch002

80 mg) was loaded into the sample container and heated to 348.2 K under a vacuum of about $10^{-9}$ MPa for 10 to 24 h to remove any trace amounts of water or other impurities. Typically, four isotherms were measured at 283.2, 298.2, 323.2, and 348.2 K over a pressure range from about 0.01 to 2.0 MPa. The upper pressure limit for each gas was dependent on the saturation pressure in the sample container at ambient temperature. To ensure sufficient time for gas-liquid equilibrium, the ionic liquid samples were maintained at each pressure set point for a minimum of 3 h with a maximum time-out of 20 h. Additional experimental details are provided in *(24)*.

An important aspect of high-quality experimental work is to carefully consider the effect of errors on the measurements. In the case of the microbalance, the instrumental uncertainties in $T$ and $P$ are within 0.1 K and 0.8 kPa, respectively. These errors do not cause any significant changes in the gas solubility (mole fraction) measurement. One of the largest sources of error in the present experiment is data reproducibility. Our best estimate for the present experimental reproducibility error, including the sample (ionic liquid) purity effect, has been <0.005 mole fraction. The next largest systematic error is attributed to the buoyancy correction in the data analysis. When gas dissolves in the ionic liquid, the liquid volume will expand. The change in liquid volume affects the buoyancy force of the sample in the gravimetric microbalance. This force is often neglected, but we have developed a method for estimating this volume change in the liquid solution *(3)*. We have estimated a systematic error attributed to this effect to be <0.002 mole fraction in our experiments. Thus, total errors in the solubility data arising from both random and systematic errors have been estimated to be <0.006 mole fractions at each given $T$ and $P$.

Downloaded by DUKE UNIV on June 28, 2012 | http://pubs.acs.org
Publication Date (Web): December 18, 2009 | doi: 10.1021/bk-2009-1030.ch002

### Mass-volume (vapour-liquid-liquid equilibria) measurements

When a binary system exhibits a liquid-liquid separation (or VLLE), it is a *univariant* state according to the Gibbs phase rule. This means that at a given intensive variable, say temperature, there is no freedom for other intensive variables. All other variables such as compositions, pressure, and densities of the system are uniquely determined regardless of any different extensive variables (volume of each phase and total mass of the system). The overall feed composition merely changes the physical volume in each phase, but the composition and density in each phase remains constant as long as the three phases exist at the fixed $T$.

This unique VLLE state of a binary system can be determined experimentally using a simple apparatus by mass-and-volume measurements *alone* without using any analytical method for the composition analysis. A set of mass-and-volume measurements of two sample containers at a constant temperature is sufficient to determine the required thermodynamic property. A detailed description of the experimental equipment, procedure, error analysis, and principle of the method is available in our previous reports *(8,9)*.

### Cloud-point measurements

To prove the existence of a lower critical solution temperature (LCST) of the VLLE curve, cloud-point measurements were performed. Starting at a temperature where two liquid phases existed, the temperature was lowered with manual mixing in a constant-temperature bath until only a single phase existed. Once the samples were single phase, the temperature was slowly (2 K $h^{-1}$) raised until a cloud layer became visible inside the tube. The cloud-point temperature was recorded when the cloud layer started to form. These experiments are not always straight-forward because the rate of temperature change, the intensity and duration of mixing, and the time required to obtain both a single phase and cloud point were important to control. Several detailed examples of the method are provided in *(8-13)*.

### Safety

The experiments described here were performed under elevated pressures; therefore all equipment should have the proper pressure ratings, relief devices, and safety factors. In some cases the fluorocarbons (*e.g.*, HFC-32, HFC-41, HFC-143a, HFC-152a, and HFC-161) are flammable and proper handling and ventilation are required.

## Modelling

### Activity model

In general, low-and-medium pressure VLE (vapour liquid equilibria) for an $N$-component system can be described by Equation (1) *(25)*:

$$y_i P \Phi_i = x_i \gamma_i P_i^s \quad (i = 1, .., N), \tag{1}$$

where, $y$ = vapour phase mole fraction,
$x$ = liquid phase mole fraction,
$P$ = system pressure,

Downloaded by DUKE UNIV on June 28, 2012 | http://pubs.acs.org
Publication Date (Web): December 18, 2009 | doi: 10.1021/bk-2009-1030.ch002

$P_i^s$ = saturated vapour pressure of *i-th* species,

$\gamma$ = activity coefficient (function of compositions and $T$),

$\Phi_i$ = a correction factor for *i-th* species (≈ 1 for sufficiently low $P$ systems).

For a binary system ($N = 2$) of gas (1) / ionic liquid (2) mixtures, it is reasonable to assume that $y_1 = 1$ (or $y_2 = 0$) at temperatures of the present interest; *i.e.* $P_2^s \approx 0$. Then, the activity coefficient for species 1 is given by Equation (2):

$$\gamma_1 = \frac{P\Phi_1}{x_1 P_1^s}. \tag{2}$$

To analyse experimental solubility data using the activity coefficient of Equation (2), we use the common non-random two liquid (NRTL) activity model. Details regarding how to properly solve for the correction factor, $\Phi_1$, second viral coefficient, $B_1(T)$ and NRTL adjustable parameters are provided in *(3,26)*.

## Equation of State Model

In order to understand the global phase behaviour of the present systems, we have employed a generic Redlich-Kwong (RK) type of cubic equation of state *(28,29)* which is written in the following form:

$$P = \frac{RT}{V-b} - \frac{a(T)}{V(V+b)} \tag{3}$$

where,

$$a(T) = 0.427480\frac{R^2T_c^2}{P_c}\alpha(T) \tag{4}$$

$$b = 0.08664\frac{RT_c}{P_c}, \tag{5}$$

Downloaded by DUKE UNIV on June 28, 2012 | http://pubs.acs.org
Publication Date (Web): December 18, 2009 | doi: 10.1021/bk-2009-1030.ch002

The temperature-dependent part of the parameter *a* in the equation of state for pure compounds is modelled by the following empirical form *(29)*:

$$\alpha(T) = \sum_{k=0}^{\leq 3} \beta_k (1/T_r - T_r)^k \text{ , for } T_r \equiv T/T_c \leq 1, \tag{6a}$$

$$\alpha(T) = \beta_0 + \beta_1 [\exp\{2(1 - T_r)\} - 1], \text{ for } T_r \geq 1. \tag{6b}$$

The coefficients, $\beta_k$, are determined so as to reproduce the vapour pressure of each pure compound. For ionic liquids, however, usually no vapour pressure data are available (practically non-volatile); and furthermore, no data for the critical parameters ($T_c$ and $P_c$) exist. The critical parameters can be estimated in various ways. As discussed in *(29)*, rough estimates for the critical parameters of non-volatile compounds are sufficient for the present purpose. On the other hand, the temperature-dependent part of the parameter *a* of the ionic liquid, Equation (6) is significantly important when we try to correlate the solubility (pressure-temperature-composition: *PTx*) data, although the vapour pressure of ionic liquid is essentially zero at the temperature of interest. Therefore, the coefficient $\beta_1$ for ionic liquids in Equation (6) are usually treated as an adjustable fitting parameter using $\beta_0 = 1$ and $\beta_2 = \beta_3 = 0$ in the solubility data analysis, together with the binary interaction parameters discussed below. However, once it was determined for a particular ionic liquid using a certain binary system, it will be used as a fixed constant for any other binary systems containing that ionic liquid.

Then, the parameters *a* and *b* for a general *N*-component mixture are modelled in terms of binary interaction parameters *(29)*:

$$a = \sum_{i,j=1}^{N} \sqrt{a_i a_j} f_{ij}(T)(1 - k_{ij}) x_i x_j, \quad a_i = 0.427480 \frac{R^2 T_{ci}^2}{P_{ci}} \alpha_i(T) \tag{7}$$

$$f_{ij}(T) = 1 + \tau_{ij}/T, \quad \text{where } \tau_{ij} = \tau_{ji}, \text{ and } \tau_{ii} = 0. \tag{8}$$

$$k_{ij} = \frac{l_{ij} l_{ji} (x_i + x_j)}{l_{ji} x_i + l_{ij} x_j}, \text{ where } k_{ii} = 0. \tag{9}$$

Downloaded by DUKE UNIV on June 28, 2012 | http://pubs.acs.org
Publication Date (Web): December 18, 2009 | doi: 10.1021/bk-2009-1030.ch002

$$b=\frac{1}{2}\sum_{i,j=1}^{N}\left(b_i+b_j\right)\left(1-k_{ij}\right)\left(1-m_{ij}\right)x_i x_j,\quad b_i=0.08664\frac{RT_{ci}}{P_{ci}}, \tag{10}$$

where, $m_{ij}=m_{ji}$, and $m_{ii}=0$, $T_{ci}$ : critical temperature of *i*-th species, $P_{ci}$ : critical pressure of *i*-th species, and $x_i$ : mole fraction of *i*-th species.

In the above model, there are a maximum of four binary interaction parameters: $l_{ij}$, $l_{ji}$, $m_{ij}$, and $\tau_{ij}$ for each binary pair. It should be noted that when $l_{ij}=l_{ji}$ in Equation (9) and $f_{ij}=1$ in Equation (8), Equation (7) becomes the ordinary quadratic-mixing rule for the *a* parameter. The present equation of state model has been successfully applied for highly non-symmetric (with respect to the polarity and size) mixtures such as various refrigerant/oil mixtures *(28,29)*. The fugacity coefficient $\phi_i$ of *i*-th species for the present EOS model, which is needed for the phase equilibrium calculation, is given by:

$$\ln\phi_i=\ln\frac{RT}{P(V-b)}+b'_i\left(\frac{1}{V-b}-\frac{a}{RTb(V+b)}\right)+\frac{a}{RTb}\left(\frac{a'_i}{a}-\frac{b'_i}{b}+1\right)\ln\frac{V}{V+b} \tag{11}$$

where,

$a'_i\equiv\left(\frac{\partial na}{\partial n_i}\right)_{n_{j\neq i}}$ and $b'_i\equiv\left(\frac{\partial nb}{\partial n_i}\right)_{n_{j\neq i}}$ : $n$ = total mole number and $n_i$ = mole number of *i*-th species (or $x_i=n_i/n$). The explicit forms of $a_i^{'}$ and $b_i^{'}$ are:

$$a_i^{'}=2\sum_{j=1}^{N}\sqrt{a_i a_j}\,f_{ij}x_j\left\{1-k_{ij}-\frac{l_{ij}l_{ji}\left(l_{ij}-l_{ji}\right)x_i x_j}{\left(l_{ji}x_i+l_{ij}x_j\right)^2}\right\}-a \tag{12}$$

$$b_i^{'}=\sum_{j=1}^{N}\left(b_i+b_j\right)\left(1-m_{ij}\right)x_j\left\{1-k_{ij}-\frac{l_{ij}l_{ji}\left(l_{ij}-l_{ji}\right)x_i x_j}{\left(l_{ji}x_i+l_{ij}x_j\right)^2}\right\}-b \tag{13}$$

Phase equilibria ($\alpha,\beta,\gamma$, …, coexisting phases) for an *N*-component system can be obtained by solving the following equilibrium conditions:

$$x_i^{\alpha}\phi_i^{\alpha}=x_i^{\beta}\phi_i^{\beta}=x_i^{\gamma}\phi_i^{\gamma}=........,\quad (i=1,\ldots,N) \tag{14}$$

Downloaded by DUKE UNIV on June 28, 2012 | http://pubs.acs.org
Publication Date (Web): December 18, 2009 | doi: 10.1021/bk-2009-1030.ch002

where,

$x_i^{\alpha}$ , $x_i^{\beta}$ , $x_i^{\gamma}$ , ….: mole fractions of $\alpha, \beta, \gamma,$ … phases for the *i-th* species

$\phi_i^{\alpha}$ , $\phi_i^{\beta}$ , $\phi_i^{\gamma}$ , …: fugacity coefficients of $\alpha, \beta, \gamma,$ … phases for the *i-th* species.

## Results and Discussion

Solubility data (*P, T*, *x*) have been measured for the fluorocarbons provided in Table 1 with several ionic liquids including [C$_4$mim][PF$_6$] and [C$_2$mim][NTf$_2$] *(3-16)*. Figure 1 shows a plot of the normalised pressures (or more precisely, normalised-fugacities at 298.15 K) *vs*. molar compositions, which measures the deviation from the ideal solubility behaviour (Raoult's law).

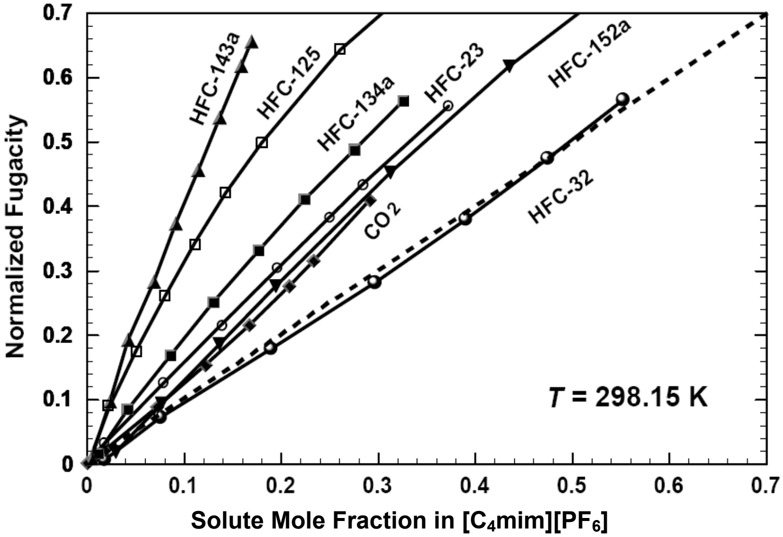

*Figure 1. Normalised fugacity versus mole fraction of refrigerant (solute) in ionic liquid [C$_4$mim][PF$_6$]. Symbols: experimental measurements, Dashed line: Raoult's law, Solid lines: trend lines. (3; used with permission).*

Surprisingly large differences in the solubility among the same family of compounds (HFCs) are clearly observed, such as from a slightly negative deviation in HFC-32 to a highly positive deviation in HFC-143a. These behaviours were quite unexpected and did not correlate with the fluorocarbon dipole moment. The large differences in solubility led us to consider the use of ionic liquids as extractants for separating close-boiling or azeotropic mixtures such as HFC-32 and HFC-125 *(6)*.

Solubility data have been modelled using both activity models (*e.g*. NRTL) *(3-5,7)* and a modified RK type EOS *(8-10)*. The advantage of using the

Downloaded by DUKE UNIV on June 28, 2012 | http://pubs.acs.org
Publication Date (Web): December 18, 2009 | doi: 10.1021/bk-2009-1030.ch002

equation of state model is the ability to predict high-pressure VLE and VLLE from only the low-pressure solubility data measurements *(10)*. For example, let us consider the binary system of HFC-23 and [$C_4$mim][$PF_6$]. Using only low pressure VLE measurements, the equation of state model predicts liquid-liquid phase separations with a LCST in the HFC-23 rich side solutions as shown in Figure 2.

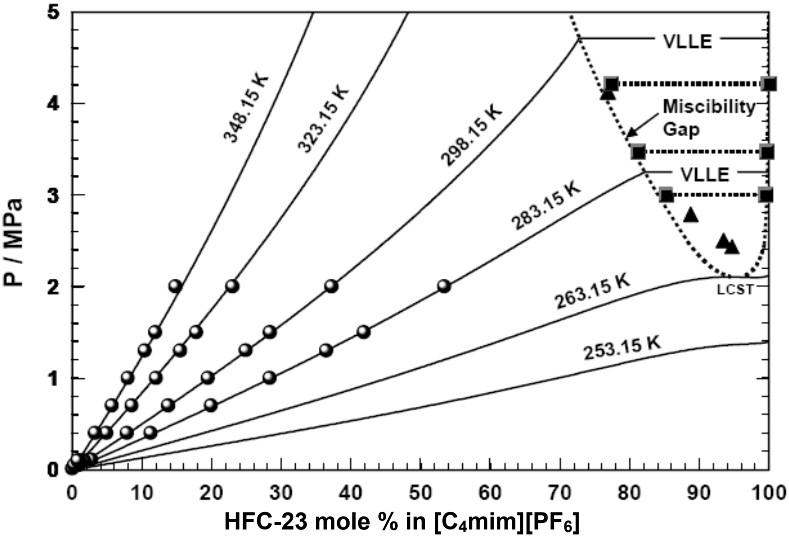

*Figure 2. Isothermal PTx phase diagrams for HFC-23 + [$C_4$mim][$PF_6$] mixtures. Solid lines and broken lines: EOS predictions. Circles: VLE experimental data (3), which were used to construct the present EOS model. Squares: experimental VLLE data (10). Triangles: experimental cloud-point data. (10; used with permission.)*

In order to verify these predictions, VLLE experiments using the mass-volume technique were measured. To prove the existence of the LCST of the VLLE curve, cloud-point measurements have also been performed. The EOS model predictions are in excellent agreement with the experimental data, showing VLLE in the HFC-23 rich-side solutions with a LCST. Figure 2 suggests the type V mixture behaviour for this binary system, according to the classification of van Konynenburg and Scott *(30,31)*. Other binary systems that have been measured which belong to the type V mixture behaviour include (HCFC-123, HFC-125, HFC-134a, and HFC-152a) + [$C_4$mim][$PF_6$] *(8,9,12)*; and (HCFC-123, HCFC-123a, HCFC-124, HCFC-124a, HFC-134, HFC-134a) + [$C_2$mim][$NTf_2$] *(13)*. However, some systems such as HFC-41 and [$C_4$mim][$PF_6$] shown in Figure 3 did not show a LCST. Therefore, this binary system belongs to the type-III mixture behaviour *(30,31)*. Other type-III

Downloaded by DUKE UNIV on June 28, 2012 | http://pubs.acs.org
Publication Date (Web): December 18, 2009 | doi: 10.1021/bk-2009-1030.ch002

systems include HFC-143a + [C$_4$mim][PF$_6$] and HFC-161 + [C$_4$mim][PF$_6$]. In the case of HFC-32 and HFC-134a isomers in [C$_4$mim][PF$_6$], the equation of state model does not predict any VLLE behaviour below the critical temperature of these fluorocarbons (Table 1). VLLE might exist above the critical temperature, which would classify these binary systems as type-V mixture behaviour, but if no VLLE exists, then these systems will be the simple type-I mixture behaviour.

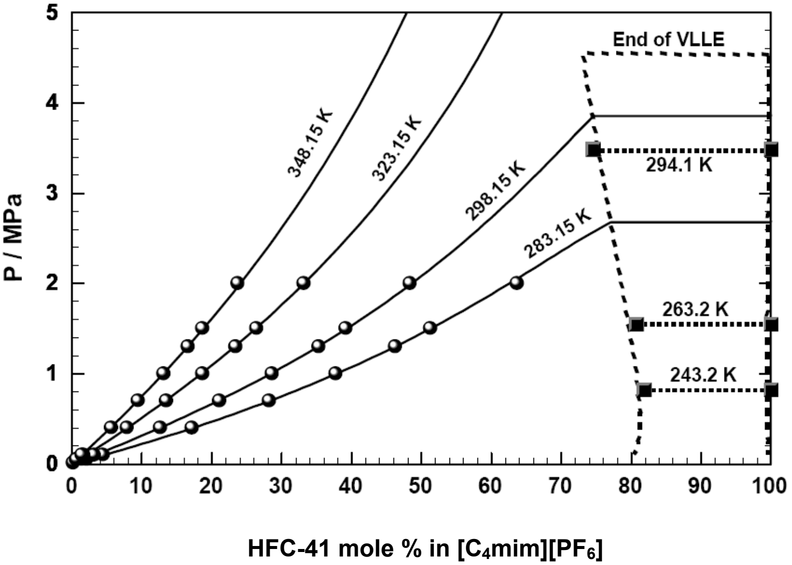

*Figure 3. Isothermal PTx phase diagrams for HFC-41 + [C$_4$mim][PF$_6$] mixtures. Solid lines and broken lines: equation of state predictions. Circles: VLE experimental data (7), which were used to construct the present EOS model. Squares: experimental VLLE data (9), Triangles: experimental cloud-point data (9).*

The mass-volume method also provides molar volumes for each liquid phase. The excess molar volume of each liquid solution ($V^{ex'}$ and $V^{ex}$) can be obtained, by use of the pure component molar volumes $V_1^0$ (fluorocarbon) and $V_2^0$ (ionic liquid) using:

$$V^{ex'} = V_m - x'_1 V_1^0 - x'_2 V_2^0 \quad \text{or} \quad V^{ex} = V_m - x_1 V_1^0 - x_2 V_2^0 \qquad (15)$$

where $V_m$ is the measured molar volume of the mixture ($V_m = V'$ for the lower phase L' *or* $V_m = V$ for the upper phase L), and ($x'_1, x'_2$ or $x_1, x_2$) are mole fractions of fluorocarbon (1) and ionic liquid (2) in phase L' and L, respectively.

Downloaded by DUKE UNIV on June 28, 2012 | http://pubs.acs.org
Publication Date (Web): December 18, 2009 | doi: 10.1021/bk-2009-1030.ch002

Saturated liquid molar volumes for many fluorocarbons were calculated using an EOS programme *(18,19)*. Molar volume for ionic liquids were calculated from known or measured liquid density data *(4,5,24)*. Many fluorocarbons have shown large negative excess molar volumes in [$C_4$mim][$PF_6$] and [$C_2$mim][$NTf_2$] rich side solutions (-2 to -15 $cm^3$ $mol^{-1}$) *(8-14)*. Although it is not clear yet, both a size effect and hydrogen bonding may be involved. We have also discovered that $CO_2$ and ionic liquids (*e.g.*, [$C_4$mim][$PF_6$], [$C_6$mim][$NTf_2$], [$C_4$mim][$O_2CCH_3$]) can exhibit large negative excess molar volumes *(24,34,35)*. In some cases a complex is formed between $CO_2$ and the anion (*e.g.* [$O_2CCH_3$]) *(35-37)*. These unique and interesting findings pose an interesting challenge for theoretical modellers to explain these phenomena.

We have also analysed the solubility data to obtain Henry's law's constants, $k_H$ *(3,7,15)* because they can provide some important insights on solute and solvent interactions. We have discovered some empirical correlations of the observed Henry's law constants and determined that ln($k_H$) is linearly correlated with the VLE critical temperature ($T_c$) of pure HFCs, which have different slopes for the methane and ethane series of HFCs. Figure 4 shows the correlation at 298.15 K; other temperatures show similar trends.

Downloaded by DUKE UNIV on June 28, 2012 | http://pubs.acs.org
Publication Date (Web): December 18, 2009 | doi: 10.1021/bk-2009-1030.ch002

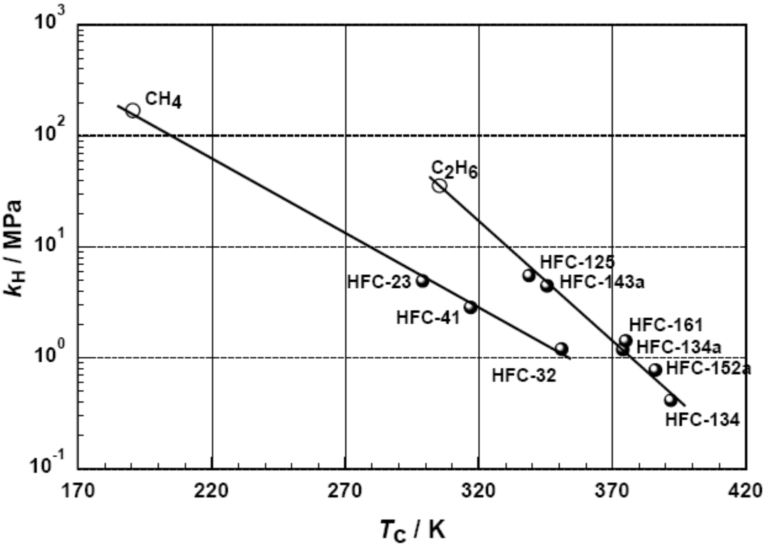

*Figure 4. Correlation of Henry's law constants, $k_H$, with respect to $T_c$, for methane- and ethane-series HFCs in [$C_4$mim][$PF_6$] at 298.15 K: Solid circles: (3,7). Open circles: (27); Solid lines: trend lines.*

There are no simple or obvious theoretical explanations for this excellent correlation. However, it is qualitatively understood in the following way: for pure compounds, $T_c$ is closely related to an intermolecular potential (attractive) well depth, $\varepsilon$ ; for example, $\varepsilon = 0.750kT_C$ for all inert gases ($k$ = Boltzmann constant) *(32,33)*. For binary solutions with the same solvent, the intermolecular potential strength between the solute and solvent will be represented by the magnitude of $\varepsilon$ of a pure solute only. On the other hand, $k_H$ is directly related to the excess chemical potential of solute at an infinitely dilute solution as shown by Equation (16).

$$k_H(T,P) = \exp\frac{\mu_1^{\infty} - \mu_1^{0}}{RT} \qquad (16)$$

where $\mu_1^{\infty}$ is the chemical potential of the solute at the infinitely dilute solution state (in the present case, at the system $T$ and $P \rightarrow 0$), and $\mu_1^0$ is the chemical potential referring to the pure gas (species 1) at the system $T$ and at a pressure of 1 atm. Therefore, $k_H$ must be related to $\varepsilon$ (or $T_c$). Then, from Equation (16), it suggests that $\ln(k_H)$ may be proportional to $T_c$. Now, we speculate that a similar linear relation ($\ln(k_H)$ *vs.* $T_c$) holds for other compounds in a given ionic liquid solvent, but having *different* slopes for *different class* of compounds. This led us to measure the solubility of $NH_3$ in ionic liquids which has a critical temperature ($T_c$ = 405.4 K). Based on our correlation, we predicted $NH_3$ would be highly soluble in room-temperature ionic liquid room-temperature ionic liquids; and our measurements have confirmed our predictions *(38,39)*. It will be interesting to continue testing this hypothesis in the future.

The results of our work have led us to examine the use of room-temperature ionic liquids (*e.g.*, $[C_4mim][PF_6]$, $[C_2mim][NTf_2]$) for separating close-boiling or azeotropic fluorocarbon mixtures. Several of the fluorocarbons shown in Table I form binary azeotropic mixtures (*e.g.,* HFC-32 / HFC-125, HFC-32 / HFC-143a, HFC-125 / HFC-143a) which are impossible to completely separate using conventional distillation techniques *(6)*. Extractive distillation has been the primary technique used in industry for the separation of mixtures, which have similar boiling points or form azeotropic compositions. A homogenous azeotropic composition is defined at a particular temperature or pressure where the liquid and vapour phase have the same composition (*i.e.*, 81.62 mol % HFC-32 / 18.38 mol % HFC-125 at 223.15 K); therefore, at this condition, rectification can no longer separate one component preferentially from the other. In an extractive distillation process, a solvent is added which selectively interacts with one or more of the components in the mixture so that separation is possible. In our case, HFC-32 is much more soluble than HFC-125 in $[C_4mim][PF_6]$ as shown in Figure 1. Process simulations using ASPEN Plus®

Downloaded by DUKE UNIV on June 28, 2012 | http://pubs.acs.org
Publication Date (Web): December 18, 2009 | doi: 10.1021/bk-2009-1030.ch002

software (40) indicate that HFC-32 / HFC-125 can be separated in good purity (> 99 mol %) with reasonable economics *(6)*. We have also studied the separation of isomer pairs (*e.g.*, HFC-134a / HFC-134 and fluorinated benzenes) and found that [$C_2$mim][$NTf_2$] is an effective extractive solvent *(13,41)*.

A unique solubility study of two diastereomers was also investigated. HF-4310mee or 2,3-dihydrodecafluoropentane ($CF_3CHFCHFCF_2CF_3$), is one of the chemical isomers of dihydrodecafluoropentane ($C_5H_2F_{10}$) consisting of two diastereomers (*threo*- and *erythro*-isomers) which are further composed of two *optical* isomers (or R and S types of D/L enantiomers), as illustrated in Figure 5.

| Chemical Name | Structures | $T_b$ /K |
|---|---|---|
| *Erythro*-2,3-dihydrodecafluoropentane | 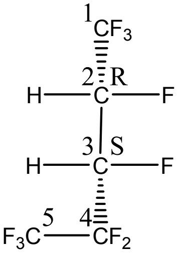<br>*Erythro* (2R,3S)<br>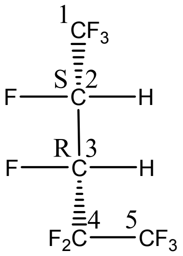<br>*Erythro* (2S,3R) | 320.1 |
| *Threo*-2,3-dihydrodecafluoropentane | 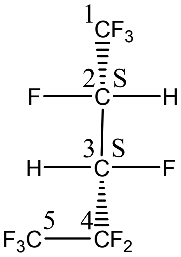<br>*Threo* (2S,3S)<br>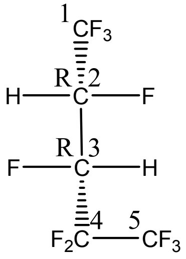<br>*Threo* (2R,3R) | 328.3 |

*Figure 5. Schematic molecular structures of HFC-4310mee (erythro- and threo-2,3-dihydrodecafluoropentanes). R and S (rectus and sinister, or right and left) refer to the configuration about the chiral (asymmetric) carbon atom. Normal boiling point ($T_b$).*

Downloaded by DUKE UNIV on June 28, 2012 | http://pubs.acs.org
Publication Date (Web): December 18, 2009 | doi: 10.1021/bk-2009-1030.ch002

HFC-4310mee was developed more than a decade ago as a replacement for ozone-depleting solvents such as 1,1,2-trichloro-1,2,2-trifluoroethane ($CFCl_2CF_2Cl$, CFC-113). These diastereoisomers (or chemical isomers) possess two *asymmetric* (or chiral) carbon atoms at the positions 2 and 3, and the *erythro*-isomer is made of the two (50/50%) optical isomers labelled (2R, 3S) and (2S, 3R), while the *threo*-isomer is composed of the two (50/50%) optical isomers labelled (2S, 3S) and (2R, 3R). The thermophysical properties between the (2R, 3S) and (2S, 3R) optical isomers are identical and similarly true for the (2S, 3S) and (2R, 3R) isomers. However, the *erythro*- and *threo*-isomers have significantly different thermodynamic properties; *e.g.*, the normal boiling points are 320.1 and 328.3 K for the former and the latter, respectively.

Liquid-liquid equilibria of HFC-4310mee diastereoisomers in ionic liquids (*e.g.*, $[C_4mim][PF_6]$, $[C_4mim][BF_4]$, $[C_2mim][BF_4]$) was measured using the mass-volume and cloud point methods *(11)*. All mixtures showed limited miscibility; however, the solubility differences between the cases of the *threo*- and *erythro*-isomers were quite dramatic, when considering the very similar chemical structures. *Tx* phase diagrams for *threo*- and *erythro*- isomers in $[C_4mim][PF_6]$ are shown in Figure 6. The *threo*-isomer has a LCST and at $T <$ 265 K is completely miscible. The *erythro*-isomer is only partially miscible (~10 mole % *erythro*-isomer) over the same temperature range. This means that not only the inclusion of a hydrogen atom, but the relative arrangement of the hydrogen atom on a carbon position is significantly important for the thermodynamic properties. Fluorocarbons (*i.e.*, HCFCs and HFCs) possess strong hydrogen-bonding (H-F-H) capability and the hydrogen bonding is highly directional; therefore, the relative positions of hydrogen-bonding atoms are important.

## Conclusions

We have studied the solubility of an important class of compounds – fluorocarbons in a variety of ionic liquids. We have found amazingly different solubilities among fluorocarbons in RTILs. Although the mechanism of the solubility difference is not clear at an intermolecular level, the engineering applications projected from the present discovery are quite significant in the field of material separations among fluorocarbons, such as extractive distillation and extraction solvents. The observed VLE ($P$, $T$, $x$) behaviours of electrolyte (ionic liquid) solutions with fluorocarbons have been well correlated with conventional solution (activity coefficient) models and a cubic equation of state. The EOS model based on low pressure VLE data alone can be highly reliable when extrapolating thermodynamic properties. Fluorocarbon + RTIL mixture behaviour indicate that these systems belong to either type III or type V according to the Scott-van Konynenburg classification. Large negative excess

Downloaded by DUKE UNIV on June 28, 2012 | http://pubs.acs.org
Publication Date (Web): December 18, 2009 | doi: 10.1021/bk-2009-1030.ch002

molar volumes indicate that the molecular size effect and hydrogen bonding capability are important. Future molecular dynamics calculations may provide further insight.

Downloaded by DUKE UNIV on June 28, 2012 | http://pubs.acs.org
Publication Date (Web): December 18, 2009 | doi: 10.1021/bk-2009-1030.ch002

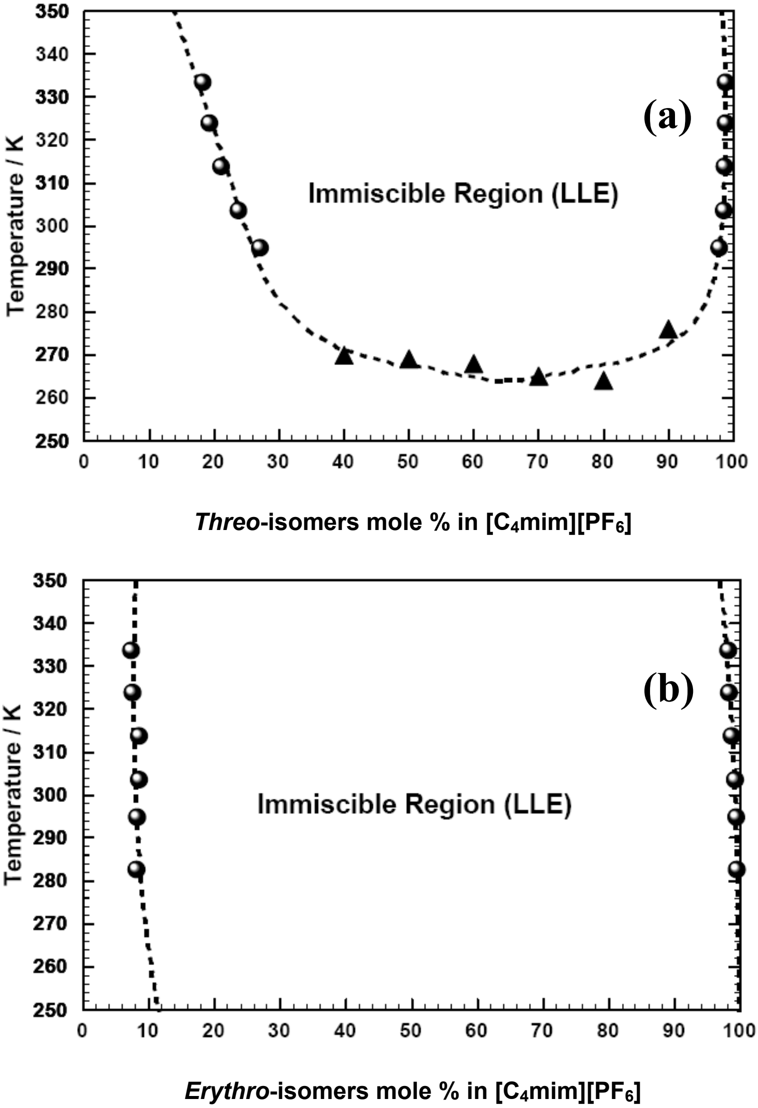

*Figure 6. Tx phase diagrams for LLE. (a) Threo-isomer + [$C_4$mim][$PF_6$] system and (b) Erythro-isomer + [$C_4$mim][$PF_6$] system. Broken line: calculated with the NRTL activity model. Symbols: experimental data (11); circles = VLLE experiments and triangles = the cloud-point method*

Downloaded by DUKE UNIV on June 28, 2012 | http://pubs.acs.org
Publication Date (Web): December 18, 2009 | doi: 10.1021/bk-2009-1030.ch002

# Acknowledgements

The authors thank Mr. Brian L. Wells and Mr. Joe Nestlerode at the DuPont Experimental Station for their assistance with the gas solubility and liquid-liquid equilibria measurements, respectively. They also appreciate Drs. Allen Sievert and Mario J. Nappa (DuPont Fluorochemicals) who kindly provided samples of CFC-113, CFC-113a, HCFC-123, *threo*- and *erythro*-isomers of HFC-4310mee and Drs. Christopher P. Junk, Mark A. Harmer, and Thomas Foo (DuPont Central Research and Development) who synthesised new ionic liquids. They also appreciate Dr. Lam H. Leung (DuPont Corporate Center for Analytical Science) for the GCMS fluorocarbon analysis. They also thank Dr. Marcia L. Huber (National Institute of Standards and Technology, Boulder, Colorado) for kindly providing new fluorocarbon data files (HFC-41, HFC-161, HFE-125, HFE-143a) for the Refprop software. DuPont Central Research and Development supported the present work.

# References

1. Downing, R. C. *Fluorocarbon Refrigerants Handbook*; Prentice Hall: Englewood Cliffs, NJ, 1988.
2. Wasserscheid, P.; Welton, T., Eds. Ionic Liquids in Synthesis, 2nd ed.; Wiley-VCH: Weinheim, Germany, 2008.
3. Shiflett, M. B.; Yokozeki, A. Solubility and Diffusivity of Hydrofluorocarbons in Room-Temperature Ionic Liquids. *AIChE J.* **2006**, *52(3)*, 1205-1219.
4. Shiflett, M. B.; Junk, C. P.; Harmer, M. A.; Yokozeki, A. Solubility and Diffusivity of Difluoromethane in Room-Temperature Ionic Liquids. *J. Chem. Eng. Data* **2006**, *51(2)*, 483-495.
5. Shiflett, M. B.; Junk, C. P.; Harmer, M. A.; Yokozeki, A. Solubility and Diffusivity of 1,1,1,2-tetrafluoroethane in Room-Temperature Ionic Liquids. *Fluid Phase Equilibr.* **2006**, *242*, 220-232.
6. Shiflett, M. B.; Yokozeki, A. Separation of difluoromethane and pentafluoroethane by extractive distillation using ionic liquid. *Chimica Oggi/Chem. Today* **2006**, *24*, 28-30.
7. Shiflett, M. B.; Yokozeki, A. Gaseous Absorption of Fluoromethane, Fluoroethane, and 1,1,2,2-Tetrafluoroethane in 1-butyl-3-methylimidazolium Hexafluorophosphate. *Ind. Chem. Eng. Res.* **2006**, *45(18)*, 6375-6382.

Downloaded by DUKE UNIV on June 28, 2012 | http://pubs.acs.org
Publication Date (Web): December 18, 2009 | doi: 10.1021/bk-2009-1030.ch002

8. Shiflett, M. B.; Yokozeki, A. Vapor-Liquid-Liquid Equilibria of Pentafluoroethane and Ionic Liquid [bmim][$PF_6$] Mixtures studied with the Volumetric Method. *J. Phys. Chem. B* **2006**, *110(29)*, 14436-14443.
9. Shiflett, M. B.; Yokozeki, A. Vapor-Liquid-Liquid Equilibria of Hydrofluorocarbons and 1-Butyl-3-Methylimidazolium Hexafluorophosphate. *J. Chem. Eng. Data* **2006**, *51(5)*, 1931-1939.
10. Yokozeki, A.; Shiflett, M. B. Global Phase Behaviors of Trifluoromethane in Room-Temperature Ionic Liquid [bmim][$PF_6$]. *AIChE J.* **2006**, *52(11)*, 3952-3957.
11. Shiflett, M. B.; Yokozeki, A. Phase Equilibria of Hydrofluorocarbon-4310mee Mixtures with Ionic Liquids: Miscibility of *Threo*- and *Erythro*-Diasteromers in Ionic Liquids. *Ind. Eng. Chem. Res*. **2008**, *47(3)*, 926-934.
12. Shiflett, M. B.; Yokozeki, A. Hydrogen Substitution Effect on the Solubility of Perhalogenated Compounds in Ionic Liquid [bmim][$PF_6$]. *Fluid Phase Equilibr*. **2007**, *259*, 210-217.
13. Shiflett, M. B.; Yokozeki, A. Solubility Differences of Halocarbon Isomers in Ionic Liquid [emim][$Tf_2N$]. *J. Chem. Eng. Data* **2007**, *52*, 2007-2015.
14. Shiflett, M. B.; Yokozeki, A. Liquid-Liquid Equilibria of Hydrofluoroethers and Ionic Liquid [emim][$Tf_2N$]. *J. Chem. Eng. Data* **2007**, *52(6)*, 2413-2418.
15. Kumełan, J.; Kamps, P.-S. Á.; Tuma, D.; Yokozeki, A. Shiflett, M. B.; Maurer, G. Solubility of tetrafluoromethane in the ionic liquid [hmim][$Tf_2N$]. *J. Phys. Chem. B* **2008**, *112(10)*, 3040-3047.
16. Shiflett, M. B.; Yokozeki, A. Binary Vapor-Liquid and Vapor-Liquid-Liquid Equilibira of Hydrofluorocarbons (HFC-125 and HFC-143a) and Hydrofluorethers (HFE-125 and HFE-143a) with Ionic Liquid [emim][$Tf_2N$]. *J. Chem. Eng. Data* **2008**, *53(2)*, 492-497.
17. Poling, B. E.; Prausnitz, J. M.; O'Connell, J. P. *The Properties of Gases and Liquids*, 5th Edit.; McGraw-Hill: New York, 2001.
18. Lemmon, E. W.; McLinden, M. O.; Huber, M. L. *NIST reference fluid thermodynamic and transport properties - REFPROP*, version 7.0, users' guide; U. S. Department of Commerce, Technology Administration, National Institute of Standards and Technology, Standard Reference Data Program: Gaithersburg, MD, 2002.
19. Yokozeki, A. *BLENDY computer program*, version 3; DuPont Fluoroproducts: Wilmington, DE, 1992.
20. Reid, R. C.; Prausnitz, J. M.; Poling, B. E. *The Properties of Gases and Liquids*, 4th ed.; McGraw-Hill: New York, 1987.
21. Chae, H. B.; Schmidt, J. W.; Moldover, M. R. Alternative Refrigerants R123a, R134, R141b, R142b, and R152a: Critical Temperature, Refractive Index, Surface Tension, and Estimates of Liquid, Vapor, and Critical Densities. *J. Phys. Chem*. **1990**, *94*, 8840-8845.

Downloaded by DUKE UNIV on June 28, 2012 | http://pubs.acs.org
Publication Date (Web): December 18, 2009 | doi: 10.1021/bk-2009-1030.ch002

22. Park, J. D.; Lycan, W. R.; Lacher, J. R. The Addition Products of Trifluoroethylene. *J. Am. Chem. Soc.* **1951**, *73*, 711-712.
23. Covalent Associates, Inc., Corvallis, OR. www.covalentassociates.com.
24. Shiflett, M. B.; Yokozeki, A. Solubilities and Diffusivities of Carbon Dioxide in Ionic Liquids: [bmim][$PF_6$] and [bmim][$BF_4$]. *Ind. Eng. Chem. Res*. **2005**, *44*, 4453-4464.
25. Van Ness, C. H.; Abbott, M. M. *Classical Thermodynamics of Nonelectrolyte Solutions*. McGraw-Hill: New York, 1982.
26. Yokozeki, A.; Sato, H.; Watanabe, K. Ideal-gas heat capacities and virial coefficients of HFC refrigerants. *Int. J Thermophys*. **1998**, *19*, 89-127.
27. Anthony, J. L.; Maginn, E. J.; Brennecke, J. F. Solubilities and Therrnodynamic Properties of Gases in the Ionic Liquid 1-*n*-Butyl-3-methylimidazolium Hexafluorophsophate. *J. Phys. Chem. B* **2002**, *106*, 7315.
28. Yokozeki, A. Solubility correlation and phase behaviors of carbon dioxide + lubricant oil mixtures. *Applied Energy* **2007**, *84*. 159-175.
29. Yokozeki, A. Solubility of refrigerants in various lubricants. *Int. J. Thermophys*. **2001**, *22*, 1057-1071.
30. Scott, R. L.; van Konynenburg, P. H. Static problems of solutions. Van der Waals and related models for hydrocarbon models. *Discuss Faraday Soc*. **1970**, *49*, 87.
31. Van Konynenburg, P. H.; Scott, R. L. Critical lines and phase equilibria in binary van der Waals mixtures. *Phil Trans*. **1980**, *A298*, 495.
32. Hirschfelder, J. O.; Curtis, C. F.; Bird, R. B. *Molecular Theory of Gases and Liquids*; Wiley: New York, 1954
33. Toda, M.; Mastuda, H.; Hiwatari, Y.; Wadachi, M. *Liquid Structures and Properties*; Iwanami: Tokyo, 1976.
34. Shiflett, M. B.; Yokozeki, A. Solubility of $CO_2$ in Room-Temperature Ionic Liquid [hmim][$Tf_2N$]. *J. Phys. Chem B* **2007**, *111(8)*, 2070-2074
35. Shiflett, M. B.; Kasprzak, D. J.; Junk, C. P.; Yokozeki, A. Phase Behavior of Carbon Dioxide + [bmim][Ac] Mixtures. *J. Chem. Thermodynamics*, **2008**, *40*, 25-31.
36. A. Yokozeki; Shiflett, M. B.; Junk, C. P.; Grieco, L. M.; Foo, T. Physical and Chemical Absorptions of Carbon Dioxide in Room-Temperature Ionic Liquids. *J. Phys. Chem. B*, **2008**, DOI: 10.1021/jp805784u.
37. Shiflett, M. B.; Yokozeki, A. Phase behavior of carbon dioxide in ionic liquids: [emim][acetate], [emim][trifluoroacetate], and [emim][acetate] + [emim][trifluoroacetate] mixtures. *J. Chem. Eng. Data*, **2008**, DOI: 10.1021/je800701j.
38. Yokozeki, A.; Shiflett, M. B. Ammonia Solubilities in Room-Temperature Ionic Liquids. *Ind. Eng. Chem. Res***. 2007**, *46(5)*, 1605-1610.

39. Yokozeki, A.; Shiflett, M. B. Vapor-Liquid Equilibria of Ammonia + Ionic Liquid Mixtures. *Applied Energy*, **2007**, *84*, 1258-1273.

40. ASPEN Plus® Simulator (v.13.1) of Aspen Technology, Inc., Cambridge, MA, 2005.

41. Shiflett, M. B.; Yokozeki, A. Liquid-Liquid Equilibria in Binary Mixtures containing Fluorinated Benzenes and Ionic Liquid 1-ethyl-3-methylimidazolium bis(trifluoromethylsulfonyl)imide. *J. Chem. Eng. Data*, **2008**, *53*, 2683-2691.

Downloaded by DUKE UNIV on June 28, 2012 | http://pubs.acs.org
Publication Date (Web): December 18, 2009 | doi: 10.1021/bk-2009-1030.ch002

Downloaded by UNIV OF GUELPH LIBRARY on June 28, 2012 | http://pubs.acs.org
Publication Date (Web): December 18, 2009 | doi: 10.1021/bk-2009-1030.ch003

## Chapter 3

# Thermophysical properties of ionic liquids

**Rile Ge[1], Christopher Hardacre[1], Johan Jacquemin[2], and David W. Rooney[1]*.**

**[1]The QUILL Research Centre, School of Chemistry and Chemical Engineering, Queen's University of Belfast, Stranmillis Road, Belfast BT9 5AG, United Kingdom**
**[2]Université François Rabelais, Laboratoire PCMB (E.A. 4244), Equipe CIME, Faculté des Sciences et Techniques, parc de Grandmont, 37200 Tours, France.**

Ionic liquids have received significant interest from research groups and industry for a range of novel applications. Many of these require a thorough knowledge of the thermophysical properties of the pure fluids and their mixtures. Despite this need, the necessary experimental data for many properties are scarce and often inconsistent between the various sources. However, by using accurate data, predictive physical models can be developed which are highly useful, and some would consider essential, if ionic liquids are to realise their full potential. This is particularly true if one can use them to design new ionic liquids which maximise key desired attributes. This paper will review some of the recent advances in our understanding, prediction and correlation of selected ionic liquid physical properties.

In Ionic Liquids: From Knowledge to Application; Plechkova, N., et al.;
ACS Symposium Series; American Chemical Society: Washington, DC, 2010.

Downloaded by UNIV OF GUELPH LIBRARY on June 28, 2012 | http://pubs.acs.org
Publication Date (Web): December 18, 2009 | doi: 10.1021/bk-2009-1030.ch003

# Introduction

Over the last number of years, there has been a dramatic increase in research relating to the use of ionic liquids as potential replacements for organic solvents in chemical processes *(1-4)*. More recently, specialised areas such as lubricants *(5)*, heat transfer fluids *(6)* and analytical applications *(7)* have been investigated. These materials are generally organic salts which have a relatively low melting point when compared to inorganic salts. For example, many are fluid at temperatures below 25 °C and these are often described as room temperature ionic liquids. However, the term ionic liquid does not exclude those salts which have higher melting points and although this description is associated with salts which melt below 100 °C, in reality there is no clear distinction between the term molten salt (often used for high temperature liquids), and the term ionic liquid. The expanding range of applications is not surprising, given that approximately $10^{18}$ anion–cation combinations exist which could generate ionic liquids *(8),* and thus these liquids could be classified as true designer materials, particularly since many of these designs include in-built functionality. Therefore, given the potential range available, it is possible for them to have properties suited to a particular application or, if desired, contradict some of the earlier perceived advantages of dealing with fluids consisting of only ionic species. For example, their negligible vapour pressure has been well lauded, yet recently there have been reports of volatile ionic liquids *(9)* and their distillation has been demonstrated *(10)*. Their biodegradability and toxicity have been questioned, yet nutritional or pharmacological ionic liquids are feasible *(11)*. Similarly, while some ionic liquids could be used as flame retardants, others are combustible and energetic ionic liquids are a reality *(12)*.

In each of the potential applications listed above, the ionic liquids often display at least one key advantage over molecular fluids. This may be simply that ionic liquids tend to have much greater liquidus temperature ranges *(13)* at atmospheric pressure than common molecular solvents, allowing for greater flexibility in processing conditions, or it could be that the chemistry within an ionic environment is sufficiently different to cause an increase in yield or selectivity. Such chemical effects have been reported for some ionic liquid facilitated reactions *(14),* although in other cases normal solvent effects can be used to describe the system behaviour *(15)*. For applications such as lubricants, heat transfer fluids and in general when considering any scale-up or process design, knowledge of their thermophysical properties and in particular their transport properties is important. The IUPAC ionic liquid database (IL Thermo) *(16),* which has been operating for approximately three years, has collected a significant amount of such data, including chemical and physical properties as well as measurement methods, *etc.* Importantly, it also contains information with regard to sample purity and the uncertainty of the quoted property values, and thus this database serves as an important tool in addressing the need to find reliable physical property data. In particular, experimental data are reported for a large range of properties with density and viscosity being the most widely examined. An additional advantage of such a repository is that it facilitates research into the development of predictive tools to generate group contribution parameters for these important physical properties, which overall increases our basic understanding of structure–property relationships of these novel fluids. Currently, very few works have systematically studied the qualitative and/or quantitative relationships between the structures of ionic liquids and their fundamental properties *(17-21)* such as melting point, viscosity, density, surface tension, thermal and electrochemical conductivity, solvent properties and speed of sound. At present, data for many other important physicochemical properties of ionic liquids are in short supply, or are currently too unreliable to allow for similar structure-property relationship studies. Group contribution models (GCMs) are commonly used as predictive tools by engineers and physical scientists in process design, and many have become an integral part of process simulation software packages, due to their wide applicability, ease of use, and relative accuracy. The basic assumptions of GCMs are that the physical properties of a component are dependent on the functional groups which make up its structure, and that each functional group provides a fixed contribution towards the physical properties, irrespective of the species involved *(22)*. Herein, we will examine a number of key ionic liquid thermophysical properties (density, heat capacity and thermal conductivity) and strategies for modelling them.

## Density

A considerable amount of experimental data has been measured for density as a function of temperature for a range of ionic liquids. For pure materials, the values vary depending on the choice of anion and cation. Typically, values range from (1.05-1.64) g cm$^{-3}$ at 293 K, decreasing with temperature to between (1.01-1.57) g cm$^{-3}$ at 363 K. Figures 1 and 2 shows a range of measured densities of dried ionic liquids as a function of temperature at 0.1 MPa, where it can be observed that the density is found to be a strong function of anion type and decreases with increasing alkyl chain length.

The most widely used method for ionic liquid density measurement is the vibrating-tube densitometer; a method which relies on a calibration as a function of temperature and pressure, using appropriate reference fluids *(23,24)*. For many reported ionic liquids, this is not routinely performed and corrections for the case of viscous fluids (*i.e.* > 100 mPa s) are often ignored *(25-27)*. Despite these factors, the densities of ionic liquids measured with vibrating tube densitometers have a standard uncertainty to within 0.1 %. Alternative methods include the calculation of density through speed of sound measurements *(28)* or piezometric methods *(23)*. Both approaches are relatively complex technically, but present the advantage of providing extra thermodynamic property data.

Downloaded by UNIV OF GUELPH LIBRARY on June 28, 2012 | http://pubs.acs.org
Publication Date (Web): December 18, 2009 | doi: 10.1021/bk-2009-1030.ch003

Downloaded by UNIV OF GUELPH LIBRARY on June 28, 2012 | http://pubs.acs.org
Publication Date (Web): December 18, 2009 | doi: 10.1021/bk-2009-1030.ch003

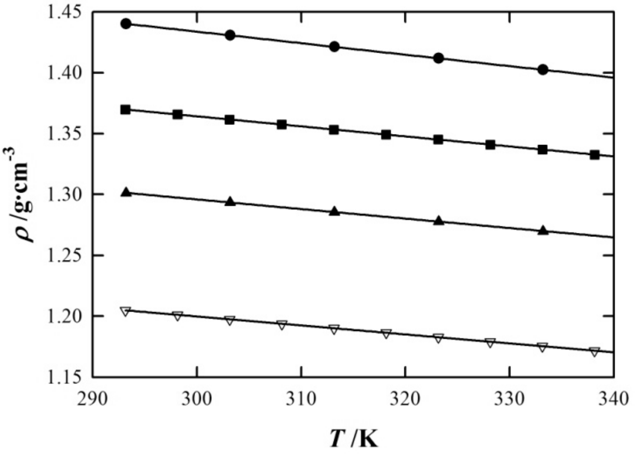

***Figure 1.*** *Effect of the anion on the densities of $[C_4mim]^+$ based ionic liquids : ●, $[NTf_2]^-$; ■, $[PF_6]^-$; ▲, $[OTf]^-$; ▽, $[BF_4]^-$ (reproduced from (30)).*

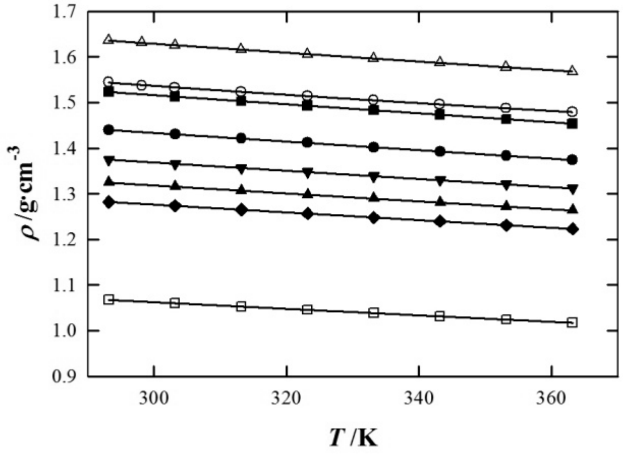

***Figure 2.*** *Effect of the cation on the densities of $[NTf_2]^-$ based ionic liquids : ■, $[C_2mim]^+$ ; ●, $[C_4mim]^+$ ; ▼, $[C_6mim]^+$ ; ▲, $[C_8mim]^+$ ; ◆, $[C_{10}mim]^+$ ; △, $[(NCCH_2)py]^+$ ; ○, $[(NCCH_2)mpyr]^+$ ; □, $[P_{6\,6\,6\,14}]^+$ (reproduced from (30)).*

As with other physical properties, impurities can have a significant effect. Jacquemin *et al.* *(29)* studied six hydrophobic and hydrophilic ionic liquids (including five imidazolium and one ammonium based) as a function of temperature up to 393 K and at atmospheric pressure and found that the densities of the water-saturated ionic liquid samples were lower when compared with dried samples. This difference was relatively small at around (1-2) % for hydrophobic ionic liquids samples containing a mole fraction of water close to 30 %. More recently, we have *(30)* reported experimental densities for a range of selected ionic liquids contaminated by a mass fraction of water ($w_w$) of $1\times10^{-3}$ at 25 °C and 0.1 MPa, shown here in Table 1. It can be observed from these data that, while the variation on the overall density is small, the change in the calculated molar volume ($\Delta V_m$) is significantly larger given the relative difference in the molecular weights between ionic liquid and water. Here the water mole fraction is given by the $x_w$ value.

**Table 1: Impact of water impurities on the calculated molar volume of ionic liquids.**

| Ionic Liquid | $\rho$ /g cm$^{-3}$ | $V_m$ /cm$^3$ mol$^{-1}$ | $x_w$ /10$^{-2}$ | $\Delta V_m$ /% |
|---|---|---|---|---|
| [$C_2$mim][$NTf_2$] | 1.5150 | 258.29 | 2.13 | − 2.0 |
| [$C_4$mim][$NTf_2$] | 1.4351 | 292.22 | 2.27 | − 2.2 |
| [$C_{10}$mim][$NTf_2$] | 1.2755 | 394.77 | 2.72 | − 2.6 |
| [$P_{6\,6\,6\,14}$][$NTf_2$] | 1.0601 | 720.70 | 4.07 | − 4.0 |

Similarly, it has been reported that increasing halide (such as chloride and bromide) contamination also tends to decrease the density over a wide range of values *(31)*.

A number of models which can estimate density at atmospheric pressure have recently been reported. For example, Rebelo *et al. (32,33)* defined the effective molar volumes of ions at 25 °C and used the assumption of "ideal behaviour" for the determination of the molar volume of ionic liquids. Yang *et al. (34)* used a theory based on the "interstice model" which correlated the density and the surface tension of the ionic liquid. Group contribution models have been reported by Kim *et al. (35,36)* for the calculation of the density and $CO_2$ gas solubility for 1-alkyl-3-methylimidazolium based ionic liquids as a function of the temperature and $CO_2$ gas pressure with reasonable accuracy over a 50 K temperature range: however, in this paper, the effect of the anion was not studied. In their work, Ye and Shreeve *(37)* observed a linear relationship between the density in solid and liquid states of ionic liquids and used a group contribution model for the calculation of the density in solid state coupled with linear regression to estimate the liquid density. Recently, Gardas and Coutinho *(38)* extended the Ye and Shreeve group contribution method for the estimation of the density over a wide range of temperatures and pressures with a determined uncertainty of 0.6 %. As in the original work, the calculation of ionic liquid density was determined from a prior knowledge of their mechanical coefficients, thus limiting the general applicability of this methodology. Alternative strategies to the GCM include that of Deetlefs *et al. (18)* which

Downloaded by UNIV OF GUELPH LIBRARY on June 28, 2012 | http://pubs.acs.org
Publication Date (Web): December 18, 2009 | doi: 10.1021/bk-2009-1030.ch003

studied the determination of refractive index, surface tension and density at 25 °C for a range of ionic liquids using a parachor function, defined by Knotts *et al.* *(39)*.

Recently, Jacquemin *et al.* *(30,40)* extended the concept proposed by Rebelo *et al.* In this method, the effective molar volume of an ionic liquid and hence density can be determined by assuming that the volumes of the ions behave as an "ideal" mixture. This strategy was used to calculate the effective molar volumes of a wide range of ions using a large set of previously reported data as a function of the temperature difference at 0.1 MPa and a reference temperature of 25 °C using Equation (1).

$$V^*_{\mathrm{ion}}(\delta T) = \sum_{i=0}^{2}\left(C_i \times \delta T^i\right) \quad (1)$$

The coefficients ($C_i$) were obtained for 44 anions and 102 cations, which achieved a high degree of accuracy when using more than 2150 data points. This approach was further extended to include pressure *(41)* by applying the commonly used Tait equation. In this case, the effective molar volumes are estimated using Equation (2).

$$V^*_{\alpha}(\delta T,\ p,\ G,\ H) = \frac{V^*_{\alpha}(\delta T,\ p_{\mathrm{ref}})}{1 - G\cdot\ln\left(\dfrac{\sum_{i=0}^{2}\left(H_i\cdot\delta T^i\right)+p}{\sum_{i=0}^{2}\left(H_i\cdot\delta T^i\right)+p_{ref}}\right)} \quad (2)$$

Here $\alpha$ can represent the cation or anion constituting an ionic liquid or an extra -$CH_2$- group in the alkyl chain length of an 1-alkyl-3-methylimidazolium based ionic liquid and $V^*_{\alpha}(\delta T,\ p_{\mathrm{ref}})$ is the effective molar volume obtained using the reference pressure ($p_{ref}$ = 0.1 MPa). The coefficients ($G$ and $H_i$) were obtained by fitting literature data and, as can be seen in Figure 3, the approach was successful in estimating the densities over a wide temperature and pressure range yielding 0.36 % error for 5080 experimental data points.

Downloaded by UNIV OF GUELPH LIBRARY on June 28, 2012 | http://pubs.acs.org
Publication Date (Web): December 18, 2009 | doi: 10.1021/bk-2009-1030.ch003

Downloaded by UNIV OF GUELPH LIBRARY on June 28, 2012 | http://pubs.acs.org
Publication Date (Web): December 18, 2009 | doi: 10.1021/bk-2009-1030.ch003

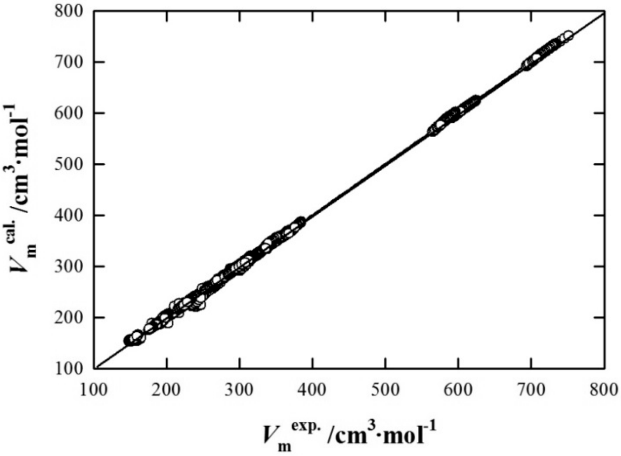

***Figure 3.*** *Predicted vs. experimental molar volumes for a range of ionic liquids at varying temperature and pressure using the group contribution method proposed by Jacquemin et al. (reproduced from (41))*

## Specific Heat capacity

Heat capacity represents the relationship between energy and temperature for a specified quantity of material. In general, this value relates to the kinetic energy stored within the vibrations of the molecule of interest and can be correlated to such. For example, Strechan *et al. (42)* reported a predictive method for determining heat capacities of six different ionic liquids by correlating this property with the intramolecular vibrational contribution, where they reported a relative deviation of 0.9 %.

The fact that these fluids are ionic should not impose a significant effect on the specific heat capacity of ionic liquids, and indeed reported values are in line with those one would expect for organic molecules. For example, the heat capacity for chlorobenzene is 152.1 J mol$^{-1}$ K$^{-1}$ or 1.36 kJ kg$^{-1}$ K$^{-1}$ when written in terms of weight, which is similar to that reported for ionic liquids such as [$C_2$mim][$NTf_2$] which has a heat capacity of 525 J mol$^{-1}$ K$^{-1}$ or 1.34 kJ kg$^{-1}$ K$^{-1}$. When written in a molar basis, the heat capacities of ionic liquids are generally higher than typical organic solvents, which is expected given their relatively large molecular weights. For example, at 25 °C the heat capacities of water, ethanol, nitromethane and benzene are between 75 and 292 J mol$^{-1}$ K$^{-1}$ *(43,44)*.

Downloaded by UNIV OF GUELPH LIBRARY on June 28, 2012 | http://pubs.acs.org
Publication Date (Web): December 18, 2009 | doi: 10.1021/bk-2009-1030.ch003

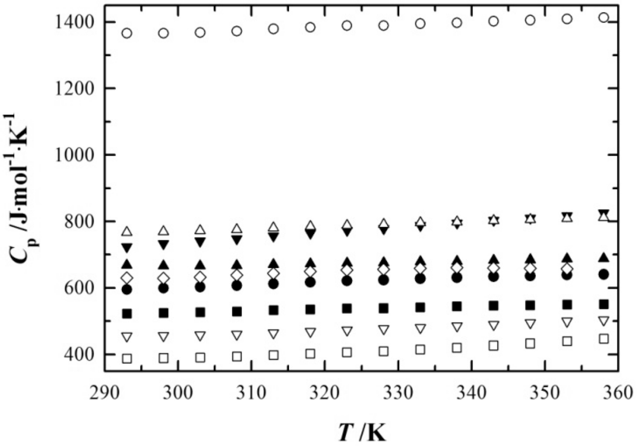

***Figure 4.*** *Heat capacities of ionic liquids as a function of temperature.* ■, *[$C_2$mim][$NTf_2$];* ●, *[$C_4$mim][$NTf_2$];* ▲, *[$C_6$mim][$NTf_2$];* ▼, *[$C_8$mim][$NTf_2$];* ○, *[$P_{6\,6\,6\,14}$][$NTf_2$];* ◇, *[$C_4$mpyr][$NTf_2$];* △, *[$C_4$mpyr][FAP];* ▽, *[$C_4$mim][OTf];* □, *[$C_2$mim][$C_2SO_4$] (reproduced from (45)).*

Figure 4 shows an example of a number of ionic liquid heat capacities as a function of temperature. Here, it is observed that an approximately linear relationship is obtained and a secondary relationship between the chain length of the [$C_n$mim][$NTf_2$] ionic liquids and heat capacity is also apparent. From the results of Ge *et al.(45)*, each additional '-$CH_2$-' group increases the heat capacity by approximately 35 J mol$^{-1}$ K$^{-1}$ at 25 °C, which is similar to the observations made by Holbrey *et al. (46)*, Archer *et al. (47)* and Paulechka *et al. (48)*, who reported incremental increases in $C_p$ of 40 J mol$^{-1}$ K$^{-1}$, 30 J mol$^{-1}$ K$^{-1}$ and 31 J mol$^{-1}$ K$^{-1}$ respectively. Ge *et al. (45)* also reported measurements on the influence of impurities on the heat capacity, where it was found that the heat capacity was lowered with increasing water or chloride and that this followed a linear relationship. Overall, it was reported that for small chloride or water mass fraction contents (*i.e.* up to $1\times10^{-3}$), a decrease in the heat capacity of ≈ 0.15 % or ≈ 1.3 % on average when compared with the halide free or dried ionic liquid, respectively, was observed.

As expected, the larger the molecular weight of the ionic liquid, the larger the molar heat capacity. For example the heat capacity of [$P_{6\,6\,6\,14}$][$NTf_2$] has been reported as 1366 J mol$^{-1}$ K$^{-1}$, compared with 525 J mol$^{-1}$ K$^{-1}$ for [$C_2$mim][$NTf_2$] at 25 °C. Similarly, the choice of anion significantly changes the heat capacity for example [$C_4$mim][OTf] < [$C_4$mim][$NTf_2$], and [$C_4$mpyr][$NTf_2$] < [$C_4$mpyr][FAP], demonstrating again that the heat capacity increases with anion size/molecular weight. As found for other properties, such as density and viscosity*,* the anion type has a greater impact than the cation on the heat capacity.

Furthermore, Ge *et al. (45)* reported an extension to the Joback *(49)* and Benson *(50)* group contribution method, a model often used for the estimation of organic materials, by developing new contributions for the ‘-SO$_2$-’, ‘P’ and ‘B’ groups which are commonly found in these liquids. This was tested against the heat capacities for a range of ionic liquids including measured values determined using a heat flux differential scanning calorimeter technique as described by Diedrichs and Gmehling *(51)*. As stated above, the Joback method is widely used to predict the ideal gas heat capacities of molecular compounds through application of following equation:

$$C_p^o(T) = \left[\sum_{i=1}^{k} n_i A_{Cpi} - 37.93\right] + \left[\sum_{i=1}^{k} n_i B_{Cpi} + 0.210\right]T + \left[\sum_{i=1}^{k} n_i C_{Cpi} - 3.91\times10^{-4}\right]T^2 + \left[\sum_{i=1}^{k} n_i D_{Cpi} - 2.06\times10^{-7}\right]T^3 \qquad (3)$$

where $A_{Cpk}$, $B_{Cpk}$, $C_{Cpk}$ and $D_{Cpk}$ are group contribution parameters, $n_i$ is the number of groups of type $i$ in the molecule, and $T$ is the temperature in K. However, in order for Ge *et al.* *(45)* to apply this equation to ionic liquids, the principle of corresponding states, Equation (4), was required *(50)*.

$$\frac{C_p^r}{R} = \frac{C_p - C_p^o}{R} = 1.586 + \frac{0.49}{1-T_r} + \omega\left[4.2775 + \frac{6.3(1-T_r)^{\frac{1}{8}}}{T_r} + \frac{0.4355}{1-T_r}\right] \qquad (4)$$

where $R$, $T_r$, are $\omega$ the gas constant, reduced temperature and acentric factor respectively. Therefore, Equation (4) requires knowledge of the critical properties of the ionic liquids which have been reported by Valderrama and Robles, who developed and applied the modified Lydersen-Joback-Reid group contribution model for the determination of normal boiling points, acentric factors and critical properties of ionic liquids *(52,53)*. One of the reasons for such a ‘complicated’ approach was due to the fact such methodologies are often employed by process simulation software such as Aspen Plus to determine heat capacity data. Since it was the authors’ intention to develop an Aspen Databank for ionic liquids, such an approach is justified and relevant. Despite the number of equations used, a relative absolute deviation of 2.9 % was observed when testing the model against 961 data points from 53 different ionic liquids reported. Overall, this is considered a highly versatile method given the range of ionic liquids which can be generated using the groups available.

An alternative approach to that of Ge *et al.* *(45)* was adopted by Gardas and Coutinho *(54)*. In this study, 2396 data points for 19 ionic liquids consisting of combinations of imidazolium, pyridinium and pyrrolidinium cations with a range of anions including $[PF_6]^-$, $[BF_4]^-$, $[NTf_2]^-$, $Br^-$, and $[OTf]^-$ anions, over a wide temperature range from 196.36 to 663.10 K was modelled using the method proposed by Ruzicka and Domalski *(55,56)*. The group contribution equation used in this study was Equation (5).

Downloaded by UNIV OF GUELPH LIBRARY on June 28, 2012 | http://pubs.acs.org
Publication Date (Web): December 18, 2009 | doi: 10.1021/bk-2009-1030.ch003

$$C_{pL} = R\left[\sum_{i=1}^{k} n_i a_i + \sum_{i=1}^{k} n_i b_i \left(\frac{T}{100}\right) + \sum_{i=1}^{k} n_i d_i \left(\frac{T}{100}\right)^2\right] \quad (5)$$

where $R$ is the gas constant (8.31 J $mol^{-1}$ $K^{-1}$) and $T$ is the absolute temperature. Again, $n_i$ represents the number of groups of type $i$, $k$ the total number of different groups. The parameters $a_i$, $b_i$, and $d_i$ were reported for three cations, six anions, as well as the $-CH_2-$, $-CH_3$ and dimethylammonium groups. Overall, a mean percent deviation of 0.36 % and a maximum deviation of < 2.5 % were reported. Therefore this approach gives a slightly higher accuracy than that proposed by Ge *et al. (45),* although the range of ionic liquids which can be generated from the groups is significantly lower.

Downloaded by UNIV OF GUELPH LIBRARY on June 28, 2012 | http://pubs.acs.org
Publication Date (Web): December 18, 2009 | doi: 10.1021/bk-2009-1030.ch003

## Thermal conductivity

At present, there are limited data available on the thermal conductivities of ionic liquids. Of those which have been reported, two main methods have been used for the measurement of this property, namely the transient hot wire method and the transient grating technique. In the former, the measurements are made by heating a probe (containing a heating element and a thermoresistor) within the sample while simultaneously monitoring the temperature change of the probe. The latter technique does not directly measure the thermal conductivity but instead estimates this value from the measured thermal diffusivity and previously reported values for heat capacity and density. This difference in methods can lead to significant differences in the calculated thermal conductivities. For example, Frez *et al. (57)* calculated a value for the thermal conductivity of $[C_4mim][BF_4]$ which was 15 % lower when using the transient gradient approach than that reported by Van Valkenburg *et al. (58)* where the transient hot wire was used. It is expected that as the transient grating technique requires additional properties, this method is more prone to errors and thus the transient hot wire method appears to be more accurate.

Reported values for ionic liquids using this technique indicate that ionic liquid thermal conductivities are similar to those of commonly used organic solvents. For example, Tomida *et al. (59)* determined the thermal conductivity for a series of $[C_n mim][PF_6]$ salts and reported values for $[C_4mim][PF_6]$ which compared well with those of benzene 0.145 and 0.16 W $m^{-1}$ $K^{-1}$, respectively. In their study, they also concluded that the thermal conductivity was not a strong function of temperature, pressure or chain length.

Ge *et al. (60)* used a similar technique for the measurement of 11 ionic liquids over the temperature range 293-353 K (Figure 5). In this study, the thermal conductivities were found to be between 0.1 and 0.2 W $m^{-1}$ $K^{-1}$. Here a slight negative and linear relationship with temperature was observed.

Downloaded by UNIV OF GUELPH LIBRARY on June 28, 2012 | http://pubs.acs.org
Publication Date (Web): December 18, 2009 | doi: 10.1021/bk-2009-1030.ch003

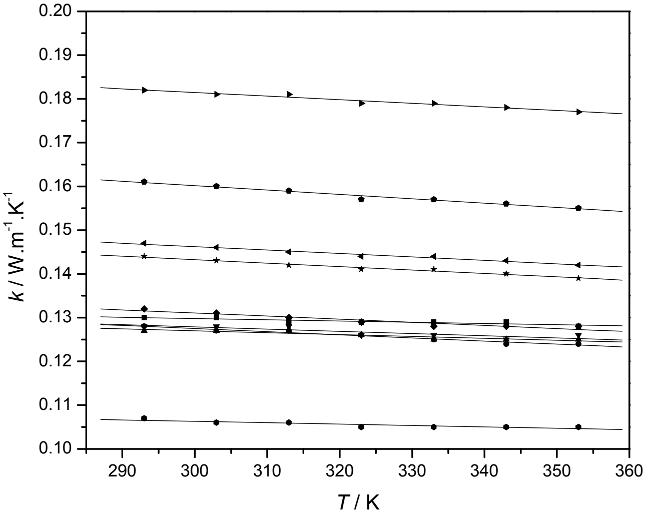

***Figure 5**. Thermal conductivities of ionic liquids as a function of temperature: ■, $[C_2mim][NTf_2]$; ✸, $[C_4mim][NTf_2]$; ▲, $[C_6mim][NTf_2]$; ▼, $[C_8mim][NTf_2]$; ◆, $[C_{10}mim][NTf_2]$; ◀$[C_4mim][OTf]$; ▶, $[C_2mim][EtSO_4]$; ⬢, $[C_4mpyrr][FAP]$; ★, $[C_6H_{13})_3P(C_{14}H_{29})][NTf_2]$; ⬟, $[C_6H_{13})_3P(C_{14}H_{29})]Cl$ (reproduced from (60)).*

Similar to that reported by Tomida *et al. (59)*, there was no significant effect on the thermal conductivity by varying the alkyl chain length, *n*, of the $[C_nmim]$ cation family. From these studies, it appears that while the chain length of a particular cation series does not appear to significantly alter the thermal conductivity, the choice of both cation and anion does have an effect. For example, when using the same $[NTf_2]^-$ anion at 25 °C, the thermal conductivity of $[P_{6\,6\,6\,14}]^+$ > $[C_4mim]^+$ > $[C_4mpyr]^+$ was 0.144, 0.128 and 0.125 W m$^{-1}$ K$^{-1}$, respectively. In contrast, while keeping the cation as $[C_4mim]^+$, the thermal conductivity of $[OTf]^- \approx [PF_6]^- > [NTf_2]^-$ was 0.146, 0.145 and 0.128 W m$^{-1}$ K$^{-1}$, respectively. The fact that the $[P_{6\,6\,6\,14}]^+$ ionic liquids have similar thermal conductivities to those of the 1-alkyl-3-methylimidazolium based liquids highlights that this property is independent of viscosity. These studies also indicate that the highest thermal conductivity is associated with $[C_2mim][C_2SO_4]$ (0.181 W m$^{-1}$ K$^{-1}$ at 298 K) while the lowest is the $[C_4mpyr][FAP]$ liquid (0.106 W m$^{-1}$ K$^{-1}$ at 298 K).

Ge *et al. (60)* also investigated the impact of both water and halide impurities where it was found that in the case of small quantities, *i.e.* up to a mass fraction of 0.01 for water and 0.05 for halide (chloride), no significant effect on thermal conductivity was observed. Above this, the thermal conductivity of the mixture could be modelled using the Jamieson correlation (Equation (6).

$$\lambda_m = w_1\lambda_1 + w_2\lambda_2 - \alpha(\lambda_2 - \lambda_1)\left(1 - \sqrt{w_2}\right)w_2, \qquad \lambda_2 > \lambda_1 \qquad (6)$$

where $w_1$ and $w_2$ are mass fractions and the adjustable parameter $\alpha$ varied depending on the system and impurity chosen. For example, values of 0.42 and 0.70 and 1.39 were obtained for the binary mixtures ([$C_4$mim][OTf] + water), ([$C_2$mim][$C_2SO_4$] + water) and ([$C_6$mim][$NTf_2$] + [$C_6$mim]Cl), respectively.

The use of thermal conductivity, heat capacity and rheological properties for [$C_4$mim][$NTf_2$] was also shown by Chen *et al. (61)* to correlate with Shah's equation for forced convective heat transfer in the laminar flow regime, indicating that knowledge of these parameters can successfully be used to model heat transfer behaviour of ionic liquid systems at the larger scale.

Downloaded by UNIV OF GUELPH LIBRARY on June 28, 2012 | http://pubs.acs.org
Publication Date (Web): December 18, 2009 | doi: 10.1021/bk-2009-1030.ch003

## Conclusions

The topic of ionic liquids has grown significantly over the last number of years, with the vast majority of this research focusing on their use as solvents for a wide range of chemical reactions. However, none of these reactions would ever be industrially exploited without some knowledge of the physical properties of these materials. In an effort to address this problem, the ionic liquid thermodynamic property database (IL Thermo) was developed, and has grown considerably over recent years to contain a variety of important physical properties such as densities, viscosities, *etc.* This database shows that ionic liquids can have a wide range of properties depending on the choice of anion and cation. Many of these are intuitively what one would expect. For example, ionic liquids containing heavy inorganic anions will be denser than those containing lighter organic anions. However, other properties such as melting points and viscosity are more difficult to predict from simple structural information. Here, we have focussed on only a small number of key ionic liquid properties including density, heat capacity and thermal conductivity. In each of these, we have attempted to provide typical values as well as show the important factors which influence the observed trends. We have also discussed some of the techniques which can be used to predict these properties from simple structural information, using techniques such as, in particular, group contributions. Over the coming years as new data become available, our understanding of the relationship between ionic liquid formulation and physical properties will increase, allowing us to design ionic liquids which maximise key desired attributes for any desired application.

### Nomenclature

Anions

| | |
|---|---|
| [$NTf_2$]$^-$ | bis(trifluoromethylsulfonyl)amide |
| [OTf]$^-$ | trifluoromethanesulfonate |
| [$C_1SO_4$]$^-$ | methylsulfate |
| [$C_2SO_4$]$^-$ | ethylsulfate |

| | |
|---|---|
| $[PF_6]^-$ | hexafluorophosphate |
| $[BF_4]^-$ | tetrafluoroborate |
| $[CTf_3]^-$ | tris(trifluoromethylsulfonyl)methide |
| $[N(CN)_2]^-$ | dicyanamide |
| $[FAP]^-$ | tris(perfluoroethyl)trifluorophosphate |

For cations *n* represents the carbon number of the alkyl chain, *i.e.* for ethyl *n* = 2, for butyl *n* = 4, *etc.*

| | |
|---|---|
| $[C_n\text{mim}]^+$ | 1-alkyl-3-methylimidazolium |
| $[C_n\text{mpy}]^+$ | 1-alkyl-3-methylpyridinium |
| $[C_n\text{mpyr}]^+$ | 1-alkyl-1-methylpyrrolidinium |
| $[P_{6\,6\,6\,14}]^+$ | trihexyl(tetradecyl)phosphonium |
| $[(NCCH_2)py]^+$ | 1-cyanomethylpyridinium |
| $[(NCCH_2)mpyr]^+$ | 1-cyanomethyl-1-methylpyrrolidinium |

Downloaded by UNIV OF GUELPH LIBRARY on June 28, 2012 | http://pubs.acs.org
Publication Date (Web): December 18, 2009 | doi: 10.1021/bk-2009-1030.ch003

## Acknowledgements

The authors would like to thank the UK EPSRC under a portfolio partnership for financially supporting this work and also P. Nancarrow (QUB) is acknowledged for useful discussions.

## References

1. *Ionic Liquids in Synthesis;* Wasserscheid, P.; Welton, T., Eds.; Wiley-VCH Verlag: Weinheim, **2003**.
2. Pârvulescu, V.I.; Hardacre, C. Catalysis in Ionic Liquids. *Chem. Rev.* **2007,** *107*, 2615-2665.
3. Silvester, D.S.; Compton, R.G. Electrochemistry in room temperature ionic liquids: A review and some possible applications. *Z. Phys. Chem.* **2006**, *220*, 1247-1274.
4. Harper, J.B.; Kobrak, M.N. Understanding organic processes in ionic liquids: Achievements so far and challenges remaining. *Mini-Reviews in Organic Chemistry* **2006**, *3*, 253-269.
5. Qu, J.; Truhan, J.J.; Dai, S.; Luo, H.; Blau, P.J. Ionic liquids with ammonium cations as lubricants or additives. Tribology Let. **2006,** *22,* 207-214
6. Holbrey, J.D. Heat capacities of common ionic liquids - Potential applications as thermal fluids? *Chim. Oggi - Chem. Today* **2007,** *25,* 24-26.
7. Liu, J.F.; Jonsson, J.A.; Jiang, G.B. Application of ionic liquids in analytical chemistry. *TRAC-Trends in Analytical Chemistry* **2005,** *24,* 20-27.

8. Katritzky, A.R.; Jain, R.; Lomaka, A.; Pertrukin, R.; Karelson, M.; Visser, A.E.; Rogers, R.D. Correlation of the melting points of potential ionic liquids (imidazolium bromides and benzimidazolium bromides) using the CODESSA program. *J. Chem. Inf. Comp. Sci.* **2002,** *42,* 225-231.
9. Widegren, J.A.; Wang, Y.M.; Henderson, W.A; Magee, J.W. Relative volatilities of ionic liquids by vacuum distillation of mixtures. *J. Phys. Chem. B* **2007,** *111,* 8959-8964.
10. Earle, M.J.; Esperanca, J.M.S.S.; Gilea, M.A,; Lopes, J.N.C.; Rebelo, L.P.N.; Magee, J.W.; Seddon, K.R.; Widegren, J.A. The distillation and volatility of ionic liquids. *Nature* **2006,** *439,* 831-834.
11. Hough, W.L.; Smiglak, M.; Rodriguez, H.; Swatloski, R.P.; Spear, S.K.; Daly, D.T.; Pernak, J.; Grisel, J.E.; Carliss, R.D.; Soutullo, M.D.; Davis, J.H.; Rogers, R.D. The third evolution of ionic liquids: active pharmaceutical ingredients. *New J. Chem.* **2007,** *31,* 1429-1436.
12. Xue, H.; Twamley, B.; Shreeve, J.M. Energetic salts of substituted 1,2,4-triazolium and tetrazolium 3,5-dinitro-1,2,4-triazolates. *J. Mat. Chem.* **2005,** *15,* 3459-3465.
13. Fredlake, C.P.; Crosthwaite, J.M.; Hert, D.G.; Aki, S.N.V.K.; Brennecke, J.F., Thermophysical properties of imidazolium-based ionic liquids. *J. Chem. Eng. Data* **2004,** *49,* 954-964.
14. Earle, M.J.; Katdare S.P.; Seddon, K.R. Paradigm confirmed: The first use of ionic liquids to dramatically influence the outcome of chemical reactions. *Org. Let.* **2004,** *6,* 707-710.
15. Crowhurst, L.; Falcone, R.; Lancaster, N.L.; Llopis-Mestre, V.; Welton, T. Using Kamlet-Taft solvent descriptors to explain the reactivity of anionic nucleophiles in ionic liquids. *J. Org. Chem.* **2006,** *71,* 8847-8853.
16. Dong, Q.; Muzny, C.D.; Kazakov, A.; Diky, V.; Magee, J.W.; Widegren, J.A.; Chirico, R.D.; Marsh, K.N.; Frenkel, M. IL Thermo: A Free-Access Web Database for Thermodynamic Properties of Ionic Liquids. *J. Chem Eng. Data* **2007,** *52,* 1151-1159.
17. Katritzky, A.R.; Lomaka, A.; Petrukhin, R.; Jain, R.; Karelson, M.; Visser, A.E.; Rogers, R.D. QSPR correlation of the melting point for pyridinium bromides, potential ionic liquids. J. Chem. Inf. Comp. Sci. 2002, 42, 71-74.
18. Deetlefs, M.; Seddon, K.R.; Shara, M. Predicting physical properties of ionic liquids. *Phys. Chem. Chem. Phys.* **2006,** *8,* 642-649.
19. Zhang, S.J.; Sun, N.; He, X.Z.; Lu, X.M.; Zhang, X.P. Physical properties of ionic liquids: Database and evaluation. *J. Phys. Chem. Ref. Data* **2006,** *35,* 1475-1517.
20. Tochigi, K.; Yamamoto, H. Estimation of ionic conductivity and viscosity of ionic liquids using a QSPR model. *J. Phys. Chem. C* **2007,** *111,* 15989-15994.

Downloaded by UNIV OF GUELPH LIBRARY on June 28, 2012 | http://pubs.acs.org
Publication Date (Web): December 18, 2009 | doi: 10.1021/bk-2009-1030.ch003

Downloaded by UNIV OF GUELPH LIBRARY on June 28, 2012 | http://pubs.acs.org
Publication Date (Web): December 18, 2009 | doi: 10.1021/bk-2009-1030.ch003

21. Matsuda, H.; Yamamoto, H.; Kurihara, K.; Tochigi, K. Computer-aided reverse design for ionic liquids by QSPR using descriptors of group contribution type for ionic conductivities. *Fluid Phase Equilib.* **2007,** *261,* 434-443.
22. Chopey, N.P. Handbook of Chemical Engineering Calculations; *McGraw-Hill, New York,* **2004.**
23. Wagner, W.; Kleinrahm, R.; Losch, H.W.; Density. Hydrostatic balance densimeters with magnetic suspension couplings. Bellows volumetry. Absolute density standards. In situ density measurements. In: Experimental Thermodynamics, Vol. VI : Measurement of the Thermodynamic Properties of Single Phases; Goodwin, A.R.H.; Marsh, K.N.; Wakeham, W.A., Eds.; *IUPAC, Elsevier, Amsterdam* **2003.**
24. Kratky, O.; Leopold, H.; Stabinger. H.Z. Density determination of liquids and gases to an accuracy of 10-6 g/cm3, with a sample volume of only 0.6 cm3. *Z. Angew. Phys.* **1969,** *27,* 273-277.
25. Kandil, M.E.; Harris, K.R.; Goodwin, A.R.H.; Hsu, K.; Marsh, K.N.; Measurement of the Viscosity and Density of a Reference Fluid, with Nominal Viscosity at T = 298 K and p = 0.1 MPa of 29 mPa s, at Temperatures between (273 and 423) K and Pressures below 275 MPa. *J. Chem. Eng. Data* **2006,** *51,* 2185-2196.
26. Dávila, M.J.; Aparicio, S,; Alcalde, R.; Garcia, B.; Leal, J.M. On the properties of 1-butyl-3-methylimidazolium octylsulfate ionic liquid. *Green Chem.* **2007,** *9,* 221-232.
27. Sanmamed, Y.A.; González-Salgado, D.; Troncoso. J.; Cerdeirina, C. A.; Romani, L. Viscosity-induced errors in the density determination of room temperature ionic liquids using vibrating tube densitometry. *Fluid Phase Equilib.* **2007,** *252,* 96-102.
28. Goodwin, A.R.H.; Trusler, J.P.M. Speed of Sound. Measurements of the speed of sound. Thermodynamic properties from the speed of sound. In: Experimental Thermodynamics, Vol. VI : Measurement of the Thermodynamic Properties of Single Phases; Goodwin, A.R.H.; Marsh, K.N.; Wakeham, W.A., Eds.; *IUPAC, Elsevier, Amsterdam* **2003.**
29. Jacquemin, J.; Husson, P.; Padua, A.A.H.; Majer, V. Density and viscosity of several pure and water-saturated ionic liquids. *Green Chem.* **2006,** *8,* 172-180.
30. Jacquemin, J.; Ge, R.; Nancarrow, P.; Rooney, D.W.; Gomes, M.F.C.; Padua, A.A.H.; Hardacre, C. Prediction of ionic liquid properties. I. Volumetric properties as a function of temperature at 0.1 MPa. *J. Chem. Eng. Data* **2008,** *53,* 716-726.
31. Troncoso, J.; Cerdeirina, C.A.; Sanmamed, Y.A.; Romani, L.; Rebelo, L.P.N. Thermodynamic Properties of Imidazolium-Based Ionic Liquids:

Densities, Heat Capacities, and Enthalpies of Fusion of [bmim][PF6] and [bmim][NTf2]. *J. Chem. Eng. Data* **2006,** *51,* 1856-1859.

32. Rebelo, L.P.N.; Najdanovic-Visak, V.; Gomes de Azevedo, R.; Phase behaviour and thermodynamic properties of ionic liquids, ionic liquid mixtures, and ionic liquid solutions. In: Ionic Liquids IIIA: Fundamentals, Progress, Challenges, and Opportunities-Properties and Structure. Rogers, R.D.; Seddon, K.R., Eds.; *ACS Symposium Series 901; American Chemical Society: Washington* **2005.**
33. Esperança, J.; Guedes, H.J.R.; Blesic, M.; Rebelo, L.P.N. Densities and Derived Thermodynamic Properties of Ionic Liquids. 3. Phosphonium-Based Ionic Liquids over an Extended Pressure Range. *J. Chem. Eng. Data* **2006,** *51,* 237-242.
34. Yang, J.; Lu, X.; Gui, J.; Xu, W.G. A new theory for ionic liquids - the interstice model Part 1. The density and surface tension of ionic liquid EMISE. *Green Chem.* **2004,** *6,* 541-543.
35. Kim, Y.S.; Choi, W.Y.; Jang, J.H.; Yoo K.P.; Lee, C.S. Solubility measurement and prediction of carbon dioxide in ionic liquids. *Fluid Phase Equilib.* **2005,** *256,* 439-445.
36. Kim, Y.S.; Jang, J.H.; Lim, D.B.; Lee, C.S. Solubility of mixed gases containing carbon dioxide in ionic liquids: Measurements and predictions. *Fluid Phase Equilib.* **2007,** *228,* 70-74.
37. Ye, C.; Shreeve, J.M. Rapid and Accurate Estimation of Densities of Room-Temperature Ionic Liquids and Salts. *J. Phys. Chem. A* **2007,** *111,* 1456-1461.
38. Gardas, R.L.; Coutinho, J.A.P. Extension of the Ye and Shreeve group contribution method for density estimation of ionic liquids in a wide range of temperatures and pressures. *Fluid Phase Equilib.* **2008,** *263,* 26-32.
39. Knotts, T.A.; Wilding, W.V.; Oscarson, J.L.; Rowley, R.L. Use of the DIPPR Database for Development of QSPR Correlations: Surface Tension. *J Chem. Eng. Data* **2001,** *46,* 1007-1012.
40. Jacquemin, J. ; Husson, P. ; Mayer, V.; Cibulka, I. High-pressure volumetric properties of imidazolium-based ionic liquids – Effect of the anion. *J Chem. Eng. Data* **2007,** *52,* 2204-2211.
41. Jacquemin, J.; Nancarrow, P.; Rooney, D.W.; Gomes, M.F.C.; Husson, P.; Majer, V.; Padua, A.A.H.; Hardacre, C. Prediction of ionic liquid properties. II. Volumetric properties as a function of temperature and pressure. *J. Chem. Eng. Data* **2008,** *53,* 2133-2143.
42. Strechan, A.A.; Paulechka, Y.U.; Blokhin, A.V.; Low-temperature heat capacity of hydrophilic ionic liquids [BMIM][CF3COO] and [BMIM][CH3COO] and a correlation scheme for estimation of heat capacity of ionic liquids. *J. Chem. Thermodyn.* **2008,** *40,* 632-639.

Downloaded by UNIV OF GUELPH LIBRARY on June 28, 2012 | http://pubs.acs.org
Publication Date (Web): December 18, 2009 | doi: 10.1021/bk-2009-1030.ch003

Downloaded by UNIV OF GUELPH LIBRARY on June 28, 2012 | http://pubs.acs.org
Publication Date (Web): December 18, 2009 | doi: 10.1021/bk-2009-1030.ch003

43. García-Miaja, G.; Troncoso, J.; Romaní, L. Density and heat capacity as a function of temperature for binary mixtures of 1-butyl-3-methylpyridinium tetrafluoroborate + water, + ethanol, and + nitromethane. *J. Chem. Eng. Data* **2007,** *52,* 2261-2265.
44. Graziano, G. On the hydration heat capacity change of benzene. *Biophys. Chem.* **2005,** *116,* 137-144.
45. Ge, R.; Hardacre, C.; Jacquemin, J.; Nancarrrow, P.; Rooney, D.W. Heat Capacities of Ionic Liquids as a Function of Temperature at 0.1 MPa - Measurement and Prediction. *J. Chem. Eng. Data* **2008,** *53,* 2148-2153.
46. Holbrey, J.D.; Reichert, W.M.; Reddy, R.G.. Heat Capacities of Ionic Liquids and Their Applications as Thermal Fluids. In: Ionic liquids as green solvents: progress and prospects. Rogers, R.D.; Seddon, K.R., Eds., *ACS Symposium Series; ACS, Washington D.C.,* **2003.**
47. Archer, D.G.; Widegren, J.A.; Kirklin, D.R.; Magee, J.W. Enthalpy of Solution of 1-Octyl-3-methylimidazolium Tetrafluoroborate in Water and in Aqueous Sodium Fluoride. *J Chem Eng Data* **2005,** *50,* 1484-1491.
48. Paulechka, Y.U.; Blokhin, A.V.; Kabo, G.J.; Strechan, A.A. Thermodynamic properties and polymorphism of 1-alkyl-3-methylimidazolium bis(triflamides). *J. Chem. Thermodyn.* **2007,** *39,* 866-877.
49. Joback, K.G. *A unified approach to physical property estimation using multivariant statistical techniques. M.Sc. Thesis in Chemical Engineering, Massachusetts Institute of Technology, Cambridge,* **1984.**
50. Poling, B.E.; Prausnitz, J.M.; O'Connell, J.P. *The Properties of Gases and Liquids;* McGraw-Hill: New York, **2001.**
51. Diedrichs, A.; Gmehling, J. Measurement of heat capacities of ionic liquids by differential scanning calorimetry. *Fluid Phase Equilib.* **2006,** 244, 68-77.
52. Valderrama, J.O.; Robles, P.A. Critical Properties, Normal Boiling Temperatures and Acentric Factors Fifty Ionic Liquids. *Ind. Eng. Chem. Res.* **2007,** *46,* 1338-1344.
53. Valderrama, J.O.; Sanga, W.W.; Lazzús, J.A. Critical Properties, Normal Boiling Temperature, and Acentric Factor of Another 200 Ionic Liquids. *Ind. Eng. Chem. Res.* **2008,** *47,* 1318-1330.
54. Gardas, R.L.; Coutinho, J.A.P. A Group Contribution Method for Heat Capacity Estimation of Ionic Liquids. *Ind. Eng. Chem. Res.* **2008,** *47,* 5751-5757.
55. Ruzicka, V.; Domalski, E.S. Estimation of the Heat-Capacities of Organic Liquids as a Function of Temperature Using Group Additivity. 1. Hydrocarbon Compounds. *J. Phys. Chem. Ref. Data* **1993,** *22,* 597-618.
56. Ruzicka, V.; Domalski, E.S. Estimation of the Heat-Capacities of Organic Liquids as a Function of Temperature Using Group Additivity. 2.

Compounds of Carbon, Hydrogen, Halogens, Nitrogen, Oxygen, and Sulfur. *J. Phys. Chem. Ref. Data* **1993,** *22,* 619-657.

57. Frez, C.; Diebold, G.J.; Tran, C.; Yu, S. Determination of thermal diffusivities, thermal conductivities, and sound speeds of room temperature ionic liquids by the transient grating technique. *J. Chem. Eng. Data* **2006,** *51,* 1250-1255.
58. Van Valkenburg, M.E.; Vaughn, R.L.; Williams, M.; Wilkes, J. Thermochemistry of ionic liquid heat-transfer fluids. *Thermochimica Acta* **2005,** *425,* 181-188.
59. Tomida, D.; Kenmochi, S.; Tsukada, T.; Qiao, K.; Yokoyama, C. Thermal Conductivities of [bmim][PF6], [hmim][PF6], and [omim][PF6] from 294 to 335 K at Pressures up to 20 MPa. *Int. J. Thermophys.* **2007,** *28,* 1147-1160.
60. Ge, R.; Hardacre, C.; Nancarrow, P.; Rooney, D.W. Thermal Conductivities of Ionic Liquids over the Temperature Range from 293 K to 353 K. *J. Chem. Eng. Data* **2007,** *52,* 1819-1823.
61. Chen, H.; He, Y.; Zhu, J.; Alias, H.; Ding, Y.; Nancarrow, P.; Hardacre, C.; Rooney, D.; Chunqing, T. Rheological and heat transfer behaviour of the ionic liquid, [C4mim][NTf2]. *Int. J. Heat Fluid Flow* **2008,** *29,* 149-155.

Downloaded by UNIV OF GUELPH LIBRARY on June 28, 2012 | http://pubs.acs.org
Publication Date (Web): December 18, 2009 | doi: 10.1021/bk-2009-1030.ch003

Downloaded by DUKE UNIV on June 28, 2012 | http://pubs.acs.org
Publication Date (Web): December 18, 2009 | doi: 10.1021/bk-2009-1030.ch004

## Chapter 4

# Chemical Speciation in Ionic Liquids and their Mixtures with Polar Solvents Using Dielectric Spectroscopy

**Glenn Hefter,[a]* Richard Buchner,[b] Johannes Hunger,[b] and Alexander Stoppa[b]**

**[a] Chemistry Department, Murdoch University, Murdoch WA 6150, Australia**
**[b] Institut für Physikalische & Theoretische Chemie, Universität Regensburg, D-93040 Regensburg, Germany**
*** e-mail: g.hefter@murdoch.edu.au**

Broadband dielectric relaxation spectroscopy (DRS) is a powerful tool for studying the nature and dynamics of room-temperature ionic liquids, as well as providing the only means to directly measure their dielectric constants. The DR spectra of neat ionic liquids exhibit many modes, especially at high frequencies, where they reflect 'intermolecular' vibrations and librations. Detailed investigations have also been made into mixtures of ionic liquids with molecular solvents of varying character. The spectra indicate that typical ionic liquids retain their chemical nature even after significant dilution by a molecular solvent such as dichloromethane. Contrary to popular belief, there is little evidence for the existence of discrete ion pairs in the neat ionic liquids; such species appear to exist only at high dilution (typically at $x_{\mathrm{IL}} <$ 0.1) in molecular solvents.

In Ionic Liquids: From Knowledge to Application; Plechkova, N., et al.;
ACS Symposium Series; American Chemical Society: Washington, DC, 2010.

# Introduction

As for *all* electrolyte solutions, chemical speciation has profound effects on the properties and behaviour of room temperature ionic liquids. Indeed, chemical speciation is likely to be especially important for ionic liquids because of the concentration of charged particles and the inevitable strong interactions among them. Despite their importance, relatively few speciation studies have been made to date on ionic liquids, either neat or mixed with other solvents *(1,2)*. This is partly because of the problematic nature of such studies: the species most widely thought to be present in ionic liquids, apart from their constituent ions, are ion pairs along with larger (charged or neutral) aggregates. Such species are often difficult to determine by the techniques routinely used for chemical speciation studies *(3,4)*. For example, traditional thermodynamic and conductometric data are often difficult to interpret at the 'molecular' level, whilst most spectroscopic methods provide only localised (chromophore-based) information and have specific weaknesses with respect to the characterisation of some types of ion pairs *(4)*.

Dielectric relaxation spectroscopy (DRS) is responsive to the motions of molecular-level dipoles and, as such, has a number of advantages over most other techniques in the study of chemical speciation in ionic liquids *(3,4)*. In particular, DRS has special capabilities for the detection and characterisation of all types of ion pairs, and it is also sensitive to longer-range cooperative motions in liquids, which are likely to be significant in ionic liquids *(1,2)*. Additionally, DRS is the only technique *(5)* currently available that can directly measure the (relative) electric permittivity or dielectric constant of conducting liquids such as ionic liquids, a very important quantity for understanding and modelling their behaviour. In favourable circumstances DRS can provide detailed thermodynamic, kinetic and even some structural information on the species present in electrolyte solutions *(3)*.

DRS measures the response of a sample to an imposed low-amplitude electric field oscillating at frequencies in the microwave (MW) and near-MW region (ideally $0.1 \lesssim \nu/\mathrm{GHz} \lesssim 10{,}000$). The quantity usually measured in DRS is the frequency-dependent complex permittivity:

$$\varepsilon^*(\nu) = \varepsilon'(\nu) - \mathrm{i}\varepsilon''(\nu)$$

where $\varepsilon'(\nu)$ is the in-phase permittivity component and $\varepsilon''(\nu)$ is the out-of phase dielectric loss component *(3)*. An electric field is transmitted through a conducting medium by just three mechanisms: the re-orientation of electric dipoles, the polarisation of electron clouds, and the movement of ions. While the second and third of these mechanisms dominate the dielectric spectrum at very high and very low frequencies respectively, it is only the first that is usually of interest in DRS, although it should be noted that for ionic liquids, librations and intermolecular vibrations are common in the THz region *(1)*.

The origin of dielectric relaxation is illustrated in Figure 1. At low field frequencies, molecular-level dipoles are able to re-orient with the oscillating electric field vector, corresponding to a (relatively) high solution permittivity. If

Downloaded by DUKE UNIV on June 28, 2012 | http://pubs.acs.org
Publication Date (Web): December 18, 2009 | doi: 10.1021/bk-2009-1030.ch004

the field frequency is increased sufficiently, it will eventually outpace the finite rate at which the molecular-level dipoles can re-orient, which is limited by their size, shape and interactions with neighbouring species. At this point, dielectric 'relaxation' occurs as the dipoles can no longer follow the field; this causes the permittivity to decrease and the dielectric loss within the sample to increase.

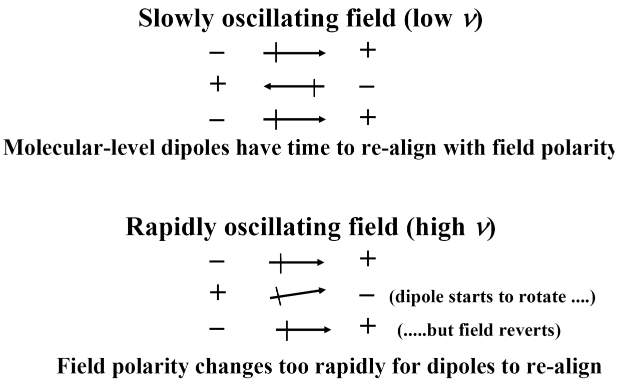
Slowly oscillating field (low ν)
– +
+ –
– +
Molecular-level dipoles have time to re-align with field polarity
Rapidly oscillating field (high ν)
– +
+ – (dipole starts to rotate ....)
– + (.....but field reverts)
Field polarity changes too rapidly for dipoles to re-align

*Figure 1. Effect of the frequency of an oscillating electric field on the rotation of molecular-level dipoles (+/– signs refer to the field polarity).*

These features of DRS are readily seen in Figure 2, which shows the dielectric spectrum of water over the frequency range ($0.4 \leq \nu/\mathrm{GHz} \leq 400$) at 25 °C (*6*). The major loss peak in liquid water, centred at ~18 GHz, corresponds to the cooperative relaxation of the three-dimensional hydrogen-bonded water network. The smaller contribution, centred at ~400 GHz and barely discernable in this spectrum, is thought to be due to the rotation of 'free' water molecules and/or possibly the effects of dielectric friction *(6)*.

DRS is particularly sensitive to the presence of ion pairs in electrolyte solutions. Indeed, DRS is one of the very few techniques that can distinguish and quantify all types of ion pairing (*4,7*). A typical example, for $MgSO_4$(*aq*), is shown in Figure 3 and reveals that all three ion-pair types (double-solvent-separated, 2SIP, solvent-shared, SIP, and contact, CIP, ion pairs) are detected in such solutions *(7)*, along with the two solvent peaks seen in Figure 2.

Downloaded by DUKE UNIV on June 28, 2012 | http://pubs.acs.org
Publication Date (Web): December 18, 2009 | doi: 10.1021/bk-2009-1030.ch004

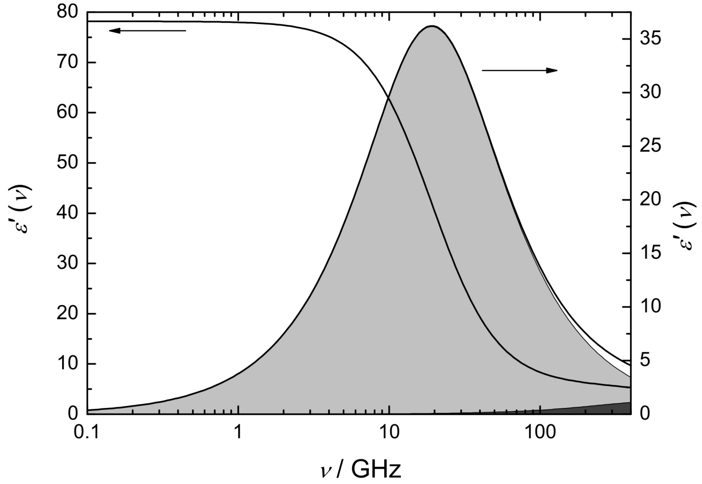

*Figure 2. DR spectrum of water at 25 °C; note the presence of two relaxation processes.*

## DR Spectra of Ionic Liquids

The great diversity of ionic liquids precludes discussion of their DR spectra in a completely generic manner. Nevertheless, useful generalisations can be drawn from a consideration of typical spectra. As with most other properties of ionic liquids the most widely studied compounds to date have been the 1,3-dialkylimidazolium salts.

A representative dielectric spectrum, for $[C_4mim][BF_4]$, is shown in Figure 4 *(1,8)*. The spectrum covers an unusually wide frequency range ($0.1 \lesssim \nu/\mathrm{GHz} \lesssim 3000$) and shows a number of interesting features that are characteristic of imidazolium-based ionic liquids.

The dominant mode in the loss spectrum occurs at rather low frequencies, being centred at ~0.6 GHz (Figure 4). Although its exact mathematical description remains somewhat controversial, it seems this mode is best described by a Cole-Cole equation *(8)*. Its location (frequency) and intensity (amplitude) have been shown to be qualitatively consistent with the rotational diffusion of the weakly dipolar imidazolium cation *(9)*. On the other hand, quantitative consideration of the DR data, including comparisons with other techniques, suggest that there may be other processes such as cooperative motions from larger aggregates also contributing to this mode *(8)*. Interestingly, and in contradiction to general belief, there appears to be no evidence in the DR spectrum (*cf.* Figure 3) for the presence of significant concentrations of ion pairs *(10)*. As will be shown below, this is consistent with evidence obtained from ionic liquid/solvent mixtures.

Downloaded by DUKE UNIV on June 28, 2012 | http://pubs.acs.org
Publication Date (Web): December 18, 2009 | doi: 10.1021/bk-2009-1030.ch004

Downloaded by DUKE UNIV on June 28, 2012 | http://pubs.acs.org
Publication Date (Web): December 18, 2009 | doi: 10.1021/bk-2009-1030.ch004

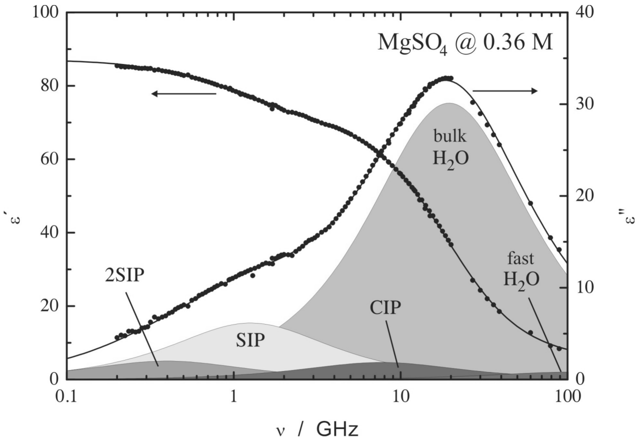

*Figure 3. DR spectrum of 0.36 M $MgSO_4(aq)$ at 25 °C, showing the simultaneous presence of double-solvent-separated (2SIP), solvent-shared (SIP) and contact (CIP) ion pairs, along with the two water relaxations ($\tau_i = 1/2\pi\nu_{max}$).*

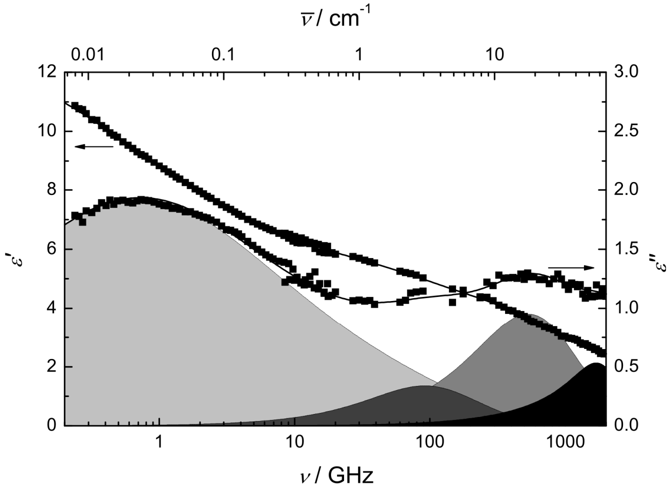

*Figure 4. DR spectrum of [$C_4$mim][$BF_4$] at 25 °C. Component modes for the loss (ε″) curve are described (left to right) by a Cole-Cole process, one Debye process and two damped harmonic oscillators.*

Extrapolation of the $\varepsilon'(\nu)$ data in Figure 4 to zero frequency provides a direct measure of the sample's dielectric constant, $\varepsilon$ (*5*). Although this extrapolation is somewhat less accurate for this particular liquid because of the location of the dominant process at such low frequencies, the value of $\varepsilon \approx 14$ is typical of most of the (largely imidazolium-based) ionic liquids investigated to date *(11,12)*. Such values of the dielectric constant, roughly equivalent to those of medium chain-length ketones and ethers, are considerably lower than the expectations of many researchers. However, they are consistent with the relatively low electrical conductivities and other solvent characteristics of many ionic liquids *(8)*.

The DR spectra of typical ionic liquids at higher frequencies ($\nu \gtrsim$ 10 GHz) exhibit a small, almost featureless, but remarkably persistent loss curve (Figure 4) *(1)*. The origin of the contributing modes (clearly many modes are required to produce the observed loss curves) are not well understood at the present time. In part, this is because of the possible influence on the spectra from contributions from even faster modes (*i.e.*, at $\nu$ > 3 THz), which makes definitive description difficult; measurements at such high frequencies require highly specialised equipment and very few studies of ionic liquids have been made in this region. Among the various possibilities, it seems likely that librations and intermolecular vibrations make some contribution, although their precise nature remains obscure at present *(1)*.

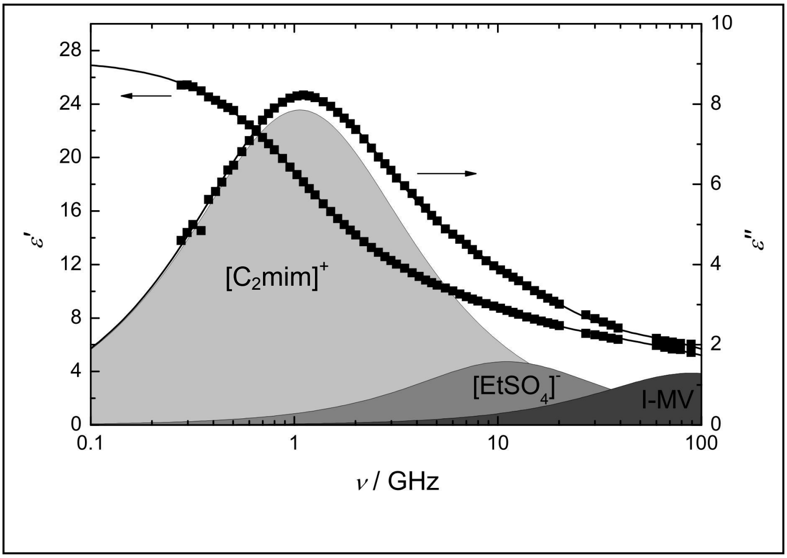

*Figure 5. DR spectrum of [$C_2$mim][$EtSO_4$] at 25 °C. Note the mode due to the rotational diffusion of the anion, centred at ~10 GHz; I-MV = inter-molecular vibration.*

As [$BF_4$]$^-$ possesses tetrahedral symmetry, it does not have a dipole moment and thus does not contribute to the spectrum of [$C_4$mim][$BF_4$] shown in Figure 4. A typical spectrum of an ionic liquid that contains a dipolar anion, [$EtSO_4$]$^-$, is shown in Figure 5 *(13)*. The mode centred at ~10 GHz is readily assigned to the rotational diffusion of the [$EtSO_4$]$^-$ anion, since all the other features of the spectrum are very similar to those of other imidazolium salts containing non-polar anions (Figure 4) *(8)*.

Downloaded by DUKE UNIV on June 28, 2012 | http://pubs.acs.org
Publication Date (Web): December 18, 2009 | doi: 10.1021/bk-2009-1030.ch004

## Mixtures of Ionic Liquids with Polar Solvents

The insights that can be obtained from a single DR (or indeed any other type of) spectrum of a neat ionic liquid is inevitably limited. Understanding can of course be extended by studying the effects of other variables, such as temperature, or by investigating a series of ionic liquids of systematically varying character. Another fruitful approach is to study the effects of mixing ionic liquids with conventional molecular solvents. In addition to the insights that can be gained about the neat ionic liquid from studying the effects of systematic variation in mixture composition, such blends are likely to have many practical applications, *e.g.*, in batteries or as reaction media, where compositional variation can be employed to produce desired properties *(2)*. The range of molecular solvents that can be used as diluents for ionic liquids is almost unlimited. Dichloromethane ($CH_2Cl_2$) is a good choice because it is fully miscible with many ionic liquids, has a reasonable dielectric constant ($\varepsilon \approx 9$ at 25 °C) and makes a relatively small, well-known contribution to the DR spectrum.

A general scheme (Figure 6) for the dilution of an ionic liquid by a molecular solvent has been proposed by Dupont *(14)* and it is interesting to investigate how far this scheme is consistent with experimental observations.

In essence, Dupont assumes a highly structured form for the neat ionic liquid. This structure is gradually broken down into smaller entities with increasing dilution, forming sequentially: large aggregates, triple ions, contact ion pairs and ultimately free ions. Some aspects of this scheme have intuitive appeal because they mimic the known effects of dilution on conventional electrolyte solutions *(7),* while other steps are more speculative but, at least in principle, should be detectable using DRS.

Relatively few studies of the DR spectra of ionic liquid/co-solvent mixtures have been made to date *(2,15)*. The best-investigated system is undoubtedly ($[C_4mim][BF_4] + CH_2Cl_2$), which has been studied over the entire composition range over the wide (but not ideal) frequency range ($0.1 \lesssim \nu/\mathrm{GHz} \lesssim 100$) at 25 °C (*2*). The DR spectra obtained for these mixtures (Figure 7) appear relatively simple, showing just two processes: a Cole-Cole (CC) mode at lower frequencies and a Debye (D) mode at much higher frequencies.

Downloaded by DUKE UNIV on June 28, 2012 | http://pubs.acs.org
Publication Date (Web): December 18, 2009 | doi: 10.1021/bk-2009-1030.ch004

Downloaded by DUKE UNIV on June 28, 2012 | http://pubs.acs.org
Publication Date (Web): December 18, 2009 | doi: 10.1021/bk-2009-1030.ch004

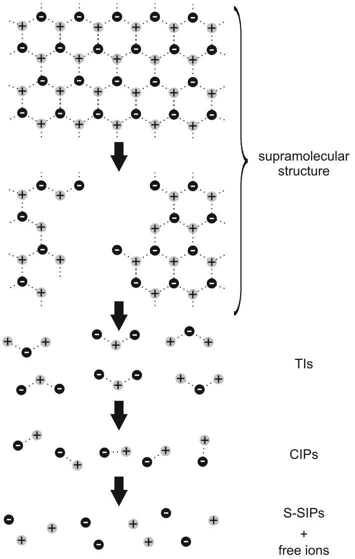

*Figure 6. Generalised scheme of Dupont (14) for the dilution of an ionic liquid with a molecular solvent (mol fraction of the ionic liquid, $x_{IL}$, decreases from top to bottom): TIs = triple ions; CIPs = contact ion pairs; S-SIPs = solvent-separated ion pairs.*

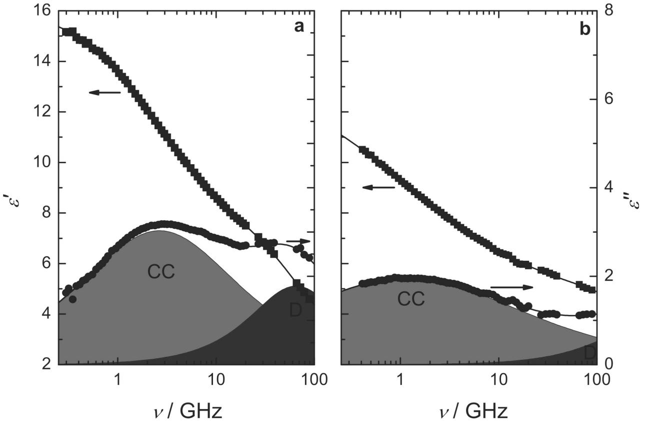

*Figure 7. DR spectra for two ([$C_4$mim][$BF_4$] + $CH_2Cl_2$) mixtures at 25 °C: (a) $x_{IL}$ = 0.1; (b) $x_{IL}$ = 0.9. Note that the Cole-Cole (CC) and Debye (D) processes are composites of more than one mode (see text).*

However, this apparent simplicity is deceptive, as is readily revealed by a closer look at the spectra as a function of composition. Focussing first on the lower frequency contribution: the data in Figure 8 illustrate the real complexity of the mixtures. Thus, the static solution permittivity $\varepsilon$ (= $\lim_{\nu\to 0}$ $\varepsilon'(\nu)$) undergoes quite dramatic changes as a function of composition {Figure 8(a)}, rather than the smooth variation that would be expected from simple mixing. The shape of the CC mode, as measured by the broadness parameter $\alpha$, also undergoes significant and complex changes with composition {Figure 8(b)}.

While a detailed interpretation of the DR spectra for these mixtures is given elsewhere *(2),* it is interesting to note the influence of composition on $\mu_{\text{eff}}$, the effective dipole moment for the low frequency process, calculated from the spectra *via* the Cavell equation *(16).* The values so obtained (Figure 9) show that at moderate and high mole fractions of the ionic liquid ($x_{\text{IL}} \gtrsim 0.3$), $\mu_{\text{eff}} \approx 4.6$ D, which agrees well with the values of $\mu([\text{C}_4\text{mim}]^+) \approx 5$ to 7 D (depending on conformation) obtained for the isolated cation from quantum mechanical calculations *(2).* Also at $x_{\text{IL}} \gtrsim 0.3$, the microscopic relaxation time for this process obtained from the spectra, $\tau_1'$, correlates (Figure 10) strongly with mixture viscosities (*17*). Taken together, these observations suggest that there is an essentially random or homogeneous dilution of the ionic liquid by the $CH_2Cl_2$ molecules over the composition range $0.3 \lesssim x_{\text{IL}} \leq 1$ and that the chemical 'character' of the ionic liquid is retained down to quite high dilutions with $CH_2Cl_2$.

Downloaded by DUKE UNIV on June 28, 2012 | http://pubs.acs.org
Publication Date (Web): December 18, 2009 | doi: 10.1021/bk-2009-1030.ch004

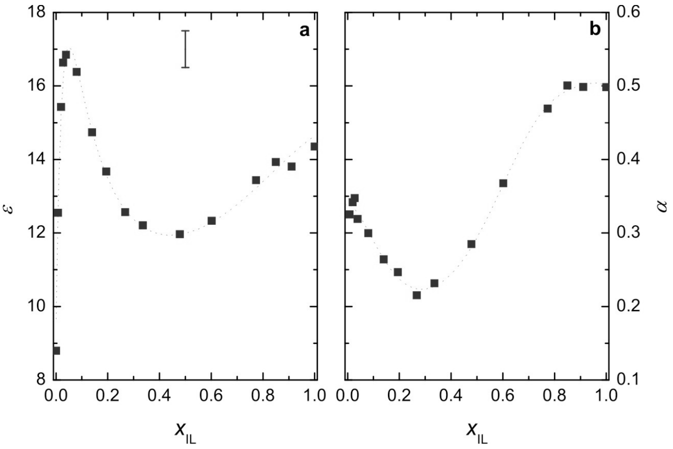

*Figure 8. Parameters derived from the DR spectra of ($[C_4mim][BF_4]$ + $CH_2Cl_2$) mixtures at 25 °C as a function of solution composition: (a) the dielectric constant, $\varepsilon$ ; (b) the Cole-Cole shape parameter, $\alpha$.*

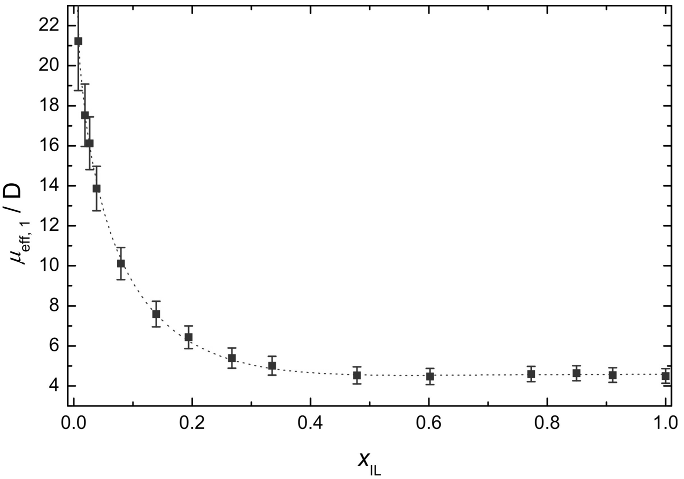

*Figure 9. The effective dipole moment, $\mu_{eff}$, of the species assumed to be responsible for the Cole-Cole process in ([$C_4$mim][$BF_4$] + $CH_2Cl_2$) mixtures at 25 °C, calculated via the Cavell equation. Note that at $x_{IL} \gtrsim 0.3$, $\mu_{eff}(obs) \approx \mu([C_4mim]^+)$.*

Similar results have been obtained with other ionic liquids mixed with $CH_2Cl_2$ *(13,15)*. At very high dilutions of [$C_4$mim][$BF_4$] in $CH_2Cl_2$, the amplitude of the low frequency CC process and thus the static permittivity, goes through a maximum (at $x_{\mathrm{IL}} \approx 0.08$, Figure 9) and there is a rapid increase in $\mu_{\mathrm{eff}}$ (*2*). These observations indicate the presence of a new relaxing species with a large dipole moment. The location, nature and magnitude of these effects are consistent with the formation of ion pairs. While the overlap of the ion pairing contribution and that of the cation rotation was too strong to allow their respective contributions to be separated *(2)*, the observed values of $\mu_{\mathrm{eff}}$ at $x_{\mathrm{IL}}\rightarrow 0$ (Figure 9) and the corresponding effective volume of rotation, $V_{\mathrm{eff}}$ *(18)*, are consistent with those calculated by quantum mechanics for contact (rather than solvent-separated) ion pairs.

As described elsewhere (*2*), these data can be used to calculate a simplified chemical speciation diagram (Figure 11) which shows that the (contact) ion pairs are significant only at high dilution ($x_{\mathrm{IL}} \lesssim 0.1$) in $CH_2Cl_2$. Of course, at even higher dilutions, these ion pairs must ultimately dissociate into free ions.

Downloaded by DUKE UNIV on June 28, 2012 | http://pubs.acs.org
Publication Date (Web): December 18, 2009 | doi: 10.1021/bk-2009-1030.ch004

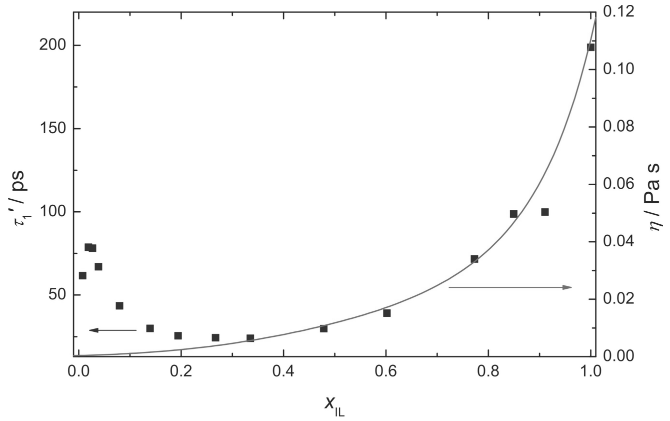

*Figure 10. Relaxation time for the Cole-Cole process, $\tau_1$ (left hand axis, points) and bulk viscosity (17), $\eta$ (right hand axis, line) for ([$C_4$mim][$BF_4$] + $CH_2Cl_2$) mixtures at 25 °C as a function of composition. Note correlation between $\tau_1$ and $\eta$ at $x_{IL} \gtrsim 0.3$.*

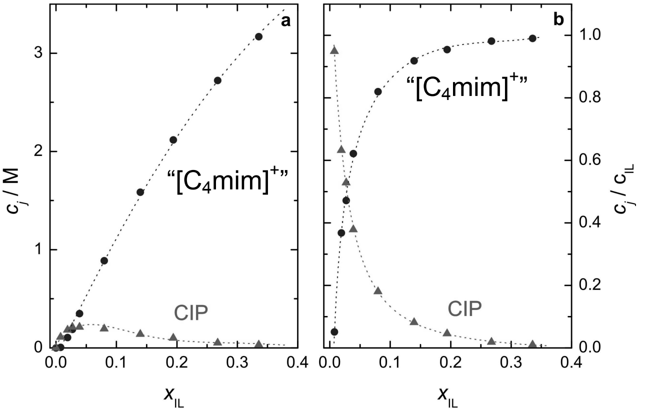

*Figure 11. Simplified chemical speciation model for ([$C_4$mim][$BF_4$] + $CH_2Cl_2$) mixtures at 25 °C at low $x_{IL}$. Note that ion pairs (CIPs) are dominant only at very low $x_{IL}$; "[$C_4$mim]$^+$" refers to all cations regardless of their immediate environment.*

Turning now to the higher frequency process, centred at *ca*. 70 to 260 GHz depending on composition (Figure 7) and which is satisfactorily described by a single Debye equation (*2*), a detailed inspection of the data again reveals this process is a composite of various modes. One of these modes is due to $CH_2Cl_2$, while there are at least two other modes associated with the ionic liquid. However, it must be remembered that higher frequency modes that are outside the range of these measurements (*cf*. Figure 4) may still contribute significantly *(1)* and care must be taken not to over-interpret the data. Even accepting this

Downloaded by DUKE UNIV on June 28, 2012 | http://pubs.acs.org
Publication Date (Web): December 18, 2009 | doi: 10.1021/bk-2009-1030.ch004

*caveat*, the behaviour of the amplitude ($S_2$) and relaxation time ($\tau_2$) for this process as a function of composition clearly show the complexity of this process (Figure 12). A full discussion of these data is given elsewhere (*2*), so only a few points of interest are noted here. At $x_{\mathrm{IL}} \lesssim 0.5$, the observed values of $S_2$ are less than the amplitude arising from the $CH_2Cl_2$ molecules, $S_{\mathrm{DCM}}$, calculated *via* the Cavell equation *(16)*. This apparent 'loss' of $CH_2Cl_2$ molecules from the mixture is possibly due to them being involved in solvation of the ions and/or higher aggregates of the ionic liquid. At $x_{\mathrm{IL}} \gtrsim 0.5$, the value of $S_2$ is > $S_{\mathrm{DCM}}$ (Figure 12). As this is physically impossible, there must be at least one ionic liquid-related mode contributing at these frequencies. This is consistent with the spectrum of the neat ionic liquid, which shows features at high frequencies that probably arise from intermolecular vibrations and/or a cross-correlation of rotational and translational modes *(2)*.

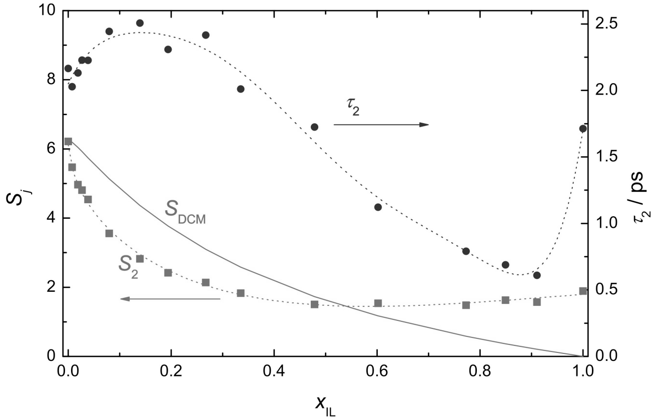

*Figure 12. Parameters calculated from the DR spectra for the Debye mode (higher frequency process in Figure 7) in ([C$_4$mim][BF$_4$] + $CH_2Cl_2$) mixtures at 25 °C: relaxation time, $\tau_2$ (circles, right hand axis); amplitude, $S_2$ (squares, left hand axis). Note $S_{DCM}$ is the expected amplitude associated with the $CH_2Cl_2$ molecules (see text).*

As a solvent, $CH_2Cl_2$ is neither particularly polar nor strongly coordinating *(19)*; nevertheless, the DR spectra of its mixtures with [C$_4$mim][BF$_4$] are remarkably similar to those observed for mixtures of [C$_4$mim][BF$_4$] with much more strongly interacting solvents such as ethanenitrile or dimethylsulfoxide *(20)*. This is illustrated in Figure 13, which plots $\mu_{\mathrm{eff}}$ values obtained for the lower frequency process *via* the Cavell equation. The results are almost identical to those shown in Figure 9. Despite the unusual properties of water as a solvent *(19)*, even mixtures of ([C$_4$mim][BF$_4$] + $H_2O$) (Figure 13) are still broadly similar to the corresponding mixtures with $CH_2Cl_2$ (Figure 9).

A fuller understanding of these spectra requires measurements on more ionic liquids and over a wider frequency range. Nevertheless, the ability of DRS to provide insights into the nature of room-temperature ionic liquids and their mixtures with molecular solvents is well demonstrated by the data presented here.

Downloaded by DUKE UNIV on June 28, 2012 | http://pubs.acs.org
Publication Date (Web): December 18, 2009 | doi: 10.1021/bk-2009-1030.ch004

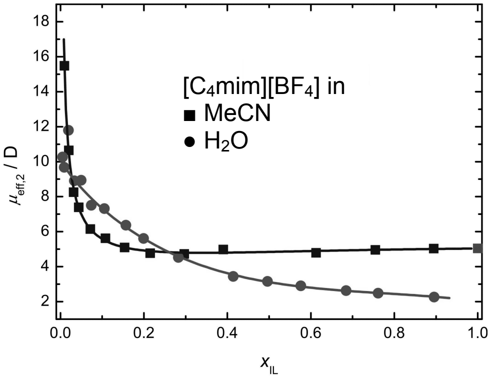

*Figure 13. Effective dipole moments, μeff, calculated from the Cavell equation for ([$C_4$mim][$BF_4$] + S) mixtures at 25 °C: with co-solvent (S) = MeCN or $H_2O$. Note similarity with data in Figure 9.*

Downloaded by DUKE UNIV on June 28, 2012 | http://pubs.acs.org
Publication Date (Web): December 18, 2009 | doi: 10.1021/bk-2009-1030.ch004

## Concluding remarks

The DR spectra presented here, along with the quantities that can be derived from them, illustrate the power of modern broadband dielectric spectroscopy to provide important insights into the nature of room-temperature ionic liquids, and their mixtures with conventional molecular solvents. While interactions in neat ionic liquids are undoubtedly dominated by multiple direct cation-anion interactions, the spectra of typical imidazolium salts show, unexpectedly, that there are few ion pairs (more precisely, few that are stable on the DRS timescale) present in the neat ionic liquids. Such species only appear to form appreciably when the ionic liquid is substantially diluted by a molecular solvent. Little direct evidence has been found to support all of the steps in Dupont's dilution scheme (Figure 6), but further work is required before the effects of mixing of ionic liquids and molecular solvents can be understood. Certainly, it appears that ionic liquids retain their chemical nature up to quite high levels of dilution, which has significant technological implications.

## Acknowledgements

GH thanks the Deutsche Forschungsgemeinschaft (DFG), Bonn, Germany, for a Visiting Mercator Professorship at the University of Regensburg during 2008; RB, JH and AS also thank the DFG for financial support within Priority Program 1191.

## References

1. Stoppa, A.; Hunger, J.; Buchner, R.; Hefter, G.; Thoman, A.; Helm, H. *J. Phys. Chem. B* 2008, *112*, 4854-4858.
2. Hunger, J.; Stoppa, A.; Buchner, R.; Hefter, G. *J. Phys. Chem. B* **2008**, *112*, 12913-12919.
3. Buchner, R. Dielectric Spectroscopy of Solutions. In *Novel Approaches to the Structure and Dynamics of Liquids: Experiments, Theories and Simulations*; J. Samios and V.A. Durov, Eds.; NATO ASI Series; Kluwer: Dordrecht, 2004; Vol. 133,pp. 265-288.
4. Hefter, G. *Pure Appl. Chem.* 2006, *78*, 1571-1586.
5. Moldover, M. R.; Marsh, K. N.; Barthel, J.; Buchner, R. Relative Permittivity and Refractive Index. In *Experimental Thermodynamics, Vol. VI, Measurement of the Thermodynamic Properties of Single Phases*, Goodwin, A. R. H., Marsh, K. N., Wakeham, W. A., Eds.; Elsevier: Amsterdam, 2003.
6. Fukasawa, T.; Sato, T.; Watanabe, J.; Hama, Y.; Kunz, W.; Buchner, R. *Phys. Rev. Lett.* **2005**, *95*, 197802, 4 pp.
7. Buchner, R.; Chen, T.; Hefter, G. *J. Phys. Chem. B* **2004**, *108*, 2365-2375.
8. Hunger, J.; Stoppa, A.; Schrödle, S.; Hefter, G.; Buchner, R. *ChemPhysChem.* **2009**, *10*, 723-733.
9. Weingärtner, H.; Sasisanker, P.; Daguenet, C.; Dyson, P. J.; Krossing, I.; Slattery, J. M.; Schubert, T. *J. Phys. Chem. B* **2007**, *111*, 4775-4780.
10. Sangoro, J.; Iacob, C.; Serghei, A.; Naumov, S.; Galvosas, P.; Kärger, J.; Wespe, C.; Bordusa, F.; Stoppa, A.; Hunger, J.; Buchner, R.; Kremer, F. *J. Chem. Phys.* **2008**, *128*, 214509, 5 pp.
11. Weingärtner, H. *Z. Phys. Chem.* **2006**, *220*, 1395-1405.
12. There are of course specific compounds with higher $\varepsilon$ values, see for example: Huang, M.-M.; Weingärtner, H. *ChemPhysChem* **2008,** *9*, 2172-2173.
13. Hunger, J.; Stoppa, A.; Buchner, R.; Hefter, G. *J. Phys. Chem. B*, submitted.
14. Dupont, J. *J. Braz. Chem. Soc.* **2004**, *15*, 341-350.
15. Schrödle, S.; Annat, G.; MacFarlane, D. R.; Forsyth, M.; Buchner, R.; Hefter, G. *J. Chem. Soc. Chem. Commun.* 2006, 1748-1750.
16. Cavell, E. A. S.; Knight, P. C.; Sheikh, M. A. *Trans. Faraday Soc.* 1971, *67*, 2225-2233.
17. Wang, J.; Tian, Y.; Zhao, Y.; Zhuo, K. *Green Chem.* **2003**, *5*, 618-622.
18. Dote, J. C.; Kivelson, D.; Schwartz, R. N. *J. Chem. Phys.* **1981**, *85*, 2169-2180.
19. Marcus, Y. *Ion Solvation*; Wiley-Interscience: New York, 1997.
20. Stoppa, A.; Hunger, J.; Buchner, R.; Hefter, G. Unpublished results.

Downloaded by DUKE UNIV on June 28, 2012 | http://pubs.acs.org
Publication Date (Web): December 18, 2009 | doi: 10.1021/bk-2009-1030.ch004

Downloaded by DUKE UNIV on June 28, 2012 | http://pubs.acs.org
Publication Date (Web): December 18, 2009 | doi: 10.1021/bk-2009-1030.ch005

## Chapter 5

# Solvation of Carbohydrates in 1,3-Dialkylimidazolium Ionic Liquids: Insights from Multinuclear NMR Spectroscopy and Molecular Dynamics Simulations

**Igor D. Petrik, Richard C. Remsing, Zhiwei Liu,
Brendan B. O'Brien, and Guillermo Moyna**

**West Center for Computational Chemistry and Drug Design and
Department of Chemistry & Biochemistry, University of the Sciences in
Philadelphia, 600 South 43rd Street, PA 19104-4495**

Multinuclear NMR spectroscopy and molecular modelling represent two of the most important tools available to study the structure, solvation, and dynamics of ionic liquids and ionic liquid-based systems. This chapter showcases the application of these techniques to the investigation of carbohydrate solvation in 1,3-dialkylimidazolium ionic liquids. We show that when used in combination, $^{13}$C and $^{35/37}$Cl relaxation data, $^{1}$H diffusion measurements, and molecular dynamics (MD) simulations can provide detailed information regarding this process at the molecular level. Our results point to a general solvation mechanism which is governed by the formation of hydrogen bonds between the ionic liquid anions and the hydroxyl group protons of the carbohydrate. Furthermore, both experimental and theoretical studies demonstrate that the interactions of the ionic liquid cation and the solutes are negligible. The application of similar approaches in the study of other relevant systems based on ionic liquids is briefly discussed.

In Ionic Liquids: From Knowledge to Application; Plechkova, N., et al.;
ACS Symposium Series; American Chemical Society: Washington, DC, 2010.

# Introduction

As evidenced by thousands of journal articles and an equally significant number of books devoted to their basic science and applications, ionic liquids have become increasingly important to the scientific community over the past decade. Originally recognised for their potential as "green" solvents, these low-melting organic salts have not only led to improvements in well established laboratory and industrial methods, but have also allowed for the development of new processes that were unattainable with traditional molecular solvents. Since it is possible to fine-tune their properties by modifying the chemical structure of their cation and anion components, ionic liquids can be in theory optimised to perform specific tasks. Consequently, these materials have found uses as battery electrolytes, lubricants, fuels, heat transport and storage fluids, and alternative media for synthesis, liquid-liquid extractions, and polymer processing, to mention a few examples. Many of these applications are described or cited in this and earlier volumes of the same series *(1)*.

The design of new ionic liquids tailored for particular applications requires knowledge of the interactions between the ionic liquid anions and cations and, more importantly, between these ions and solutes. A variety of techniques, including diffraction, spectroscopic, and computational methods, have been employed to investigate interionic interactions, dynamics, and solvation phenomena in these materials *(2-6)*. Among these, NMR spectroscopy and molecular dynamics (MD) simulations have found widespread use. Through the measurement of chemical shift perturbations *(7,8)*, nuclear Overhauser effects (nOes) *(9)*, relaxation rates *(10-13)*, and diffusion coefficients *(14,15)*, NMR experiments allow for the straightforward evaluation of the structure and dynamics of both the local and bulk environments of ionic liquids and ionic liquid-based solutions. While these experiments alone cannot explain certain phenomena atomistically, a variety of parameters obtained from NMR studies can be employed to validate results from MD simulations on these systems *(8,16)*. These experimentally supported models provide accurate atomic-level depictions of structure, dynamics, and intraionic and intermolecular interactions which are critical in the rational design and utilisation of ionic liquids and ionic liquid-based systems.

In this chapter, we showcase the application of some of these techniques to systems based on 1,3-dialkylimidazolium ionic liquids. In particular, we describe the use of $^{13}$C and $^{35/37}$Cl relaxation data, $^{1}$H diffusion measurements, and MD simulations in the study of carbohydrate solvation in two imidazolium salts known to dissolve polysaccharides efficiently, 1-butyl-3-methylimidazolium chloride and 1-ethyl-3-methylimidazolium ethanoate ([$C_4$mim]Cl and [$C_2$mim][$O_2$CMe], Figure 1). As detailed in the following sections, results obtained using cellobiose as a model solute point to a general solvation mechanism in which the ionic liquids interact with carbohydrates through the formation of hydrogen bonds between the non-hydrated ionic liquid anions and the hydroxyl group protons of the sugar. In addition, our experimental and theoretical findings also confirm that the interactions between the ionic liquid cations and the carbohydrate are negligible.

Downloaded by DUKE UNIV on June 28, 2012 | http://pubs.acs.org
Publication Date (Web): December 18, 2009 | doi: 10.1021/bk-2009-1030.ch005

The application of similar methodology to the study of other relevant ionic liquid-based systems is briefly discussed.

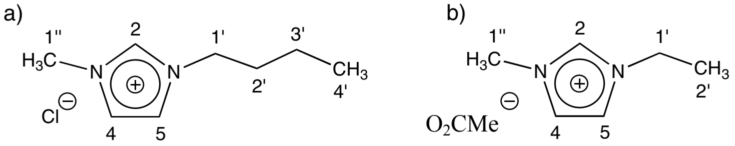

*Figure 1. Structure and numbering of (a)[$C_4$mim]Cl and (b)[$C_2$mim][$O_2$CMe].*

# Materials and Methods

## General

[$C_4$mim]Cl was prepared following reported procedures *(17)*. [$C_2$mim][$O_2$CMe] (97%) and D-cellobiose (98%) were purchased from Sigma-Aldrich (Milwaukee, WI). The ionic liquids were dried *in vacuo* ($1 \times 10^{-4}$ Torr) under vigorous stirring at 110 ºC for at least 16 h, and all materials were kept under vacuum until used. The absolute viscosities of the ionic liquids and ionic liquid solutions were determined using a ViscoLab 3000 temperature-controlled piston-type viscometer (Cambridge Applied Systems, Inc., Medford, MA).

## NMR Experiments

Solutions of cellobiose in [$C_4$mim]Cl and [$C_2$mim][$O_2$CMe] were prepared by heating a mixture of the carbohydrate and the ionic liquid to 80 ºC with constant stirring. Upon complete dissolution, the samples were transferred to 5 mm NMR tubes that were then fitted with 60 μL co-axial inserts containing dmso-$d_6$ required for field-frequency lock. Samples of the neat ionic liquids were prepared analogously.

Longitudinal ($T_1$) relaxation data for the $^{13}$C nuclei in [$C_4$mim]$^+$, [$C_2$mim]$^+$, and [$O_2$CMe]$^-$ ions were obtained with a standard $^{13}$C-{$^1$H} inversion recovery (180º - $t_d$ - 90º - Acq) pulse sequence, using eight $t_d$ increments. The $T_1$ times were computed by fitting the raw data to exponential functions of the form:

$$I(t_d) = I_o \cdot (1 - 2 \cdot e^{-t_d/T_1})$$

where $I_o$ and $T_1$ are the fit variables. $^{35/37}$Cl longitudinal relaxation measurements for the chloride ion were performed using an inversion recovery sequence in which the 90º read pulse was substituted by a 90º-90º-90º ARING pulse train to reduce acoustic ringing effects *(12)*. Twelve $t_d$ increments were employed in this case, and the values of $T_1$ were also estimated using the equation shown above. When necessary, nOe factors for $^{13}$C nuclei of the ionic

Downloaded by DUKE UNIV on June 28, 2012 | http://pubs.acs.org
Publication Date (Web): December 18, 2009 | doi: 10.1021/bk-2009-1030.ch005

liquid ions were computed from the ratio of the $^{13}C$-{$^{1}H$} signal area recorded with continuous decoupling relative to that obtained using inverse-gated decoupling *(18)*. Experiments for the neat ionic liquids were performed in 10 ºC increments at temperatures ranging from 40 to 90 ºC for [$C_4$mim]Cl and 30 to 80 ºC for [$C_2$mim][$O_2$CMe]. Measurements for [$C_4$mim]Cl solutions were carried out at 90 ºC, and at 80 ºC in the case of [$C_2$mim][$O_2$CMe] solutions. It is worth noting that although its melting point is approximately 70 ºC *(2,17)*, [$C_4$mim]Cl and its solutions behave as supercooled fluids and remain liquid below this temperature for prolonged periods.

Diffusion coefficients for ions in the neat ionic liquids and ionic liquid/carbohydrate solutions were obtained using the $^{1}H$-detected PFG-STE sequence 90º - $G$ - 90º - $\Delta$ - 90º - $G$ - Acq *(19)*, where $\Delta$ is the diffusion time and $G$ represents a bipolar $z$-gradient block of the form $G_{+z}$ - 180º - $G_{-z}$ with overall duration $\delta$ and strength $g$ *(20)*. For each measurement, a total of 16 data points were recorded by varying the gradient strength linearly while keeping the $\Delta$ and $\delta$ diffusion parameters constant. Self-diffusion coefficients ($D$) were estimated by fitting the $^{1}H$ signal intensity versus gradient strength to mono-Gaussian curves of the form *(21)*:

$$I(g) = I_o \cdot e^{-\gamma^2 g^2 \delta^2 D \cdot (\Delta - \delta/3)}$$

where $I_o$ and $D$ are the fit variables, $\gamma$ represents the $^{1}H$ gyromagnetic ratio, and the remaining parameters were previously defined. The self-diffusion coefficient for any given ion was computed as the average of the $D$ values obtained for all its protons. Diffusion measurements were carried out in 10 ºC increments at temperatures ranging from 40 to 100 ºC for [$C_4$mim]Cl and from 30 to 90 ºC for [$C_2$mim][$O_2$CMe] solutions.

All experiments were carried out on a Bruker AVANCE 400 NMR spectrometer equipped with 5 mm BBO and QNP $z$-gradient shielded probes, operating at $^{1}H$, $^{13}C$, $^{35}Cl$, and $^{37}Cl$ frequencies of 400.13, 100.61, 39.21, and 32.64 MHz, respectively.

## Simulation Details

MD simulations were performed employing the CM3D software package and the OPLS-AA force field with optimised van der Waals parameters for the chloride ion described earlier *(8,22-24)*. Partial charges for cellobiose, [$C_4$mim]Cl, and [$C_2$mim][$O_2$CMe] were computed from fits to their electrostatic potentials (ESPs) derived from *ab initio* calculations at the B3LYP/6-311+G* level of theory *(24)*. The initial configurations of all systems were obtained from previously equilibrated [$C_4$mim]Cl and [$C_2$mim][$O_2$CMe] simulation boxes. The cellobiose solutions were created by patching sugar molecules to the sides of the ionic liquid boxes until the correct concentration was obtained. In the case of the 5 wt% cellobiose solutions discussed below, a total of six sugar molecules were required in both cases. Periodic boundary conditions were employed, using the Ewald method to treat long-range electrostatic interactions

Downloaded by DUKE UNIV on June 28, 2012 | http://pubs.acs.org
Publication Date (Web): December 18, 2009 | doi: 10.1021/bk-2009-1030.ch005

*(25,26)*. The reversible reference system propagator algorithm (r-RESPA) with time steps of 0.5 and 2 fs was employed to evaluate short-range intramolecular forces and long-range interactions, respectively *(27)*. The systems were first equilibrated in the canonical ensemble (NVT) for 1 ns, followed by period of a 1 to 2 ns in the isothermal-isobaric ensemble (NPT) required to stabilise their densities. After an additional 1 ns equilibration period in the NVT ensemble, 10 ns production runs used in the analyses discussed below were performed under the same conditions. Simulations of [$C_4$mim]Cl and [$C_2$mim][$O_2$CMe] solutions were carried out at 363.15 and 353.15 K, respectively.

## 3. Results and Discussion

### NMR Studies of Ionic Liquid/Cellobiose Systems

As we have recently reported, the relaxation of NMR-active nuclei in an ionic liquid depends on the dynamics of both ions and their interactions with solutes. In the case of imidazolium chlorides, the marked variation in the $^{35/37}$Cl relaxation parameters with changes in the environment of the chloride ion makes these quadrupolar nuclei ideal to investigate sugar/ionic liquid solutions *(12,28)*. As a matter of fact, the dependency of $^{35/37}$Cl transverse ($T_2$) relaxation times with carbohydrate concentration allowed us to establish that the solvation of sugars in [$C_4$mim]Cl occurs through the formation of hydrogen bonds between the chloride ion and the solute hydroxyl group protons *(12)*. While the concentration dependency of the relaxation times of the ethanoate carbons is not expected to be as marked as that of the anions in imidazolium chloride salts, a similar approach should also be suitable to study [$C_2$mim][$O_2$CMe]/carbohydrate solutions.

We first investigated longitudinal relaxation times as a function of temperature and in the absence of solutes. Results for selected carbons of the [$C_4$mim]$^+$ and [$C_2$mim]$^+$ ions are presented in Figure 2. For [$C_4$mim]$^+$, the $T_1$ minima observed for the imidazolium ring carbons, C-1', and C-1" indicate that these nuclei transition from the extreme narrowing ($\omega_o \tau_c < 1$) to the diffusion limit ($\omega_o \tau_c > 1$) relaxation regime at ~70 ºC, Figure 2(a). Due to their higher mobility, the remaining butyl chain carbons fail to undergo this transition in the range of temperatures studied. In the case of [$C_2$mim]$^+$, all carbons remain in the extreme narrowing regime, Figure 2(b).

Downloaded by DUKE UNIV on June 28, 2012 | http://pubs.acs.org
Publication Date (Web): December 18, 2009 | doi: 10.1021/bk-2009-1030.ch005

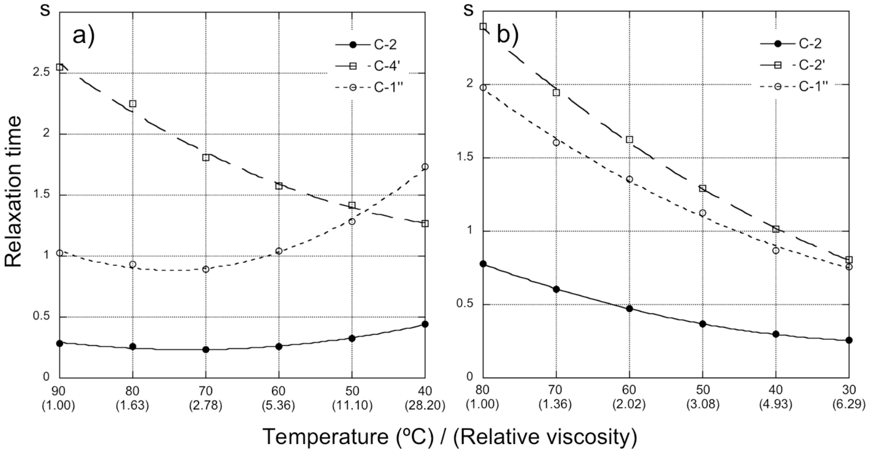

*Figure 2.* $^{13}C$ $T_1$ *relaxation as a function of temperature for (a) C-2, C-4', and C-1" in* $[C_4mim]Cl$*, and (b) C-2, C-2', and C-1" in* $[C_2mim][O_2CMe]$*.*

Due to the smaller size of the ethyl side chain, the C-2' and C-1" carbons of this cation have similar mobilities. Overall, and in agreement with previous NMR and molecular dynamics simulation studies on analogous systems *(11,13)*, the temperature dependency of the $^{13}C$ relaxation rates for both imidazolium cations reflects the variations observed in the viscosities of the neat ionic liquids. Longitudinal relaxation data as a function of temperature for the anions for the two ionic liquids are presented in Figure 3. The pronounced increase in the $T_1$ times with rising temperature also correlates with changes in viscosity and is consistent with a weakening of interionic interactions *(12)*. It is also worth noting that in the range of temperatures considered, the anions of both ionic liquids remain in the extreme narrowing relaxation regime. This is evidenced by the fact that the chloride ion in $[C_4mim]Cl$ has virtually indistinguishable $T_1$ and $T_2$ values, and that no $T_1$ minima are observed for the carbons of the ethanoate ion *(18)*. Based on these results, carbohydrate dissolution in $[C_4mim]Cl$ and $[C_2mim][O_2CMe]$ was studied at 90 and 80 ºC, respectively. All nuclei in the neat ionic liquids are in the extreme narrowing region at these temperatures, and thus pronounced changes in relaxation rates as a function of concentration are likely to indicate specific ionic liquid-solute interactions.

Downloaded by DUKE UNIV on June 28, 2012 | http://pubs.acs.org
Publication Date (Web): December 18, 2009 | doi: 10.1021/bk-2009-1030.ch005

Downloaded by DUKE UNIV on June 28, 2012 | http://pubs.acs.org
Publication Date (Web): December 18, 2009 | doi: 10.1021/bk-2009-1030.ch005

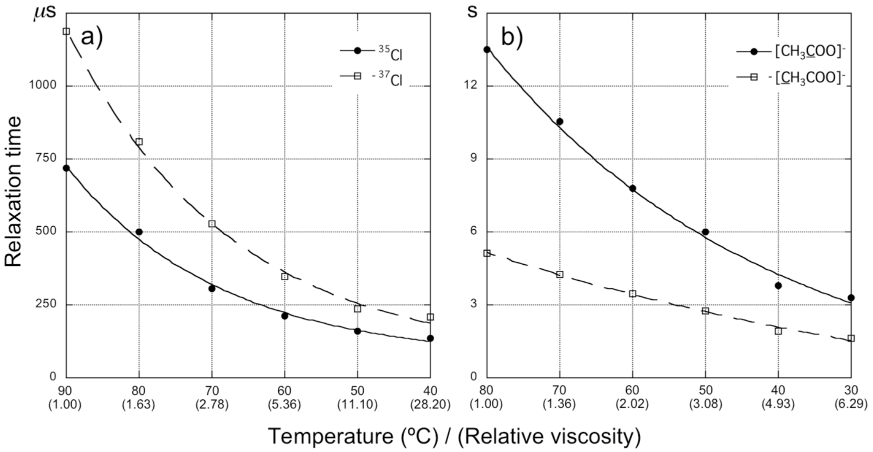

*Figure 3. Temperature dependence of the $^{35/37}$Cl $T_1$ relaxation of the chloride ion in (a) [$C_4$mim]Cl, and (b) $^{13}$C $T_1$ for the carbonyl and methyl carbons of the [$O_2$CMe]$^-$ ion in [$C_2$mim][$O_2$CMe].*

As shown in Figure 4, there are only slight variations in the longitudinal relaxation of the carbons in both ionic liquid cations as a function of cellobiose content. In all cases, the changes in $T_1$ times over the whole concentration range are comparable with those observed upon varying the temperature of the neat ionic liquids by 10 ºC or less, and can be rationalised satisfactorily on the basis of changes in solution viscosity.

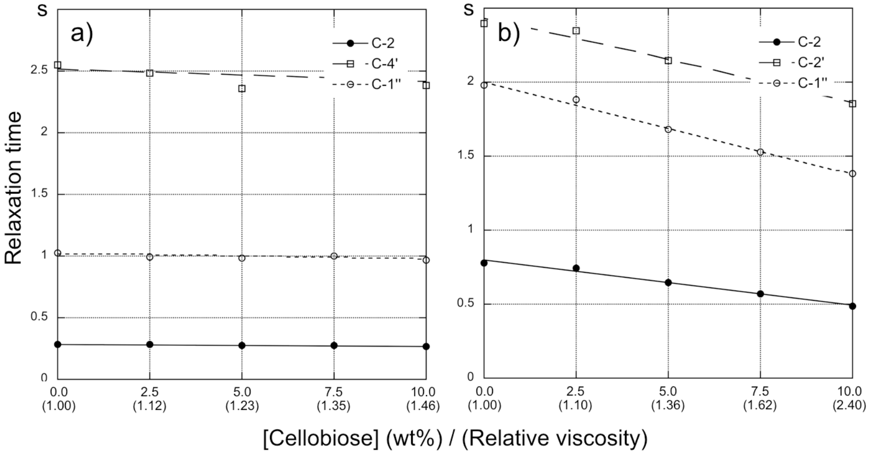

*Figure 4. $^{13}$C $T_1$ relaxation versus cellobiose concentration for C-2, C-4', and C-1" in (a)[$C_4$mim]Cl, and (b) C-2, C-2', and C-1" in [$C_2$mim][$O_2$CMe].*

Conversely, the relaxation parameters of the ionic liquid anions are strongly influenced by the presence of sugars. For [$C_4$mim]Cl solutions, the changes in the longitudinal relaxation rates of the chloride ion as a function of carbohydrate concentration are vastly larger than those expected based on the variation of the solution viscosity alone, Figure 5(a). For example, the $T_1$ times for the anion in 10 wt% cellobiose solutions in [$C_4$mim]Cl at 90 ºC, which has a viscosity of 112.3 cP, are considerably lower than in the neat ionic liquid at 40 ºC, which has a viscosity of 1716.0 cP. These large changes in the $^{35/37}$Cl relaxation parameters point to the disruption of the spherical symmetry around the quadrupolar nuclei, and are consistent with the formation of hydrogen bonds between the chloride ions and the carbohydrate hydroxyl group protons *(12)*. Although less pronounced, the dependency of the $T_1$ times of the ethanoate carbons with sugar concentration in [$C_2$mim][$O_2$CMe] solutions at 80 ºC is also clear, Figure 5(b).

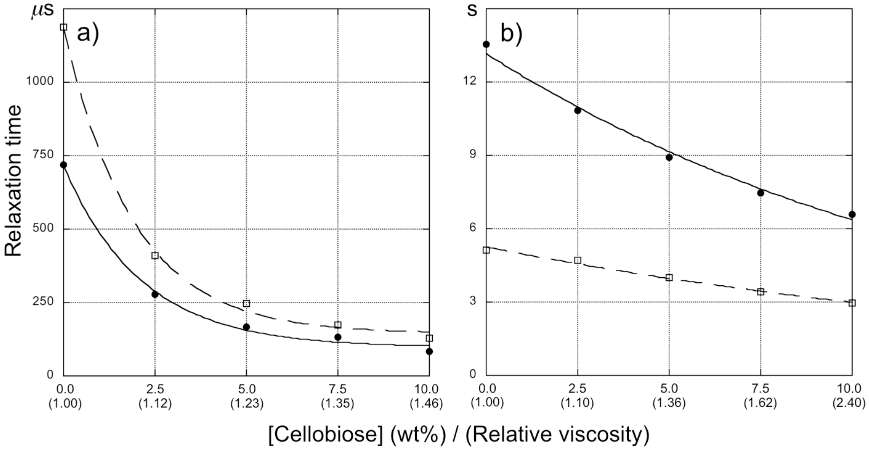

*Figure 5. $^{35/37}$Cl $T_1$ relaxation for the chloride ion in (a)[$C_4$mim]Cl, and (b) $^{13}$C $T_1$ relaxation times for the carbonyl and methyl carbons of the [$O_2$CMe]$^-$ ion in [$C_2$mim][$O_2$CMe] as a function of cellobiose concentration.*

Further analysis of the $^{13}$C and $^{35/37}$Cl relaxation data can provide detailed information regarding changes in the mobilities of the ions in both ionic liquids as a function of cellobiose concentration. The measured longitudinal relaxation times are the combination of a variety of relaxation processes *(18)*. These include, for example, dipolar interactions ( $R_1^D$ ), chemical shift anisotropy ( $R_1^{CSA}$ ), and quadrupolar coupling ( $R_1^Q$ ):

$$\frac{1}{T_1} \equiv R_1 = R_1^D + R_1^{CSA} + R_1^Q + \ldots$$

In the case of protonated carbons, which applies to [$C_4$mim]$^+$ and both ions in [$C_2$mim][$O_2$CMe], $R_1^D$ and $R_1^{CSA}$ dominate. The two are related to the correlation time ($\tau_c$) of the nuclei under scrutiny by the following expressions *(18)*:

Downloaded by DUKE UNIV on June 28, 2012 | http://pubs.acs.org
Publication Date (Web): December 18, 2009 | doi: 10.1021/bk-2009-1030.ch005

$$R_1^D = \frac{N_H}{40} \cdot \frac{\gamma_C^2 \gamma_H^2 \mu_o^2 \hbar^2}{r_{CH}^6} \cdot \left( \frac{\tau_c}{1+(\omega_C-\omega_H)^2 \tau_c^2} + \frac{3\tau_c}{1+\omega_C^2 \tau_c^2} + \frac{6\tau_c}{1+(\omega_C+\omega_H)^2 \tau_c^2} \right)$$

$$R_1^{CSA} = \frac{1}{15} \cdot \gamma_C^2 B_o^2 \Delta\sigma^2 \cdot \left( \frac{2\tau_c}{1+\omega_C^2 \tau_c^2} \right)$$

$N_H$ represents the number of attached protons and $r_{CH}$ the C-H bond distance, $\mu_o$ is the permeability of vacuum, $\gamma_C$ and $\gamma_H$ are the gyromagnetic ratios of $^{13}$C and $^1$H and $\omega_C$ and $\omega_H$ their Larmor frequencies, respectively, $\hbar$ is the reduced Planck constant, $B_o$ is the spectrometer magnetic field, and $\Delta\sigma$ is the chemical shift anisotropy of the nucleus under consideration. The $\tau_c$ values for protonated carbons in [C$_4$mim]Cl and [C$_2$mim][O$_2$CMe] solutions can be determined using the experimental $^{13}$C $T_1$ data as input for these equations following the approach of Carper and coworkers *(11,13)*.

As stated earlier, the relaxation of the chloride ion in [C$_4$mim]Cl solutions is dominated by $R_1^Q$, which can also be expressed as a function of the correlation time of the anion *(18)*:

$$R_1^Q = \frac{1}{10} \cdot \left(1 + \frac{\eta^2}{3}\right) \cdot \left(\frac{e^2 Qq}{\hbar}\right) \cdot \tau_c$$

In this equation, $\eta$ represents the assymetry parameter and $e^2Qq\,/\,\hbar$ the quadrupole coupling constant. These parameters have been recently reported for the chloride ion $^{35}$Cl isotope in solid [C$_4$mim]Cl *(29)*, and they could in principle be used in the estimation of $\tau_c$ from experimental $T_1$ data. However, the changes in $\tau_c$ values measured in the ionic liquid/cellobiose solutions relative to those obtained for the neat ionic liquids are better suited to investigate changes in the mobility of the ions. This not only circumvents the need to compute correlation times in the case of the chloride ion, but also allows for clear comparisons of the variations in the mobilities of cations versus anions as a function of solute concentration.

As shown in Figure 6, the changes in $\tau_c$ as a function of sugar concentration are modest and comparable for all carbons in both imidazolium ions. Indeed, there is virtually no variation in the correlation times of the [C$_4$mim]Cl carbons. This not only indicates that the rotational mobilities of different regions of the cations are affected similarly by the presence of cellobiose, but is consistent with a lack of strong interactions between the cation and the carbohydrate. On the other hand, the variation of the $\tau_c$ values of the ethanoate ion methyl carbon and chloride ion reveals that the reorientation rate of the anions decreases sharply with increasing sugar concentration. In [C$_2$mim][O$_2$CMe] solutions, the tumbling rate of the anion decreases nearly twice as much as that of the cation when the concentration of cellobiose increases, while for [C$_4$mim]Cl solutions the change in the rotational mobility of the anion is nearly eight times larger than that observed for the cation. These results agree well with the preliminary conclusions derived from raw longitudinal relaxation data presented earlier, and

Downloaded by DUKE UNIV on June 28, 2012 | http://pubs.acs.org
Publication Date (Web): December 18, 2009 | doi: 10.1021/bk-2009-1030.ch005

provide further evidence regarding the presence of specific interactions between the ethanoate ion and the sugar solute.

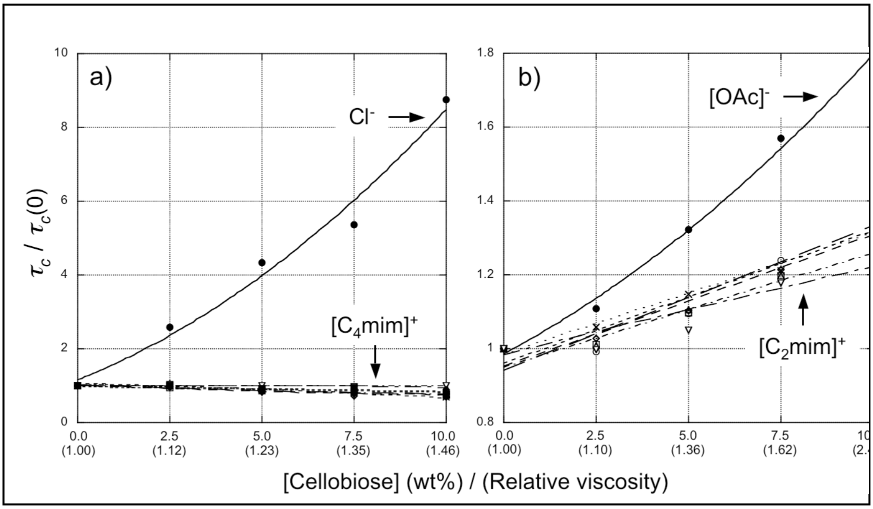

*Figure 6. Relative variation in the $\tau_c$ values of nuclei in (a) [$C_4$mim]Cl and (b) [$C_2$mim][$O_2$CMe] as a function of cellobiose concentration.*

[$O_2$CMe]$^-$

Additional information regarding the effects of the sugar on the dynamics of the ionic liquid ions can be obtained by studying variations in their translational mobility *(15,16,30,31)*. This was done through the estimation of the self-diffusion coefficients of the [$C_4$mim]$^+$, [$C_2$mim]$^+$, and [$O_2$CMe]$^-$ ions as a function of temperature in the neat ionic liquids, as well as in 5 and 10 wt% cellobiose ionic liquid solutions (Figure 7). The relatively high viscosities of these systems lead to short $^1$H $T_2$ times, and thus PFG-STE techniques were employed to carry out all measurements (*16*). Regardless of the method, the fast transverse relaxation of $^{35/37}$Cl nuclei precludes the estimation of the anion self-diffusivity in [$C_4$mim]Cl solutions using this or related techniques.

Not surprisingly, there is an inversely proportional relationship between the self-diffusivity of the cations and the viscosity of the neat ionic liquids, with $D_{[C2mim]+} >> D_{[C4mim]+}$. In the case of [$C_2$mim][$O_2$CMe], it is worth noting that the smaller ethanoate ion diffuses slower than the imidazolium cation. This behaviour has been observed for other ionic liquids, and suggests that the anions do not diffuse as isolated species but as part of larger ion aggregates *(30,31)*. Together with the increase in the viscosity of the systems, there is a substantial drop in the diffusion coefficients of all species as sugars are dissolved in the ionic liquids. In [$C_2$mim][$O_2$CMe] solutions, the diffusion of the ethanoate ion is affected more than that of the imidazolium cation by the dissolved carbohydrates. However, the differences are minimal and considerably smaller than those observed through analysis of $^{13}$C relaxation data. This is not unexpected considering that even when their local mobility may be affected

Downloaded by DUKE UNIV on June 28, 2012 | http://pubs.acs.org
Publication Date (Web): December 18, 2009 | doi: 10.1021/bk-2009-1030.ch005

differently by their interactions with carbohydrates (*vide supra*), anion and cation co-migration is required to maintain the charge balance of the systems.

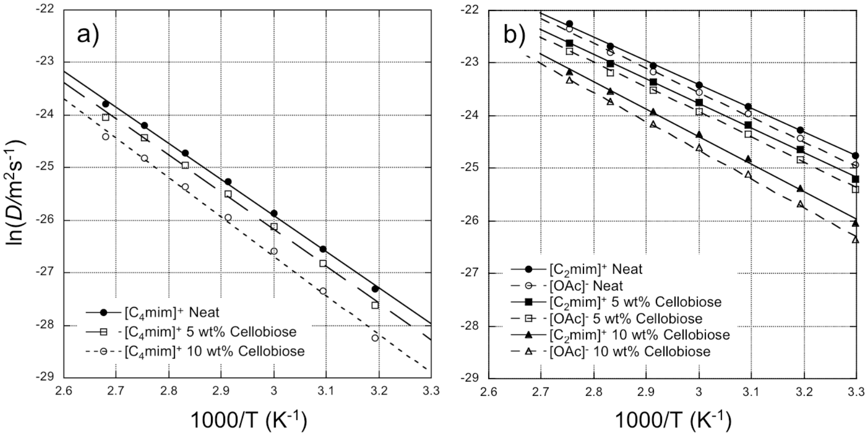

*Figure 7. Arrhenius plots for the (a) $[C_4mim]^+$, (b) $[C_2mim]^+$ and $[O_2CMe]^-$ ions in the neat ionic liquids, as well as their 5 and 10 wt% cellobiose solutions.*

## MD Simulations of Ionic Liquid/Cellobiose Systems

We and others have recently employed MD simulations to investigate carbohydrate dissolution in imidazolium ionic liquids *(24,32,33)*. The results summarised in these reports, which considered exclusively $[C_4mim]Cl$ and $[C_1mim]Cl$, were in good agreement with NMR studies and corroborated that sugar solvation is governed by hydrogen bonding between the ionic liquid chloride ion and the solute hydroxyl groups. Since the results presented in the previous section of this chapter indicate that the process is analogous for chloride and ethanoate anions, we here extend our MD studies to $[C_2mim][O_2CMe]$/cellobiose solutions. In addition, we pay considerable attention to potential interactions between the ionic liquid cations and the solute, as these have been suggested to be of importance in some of the previous studies *(32,33)*. While MD simulations were carried out for all the solutions investigated by NMR, the results obtained for the 5 wt% ionic liquid/cellobiose solutions are representative and we limit our analyses to these systems.

Figure 8a shows the radial distribution functions (RDFs) between the sugar primary and secondary hydroxyl group protons and the chloride ion in the $[C_4mim]Cl$/cellobiose system. There is a prominent peak in the OH···Cl RDFs, or $g_{OH\cdots Cl}(r)$ functions, centred at 1.85 Å which indicates a strong interaction between the chloride ion and the hydroxyl protons. Similarly, analysis of the angular distribution functions (ADFs) for the O–H···Cl angle shows a strong maximum centred at ~170°, Figure 8(b). This distance and angle combination are in the ideal hydrogen bonding range, and thus our results clearly indicate the presence of hydrogen bonds between the hydroxyl protons and the chloride ion.

Downloaded by DUKE UNIV on June 28, 2012 | http://pubs.acs.org
Publication Date (Web): December 18, 2009 | doi: 10.1021/bk-2009-1030.ch005

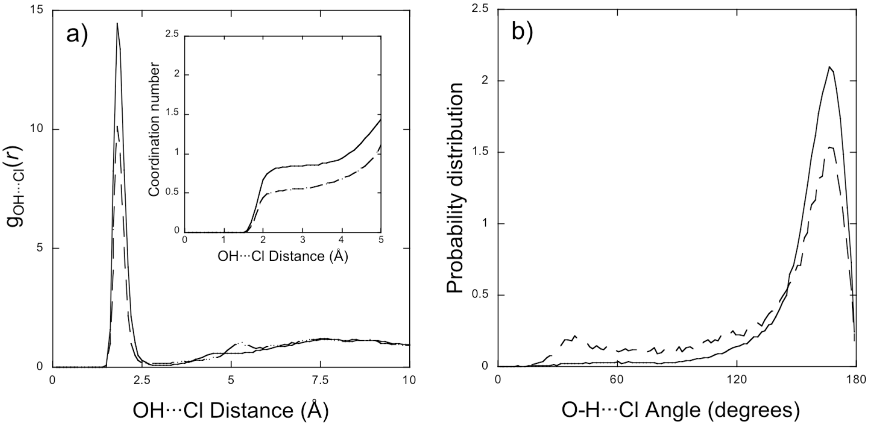

*Figure 8. (a) OH···Cl RDFs and coordination numbers, and (b) O–H···Cl ADFs for the [$C_4$mim]Cl/cellobiose system. Results for secondary and primary hydroxyl groups are presented as solid and dashed lines, respectively.*

The stoicheiometry of the interaction can be established by calculation of the coordination numbers, which is done by integration of the RDFs out to the first solvation shell, Figure 8(a). The coordination numbers of secondary and primary hydroxyl groups to chloride ions in the first shell are 0.85 and 0.56, respectively. If the coordination numbers are averaged over all types of hydroxyl groups, a OH···Cl hydrogen bonding stoicheiometry of 1:0.78 is obtained. This is close to the ideal 1:1 ratio expected for these systems, and agrees well with results from NMR experiments *(12)*. The slight deviation from ideality can be explained by analysis of the ion spatial distribution around the solute presented in Figure 9. The most populated cellobiose conformer observed in the simulation, which accounts for ~60% of the total, displays a lack of chloride ion density around some hydroxyl groups. Closer inspection reveals that these groups hydrogen bond intramolecularly to oxygen atoms within the carbohydrate, therefore reducing the number of OH···Cl interactions.

The spatial distribution also shows that while the anions are in close proximity to the solute, the [$C_4$mim]$^+$ ions lie in the periphery. This would indicate weak interactions between the cations and the sugar, in agreement with the NMR results discussed above, and can be corroborated by analysis of the RDF from the sugar oxygens to the imidazolium H-2 proton, or $g_{O\cdots H2}(r)$, and the corresponding O···H2–C2 ADF. As seen in Figure 10, there are no significant peaks above the ideal gas distribution threshold in neither the RDF nor the ADF. Contrary to what has been previously proposed *(32,33)*, this demonstrates that there are no specific interactions between the cations and the solute.

Similar analyses were carried out for the [$C_2$mim][$O_2CMe$]/cellobiose system. Once again, there is a pronounced peak in the OH···$O_2CMe$ RDFs at 1.55 Å, Figure 11(a). Since both oxygen atoms in the anion were analysed independently, a minor peak at 3.30 Å, which corresponds to the non-interacting oxygen in each ethanoate ion, can be observed. The O–H···$O_2CMe$ ADFs, shown in Figure 11(b), also show a maximum centred at ~170°. As was the case in the [$C_4$mim]Cl/cellobiose system, these distance and angle values correspond

Downloaded by DUKE UNIV on June 28, 2012 | http://pubs.acs.org
Publication Date (Web): December 18, 2009 | doi: 10.1021/bk-2009-1030.ch005

to ideal hydrogen bonding geometry between the hydroxyl group protons and the ethanoate ions. The coordination numbers reveal that the $OH\cdots O_2CMe$ interactions are nearly stoicheiometric and virtually identical for primary and secondary hydroxyl groups (0.93 and 0.91, respectively). Consistent with the profile of the RDFs, there is a second plateau in the RDF integrals that corresponds to the non-interacting ethanoate oxygen atom.

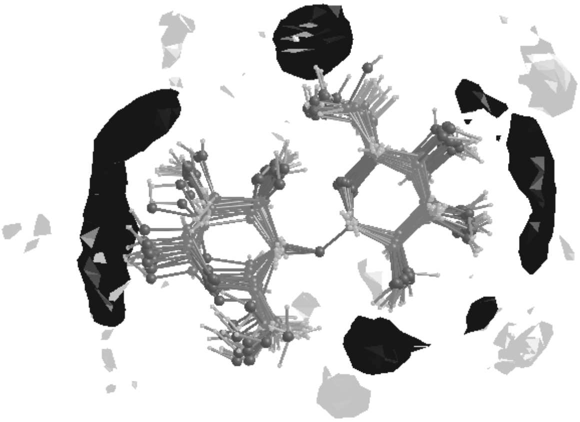

*Figure 9. Spatial distribution of $Cl^-$ (dark grey) and $[C_4mim]^+$ ions (light grey) around cellobiose in a 5 wt% $[C_4mim]Cl$/cellobiose solution. The centre of mass of the imidazolium ring was used to compute the distributions.*

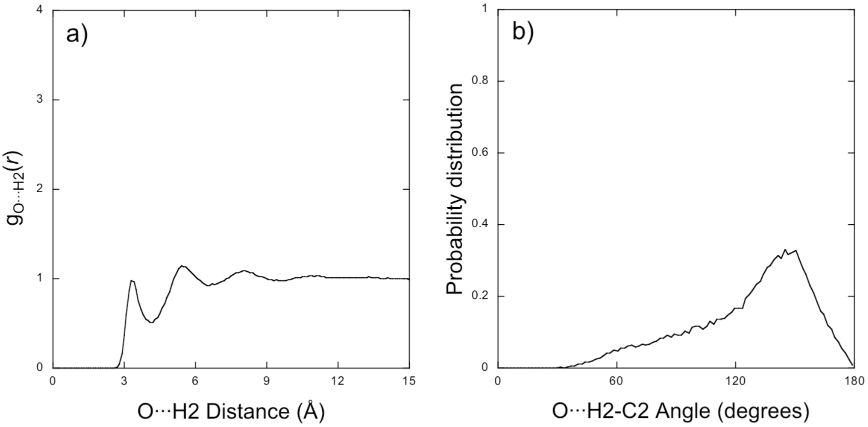

*Figure 10. (a) O···H2 RDFs and (b) O···H2–C2 ADFs for the $[C_4mim]Cl$/cellobiose system*

Downloaded by DUKE UNIV on June 28, 2012 | http://pubs.acs.org
Publication Date (Web): December 18, 2009 | doi: 10.1021/bk-2009-1030.ch005

Downloaded by DUKE UNIV on June 28, 2012 | http://pubs.acs.org
Publication Date (Web): December 18, 2009 | doi: 10.1021/bk-2009-1030.ch005

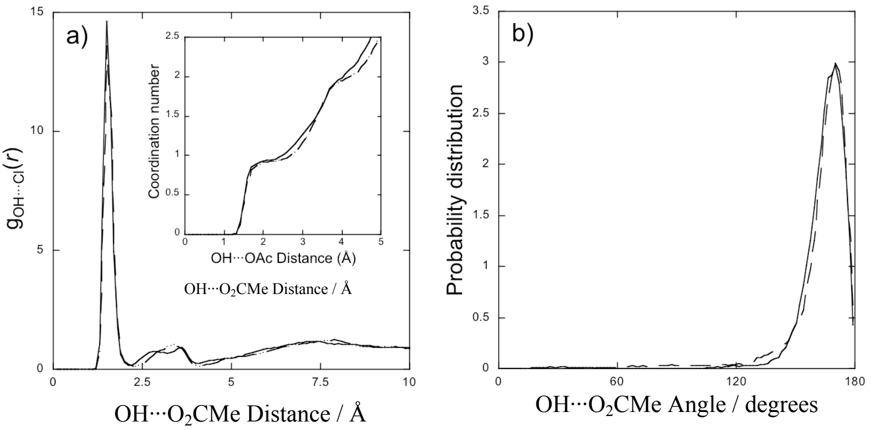

*Figure 11. (a) OH···$O_2CMe$ RDFs and coordination numbers, and (b) O-H···$O_2CMe$ ADFs for the [$C_2mim$][$O_2CMe$]/cellobiose system. Results for secondary and primary hydroxyl groups are presented as solid and dashed lines, respectively.*

The near-ideal OH···$O_2CMe$ interaction ratio can be rationalised if the distribution of cellobiose conformers in this system is analysed. In this case, the hydroxyl groups in most of the conformer families do not display intramolecular hydrogen bonds, but instead participate in intermolecular hydrogen bonding with the ethanoate ions. Indeed, the spatial distribution of ions around the most populated cellobiose conformer shows anion density near all hydroxyl groups (Figure 12).

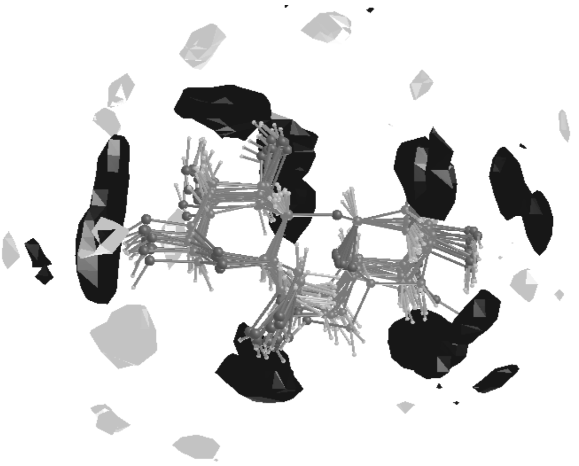

*Figure 12. Spatial distribution of [$O_2CMe$]$^-$ (dark grey) and [$C_2mim$]$^+$ (light grey) ions around cellobiose in a 5 wt% [$C_2mim$][$O_2CMe$]/cellobiose solution. The centre of mass of the imidazolium ring was used to compute the distributions.*

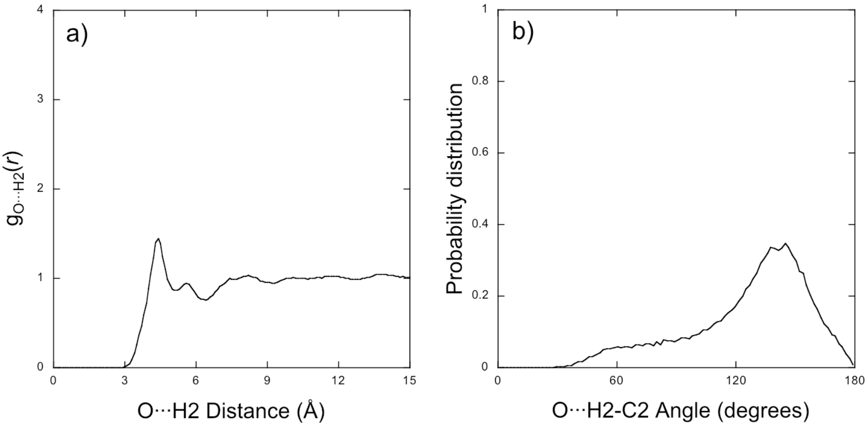

*Figure 13. (a) O···H2 RDFs and (b) O···H2–C2 ADFs for the [$C_2$mim][$O_2$CMe]/cellobiose system.*

By analogy to the [$C_4$mim]Cl/cellobiose system, further inspection of the ion spatial distribution shows limited cation density around the solute. This is also consistent with results from our NMR experiments, is again corroborated by analysis of the $g_{O\cdots H2}(r)$ and the corresponding ADF (Figure 13), and indicates a lack of specific interaction between the [$C_2$mim]$^+$ ion and the solute.

## 4. Conclusions

In summary, this chapter outlined the use of NMR spectroscopy in combination with molecular modelling simulations in the study of carbohydrate dissolution by 1,3-dialkylimidazolium ionic liquids at the molecular level. Our results conclusively show that the solvation mechanism is based on the interaction of the ionic liquid anion with the hydroxyl group protons of the sugar solute. More importantly, both experimental and theoretical methods demonstrate that the ionic liquid cation does not play a primary role in the process. Therefore, these findings suggest that while the structure of the anion is critical, that of the cation may be modified to fine tune the physicochemical properties of the ionic liquid without affecting its carbohydrate dissolving ability.

Our MD simulation analyses for the ionic liquid/sugar systems concentrated on structural parameters. These are sufficient to explain most of the experimental observations adequately in this case, but computation of dynamic properties such as ion diffusivities and correlation times of NMR-active nuclei can also be undertaken to further validate theoretical results *(6,24,34)*. Given the long simulation times required to properly reproduce the dynamics of viscous fluids such as ionic liquids, the accuracy of these estimations is generally semi-quantitative. However, they are in most cases able to reproduce

Downloaded by DUKE UNIV on June 28, 2012 | http://pubs.acs.org
Publication Date (Web): December 18, 2009 | doi: 10.1021/bk-2009-1030.ch005

experimental trends satisfactorily and can therefore be used in the *a priori* prediction of properties of ionic liquids.

The methodology outlined here can also be applied to other systems based on ionic liquids. For example, we have employed a similar combination of NMR experiments and MD simulations to explain the effects of co-solvents on the macroscopic properties of ionic liquids *(8)*. The findings from these and other studies thus indicate that the approach should be suitable to investigate ionic liquid interactions with a wide range of materials in a variety of processes. Work in several of these areas is ongoing, and our results will be reported in due course.

Downloaded by DUKE UNIV on June 28, 2012 | http://pubs.acs.org
Publication Date (Web): December 18, 2009 | doi: 10.1021/bk-2009-1030.ch005

## Acknowledgments

Funding from the NSF CCLI-A&I and MRI programs (Grants DUE-9952264 and CHE-0420556), the Camille and Henry Dreyfus Foundation (Award TH-04-008), the H. O. West Foundation, the Merck/AAAS Undergraduate Summer Research Program, and W. R. Grace & Company is greatly acknowledged.

## References

1. *Ionic Liquids IV: Not Just Solvents Anymore*, Brennecke, J. F., Rogers, R. D., Seddon, K. R., Eds. ACS Symposium Series 975, American Chemical Society: Washington, DC, 2007. See also volumes 818, 856, 901, and 902 of the same series.
2. Holbrey, J. D.; Reichert, W. M.; Nieuwenhuyzen, M.; Johnston, S.; Seddon, K. R.; Rogers, R. D. *Chem. Commun.* **2003**, 1636-1637.
3. Hardacre, C.; Holbery, J. D.; McMath, S. E. J.; Bowron, D. T.; Soper, A. K. *J. Chem. Phys.* **2003**, *118*, 273-278.
4. Dieter, K. M.; Dymek, C. J., Jr.; Heimer, N. E.; Rovang, J. W.; Wilkes, J. S. *J. Am. Chem. Soc.* **1988**, *110*, 2722-2726.
5. Bankmann, D.; Giernoth, R. *Prog. Nucl. Magn. Reson. Spectrosc.* **2007**, *51*, 63-90.
6. Margulis, C. J.; Stern, H. A.; Berne, B. J. *J. Phys. Chem. B* **2002**, *106*, 12017-12021.
7. Consorti, C. S.; Suarez, P. A. Z.; de Souza, R. F.; Burrow, R. A.; Farrar, D. H.; Lough, A. J.; Loh, W.; da Silva, L. H. M.; Dupont, J. *J. Phys. Chem. B* **2005**, *109*, 4341-4349.
8. Remsing, R. C.; Liu, Z.; Sergeyev, I.; Moyna, G. *J. Phys. Chem. B* **2008**, *112*, 7363-7369.
9. Mele, A.; Romanò, G.; Giannone, M.; Ragg, E.; Fronza, G.; Raos, G.; Marcon, V. *Angew. Chem. Int. Ed.* **2006**, *45*, 1123-1126.
10. Carper, W. R.; Wahlbeck, P. G.; Dölle, A. *J. Phys. Chem. A* **2004**, *108*, 6096-6099.
11. Remsing, R. C.; Swatloski, R. P.; Rogers, R. D.; Moyna, G. *Chem. Commun.* **2006**, 1271-1273.

12. Heimer, N. E.; Wilkes, J. S.; Wahlbeck, P. G.; Carper, W. R. *J. Phys. Chem. A* **2006**, *110*, 868-874.
13. Remsing, R. C.; Hernandez, G.; Swatloski, R. P.; Massefski, W. W.; Rogers, R. D.; Moyna, G. *J. Phys. Chem. B* **2008**, *112*, 11071-11078.
14. Noda, A.; Hayamizu, K.; Watanabe, M. *J. Phys. Chem. B* **2001**, *105*, 4603-4610.
15. Annat, G.; MacFarlane, D. R.; Forsyth, M. *J. Phys. Chem. B* **2007**, *111*, 9018-9024.
16. Moreno, M.; Castiglione, F.; Mele, A.; Pasqui, C.; Raos, G. *J. Phys. Chem. B* **2008**, *112*, 7826-7836.
17. Huddleston, J. G.; Visser, A. E.; Reichert, W. M.; Willauer, H. D.; Broker, G. A.; Rogers, R. D. *Green Chem.* **2001**, *3*, 156-164.
18. Farrar, T. C.; Becker, E. D. *Pulse and Fourier Transform NMR. Introduction to Theory and Methods*, Academic Press, New York, 1971.
19. Pelta, M. D.; Barjat, H.; Morris, G. A.; Davis, A. L.; Hammond, S. J. *Magn. Reson. Chem.* **1998**, *36*, 706-714.
20. Wider, G.; Dötsch, V.; Wüthrich, K. *J. Magn. Reson. A* **1994**, *108*, 255-258.
21. Stejskal, E. O.; Tanner, J. E. *J. Chem. Phys.* **1965**, *42*, 288-292.
22. Moore, P. B. Code for Molecular Modeling and Molecular Dynamics (CM3D). http://hydrogen.usp.edu/moore/code/cm3d.html (accessed Feb 2008).
23. Jorgensen, W. L.; Maxwell, D. S.; Tirado-Rives, J. *J. Am. Chem. Soc.* **1996**, *118*, 11225-11236.
24. Liu, Z.; Remsing, R. C.; Moore, P. B.; Moyna, G. In *Ionic Liquids: Not Just Solvents Anymore*, Brennecke, J. F., Rogers, R. D., Seddon, K. R., Eds. ACS Symposium Series, American Chemical Society: Washington, DC, 2007, pp. 335-350.
25. Darden, T. A.; York, D. M.; Pedersen, L. G. *J. Chem. Phys.* **1993**, *98*, 10089-10092.
26. Essmann, U.; Perera, L.; Berkowitz, M. L.; Darden, T.; Lee, H.; Pedersen, L. G. *J. Chem. Phys.* **1995**, *103*, 8577-8593.
27. Tuckerman, M.; Berne, B. J.; Martyna, G. *J. Chem. Phys.* **1992**, *97*, 1990-2001.
28. Hedin, N.; Furó, I.; Eriksson, P. O. *J. Phys. Chem. B* **2000**, *104*, 8544-8547.
29. Gordon, P. G.; Brouwer, D. H.; Ripmeester. J. A. *J. Phys. Chem. A* **2008**, *112*, 12527-12529.
30. Hayamizu, K.; Aihara, Y.; Nakagawa, H.; Nukuda, T.; Price, W. S. *J. Phys. Chem. B* **2004**, *108*, 19527-19532.
31. Chung, S. H.; Lopato, R.; Greenbaum, S. G.; Shirota, H.; Castner, E.W. Jr.; Wishart, J. F. *J. Phys. Chem. B* **2007**, *111*, 4885-4893.
32. Youngs, T. G. A.; Holbrey, J. D.; Deetlefs, M.; Nieuwenhuyzen, M.; Costa Gomes, M. F.; Hardacre, C. *ChemPhysChem* **2006**, *7*, 2279-2281.
33. Youngs, T. G. A.; Hardacre, C.; Holbrey, J. D. *J. Phys. Chem. B* **2007**, *111*, 13765-13774.
34. Ködderman, T.; Ludwig, R.; Paschek, D. *ChemPhysChem* **2008**, *9*, 1851-1858.

Downloaded by DUKE UNIV on June 28, 2012 | http://pubs.acs.org
Publication Date (Web): December 18, 2009 | doi: 10.1021/bk-2009-1030.ch005

## Chapter 6

# The Development of Ionic Liquids for Biomedical Applications – Prospects and Challenges

**Gloria D. Elliott,[1] Regina Kemp,[1] and Douglas R MacFarlane[2]**

**[1] Department of Mechanical Engineering, University of North Carolina at Charlotte, 9201 University City Blvd., Charlotte, NC 28223-0001, gdelliot@uncc.edu,**
**[2] School of Chemistry, Monash University, Clayton VIC 3800, Australia**

Downloaded by COLUMBIA UNIV on June 28, 2012 | http://pubs.acs.org
Publication Date (Web): December 18, 2009 | doi: 10.1021/bk-2009-1030.ch006

Ionic liquids have considerable potential to advance formulation science for protein-based pharmaceutical preparations and cellular therapies. Extended shelf life has been reported for a number of model proteins in rationally designed ionic liquid formulations *(1-4)*. Biocompatibility is also an important aspect of rational design of pharmaceutical additives that are co-delivered into the body with a therapeutic. Using mouse macrophage cells as models for toxicity testing, biocompatibility has been established for a number of these bio-inspired ionic liquids, including salts based on the choline cation. Other important facets of clinical translation have also been elucidated. Here, we overview progress towards clinical application of ionic liquids and identify some of the challenges that remain.

## Introduction

Ionic liquids (ILs) are a class of materials that have considerable potential to provide advances in a variety of biomedical fields, including the formulation of biologics intended for delivery into the human body. Progress in genomics and metabolomics have advanced our understanding of human disease, and as a result protein and peptide-based drugs and cellular therapies are complementing

In Ionic Liquids: From Knowledge to Application; Plechkova, N., et al.;
ACS Symposium Series; American Chemical Society: Washington, DC, 2010.

traditional small molecule chemical approaches to treating disease. Protein-based drugs have become a major component of pharmaceutical R&D. Furthermore, successes with stem-cell transplants for cancer and other diseases are paving the way for a range of other cell-based treatments. As demand increases for such interventions, there is a need to ensure adequate supply, and improve the ease-of-use of such therapies.

Ultimately, to retain therapeutic efficacy, the structural elements of protein and cellular therapies that are critical to their biological function need to be retained. Proteins generally need to remain folded, a state that results from a delicate balance of the energetic drives to minimise the exposure of hydrophobic regions to solvent water, neutralise electrical charges, maximise hydrogen bonding, and maximise van der Waals interactions *(5)*. In the case of cellular therapies, membranes need to remain intact, as does the cellular machinery to grow, reproduce, and perform specialised cellular functions. Storage solutions must be chosen to ensure that biomolecules such as proteins and lipids in the membrane remain in their native state, and that larger cellular assemblies are also preserved. Because of the necessity of preserving molecular structure in both cases, it is not surprising that many of the same excipients are used in the storage formulations of both proteins and cells. Examples include physiologic buffering agents and disaccharides, such as trehalose *(6)*.

Although traditional ionic liquids are synthesised from imidazolium-based cations and highly fluorinated anions, ionic liquids can also be formulated from salts, sugars, amino acids, and biomolecules that exist in nature - many of which have already been approved as pharmaceutical additives (excipients) *(1-4,7)*. Because ionic liquids consist of chemically distinct ions, by appropriate selection of cation and anion, the hydrogen-bonding character and the water miscibility can be rationally designed into the material, to enable a particular application. For example, the organic cations can be ammonium, imidazolium, or phosphonium based *(8)*. Many of these cations, such as choline, can have important biochemical roles. The anions can be selected from the large family of atomic and molecular anions, such as chloride, ethanoate, phosphate, gluconate, citrate, and sulfonate. As individual ions, many of these are well known substances, and have even been derived from natural amino acids *(9)*. Thus, in many cases, the component ions are known to be quite biocompatible and are listed on the FDA Inactive Ingredients list. The combinations of the anions and cations produce a huge family of potential salts of varied properties and it is this breadth of scope in properties that has generated such wide interest in these materials in recent years. These organic salts vary across the spectrum from those that are clearly hydrophobic, to those that are nearly miscible with water, to organic salts that are actually more hydrophilic than water itself. The ability to rationally design solvents with desirable features for biological solutions, by judicious optimisation of the cation and anion, is opening up an entirely new area of fruitful biomedical exploration. In this paper, we present an overview of progress towards biomedical applications of ionic liquids and discuss the challenges that remain.

Downloaded by COLUMBIA UNIV on June 28, 2012 | http://pubs.acs.org
Publication Date (Web): December 18, 2009 | doi: 10.1021/bk-2009-1030.ch006

## Maximising Shelf-life

A challenge in the development of protein drugs is the necessity of ensuring that the protein emerges in its folded native state at the end of production, and that it can be effectively delivered to the patient in an active functional state. Many protein therapeutics are not stable enough to be stored and delivered in liquid formulation, and are instead formulated and stored in the costlier lyophilised form. For example, Enbrel *(etanercept)* produced by Wyeth, and Basiliximab *(Simulect)* produced by Novartis, each are lyophilised products that require reconstitution at the end point of use (www.enbrel.com; www.basiliximab.com). These efforts often result in an increase in development time and manufacturing cost when compared to a liquid formulation. An example of the specialised packaging that is utilised to enable sterile reconstitution of lyophilised therapeutics is shown in Figure 1. Patient compliance decreases as the complexity of administration increases, consequently liquid formulation of parenterals (drugs intended for injection) is highly preferred over lyophilised dosages that require sterile reconstitution by the patient. Although the current list of FDA-approved additives provides an adequate panel for stabilising many proteins in liquid formulation, there still are numerous proteins that must be lyophilised in order to achieve a reasonable shelf-life, and others still that cannot be effectively stabilised by any means.

Currently, long-term storage of cellular therapies is achieved by storing cells at cryogenic temperatures. This requires the use of chemicals such as dimethylsulfoxide (DMSO), a cryoprotectant (CPA), to minimise damage caused by ice formation. Such CPAs are toxic at room temperature, thus the cellular therapy requires special handling before and after storage. Due to challenges with washing out the CPA, some amount is ultimately delivered into the body, which is a very unpleasant experience for the patient. As such, there is considerable interest in identifying formulations that are bio-compatible, but still provide superior cryo-protection *(10)*. It is possible that the stabilising characteristics of biocompatible ionic liquids can also afford protection to cells in storage formulations.

Downloaded by COLUMBIA UNIV on June 28, 2012 | http://pubs.acs.org
Publication Date (Web): December 18, 2009 | doi: 10.1021/bk-2009-1030.ch006

Downloaded by COLUMBIA UNIV on June 28, 2012 | http://pubs.acs.org
Publication Date (Web): December 18, 2009 | doi: 10.1021/bk-2009-1030.ch006

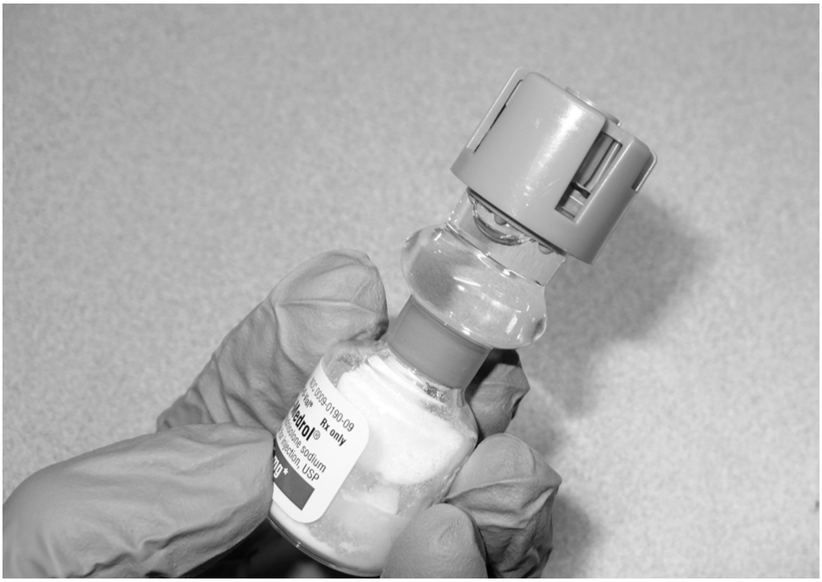

*Figure 1. Specialised packaging enables sterile reconstitution of lyophilised medicine at the point-of use.*

## Biological Formulation

A judicious choice of additives is necessary to stabilise a protein in liquid formulation to prevent adverse protein denaturation and precipitation. These excipients have many roles in optimising the liquid protein formulation, such as increasing the solubility of the protein, acting as an antioxidant or antimicrobial, adjusting the osmolality of the solution, and protecting hydrophobic regions of the protein *(11)*. Surfactants such as Tween 20 (polyoxyethylene sorbitan monolaurate) stabilise the protein in the folded state by preventing protein aggregation *(11,12)*. To prevent oxidation reactions from occurring at amino acid sites within the protein, methionine can be added to competitively inhibit the undesired protein oxidation *(13)*. EDTA can also be added to chelate metals that contribute to these unfavourable oxidation reactions. Sometimes a single excipient can fulfil several roles. For example, co-solvents such as glycerol increase solubility, while modulating the osmolality of the solution *(11)*. Excipients for liquid formulation are thus typically selected to enhance both the solubility and the stability of proteins, as well as to prevent aggregation or oxidation. In order to increase solubility and/or increase stability, an excipient molecule must be physiologically inactive, non-toxic *(14)* and provide some detectable benefit *(15)*. In the case of cellular therapeutics, additional criteria, such as buffering capacity and osmolality of the solution are important to avoid loss of therapeutic potential. Approved excipients in the U.S.A. can be found in the Food and Drug Administration's (FDA) database (http://www.accessdata.fda.gov/scripts/cder/iig/index.cfm). Many sugars, salts and amino acids appear on this list. However, these alone are insufficient to provide adequate stability for some protein therapeutics to be considered for drug applications. Novel molecules that can increase biomolecule stability and satisfy FDA requirements would enable advances in the formulation of biologics.

## Biocompatibility of Ionic Liquids

Different methods have been adopted to test ionic liquid toxicity, from standard WST1 cell viability assays *(16)* to assays on soil nematode *Caenorhabditis elegans (17)*. Alkylimidazolium salts have been most extensively tested, revealing a direct link between alkyl side chain length and toxicity. It is thought that the ionic liquid toxicity may be linked to lipophilicity, in that the hydrophobic side chains may increase membrane permeability, causing necrotic effects *(16,18)*. Ranke *et al. (19)* have also recently identified a relationship between the choice of anion and cytotoxicity. Structure-Activity-Relationship (QSAR and TSAR) studies have been developed *(20)* to rapidly screen for ionic liquids toxicity, revealing that specific ionic liquids inhibit acetylcholinesterase activity *(21)*. This method studies the $LC_{50}$ level of the ionic liquids, treating the ionic liquid as a solute. Much of this research is current, dating back only a few years.

Ranke *et al. (16,19)* have recently determined $EC_{50}$ values for a range of "traditional" organic salts (*i.e.* those designed for chemical rather than biological applications). In our work with biologically inspired ionic liquids, we have tested a number of organic salts purposely designed for biocompatibility including 1-butyl-3-methylimidazolium lactate, choline saccharinate, and choline dihydrogenphosphate ($[N_{1\,1\,1}(CH_2OH)][H_2PO_4]$) *(22)*. An assay similar to that of Ranke *et al. (16,19)* was used to assess toxicity to J774 mouse macrophage cells. The calculated $EC_{50}$ levels were 16 mM for the choline saccharinate, 2 mM for the bmim lactate, and there was no loss of viability observed in $[N_{1\,1\,1}(CH_2OH)][H_2PO_4]$ up to the maximum tested concentration of 50 mM. $[N_{1\,1\,1}(CH_2OH)][H_2PO_4]$ actually demonstrated a hormetic effect on cells, with cell growth being stimulated compared to control *(22)*. These values meet or exceed those of the least toxic ionic liquids reported in Ranke *et al. (16)*, thus supporting the hypothesis that biocompatibility can be designed into ionic liquids.

## Solubility of Proteins in Ionic Liquids

Proteins need to be in a sufficient concentration to effectively reach and act on their target destination. The issue of solubility arises when trying to concentrate proteins to desired therapeutic dosage levels. In a crowded protein environment, the potential for proteins to self associate is increased. Hydrophobic regions within proteins interact with regions from neighbouring proteins, and this in turn leads to protein unfolding and ultimately to aggregation

Downloaded by COLUMBIA UNIV on June 28, 2012 | http://pubs.acs.org
Publication Date (Web): December 18, 2009 | doi: 10.1021/bk-2009-1030.ch006

and loss of protein function *(13,23)*. This can also lead to irreversible precipitation of protein, creating a loss of available protein and visual particulate, which is unacceptable in the final formulation dispensed to patients. While precipitate can be filtered out of solution for purposes of drug delivery, the loss of concentration is significant and more difficult to overcome.

A potential impact of combining proteins with ionic liquids involves increasing the protein solubility over typical aqueous formulation, and thereby increasing the maximum protein concentration that can be achieved. This advantage would greatly aid in the administration of drug dosages. Many protein drugs are difficult to formulate at high concentrations, which in turn requires administering large volumes of liquid to meet the recommended dosage. This typically requires clinical visits for intravenous (IV) administration *(24)*. Increasing the protein concentration in liquid formulation may enable subcutaneous injections and dosing at home, thereby avoiding a clinical visit. Smaller volumes can be used resulting in less painful and/or less frequent injections, which further results in more convenience and increased patient compliance.

As described in the previous section, a number of new ionic liquids have been prepared based on the biocompatible anions saccharinate and dihydrogenphosphate *(1,2)*. The cations chosen included 1-butyl-1-methylpyrrolidinium ($[C_4mpyr]^+$) and an important biochemical cation, choline. A key feature of these new ionic liquids is their ability to dissolve significant amounts of cytochrome c (cyt c). For example, $[C_4mpyr][H_2PO_4]$ will dissolve up to 3 mM cyt c when a small amount (10-20 wt%) of water is added *(1,2)*. Cyt c solubility in this family of ionic liquids has indicated the importance of the choice of anion on the protein solubility *(1)*. Recent molecular modelling studies have shown that the cations and anions of ionic liquids can interact directly with proteins, displacing hydrogen-bonded water to a large extent *(25)*. The anion interaction was observed to dominate the non-bonded interactions with the enzyme serine protease cutinase. Notably, the anion $[NO_3]^-$ of the ionic liquid was observed to interact directly with the main chain of the protein, an interaction that led to a destabilisation of the protein. Such modelling studies have provided considerable insight into the nature of interactions between the protein and ionic liquid solvent, and could potentially predict ionic liquids that have the potential to solvate and stabilise therapeutic proteins.

## Thermal Stability and Shelf Life

Although the shape and characteristics of a protein are primarily determined by the amino acid sequence, the environment (solvent, salts, enzymes, other excipients) surrounding the protein during and after folding determines the final folded state. The organic salt $[N_{1\,1\,1}(CH_2OH)][H_2PO_4]$ has been shown to impart excellent thermal stability to the model protein horse heart cyt c *(1,2)*. Very significantly, the secondary structure is retained in the ionic liquid solubilised protein, as evidenced by the second derivative ATR FT-IR spectrum in the amino I region of the vibrational spectrum. Upon heating the protein solution, the key peak at 1657 $cm^{-1}$ arising from the $\alpha$–helix in the

Downloaded by COLUMBIA UNIV on June 28, 2012 | http://pubs.acs.org
Publication Date (Web): December 18, 2009 | doi: 10.1021/bk-2009-1030.ch006

folded structure is retained in ionic liquids, whereas in aqueous formulation it is no longer present, and a new band at 1620 $cm^{-1}$ corresponding to unstructured amide groups appears. Multi-year preservation of cyt c activity in this ionic liquid has also been achieved. By comparison cyt c in aqueous buffer showed substantial loss of activity after only two weeks of storage. Hen egg white lysozyme formulated in this same 80 wt% ionic liquid solution was tested for its ability to lyse the bacterial wall of *micrococcus lysodeikticus.* Activity levels were observed to be near control activity levels after 1 month of storage *(22)*. Others have also reported excellent protein stabilisation in ionic liquids. A pyrrolidinium-based ionic liquid has been shown to increase the transition temperature of the sweet protein monellin by over 100% *(26)*. Ethylammonium nitrate, $[EtNH_3][NO_3]$, a protic ionic liquid, has also been found to prevent aggregation of lysozyme upon denaturation *(3,26)* with multi-year stability reported with concentrations of protein in the range of 200 mg $cm^{-3}$ *(3)*.

An important observation with respect to protein stabilisation in ionic liquids is that some amount of ionic liquid hydration may be necessary to maintain a critical number of protein surface water molecules *(25)*. Molecular modelling studies suggest that a fraction of this critical water is located on the surface, while the excess of water molecules interact with the bulk ionic liquid solvent through hydrogen bonding with the anion. These studies also revealed that the anion interaction with the protein may become detrimental to protein stability if it is strong enough to disrupt essential internal hydrogen bonding *(25)*.

## Anti-Microbial Activity

Another desirable feature of excipients or solvents for liquid formulation is the ability to resist bacterial contamination. Cieniecka-Rosonkiewicz *et al.* have shown that the biocidal activity of ionic liquids can be altered based on the choice of cations and anions *(27)*. For example, in their studies with a family of alkyltrihexylphosphonium halides, anti-microbial activity was observed for pentyl to tetradecyl alkyl groups, but the biocidal activity was attenuated as the number of carbons in the alkyl group was increased or decreased. In the case of protein or cellular formulations, the biological functionality can be adversely affected by the presence of bacteria, and clearly any agent intended for injection should be contaminant free. It would be desirable if ionic liquid based formulations could provide some resistance to bacterial contamination while maintaining general mammalian cell biocompatibility. While bacterial and mammalian cell compatibility have been independently studied by various groups, studies involving a synergistic modulation of these effects have not been reported (to the authors' best knowledge). The selective activity against certain bacteria observed by Cieniecka-Rosonkiewicz *et al.* *(27)* suggests that such a mixed role could be possible. It should be noted that strong biocidal ionic liquids could potentially pose adverse health and environmental risks if used as additives in formulations not intended for use as biocides. Mild to moderate anti-microbial activity against harmful bacteria would be the desired route for pharmaceutical formulations. Research of this nature is encouraged.

Downloaded by COLUMBIA UNIV on June 28, 2012 | http://pubs.acs.org
Publication Date (Web): December 18, 2009 | doi: 10.1021/bk-2009-1030.ch006

In our work with $[N_{1\,1\,1}(CH_2OH)][H_2PO_4]$-protein formulations, the vials and liquid formulations were autoclaved before use, and aliquots of the formulation were added to nutrient rich bacterial broth (0.5 g $l^{-1}$ bactopeptone, 0.5 g $l^{-1}$ yeast extract, 0.5 g $l^{-1}$ glucose in phosphate buffered saline) to screen for possible bacterial contamination *(28)*. As illustrated in Figure 2, the ionic liquid has performed equally as well as a buffer in experiments performed to date. Bacterial contamination in experimental samples has not been observed. Although this does not suggest that $[N_{1\,1\,1}(CH_2OH)][H_2PO_4]$ has biocidal activity, it does suggest that the ionic liquid can be suitably sterilised for pharmaceutical applications. This is also an important consideration for agents intended for delivery into the body.

Downloaded by COLUMBIA UNIV on June 28, 2012 | http://pubs.acs.org
Publication Date (Web): December 18, 2009 | doi: 10.1021/bk-2009-1030.ch006

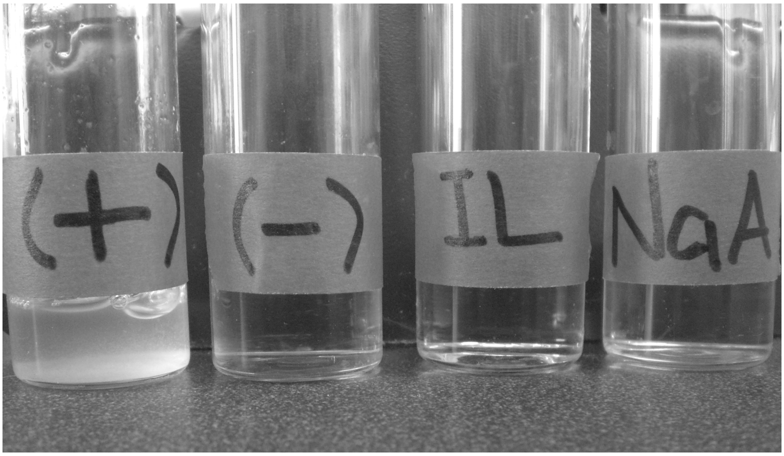

*Figure 2. Broth inoculated with an aliquot (10 μl ) of liquid formulation. Innoculum from left to right: contaminated culture media, nothing added, lysozyme in 80 wt% $[N_{1\,1\,1}(CH_2OH)][H_2PO_4]$, and lysozyme in sodium ethanoate buffer.*

## Osmolality of Formulations

While many of the rationally designed ionic liquids studied to date appear to be as benign as basic sugars, the osmotic strength must be considered in the development of the storage formulation to ensure that a final delivery formulation falls within acceptable limits for injection. This is especially true when the ionic liquid is the major cosolvent. Recent work has shown that many of the ionic liquids that are of interest in bio-applications do not behave as a medium comprised of separated ions; instead they exist as ion pairs in the neat liquid *(29)*. This observation creates an intermediate concept between conventional ionic liquids, and molecular solvents such as water. Practically, it means that the osmolality of the liquid could be much lower than one would expect for a simple salt.

Downloaded by COLUMBIA UNIV on June 28, 2012 | http://pubs.acs.org
Publication Date (Web): December 18, 2009 | doi: 10.1021/bk-2009-1030.ch006

The toxicity studies described previously were carried out using the ionic liquid as a solute in full-complement media with no reduction in the physiologic salt composition of the media. Using this approach $EC_{50}$ values in the >10-20 mM range are generally reflecting osmotic stresses, not necessarily chemical toxicities. Because some of the ionic liquids (including choline dihydrogenphosphate) were as benign as trehalose and glucose, it is possible that concentrations of ionic liquid greater than the $EC_{50}$ value can be tolerated in the final formulation, much the same way as sugar concentrations can be tolerated in the 100 mM range if other osmolytes in the formulation are reduced. In the case of $[N_{1\,1\,1}(CH_2OH)][H_2PO_4]$, no loss of viability was observed up to 50 mM, the highest tested concentration. This would suggest that a high concentration of $[N_{1\,1\,1}(CH_2OH)][H_2PO_4]$ could possibly be tolerated in a formulation designed for parenteral injection, as long as total osmolality limits are not exceeded.

The question then remains as to how much ionic liquid is needed to maintain protein stability. Although evidence suggests that ionic liquid water contents in the range of 5-20% yield maximal stability of the protein *(1,2,25),* it is possible that adequate shelf-life (1-2 years) can be achieved at higher moisture contents, thus enabling the creation of formulations with osmolalities nearer to physiologic values (~300 mOsm). $[N_{1\,1\,1}(CH_2OH)][H_2PO_4]$ stability studies were performed at 80 wt%, which would require a dilution of ~1:10 to 1:20 to achieve an isotonic formulation suitable for injection *(1-2).* Under these circumstances, the protein would need to be reasonably concentrated to accommodate such a dilution prior to delivery. However, even though excellent real-time storage data has been reported with the 80 wt% $[N_{1\,1\,1}(CH_2OH)][H_2PO_4]$ solution, it is likely that an adequate shelf life can be retained at an even lower concentration of ionic liquid. A goal of future studies is to develop ionic liquid formulations and strategies that can provide acceptable therapeutic shelf-life without requiring dilution prior to administration.

Osmolality of the formulation is also an important consideration for cellular therapies. Solution osmolality must stay within a certain range to avoid osmotically-induced volumetric excursions that can cause shrinking or swelling of the cell beyond tolerable limits, thus leading to cell lysis, and concomitantly a lack of function. Progress in this direction thus has implications for a wide range of therapies.

## Clinical Translation: Remaining Challenges

As described above, a number of criteria must be met in order to deem an ionic liquid suitable as a possible liquid protein formulation candidate. The different ionic liquids must produce a significant increase in either protein stability or solubility as compared to the protein's original best known formulation. If an ionic liquid does show the ability to increase stability or solubility, this may not be sufficient to establish its acceptance as a viable solvent or excipient. It must also not pose any toxic threat and approach the safety levels demanded by drug monitoring organisations like the FDA. Although cytotoxicity studies can enable the elimination of highly toxic ionic liquids early in a development process, continued toxicology studies are necessary to ensure safety for parenteral drug administration.

To enable the development of a formulation that is suitable for clinical translation, it will be important to determine the optimum level of ionic liquid to allow adequate shelf-life while minimising the osmolality of the storage solution. With continued development and optimisation, it is reasonable to expect that some formulations would enable direct injection with minimal dilution. Even with a moderate dilution requirement, practical subcutaneous dosing by the patient may still be possible, as recent developments are enabling injections that exceed the standard 1-2 $cm^3$ bolus *(30)*. Furthermore, many commercial and experimental strategies exist to enable the delivery and slow release of protein formulations, including encapsulation within polymers, liposomes, hydrogels, and other microparticles *(e.g. 31)*. If proteins can be suitably stabilised in liquid formulation with molecules that are as benign as simple salts and sugars in cell-based *in vitro* assays, but osmolality issues remain a concern, delivery into the body can potentially be facilitated by many of the encapsulation technologies that already exist on the market (*e.g.* Lupron Depot® or Nutropin Depot®), as well as other emerging approaches.

Clearly certain ionic liquids offer a range of interesting and very useful properties that can be exploited in the formulation and storage of protein-based pharmaceuticals. Many of these same ionic liquids may have potential as stabilisers in non-toxic cryoprotectant and lyoprotectant formulations. It is likely that the stabilising effects observed thus far are ionic liquid-protein combination specific, thus considerable work is still needed to understand the underlying mechanisms responsible for these effects. Continued toxicity assessments will also need to be an integral component of gaining FDA clearance for any ionic liquid intended for use in the human body. Despite the need for detailed studies in these areas, investigations with model proteins have shown enough promise to warrant studies with therapeutic proteins that are currently unstable in liquid formulation. With continued research into the stabilisation of therapeutic proteins and appropriate delivery strategies, this relatively new area of investigation has considerable potential for clinical translation.

Downloaded by COLUMBIA UNIV on June 28, 2012 | http://pubs.acs.org
Publication Date (Web): December 18, 2009 | doi: 10.1021/bk-2009-1030.ch006

## References

1. Fujita, K.; MacFarlane, D.R.; Forsyth, M. *Chem. Commun.* **2005**, 4804-4806.
2. Fujita, K.; Forsyth, M.; MacFarlane, D.R.; Reid, R.W.; Elliott, G.D. *Biotech. Bioeng.* **2006,** *94(6)*, 1209-1213.
3. Byrne, N.; Wang L.-M.; Belieres J.-P.; Angell, C.A. *Chem. Commun.* **2007**, 2714-2716.
4. Baker, S.N.; McCleskey, T.M., Pandey, S., Baker, G.A. *Chem. Commun.* **2004,** *8,* 940-941.
5. Stryer, L. *Biochemistry, 4th Edition*, W.H. Freeman and Company: New York, 1996.
6. Carpenter, J.F.; Pikal, M.J.; Chang, B.S.; Randolph, T.W. *Pharmaceutical*

*Research*, **1997,** *14(8)*, 969-975.

7. Carter, E.B.; Culver, S.L.; Fox, P.A.; Good, D.A.; Ntai, I.; Tickell, M.D.; Traylor, R.K.; Hoffman, N.W.; Davis, J.H. *Chem. Commun.* **2004,** *6*, 630-631.
8. Forsyth, S.A.; Pringle, J.M.; MacFarlane, D.R. *Aust. J. Chem.* **2004,** *57* 113-119.
9. Fukumoto, K.; Yoshizawa, M.; Ohno, H. *J. Am. Chem. Soc.* **2005,** *127*, 2398-2399.
10. Wusteman, M.; Rauen, U.; Simmonds, J.; Hunds, N.; Pegg, D.E. *Cryobiology* **2008**, *56(1)*, 72-79.
11. Akers, M.J. *J. Pharm. Sci.,* **2002,** *91(11)*, 2283-2300.
12. Krielgaard, L.; Jones, L.S.; Randolph, T.W.; Frokjaer, S.; Flink, J.M.; Manning, M.C.; Carpenter, J.F. *J. Pharm. Sci.* **1998,** *87*, 1593-1603.
13. Wang, W. *Int. J. Pharm.,***1999,** *185(2)* 129-188.
14. Osterberg, R.E.; See, N.A. *Int. J. Toxicol.* **2003**, *22(5)*, 377-380.
15. Nema, S.; Washkuhn, R.J.; Brendel, R.J. *PDA J. Pharm. Sci. Technol.* **1997,** *51(4)*, 166-171.
16. Ranke, J.; Mölter, K.; Stock, F.; Bottin-Weber, U.; Poczobutt, J.; Hoffmann, J.; Ondruschka, B.; Filser, J.; and Jastorff, B. *Ecotoxicol. Environ. Saf.* **2004**, *28(3)*, 396-404.
17. Swatloski, R.P.; Holbrey, J.D.; Memon, S.B.; Caldwell, G.A.; Caldwell, K.A.; and Rogers, R D. *Chem. Commun.* **2004**, *6*, 668-669.
18. Brown, R.S.; Akhtar, P.; Akerman, J.; Hamper, L.; Kozin, I.S.; Villerius, L.A.; Klamer, H.J. *Environ. Sci. Tech.* **2001,** *35*, 4097-4102.
19. Stolte, S.; Arning, J.; Bottin-Weber, U.; Matzke, M.; Stock, F.; Thiele, K.; Uerdingen, M.; Welz-Bierman, U.; Jastorff, B.; Ranke, J. *Green Chem.* **2006,** *8*, 621-629.
20. Jastorff, B.; Störmann, R.; Ranke, J.; Mölter, K.; Stock, F.; Oberheitmann, B.; Hoffmann, W.; Hoffmann, J.; Nüchter, M.; Ondruschka, B.; and Filser, J. *Green Chem.* **2003,** *5*, 136-142.
21. Stock, F; Hoffmann, J.; Ranke, J.; Stormann, R.; Ondruschka, B.; Jastroff B.; *Green Chem.* **2004**, *6(6)*, 286-290.
22. Kemp, R.; Fraser, K.; Fujita, K.; MacFarlane, D.; Elliott, G. Proceedings of the 2008 ASME Summer Bioengineering Conference, June 25-29, Marco Island, Florida USA. Published on CD (ISBN 0-7918-3825-0).
23. Stirling, P.C.; Lundin, V.F.; Leroux, M.R. *EMBO Rep.* **2003,** *4(6)*, 565-570.
24. Shire, S.J.; Shakrokh, Z.; and Liu, J. *J. Pharmaceutical Sci.* **2004,** *93(6)*, 1390-1402.
25. Micalo, N. M.; Soares, C. M. *J. Phys. Chem. B* **2008,** *112(9)*, 2566-2572.
26. Summers, C.A.; Flowers, R.A. II; *Protein Science* **2000,** *9,* 2001-2008.
27. Cieniecka-Rosonkiewicz, A.; Pernak, J.; Kubi-Feder, J.; Ramani, A.; Robertson, A.J.; Seddon, K.R.; *Green Chem.* **2005,** *7,* 855-862.
28. Parrow, M.W.; Burkholder, J.M.; Deamer, N.D.; Ramsdell, J.S.; *Aquat. Microb. Ecol.,* **2005**, *39*, 97-105.
29. Fraser, K.J.; Izgorodina, E.I.; Forsyth, M.; Scott, J.L.; MacFarlane, D.R. *Chem. Comm.* **2007,** 3817-3819.
30. Wilson, M.S. *Drug Delivery Technology* **2006,** *6(6)*, 64-66.
31. Varde, N.K., Pack, D. *Expert Opin. Biol. Ther.* **2004,** *4(1),* 35-51.

Downloaded by COLUMBIA UNIV on June 28, 2012 | http://pubs.acs.org
Publication Date (Web): December 18, 2009 | doi: 10.1021/bk-2009-1030.ch006

## Chapter 7

# Protein Denaturation by Ionic Liquids and the Hofmeister Series

**Diana Constantinescu, Christian Herrmann, and Hermann Weingärtner***

**Department of Physical Chemistry, Faculty of Chemistry and Biochemistry, Ruhr-University of Bochum, D-44780 Bochum, Germany**

Downloaded by STANFORD UNIV GREEN LIBR on June 28, 2012 | http://pubs.acs.org
Publication Date (Web): December 18, 2009 | doi: 10.1021/bk-2009-1030.ch007

We have used differential scanning calorimetry (DSC) for studying how ionic liquids affect the thermal stability of proteins. Most 1,3-dialkylimidazolium, 1,1-dialkyl pyrrolidinium and tetraalkylammonium salts decrease the thermal stability, but some protic ionic liquids stabilise the native state. The effects can be systematised by the Hofmeister ion series. Depending on the nature of the ions, ionic liquids can also suppress the formation of misfolded proteins and the irreversible deactivation of proteins at high temperatures.

## Introduction

The unique physical and chemical properties of ionic liquids open fascinating prospects for chemical and technological processes *(1-3)*. Ionic liquids are also of interest in biochemistry, for example in biocatalysis, biopreservation, or drug transportation *(1,4,5)*. In such applications, native proteins are often exposed to high ionic liquid concentrations.

How an ionic liquid affects the enzymatic function of a protein can vary sharply according to its ionic composition *(1,5-14)*. The high specificity of salt effects was first noted by Hofmeister *(15)*, who ranked salts according to their effect on the precipitation of hen egg white proteins. Essentially the same ranking is observed for other enzyme properties such as the thermal and functional stability and for many phenomena in other fields such as colloid or surface chemistry *(11,17-21)*. Ionic liquids open options for steering such

In Ionic Liquids: From Knowledge to Application; Plechkova, N., et al.;
ACS Symposium Series; American Chemical Society: Washington, DC, 2010.

processes because their variability allows to impart the solvent properties of interest. For example, ionic liquids can be hydrophobic or hydrophilic. The subclass of protic ionic liquids composed of Brønsted acids and Brønsted bases *(22,23)* involves some salts which offer prospects as highly hydrophilic media for biomolecular processes *(6,7)*.

Here, we use differential scanning calorimetry (DSC) to study how ionic liquids affect the thermal stability of native proteins. In the simplest case these processes follow the Lumry-Eyring scheme *(24)* for the reaction $N \Leftrightarrow U \rightarrow I$ between the native state (A), unfolded state (U), and irreversibly deactivated state (I). The unfolding/refolding equilibrium $N \Leftrightarrow U$ is completely reversible, so that after cooling the enzymatic activity is regained. Prolongated heating may, however, result in irreversible processes $U \rightarrow I$, which lead to a loss of the enzymatic function. Such irreversible deactivation plagues many processes in enzyme technology. The mechanisms of irreversible deactivation are highly specific to the protein and to solvent conditions such as pH and buffer. They also depend on experimental conditions such as temperature and incubation time. Rather than exploring these mechanisms, we focus here on possibilities to improve the thermal and functional stability by adding suitably chosen ionic liquids.

## Protein Unfolding

Most of the experiments reported here were conducted with bovine ribonuclease A (RNase A), generally at a protein concentration of 0.36 mM in buffered solutions (25 mM phosphate buffer), with the pH value adjusted to the desired value. RNase A is a relatively small, monomeric enzyme, which is widely used in studies of protein denaturation *(25-27)*.

Figure 1 shows the DSC profile of a single scan of a freshly prepared solution of ribonuclease A (RNase A) at pH 7.0 and two profiles of solutions containing choline dihydrogenphosphate ([chol][$H_2PO_4$]) at concentrations $C$ = 1 M and 2 M, respectively. In the freshly prepared, ionic liquid-free solution thermal denaturation sets on near 50 $^{o}$C and is essentially complete at 75 $^{o}$C, with a midpoint temperature of the transition ('melting temperature') of $T_m$ = 63.5 $^{o}$C.

Downloaded by STANFORD UNIV GREEN LIBR on June 28, 2012 | http://pubs.acs.org
Publication Date (Web): December 18, 2009 | doi: 10.1021/bk-2009-1030.ch007

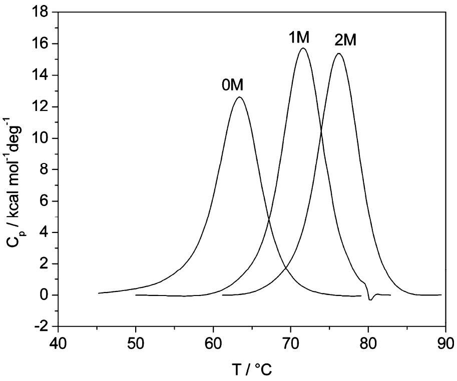

*Figure 1. Base line-corrected DSC profiles of RNase A (pH 7.0) in an ionic liquid-free solution and in 1 M and 2 M solutions of [chol][$H_2PO_4$], respectively.*

The DSC profile of the ionic liquid-free solution is symmetric and can be described by a two-state approximation. The two-state model assumes a transition reaction N ⇔ U without intermediates. For its physical foundations we refer to a review by Chan *et al.* *(28)*. For RNase A the adequacy of the two-state approach is well established *(25)*. Upon addition of [chol][$H_2PO_4$], the symmetric shape of the DSC profile is retained, but the denaturation transition is displaced to higher temperatures, thus indicating the thermal stabilisation of the native state of RNase A.

Figure 2 shows the dependence of the melting temperature $T_m$ on the [chol][$H_2PO_4$] concentration up to $C = 4$ M, above which the solubility of RNase A became too low for DSC experiments. At $C = 4$ M, the solvent conditions already resemble those in the neat ionic liquid *(6,7,29)*. $T_m$ is increased up to about 20 $^{o}$C relative to the ionic liquid-free solution. Similar effects were observed by us when adding [chol][$H_2PO_4$] to solutions of alcohol dehydrogenase and myoglobin. Fujita *et al.* reported an even larger stabilisation of cytochrome *c* by [chol][$H_2PO_4$] *(6,7)*.

The stabilising effect of [chol][$H_2PO_4$] contrasts to an enhanced unfolding induced by most aprotic ionic liquids, for example comprising 1,3-dialkylimidazolium, 1,1-dialkylpyrrolidinium and tetraalkylammonium ions *(10)*. Figure 2 illustrates this behaviour for 1-ethyl-3-methylimidazolium dicyanamide ([$C_2$mim][$N(CN)_2$]). This ionic liquid is liquid at room temperature, and is hydrophilic enough to be completely miscible with water, but again, the solubility of RNase A prevented experiments at ionic liquid concentrations above $C = 4$ M. $T_m$ decreases monotonously, displacing the denaturation transition at $C = 4$ M to room temperature. Density data *(30)* imply for anhydrous [$C_2$mim][$N(CN)_2$] $C = 5.98$ M. The tentative extrapolation to this concentration (Figure 2) predicts $T_m \cong 20$ $^{o}$C.

Downloaded by STANFORD UNIV GREEN LIBR on June 28, 2012 | http://pubs.acs.org
Publication Date (Web): December 18, 2009 | doi: 10.1021/bk-2009-1030.ch007

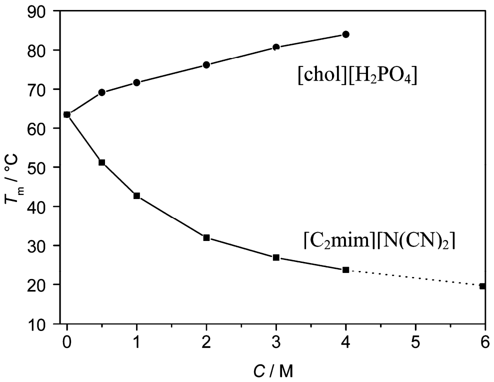

*Figure 2. Dependence of the melting temperature $T_m$ of RNase A (pH 7.0) on the concentration of added [chol][$H_2PO_4$] and [$C_2$mim][$N(CN)_2$]. The curve for [$C_2$mim][$N(CN)_2$] is tentatively extrapolated to the neat ionic liquid ($C$ = 5.98 M).*

Our observation contrasts with reports *(5,12-14)* on a surprisingly high thermal and functional stability of some proteins in neat aprotic ionic liquids similar to [$C_2$mim][$N(CN)_2$], where in part, protein functions were found to be retained well above 100 °C. A turnover to protein stabilisation in anhydrous [$C_2$mim][$N(CN)_2$] cannot be inferred from our data, and would imply a sharp break in the concentration dependence of $T_m$ above $C$ = 4 M. In anhydrous ionic liquids (or ionic liquids with little water) proteins are little soluble, and the reported effects may refer to dispersed states *(5)*, which renders comparison with our data meaningless.

## The Hofmeister Series

Salt effects on properties of biomolecular solutes often obey the Hofmeister ion series *(15-20)*. It is therefore apt to systematise our observations by ranking the cations and anions in the Hofmeister series. Usually, ion series reported in the literature are limited to inorganic salts. An exception is the work by von Hippel and Wong *(16,17)* on effects of guanidinium and tetraalkylammonium salts on the thermal stability of RNase A *(17)* and of other native biomolecules as diverse as collagen, DNA and myosin *(16)*. We have recently extended their work by considering Hofmeister effects on the melting temperature of RNase A induced by some major cations and anions of ionic liquids *(10)*. Figure 3 shows our results for chlorides combined with $Li^+$, $Na^+$, choline, 1-ethyl-3-methylimidazolium ([$C_2$mim]$^+$), 1-butyl-3-methylimidazolium ([$C_4$mim]$^+$) and guanidinium ([gua]$^+$), respectively.

Downloaded by STANFORD UNIV GREEN LIBR on June 28, 2012 | http://pubs.acs.org
Publication Date (Web): December 18, 2009 | doi: 10.1021/bk-2009-1030.ch007

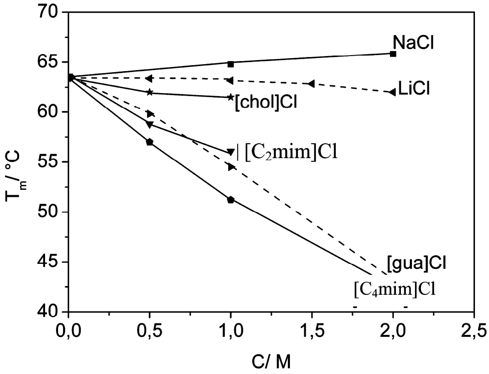

*Figure 3. Melting temperatures $T_m$ of RNase A (pH 7.0) as a function of the concentration of added ionic liquids with $Cl^-$ as a common anion.*

From the salts shown in Figure 3 only NaCl exerts a stabilising effect. The organic chlorides act as denaturating agents. Note that [chol]Cl destabilises RNase A, so that the stabilisation by [chol][$H_2PO_4$] reported above must result from the [$H_2PO_4$]$^-$ anion, perhaps in conjunction with cation–anion synergetic effects. Results for other ion families are documented in reference *(10)*.

The concentration dependence of $T_m$ may be nonlinear, and adjacent curves may intersect at high concentrations. A well-defined ion ranking has to resort to the limiting slope of the concentration dependence of $T_m$. A comprehensive survey of our data for RNase A *(10)* in conjunction with data reported by von Hippel and Wong *(17)* yields the cation series

$$Cs^+ > Rb^+ > K^+ > Na^+ \approx [NMe_4]^+ > Li^+ > [chol]^+ > [NEt_4]^+ \approx [C_2mim]^+$$
$$\approx [gua]^+ > [C_4mpyr]^+ > [C_4mim]^+ \approx [NPr_4]^+ > [C_6mim]^+ \approx [NBu_4]^+.$$

where [$C_6$mim]$^+$ stands for 1-hexyl-3-methylimidazolium, [$C_4$mpyr]$^+$ for 1-butyl-1-methylpyrrolidinium, and [$NR_4$]$^+$ for tetrahedral tetraalkylammonium ions with methyl (Me), ethyl (Et), propyl (Pr), and butyl (Bu) residues. The stronger the hydrophobicity of the cation, the stronger is the thermal destabilisation. Protein denaturation studies often resort to guanidinium salts such as [gua]Cl or [gua][SCN] as denaturating agents *(31)*, but among the hydrophobic cations considered [gua]$^+$ adopts only an intermediate position.

For the most widely used anions of ionic liquids, the Hofmeister series reads

$$[SO_4]^{2-} > [H_2PO_4]^- > [O_2CMe]^- > Cl^- > [EtOSO_3]^- > [BF_4]^- \approx Br^-$$
$$> [OTf]^- > [SCN]^- \approx [N(CN)_2]^- >> [NTf_2]^-$$

where [$O_2$CMe]$^-$ stands for ethanoate, [OTf]$^-$ for trifluoromethylsulfonate, [$EtOSO_3$]$^-$ for ethylsulfate, and [$NTf_2$]$^-$ for bis(trifluoromethylsulfonyl)amide. Because most anions are not interrelated by homologous series, the interpretation of the Hofmeister anion series is not straightforward, but it seems that weakly hydrated and hydrophobic anions exert a destabilising effect.

Downloaded by STANFORD UNIV GREEN LIBR on June 28, 2012 | http://pubs.acs.org
Publication Date (Web): December 18, 2009 | doi: 10.1021/bk-2009-1030.ch007

Reported Hofmeister anion series usually quote $[SCN]^-$ as the most destabilising anion. However, among the widely used anions of ionic liquids, $[N(CN)_2]^-$ is a similarly strong denaturant as $[SCN]^-$, and the destabilising effect of hydrophobic $[NTf_2]^-$ is even larger.

The interpretation of Hofmeister effects at the molecular level is complex, and it is unlikely that the observations can be rationalised by a single or a few molecular properties. Traditional explanations use the concept of kosmotropic (structure-making) and chaotropic (structure-breaking) ions, which differently affect protein hydration *(18,19,32)*. Even for simple ions there is, however, little consensus on what these properties actually entail *(21)*. It is therefore not surprising that the extension to more complex ions is difficult to rationalise in terms of the chaotrope/kosmotrope terminology. Even without a detailed molecular understanding, such ion series seem, however, sufficiently general to provide a valuable phenomenological guide for assessing salt effects on enzyme stability *(16,18)* and enzymatic functions *(11,18,19)*.

It is important to recall that our rankings rely on the limiting slopes of $T_m$, whereas many applications resort to ionic liquid-rich solutions. However, in the cases studied here, $T_m$ behaves monotonously, and intersections of adjacent curves are rare. Thus, the quoted series may also form a qualitative guide for assessing the behaviour of concentrated ionic liquids. Extrapolation to neat ionic liquids is, however, difficult.

Downloaded by STANFORD UNIV GREEN LIBR on June 28, 2012 | http://pubs.acs.org
Publication Date (Web): December 18, 2009 | doi: 10.1021/bk-2009-1030.ch007

## Irreversible Protein Deactivation

Refolding of the protein to the native state is often not complete. Whereas the denaturation equilibrium itself is reversible, additional processes may cause an irreversible loss of the enzymatic function. Depending on sample-specific conditions such as the pH and experimental conditions such as the incubation time at high temperatures, the irreversible deactivation can be founded in a variety of processes. Zale and Klibanov *(27)* have shown that in RNase A the most important processes are the hydrolysis of amide side chain functions at the aspartic residues, disulfide interchange and the formation of incorrectly folded and kinetically trapped structures. Note that the amyloidal aggregation of incorrectly folded proteins is a well-known phenomenon with regard to some pathological diseases such as Alzheimer's disease *(33)*.

For RNase A the pathways for irreversible deactivation *(27)* depend on the properties of the sample, such as protein concentration, buffer and pH. In addition, pathways for deactivation depend on conditions imposed by the experiments such as the scan rate and maximum temperature of the DSC scan and the conditions imposed by cooling. Rather than considering these details of the deactivation process, we focus here on the effect induced by added ionic liquids.

In the DSC profile deactivation reveals itself by a decrease of the area under the endothermic DSC peak. This area reflects the enthalpy of unfolding, $\Delta_u H$, which is proportional to the number of proteins participating in the denaturation equilibrium. In repeated DSC cycles, the number of deactivated molecules will accumulate.

Figure 4 shows as a typical example the DSC profile of RNase A at pH 5.5 in the third DSC cycle (maximum temperature 110 °C, scan rate 60 K $h^{-1}$ after shock-freezing to −80 °C). Under these conditions the behaviour is no more two-state. The endothermic peak shows a low-temperature shoulder, which indicates that some fraction of RNase A undergoes a reversible reaction to a less stable form. This second form may be a misfolded structure or a reversibly unfolding aggregate. Compared to the initial scan, the area under the total endothermic DSC peak is largely reduced, indicating a large fraction of deactivated RNase A. In addition, there is a strong peak above 100 °C due to an exothermic reaction. While these phenomena have not yet been explored by us in detail, in the present context the main observation is the ability of ionic liquids to drastically affect these phenomena. As an example, we show in Figure 4 the DSC of a 1 M solution of [chol][$H_2PO_4$], all other conditions being identical to those imposed to the ionic liquid-free solution. Addition of [chol][$H_2PO_4$] suppresses the exothermic peak, and increases the fraction of properly refolded RNase A.

For further illustration we consider in Figure 5 the denaturation of RNase A at pH 5.5 and 7.0 at milder conditions than in Figure 4. The upper temperature of the DSC scan was set to 90 °C. Cooling was performed to room temperature. At pH 5.5 unfolding is now largely reversible. The area of the second scan differs by less than 10% from that in the initial scan. Addition of [chol][$H_2PO_4$] leaves the profiles unaffected (not shown). If the pH is increased to 7.0, denaturation is almost irreversible. The area in the second scan (dashed line) is less than 5% of that in the initial scan (solid line). [chol][$H_2PO_4$] restores, however, the reversibility. The thermal stabilisation of RNase A by [chol][$H_2PO_4$] is accompanied by a drastic increase in reversibility of the denaturation process.

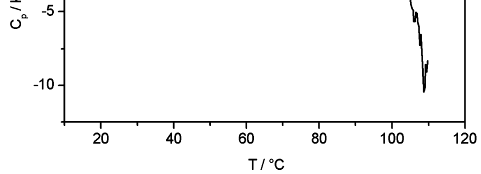

*Figure 4. DSC profiles of the third DSC cycle of RNase A (pH 5.5) in the ionic liquid-free solution and with 1 M [chol][$H_2PO_4$].*

Downloaded by STANFORD UNIV GREEN LIBR on June 28, 2012 | http://pubs.acs.org
Publication Date (Web): December 18, 2009 | doi: 10.1021/bk-2009-1030.ch007

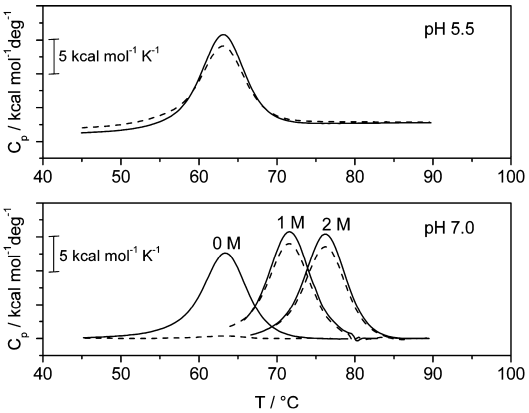

*Figure 5. DSC profiles of the initial scans (solid lines) and the first rescans (dashed lines) for RNase A in ionic liquid-free samples at pH 5.5 and 7.0, and in samples containing 1 M and 2 M [chol][$H_2PO_4$] at pH 7.0.*

To further study the effect of ionic liquids on enzyme stability, we have considered the development of the DSC profiles of RNase A (0.36 mM, 10 mM phosphate buffer, pH 5.5) in successive DSC scans to 110 °C after shock-freezing to −80 °C. Figure 6 shows the fraction of deactivated proteins deduced from the area of the endothermic peak for ionic liquid-free RNase A and for solutions of three prototypical ionic liquids at $C = 1$ M. The fraction of deactivated proteins largely increases in progressive scans. Addition of ionic liquids can suppress or enhance deactivation. It appears that some basic trends in the Hofmeister series are also relevant for protein deactivation. The thermal destabilisation of RNase A by [$C_4$mim]Cl is accompanied by an increase in the fraction of deactivated proteins. The weakly denaturating ionic liquid [chol]Cl slightly suppresses the deactivation of RNase A. The thermal stabilisation of proteins by [chol][$H_2PO_4$] is accompanied by strong suppression of protein deactivation.

Downloaded by STANFORD UNIV GREEN LIBR on June 28, 2012 | http://pubs.acs.org
Publication Date (Web): December 18, 2009 | doi: 10.1021/bk-2009-1030.ch007

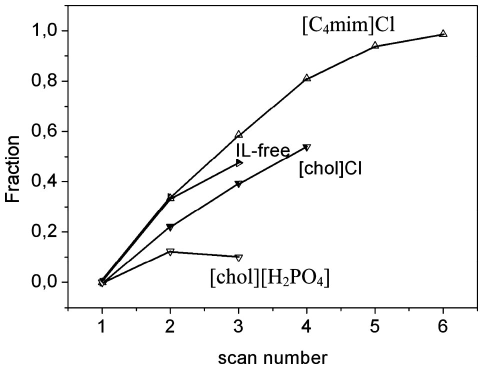

*Figure 6. Fraction of irreversibly deactivated RNase A (pH 5.5) after successive scans for the ionic liquid-free (IL-free) solution and with 1 M , [chol]Cl, and [$C_4$mim]Cl, respectively.*

Finally, we mention similar observations by us for myoglobin, insulin and yeast alcohol dehydrogenase (ADH) and by Byrne *et al. (9)* for hen egg white lysozyme. Figure 7 shows results for ADH (protein concentration 0.012 mM, 25 mM phosphate buffer, pH 7.6). ADH enables the biocatalytic transformation of alcohols to aldehydes and ketones. It aggregates at comparatively mild conditions, here already during the first DSC cycle (19). [chol][$H_2PO_4$] suppresses the exothermic peak and increases the fraction of properly refolded ADH.

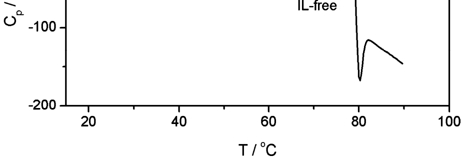

*Figure 7. DSC profiles of 0.012 mM yeast ADH (pH 7.6, 25 mM phosphate buffer) without ionic liquid and with 0.5 M [chol][$H_2PO_4$].*

Downloaded by STANFORD UNIV GREEN LIBR on June 28, 2012 | http://pubs.acs.org
Publication Date (Web): December 18, 2009 | doi: 10.1021/bk-2009-1030.ch007

## Conclusions

By creating a hydrophilic environment, some protic ionic liquids as co-solvents to water can lead to thermal stabilisation of proteins. By contrast, the most widely used hydrophobic ionic liquids exert a destabilising effect. In addition, ionic liquids may largely affect the irreversible deactivation of denaturated proteins induced at high temperatures. Carefully selected ionic liquids can suppress this deactivation. The factors controlling the effect of ionic liquids on protein deactivation seem to be intrinsically connected with those controlling the thermal stability of native proteins.

Downloaded by STANFORD UNIV GREEN LIBR on June 28, 2012 | http://pubs.acs.org
Publication Date (Web): December 18, 2009 | doi: 10.1021/bk-2009-1030.ch007

## References

1. *Ionic Liquids in Synthesis.* Wasserscheid, P.; Welton, T., Eds.; Wiley-VCH, Weinheim, **2008**, 2nd ed.
2. *Ionic Liquids IIIA: Fundamentals, Progress, Challenges, and Opportunities. Properties and Structure.* Rogers, R. D.; Seddon, K. R. Eds.; American Chemical Society: Washington, DC, **2005**.
3. *Ionic Liquids IIIB: Fundamentals, Progress, Challenges, and Opportunities. Transformations and Processes.* Rogers, R. D., Seddon, K. R. Eds.; American Chemical Society: Washington, DC, **2005**.
4. Kragl, U.; Eckstein, B.; Kaftzik, N. *Current Opinions Biotechn.* **2002**, 13, 565-571.
5. Van Rantwijk, F.; Sheldon, R. A. *Chem. Rev.* **2007**, *107*, 2757-2785.
6. Fujita, K.; MacFarlane, D. R.; Forsyth, M. *Chem. Comm.* **2005**, 4804-4806.
7. Fujita, K.; MacFarlane, D. R.; Forsyth, M.; Yoshizawa-Fujita, M.; Murata, K.; Nakamura, N.; Ohno, H. *Biomacromolecules* **2007**, *8*, 2080-2086.
8. Byrne, N.; Angell, C. A. *J. Mol. Biol.* **2008**, *378*, 707-714.
9. Byrne, N.; Wang, L.-M.; Belieres, J.-P.; Angell, C. A. *Chem. Comm.* **2007**, 2714-2716.
10. Constantinescu, D.; Hermann, C.; Weingärtner, H. *Angew. Chem. Int. Ed.* **2007**, *46*, 8887-8889.
11. Zhao, H. J. *Chem. Technol. Biotechnol.* **2006**, *81*, 877-891.
12. Ohno, H.; Suzki, C.; Fukumoto, K.; Yoshizawa, M.; Fujita, K. *Chem. Lett.*, **2003**, 450-451.
13. Baker, N.; McCleskey, T. M.; Pandey S.; Baker, G. A. *Chem. Commun.*, **2004**, 940-941.
14. Fujita, K.; MacFarlane, D. R.; Forsyth, M. *Chem. Comm.* **2005**, 4804-4806.
15. Hofmeister, F. *Arch. Exp. Patol. Pharmakol.* **1888**, *64*, 247-260.
16. Von Hippel, P. H.; Wong, K.-Y. *Science* **1964**, *145*, 577-580.
17. Von Hippel, P. H.; Wong, K.-Y. *J. Biomol. Chem.* **1965**, *240*, 3909-3923.
18. Collins, K. D.; Washabaugh, M. W. *Quart. Rev. Biophys.* **1985**, *18*, 323-422.
19. Broering, J. M.; Bommarius, A. S. *J. Phys. Chem. B* **2005**, *109*, 20612-20619.
20. Kunz, W.; Lo Nostro, P.; Ninham, B. W. *Curr. Opinion Coll. Interface Sci.* **2004**, *9*, 48-52.

21. Ball, P. *Chem. Rev.* **2008**, *108*, 74-108.
22. Greaves T.L.; Drummond, C. J. *Chem. Rev.* **2008**, *108*, 206-237.
23. Belieres, J.-P.; Angell, C. A. *J. Phys. Chem. B* **2007**, *111*, 4926-4937.
24. Lumry, R.; Eyring, H. *J. Phys. Chem.* **1954**, *58*, 110-120.
25. Privalov, P. L.; Khechinashvili, N. N. *J. Mol. Biol.* **1974**, *86*, 665-684.
26. Navon, A.; Ittah, V.; Laity, J. H.; Scheraga, H. A.; Haas, E.; Gussakovsky, E. E. *Biochemistry*, **2001**, *40*, 93-104.
27. Zale, S. E.; Klibanov, A. M. *Biochemistry*, **1986**, *25*, 5432-5444.
28. Chan H. S.; Bromberg, S.; Dill K. A. *Philos. Trans. Roy. Soc. B*, **1995**, *348*, 61-70.
29. M.-M. Huang, M.-M.; Weingärtner, H. *ChemPhysChem* **2008**, *9*, 2172-2173.
30. MacFarlane, D. R.; Golding, J.; Forsyth, S.; Forsyth, M.; Deacon, G. B. *Chem. Comm.* **2001**, 1430-1431.
31. Lapange, S. *Physicochemical Aspects of Protein Denaturation*. Wiley, New York, **1978**.
32. Baldwin, R. L. *Biophys. J.* **1996**, *71*, 2056-2063.
33. Serpell, L. C. *Biochim. Biophys. Acta* **2000**, *1502*, 16-30.

Downloaded by STANFORD UNIV GREEN LIBR on June 28, 2012 | http://pubs.acs.org
Publication Date (Web): December 18, 2009 | doi: 10.1021/bk-2009-1030.ch007

Downloaded by UNIV OF GUELPH LIBRARY on June 28, 2012 | http://pubs.acs.org
Publication Date (Web): December 18, 2009 | doi: 10.1021/bk-2009-1030.ch008

## Chapter 8

# The Radiation Chemistry of Ionic Liquids and its Implications for their Use in Nuclear Fuel Processing

**James F. Wishart[1] and Ilya A. Shkrob[2]**

[1]**Chemistry Department, Brookhaven National Laboratory, Upton, NY 11973**
[2]**Chemistry Division, Argonne National Laboratory, 9700 S. Cass Ave, Argonne, IL 60439**

The use of ionic liquids as a medium for the processing of spent nuclear fuel, where their safety and process improvement advantages could be significant, promises to contribute substantially to the development of advanced nuclear fuel cycles to improve the world's energy posture. It is therefore important to study the radiation chemistry of ionic liquids, to determine their radiolytic products and degradation pathways, and to describe how the radiolysis may affect or interfere with separation processes. As it turns out, many of the important features of ionic liquid radiation chemistry can be traced back to unique aspects of their physical chemistry.

In recent years, growing concerns over the condition of the global climate and the increasing energy requirements of developing and developed nations have greatly spurred interest in non-carbon-based energy sources such as solar, wind, geothermal, wave, hydroelectric and nuclear power. Many of the renewable energy sources (to which biofuel production can be included) have promising upward trends in capacity that will need to be scaled up significantly to meet expected future demand, although their environmental impacts at those scales of operation need to be taken into account.

Nuclear power is already a major source of carbon-free energy in many countries. Like the carbon-based electricity sources oil, gas and coal, it provides a reliable base supply of power irrespective of environmental conditions, while

In Ionic Liquids: From Knowledge to Application; Plechkova, N., et al.;
ACS Symposium Series; American Chemical Society: Washington, DC, 2010.

renewables have diurnal or seasonal variations in availability, and are subject to constraints on geographic distribution that necessitate the development of new transmission infrastructures. Thus, nuclear power can play a unique role in replacing greenhouse gas-generating base supply sources. However, the installation of new nuclear power stations was generally curtailed worldwide in the 1980s in response to public concerns over safety and waste disposal. The gravity of the World's future energy situation, and the expectation that future transportation modalities based on batteries or hydrogen fuels will place extra demands on electrical power generation, have motivated policy makers in many countries, including some that had previously decided to exit from nuclear power generation, to plan the construction of a new generation of nuclear power plants with advanced designs to enhance safety and security.

Despite the renewed interest in building power stations, nuclear energy as it had been practiced in the past is simply not sustainable on a long-term basis because of limitations in the nuclear fuel and waste cycle as it exists today. The underlying problem is that currently most spent fuel from commercial power reactors is not recycled, but is intended instead for long-term geological storage (some countries are exceptions). At the production end, this means more environmental degradation from uranium mining to meet demand, and pessimistic estimates of the duration of uranium reserves (on the order of decades). At the disposal end, this places tremendous burdens on the capacity and technical performance of geological repositories, which present huge engineering and political challenges. As presently constituted, these repositories must be designed to sequester their contents for hundreds of thousands of years.

Downloaded by UNIV OF GUELPH LIBRARY on June 28, 2012 | http://pubs.acs.org
Publication Date (Web): December 18, 2009 | doi: 10.1021/bk-2009-1030.ch008

## A fresh approach

To overcome these problems, schemes for the detailed chemical separation of spent nuclear fuel into its components have been proposed under the rubric of the Advanced Fuel Cycle (AFC). The aim is to recover the fissile and fertile (capable of being converted to fissile) materials for conversion into recycled nuclear fuel, and to separate the accumulated fission products for conversion into permanent waste forms that are appropriate for their chemistry and radioactive characteristics. The benefits to the supply side of the cycle are that the rate of uranium mining could be reduced dramatically, and that the known reserves would last for hundreds of years. On the disposal side, the volume of waste would be reduced significantly and the transuranic elements (Np, Pu, Am, and Cm) that are primarily responsible for the long-term radioactivity of unprocessed spent nuclear fuel would be burned up in a second tier of fast neutron reactors instead of going to the repository. Thus, the useful capacity of the repository would be increased greatly and the period of radiological concern would be hundreds of years instead of hundreds of thousands. The closure of the nuclear fuel cycle, and the quantitative destruction of fissile $^{239}$Pu in the fast neutron reactor stage, would prevent the accumulation of material that could be converted to weapons, making the World safer now and in the future.

Research into detailed nuclear fuel reprocessing for the AFC has been ongoing in several countries for some time. Most of the proposed processing schemes involve liquid/liquid extraction steps, although electrochemical deposition from high-temperature molten salts ("pyroprocessing") is considered a potential alternative. Despite the substantial groundwork that has been laid, opportunities still abound at this time for process optimisation, or even the wholesale substitution of process steps with better performing ones, for example using neoteric solvents such as ionic liquids. It is therefore a potentially fruitful and rewarding field of study for chemists with a real opportunity to positively impact the World's energy posture.

## Ionic liquids for nuclear separations

The fundamentals of ionic liquids should be familiar to the readers of the book to which this chapter belongs, so they will not be repeated here. However, many properties of ionic liquids can be beneficial for nuclear fuel reprocessing. Their greatest asset is the flexibility granted by the practically infinite possible variations of anions, cations and functional groups that can be used to tune the physical, solubility/solvation, separations, and electrochemical properties of ionic liquids. In addition to boosting performance, this flexibility permits the selection of ionic liquids with process safety advantages relative to conventional solvents, such as low volatility and combustion resistance. Also, functional groups may be added to improve extraction efficiency and stabilise particular metal ion oxidation states *(1-4)*. Finally, the inherent conductivity of ionic liquids and the ability to control their electrochemical windows over a wide range enables the linkage of liquid/liquid separations with selective electrodeposition of particular elements in their metallic form, even for very electropositive metals such as caesium *(5)*. Direct electrodeposition from ionic liquid solution provides a valuable "back door" for the separations process, because it allows the optimisation of the forward aqueous-to-ionic-liquid extraction process without the need to balance it against the efficiency of the organic-to-aqueous back extraction step that usually follows in conventional extraction systems.

When working with fissile materials such as $^{233}$U, $^{235}$U and $^{239}$Pu, an enormous advantage in process safety can be gained by using ionic liquids containing boron or chlorine, because $^{10}$B (20% natural abundance) and $^{35}$Cl (76% natural abundance) have large thermal neutron capture cross sections that can effectively quench nuclear chain reactions and thereby prevent potentially dangerous criticality accidents such as the one that occurred in Tokai-mura, Japan in 1999 *(6)*. A group from Los Alamos National Laboratory *(7)* calculated that the ionic liquids 1-ethyl-3-methylimidazolium tetrachloroaluminate ($[C_2mim][AlCl_4]$) and $[C_2mim][BF_4]$ have minimum critical $^{239}$Pu concentrations (at infinite volume) that are 20 and 100 times larger, respectively, than in water. Although neither of these ionic liquids is stable enough for process use in contact with water because of anion hydrolysis, the principle still applies that boron and chlorine can be incorporated into other families of ionic liquids that would be used to make inherently criticality-safe processing systems that would be resistant to human error and design flaws.

Downloaded by UNIV OF GUELPH LIBRARY on June 28, 2012 | http://pubs.acs.org
Publication Date (Web): December 18, 2009 | doi: 10.1021/bk-2009-1030.ch008

## Progress in ionic liquid-based separations schemes for nuclear applications

As mentioned above, conventional nuclear separations schemes employ liquid/liquid extraction and reverse extraction stages, often modulated by control of pH, using immiscible combinations of aqueous solutions and hydrocarbon solvents with added extractants such as tributylphosphate (TBP), octyl(phenyl)-*N,N*-diisobutylcarbamoylmethyl phosphine oxide (CMPO) or dicyclohexano-18-crown-6 (DCH18C6), that complex specific metal ions to increase their partition into the organic phase.

In separation schemes, ionic liquids can substitute for either the aqueous or the organic phase; however, since the standard spent fuel recycling process begins with the dissolution of zirconium-clad uranium oxide fuel rod pieces in concentrated aqueous nitric acid solution, all work to date has focussed on ionic liquids as replacements for the hydrocarbons. Near the end of this chapter, it will be explained why this substitution can have beneficial effects on the radiation stability of an extraction system, in addition to any separation performance benefits that may result. Space does not permit a detailed recitation of the growing amount of work in the separations of actinides and fission products using ionic liquids. Gutowski *et al. (8)* and Stepinski *et al. (9)* have provided general overviews of the subject. Binnemans *(10)* and Cocalia *et al. (11)* have written reviews of the chemistry of actinides and lanthanides in ionic liquids, including studies relevant to spent fuel reprocessing. To summarise, ionic liquids containing extractant solutes *(12-15)* or extractive functional groups *(3,4)* have been shown to be effective at extraction of uranium complexes from aqueous solutions. Likewise, extractions of fission products, such as selected lanthanides *(14,16,17)* and strontium *(17,18)*, have also been demonstrated.

Extractions of ionic metal complexes into organic solvents occur through the transfer of neutral ion pairs or complexes from the aqueous solution. This mechanism also works in the case of ionic liquids, however a second mechanism involving exchange of the constituent ions of the ionic liquid for a metal complex of like charge may operate as well *(16,17,19)*. Although the recognition of this complication had a mildly sobering effect on expectations for ionic liquid-based separations, it was soon proven that the balance between the two mechanisms could be controlled and even exploited. Increasing the hydrophobicity of ionic liquid cations can convert a cation exchange mechanism to neutral complex extraction *(20)*. Increasing the concentration of nitrate ion in the aqueous phase can have a similar effect *(21)*. Selectivity for strontium ion partition *via* ion exchange depends on the solubility of the ionic liquid in the aqueous phase; increasing the hydrophobicity of the anion promotes cation exchange and strontium extraction selectivity over potassium *(22)*.

The progress to date, while still preliminary, has shown that ionic liquids remain a viable and perhaps transformative alternative medium for spent nuclear fuel processing under the detailed separations schemes required by the advanced fuel cycle concept. However, the history of nuclear separations processing worldwide is littered with examples of systems that worked well with non-radioactive simulants, but failed to perform or caused even bigger headaches when exposed to a real-world radioactive system. Therefore, it is essential to

Downloaded by UNIV OF GUELPH LIBRARY on June 28, 2012 | http://pubs.acs.org
Publication Date (Web): December 18, 2009 | doi: 10.1021/bk-2009-1030.ch008

understand how radiation affects ionic liquids and what effects it may have on separations processes in ionic liquids. In the following sections, it will be attempted to link the radiolytic processes that occur on the earliest time scales with intermediate reaction chemistry and ultimately attempt to rationalise product distributions observed by bulk radiolysis studies of ionic liquids.

## Ionic Liquid Radiation Chemistry

### Radiation-induced reactivity on early time scales *(23,24)*

Radiation chemistry is the study of the products formed and the chemical reactions induced when ionising radiation interacts with matter *(25-28)*. It should be distinguished from radiochemistry, which is the chemistry of radioactive materials, although both areas are essential for success in designing nuclear separations processes. High-energy photons (X-rays or gamma rays) and energetic subatomic particles (electrons, alpha particles, neutrons, *etc.*) are classified as ionising radiation because they transfer energy to materials through interactions that cause electrons to be ejected from molecules within the medium they traverse, thereby producing ions if the starting medium is neutral. The immediate products of ionisation are electrons with excess kinetic energy and "holes" (the atoms or molecules from which the electron was ejected, Figure 1). The electrons lose their excess energy through collisions with the medium until they become "thermalised" and come to rest at a distribution of distances from the holes they originated from. Many interactions between the incident radiation and the medium impart less energy than required for ionisation; in those cases the molecules may be placed in highly excited states that also result in chemistry (*vide infra*).

Downloaded by UNIV OF GUELPH LIBRARY on June 28, 2012 | http://pubs.acs.org
Publication Date (Web): December 18, 2009 | doi: 10.1021/bk-2009-1030.ch008

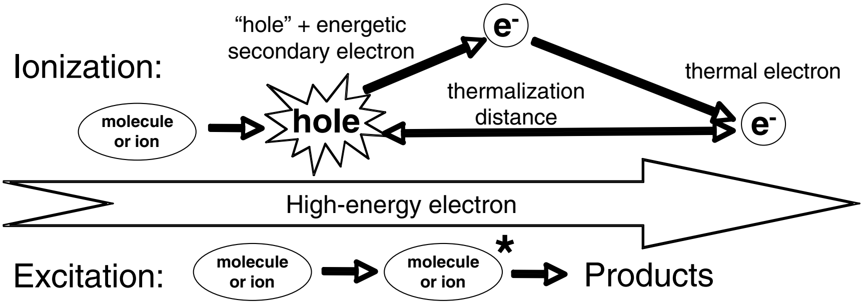

*Figure 1. Initial processes induced in materials by ionising radiation.*

When the "thermal" electrons come to rest, they may localise in pre-formed electrostatic traps of varying depth, but they are yet not in equilibrium with their environment, or "solvated". During the solvation process, the surrounding medium rearranges to adjust to the presence of an excess negative charge (wavy arrows in Figure 2).

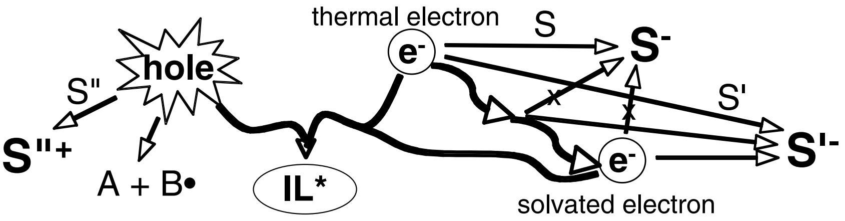

*Figure 2. Early chemical events in the radiolysis of ionic liquids. S, S' and S'' are scavengers of electrons or holes. A and B• are fragments from bond breakage of the hole transient species. X indicates no reaction.*

In normal liquids, such as water or organic solvents, this process is complete within a few picoseconds; however, the higher viscosity of ionic liquids makes the overall solvation process hundreds or thousands of times slower *(29-32)*. This difference may have significant consequences for nuclear fuel process chemistry in radiation environments. Incompletely solvated ("pre-solvated" or "dry") electrons may persist on time scales up to tens of nanoseconds in ionic liquids *(33,34)*. They are more mobile than solvated ones because they are less deeply trapped, and they exist at higher chemical potentials. Therefore, they may react more rapidly with solutes in general, they may have the energy to react with certain solutes that are unreactive with fully solvated electrons (S *vs.* S' in Figure 2), and they may even be less reactive than solvated electrons with some substrates. In some cases S or S' may be a constituent of the ionic liquid itself, such as imidazolium or pyridinium cations. In these situations, electron capture is quantitative and radical reactions dominate the chemistry *(35-38)*, as described in a later section.

Both aspects of pre-solvated electron reactivity manifest themselves to a much greater degree in ionic liquids than in conventional solvents because the pre-solvated electron lifetimes are much longer in the case of ionic liquids. In a processing solution containing moderate amounts of reagents and metal ions, this can result in new products and altered product distributions that could not have been predicted from the chemistry of the solvated electron alone. Direct evidence for pre-solvated electron scavenging in aliphatic-cation ionic liquids by aromatic hydrocarbons *(33,39,40)*, imidazolium cations *(41,42)*, and bis(oxalato)borate anions *(43)* has been reported in the literature. It was necessary to account for the contribution from pre-solvated electron scavenging to explain the yields of hydrogen-atom adducts of aromatic hydrocarbons in acidified ionic liquid solution *(44)*. In lower-viscosity ionic liquids, the efficiency of pre-solvated electron scavenging is reduced because of increased competition from the electron solvation process. It is possible in some circumstances to observe the solvation process directly through the blue shift of the electron absorption spectrum using ultrafast accelerator facilities *(45,46)*. In other cases, where that is not possible, the electron solvation lifetime can be estimated from the solvation dynamics of solvatochromic dye molecules in the same ionic liquids because of the similarity between the two processes *(47)*.

Downloaded by UNIV OF GUELPH LIBRARY on June 28, 2012 | http://pubs.acs.org
Publication Date (Web): December 18, 2009 | doi: 10.1021/bk-2009-1030.ch008

Downloaded by UNIV OF GUELPH LIBRARY on June 28, 2012 | http://pubs.acs.org
Publication Date (Web): December 18, 2009 | doi: 10.1021/bk-2009-1030.ch008

Returning to Figure 2, another important observation from time-resolved radiolysis studies is that apparently diffusion-controlled reaction rates of the solvated electron ($e^-_{solv}$) with scavengers (S') in ionic liquids tend to be significantly slower (~2-8 x $10^8$ $M^{-1}$ $s^{-1}$) *(33,39-42)* than in conventional solvents, by a couple orders of magnitude versus water (~5 x $10^{10}$ $M^{-1}$ $s^{-1}$), for example. In contrast, the hydrogen atom reacts with aromatic hydrocarbons at approximately the same rate in ionic liquids as in water or alcohols (~3 x $10^9$ $M^{-1}$ $s^{-1}$) and ten times faster than the $e^-_{solv}$ reaction for the same ionic liquid and substrate *(44)*. These findings are consistent with charge- and ionic liquid-viscosity-dependent diffusion rates of $O_2$ and $[O_2]^-$ inferred from electrochemical measurements *(48)*. Despite the fact that the electron is a quantum particle, it is trapped within its solvation sphere, and its diffusion is subject to the slower dynamics of the ionic liquid environment. In designing separations systems and extractants for spent fuel processing in ionic liquids, it is important to take the anomalous reactivities of *both* the solvated and pre-solvated electrons into account.

Returning again to Figure 2, the electron in any state of solvation may also react with the hole, or one of its successors such as $S''^{+}$. In such cases it is possible that the radiolytic energy deposited as an ionisation event is ultimately dissipated as heat without nett chemical effect. However, recombination of holes and electrons can lead to excited states that may be reactive as well, such as the case of the $[NTf_2]^-$ anion described in the next section. The probability of recombination is increased by the high mobilities of pre-solvated electron states that are more persistent in ionic liquids. This may help to explain the quantitative and qualitative observations of radiation resistance attributed to ionic liquids in bulk radiolysis product studies *(49-52)*. Despite the attributed radiation resistance, decomposition products do accumulate with dose, particularly in ionic liquids with aromatic cations. Detailed electrospray-mass spectrometry studies of ionic liquid radiolysis products, by the group of Moisy at CEA Marcoule, have revealed evidence of numerous radiation-induced radical reactions *(50,51)*. Unfortunately, the time-resolved transient absorption radiolysis techniques, that work so well for following fast reactions of electrons in ionic liquids, do not work well to detect most organic radicals because they absorb in the UV where there is often considerable interference from absorption bands of the ionic liquid itself, or impurities, or radiolysis products. Fortunately, EPR spectroscopy is a structure-sensitive detection technique well-suited for elucidation of the radical chemistry of ionic liquid radiolysis.

## The unseen chemistry of radicals in irradiated ionic liquids revealed by Electron Paramagnetic Resonance (EPR)

In the course of radiolysis, superexcited molecules generated *via* electron-molecule scattering, and having the excess energies of 10-20 eV, ionise yielding primary charges: the electrons and electron deficiencies (holes). In ionic liquids, the ions forming the ionic liquid serve as deep Coulomb traps for these charges: the electrons are trapped by the cations ($C^+$) and/or anion vacancies ($V^+$), and the holes are trapped by the anions ($A^-$) and/or cation vacancies ($V^-$). Such a

Downloaded by UNIV OF GUELPH LIBRARY on June 28, 2012 | http://pubs.acs.org
Publication Date (Web): December 18, 2009 | doi: 10.1021/bk-2009-1030.ch008

situation is also typical for ionic crystals that serve as reference systems; another reference system is organic solvents. The charges trapped by the ions are *neutral radicals* and the charges trapped by the vacancies are *radical ions* (including the solvated electrons that were described in the previous sections). Given that many of these radicals do not exhibit strong absorption bands in their optical spectra, EPR is a complementary method of choice for studying the structure and reactions of these reactive intermediates. The structural information is extracted from the pattern of hyperfine coupling constants (hfcc) for magnetic nuclei, such as $^1$H, $^{14}$N, $^{31}$P, and $^{11}$B; the observed patterns can be compared with the hfcc parameters calculated using quantum chemistry methods, such as density functional theory (DFT). The approach takes advantage of this interplay between the theoretical and experimental methods to gain structural and mechanistic insight.

EPR studies indicate that the radicals are generated through multiple chemical routes. One of these is neutralisation of the ions. For example, the irradiation of bistriflamide, $[NTf_2]^-$, ionic liquids yields an *N*-centred radical obtained *via* neutralisation of this anion by a hole. However, this mode of hole-trapping appears to be more of an exception than the rule. This has a well-known precedent in crystalline alkali halides, where the holes are trapped as $V_K$ centres (dimeric $[X_2]^{-\bullet}$ ions) rather than halogen atoms: the $X^\bullet$ atom forms a three-electron $(\sigma)^2(\sigma^*)^1$ bond with a nearby $X^-$ anion at a $V^+$ site. The tendency to form such dimers is also present in the ionic liquids, and the $[X_2]^{-\bullet}$ ions have been observed in photolysed and radiolysed halide anion ionic liquids *(53-55)* through their strong $\sigma \leftarrow \sigma^*$ absorption band in the visible part of the spectrum. For large ionic liquid anions such as $[NTf_2]^-$, this binding is sterically hindered, but for smaller anions such as dicyanamide it is very facile and results in the formation of dimeric radical anions *(56)*.

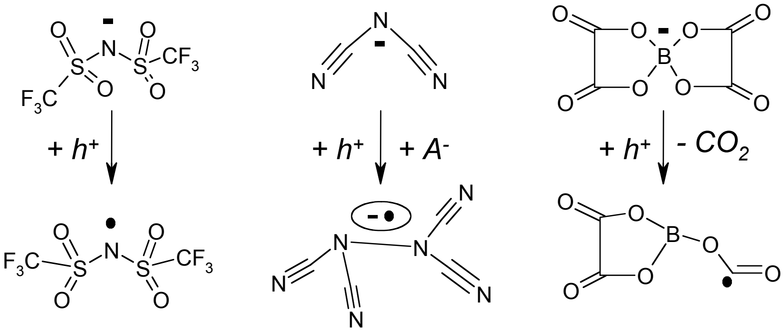

The neutral radicals generated by the neutralisation of the parent anion can be unstable. An important example of this kind is bis(oxalato)borate, $[BOB]^-$, ionic liquids. Such liquids are attractive solvents for plutonium processing, due to the presence of $^{10}$B, which has high neutron cross section and, thus, reduces the criticality risks *(7)*. Irradiation of these ionic liquids leads to evolution of $CO_2$. EPR spectra suggest that the gas is evolved *via* decarboxylation of the $[BOB]^\bullet$ radical, generated by neutralisation of $[BOB]^-$: the B-O bond dissociates and the tetrahedral boron becomes trigonal in the resulting $[(C_2O_4)B(OC\bullet{=}O)]$ radical *(56)*. Thus, the stability of the radicals is a significant factor for durability of the ionic liquids in high radiation fields.

The stability of the excited states of the ions and radicals is also important. For example, radiolysis of $[NTf_2]^-$ ionic liquids yields $[CF_3]^\bullet$ radicals that are readily observed by EPR *(56)*. The yield of these trifluoromethyl radicals is only 5% of the $[NTf_2]^\bullet$ radicals, but these trifluoromethyl radicals are small, diffusive, and very reactive. Product analyses suggest that these radicals are critically involved in the radiolytic degradation of ionic liquids *(50,51)*. Since the $[NTf_2]^\bullet$ radical is relatively stable, the S-C bond fragmentation can only occur in the excited radical (which gains excess electronic energy in the highly exothermic electron attachment) or the excited state of the anion. Thus, not only ground states of the anions and radicals are important chemically, but also their excited states. The same is suggested by “dry” electron reactions in the ionic liquids composed of ammonium cations *(33,40-42,44)*: the excess energy possessed by the electron before it is fully solvated and relaxed makes this species much more reactive than the corresponding relaxed electron, and so it accounts for the high yield of electron attachment reactions occurring in these ionic liquids.

Similarly to the anions, the cations also exhibit a multiplicity of reaction paths. It was found that the ionic liquids composed of aliphatic cations (such as ammonium and phosphonium) show different chemistry than the ionic liquids composed of aromatic cations (such as imidazolium), as the latter have π−systems accessible to the electrons *(35-37)*. Consequently, the aromatic cations are efficient electron acceptors, whereas the aliphatic cations trap electrons electrostatically, at anion vacancy sites *(23,33)*. As the electron pathway is blocked, the radiolytic degradation of these aliphatic cations occurs *via* the hole pathway. Specifically, EPR spectroscopy indicates that the aliphatic cations yield *C*-centred radical cations, $[C(\text{-}H)]^{+\bullet}$, generated by deprotonation of terminal methyl and penultimate methylene groups in the aliphatic chains *(56)*. This site specificity has been previously observed in deprotonation of radical cations of alkanes, as the loss of the proton occurs at the site of maximum spin density. By this analogy, the formation of the *C*-centred radicals should also involve a trapped hole, *i.e.* the radical dication, $[C]^{2+\bullet}$, generated by the ionisation of the parent cation. DFT calculations indicate that, in this radical dication, the sites of the maximum spin density are indeed in the terminal and penultimate hydrogen atoms of the extended aliphatic chains *(56)*. This is easily understood, as the excess positive charge is repelled by the positive charge at the heteroatom (N or P). The proximity of the proton acceptor (the anion) to the chain termini also contributes to the observed selectivity of the proton transfer. The same proximity, however, also facilitates charge transfer from the radical dication, so there is a competition:

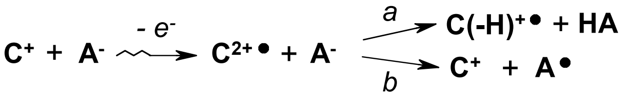

$$C^+ + A^- \xrightarrow{-\,e^-} C^{2+\bullet} + A^- \begin{array}{l} \xrightarrow{a} C(\text{-H})^{+\bullet} + HA \\ \xrightarrow[b]{} C^+ + A^\bullet \end{array}$$

Downloaded by UNIV OF GUELPH LIBRARY on June 28, 2012 | http://pubs.acs.org
Publication Date (Web): December 18, 2009 | doi: 10.1021/bk-2009-1030.ch008

Downloaded by UNIV OF GUELPH LIBRARY on June 28, 2012 | http://pubs.acs.org
Publication Date (Web): December 18, 2009 | doi: 10.1021/bk-2009-1030.ch008

EPR spectroscopy suggests that for aliphatic cations, the yield of the deprotonation and charge transfer (as suggested by the relative yields of the deprotonated radical cation, $[C(-H)]^{+\bullet}$, and the neutral radical, $A^{\bullet}$) are comparable, *i.e.* both reaction pathways are equally rapid *(56)*. By contrast, no *C*-centred radicals are observed for aromatic cations, suggesting that either the charge transfer is much faster than the deprotonation or that deprotonation does not occur. The latter seems very likely, as DFT calculations indicate that the excess positive charge and the spin density in the corresponding radical dication are spread over the π−system of the imidazole ring. As a result, the EPR spectra of irradiated aliphatic ionic liquids are dominated by the resonance signals from $[C(-H)]^{+\bullet}$ and $A^{\bullet}$ (or, alternatively, $[A_2]^{-\bullet}$) that account for 95+% of all paramagnetic species generated in radiolysis and laser photoionisation *(56)*. For irradiated aromatic ionic liquids, the EPR spectrum is dominated by $A^{\bullet}$ radicals and another species that was originally attributed to a neutral radical derived from the parent cation as it traps the electron ($C^{\bullet}$). However, this attribution poorly corresponds to the observed properties of the species. In this radical, the imidazole ring undergoes Jahn-Teller distortion *(57)* so that the radical becomes a σ-radical with the pyramidal C(2) atom. Such σ-radicals do not absorb in the visible and the radical would also have large hfcc at the C(2)-H proton, due to the spin bond polarisation. This large hfcc is not observed in the EPR spectra *(56)*, and the species that is formed by photoexcitation of imidazolium halide ionic liquids absorbs in the near infrared (NIR) *(58)*. DFT calculations suggest that both of these observations can be rationalised by assuming that the radical and its parent form a three-electron bond $(\sigma)^2(\sigma^*)^1$ between their C(2) carbons *(57)*.

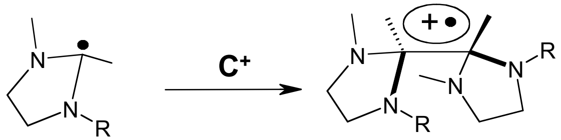

$C^{\bullet}$ $C_2^{+\bullet}$

The spreading of the spin density naturally accounts for reduced hfccs at the protons and $^{14}N$ nuclei, explaining the observed EPR spectra, and the σ←σ* transition accounts for the low energy absorption bands. These observations point to the general tendency of the ionised ionic liquids to stabilise the excess positive and negative charges, not only through the production of neutral radicals, but also through the formation of radical ions, either *via* deprotonation of the parent cations or sharing of the excess charge between the ions through three electron σσ* bonding. The formation of solvated electrons in aliphatic cation ionic liquids *(33,34,40-42)* can also be viewed as the manifestation of *collective stabilisation of the excess charge* by anion vacancies, $V^+$. Importantly, the $[A_2]^{-\bullet}$ and $[C_2]^{+\bullet}$ dimer radical ions can also be viewed as examples of the stabilisation of the excess charge by cation and anion vacancies, respectively.

Downloaded by UNIV OF GUELPH LIBRARY on June 28, 2012 | http://pubs.acs.org
Publication Date (Web): December 18, 2009 | doi: 10.1021/bk-2009-1030.ch008

The fact that the ionic liquid ions have relatively low ionisation potentials and high electron affinities accounts for their properties as "antirads" *(56)*. This is relevant to potential applications of the ionic liquids for processing of spent nuclear fuel, including the main [P]UREX process in which dioxouranium(VI) nitrate is extracted by tributylphosphate (TBP) into dodecane *(59-61)*. Since the ionisation potential and the excitation energy for the alkanes are higher than the ionisation potential and the excitation energy for the TBP, the damage is channelled from the solvent to the solute, and so the radiolytic damage of TBP is very efficient, occurring mainly *via* electron attachment followed by dealkylation of TBP *(56,62)*.

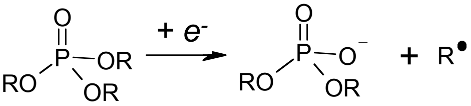

The resulting dibutylphosphate extracts Zr-Nb fission products from the aqueous raffinate into the organic phase, thereby contaminating this phase and necessitating costly scrubbing of the acidic product and recycling of TBP. In contrast, irradiation of $(MeO)_3PO$ in several ionic liquids produced a very low yield of methyl radicals, even at high irradiation exposure and loading of the solute (20-40%). This is due to the reversal of the excitation and charge flow in these solutions (from solute to the solvent) and efficient trapping of electrons and holes by the ionic liquid solvent *(56)*.

## A sketch of the early events in radiation damage of ionic liquids.

Combining the insights obtained using different methods, Scheme 1 shows a general scenario of the early events in the radiation chemistry of ionic liquids. The interaction of ionising radiation with the ionic liquids yields the excited states of the parent ions. Some of these states promptly fragment, yielding radicals and other reactive intermediates, whereas the majority ionise to yield short-lived electrons and holes which are rapidly trapped by the parent ions and ion vacancies in the ionic liquids. These reactions are different for aromatic and aliphatic cation ionic liquids. *In ionic liquids containing aromatic cations,* the electrons are trapped by the cations and/or anion vacancies; in both cases the final product is the dimeric radical cation, $[C_2]^{+\bullet}$. The hole is trapped by either ionic liquid parent ion or the anion vacancy; in all of these cases, the final radical product is either $A^\bullet$ or $[A_2]^{-\bullet}$ (if hemicolligation is possible). *In ionic liquids containing aliphatic cations*, the electrons are trapped by cation vacancies yielding solvated electrons, which are fully analogous to *F*-centres in ionic crystals. The holes are trapped by the ionic liquid parent ions and also by anion vacancies.

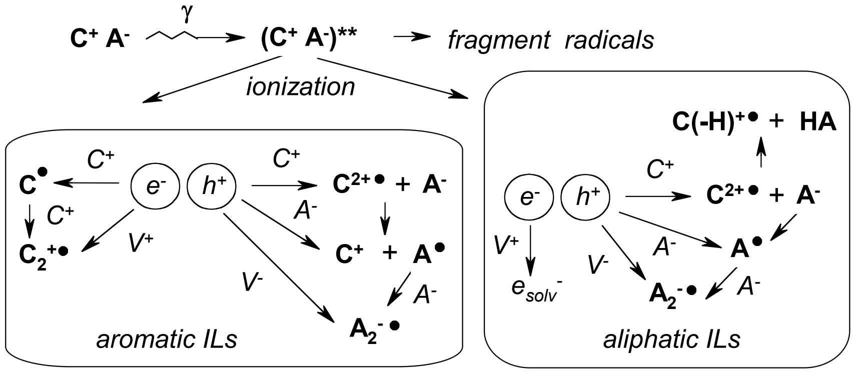

*Scheme 1. After irradiation (γ) the excited ionic liquid components may fragment or ionise to produce electrons and holes. The ensuing reactions depend on whether the cations ($C^+$) are aromatic or fully saturated, and the structure of the anions ($A^-$). $V^+$ and $V^-$ represent cation and anion vacancies.*

The holes trapped by the anions and the anion vacancies yield $A^\bullet$ and $[A_2]^{-\bullet}$. The holes trapped by the cations either transfer electrons from nearby anions, yielding the same anion-derived radicals, or undergo deprotonation yielding *C*-centred radical cations.

This scenario is consistent with the EPR and pulse radiolysis data, but product analyses suggest that there are also reaction channels that are not included in this scheme. For example, radiolysis of $[N_{1\,4\,4\,4}][NTf_2]$ was shown to yield products indicative of C-C and C-N scission in the aliphatic chains of the cations and N-S scission in the $[NTf_2]^-$ *(51)*; none of the paramagnetic species corresponding to such fragmentation patterns has been observed using EPR spectroscopy. In particular, EPR spectroscopy positively excludes the formation of chain-loss alkyl radicals by C-N scission, such as the dissociation of the excited state of $[NR'R_3]^+$ to $[NR_3]^{+\bullet}$ + $R^\bullet$, although such reactions have been observed in crystalline ionic solids. The fact that no paramagnetic species that account for some of the combination products observed by mass spectrometry have been observed using EPR spectroscopy points to generation of *diamagnetic* reactive intermediates, such as carbonium ions and nitrenes, *via* the fragmentation of electronically excited parent ions, *e.g.*

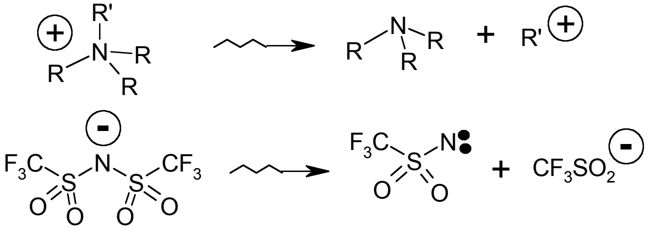

Downloaded by UNIV OF GUELPH LIBRARY on June 28, 2012 | http://pubs.acs.org
Publication Date (Web): December 18, 2009 | doi: 10.1021/bk-2009-1030.ch008

In the gas phase, the dissociation to $[CF_3SO_2]^-$ and $[^1TfN]$**:** is 0.73 eV less energetic than the ionisation of $[NTf_2]^-$, which may explain the occurrence of such fragmentation. Therefore, Scheme 1 is incomplete, and more work is needed to understand the observed product distribution. Further progress in delineating the complex chemistry of irradiated ionic liquids may require new experimental approaches, such as time-resolved vibrational spectroscopy.

# Conclusion

The factors that control radiolytic product distributions and radiation-induced chemical reactivity are being identified through the combination of time-resolved absorbance pulse radiolysis, electron paramagnetic resonance characterisation of radiolytically-produced radicals, and detailed structural identification of final products. The work has revealed uncommon reactivity patterns that stem from the unusual physical properties of ionic liquids. A potential radioprotective role for the ionic liquid solvent has been identified. The results to date have exposed several intriguing differences with conventional solvent systems that could be exploited to design radiolytically-robust separations systems for spent nuclear fuel. While there is still much work to be done on the separations and radiation chemistry aspects of the problem, the possibility of using ionic liquids in this important energy application remains strong.

Downloaded by UNIV OF GUELPH LIBRARY on June 28, 2012 | http://pubs.acs.org
Publication Date (Web): December 18, 2009 | doi: 10.1021/bk-2009-1030.ch008

# Acknowledgments

This work was performed at Brookhaven National Laboratory and Argonne National Laboratory under contracts DE-AC02-98CH10886 and DE-AC02-06CH11357, respectively, with the U.S. Department of Energy and supported by its Division of Chemical Sciences, Office of Basic Energy Sciences.

# References

1. Visser, A. E.; Swatloski, R. P.; Reichert, W. M.; Mayton, R.; Sheff, S.; Wierzbicki, A.; Davis, J. H.; Rogers, R. D., *Chem. Commun.* **2001**, 135-136.
2. Ouadi, A.; Gadenne, B.; Hesemann, P.; Moreau, J. J. E.; Billard, I.; Gaillard, C.; Mekki, S.; Moutiers, G., *Chem. Eur. J.* **2006,** *12*, 3074-3081.
3. Ouadi, A.; Klimchuk, O.; Gaillard, C.; Billard, I., *Green Chem.* **2007,** *9*, 1160-1162.
4. Rao, C. J.; Venkatesan, K. A.; Nagarajan, K.; Srinivasan, T. G., *Radiochim. Acta* **2008,** *96*, 403-409.
5. Chen, P. Y.; Hussey, C. L., *Electrochim. Acta* **2004,** *49*, 5125-5138.
6. Komura, K*., et al.*, *J. Environ. Radioact.* **2000,** *50*, 3-14.

7. Harmon, C. D.; Smith, W. H.; Costa, D. A., *Radiat. Phys. Chem.* **2001,** *60*, 157-159.
8. Gutowski, K. E.; Bridges, N. J.; Cocalia, V. A.; Spear, S. K.; Visser, A. E.; Holbrey, J. D.; Davis, J. H.; Rogers, R. D., In *Ionic Liquids IIIb: Fundamentals, Progress, Challenges and Opportunities: Transformations and Processes*, Amer. Chem. Soc.: Washington, 2005; ACS Symp. Ser. Vol. 902, pp 33-48.
9. Stepinski, D. C.; Young, B. A.; Jensen, M. P.; Rickert, P. G.; Dzielawa, J. A.; Dilger, A. A.; Rausch, D. J.; Dietz, M. L., In *Separations for the Nuclear Fuel Cycle in the 21st Century*, Lumetta, G. J.; Nash, K. L.; Clark, S. B.; Friese, J. I., Eds. Amer. Chem. Soc.: Washington, 2006; ACS Symp. Ser. Vol. 933, pp 233-247.
10. Binnemans, K., *Chem. Rev.* **2007,** *107*, 2592-2614.
11. Cocalia, V. A.; Gutowski, K. E.; Rogers, R. D., *Coord. Chem. Rev.* **2006,** *250*, 755-764.
12. Visser, A. E.; Jensen, M. P.; Laszak, I.; Nash, K. L.; Choppin, G. R.; Rogers, R. D., *Inorg. Chem.* **2003,** *42*, 2197-2199.
13. Visser, A. E.; Rogers, R. D., *J. Solid State Chem.* **2003,** *171*, 109-113.
14. Cocalia, V. A.; Jensen, M. P.; Holbrey, J. D.; Spear, S. K.; Stepinski, D. C.; Rogers, R. D., *Dalton Trans.* **2005**, 1966-1971.
15. Giridhar, P.; Venkatesan, K. A.; Subramaniam, S.; Srinivasan, T. G.; Rao, P. R. V., *J. Alloy. Compd.* **2008,** *448*, 104-108.
16. Jensen, M. P.; Neuefeind, J.; Beitz, J. V.; Skanthakumar, S.; Soderholm, L., *J. Am. Chem. Soc.* **2003,** *125*, 15466-15473.
17. Dietz, M. L.; Dzielawa, J. A.; Jensen, M. P.; Beitz, J. V.; Borkowski, M., In *Ionic Liquids IIIb: Fundamentals, Progress, Challenges and Opportunities: Transformations and Processes*, Amer. Chem. Soc.: Washington, 2005; ACS Symp. Ser. Vol. 902, pp 2-18.
18. Stepinski, D. C.; Jensen, M. P.; Dzielawa, J. A.; Dietz, M. L., *Green Chem.* **2005,** *7*, 151-158.
19. Cocalia, V. A.; Holbrey, J. D.; Gutowski, K. E.; Bridges, N. J.; Rogers, R. D., *Tsinghua Sci. Tech.* **2006,** *11*, 188-193.
20. Dietz, M. L.; Dzielawa, J. A.; Laszak, I.; Young, B. A.; Jensen, M. P., *Green Chem.* **2003,** *5*, 682-685.
21. Dietz, M. L.; Stepinski, D. C., *Talanta* **2008,** *75*, 598-603.
22. Luo, H.; Dai, S.; Bonnesen, P. V.; Haverlock, T. J.; Moyer, B. A.; Buchanan, A. C., *Solvent Extr. Ion Exch.* **2006,** *24*, 19-31.
23. Wishart, J. F., In *Ionic Liquids as Green Solvents: Progress and Prospects*, Rogers, R. D.; Seddon, K. R., Eds. Amer. Chem. Soc.: Washington, 2003; ACS Symp. Ser. Vol. 856, pp 381-396.
24. Wishart, J. F.; Funston, A. M.; Szreder, T., In *Molten Salts XIV*, Mantz, R. A.; Trulove, P. C.; De Long, H. C.; Stafford, G. R.; Hagiwara, R.; Costa, D. A., Eds. The Electrochemical Society: Pennington, NJ, 2006; pp 802-813.
25. Farhataziz; Rodgers, M. A. J., *Radiation Chemistry: Principles and Applications*. VCH: New York, 1987.
26. Wishart, J. F.; Nocera, D. G., *Photochemistry and Radiation Chemistry: Complementary Methods for the Study of Electron Transfer*. Adv. Chem Ser. Vol. 254, Amer. Chem. Soc.: Washington, DC, 1998.

Downloaded by UNIV OF GUELPH LIBRARY on June 28, 2012 | http://pubs.acs.org
Publication Date (Web): December 18, 2009 | doi: 10.1021/bk-2009-1030.ch008

27. Jonah, C. D.; Rao, B. S. M., *Radiation Chemistry: Present Status and Future Trends*. Studies in Physical and Theoretical Chemistry Vol. 87, Elsevier Science: Amsterdam, 2001.
28. Spotheim-Maurizot, M.; Mostafavi, M.; Douki, T.; Belloni, J., *Radiation Chemistry: From Basics to Applications in Materials and Life Sciences*. EDP Sciences: Les Ulis, France, 2008.
29. Ito, N.; Arzhantsev, S.; Heitz, M.; Maroncelli, M., *J. Phys. Chem. B* **2004,** *108*, 5771-5777.
30. Arzhantsev, S.; Jin, H.; Baker, G. A.; Maroncelli, M., *J. Phys. Chem. B* **2007,** *111*, 4978-4989.
31. Funston, A. M.; Fadeeva, T. A.; Wishart, J. F.; Castner, E. W., *J. Phys. Chem. B* **2007,** *111*, 4963-4977.
32. Paul, A.; Samanta, A., *J. Phys. Chem. B* **2007,** *111*, 4724-4731.
33. Wishart, J. F.; Neta, P., *J. Phys. Chem. B* **2003,** *107*, 7261-7267.
34. Wishart, J. F.; Lall-Ramnarine, S. I.; Raju, R.; Scumpia, A.; Bellevue, S.; Ragbir, R.; Engel, R., *Radiat. Phys. Chem.* **2005,** *72*, 99-104.
35. Behar, D.; Gonzalez, C.; Neta, P., *J. Phys. Chem. A* **2001,** *105*, 7607-7614.
36. Marcinek, A.; Zielonka, J.; Gebicki, J.; Gordon, C. M.; Dunkin, I. R., *J. Phys. Chem. A* **2001,** *105*, 9305-9309.
37. Behar, D.; Neta, P.; Schultheisz, C., *J. Phys. Chem. A* **2002,** *106*, 3139-3147.
38. Skrzypczak, A.; Neta, P., *J. Phys. Chem. A* **2003,** *107*, 7800-7803.
39. Yang, J.; Kondoh, T.; Norizawa, K.; Nagaishi, R.; Taguchi, M.; Takahashi, K.; Katoh, R.; Anishchik, S. V.; Yoshida, Y.; Tagawa, S., *Radiat. Phys. Chem.* **2008,** *77*, 1233-1238.
40. Asano, A.; Yang, J.; Kondoh, T.; Norizawa, K.; Nagaishi, R.; Takahashi, K.; Yoshida, Y., *Radiat. Phys. Chem.* **2008,** *77*, 1244-1247.
41. Katoh, R.; Yoshida, Y.; Katsumura, Y.; Takahashi, K., *J. Phys. Chem. B* **2007,** *111*, 4770-4774.
42. Takahashi, K.; Sato, T.; Katsumura, Y.; Yang, J.; Kondoh, T.; Yoshida, Y.; Katoh, R., *Radiat. Phys. Chem.* **2008,** *77*, 1239-1243.
43. Lall-Ramnarine, S. I.; Castano, A.; Subramaniam, G.; Thomas, M. F.; Wishart, J. F., *Radiat. Phys. Chem.* **2009**, in press, DOI: 10.1016/j.radphyschem.2009.02.007.
44. Grodkowski, J.; Neta, P.; Wishart, J. F., *J. Phys. Chem. A* **2003,** *107*, 9794-9799.
45. Wishart, J. F.; Cook, A. R.; Miller, J. R., *Rev. Sci. Instrum.* **2004,** *75*, 4359-4366.
46. Cook, A. R.; Shen, Y., *Rev. Sci. Instrum.* **2009**, in press.
47. Funston, A. M.; Wishart, J. F., In *Ionic Liquids IIIa: Fundamentals, Progress, Challenges, and Opportunities, Properties and Structure*, Amer. Chem. Soc.: Washington, 2005; ACS Symp. Ser. Vol. 901, pp 102-116.
48. Buzzeo, M. C.; Klymenko, O. V.; Wadhawan, J. D.; Hardacre, C.; Seddon, K. R.; Compton, R. G., *J. Phys. Chem. A* **2003,** *107*, 8872-8878.
49. Allen, D.; Baston, G.; Bradley, A. E.; Gorman, T.; Haile, A.; Hamblett, I.; Hatter, J. E.; Healey, M. J. F.; Hodgson, B.; Lewin, R.; Lovell, K. V.; Newton, B.; Pitner, W. R.; Rooney, D. W.; Sanders, D.; Seddon, K. R.; Sims, H. E.; Thied, R. C., *Green Chem.* **2002,** *4*, 152-158.

Downloaded by UNIV OF GUELPH LIBRARY on June 28, 2012 | http://pubs.acs.org
Publication Date (Web): December 18, 2009 | doi: 10.1021/bk-2009-1030.ch008

50. Berthon, L.; Nikitenko, S. I.; Bisel, I.; Berthon, C.; Faucon, M.; Saucerotte, B.; Zorz, N.; Moisy, P., *Dalton Trans.* **2006**, 2526-2534.
51. Bosse, E.; Berthon, L.; Zorz, N.; Monget, J.; Berthon, C.; Bisel, I.; Legand, S.; Moisy, P., *Dalton Trans.* **2008**, 924-931.
52. Qi, M. Y.; Wu, G. Z.; Li, Q. M.; Luo, Y. S., *Radiat. Phys. Chem.* **2008,** *77*, 877-883.
53. Grodkowski, J.; Neta, P., *J. Phys. Chem. A* **2002,** *106*, 11130-11134.
54. Grodkowski, J.; Nyga, M.; Mirkowski, J., *Nukleonika* **2005,** *50*, S35-S38.
55. Takahashi, K.; Sakai, S.; Tezuka, H.; Hiejima, Y.; Katsumura, Y.; Watanabe, M., *J. Phys. Chem. B* **2007,** *111*, 4807-4811.
56. Shkrob, I. A.; Chemerisov, S. D.; Wishart, J. F., *J. Phys. Chem. B* **2007,** *111*, 11786-11793.
57. Shkrob, I. A.; Wishart, J. F., *J. Phys. Chem. B* **2009,** *113*, 5582-5592.
58. Chandrasekhar, N.; Schalk, O.; Unterreiner, A. N., *J. Phys. Chem. B* **2008,** *112*, 15718-15724.
59. Mathur, J. N.; Murali, M. S.; Nash, K. L., **2001,** *19*, 357 - 390.
60. Nash, K. L., In *Separations for the Nuclear Fuel Cycle in the 21st Century*, Lumetta, G. J.; Nash, K. L.; Clark, S. B.; Friese, J. I., Eds. Amer. Chem. Soc.: Washington, 2006; ACS Symp. Ser. Vol. 933, pp 21-40.
61. Fox, O. D.; Jones, C. J.; Birkett, J. E.; Carrott, M. J.; Crooks, G.; Maher, C. J.; Roube, C. V.; Taylor, R. J., In *Separations for the Nuclear Fuel Cycle in the 21st Century*, Lumetta, G. J.; Nash, K. L.; Clark, S. B.; Friese, J. I., Eds. Amer. Chem. Soc.: Washington, 2006; ACS Symp. Ser. Vol. 933, pp 89-102.
62. Shkrob, I. A.; Marin, T. W., *Chem. Phys. Lett.* **2008,** *465*, 234-237.

Downloaded by UNIV OF GUELPH LIBRARY on June 28, 2012 | http://pubs.acs.org
Publication Date (Web): December 18, 2009 | doi: 10.1021/bk-2009-1030.ch008

Downloaded by UNIV OF GUELPH LIBRARY on June 28, 2012 | http://pubs.acs.org
Publication Date (Web): December 18, 2009 | doi: 10.1021/bk-2009-1030.ch009

## Chapter 9

# Ionic liquids: Solutions for Electrospray Ionisation Mass Spectrometry

**Paul J. Dyson[1], Matthew A. Henderson[2], J. Scott McIndoe[2]**

**[1]Institut des Sciences et Ingénierie Chimiques, Ecole Polytechnique Fédérale de Lausanne (EPFL), BCH-SB-LCOM, CH-1015 Lausanne, Switzerland**
**[2]Department of Chemistry, University of Victoria, P.O. Box 3065 Victoria, BC V8W 3V6, Canada**

Ionic liquids pose challenges and provide solutions for electrospray ionisation mass spectrometry (ESI-MS). Being inherently charged, they are themselves easy to characterise in both positive- and negative-ion mode by ESI-MS, but the challenge arises when using the ionic liquid as a solvent – how does one then identify the solute? Fortunately, an excess of one charged species does not preclude the detection of others, and good data on charged analytes dissolved in ionic liquids can be obtained. In return, ionic liquids can also be used to solve problems in ESI-MS, most notably removing the restriction that only polar solvents can support the electrospray ionisation process.

## Introduction

The huge growth witnessed in the field of ionic liquids over that last few years has been facilitated by new synthetic routes to ionic liquids, new ionic liquids with tailored physical and chemical properties, and an increasing scope of potential applications *(1)*. Notably, with the discovery of the air and moisture stable imidazolium based ionic liquids *(2),* the field has seen incredible growth, especially, but not exclusively, in the use of ionic liquids as alternative reaction media *(3)*. For example, ionic liquids are under investigation in energy research

In Ionic Liquids: From Knowledge to Application; Plechkova, N., et al.;
ACS Symposium Series; American Chemical Society: Washington, DC, 2010.

as electrolytes in solar cells and batteries, in materials science, in analytical and separation processes and elsewhere *(4)*.

All the applied aspects of ionic liquid research are strongly facilitated by the development of analytical, spectroscopic and theoretical methods to probe their fundamental properties. In this respect, an increasing body of papers devoted to these topics have been published. In turn, these studies have actually led to new applications of ionic liquids, such as matrices for matrix-assisted laser desorption ionisation mass spectrometry (MALDI-MS) *(5)* – and an example of such a case concerning electrospray ionisation (ESI) mass spectrometry is described herein.

Downloaded by UNIV OF GUELPH LIBRARY on June 28, 2012 | http://pubs.acs.org
Publication Date (Web): December 18, 2009 | doi: 10.1021/bk-2009-1030.ch009

## Electrospray Ionisation Mass Spectrometry

ESI is a well-established method for the generation of gas-phase ions from solution for subsequent analysis by mass spectrometry *(6)*. The technique gained rapid prominence for its ability to analyse high molecular weight, polar biomolecules as multiply-charged ions *(7)*. It has also found favour among chemists interested in characterising small molecules, in metabolomics, proteomics, trace analysis and quantification. ESI essentially involves pumping a solution through a charged (3-5 kV) stainless steel capillary into the atmospheric pressure source region. Under these conditions, the solution separates at the tip into a fine spray of charged droplets, from which the solvent is evaporated by a counterflow of warm nitrogen gas. The charge density on the droplets increases to the point that the droplet begins to divide, either by Coulomb explosion (in which the droplet splits into roughly equal parts) or by ion evaporation (in which individual solvated ions depart from the surface of the droplet). The ions are ultimately completely desolvated, and are transferred through a series of differentially pumped chambers into the mass analyser, where the ions are separated by *m/z* in entirely conventional fashion. The description of ESI as a “soft” ionisation technique comes from the fact that little energy is imparted to the ion in the process of transferring it from solution to gas phase, so minimal fragmentation occurs and spectra are dominated by intact ions.

### Ionic liquids in ESI-MS

For relatively concentrated solutions of ionic compounds, including ionic liquids, it is entirely plausible that a small droplet contains a single nett positive (the same applies to negative ions) charge along with a number of paired cations and anions. A nett double charge is unfavoured, as charge repulsion will break the droplet apart. A nett surplus of one cation generates a series of aggregated ions of the type $[\{\text{cation}\}_{n+1}\{\text{anion}\}_{n}]^{+}$, and spectra of ionic liquids at all but the lowest concentrations contain exactly these series. Interestingly, this phenomenon means spectra in both ionisation modes can readily characterise both cation and anion by molecular weight, since the difference in *m/z* between each ion in the series is equal to the mass of cation plus anion, and the first *m/z* value provides the mass of the cation (or anion, if in the negative ion mode). Figure 1 illustrates a typical ESI mass spectrum of an ionic liquid, in this case [$C_4$mim][$BF_4$].

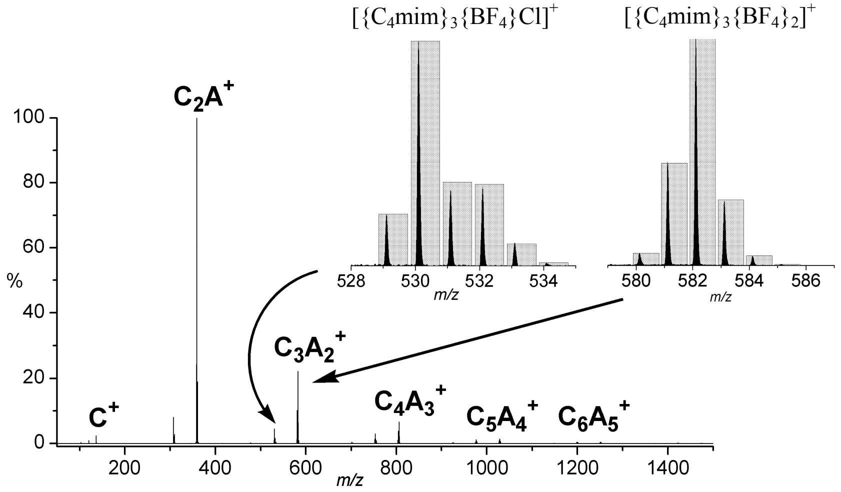

*Figure 1. Positive-ion ESI-MS spectrum of the benchmark ionic liquid [$C_4$mim][$BF_4$], contaminated with chloride. "C" corresponds to the cation, "A" to the anion. The inset spectra are expansions of the isotope patterns (black line is experimental, histogram is calculated) of two of the aggregated ions, one with $Cl^-$ and one with $[BF_4]^-$ only. The combination of m/z and isotope pattern identifies the ions unambiguously.*

The aggregates $[\{\text{cation}\}_{n+1}\{\text{anion}\}_n]^+$ can be clearly observed, and in this case, the presence of chloride ions in addition to the tetrafluoroborate ions can be detected, as an additional series of ions, $[\{C_4\text{mim}\}_{n+1}\{BF_4\}_{n-1}\{Cl\}]^+$. ESI-MS is therefore a rapid method not only for characterisation of ionic liquids, but is also capable of giving an indication of impurities that are *ionic* in nature. ESI-MS can not, of course, reveal the presence of neutral molecules, including solvent.

ESI-MS has also identified anion decomposition reactions of [$C_4$mim][$PF_6$], with $[PF_4O]^-$ and $[PF_2O_2]^-$ ions being observed from the hydrolysis of $[PF_6]^-$ *(8)*. The presence of the oxygen-containing ions could be correlated to the water content of the ionic liquid, and provided similar results to a Karl-Fischer titration.

The relative strength of anion-cation interaction in various ionic liquids has been probed using ESI-MS/MS, and "magic numbers" observed for some aggregates *(9)*. By selecting the mixed aggregate species $[C^1\cdots Br\cdots C^2]^+$ in the positive ion mode and $[A^1\cdots C_4\text{mim}\cdots A^2]^-$ in the negative ion mode and subjecting them to fragmentation *via* collision-induced dissociation, a qualitative order of interaction strength can be established *(10)*.

Downloaded by UNIV OF GUELPH LIBRARY on June 28, 2012 | http://pubs.acs.org
Publication Date (Web): December 18, 2009 | doi: 10.1021/bk-2009-1030.ch009

## Characterisation of Ionic Liquid Solutes

Ionic liquids are currently undergoing extensive study as media for catalyst immobilisation in multiphasic catalysis. A diverse array of transformations are under investigation employing modified homogeneous catalysts *(11)*. Although a wide range of catalysts and reactions have been screened across a range of ionic liquids, a limited amount of *in situ* spectroscopic information regarding the fate of the catalyst is available. Extraction of the catalyst after reaction is difficult or impossible (at least for catalysts that do not easily leach), hampering post-reaction analysis by spectroscopic techniques. It has become apparent that often the optimum catalysts that operate in ionic liquids are those that are themselves ionic, with the charge either located on the metal centre or on a ligand. Such species lend themselves well to ESI-MS analysis *(12)*, but since the solvent is also ionic and present in a vast excess, swamping of the compound of interest and saturation of the detector makes analysis seem, at first glance, to be highly problematic. The question becomes whether or not the technique is sensitive enough to detect the trace quantities of ionic catalyst in the presence of large quantities of the ionic liquid solvent. The answer, fortunately, is yes, although the ionic liquid/ionic catalyst mixture must be diluted in a molecular solvent to enable the analysis to proceed *(13)*. The degree of dilution can be very high, and needs to be, since pure ionic liquids (usually) have a concentration of >1 mol $l^{-1}$. ESI-MS, in comparison, routinely characterises analytes at the micromolar level and is capable of much lower detection limits; indeed, one of the challenges in analysing ionic compounds by ESI-MS is to ensure that dilution is sufficient that lingering contamination of the source does not occur. For the type of analysis described here, a balance has to be struck between appropriate dilution and successful detection of the dissolved catalyst. The range has been tested on the ionic liquid active catalyst [Ru($\eta^6$-4-isopropyltoluene)($\eta^2$-triphos)Cl][$PF_6$] (**1**), dissolved in the ionic liquid [$C_4$mim][$PF_6$] at 0.1 mmol $l^{-1}$. The catalyst solution was diluted in methanol to concentrations of 10, 1, 0.1, 0.01 and 0.001 mmol $l^{-1}$. The corresponding concentration of catalyst was 4 orders of magnitude lower in each case, *i.e.* 1000, 100, 10, 1 and 0.1 pmol $l^{-1}$. The spectrum collected at the highest concentration is depicted in Figure 2. Despite the overwhelming dominance of ionic liquid species (the cation itself and cation/anion aggregates), the presence of the catalyst can easily be detected. Even at the lowest concentrations used, the catalyst was still detectable.

The issue of overlap between ionic liquid aggregate ions and species of interest is potentially a problem, but one that may be overcome readily by making a slight change to either the cation or the anion of the ionic liquid; thus changing the *m/z* intervals at which the ionic liquid aggregates appear and removing the overlap problem.

Downloaded by UNIV OF GUELPH LIBRARY on June 28, 2012 | http://pubs.acs.org
Publication Date (Web): December 18, 2009 | doi: 10.1021/bk-2009-1030.ch009

Downloaded by UNIV OF GUELPH LIBRARY on June 28, 2012 | http://pubs.acs.org
Publication Date (Web): December 18, 2009 | doi: 10.1021/bk-2009-1030.ch009

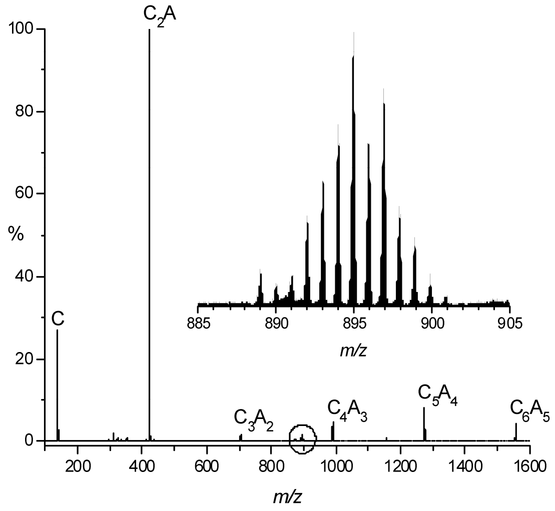

*Figure 2. The positive ion ESI mass spectrum of [Ru($\eta^6$-4-isopropyltoluene)($\eta^2$-triphos)Cl][$PF_6$] in the ionic liquid [$C_4$mim][$PF_6$], diluted in methanol to a concentration of 1000 pmol $l^{-1}$. "C" corresponds to the cation, "A" to the anion, so "$C_5A_4$" is the aggregated ion [{$C_4$mim}$_5${$PF_6$}$_4$]$^+$. The circled peak and enlarged isotope pattern correspond to [Ru($\eta^6$-4-isopropyltoluene)($\eta^2$-triphos)Cl]$^+$. (Modified from (13). Copyright Royal Society of Chemistry.)*

It has been pointed out that a potential problem with the ESI-MS approach is the need to dilute the catalyst solution with a polar (nonionic) solvent. This alters the medium and may, under some circumstances, cause the species in solution to change *(14)*. This perceived weakness attracted attention from Jackson and Duckworth *(15)*, who showed that in fact it perhaps *was* possible to analyse ionic liquids directly, without dilution, using ESI-MS. An experiment in which ionic liquids were infused directly into the source (desolvation gas heated to 250°C) allowed spectra to be collected that showed not only ionic liquid aggregates but also tetraalkylammonium ions dissolved in the ionic liquid. Such an approach has advantages, especially for reactive ionic liquids such as chloroaluminate salts, but has some practical deficiencies: injecting such a high concentration of ionic material into the instrument inevitably leads to serious contamination issues requiring thorough cleaning of the source after each experiment.

Seeking ways to mitigate this disadvantage, we evaluated two alternative experimental methods *(16)*: the first used a hanging drop of ionic liquid mounted on the charged capillary (a modification of Shiea's direct probe method) *(17)*, and the second, nanospray from a preloaded microcapillary, both drastically reducing the amount of ionic liquid entering the instrument. The first method provided interesting results, because ion generation could be monitored over time as the temperature of the desolvation gas was increased. Ion production proved to be copious upon applying a high voltage to the capillary (the normal operating mode of ESI-MS), then tapered to zero, and could be recovered only upon heating the desolvation gas. Further, sporadic bursts of ion production were observed, and at very high desolvation temperatures (>300 °C), the ion current became high and steady. These three regimes of ion production **A**, **B**, and **C** (see ion chromatogram in Figure 3) were attributed as follows. Regime **A** represents residual molecular solvent departing from the droplet, taking with it small quantities of ions in a process reminiscent of conventional ESI. Once the residual solvent (or water, *etc.*) is exhausted, ion production nearly shuts down, but some ions and ion aggregates are able to periodically evaporate directly from the drop of heated ionic liquid (regime **B**). Finally, at very high temperature (regime **C**), the ionic liquid begins to decompose and a wide range of ions is observed in the mass spectrum.

The nanospray studies confirmed the importance of the presence of molecular solvent to the success of the ESI-MS experiment. The spectra of $[Ru(\eta^6\text{-4-isopropyltoluene})(\eta^2\text{-triphos})Cl][PF_6]$ in $[C_4mim][PF_6]$, $[C_4mim][PF_6]$/MeOH (1:1) and MeOH recorded under identical conditions are compared in Figure 4, illustrating the benefit of dilution. The presence of a molecular solvent results in a much higher ion current leading to a vast improvement in signal-to-noise ratio and hence detection limit.

It therefore seems highly probable that at least some molecular solvent is required to obtain satisfactory data from species dissolved in ionic liquids. Directly infusing ionic liquids may contain enough water or other solvent contamination for the purpose (assuming the ionic liquid has not been scrupulously dried), but has the downside of resulting in considerable contamination of the source. As such, the most reliable method is to dilute the ionic liquid with molecular solvent. The next section demonstrates just how wide a choice chemists have; essentially, the very presence of an ionic liquid facilitates the ESI process to the extent that practically any volatile solvent will do, regardless of its polarity. If it is suspected that catalyst speciation is being perturbed by the molecular solvent, this aspect can be investigated by choosing different diluents.

Downloaded by UNIV OF GUELPH LIBRARY on June 28, 2012 | http://pubs.acs.org
Publication Date (Web): December 18, 2009 | doi: 10.1021/bk-2009-1030.ch009

Downloaded by UNIV OF GUELPH LIBRARY on June 28, 2012 | http://pubs.acs.org
Publication Date (Web): December 18, 2009 | doi: 10.1021/bk-2009-1030.ch009

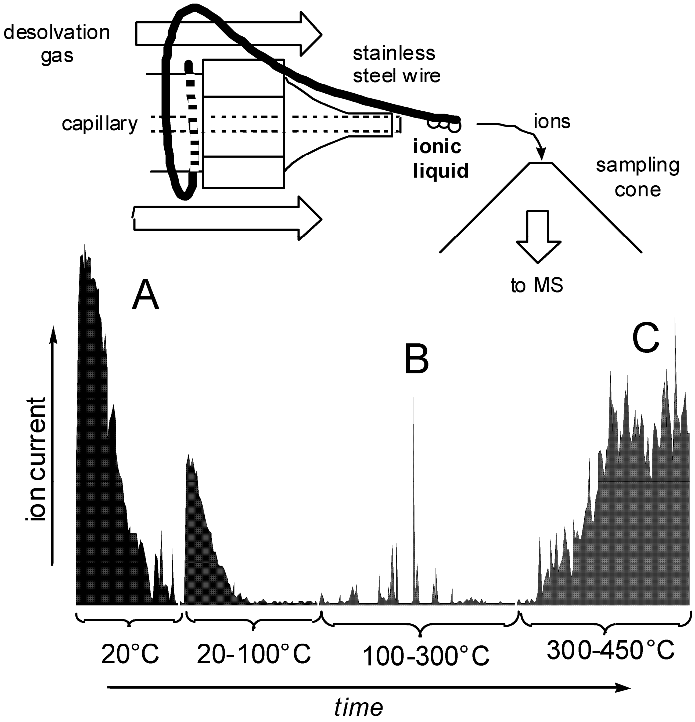
desolvation gas
stainless steel wire
capillary
ionic liquid
ions
sampling cone
to MS
A
B
C
ion current
20°C
20-100°C
100-300°C
300-450°C
time

*Figure 3. Top: Suspension of ionic liquid in the path of desolvation gas to enable direct probe analysis. Bottom: plot of ion current vs. time (temperature) for the direct probe analysis of neat [$C_4$py][$BF_4$]. Total acquisition time of seven minutes. (Modified from (16). Copyright Royal Society of Chemistry.)*

Downloaded by UNIV OF GUELPH LIBRARY on June 28, 2012 | http://pubs.acs.org
Publication Date (Web): December 18, 2009 | doi: 10.1021/bk-2009-1030.ch009

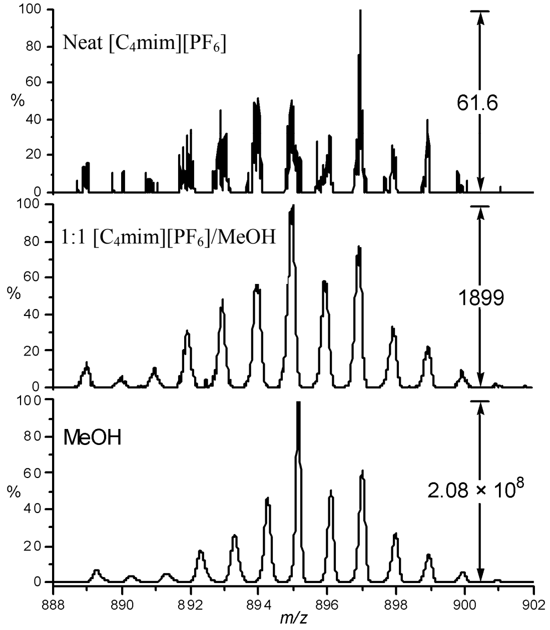

*Figure 4. The positive-ion nanospray mass spectra of [Ru($\eta^6$-p-cymene)-($\eta^2$-triphos)Cl][$PF_6$] in (top) neat [$C_4$mim][$PF_6$], 1 mM; (middle) [$C_4$mim][$PF_6$]-methanol 1:1, 0.5 mM; (bottom) neat MeOH, 0.5 mM. Acquisition time 5 min per spectrum. Absolute intensity (ion count) is indicated to the right of each spectrum. (Modified from (16). Copyright Royal Society of Chemistry.)*

## ESI-MS of Non-Polar Solvents

Our efforts to use ESI-MS to probe ionic liquids and solutes in ionic liquids led us to investigate the range of diluting molecular solvents that might be used. Ionic liquids themselves have a huge range of solvation properties, ranging from miscibility in all proportions with water to miscibility with entirely non-polar solvents such as hexane or tetrachloromethane. Insofar as ESI-MS is concerned, the ionic liquid must be at least slightly soluble in the diluting molecular solvent, immediately restricting the range of solvents that can be employed. Furthermore, ESI-MS is most amenable to polar solvents such as water, methanol and ethanenitrile, and it is widely accepted that non-polar solvents such as hydrocarbons are essentially "off-limits" to the technique. It is less clear from the literature why this should be the case, but one possibility is that because ESI-MS is essentially an electrochemical process – the same number of ions are discharged at the capillary as are generated in the source – non-polar solvents may inhibit this process due to high resistance *(18)*. In electrochemistry, the problem is dealt with in a straightforward way: a supporting electrolyte is added *(19)*. Ionic liquids themselves are, of course, electrolytes, so an obvious experiment suggested itself: add a lipophilic ionic liquid to a non-polar solvent to examine its effect on the ESI-MS process (Figure 5) *(20)*. We were encouraged in this approach by the fact that ionic liquids had been successfully characterised from benzene using ESI-MS *(21)*.

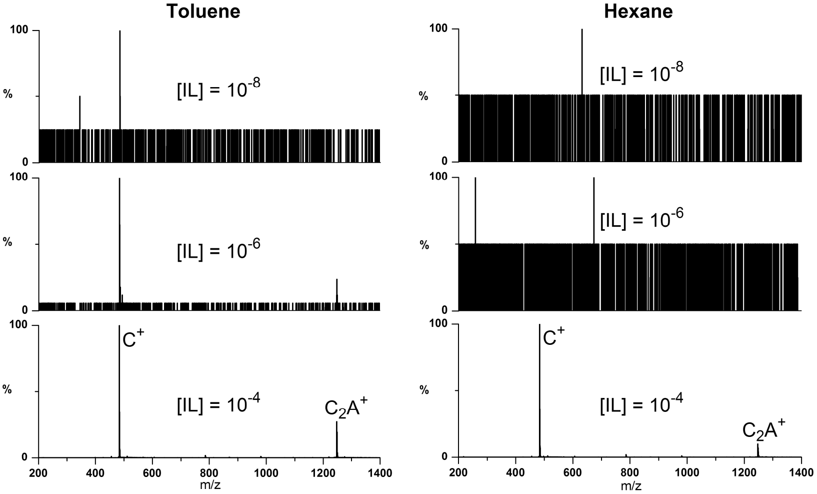

*Figure 5. (left) $[P(C_6H_{13})_3(C_{14}H_{29})][NTf_2]$ in toluene and (right) $[P(C_6H_{13})_3(C_{14}H_{29})][NTf_2]$ in hexane. Reasonable quality spectra are obtained at different threshold concentrations for the two solvents. For toluene, approximately $10^{-6}$ mol $l^{-1}$ $[P(C_6H_{13})_3(C_{14}H_{29})][NTf_2]$ is required, whereas $10^{-5}$ mol $l^{-1}$ of the same ionic liquid is needed for hexane.*

From Figure 5, it can been seen that the approach works quite satisfactorily using the lipophilic ionic liquid $[P(C_6H_{13})_3(C_{14}H_{29})][NTf_2]$, facilitating the collection of good quality data under quite conventional conditions (cone voltage, temperature, desolvation gas flow, *etc.*) for toluene and hexane. In the case of non-polar hexane, the highest concentration is required, approximately $10^{-5}$ mol $l^{-1}$, or preferably, $10^{-4}$ mol $l^{-1}$. Because the ionic liquid has a relatively high molecular weight, the higher concentration corresponds to about 0.1 mg $cm^3$, high by MS standards but sufficiently low that source contamination is not a disabling problem. For more polar solvents such as diethyl ether, fluorobenzene and dichloromethane, good spectra of the ionic liquid could be collected down to the detection limits of the instrument and there appears to be no minimum concentration of ionic liquid required for a stable spray.

Investigation of other ionic liquids showed the same enabling behaviour. Careful choice of cation and anion could almost completely shut down the appearance of aggregate ions in the mass spectrum: the combination of a $[P(C_6H_{13})_3(C_{14}H_{29})]^+$ cation with a $[B(C_6H_3\{CF_3\}_2)_4]^-$ anion (a large, non-coordinating, lipophilic counterion) resulted in almost complete suppression of the aggregate ions $[C_2A]^+$ and $[CA_2]^-$ (present at <0.5 % of the base peak).

Downloaded by UNIV OF GUELPH LIBRARY on June 28, 2012 | http://pubs.acs.org
Publication Date (Web): December 18, 2009 | doi: 10.1021/bk-2009-1030.ch009

Provided a stable spray is obtained, any other soluble species can come along for the ride. So the circumstance in which a charged compound is only stable in a non-polar solvent is no longer a barrier to a successful analysis; addition of an ionic liquid enables ESI-MS detection of the ionic liquid and anything else present. Figure 6 demonstrates this approach; addition of a lipophilic ionic liquid to a small amount of a rhodium catalyst in cyclohexane results in a spectrum that is dominated by the ionic liquid and aggregates thereof, but the catalyst is visible and good quality data can be obtained on this species.

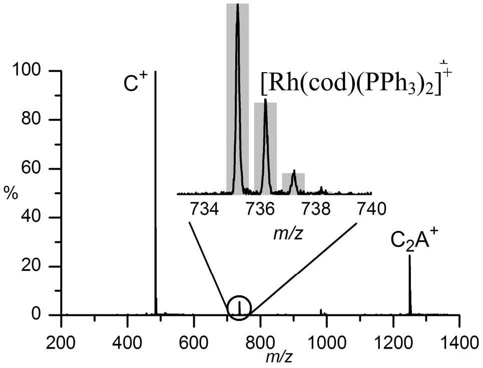

*Figure 6. Facilitation of the ESI process in non-polar solvents by the presence of a lipophilic ionic liquid also enable the ready detection of analytes dissolved in the ionic liquid. Here, high quality positive-ion ESI-MS data has been obtained on (cod= 1,4-cyclooctadiene) dissolved in* $[P(C_6H_{13})_3(C_{14}H_{29})][NTf_2]$ *and diluted in cyclohexane. Inset: expansion of isotope pattern match for the analyte. (Modified from (20). Copyright Royal Society of Chemistry.)*

The addition of the ionic liquid has some other, less immediately obvious but still useful, benefits. Firstly, the ionic liquid aggregates make excellent calibrants for obtaining accurate mass determinations. Secondly, in circumstances where the ionic compound of interest is not especially soluble in the non-polar solvent, addition of a lipophilic ionic liquid serves to dissolve the insoluble material, presumably through counterion exchange. An example of this behaviour is shown in Figure 7, where the hexane-insoluble $[HNEt_3][HFe_3(CO)_{11}]$ is dissolved rapidly upon addition of a small amount of ionic liquid.

Downloaded by UNIV OF GUELPH LIBRARY on June 28, 2012 | http://pubs.acs.org
Publication Date (Web): December 18, 2009 | doi: 10.1021/bk-2009-1030.ch009

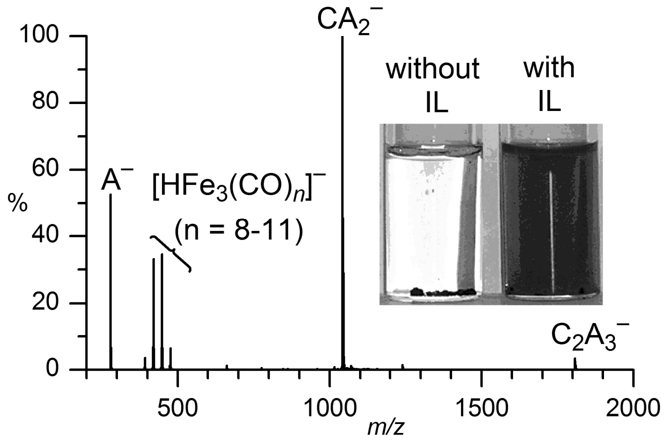

*Figure 7. Negative ion ESI-MS of $[HNEt_3][HFe_3(CO)_{11}]$ in hexane, with $10^{-4}$ mol $l^{-1}$ of $[P(C_6H_{13})_3(C_{14}H_{29})][NTf_2]$ added. Inset shows how the salt is insoluble in hexane prior to the addition of the ionic liquid. (Modified from (20). Copyright Royal Society of Chemistry.)*

## Conclusions

ESI-MS is a convenient method for characterising not only ionic liquids, but also charged analytes dissolved therein. Aggregate ions are observed in spectra of ionic liquids, appearing at regular intervals separated by the combined mass of cation and anion. Provided these ions do not coincide with the *m/z* of the species of interest, analysis is routine.

Lipophilic ionic liquids have the useful property of facilitating the electrospray process in non-polar solvents such as toluene or hexane. Broadening the scope of the ESI-MS technique in this way is most likely to be useful in cases where other molecular solvents either do not dissolve the analyte, or react with it to change the solution speciation.

## References

1. (a) Chum, H. L.; Koch, V. R.; Miller, L. L.; Osteryoung, R. A. *J. Am. Chem. Soc.* **1975**, *97*, 3264-3265. (b) Robinson, J.; Osteryoung, R. A. *J. Am. Chem. Soc.* **1979**, *101*, 323-327. (c) Wilkes, J. S.; Levisky, J. A.; Wilson, R. A.; Hussey, C. L. *Inorg. Chem.* **1982**, *21*, 1263-1264. (d) Scheffler, T. B.; Hussey, C. L.; Seddon, K. R.; Kear, C. M.; Armitage, P. D. *Inorg. Chem.* **1983**, *22*, 2099-2100. (e) Appleby, D.; Hussey, C. L.; Seddon, K. R.; Turp, J. E. *Nature* **1986**, *323*, 614-616. (f) Boon, J. A.; Levisky, J. A.; Pflug, J. L.; Wilkes, J. S. *J. Org. Chem.* **1986**, *51*, 480-483.

Downloaded by UNIV OF GUELPH LIBRARY on June 28, 2012 | http://pubs.acs.org
Publication Date (Web): December 18, 2009 | doi: 10.1021/bk-2009-1030.ch009

2. Wilkes, J. S. ; Zaworotko, M. J. *J. Chem. Soc., Chem. Commun.* **1992**, 965-967.
3. (a) Chauvin, Y.; Gilbert, B.; Guibard, I. *J. Chem. Soc. Chem. Commun.* **1990**, 1715-1716; (b) Carlin, R. T.; Osteryoung, R. A. *J. Mol. Catal.* **1990**, *63*, 125-129; (c) Dyson, P. J. *Appl. Organometal. Chem.* **2002**, *16*, 495-500.
4. (a) Wu, J.; Zhang, J.; Zhang, H.; He, J.; Ren, Q.; Guo, M. *Biomacromolecules* **2004**, *5*, 266-268; (b) Davis Jr, J. H. *Chem. Lett.,* **2004**, *33*, 1072-1077. (c) Fei, Z.; Geldbach, T. J.; Zhao, D.; Dyson, P. J. *Chem. Eur. J.*, **2006**, *12*, 2122-2130. (d) Plechkova, N. V.; Seddon, K. R. *Chem. Soc. Rev.* **2008**, *31,* 123-150. (e) Nakamoto, H.; Watanabe, M. *Chem. Commun.* **2007**, 2539-2541. (f) Nakamoto, H.; Noda, A.; Hayamizu, K.; Hayashi, S.; Hamaguchi, H.; Watanabe, M. *J. Phys. Chem. C* **2007**, *111*, 1541-1548.
5. Armstrong, D. W.; Zhang, L. K.; He, L.; Gross, M. L. *Anal. Chem.* **2001**, 73, 3679-3686.
6. (a) *Electrospray Ionization Mass Spectrometry*, Cole, R. B., Ed. Wiley: New York, NY, 1997. (b) Henderson, W.; McIndoe, J. S. *Mass Spectrometry of Inorganic and Organometallic Compounds: Tools - Techniques - Tips* John Wiley & Sons: Chichester, UK, 2005.
7. Fenn, J. B.; Mann, M.; Meng, C.K.; Wong, S.F.; Whitehouse, C.M. *Mass Spectrom. Rev.* **1990**, *9*, 37-70.
8. Lu, Y. C.; King, F. L.; Duckworth, D. C. *J. Am. Soc. Mass Spectrom.*, **2006**, *17*, 939-944.
9. Gozzo, F. C.; Santos, L. S.; Augusti, R.; Consorti, C. S.; Dupont, J.; Eberlin, M. N. *Chem. Eur. J.* **2004**, *10*, 6187-6193.
10. Bini, R.; Bortolini, O.; Chiappe, C.; Pieraccini, D.; Siciliano, T. *J. Phys. Chem. B*, **2007**, *111*, 598-604.
11. (a) Parvulescu, V. I.; Hardacre, C. *Chem. Rev.* **2007**, 107, 2615-2665. (b) Liu, S.; Xiao, J. *J. Mol. Catal. A: Chem.*, **2007**, *270*, 1-43. (c) Sebesta, R.; Kmentova, I.; Toma, S. *Green Chem.* **2008**, *10*, 484-496.
12. Chisholm, D. M.; McIndoe, J. S. Dalton Trans. **2008**, 3933-3945.
13. Dyson, P. J.; McIndoe, J. S.; Zhao, D. *Chem. Commun.* **2003**, 508-509.
14. Cole-Hamilton, D. J. *C&EN*, February 24, 2003, p 31.
15. Jackson, G. P.; Duckworth, D. C. *Chem. Commun.* **2004**, 522-523.
16. Dyson, P. J.; Khalaila, I.; Luettgen, S.; McIndoe, J. S.; Zhao Chemical Communications, **2004**, 2204-2205.
17. C.-M. Hong, C.-T. Lee,Y-M. Lee,C.-P. Kuo, C.-H. Yuan and J. Shiea, *Rapid Commun. Mass Spectrom.* **1999**, *13*, 21-25.
18. (a) de la Mora, J. F.; Van Berkel, G. J.; Enke, C. G.; Cole, R. B.; Martinez-Sanchez, M.; Fenn, J. B. *J. Mass Spectrom.* **2000**, *35*, 939-952; (b) Kebarle, P. *J. Mass Spectrom.* **2000**, *35*, 804-817.
19. Newman, J.; Thomas-Alyea, K. E. *Electrochemical Systems* Wiley: Hoboken, NJ, 2004.
20. Henderson, M. A.; McIndoe, J. S. *Chem. Commun.* **2006**, 2872-2973.
21. Łachwa, J.; Szydłowski, J.; Makowska, A.; Seddon, K. R.; Esperança, J. M. S. S.; Guedes, H. J. R.; Rebelo, L. P. N. *Green Chem.* **2006**, *8*, 262-267.

Downloaded by UNIV OF GUELPH LIBRARY on June 28, 2012 | http://pubs.acs.org
Publication Date (Web): December 18, 2009 | doi: 10.1021/bk-2009-1030.ch009

Downloaded by STANFORD UNIV GREEN LIBR on June 28, 2012 | http://pubs.acs.org
Publication Date (Web): December 18, 2009 | doi: 10.1021/bk-2009-1030.ch010

## Chapter 10

# Smart Materials Based on Ionic Liquids: the Magnetorheological Fluid Case

**Carlos Guerrero-Sanchez,[a,b,c], Tina Erdmenger,[a,b] Tania Lara-Ceniceros,[d] Enrique Jimenez-Regalado[d], and Ulrich S. Schubert[a,b,e*]**

**[a]Laboratory of Macromolecular Chemistry and Nanoscience, Eindhoven University of Technology, P.O. Box 513, 5600 MB Eindhoven, The Netherlands, E-Mail: u.s.schubert@tue.nl**
**[b]Dutch Polymer Institute, P.O. Box 902, 5600 AX Eindhoven, The Netherlands**
**[c]Ioniqa Technologies, Eindhoven, The Netherlands**
**[d]Centro de Investigacion en Quimica Aplicada, Blvd. Enrique Reyna Hermosillo No. 140, 25253 Saltillo, Coahuila, Mexico**
**[e]Laboratory of Organic and Macromolecular Chemistry, Friedrich-Schiller-University Jena, Humboldtstr. 10, D-07743 Jena, Germany**

Ionic liquids were investigated as novel carriers and/or stabilisers of magnetorheological fluids (MRFs). Ionic liquids have revealed low sedimentation rates in the absence of stabilising agents, showing their combined function as carrier and stabiliser. In addition, the properties of the MRFs can be tuned due to the specific properties of the applied ionic liquids, the particle size and particle concentration. These new smart systems may find applications in several fields of science and technology (*e.g.*, medical therapies and engineering devices).

## Introduction

Smart materials and systems are mainly characterised by being able to respond to external stimuli in their environments, and to significantly change one or more of their properties and/or configurations. For instance, changes in stress, temperature, moisture, pH, chemical composition, light, radiation, electric

In Ionic Liquids: From Knowledge to Application; Plechkova, N., et al.;
ACS Symposium Series; American Chemical Society: Washington, DC, 2010.

and magnetic fields can show a strong and predictable influence on the properties of smart materials and systems. Due to these properties, smart materials and systems have been topics of increasing research interest in recent years for the development of diverse stimuli-responsive micro and nanotechnologies in different fields, such as polymers, electronics, biotechnology, medicine and microelectromechanical systems (MEMS) (*1-11*).

The availability of physically and chemically stable substances, as well as the possibility to fine-tune their properties, must be considered as a key aspect in the development of smart materials and systems. In this regard, ionic liquids might be very suitable compounds for such purposes. Ionic liquids are entirely composed of ions, which are in a liquid state at temperatures below 100 °C. Ionic liquids are, in general, very stable substances in a broad range of temperature and other condition. Furthermore, ionic liquids have negligible vapour pressure and negligible flammability and due to these properties, in some cases, they are considered as "environmental friendly compounds" (*12*). In addition, the properties of ionic liquids (*e.g.*, viscosity, solubility, electric conductivity, melting point, compatibility with other chemical substances, *etc.*) can be fine-tuned by varying the composition of their ions which has lead to a broad range of applications in science, technology and industry (*12,13*). Currently, there are more than three hundred ionic liquids commercially available to be investigated and exploited in diverse applications, and it is believed that about a trillion different ionic liquids could be prepared (*12*) covering a wide range of properties. Based on the broad range of properties of ionic liquids, it is believed that in the near future the development of smart materials can significantly be improved by incorporating ionic liquids in their designs, which may lead to remarkable advances in terms of applications in diverse fields of science and technology.

In this work, ionic liquids were utilised as carriers for magnetorheological fluids (MRFs). MRFs are dispersions of magnetic particles (typically with sizes from 1 to 20 microns) in a liquid carrier, whose rheological properties can be reversibly controlled by the means of a magnetic field (*14–16*). Due to this characteristic, the consistency of MRFs can instantaneously be changed from liquid to solid-like in the presence of a magnetic field (and *vice versa* in the absence of the magnetic field). This process is fully reversible, and the viscosity changes observed in the dispersions mainly depend on the strength of the magnetic field. MRFs were originally investigated by Winslow and Rabinow (*17,18*) around sixty years ago, and have been utilised in various technological applications including semi-active shock absorbers for the automotive industry, dampers for seismic damage controls in civil engineering, seals, valves, robotics, microelectronic devices, and medical therapies and devices (*5–10*). Since the pioneering works of Winslow and Rabinow (*17,18*), the liquid carriers utilised in the formulation of MRFs have been restricted to the use of water, glycols and different synthetic oils (hydrocarbon and silicon based oils) using a wide variety of additives (*19–21*) as dispersing agents, to avoid the settling of the magnetic particles. However, the use of ionic liquids has recently been proposed for the preparation of MRFs with improved properties (*16,22*). In this regard, it is thought that the use of ionic liquids as carriers of MRFs may help to overcome some of the main drawbacks of "conventional" MRFs - such as sedimentation,

Downloaded by STANFORD UNIV GREEN LIBR on June 28, 2012 | http://pubs.acs.org
Publication Date (Web): December 18, 2009 | doi: 10.1021/bk-2009-1030.ch010

durability, cavitations, chemical compatibility with other substances, restricted range of physical properties (*e. g.*, viscosity, and melting and boiling points) and thermal stability - which restrict their application in different technologies and devices. This new approach seems very promising due to the fact that ionic liquids, unlike conventional carriers of MRFs, have tuneable properties, which might expand and/or improve the applications of both ionic liquids and MRFs in different areas of science and technology. Thus, this contribution addresses the effect of the concentration of magnetic particles dispersed in a hydrophilic ionic liquid on the magnetorheological properties of the corresponding MRFs.

## Experimental

### Materials

1-Ethyl-3-methylimidazolium diethylphosphate ($[C_2mim][Et_2PO_4]$) was kindly gifted by Solvent Innovation. Iron(II,III) oxide (magnetite) powder (< 5 μm (micro), 98 %, density 4.8–5.1 g $cm^{-3}$ (25 °C), Aldrich) were chosen as magnetic particles for the preparation of MRFs based on ionic liquids.

### Preparation of MRFs

The MRFs based on ionic liquids utilised in this investigation were prepared by mixing $[C_2mim][Et_2PO_4]$ with the magnetite particles at different concentrations. The mixing process was performed by mechanical stirring (utilising a mixing rate of 2400 rpm for 15 min at room temperature) in cylindrical polyethylene containers using polyethylene stirring paddles.

### Characterisation techniques

Magnetorheological measurements of the prepared MRFs were performed at 25 °C at different shear rates using a Physica UDS200 rheometer (Anton Paar) coupled with a commercial magnetorheological device (MRD180-C, magnetorheological cell PP20/MR). The homogeneous magnetic field was oriented perpendicular to the shear flow direction. A circular parallel plate measuring system (PP20/MR made of non-magnetic metal to prevent the occurrence of radial component of magnetic forces on the shaft of the measuring system) with a diameter of 20 mm and a gap of 1 mm between the plates was used.

Images of selected MRFs were recorded with an optical microscope using an Axioplan 2 imaging system (Zeiss). The samples were placed between glass microscope slides and the images were acquired with a charge-coupled device (CCD) camera.

Before performing the described characterisation techniques, the prepared MRFs were additionally remixed in order to ensure the homogeneity of the dispersions (*e.g.*, no supernatant clear layer formation (sedimentation of the dispersed magnetic particles) was observed for at least two days).

Downloaded by STANFORD UNIV GREEN LIBR on June 28, 2012 | http://pubs.acs.org
Publication Date (Web): December 18, 2009 | doi: 10.1021/bk-2009-1030.ch010

## Results and Discussion

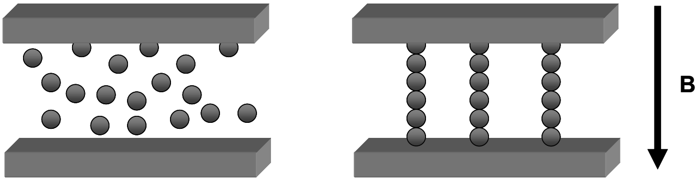

*Figure 1. Schematic representation of the interactions between magnetic particles dispersed in a liquid carrier in the absence (left) and in the presence (right) of a magnetic field.*

As mentioned above, MRFs consist of magnetic particles suspended in a liquid carrier (*19–21*). As a magnetic field is applied to these fluids ("on-state"), their magnetic particles align parallel to the direction of the applied magnetic field allowing for considerable changes in their rheological properties (*e.g.*, viscosity, shear stress, and development of a yield stress) (*19–21*). In the absence of the magnetic field ("off-state"), the magnetic particles are reversibly and homogeneously redistributed in the liquid carries allowing the MRFs to recover their original rheological properties. This phenomenon is schematically depicted in Figure 1.

So far conventional MRFs have mainly been prepared in limited carriers such as oils, water or glycols using different additives to discourage sedimentation and to promote the dispersion of their magnetic particles (*19–21*). However, the use of ionic liquids as new carriers for the preparation of MRFs has been recently proposed, and it was demonstrated that the utilisation of ionic liquids for this specific purpose may lead to MRFs with a higher durability and a better stability against sedimentation due to a dual nature shown by ionic liquids, *i.e.* as liquid carriers and as stabilising agents (*16*). In this regard, similar observations have already been reported where ionic liquids have been simultaneously used as solvents and as stabilising agents in heterogeneous polymerisation reactions (*23*). For the particular case of MRFs based on ionic liquids, apart from the expected and known magnetorheological behaviour of these stimuli-responsive dispersions, it was observed that the use of certain combinations of ionic liquids and magnetic particles allows for the preparation of MRFs with negligible sedimentation, even in the absence of any and stabilising agent. This confirms the dual nature of ionic liquids to act as liquid carriers and as novel stabilising agents.

Even though this new approach to prepare MRFs by utilising ionic liquids as novel liquid carriers seems very promising for the development and/or improvement of applications, this research field is still in its infancy. Hence, additional investigations have still to be performed to reach an acceptable understanding of these "new" smart materials. This contribution briefly addresses the influence of the content of magnetite particles dispersed in the ionic liquid [$C_2$mim][$Et_2PO_4$] on the rheological properties of the corresponding MRFs. This investigation is particularly focussed on the use of relatively high concentrations of magnetite particles dispersed in an ionic liquid, which has not

Downloaded by STANFORD UNIV GREEN LIBR on June 28, 2012 | http://pubs.acs.org
Publication Date (Web): December 18, 2009 | doi: 10.1021/bk-2009-1030.ch010

been addressed in previous reports (*16,22*). The particular selection of [$C_2$mim][$Et_2PO_4$] to perform the present study was based on the fact that this ionic liquid is readily available (*i.e.*, simple to synthesise), it has an acceptable thermal stability, and it is relatively inexpensive when compared to other ionic liquids. From the point of view of applications, these latter characteristics are important for liquid carriers and must be taken into account when formulating MRFs.

Figure 2 displays optical micrographs of dispersed magnetite particles in an ionic liquid. Figure 2(a) shows an optical micrograph of an MRF composed of 25 wt % of magnetite particles dispersed in an ionic liquid; note that the particles are homogeneously dispersed in the corresponding liquid carrier. Figure 2(b) reveals that utilised magnetite particles in this work have a spherical shape and a relatively mono-dispersed distribution with particle sizes in the range from 1.00

Downloaded by STANFORD UNIV GREEN LIBR on June 28, 2012 | http://pubs.acs.org
Publication Date (Web): December 18, 2009 | doi: 10.1021/bk-2009-1030.ch010

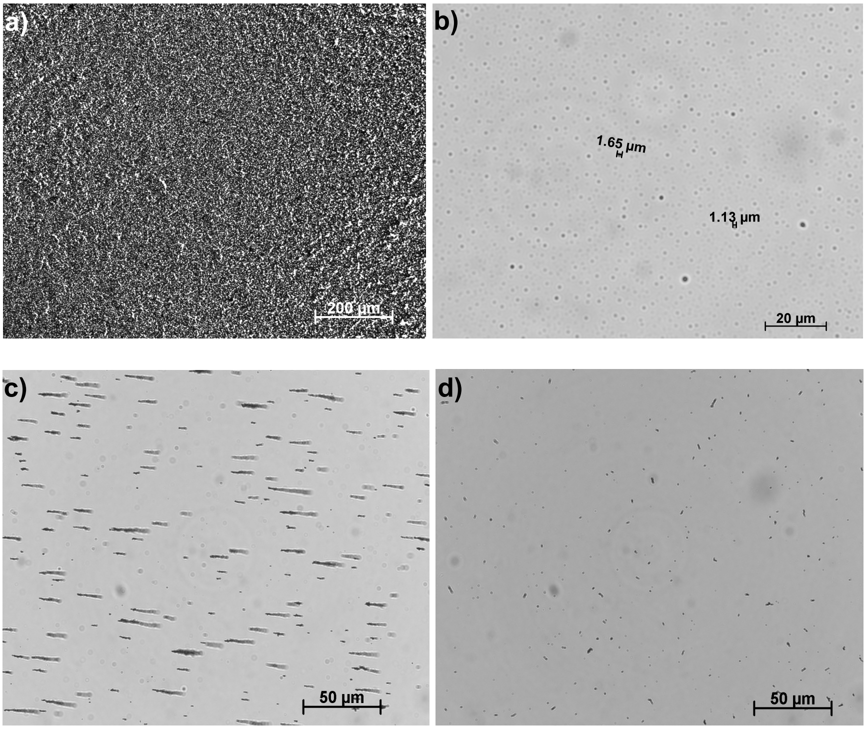

*Figure 2. Optical microscopy images of dispersed magnetite particles in an ionic liquid at room temperature are displayed. (a) Magnetorheological fluid composed of 25 wt % of magnetite particles in an ionic liquid showing a homogenous dispersion. (b) The particles (2 wt %) are randomly distributed in the ionic liquid in the absence of a magnetic field. (c) The particles (2 wt %) self-assemble and align parallel to the direction of a magnetic field applied horizontally. (d) The self-assembled structures shown in (c) disappear as soon as the magnetic field is removed.*

to 1.75 µm. Similar to the schematic representation shown in Figure 1, Figures 2(b) to 2(d) illustrate the magnetorheological phenomenon observed in dispersions of magnetite particles in ionic liquid. Figure 2(b) shows that the magnetite particles are randomly distributed in the ionic liquid in the absence of a magnetic field, whereas Figure 2(c) demonstrates that the particles align parallel to the direction of an applied magnetic field (horizontally for the specific case of Figure 2(c). Figure 2(d) shows that the self-assembled structures of particles formed in the presence of a magnetic field {*i.e.* Figure 2(c)} disappear as soon as the magnetic field is removed. Figure 2(d) also shows a remnant aggregation of magnetite particles after the elimination of the magnetic field; this observation can be attributed to the remnant magnetisation properties of the utilised magnetic material as addressed elsewhere (*16*). These observed small aggregates still demonstrated a magnetic moment, but it is practically negligible (in term of rheological properties) when compared to the considerably stronger interactions between the magnetite particles in the presence of a magnetic field. Note that, for visualisation purposes of the self-assembled structures of magnetic particles under the optical microscope, Figures 2(b) to 2(d) were recorded for a dispersion formed of 2 wt % of magnetite particles in an ionic liquid.

Figure 3 depicts the results of rheological measurements in the absence of a magnetic field for pure ionic liquid [$C_2$mim][$Et_2PO_4$] and for two concentrations of magnetic particles. In Figure 3, it is observed that the particle concentration has an important influence on the rheological properties of the investigated fluids in the absence of a magnetic field. For instance, the viscosity {Figure 3(a)} and the shear stress {Figure 3(b)} of the MRFs increase as the amount of the dispersed particles increases for a fixed shear rate. In this regard, similar findings have been addressed elsewhere for low concentrations of magnetic particles dispersed in ionic liquids (*16,24*). The measurements displayed in Figure 3 also reveal that pure ionic liquid [$C_2$mim][$Et_2PO_4$] shows a Newtonian behaviour (*16*), whereas the corresponding dispersions of magnetic particles in this ionic liquid resemble more a "*quasi*-Newtonian" fluid (*16,24*). Note that at low shear rates, the corresponding MRFs can be classified as *pseudo*-plastic fluids that become Newtonian-like as the shear rate increases.

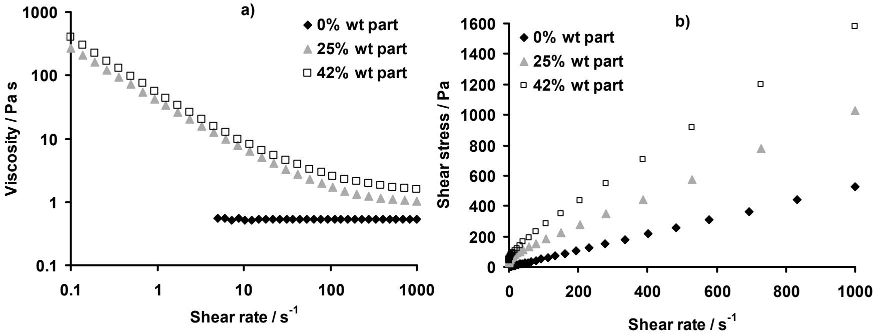

*Figure 3. Effect of the particle concentration on the rheological properties of magnetorheological fluids composed of magnetite particles dispersed in ionic liquid [$C_2$mim][$Et_2PO_4$] in the absence of a magnetic field.*

Downloaded by STANFORD UNIV GREEN LIBR on June 28, 2012 | http://pubs.acs.org
Publication Date (Web): December 18, 2009 | doi: 10.1021/bk-2009-1030.ch010

As a magnetic field is applied to the investigated MRFs, their viscosity and the shear stress significantly change; this effect can be observed in Figure 4. In connection with this phenomenon, the investigated MRFs show a Bingham-type or *pseudo*-plastic behaviour when a magnetic field is applied (*14–22*), in which the developed yield stress mainly depends on the strength of the applied magnetic field as well as on the content of the dispersed magnetic particles. In this regard, the lower the content of magnetic particles dispersed in [$C_2$mim][$Et_2PO_4$] is, the lower the aggregation and interaction is between the magnetite particles, and as a result, lower values of apparent viscosity, shear stress, and yield stress (less pronounced magnetorheological effects) are observed for a fixed strength of magnetic field. As observed in Figure 4, the mentioned magnetorheological effects increase with the strength of the magnetic field until the magnetic saturation of the utilised iron particles is reached (*16*).

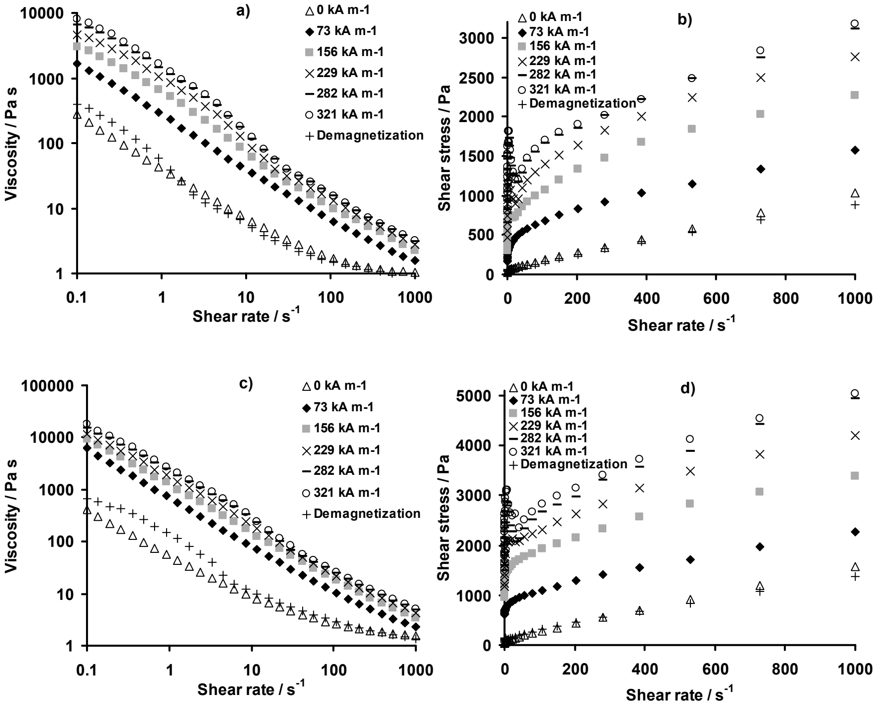

*Figure 4. Rheological measurements of magnetorheological fluids based on [$C_2$mim][$Et_2PO_4$] with different particle concentrations: (a) and (b) 25 wt % of magnetite particles; (c) and (d) 42 wt % of magnetite particles in the presence of a magnetic field (different strengths of magnetic field were utilised in this investigations).*

Figure 4 also shows initial rheological measurements of the investigated MRFs performed before the application of any magnetic field as well as measurements of the samples after being temporarily magnetised for the

Downloaded by STANFORD UNIV GREEN LIBR on June 28, 2012 | http://pubs.acs.org
Publication Date (Web): December 18, 2009 | doi: 10.1021/bk-2009-1030.ch010

magnetorheological measurements followed by a demagnetisation process. In connection to this, Figure 4 reveals that both investigated MRFs show only small differences between the initial and the demagnetised measurements, confirming that the observed magnetorheological effect is a reversible process (which is not observed in the absence of a magnetic field) in these stimuli-responsive materials. The observed small differences between the mentioned measurements can be attributed to the remnant magnetisation shown by the utilised magnetic material, which is related to the presence of residual small aggregates of magnetic particles as discussed elsewhere (*16*) (see, for instance, Figure 2). The vanishing of these small aggregates may occur when the time between initial and demagnetised measurement is sufficiently long and/or when the shear rates applied to the MRF are strong enough to break these remaining small aggregates apart. This effect is seen in Figures 4(a) and 4(c), where the viscosity values of the MRFs in the demagnetisation curve equals the values of the initial (0 kA $m^{-1}$) curve at high shear rates.

Downloaded by STANFORD UNIV GREEN LIBR on June 28, 2012 | http://pubs.acs.org
Publication Date (Web): December 18, 2009 | doi: 10.1021/bk-2009-1030.ch010

## Conclusion

This contribution addresses an important example of smart materials which take advantage of the novel properties of ionic liquids. Thus, the preparation of MRFs with a good stability was achieved utilising an inexpensive approach which makes use of the properties of ionic liquids to act simultaneously as solvents and as stabilising agents. Based on these facts, it is expected that the use of ionic liquids as carriers of MRFs will open new possibilities of application for these smart fluids, because their physical and chemical properties can be fine-tuned in a broad range by mainly varying the nature of the ionic liquids. Hence, novel stimuli-responsive materials can be efficiently developed based on the unique properties offered by ionic liquids. It is thought that, in the near future, ionic liquids will find more and more applications in the development of smart materials for different applications (*e.g.*, as novel magneto- and electro-responsive fluids, and actuators).

## Acknowledgements

This research is supported by the Technology Foundation STW and the technology program of the Ministry of Economic Affairs. The authors also thank the Fonds der Chemischen Industrie and the Dutch Polymer Institute for financial support, as well as Solvent Innovation for their collaboration.

# References

1 He, Y.; Lodge, T. P. *J. Am. Chem. Soc.* **2006**, *128*, 12666–12667.

2 Guerrero-Sanchez, C.; Gohy, J.-F.; D'Haese, C.; Thijs, H.; Hoogenboom, R.; Schubert, U. S. *Chem. Commun.* **2008**, 2753–2755.

3 André, X.; Zhang, M.; Müller, A. H. E. *Macromol. Rapid Commun.* **2005**, *26*, 558–563.

4 Neagu, C. R.; Gardeniers, J. G. E.; Elwenspoek, M.; Kelly, J. J. *J. Microelectromech. Syst.* **1996**, *5*, 2–9.

5 Phillips, T.; Barry, P. L. *Robot Blood?*, http://www.firstscience.com/home/articles/big-theories/robot-blood_1231.html (last accessed November 2008).

6 Bica, I. *J. Magn. Magn. Mater.* **2002**, *241*, 196–200.

7 Jolly, M. R.; Bender, J. W.; Carlson, J. D. *J. Intell. Mater. Syst. Struct.* **1999**, *10*, 5–13.

8 Häfeli, U. O.; Pauer, G. J. *J. Magn. Magn. Mater.* **1999**, *194*, 76–82.

9 Liu, J.; Flores, G. A.; Sheng, R. *J. Magn. Magn. Mater.* **2001**, *225*, 209–217.

10 Meretei, A. Eur. Patent Appl. EP 1676 534 A1, 2006.

11 Koch, M.; Evans, A. G. R.; Brunnschweiler, A. *J. Micromech. Microeng.* **1998**, *8*, 119–122.

12 Deetlefs, M.; Seddon, K. R. *Chim. Oggi* **2006**, *24*, 16–23.

13 Jess, A.; Große Böwing, A.; Wasserscheid, P. *Chemie Ingenieur Technik* **2005**, *77*, 1430–1439.

14 Lim, S. T.; Cho, M. S.; Jang, I. B.; Choi, H. J. *J. Magn. Magn. Mater.* **2004**, *282*, 170–173.

15 Bossis, G.; Lacis, S.; Meunier, A.; Volkova, O. *J. Magn. Magn. Mater.* **2002**, *252*, 224–228.

16 Guerrero-Sanchez, C.; Lara-Ceniceros, T; Jimenez-Regalado, E.; Rasa, M.; Schubert, U. S. *Adv. Mater.* **2007**, *19*, 1740–1747.

17 Rabinow, J. U.S. Patent 2,573,360, 1951.

18 Winslow, W. M. *J. Appl. Phys.* **1949**, *20*, 1137–1140.

19 Lopez-Lopez, M. T.; Zugaldia, A.; Gonzalez-Caballero, F.; Duran, J. D. G. *J. Rheol.* **2006**, *50*, 543–560.

20 Rakin, P. J., Horvath, A. T.; Klingenberg, D. J. *Rheol. Acta* **1999**, *38*, 471–477.

21 Goncalves, F. D.; J. Koo, J. H.; Ahmadian, M. *Shock and Vibration Digest* **2006**, *38*, 203–219.

22 Dodbiba, G.; Park, H. S.; Okaya, K.; Fujita, T. *J. Magn. Magn. Mater.* **2008**, *320*, 1322–1327.

23 Guerrero-Sanchez, C.; Erdmenger, T.; Sereda, P.; Wouters D.; Schubert, U. S. *Chem.–Eur. J.* **2006**, *12*, 9036–9045.

24 Altin, E.; Gradl, J.; Peukert, W. *Chem. Eng. Technol.* **2006**, *29*, 1347–1354.

Downloaded by STANFORD UNIV GREEN LIBR on June 28, 2012 | http://pubs.acs.org
Publication Date (Web): December 18, 2009 | doi: 10.1021/bk-2009-1030.ch010

Downloaded by UNIV OF DELAWARE MORRIS LIB on June 28, 2012 | http://pubs.acs.org
Publication Date (Web): December 18, 2009 | doi: 10.1021/bk-2009-1030.ch011

## Chapter 11

# Ionic Liquids for Microfluidic Actuation

## Multiplexed Hydraulic Valve Actuation Using Ionic Liquid Filled Soft Channels and Braille Displays

**Yi-Chung Tung and Shuichi Takayama**

**Department of Biomedical Engineering, University of Michigan, Ann Arbor, USA**

Use of ionic liquids has grown in recent years, particularly as environmentally friendly chemical solvents, in part because they have no detectable vapour pressure. Microfluidics has also been obtaining great attention for biological and chemical research; its actuation scheme plays a critical role to manipulate small amount of samples within channels. However, the existing microfluidic actuation mechanisms have drawbacks, such as complicated fabrication, tedious operation, and difficulty for scaling up. Here, several representative microfluidic actuation schemes are reviewed based on whether they require channel deformation. This is followed by a demonstration of a newly developed microfluidic actuation scheme based on ionic liquid filled poly(dimethylsiloxane) (PDMS) hydraulic microchannels actuated by Braille displays. Exploiting ionic liquids in a microfluidic device helped to solve the evaporation problem commonly faced in the PDMS microfluidic systems. Thus, the developed actuation scheme allows multiplexed hydraulic actuation while preserving all the associated advantages of using PDMS microchannels. Such integration will be useful for future development of new types of microfluidic systems.

In Ionic Liquids: From Knowledge to Application; Plechkova, N., et al.;
ACS Symposium Series; American Chemical Society: Washington, DC, 2010.

## Introduction of Microfluidics

The manipulation of fluids in channels with dimensions of tens of micrometers, microfluidics, has emerged as a distinct new field. Due to the unique characteristics of microfluidics, such as small size and laminar flow, it offers a number of useful capabilities compared to macro-scale fluidics: the ability to use very small quantities of samples and reagents, to perform analysis within short times, and to carry out separations and detections with high resolution and sensitivity. It also offers fundamentally new capabilities in the control of concentrations of molecules in space and time. Moreover, the microfluidic systems can be low cost and have small footprints for analytical devices. Consequently, microfluidics has the potential to influence subject areas from chemical synthesis and biological analysis to optics and information technology *(1)*.

In order to precisely manipulate the small amount of flow within the channels, fluidic actuation schemes play essential roles in all microfluidic systems. To facilitate better integration, easier fabrication and operation for practical use, various microscale fluidic pumps and valves have been developed over the past decades *(2)*. Research into ionic liquids is also expanding rapidly due to their unique and advantageous materials properties. Useful properties of ionic liquids include no detectable vapour pressure, high conductivity, thermal and oxidative stability, air and moisture stability, nonflammability, and excellent heat transfer properties *(3-5)*. To take advantage of these features, in recent years, researchers have been actively working to utilise ionic liquids in microfluidic systems *(6-9)*. In this article, an overview of existing microfluidic actuators is presented, followed by introduction of a new microfluidic actuation scheme, exploiting ionic liquids for their ability to serve as low volume (nanolitres to microlitres) hydraulic fluids that do not evaporate in deformation-based microfluidic actuation schemes. We divide the microfluidic pumps and valves into two sections, depending on whether or not they utilise deformable structures comprised of poly(dimethylsiloxane). Then finally, we describe the details of how ionic liquids can play a critical role in poly(dimethylsiloxane) deformation based microfluidic actuation schemes.

## Microfluidic Actuation Schemes

The most common way to drive microfluidic flow is to use syringe pumps attached through tubes and fluidic interconnections to a microfluidic device. Although syringe pumps are well-designed and straightforward to implement, they have some disadvantages that retard their exploitation in microfluidic

Downloaded by UNIV OF DELAWARE MORRIS LIB on June 28, 2012 | http://pubs.acs.org
Publication Date (Web): December 18, 2009 | doi: 10.1021/bk-2009-1030.ch011

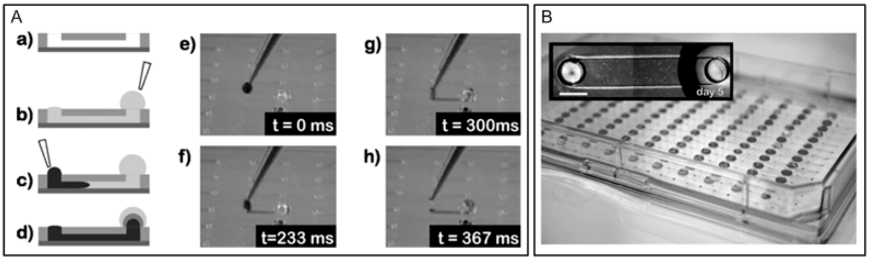

*Figure 1. (A) Schematic drawing and experimental photographs of the droplet-based passive pumping process. (Reproduced from (14). Copyright 2007 Royal Society of Chemistry.) (B) An array of 192 microfluidic channels each with two access ports positioned according microtitre plate standards. Inset: Pre-adipocytes (3T3-L1) on day 5 in culture using the developed device (scalebar: 1 mm.) (Reproduced from (15). Copyright 2008 Royal Society of Chemistry.)*

systems *(10)*. For example, they are quite bulky, expensive, not scalable, and are not amenable to miniaturisation, especially for point-of-care, biometric and biowarfare applications. Moreover, syringe pump-based systems do not allow recirculation of fluid within the microfluidic chip, a desirable requirement for certain applications in cell biology and sensing. The syringe pump on its own lacks on-chip valves, further limiting microscale fluid manipulation. In order to alleviate these problems, a large number of microfluidic actuation schemes have been developed based on actuation mechanisms, such as electroosmosis pumps *(11,12)*, bimorph piezoelectric actuators *(13)*, surface tension-driven flows *(14,15)*, and external magnetic fields *(16-18)*. Below are just a few representative examples.

## Droplet-Based Passive Pumping

To eliminate complex external connections and equipment, Beebe's group has developed droplet-based passive pumping systems *(14,15)*. In this passive pumping system, the surface energy presented in a small drop of liquid is used to pump the liquid through a microchannel. The amount of pressure present within a drop of liquid at an air/liquid interface is given by the Young-Laplace equation. A consequence of the Young-Laplace equation is that smaller drops have a higher internal pressure than larger drops. Therefore, if two drops of different size are connected *via* a fluid-filled microfluidic channel, the smaller drop will shrink while the larger one grows as shown in Figure 1(A). The group demonstrated a microfluidic platform based on the method, and the only skill needed to operate the platform is the use of the pipette to touch drops onto a

Downloaded by UNIV OF DELAWARE MORRIS LIB on June 28, 2012 | http://pubs.acs.org
Publication Date (Web): December 18, 2009 | doi: 10.1021/bk-2009-1030.ch011

Downloaded by UNIV OF DELAWARE MORRIS LIB on June 28, 2012 | http://pubs.acs.org
Publication Date (Web): December 18, 2009 | doi: 10.1021/bk-2009-1030.ch011

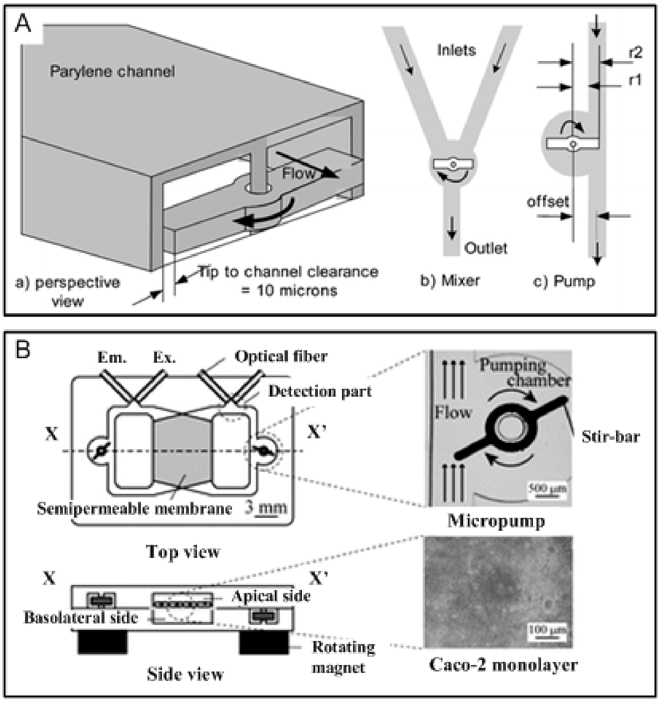
A
Parylene channel
Flow
a) perspective view
Tip to channel clearance = 10 microns
Inlets
Outlet
b) Mixer
r2
r1
offset
c) Pump
B
Em.
Ex.
Optical fiber
Detection part
X
X'
Semipermeable membrane
3 mm
Top view
Apical side
Basolateral side
Rotating magnet
Side view
Pumping chamber
Flow
Stir-bar
500 μm
Micropump
100 μm
Caco-2 monolayer

*Figure 2. (A) Schematic diagram of a single micro stir-bar in microfluidic channel. An external magnet was used to drive the magnetic bar. (Reproduced from (17). Copyright 2004 Royal Society of Chemistry.) (B) Schematic illustration of the integrated magnetic stir-bar driven microfluidic device for long-term perfusion cell culture. The semipermeable membrane on which the cells are cultivated is sandwiched between two PDMS chips. (Reproduced from (18). Copyright 2008 Royal Society of Chemistry.)*

surface. They also demonstrate a high degree of parallelisation (96-192 channels per array) while retaining basic microfluidic operations including routing, compartmentalisation, and laminar flow, Figure 1(B). Although limited in the types of fluid manipulation that can be performed, this method is elegant in its simplicity and scalability.

## Actuation by External Magnetic Field

Active magnetic microfluidic components have been embedded within microfluidic devices to create flow. Inspired by large-scale magnetic bar-stirrers, various micro magnetic stir-bar mixers and pumps have been developed. For instance, Liu's group has developed a micro stir-bar in surface-micromachined Parylene housings and channels for rapid mixing. They also demonstrated the feasibility of pumping using a similar device, Figure 2(A) *(16,17)*.

Exploiting the same concept, Kimura *et al.* developed an integrated microfluidic device with fluidic pumping and optical detection system for long-term perfusion cell culture, Figure 2(B) *(18)*. The fluidic pumping is achieved by rotating stir-bars embedded within the microfluidic devices using an external magnetic field. Another interesting example uses ferroelectric plugs in microfluidic channels as pistons. Hatch *et al.* reported the first micropump using ferrofluid plugs as pistons, which are driven by external magnets as shown in Figure 3(A) *(19)*. Recently, Sun *et al.* developed a circular ferrofluid driven PCR microfluidic device as shown in Figure 3(B) *(20)*.

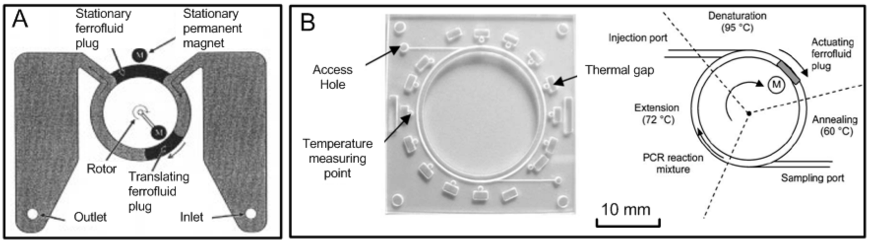

*Figure 3. (A) Schematic of the operating principle for the circular ferrofluidic pump. One plug of ferrofluid, held in place by a stationary magnet, acts as a closed valve between the inlet and outlet chambers. A second plug translates through the channel, pulling fluid in the inlet and pushing it out the outlet. (Reproduced from (19). Copyright 2001* Institute of Electrical and Electronics Engineers, Inc.*) (B) Photograph of the circular micro PCR device fabricated in PMMA, and its operation concept. The PCR reaction mixture is pushed around the circular channel by a ferrofluid plug and flows continuously through the three temperature zones. (Reproduced from (20). Copyright 2007 Royal Society of Chemistry.)*

## Polydimethylsiloxane (PDMS) Microfluidic System and Its Actuation

One of the most common ways to drive fluidic flows, other than by using a syringe pump, is to use peristaltic pumps. These types of pumps move fluids by sequentially squeezing liquid through deformable tubing. This concept of fluid actuation by channel deformation has been adapted to the microscale to achieve highly versatile, scalable, and complex microfluidic actuation. Currently, the elastomer material, polydimethylsiloxane (PDMS), is one of the most popular materials for constructing such deformable microfluidic devices because of its unique material properties and mouldability suited for low-cost rapid prototyping based on a fabrication technique called soft lithography. PDMS is inexpensive, easily moulded, mechanically robust, disposable, chemically inert, non-toxic, optically transparent, and the properties of the surface is readily modified chemically. These properties result from the presence of an inorganic siloxane backbone and organic methyl groups which branch off of the silicon in the polymer backbone.

Downloaded by UNIV OF DELAWARE MORRIS LIB on June 28, 2012 | http://pubs.acs.org
Publication Date (Web): December 18, 2009 | doi: 10.1021/bk-2009-1030.ch011

Downloaded by UNIV OF DELAWARE MORRIS LIB on June 28, 2012 | http://pubs.acs.org
Publication Date (Web): December 18, 2009 | doi: 10.1021/bk-2009-1030.ch011

## Rapid Prototyping of Microfluidic Channels in PDMS

A fabrication technique called soft lithography has been widely adapted to design and fabricate PDMS microfluidic systems in a relative short time (less than 24 h). Soft lithography is a non-photolithographic microfabrication technique that is based upon replica moulding. It provides a convenient, effective, and low-cost method for the manufacturing of microfluidic systems *(21,22)*.

In a typical procedure, a network of microfluidic channels is designed using a computer-aided design (CAD) program that is then converted into a transparency by a high-resolution printer. The transparency can be used as a photomask in photolithography to create a mould with positive relief patterns. The use of a thick photoresist called SU-8 as the mould material is a very attractive option for PDMS microfluidic devices since it allows the micromoulds to easily be patterned using conventional photolithography *(22-24)*.

Figure 4 shows the basic process steps of soft lithographic PDMS fabrication using an SU-8 mould created on a silicon wafer. First, an SU-8 photoresist is spun onto a silicon wafer to form a film of specific thickness, using a highly controlled spinning speed. Then, the SU-8 photoresist is soft baked to evaporate the solvent. Afterwards, the SU-8 is exposed to ultraviolet light using optical lithography and photomasks. A post-exposure bake is then applied on the wafer to increase the cross-linking of the exposed SU-8 parts followed by developing which removes uncross-linked resist.

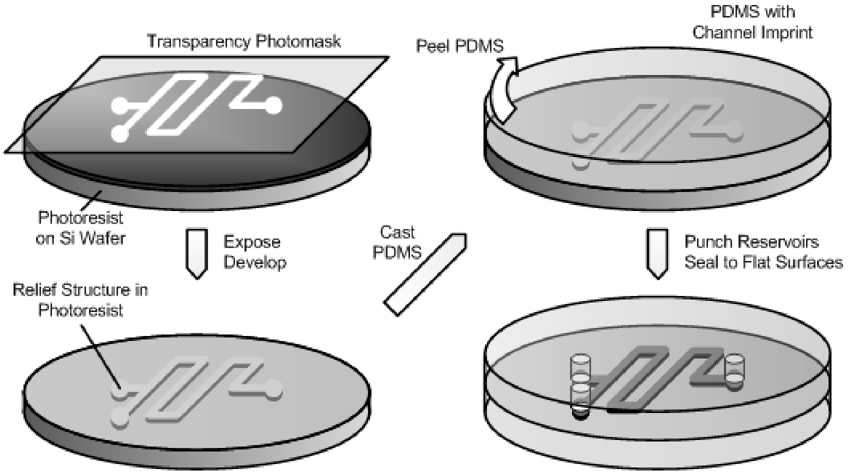

*Figure 4. PDMS microfluidic device fabrication process.*

After producing the SU-8 mould on the substrate, the wafer is silanised to promote parting of the PDMS structure from the mould after curing. Then, the PDMS precursor liquid is well mixed with the curing agent before pouring it onto the wafer mould. The cured PDMS can be easily separated from the master moulds and attached onto another substrate, which could be another PDMS layer, glass, or silicone substrate, to form enclosed microchannels. An oxygen-plasma surface treatment can be applied to form a permanent PDMS bonding to a variety of substrate materials *(25)*.

PDMS possesses great mechanical flexibility; therefore, many actuation schemes have been developed for PDMS microfluidic systems based on channel deformation. Below, this article will briefly review some of the channel deformation-based actuation methods utilised for PDMS microfluidic devices.

## Multilayer Soft Lithography with Pneumatic Actuation

By bonding multiple layers of elastomer, Quake's group has developed a fabrication technique, Multilayer Soft Lithography (MSL), to build active microfluidic systems containing on-off valves, switching valves, and pumps using pneumatic actuation, Figures 5(A) and (B) *(26)*. Moreover, exploiting the same technique, a large-scale integration of microfluidic components onto a single chip (containing more than 2000 microvalves), which is comparable to integrated circuit (IC) architecture, has been demonstrated, Figure 5(C) *(27)*.

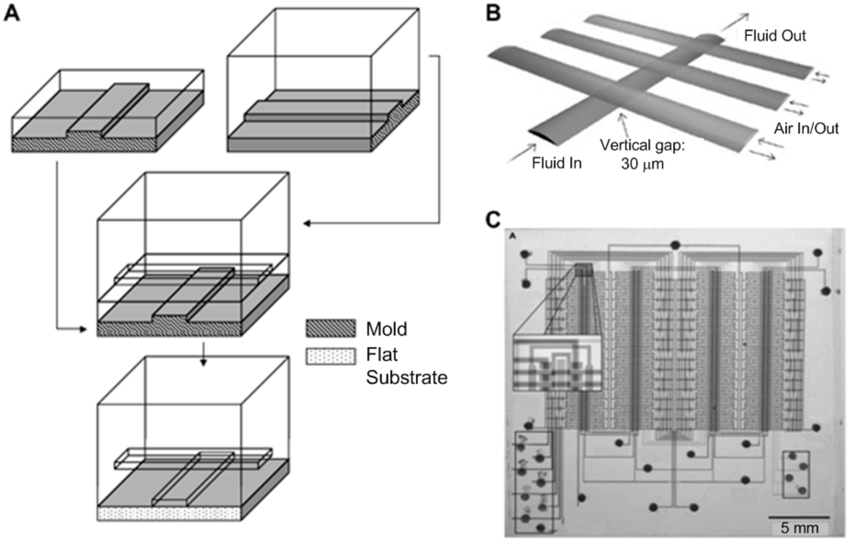

*Figure 5. (A) Process flow for multilayer soft lithography. (B) A 3D diagram of an elastomeric peristaltic pump. Peristalsis was typically actuated by the pattern 101, 100, 110, 010, 011, 001, where 0 and 1 indicate "valve open" and "valve closed," respectively. (Reproduced from (26). Copyright 2000 American Association for the Advancement of Science.) (C) Optical micrograph of a microfluidic large-scale integration example device: a microfluidic comparator chip. The various inputs have been loaded with food dyes to visualise the channels and sub-elements of the fluidic logic. (Reproduced from (27). Copyright 2002 American Association for the Advancement of Science.)*

Downloaded by UNIV OF DELAWARE MORRIS LIB on June 28, 2012 | http://pubs.acs.org
Publication Date (Web): December 18, 2009 | doi: 10.1021/bk-2009-1030.ch011

### Thermally Actuated Phase-Change Microfluidic Components

Taking advantage of materials that exhibit large volumetric change during phase change (*e.g.* polyethylene glycol (PEG), and paraffin), temperature regulated active microfluidic components have been developed. Carlen *et al.* first introduced a microvalve using a paraffin microactuator as the active component as shown in Figure 6(A) *(28)*. The device was fabricated by simple surface micromachining techniques at low temperatures, which allows other electronic components to be fabricated on the same chip beforehand. Kaigala *et al.* developed an integrated polymerase chain reaction (PCR) and capillary electrophoresis chip using electrically controlled phase-change microvalves *(29)*. The actuation is achieved by the volumetric expansion of PEG during its phase transition. The device consists of three layers: the glass control layer, the PDMS flexible membrane and a glass fluidic layer as shown in Figure 6(B).

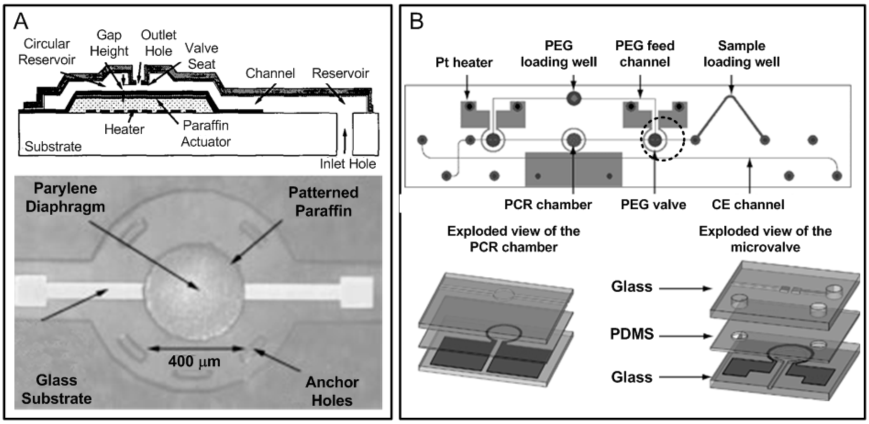
A
Circular Reservoir
Gap Height
Outlet Hole
Valve Seat
Channel
Reservoir
Heater
Paraffin Actuator
Substrate
Inlet Hole
Parylene Diaphragm
Patterned Paraffin
400 μm
Glass Substrate
Anchor Holes
B
Pt heater
PEG loading well
PEG feed channel
Sample loading well
PCR chamber
PEG valve
CE channel
Exploded view of the PCR chamber
Exploded view of the microvalve
Glass
PDMS
Glass

*Figure 6. (A) Cross-sectional view of a surface micromachined paraffin-actuated microvalve, and photograph of and actual paraffin actuator part. (Reproduced from (28). Copyright 2002* Institute of Electrical and Electronics Engineers, Inc.*) (B) Design of the glass-PDMS-glass integrated RT-PCR-CE-microvalves chip, and cross-sectional and top views of the microvalve structure. (Reproduced from (29). Copyright 2008 Royal Society of Chemistry.)*

Downloaded by UNIV OF DELAWARE MORRIS LIB on June 28, 2012 | http://pubs.acs.org
Publication Date (Web): December 18, 2009 | doi: 10.1021/bk-2009-1030.ch011

### Shape memory Alloy Actuators

A shape memory alloy (SMA) is an alloy that “remembers” its shape, and can be returned to that shape after being deformed, by applying heat to the alloy. The most effective and widely used alloys include NiTi, CuZnAl, and CuAlNi. These unusual properties are being applied to a wide variety of applications in a number of different fields, including microfluidic actuation.

Vyawahare *et al.* report a microfluidic device that is actuated using SMA. The devices combine multi-layer soft-lithography with SMA wires on printed circuit boards (PCBs) as control element for microfluidic manipulation

(Figure 7) *(30)*. The electronically activated microfluidic components such as valves, pumps, latches and multiplexers were demonstrated.

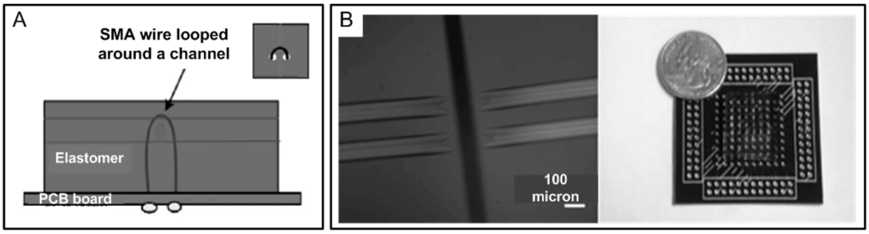
A
SMA wire looped around a channel
Elastomer
PCB board
B
100 micron

*Figure 7. (A) Design of an SMA valve. An SMA wire is looped around a rounded channel, soldered to a PCB and embedded in PDMS. (B) Operation of an SMA wire squeezing two microfluidic channels shut, and a photograph of a PDMS chip with several SMA valves on a PCB. (Reproduced from (30). Copyright 2008 Royal Society of Chemistry.)*

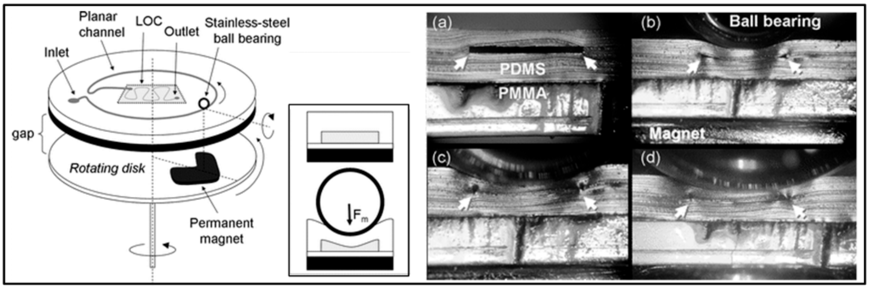
Planar channel
LOC
Outlet
Stainless-steel ball bearing
Inlet
gap
Rotating disk
Permanent magnet
$F_m$
(a)
PDMS
PMMA
(b)
Ball bearing
Magnet
(c)
(d)

*Figure 8. Schematics of a planar peristaltic pump integrated with a microfluidic device. Cross-sectional photographs of a microfluidic channel in open and close states where stainless-steel ball bearing with various diameters are used to deform the channel. The bearing is attracted to the magnet positioned below the bottom substrate. (Reproduced from (31). Copyright 2008 Royal Society of Chemistry.)*

## Peristaltic Pumping by Magnetic Actuation

Yobas *et al.* took advantage of the magnetic actuation method and used readily-available stainless-steel ball bearings coupled with rotating/translating rare-earth magnets as reconfigurable actuating elements on soft-state microfluidic devices (Figure 8) *(31)*. They demonstrated a disposable planar peristaltic pump suitable for microfluidic integration into lab-on-a-chip using the developed actuation scheme. The pump is capable of delivering a relatively large range of flow rates (up to ml min$^{-1}$). The utilisation of non-contact magnetic force preserves the simplicity, reliability, and stability of the mechanical hardware.

Downloaded by UNIV OF DELAWARE MORRIS LIB on June 28, 2012 | http://pubs.acs.org
Publication Date (Web): December 18, 2009 | doi: 10.1021/bk-2009-1030.ch011

Downloaded by UNIV OF DELAWARE MORRIS LIB on June 28, 2012 | http://pubs.acs.org
Publication Date (Web): December 18, 2009 | doi: 10.1021/bk-2009-1030.ch011

## Braille Display Microfluidics with Ionic Liquid Filled Hydraulic Channels

The existing actuation methods provide great potential for constructing practical microfluidic devices; however, they do have some disadvantages depending on the application. For example, the MSL system has capability for large-scale integration of valves and pumps, which provides versatile functions for microscale fluid manipulation. Conversely, the requirement of an external pneumatic source, and the often large numbers of tubing connections for each chip, makes the system bulky and the operation tedious. In addition, the pressurised air may dry up the liquid in the fluidic channels and cause serious problems in long term experiments. Magnetic and thermal actuation methods have poor spatial resolution due to interference from another actuation source when placing two valves too close. The integration of on-chip actuation mechanism such as SMA wires and stainless steel components makes the fabrication process more complicated, and also makes the entire system less disposable.

### Braille Display Microfluidics

Braille display microfluidics is a method to precisely control fluid flow inside elastomeric microfluidic channels by using multiple (tens to hundreds) computer-controlled, piezoelectric, movable pins. These pins are positioned as a grid on a refreshable Braille display, which is a tactile device used by the visually impaired to read computer text. Each pin can act as a valve and be shifted upward to push against channels contained in silicone rubber and completely shut the channel. Utilising synchronous control of multiple pins through Braille display software, *in situ*, integrated microfluidic pumps and valves can be achieved. In these systems, microfluidic channels have a deformable PDMS membrane (thickness: 100~200 μm) at the bottom and channels with a smooth curved wall. The channel acts as a valve when the membrane is pressed by a pin of a Braille display and deformed. Also, three (or more) pins on a channel placed in series act as a pump by a peristaltic actuation sequence of the Braille pins (Figure 9) *(32)*.

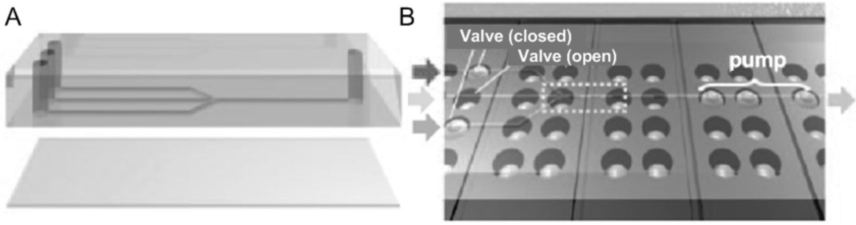

*Figure 9. Schematic representation of Braille display-based microfluidic systems. (A) A typical microfluidic channel design for use with Braille displays. The channel is constructed by a PDMS slab with channel features bonded with a PDMS deformable membrane at the bottom. (B) Overview of the typical experimental setup. The microfluidic device is positioned on top of the Braille display so that channels are aligned about Braille pins, facing down. (Reproduced from (32). Copyright 2004 National Academy of Science.)*

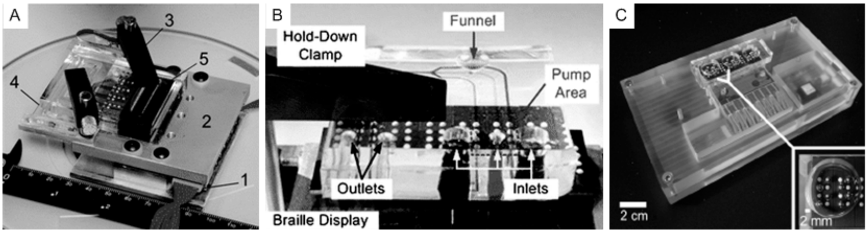

*Figure 10. Photographs of Braille display-based microfluidic devices: (A) recirculation microfluidic system for long-term culture and imaging of cells (Reproduced from (34). Copyright 2006 Royal Society of Chemistry), (B) microfluidic flow cytometry system designed for efficient and non-damaging cell analysis (Reproduced from (35). Copyright 2007 Royal Society of Chemistry), and (C) individually programmable cell stretching microwell array system (Reproduced from (36). Copyright 2008 Elsevier Ltd.)*

Various microfluidic devices have been developed using Braille Display microfluidics. For instance, cell culture systems using commercially-available refreshable Braille displays with microfluidic circulation architectures that eliminate the need for external media pumps and tanks have been developed as shown in Figure 10(A) *(32-34)*. A microflow cytometer system utilising actuation of Braille-display pins for microscale fluid manipulation has also been developed as shown in Figure 10(B) *(35)*. The system was designed for efficient and non-damaging analysis of samples with small numbers of precious cells. Moreover, a device consisting of twenty-four miniature cell stretching chambers with flexible bottom membranes that are deformed using the computer-controlled, piezoelectrically actuated pins of a Braille display has been demonstrated as shown in Figure 10(C) *(36)*. The system is a fast and easy-to-fabricate device that is capable of simultaneously exposing various cells to cyclical stretch at different frequencies.

Downloaded by UNIV OF DELAWARE MORRIS LIB on June 28, 2012 | http://pubs.acs.org
Publication Date (Web): December 18, 2009 | doi: 10.1021/bk-2009-1030.ch011

Using Braille displays as active fluidic controllers allows the basic function of microfluidic systems to be readily accessible and programmable without the need for large and expensive laboratory facilities. The total fluid actuation system is compact in size and can be powered by batteries or computer interfaces such as Universal Serial Bus (USB), which makes Braille display microfluidics portable. The Braille display microfluidics completely eliminates the requirement of fluidic interconnections between the microfluidic chips and external fluid manipulation systems. Furthermore, functions of microfluidic systems can be easily modified by reprogramming the software that controls a Braille display and/or the microfluidic channel design. As a result, this method of fluidic control is versatile and cost-effective.

Downloaded by UNIV OF DELAWARE MORRIS LIB on June 28, 2012 | http://pubs.acs.org
Publication Date (Web): December 18, 2009 | doi: 10.1021/bk-2009-1030.ch011

## Ionic Liquid Filled Hydraulic Valve

Although convenient, versatile, and overall compact, there are limitations in the usage of Braille-display actuators for microfluidic manipulation. Since Braille pins have a constant contact diameter on PDMS deformable membranes and are arranged in a regular grid, there is limited flexibility in the organised placement of pins as active microfluidic components (*e.g.* valves and pumps). The arrangement lacks multiplexing capability as each pin operates one valve, thus limiting the number of valves on a chip to the number of Braille pins. The Braille pin valve strategy also limits imaging capabilities, such as transmitted light phase contrast microscopy because the actuators are opaque.

### *Device Design*

In order to alleviate the drawbacks of the Braille Display Microfluidics, Gu *et al.* developed hydraulic valves that are analogous to the MSL pneumatic valves but are instead pressurised mechanically by movable Braille pins rather than by externally delivered and gated high pressure gas, Figure 11(A-C) *(37)*. Each pin movement compresses an on-chip piston and pressurises the connected control channel. Due to the reversible pressurisation of the control channel, it can close and reopen regions of fluidic channels directly below. A typical Braille pin is ~0.49 mm$^2$ in contact area, and delivers 0.18 N of force to a piston (KGS Co., Saitama, Japan). Pistons compressed by the mechanical pins are approximately 0.83 mm$^2$ in area and 150 μm in height. Typical cross-sectional dimensions are approximately 16 μm high and 95 μm wide for control channels and 8.5 μm high and 95 μm wide for fluidic channels making valve intersections approximately 100 x 100 μm$^2$. Similar to MSL pneumatic valves, the hydraulic valves can act on multiple fluidic channels in parallel and are able to skip fluidic channels by decreasing the width of the control channel from 100 μm to 40 μm, Fig. 11(D). For full optical accessibility, the location of hydraulic valves can be removed away from the site of the Braille pins and pistons, Figure 11(E). Thus, the multiplexing ability and flexibility in high density valve placement that MSL pneumatic actuation schemes provide is retained, while the advantages of interconnect-free hydraulic actuation using Braille pin actuation are realised as shown in Figure 11(F).

Each device is composed of three bonded PDMS layers with the top control layer serving as a mould with features for both pistons and control channels Figure 11(A). A middle layer serves as a mould for the fluidic channels as well as the membrane separating the control and fluidic channels. A bottom sheet closes the fourth side of the fluidic channels and along with the middle layer serves as the separation between the pistons and their corresponding Braille pins.

### *Ionic Liquid Critical for Sustained Stable Actuation*

Because the volume of the fluid in the hydraulic channels is small (nanolitres to microlitres), it is crucial to eliminate any losses due to evaporation and permeation of the hydraulic fluid through the PDMS. Air and water are not

Downloaded by UNIV OF DELAWARE MORRIS LIB on June 28, 2012 | http://pubs.acs.org
Publication Date (Web): December 18, 2009 | doi: 10.1021/bk-2009-1030.ch011

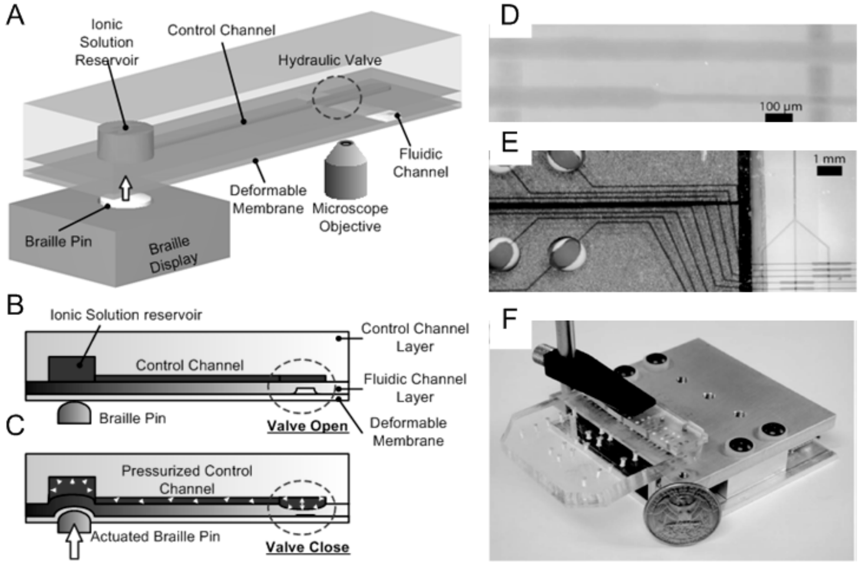
A
Ionic Solution Reservoir
Control Channel
Hydraulic Valve
Fluidic Channel
Deformable Membrane
Microscope Objective
Braille Pin
Braille Display
B
Ionic Solution reservoir
Control Channel
Control Channel Layer
Fluidic Channel Layer
Braille Pin
C
Valve Open
Deformable Membrane
Pressurized Control Channel
Actuated Braille Pin
Valve Close
D
100 µm
E
1 mm
F

*Figure 11. Schematic representation of Braille display-based microfluidic with ionic liquid filled hydraulic valves. (A) The arrangement of a microfluidic device with a hydraulic valve actuated by a Braille pin. (B) and (C) The operation of hydraulic valves. At the normal (not-actuated) situation, the hydraulic valve will maintain its open status (B) to allow fluid flowing through the fluidic channel. While the Braille pin is actuated, the control channel will be pressurised. As a result, the membrane between the control and fluidic channels will be deformed and pushed down to seal the fluidic channel creating close status (C). (D) A top-down view of the intersections of pressurised control (red) and fluidic (green) channels. (E) A top-down view of the Braille pins aligned underneath pistons (left) and microfluidic valves (right). (F) Photograph of a PDMS device with multiple hydraulic valves mounted on a computer-controlled Braille display with 64 pins. (Reproduced from (37). Copyright 2007 American Institue of Physics.)*

well-suited as actuating fluids, because gas permeation through the PDMS or direct evaporation of water causes rapid loss of pressure in the actuation channel, Figure 12(A). To overcome this fluid loss problem, an ionic liquid (1-butyl-3-methylimidazolium tetrafluoroborate) was used as an incompressible piston fluid. Unlike gases such as air and vaporisable water, no decrease in ionic liquid volume was observed within the microfluidic channels, or when open to the atmosphere for more than ten days. In contrast to air and water, the ionic liquid was the only hydraulic fluid that was able to keep valves closed over a significant time period, Figure 12(A). Figure 12(B) shows repetitive opening and closing of an ionic-liquid filled hydraulic valve. Despite the successful demonstration of the actuation mechanism, the ionic liquid used contains an expensive cation and is known to hydrolyse to form hydrogen fluoride in the presence of water, which may chemically react with PDMS. Therefore, the compatibility of the ionic liquid and PDMS may need to be tested, and more stable and less expensive ionic liquids may need to be chosen.

Downloaded by UNIV OF DELAWARE MORRIS LIB on June 28, 2012 | http://pubs.acs.org
Publication Date (Web): December 18, 2009 | doi: 10.1021/bk-2009-1030.ch011

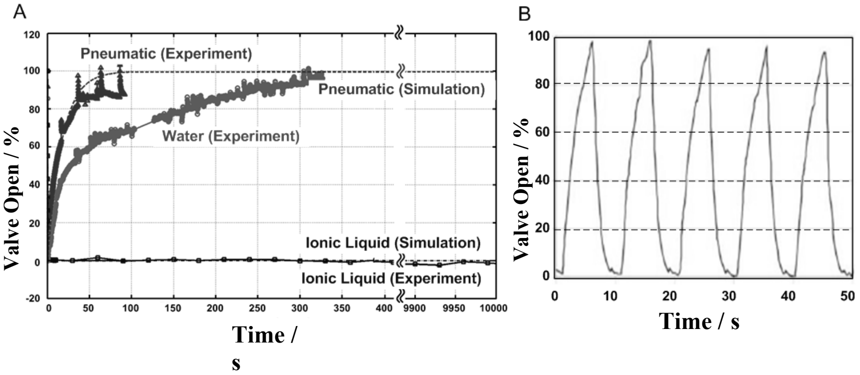

*Figure 12. (A) Graph of the abilities of valves to stay closed when actuated by different control channel fluids at zero time. The ionic liquid filled control channels consistently sustain valve closure over all observed periods. (B) Graph of a valve filled with ionic liquid repeatedly actuated. (Reproduced from (37). Copyright 2007 American Institue of Physics.)*

### *Device Fabrication and Preparation*

A schematic of the fabrication process is shown in Figure 13. Silicon moulds (i) and (iii) are fabricated through photolithography techniques *(1)*. The photoresist AZ 9260 (Microchem Co., Newton, MA) for control and fluidic channels are spun on silicon wafers at 2000 and 3500 rpm respectively for 35 s and cured. The final control layer mould (ii) is made by punching holes in a thin (~150 um thick) replica (a) of the original control channels on silicon (i) and then incorporating the space of the punched hole as a piston. Photocurable epoxy (Epoxy Technology, Billerica, MA) was used as the second mould (ii) and this mould was cast while the original PDMS replica (b) was placed upside down.

With the 3 layers (c) derived from the final control mould (ii), the fluidic mould (iii), and another flat substrate (glass or outside of a Petri dish), all three are sequentially bonded together with plasma oxidation (50 W, 300 mTorr, 30 seconds). In (d), a side-view showing three layers: top layer for control piston and channel, middle for the fluidic channels, and a last layer to seal the fluidic channels. The control channels are primed with hydraulic liquid immediately after plasma oxidation then sealed with superglue. The liquid enters spontaneously but can also be introduced with positive pressure before permanently sealing the channel input with superglue or other suitable sealants (silicone).

Downloaded by UNIV OF DELAWARE MORRIS LIB on June 28, 2012 | http://pubs.acs.org
Publication Date (Web): December 18, 2009 | doi: 10.1021/bk-2009-1030.ch011

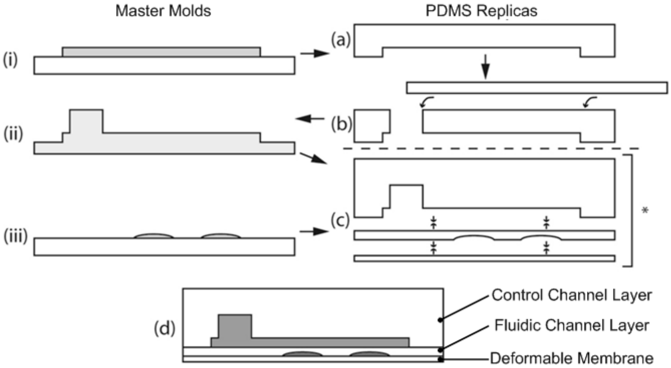

*Figure 13. Fabrication process of a microfluidic device with ionic liquid filled channels for Braille display actuation. (Reproduced from (37). Copyright 2007 American Institue of Physics.)*

## Conclusion

A novel microfluidic actuation scheme based on ionic liquid filled PDMS hydraulic microchannels actuated by Braille displays is presented here. The key enabling breakthrough is the use of non-volatile ionic liquids as the hydraulic fluid. Use of any other type of gas or liquid leads quickly to volatilisation and escape of fluid from the actuation microchannels because of the porosity of PDMS. By using ionic liquids, hydraulic microchannel actuation is realised even in PDMS materials, preserving all the associated advantages of using PDMS microchannels. The system overcomes the need for potentially numerous leak-proof interconnections found on various other microfluidic actuation methods. The described hydraulic valve control strategy has the shared advantages of both MSL pneumatic and mechanical Braille valves through the availability of parallel, arbitrarily arranged valves that are powered by potentially many independent actuators available in a portable format. Like MSL pneumatic valves, ionic liquid hydraulic control microchannels can control multiple fluidic channels and yet skip others. The functionality of Braille valves and pumps can be readily used in conjunction with hydraulic control valves. In addition, the separation between the actuation mechanism and microfluidic channels makes the microfluidic device fully disposable, eliminates the cross contamination between chips, and reduces the device fabrication complexity.

## References

1. Whitesides, G. M. *Nature*, **2006**, *442*, 368-373.
2. Laser, D. J.; Santiago, J. G. *J. Micromech. Microeng.*, **2004**, *14*, R35-R64.
3. Rogers, R. D.; Seddon, K. R. *Science*, **2003**, *302*, 792-793.
4. Baker, G. A.; Baker, S. N.; Pandey, S.; Bright, F. V. *Analyst*, **2005**, *130*, 800-808.
5. Pandey, S. *Anal. Chim. Acta*, **2006**, *556*, 38-45.
6. de Mello, A. J.; Habgood, M.; Lancaster, N. L.; Welton, T., Wooton, R. C. R. *Lab Chip*, **2004**, *4*, 417-419.
7. Mary, P.; Studer, V.; Tabeling, P. *Anal. Chem.*, **2008**, *80*, 2680-2687.
8. Nanayakkara, Y. S.; Moon, H.; Payagala, T,; Wijeratne, A. B.; Crank, J. A.; Sharma, P. S.; Armstrong, D. W. *Anal. Chem.*, **2008**, *80*, 7690-7698.
9. Wang, W.-H.; Zhang, Z.-L.; Xie, Y.-N.; Wang, L.; Yi, S.; Liu, K.;Liu, J.; Pang, D.-W.; Zhao, X.-Z. *Langmuir*, **2007**, *23*, 11924-11931.
10. Pennathur, S. *Lab Chip*, **2008**, *8*, 383-387.
11. Lazar, I. M.; Karger, B. L. *Anal. Chem.*, **2002**, *74*, 6259-6268.
12. Zhao, H.; Bau, H. H. *Phys. Rev. E*, **2007**, *75*, 066217.
13. Olsson, A.; Enoksson, P.; Stemme, G.; Stemme, E. *J. Microelectromech. Syst.*, **1997**, *6*, 161-166.
14. Berthier, E.; Beebe, D. J. *Lab Chip*, **2007**, *7*, 1475-1478.
15. Meyvantsson, I.; Warrick, J. W.; Hayes, S.; Skoien, A.; Beebe, D. J. *Lab Chip*, **2008**, *8*, 717-724.
16. Lu, L.; Ryu, K. S.; Liu, C. *J. Microelectromech. Syst.*, **2002**, *11*, 462-469.
17. Ryu, K. S.; Shaikh, K.; Goluch, E.; Fan, Z.; Liu, C. *Lab Chip*, **2004**, *4*, 608-613.
18. Kimura, H.; Yamamoto, T.; Sakai, H.; Sakai, Y.; Fujii, T. *Lab Chip*, **2008**, *8*, 741-746.
19. Hatch, A.; Kamholz, A. E.; Holman, G.; Yager, P.; Böhringer, K. F. *J. Microelectromech. Syst.*, **2001**, *10*, 215-221.
20. Sun, Y.; Kwok, Y. C.; Nguyen, N. T. *Lab Chip*, **2007**, *7*, 1012-1017.
21. Xia, Y.; Whitesides, G. M. *Annu. Rev. Mater. Sci.*, **1998**, *28*, 153-184.
22. Duffy, D. C.; McDonald, J. C.; Schueller, O. J. A.; Whitesides, G. M. *Anal. Chem.*, **1998**, *70*, 4974-4984.
23. Duffy, D. C.; Schueller, O. J. A.; Brittain, S. T.; Whitesides, G. M. *J. Micromech. Microeng.*, **1999**, *9*, 211-217.
24. Jo, B.-H.; van Lerberghe, L. M.; Motsegood, K. M.; Beebe, D. J. *J. Microelectromech. Syst.*, **2000**, *9*, 76-81.

Downloaded by UNIV OF DELAWARE MORRIS LIB on June 28, 2012 | http://pubs.acs.org
Publication Date (Web): December 18, 2009 | doi: 10.1021/bk-2009-1030.ch011

25. De Mello, A. *Lab Chip*, **2002**, *2*, 31N-36N.
26. Unger, M. A.; Chou, H.-P.; Thorsen, T.; Scherer, A.; Quake, S. R. *Science*, **2000**, *288*, 113-116.
27. Thorsen, T.; Maerkl, S. J.; Quake, S. R. *Science*, **2002**, *298*, 580-584.
28. Carlen, E. T.; Mastrangelo, C. H. *J. Microelectromech. Syst.*, **2002**, *11*, 408-420.
29. Kaigala, G. V.; Hoang, V. N.; Backhouse, C. J. *Lab Chip*, **2008**, *8*, 1071-1078.
30. Vyawahare, S.; Sitaula, S.; Martin, S.; Adalian, D.; Scherer, A. *Lab Chip*, **2008**, *8*, 1530-1535.
31. Yobas, L.; Tang, K.-C.; Yong, S.-E.; Ong, E. K.-Z. *Lab Chip*, **2008**, *8*, 660-662.
32. Gu, W.; Zhu, X.; Futai, N.; Cho, B. S.; Takayama, S. *Proc. Natl. Acad. Sci. U.S.A.*, **2004**, *45*, 15861-15866.
33. Song, J. W.; Gu, W.; Futai, N.; Warner, K. A.; Nor, J. E.; Takayama, S. *Anal. Chem.*, **2005**, *77*, 3993-3999.
34. Futai, N.; Gu, W.; Song, J. W.; Takayama, S. *Lab Chip*, **2006**, *6*, 149-154.
35. Tung, Y.-C.; Torisawa Y.-S.; Futai, N.; Takayama, S. *Lab Chip*, **2007**, *7*, 1497-1503.
36. Kamotani, Y.; Bersano-Begey, T.; Kato, N.; Tung, Y.-C.; Huh, D.; Song, J. W.; Takayama S. *Biomaterials*, **2008**, *29*, 2646-2655.
37. Gu, W.; Chen, H.; Tung, Y.-C.; Meiners, J.-C.; Takayama, S. *Appl. Phys. Lett.*, **2007**, *90*, 033505.

Downloaded by UNIV OF DELAWARE MORRIS LIB on June 28, 2012 | http://pubs.acs.org
Publication Date (Web): December 18, 2009 | doi: 10.1021/bk-2009-1030.ch011

Downloaded by COLUMBIA UNIV on June 29, 2012 | http://pubs.acs.org
Publication Date (Web): December 18, 2009 | doi: 10.1021/bk-2009-1030.ch012

## Chapter 12

# Nanoparticle Synthesis in Ionic Liquids

**Anja-Verena Mudring, Tarek Alammar, Tobias Bäcker, and Kai Richter**

**Anorganische Chemie I – Festkörperchemie und Materialien, Ruhr-Universität Bochum, D-44780 Bochum, Germany**

Ionic liquids are able to offer outstanding properties as media for the synthesis of nanoparticles. The low surface tension of many ionic liquids leads to high nucleation rates and, in consequence, to small particles. The ionic liquid itself can act as an electronic as well as a steric stabiliser and depress particle growth. As highly structured liquids, ionic liquids have a strong effect on the morphology of the particles formed.

Three synthetic techniques make special use of the unique properties that ionic liquids offer when compared to conventional VOCs (volatile organic solvents). Firstly, direct microwave synthesis can be used because of the ionic character and high polarisability of the synthetic medium. Secondly, physical vapour deposition (PVD) under high vacuum becomes possible due to the low vapour pressure of some ionic liquids. In order to make full use of the possibilities that ionic liquids offer we have designed a set of reducing ionic liquids which can be used as direct reaction partners for the generation of metal nanoparticles. Thirdly, sonochemistry has proven an especially powerful route towards oxidic nanomaterials.

In Ionic Liquids: From Knowledge to Application; Plechkova, N., et al.;
ACS Symposium Series; American Chemical Society: Washington, DC, 2010.

## Nanoparticles and Ionic Liquids

Bringing materials to the nanoscale has been occupying chemists and materials scientists, as well as engineers, for quite some time *(1)*. When a material is brought to the nanoscale, its chemical and physical properties can change significantly. These size-dependent properties make nanostructures of various compounds extraordinarily valuable.

In recent years, ionic liquids have also been discovered to be excellent media for the preparation and stabilisation of nanoparticles *(2)*. Even though this kind of nanochemistry in ionic liquids is still in its infancy, many signs imply that it is an important emerging field with a huge potential, because ionic liquids offer many advantages for the synthesis of inorganic nanomaterials:

1. Ionic liquids can be designed to be good solvents for inorganic salts which are the starting materials to nanoparticle synthesis.
2. Ionic liquids can be chosen in such a way that inorganic syntheses with polar/ionic starting materials can be carried out under ambient and anhydrous or water-poor conditions, thereby suppressing the undesired formation of hydroxides or oxyhydrates.
3. Although polar, ionic liquids can have low interfacial tensions. Since low interfacial tensions result in high nucleation rates, very small particles can be generated which undergo Ostwald ripening to a small degree.
4. As they consist of cations and anions, ionic liquids can form a protective electrostatic shell around nanoparticles to prevent agglomeration. In addition, the resemblance of many ionic liquids to well-known surface active substances is clear and ionic liquids may, in addition, stabilise nanoparticles through coordination *via* the cation or anion (ionic or covalent bonds). In particular, cations and anions with long or bulky alkyl chains can also sterically stabilise nanoparticles in solution.
5. High dispersion force components of the surface tension enhance the differences between the interfacial energies of different crystal faces, and thus morphology control is ensured in these media.
6. Ionic liquids may form extended hydrogen-bonded systems in the liquid state; in this sense, ionic liquids may be regarded "supramolecular" solvents. This special quality can be utilised in the synthesis of extended ordered nanoscale structures, or for morphology control through the templating effect of various ionic liquids.
7. Properties and property combinations of ionic liquids can be tuned through the respective cation/anion combination, for example hydrophilic/hydrophobic nature, gas solubilities, the extent of hydrogen bonding, or mesogenic character.
8. Ionic liquids can become a reactive agent, *e.g.* hydroxyl-functionalised ionic liquids can act both as a reducing agent, solvent and nanoparticle stabiliser.
9. Depending on the chosen ionic liquid, it is expected that the synthesised nanoparticles can be tailored to be either soluble in water (high charge concentration, polar functionalities like carboxyl groups, *etc.*) or be hydrophobic solvents (long alkyl chains, perfluorinated moieties).

Downloaded by COLUMBIA UNIV on June 29, 2012 | http://pubs.acs.org
Publication Date (Web): December 18, 2009 | doi: 10.1021/bk-2009-1030.ch012

10. The extremely low vapour pressure and non-flammability of most ionic liquids makes reactions at elevated temperatures and under vacuum possible and safe, which are impossible to conduct in conventional solvents.
11. Although ionic liquids are not generally green – and one has to be aware that there exist about $10^{18}$ possible cation/anion combinations for potential ionic liquids *(3)* – they can be designed in such a way that the twelve principles of green chemistry developed by Anastas and Warner *(4)* are followed. Relevant green aspects include not only the volatility, non-flammability, non-corrosiveness and low toxicity, but, most importantly, the use of any auxiliary substances such as solvents, separation agents, *etc.*, should be unnecessary.

Downloaded by COLUMBIA UNIV on June 29, 2012 | http://pubs.acs.org
Publication Date (Web): December 18, 2009 | doi: 10.1021/bk-2009-1030.ch012

The developments in the use of ionic liquids as reaction media for inorganic nanomaterials have so far mainly focussed on (1) the intrinsic high charge and polarisability of the ionic liquid to create electrostatic and steric stabilisation for nanoparticles and to favour phase transfer of the nanoparticles from water to water-immiscible solvents, and (2) using the pre-organised structure of the ionic liquid as a template for porous inorganic nanomaterials. Transition metal nanoparticles, such as iridium, rhodium, palladium, platinum and gold nanoparticles, have been generated by standard reduction methods, where the ionic liquid acts both, as a (co-)solvent and stabiliser for these nanoparticles *(5)*. Moreover, alloy nanoparticles, such as $CoPt_3$, have been prepared *via* thermolysis in ionic liquids *(6)*. However, in the majority of cases, ionic liquids were used together with co-solvents which significantly alter the properties of the solvent compared to the neat ionic liquid. In our work, we strive for make full use of the unique possibilities that ionic liquids offer compared to conventional volatile organic solvents, and aim at carrying out the reactions in neat ionic liquids with the least possible number of additional chemicals. This reduces the number of parameters that influence the reaction and gives an understanding of the reaction mechanism, and not only allows fine-tuning of the reaction parameters (as well as the ionic liquid itself), but also permits formation of purer, less contaminated compounds.

## Nanoparticle Synthesis *via* Physical Vapour Deposition

As many ionic liquids have negligible vapour pressure, they can be handled under high vacuum conditions, even at elevated temperatures. This allows employment of PVP (physical vapour deposition) methods to prepare nanoparticles *(7)*. The experimental setup that we use in our laboratory is a commercial evaporation apparatus (Torrovap TVP 800) which consists essentially of a rotating reaction flask in which either a resistive or electron beam evaporation source can be mounted (Figure 1). The system is based on the experimental experience of Timms, Skell, Klabunde and Green for the synthesis of low-valent main-group halides and transition metal arene complexes, and the work of Ozin, Burdett and Turner in matrix cryochemistry *(8)*. The reaction chamber is maintained under high vacuum by a high speed pump assembly (rotary oil pump combined with an oil diffusion pump). A quantity of the respective ionic liquid is introduced into the rotating reaction vessel, thereby creating a liquid film over the inside wall of the flask.

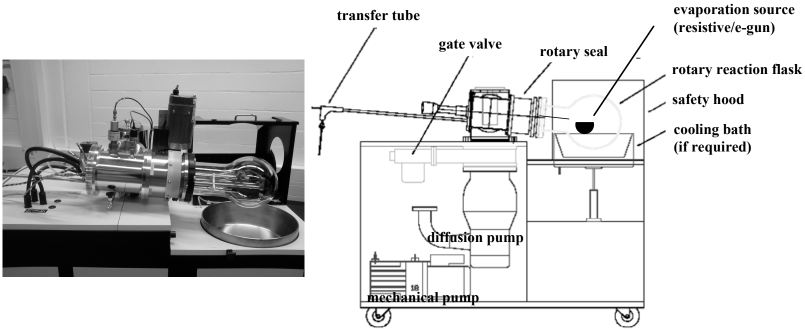

*Figure 1. Experimental setup for physical vapour deposition of substrates into ionic liquids.*

After the system has been evacuated, a metal, an intermetallic phase, or a metal salt is evaporated either *via* resistive heating from a molybdenum or tungsten container (300 A source) or *via* an electron gun (6.0 kW) and condensed into the ionic liquid film. Resistive heating is used for evaporation in the temperature regime of 25-2000 °C, whereas electron beam vaporisation is best suited for the high temperature region (1000-2500 °C). Evaporation *via* an electron beam has the advantage that it is a containerless method and can be applied whenever the reaction of the materials to be evaporated with the container might become a problem. The electron beam can be focused on the central portion of the sample, and only the inner portion of the sample is first melted and then evaporated. This method can be used for large scale vaporisation (kg $h^{-1}$) of metal halides, carbides, or oxides, as well as refractory metals and their alloys. Fortunately, many physicochemical and physical data (such as evaporation conditions, boiling points under vacuum or gas phase compositions) are well-known from matrix-isolation spectroscopic studies. A microbalance quartz crystal is used to monitor the progress of evaporation. The naked particles react with ionic liquid ions faster than they react with each other to form a bulk product. As the ionic liquid is present in large quantities, formation of larger particles can be prevented by blocking the growth and by disturbing the film formation through flask rotation. The resulting reaction product can then be transferred anaerobically from the reaction flask for subsequent examination and experiments. To our knowledge, this described PVP method has never been applied to ionic liquids.

Figure 2 shows a TEM (transmission electron microscopy) micrograph of copper particles in the ionic liquid 1-butyl-3-methylimidazolium hexafluorophosphate, [$C_4$mim][$PF_6$], as a typical result of metal evaporation experiments. These particles have been obtained by evaporating copper under thermodynamic equilibrium in high vacuum into the ionic liquid. The particles have a narrow size distribution of around 3 nm. Interestingly, the single copper

Downloaded by COLUMBIA UNIV on June 29, 2012 | http://pubs.acs.org
Publication Date (Web): December 18, 2009 | doi: 10.1021/bk-2009-1030.ch012

particles form a quite regular assembly on the TEM grid. Frequently, areas which are strongly reminiscent of a 2D-ordered close-packing of spheres can be detected. However, the copper particles never come closer than 20 nm. This might be indicative of the formation of charged, structured ionic liquid regions around the particle that lead to repulsion of the single nanoparticles.

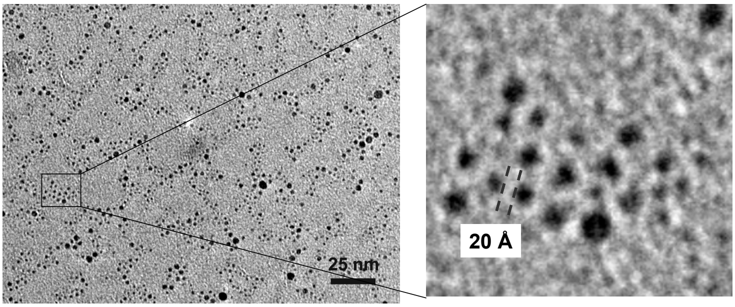

*Figure 2. Transmission electron microscopic micrograph of copper particles in [$C_4$mim][$PF_6$] synthesised via physical vapour deposition.*

It is not only possible to deposit the naked metal into an ionic liquid, but metal nanoparticles can also deposited onto materials dispersed in the ionic liquid. The formation of Cu/ZnO nanocomposites may serve as an example. First, ZnO nanorods were dispersed in [$C_4$mim][$NTf_2$] (1-butyl-3-methylimidazolium bis{(trifluoromethyl)sulfonyl}amide and then copper was evaporated into this dispersion similar to the experiment described above. Astonishingly, TEM investigations (Figure 3) show only a few free standing copper particles in the solution. Most of the particles are found on the surface of the ZnO nanorods. Again, the size distribution is quite narrow, around 3-4 nm. We are currently exploring the nature of the Cu/ZnO interactions.

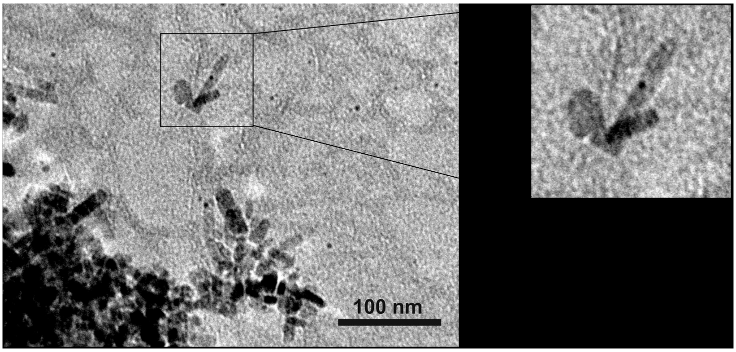

*Figure 3. Transmission electron micrograph of a sample where copper was evaporated into a dispersion of ZnO nanorods in [$C_4$mim][$NTf_2$].*

Downloaded by COLUMBIA UNIV on June 29, 2012 | http://pubs.acs.org
Publication Date (Web): December 18, 2009 | doi: 10.1021/bk-2009-1030.ch012

In summary, PVD is an extremely powerful way for synthesising neat compounds compared to conventional nanoparticle preparation in solution. Firstly, no other stabilising agents other than the ionic liquid itself are needed. Secondly, no other reactants, such as a reducing agent (or its reaction product), will be present in solution.

## Microwave Synthesis

From the perspective of microwave chemistry, one of the key advantages of ionic liquids is the presence of large ions with high polarisability and conductivity. Therefore, ionic liquids are good media for absorbing microwaves, leading to high heating rates which results in a high formation rate of nuclei (nanoparticles!) *(9)*. Short reaction times ranging from seconds to a few minutes can be achieved. This gives ionic liquids an additional advantage over conventional solvents in the synthesis of inorganic nanomaterials. In contrast to the conventional high temperature reactions which are often employed for the synthesis of inorganic materials and which preclude the formation of metastable and low-temperature phases, the temperature impact can be carefully controlled *via* microwave irradiation – microwave synthesis at sub-ambient temperatures can even be achieved. Control over particle size can be achieved by reaction temperature and time as well as reactant concentration and choice of the ionic liquid. For our experiments, we have use a CEM Discover microwave system. It has a circular single mode cavity which allows focussing the microwaves on the reactants in such a way that the sample is in a homogeneous, highly dense microwave field. In consequence, heating spreads uniformly through the sample which should lead to a narrow nanoparticle size distribution.

Ionic liquids can even be designed to act as a metal reductant *(10)*. In order to access nanostructured coin metals, and a set of different highly reducing ionic liquids was synthesised based on the choline cation and its derivatives in combination with methanoate or bis{(trifluoromethyl)sulfonyl}amide as the counter anion (Figure 4). Potentially, the hydroxyl group, as well as the methanoate anion, can act as reductant.

Downloaded by COLUMBIA UNIV on June 29, 2012 | http://pubs.acs.org
Publication Date (Web): December 18, 2009 | doi: 10.1021/bk-2009-1030.ch012

Downloaded by COLUMBIA UNIV on June 29, 2012 | http://pubs.acs.org
Publication Date (Web): December 18, 2009 | doi: 10.1021/bk-2009-1030.ch012

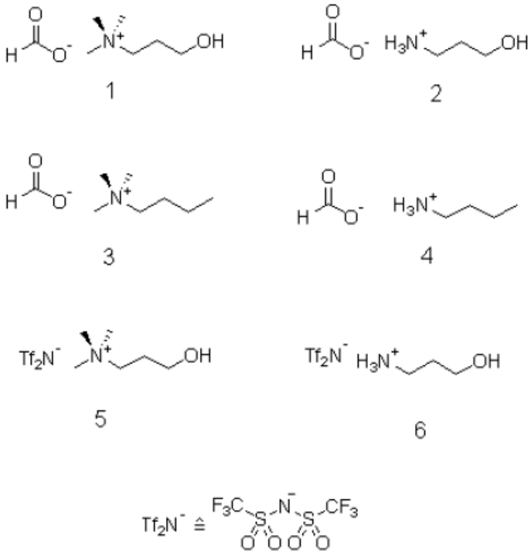

*Figure 4. Ionic liquids as reducing agents for coinage metal salts.*

2-Hydroxyethylammonium methanoate proved to be the most powerful reducing agent amongst the investigated ionic liquids, as it is able to reduce copper, silver and gold salts to the metal. Figure 5 shows the result of heating a solution of copper(II) pentane-2,4-dionate in 2-hydroxyethylammonium methanoate for five minutes at 80 °C by microwave irradiation under argon. A brownish-yellow solution of a copper colloid is formed; as soon as the sample is exposed to air, the copper particles are oxidised, which can be monitored by the colour change to green.

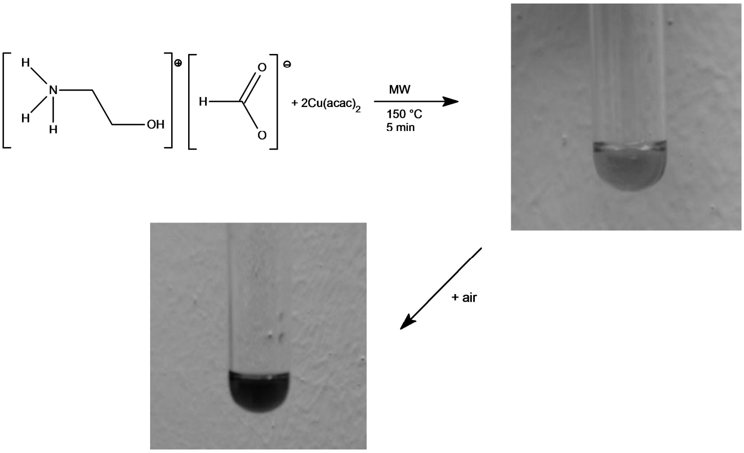

*Figure 5. Synthesis of a colloidal copper solution from copper(II) pentane-2,4-dionate and 2-hydroxyethylammonium methanoate by microwave irradiation.*

Similar reaction procedures with silver(I) ($Ag[NO_3]$) and gold(III) ($K[AuCl_4]$) salt solutions resulted (for silver) in the formation of large monoliths with a high surface area *(11)* and (for gold) in the formation of films. Analysis of the reaction by-products showed that the methanoate anion acts as the reducing agent in all of these reactions. However, if 2-hydroxyethyl-*N,N,N*-trimethylammonium bis{(trifluoromethyl)sulfonyl}amide is used as a reducing agent for silver and gold salts, the formation of small particles could be achieved. Alas, as can be grasped from the transmission electron micrographs, the particle size distribution in the case of silver is wide. For the more reactive gold, the formation of large particles which might result form the coalescence of smaller particles under the reaction conditions, is observed.

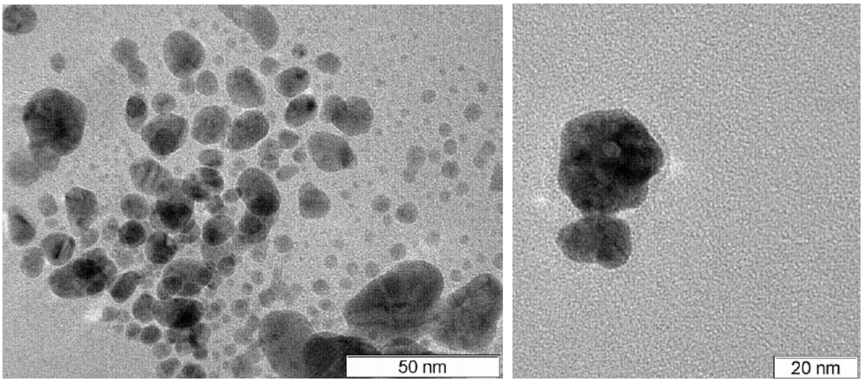

*Figure 6. Silver (left) and gold (right) particles derived from microwave synthesis in 2-hydroxyethyl-N,N,N-trimethylammonium bis{(trifluoromethyl)sulfonyl}amide.*

## Ultrasound Synthesis

Sonochemical synthesis can be an alternative means to the above mentioned synthetic methods. It has been used in the preparation of many materials such as metal, oxide, sulfide, and carbide nanoparticles, and has recently become popular in combination with ionic liquids as the reaction medium *(12)*. However, for the sonochemical synthesis of ZnO nanostructures, so far only dilute aqueous solutions of ionic liquids were used, which did not use the ionic liquid as a solvent and reaction medium, but rather as a stabiliser and surface active substance *(13)*. However, direct synthesis of ZnO nanorods from $Zn(CH_3COO)_2.2H_2O$ and NaOH in the neat ionic liquid $[C_4mim][NTf_2]$ can be achieved without further use of organic solvents, water, surfactants or templates, by irradiating the reaction mixture with ultrasound in a conventional ultrasonic bath (USC200T, VWR International; 45 KHz and 60 W) for 12h *(14)*. The selected area electron diffraction (SAED) pattern in Figure 7 (right) shows unambigiously the formation of crystalline, hexagonal ZnO. The TEM images (Figure 7) reveal that the sample is composed of crystalline nanorods of about 20 nm in diameter and 50-100 nm in length.

Downloaded by COLUMBIA UNIV on June 29, 2012 | http://pubs.acs.org
Publication Date (Web): December 18, 2009 | doi: 10.1021/bk-2009-1030.ch012

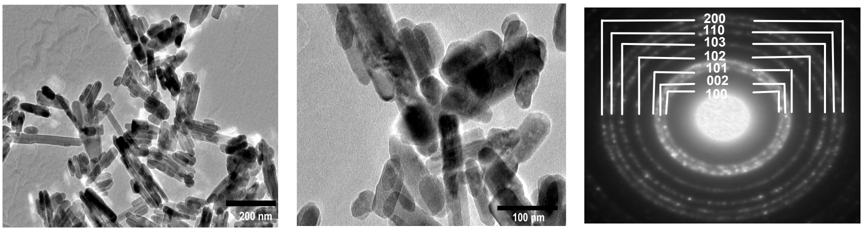

*Figure 7. TEM images of ZnO powder samples (left and middle) and an SAED diffraction pattern of a particle (right).*

Downloaded by COLUMBIA UNIV on June 29, 2012 | http://pubs.acs.org
Publication Date (Web): December 18, 2009 | doi: 10.1021/bk-2009-1030.ch012

The UV-Vis absorption spectrum of the ZnO nanorods shows an absorption peak at about 365 nm from which a band gap of 3.31 eV can be derived. This is smaller than that of the bulk material *(15)*. The room temperature photoluminescence spectrum of the ZnO nanorods shows the typical strong green-yellow emission with the peak maximum at 563 nm. Dinitrogen adsorption-desorption measurements give a specific surface area of a typical ZnO nanorod sample of 49.93 $m^2 g^{-1}$.

Nanostructured lanthanide(III) oxides can be easily synthesised by a similar reaction procedure from their (hydrous) ethanoates. Figure 8 shows a typical TEM micrograph of as-prepared $Tb_2O_3$ nanospindles. The particles are about 40 nm in diameter and 200-800 nm in length.

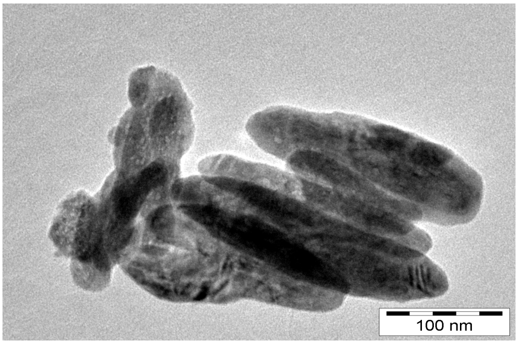

*Figure 8. TEM image of $Tb_2O_3$ nanospindles.*

Figure 9 shows an emission spectrum of the $Tb_2O_3$ nanospindles upon excitation with $\lambda_{ex}$=395 nm. The narrow band can be assigned to the typical intraconfigurational f-f transitions *(16)*. The most intense peak is located at 543 nm corresponding to the $^5D_4 \rightarrow {}^7F_5$ transition. Due to the good colour purity of the obtained samples, this synthetic route may prove to be valuable for the easy and fast preparation of phosphors.

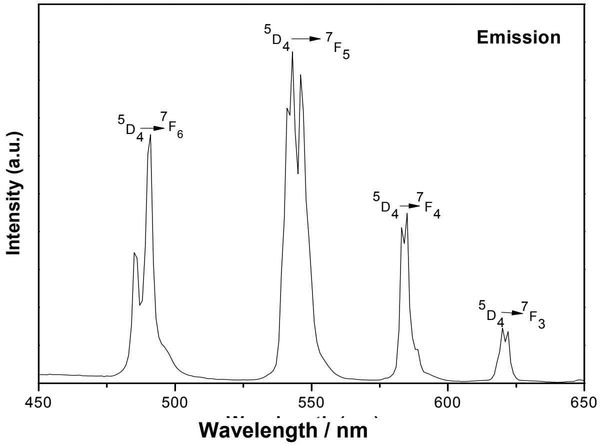

*Figure 9. Photoluminescence spectrum of $Tb_2O_3$ nanospindles.*

## Green Aspects of Nanoparticle Synthesis in Ionic Liquids

The three different techniques presented here are fast and efficient ways to synthesise nanomaterials from ionic liquids. All three techniques make use of the unique properties ionic liquids can offer as reaction media. As molten salts, they not only provide an excellent environment for the synthesis and stabilisation of nanoparticles (as mentioned before), but it is possible to work at ambient temperature under high vacuum due to the virtually non-existent vapour pressure of some ionic liquids. As salts composed of highly polarisable ions, ionic liquids couple in an excellent way to microwave radiation and finally, as chemically robust media of tuneable viscosity, sonochemistry is possible. In addition, it has been shown that ionic liquids can be designed in such a way that they serve not only as a reaction medium but also as a reaction partner. Altogether, it can be stated that nanoparticle syntheses comply with many of the twelve principles of Green Chemistry, as summarised by Anastas and Warner *(4)*. The synthetic routes are atom and energy efficient: due to the fewer reaction components involved, they are much cleaner and less waste is produced. The ionic liquids presented here are indeed inherently safer materials for nanoparticle synthesis.

Downloaded by COLUMBIA UNIV on June 29, 2012 | http://pubs.acs.org
Publication Date (Web): December 18, 2009 | doi: 10.1021/bk-2009-1030.ch012

## Acknowledgements

This research was supported by the Deutsche Forschungsgemeinschaft within the framework of the collaborative research program SFB 558 “Substrate-catalyst interaction in heterogeneous catalysis” and the European Research Starting Grant “EMIL – Exceptional Materials from Ionic Liquids”. AVM thanks the Fonds der Chemischen Industrie for a Chemiedozenten-Stipendium.

## References

1. Ozin, G. A.; Arsenault, A.C.; Cademartiri, L *Nanochemistry: A Chemical Aproach,* Royal Society of Chemistry, 2nd Ed. 2008.
2. Dupont, J.; Fonseca, G. S.; Umpierre, A. P.; Fichtner, P. F. P.; Teixeira, S. R., *J. Am. Chem. Soc.* **2002**, *124*, 4228; Huang, J.; Jiang, T.; Gao, H. X.; Han, B. X.; Liu, Z. M.; Wu, W. Z.; Chang, Y. H.; Zhao, G. Y., *Angew. Chem. Int. Ed.* **2004**, *43*, 1397; Antonietti, M.; Smarsly, B., Zhou, Y., *Angew. Chem. Int. Ed.* **2004**, *43*, 4228; Miao, S. D.; Liu, Z. M.; Han, B. X.; Huang, J.; Sun, Z. Y.; Zhang, J. L.; Jiang, T., Ru *Angew. Chem. Int. Ed* **2006**, *45*, 266; Zhou, Y., *Curr. Nanosc.* **2005**, *1*, 35.
3. Holbrey, J. D.; Seddon, K. R. *Clean Products and Processes*, **1999**, *1*, 223.
4. Anastas, P. T.; Warner, J. C.; *Green Chemistry: Theory and Practice*, Oxford University Press, New York, **1998**.
5. Fonseca, G. S.; Scholten, J. D.; Dupont, J., *Synlett* **2004**, 1525; Fonseca, G. S.; Machado, G.; Teixeira, S. R.; Fecher, G. H.; Morais, J.; Alves, M. C. M.; Dupont, J., *J. Coll. Int. Sci.* **2006,** 301, 193; Fonseca, G. S.; Umpierre, A. P.; Fichtner, P. F. P.; Teixeira, S. R.; Dupont, J., *Chem. Eur. Journal* **2003**, *9*, 3263; Mu, X. D.; Evans, D. G.; Kou, Y. A., *Cat. Lett.* **2004,** 97, 151; Scheeren, C. W.; Machado, G.; Dupont, J.; Fichtner, P. F. P.; Texeira, S. R., *Inorg. Chem.* **2003,** *42*, 4738; Itoh, H.; Naka, K.; Chujo, Y., *J. Am Chem. Soc.* **2004,** *126*, 3026; Scheeren, C. W.; Machado, G.; Teixeira, S. R.; Morais, J.; Domingos, J. B.; Dupont, J., *J. Phys. Chem. B* **2006**, *110*, 13011; Kim, K. S.; Demberelnyamba, D.; Lee, H., *Langmuir* **2004**, *20*, 556; Dahl, J.A.; Maddux, B.L.S.; Hutchinson, J.E. *Chem. Rev.* **2007**, *107*, 2228.
6. Wang, Y.; Yang, H., *J. Am. Chem. Soc.* **2005,** *127*, 5316.
7. For PVP synthesis of metal nanoparticles *via* sputtering under atmospheric pressure see: Torimoto, T., Okazaki, K., Kiyama, T., Hikahara, K., Tanaka, N., Kuwabata, S., *Appl. Phys. Lett.*, **2006,** *89*, 243117.
8. Timms, P.L, *Angew. Chem.* **1975**, *87*, 295; Schmidt, E., Klabunde*,* K.J., *Metal Vapor Synthesis of Transition Metal Compounds* in: King I., Bruce, R. *Encyclopaedia of Inorganic Chemistry*, John Wiley & Son, Chichester, New York, **1994**; Zenneck, U., *Angew. Chem.* **1990**, *102*, 171.
9. MAIL methods which make use of adding a small amount of ionic liquid to an conventional solvent to enhance its susceptibility for microwave reaction shall not be explored! *Cf.* Zhu, Y.-J., Wang, W.-W., Hu, X.-L.,

Downloaded by COLUMBIA UNIV on June 29, 2012 | http://pubs.acs.org
Publication Date (Web): December 18, 2009 | doi: 10.1021/bk-2009-1030.ch012

*Angew. Chem. Int. Ed.* **2004**, *43*, 1410; Buehler, G.; Feldmann, C; *Angew. Chem. Int. Ed.* **2006**, *45*, 4864.

10. Kim, K. S.; Choi, S.; Cha, J. H.; Yeon, S. H.; Lee, H., *J. Mater. Chem.* **2006**, *16*, 1315.
11. Richter, K.; Bäcker, T.; Mudring, A.-V., *Chem. Commun.* **2009**, in press.
12. Flannigan, D. J.; Hopkins; S.D.; Suslick, K.S. *J. Organomet. Chem.* **2005**, *690*, 3513.
13. Hou, X.; Zhou, F.; Sun, Y.; Liu, W. *Mater. Lett.* **2007**, *61,* 1789.
14. Alammar, T. ; Mudring, A.-V. *Mater. Lett.* **2009**, in press.
15. Cao, J. ; Wang, J. ; Fang, B. ; Chang, X. ; Zheng, M.; Wang, H., *Chem. Lett.* **2004** , *33*, 10.
16. Dieke, G.H. *Spectra and energy levels of rare earth ions in crystals*, Interscience Publishers, New York, **1968**; Carnall, W.T.; Crosswhite, H.M.; Crosswhite, H. *Energy level structure and transition probabilities in the spectra of trivalent lanthanides in* $LaF_3$. Special Report **1977** (Argonne, IL: Chemistry Division, Argonne National Laboratory).

Downloaded by COLUMBIA UNIV on June 29, 2012 | http://pubs.acs.org
Publication Date (Web): December 18, 2009 | doi: 10.1021/bk-2009-1030.ch012

Downloaded by PENNSYLVANIA STATE UNIV on June 28, 2012 | http://pubs.acs.org
Publication Date (Web): December 18, 2009 | doi: 10.1021/bk-2009-1030.ch013

## Chapter 13

# Influences of Side Chain Length of 1-Alkyl-3-methylimidazolium Bromide on Silica Saturation

**Xin Sun and Jennifer L. Anthony**[*]

**Department of Chemical Engineering, Kansas State University, Kansas, U.S.A.**

The saturation limits of fumed silicon dioxide in six 1-alkyl-3-methylimidazolium bromide ionic liquids [$C_n$mim]Br ($n = 2, 4, 6, 8, 10$ or 12) were measured and compared in order to get the influence of side chain length on silica saturation solubility. A maximum saturation point was observed when the alkyl chain is eight carbon atoms long. This trend is explained in terms of cation - anion interactions in ionic liquids, such as van der Waals forces, hydrogen bonding and electrostatic forces. This result is then comparable to the side chain's influence on the melting points of corresponding ionic liquids.

## Introduction

Room temperature ionic liquids, a group of novel solvents, have received significant attention in the last twenty years. In recent work, ionic liquids have been utilised in the synthesis of molecular sieves, taking advantage of the ionic liquid thermal stability and negligible vapour pressure *(1-3)*. A molecular sieve is a material containing tiny pores of a precise and uniform size. They can be used as absorbents, desiccants, water softeners, reaction media, *etc. (4-7)*. Molecular sieves are commonly synthesised hydrothermally, which means that in order to get crystals of molecular sieves, the mixture of precursors, water, structure directing agent, and mineralising agent needs to be heated at an elevated temperature *(8,9)*. A challenge with this method results since the reaction temperature is typically above the boiling point of the solvent (*i.e.* water), thus necessitating the use of a pressurised reaction vessel. However, if ionic liquids are substituted as the solvents, molecular sieves can be synthesised at ambient pressure. Morris and coworkers have published several papers on the synthesis of aluminophosphates (AlPOs), a group of molecular sieves, in imidazolium-based ionic liquids *(2,3,10,11)*. In these studies, the ionic liquids not only served as the reaction solvent, but the ionic liquids also served as structure directing agents (SDAs), which play a significant role in determining the final zeolite structure. These systems generated several new framework structures. The successful synthesis of these AlPOs suggests the possibility of synthesising silica-based zeolites, another group of molecular sieves, in ionic liquids.

Downloaded by PENNSYLVANIA STATE UNIV on June 28, 2012 | http://pubs.acs.org
Publication Date (Web): December 18, 2009 | doi: 10.1021/bk-2009-1030.ch013

It has been only in the recent literature that researchers are beginning to report applications of ionic liquids with silica-based advanced materials. For example, Itoh and coworkers developed an electrochemical light-emitting gel using a ruthenium complex, an ionic liquid, and fumed silica nanoparticles. The gel produced can be used in flexible displays, three-dimensional displays, and other lighting applications *(12)*. Other groups have synthesised silica xerogels with highly distinct morphologies in the presence of ionic liquids *(13,14)*. Our group recently reported the synthesis of porous silicate materials in the presence of ionic liquids and similar molten salts *(15)*. Watanabe and coworkers have been one of the only groups to consider the behaviour of silica particles in ionic liquids *(16,17)*. They investigated colloidal stability and rheology of the dispersions of hydrophilic and hydrophobic silica nanoparticles in different ionic liquids *(16,17)*. However, there is still a lack of systematic studies investigating the saturation solubility of silica as a function of ionic liquid properties. In this work, we report results on the solubility of fumed silica particles in ionic liquids and the influence of cation alkyl-chain length on the solubility.

## Experimental

### Ionic liquids

The ionic liquids used in this paper are of the family 1-alkyl-3-methylimidazolium bromide [$C_n$mim]Br where $n = 2, 4, 6, 8, 10$, or 12. Their names and abbreviations are listed in Table 1. These ionic liquids were selected as both [$C_2$mim]Br and [$C_4$mim]Br have been successfully used in the synthesis of zeolitic molecular sieves *(2,3,10)*.

Each [$C_n$mim]Br was synthesised in the lab according to methods reported in the literature (18). This typically involves reacting 1-methylimidazole and 1-bromoalkane in ethanenitrile for two to eight days, and drying the mixture for another three days. All of the reactants were distilled before the reaction to ensure the purity of ionic liquids. The products were passed through columns of granular activated carbon, and also an acidic activated aluminium oxide column, to remove colour. Before each trial, the ionic liquid was dried for 6-12 h at 60–100 °C to reduce the water content below 200 ppm, which was tested by Karl-Fischer titration.

**Table 1 Ionic liquids used in this study**

| *Name of ionic liquids* | *Abbreviation* |
|---|---|
| 1-ethyl-3-methylimidazolium bromide | [$C_2$mim]Br |
| 1-butyl-3-methylimidazolium bromide | [$C_4$mim]Br |
| 1-hexyl-3-methylimidazolium bromide | [$C_6$mim]Br |
| 1-octyl-3-methylimidazolium bromide | [$C_8$mim]Br |
| 1-decyl-3-methylimidazolium bromide | [$C_{10}$mim]Br |
| 1-dodecyl-3-methylimidazolium bromide | [$C_{12}$mim]Br |

Downloaded by PENNSYLVANIA STATE UNIV on June 28, 2012 | http://pubs.acs.org
Publication Date (Web): December 18, 2009 | doi: 10.1021/bk-2009-1030.ch013

### Silica source

Syloid 63FP (from GRACE Davison Company) was the source of silica used in this work. Syloid 63 is pure, fumed silicon dioxide and has been used as the silica source for the hydrothermal synthesis of silica-based zeolites. Silica particles were dried at 100 °C for 2 h and ground into a fine powder. The average diameter of single silica particle is 9 µm, which is confirmed through SEM analysis.

### Determination of the saturation point

The saturation point of the silica in the ionic liquid was determined gravimetrically by slowly adding the silicon dioxide powder in approximately 0.05 g increments to the initial 5 g sample of ionic liquid. The silica was mixed until fully dissolved in the ionic liquid (*i.e.* became a homogenous clear solution) before continuing with subsequent additions. The viscosity of the solution would increase until the saturation point was reached and the $SiO_2$/ionic liquid mixture became a gel. At this point, any additional silica would just remain in a second solid phase.

All measurements were made at 80 °C, which is above the melting points for all of the ionic liquids used.

## Results and discussion

### Solution behaviour

The saturation solubility of silicon dioxide particles was measured in six ionic liquids. Table 2 summarised the results in terms of mole fraction and weight percent. In each case, a rather large amount of silicon dioxide could be added to the ionic liquid before the saturation/gelation point was reached. The largest amount of silica could be added to [$C_8$mim]Br: a ratio of 3.58 moles silicon dioxide to every 1 mole ionic liquid (equivalent to 44 wt% $SiO_2$ in [$C_8$mim]Br). This ability of ionic liquids to stabilise $SiO_2$ particles in such high concentrations bodes well for the use of ionic liquids in the synthesis of silica-based materials. Preliminary characterisation efforts on dilute $SiO_2$/ionic liquid solutions dynamic light scattering indicate that the size of the silica particles usually remains unchanged; however these investigations are still ongoing. These early DLS results suggest that these saturated gels are stable colloid systems.

**Table 2. Silica saturation solubility result.**

| *Ionic liquid* | *Mole ratio of silica to IL* | *Mole %* | *Weight % of silica* |
|---|---|---|---|
| [$C_2$mim]Br | 1.95 | 66.10 | 40.16 |
| [$C_4$mim]Br | 2.65 | 72.60 | 42.09 |
| [$C_6$mim]Br | 3.10 | 75.61 | 42.98 |
| [$C_8$mim]Br | 3.58 | 78.17 | 43.88 |
| [$C_{10}$mim]Br | 3.05 | 75.31 | 37.68 |
| [$C_{12}$mim]Br | 1.81 | 64.41 | 24.72 |

## Influence of side-chain length

The solubilities of silica particles in bromide-based ionic liquids with different cationic side-chain lengths were tested to elucidate the influence of the cation. The relationship is shown in Figure 1. As the alkyl chain increases from an ethyl group to an octyl group, the amount of silica that could be added increased from 66 to 78 mol %. Then, increasing the chain length further resulted in a decrease in affinity for the $SiO_2$ particles, reaching 64 mol% at a chain length of twelve carbons.

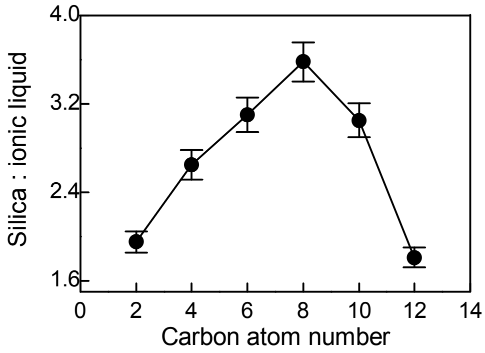

*Fig. 1. Relationship between silica molar saturation solubility and number of carbon atoms in the cationic side chain at 80 °C*

Downloaded by PENNSYLVANIA STATE UNIV on June 28, 2012 | http://pubs.acs.org
Publication Date (Web): December 18, 2009 | doi: 10.1021/bk-2009-1030.ch013

Downloaded by PENNSYLVANIA STATE UNIV on June 28, 2012 | http://pubs.acs.org
Publication Date (Web): December 18, 2009 | doi: 10.1021/bk-2009-1030.ch013

### Comparison to trends seen with melting points

The observation of an optimum solubility when the alkyl chain contains eight carbons is similar to trends previously observed with ionic liquid melting points *(19-26)*. The reported melting point values for the [$C_n$mim]Br family are summarised in Table 3. Figure 2 illustrates the trends as a function of chain length. It has been observed that the same intermolecular interactions governing the pure ionic liquid melting points are affecting the ionic liquid's affinity for the $SiO_2$ particles. Melting points of 1-alkyl-3-methylimidazolium ionic liquids are mainly influenced by the packing ability of cations and anions, which is a function of the cation symmetry *(27,28)*. Symmetric cations and anions facilitate better crystal packing, leading to stronger cation-anion interaction and thus higher melting points. When the alkyl group contains only one or two carbon atoms, the imidazolium ring is symmetrical and the melting points are higher for [$C_1$mim]Br and [$C_2$mim]Br. However, with the increase in alkyl chain length, the symmetry is broken and the melting points are lower. When the chain is longer than eight carbon atoms, researchers attribute the increase in melting point to the increase of van der Waals forces *(29)*. The increased van der Waals force between cations and anions also leads to smaller silica affinity in ionic liquids after the side chain length is eight carbons long.

**Table 3. Observed melting points of [$C_n$mim]Br**

| *Ionic liquids* | *Melting point observed* | *Lit.* |
|---|---|---|
| [$C_2$mim]Br | 76.9 | (*19*) |
| [$C_4$mim]Br | 69 | (*20*) |
| [$C_6$mim]Br | -54.9 | (*21*) |
| [$C_8$mim]Br | -61.9 | (*21*) |
| [$C_{10}$mim]Br | 10.5 | (*21*) |
| [$C_{12}$mim]Br | 39.7 | (*22*) |

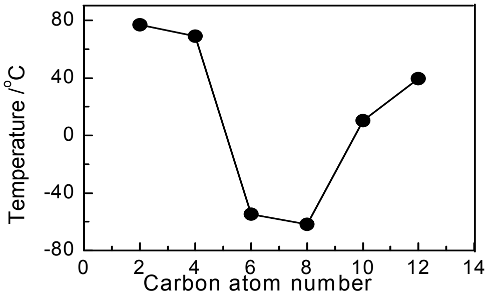

*Figure 2. Melting points of 1-alkyl-3-methylimidazolium bromides.*

## Intermolecular forces driving $SiO_2$ solubility

The relative solubility of the silica particles in the ionic liquids tested correlates with the degree of interactions between the cation and anion expected within pure ionic liquids (exhibited by the melting point). The stronger the cation/anion interactions are, the lower the observed solubility of silica particles becomes. The primary intermolecular interactions in ionic liquid systems are electrostatic forces, hydrogen bonding and van der Waals forces *(30-32)*. The electrostatic forces occur between the negative charge of anion and the positive charge on the imidazolium ring. Hydrogen bonding can occur with the hydrogen on the carbon between the two nitrogen atoms in the cation. This hydrogen has been shown to be acidic due to the electron-withdrawing effect of the two nitrogen atoms in the imidazolium ring; it can form strong hydrogen bonds with halide ions, such as bromide and chloride *(33-35)*. The final significant category of intermolecular interactions includes the van der Waals forces, which can occur between cation and anion, the cation and cation, and the ionic liquid and solute.

When the carbon number of the side chain increases from two to eight, the silica solubility also increases. This trend is explained with the decrease of electrostatic force with longer alkyl chains. According to Coulomb's law, which states that the electrostatic force is proportional to the magnitudes of positive and negative charge, and inversely proportional to the squared distance between charges: the distance between charges is the primary influence on electrostatic force. The positive imidazolium ring not only has attractive interaction with the negative bromide ion next to it, but also attracts bromide anions next to other rings. When the side chain contains one or two carbon atoms, the symmetry of anion and cation allows the ions to pack very closely, which means that the electrostatic attractive force is larger. But when the side chain becomes longer, the steric effect hinders the packing ability, decreasing the attractive forces between ions. This decrease in attractive forces leads to larger free volume cavities and enables the increase of dissolution of silica particles.

Although much weaker than the electrostatic forces for the shorter alkyl chains, the van der Waals forces and hydrogen bonding are also worthy of addressing. With the increase in side chain length, van der Waals forces also increase. Additionally, since the side chain is an electron-donor group, with the increase in alkyl chain length, nitrogen atoms in the imidazolium ring become more negative and, accordingly, the hydrogen atom on the carbon is more positive, thus leading to stronger hydrogen bonding. Although an increase in chain length from two to eight carbon atoms will increase the effective van der Waals forces and hydrogen bonding ability (and therefore increase the strength of interactions between the anion and cation), the influence of these forces compared to electrostatic effects do not become relevant in terms of silica particle solubility until the chain length is increased beyond eight carbon atoms.

After the carbon number reaches eight, the electrostatic force between the imidazolium ring and the bromide ions around it becomes smaller, since the distance between them is increased. Increasing the alkyl chain length from eight to ten to twelve will not have so great an effect as that from two to four. At this point, van der Waals forces and hydrogen bonding begin to dominate silica

Downloaded by PENNSYLVANIA STATE UNIV on June 28, 2012 | http://pubs.acs.org
Publication Date (Web): December 18, 2009 | doi: 10.1021/bk-2009-1030.ch013

Downloaded by PENNSYLVANIA STATE UNIV on June 28, 2012 | http://pubs.acs.org
Publication Date (Web): December 18, 2009 | doi: 10.1021/bk-2009-1030.ch013

solubility. When the side chain becomes longer, the larger, more dispersed electron clouds lead to increased polarisability of the cation, thus increasing the van der Waals force. Hydrogen bonding strength also increases due to the increase in the electron-withdrawing capability of nitrogen atoms in the imidazolium ring. As a result, when the distance between cation and anions are further increased, the increased strengths of van der Waals force and hydrogen bonding overrides the decreased strength of electrostatic force in determining the overall force between cations and anions. With the increase in the overall interaction between cations and anions, it becomes much harder for silica particle to overcome the force and become solubilised in liquid phase.

## Conclusion

Silica saturations in 1-alkyl-3-methylimidazolium bromide ionic liquids are greatly influenced by the side-chain length. Silica saturation increases with the increase in carbon number of the side chain at first. However, when the carbon number reaches eight, it begins to decrease. Change in solubility is explained with respect to electrostatic interaction, van der Waals forces and hydrogen bonding between cations and anions. When the side chain of the imidazolium ring contains two to eight carbon atoms, the decreased electrostatic interaction still overrides the increased hydrogen bonding and van der Waals forces, which results in the increased silica solubility. However, when the chain becomes longer, the effect of the electrostatic force becomes smaller and the increased hydrogen bonding and van der Waals forces begin to dominate the silica solubility.

## References

1. Han, L. J.; Wang, Y. B.; Li, C. X.; Zhang, S. J.; Lu, X. M.; Cao, M. J., Simple and safe synthesis of microporous aluminophosphate molecular sieves by inothermal approach. *AIChE J.* , **2008,** 54, 280-288.
2. Parnham, E. R.; Morris, R. E., Ionothermal synthesis of zeolites, metal-organic frameworks, and inorganic-organic hybrids. *Acc. Chem. Res.*, **2007,** 40, 1005-1013.
3. Xu, L.; Choi, E. Y.; Kwon, Y. U., Ionothermal syntheses of six three-dimensional zinc metal-organic frameworks with 1-alkyl-3-methylimidazolium bromide ionic liquids as solvents. *Inorg. Chem.* , **2007,** 46, 10670-10680.
4. Cooney, E. L.; Booker, N. A.; Shallcross, D. C.; Stevens, G. W., Ammonia removal from wastewaters using natural Australian zeolite. I. Characterization of the zeolite. *Sep. Sci. Technol.*, **1999,** 34, 2307-2327.
5. Lin, C. F.; Lo, S. S.; Lin, H. Y.; Lee, Y. C., Stabilization of cadmium contaminated soils using synthesized zeolite. *J. Hazard. Mater.*, **1998,** 60, 217-226.
6. Oshima, K.; Yamazaki, M.; Takewaki, T.; Kakiuchi, H.; Kodama, A., Application of novel FAM adsorbents in a desiccant system. *Kagaku*

Downloaded by PENNSYLVANIA STATE UNIV on June 28, 2012 | http://pubs.acs.org
Publication Date (Web): December 18, 2009 | doi: 10.1021/bk-2009-1030.ch013

*Kogaku Ronbunshu*, **2006,** 32, 518-523.

7. Yang, J.; Ma, L. L.; Shen, B.; Zhu, J. H., Capturing nitrosamines in environment by zeolite. *Mater. Manuf. Processes*, **2007,** 22, 750-757.
8. Corma, A.; Davis, M. E., Issues in the synthesis of crystalline molecular sieves: Towards the crystallization of low framework-density structures. *Chemphyschem*, **2004,** 5, 304-313.
9. Cundy, C. S.; Cox, P. A., The hydrothermal synthesis of zeolites: Precursors, intermediates and reaction mechanism. *Microporous and Mesoporous Mater.*, **2005,** 82, 1-78.
10. Parnham, E. R.; Morris, R. E., The ionothermal synthesis of cobalt aluminophosphate zeolite frameworks. *J. Am. Chem. Soc.*, **2006,** 128, 2204-2205.
11. Parnham, E. R.; Wheatley, P. S.; Morris, R. E., The ionothermal synthesis of SIZ-6 - a layered aluminophosphate. *Chem. Commun.*, **2006**, 380-382.
12. Itoh, N., Electrochemical light-emitting gel made by using an ionic liquids as the electrolyte. *J. Electrochem. Soc.*, **2009,** 156, J37-J40.
13. Donato, R. K.; Migliorini, M. V.; Benvegnu, M. A.; Stracke, M. P.; Gelesky, M. A.; Pavan, F. A.; Schrekker, C. M. L.; Benvenutti, E. V.; Dupont, J.; Scherekker, H. S., Synthesis of silica xerogels with highly distinct morphologies in the presence of imidazolium ionic liquids. *J. Sol-Gel Sci. Technol*, **2009**, 71-77.
14. Gelesky, M. A.; Chiaro, S. S. X.; Pavan, F. A.; dos Santos, J. H. Z.; Dupont, J., Supported ionic liquid phase rhodium nanoparticle hydrogenation catalysts. *Dalton Transactions*, **2007**, 5549-5553.
15. Sun, X.; King, J.; Anthony, J. L., Molecular sieve synthesis in the presence of tetraalkylammonium and dialkylimidazolium molten salts. *Chem. Eng. J.*, **2009,** in press, in press.
16. Ueno, K.; Lnaba, A.; Kondoh, M.; Watanabe, M., Colloidal stability of bare and polymer-grafted silica nanoparticles in ionic liquids. *Langmuir*, **2008,** 24, 5253-5259.
17. Ueno, K.; Imaizumi, S.; Hata, K.; Watanabe, M., Colloidal interaction in ionic liquids: effects of ionic structures and surface chemistry on rheology of silica colloidal dispersions. *Langmuir*, **2009,** in press, in press.
18. Gaillon, L.; Sirieix-Plenet, J.; Letellier, P., Volumetric study of binary solvent mixtures constituted by amphiphilic ionic liquids at room temperature (1-alkyl-3-methylimidazolium bromide) and water. *J. Solution Chem.*, **2004,** 33, 1333-1347.
19. Golovanov, D. G.; Lyssenko, K. A.; Vygodskii, Y. S.; Lozinskaya, E. I.; Shaplov, A. S.; Antipin, M. Y., Crystal structure of 1,3-dialkyldiazolium bromides. *Russ. Chem. Bull.*, **2006,** 55, 1989-1999.
20. Golovanov, D. G.; Lyssenko, K. A.; Antipin, M. Y.; Vygodskii, Y. S.; Lozinskaya, E. I.; Shaplov, A. S., Cocrystal of an ionic liquid with organic molecules as a mimic of ionic liquid solution. *Cryst. Growth Des.*, **2005,** 5, 337-340.
21. Wang, J. J.; Wang, H. Y.; Zhang, S. L.; Zhang, H. H.; Zhao, Y., Conductivities, volumes, fluorescence, and aggregation behavior of ionic liquids [C(4)mim][BF4] and [C(n)mim]Br(n = 4, 6, 8, 10, 12) in aqueous solutions. *J. Phys. Chem. B*, **2007,** 111, 6181-6188.

22. Yan, F.; Texter, J., Surfactant ionic liquid-based microemulsions for polymerization. *Chem. Commun.*, **2006**, 2696-2698.
23. Nishida, T.; Tashiro, Y.; Yamamoto, M., Physical and electrochemical properties of 1-alkyl-3-methylimidazolium tetrafluoroborate for electrolyte. *J. Fluorine Chem.*, **2003,** 120, 135-141.
24. Ruiz-Angel, M. J.; Berthod, A., Reversed phase liquid chromatography of alkyl-imidazolium ionic liquids. *J. Chromatogr. A*, **2006,** 1113, 101-108.
25. Holbrey, J. D.; Seddon, K. R., The phase behaviour of 1-alkyl-3-methylimidazolium tetrafluoroborates; ionic liquids and ionic liquid crystals. *J. Chem. Soc. , Dalton Trans.*, **1999**, 2133-2139.
26. Reichert, W. M.; Holbrey, J. D.; Swatloski, R. P.; Gutowski, K. E.; Visser, A. E.; Nieuwenhuyzen, M.; Seddon, K. R.; Rogers, R. D., Solid-state analysis of low-melting 1,3-dialkylimidazolium hexafluorophosphate salts (ionic liquids) by combined x-ray crystallographic and computational analyses. *Cryst. Growth Des.*, **2007,** 7, 1106-1114.
27. Krossing, I.; Slattery, J. M.; Daguenet, C.; Dyson, P. J.; Oleinikova, A.; Weingartner, H., Why are ionic liquids liquid? A simple explanation based on lattice and solvation energies. *J. Am. Chem. Soc.*, **2006,** 128, 13427-13434.
28. Trohalaki, S.; Pachter, R., Prediction of melting points for ionic liquids. *QSAR Comb. Sci.*, **2005,** 24, 485-490.
29. Lopez-Martin, I.; Burello, E.; Davey, P. N.; Seddon, K. R.; Rothenberg, G., Anion and cation effects on imidazolium salt melting points: A descriptor modelling study. *Chemphyschem*, **2007,** 8, 690-695.
30. Tsuzuki, S.; Tokuda, H.; Hayamizu, K.; Watanabe, M., Magnitude and directionality of interaction in ion pairs of ionic liquids: Relationship with ionic conductivity. *Journal of Physical Chemistry B*, **2005,** 109, 16474-16481.
31. Lynden-Bell, R. M.; Del Popolo, M. G.; Youngs, T. G. A.; Kohanoff, J.; Hanke, C. G.; Harper, J. B.; Pinilla, C. C., Simulations of ionic liquids, solutions, and surfaces. *Accounts of Chemical Research*, **2007,** 40, 1138-1145.
32. Del Popolo, M. G.; Kohanoff, J.; Lynden-Bell, R. M.; Pinilla, C., Clusters, liquids, and crystals of dialkyimidazolium salts. A combined perspective from a initio and classical computer simulations. *Accounts of Chemical Research*, **2007,** 40, 1156-1164.
33. Crowhurst, L.; Mawdsley, P. R.; Perez-Arlandis, J. M.; Salter, P. A.; Welton, T., Solvent-solute interactions in ionic liquids. *Phys. Chem. Chem. Phys.*, **2003,** 5, 2790-2794.
34. Morrow, T. I.; Maginn, E. J., Molecular dynamics study of the ionic liquid 1-n-butyl-3-methylimidazolium hexafluorophosphate. *J. Phys. Chem. B*, **2002,** 106, 12807-12803.
35. Hardacre, C.; McMath, S. E. J.; Nieuwenhuyzen, M.; Bowron, D. T.; Soper, A. K., Liquid structure of 1,3-dimethylimidazolium salts. *J. Phys-Condens. Mater.*, **2003,** 15, S159-S166.

Downloaded by PENNSYLVANIA STATE UNIV on June 28, 2012 | http://pubs.acs.org
Publication Date (Web): December 18, 2009 | doi: 10.1021/bk-2009-1030.ch013

Downloaded by DUKE UNIV on June 29, 2012 | http://pubs.acs.org
Publication Date (Web): December 18, 2009 | doi: 10.1021/bk-2009-1030.ch014

## Chapter 14

# Silica Colloidal Suspensions in Ionic Liquids: Colloidal Stability and Fabrication of Ion Gels on the basis of Colloidal Self-Assembly

**Kazuhide Ueno and Masayoshi Watanabe***

**Department of Chemistry and Biotechnology, Yokohama National University, 79-5 Tokiwadai, Hodogaya-ku, Yokohama 240-8501, Japan**

On account of their remarkable physicochemical properties, ionic liquids are finding a wide range of applications as media for colloidal suspensions. However, colloidal stability in ionic liquids, determined by interactions between particles, is not well-understood. In this study, colloidal stability in ionic liquids was investigated using colloidal silica as a model colloid. Moreover, on the basis of the colloidal stability in ionic liquids, a functional soft material consisting of silica nanoparticles and an ionic liquid was fabricated.

## Introduction

Colloidal dispersions are major components in a wide variety of well-established applications such as foods, paints, and cosmetics, and hence play an important role. The growing interest in nanomaterials (*e.g.*, metal nanoparticles, semiconductor nanoparticles, and carbon nanotubes) has encouraged several studies on their colloidal dispersions. In general, the characteristic properties of such colloidal systems (*e.g.*, electrical, optical, and rheological properties) are strongly affected by the dispersibility of the particles. Therefore, it is very important to elucidate the colloidal interaction between the particles and improve their stability in the dispersed system.

On account of their unique physicochemical properties, ionic liquids are expected to function as colloidal dispersion media for nanomaterials. A number of colloidal systems with ionic liquids have recently been developed by focussing on the dispersion of metal and semiconductor nanoparticles, including *in situ* nanomaterial synthesis in ionic liquids *(1)*, enhancement of colloidal stability in ionic liquids *(2)*, phase transfer to ionic liquids from other dispersed media *(3)*, and catalytic reactions using metal nanoclusters in ionic liquids *(4)*. Furthermore, composite materials based on nanomaterials and ionic liquids have been extensively studied. Fukushima *et al.* have produced the carbon nanotube-ionic liquid composites, wherein the carbon nanotubes were well-dispersed *(5)*. These composites have been used to develop electroactive polymer actuators that can be operated in air at low operational voltages. Semiconductor nanoparticle-ionic liquid composites produced by Nakashima *et al.* constitute another example of colloidal systems with ionic liquids. The dispersion of CdTe semiconductor nanoparticles, covered with a cationic thiol stabiliser, showed enhanced photoluminescence in a hydrophobic ionic liquid *(6)*. Recently, Schubert and co-workers have prepared magnetorheological fluids on the basis of dispersions of magnetic particles in ionic liquids *(7)*. Since ionic liquids have in general high ionic conductivities and wide electrochemical windows, the use of colloidal systems with ionic liquids constitutes an attractive subject of research pertaining to future electrochemical devices. For example, ionic liquid-based electrolytes have been solidified by adding inorganic nanoparticles in ionic liquids for use in high-performance dye-sensitised solar cells *(8)*.

In contrast to such advances in the application of ionic liquids with nanomaterials, there have been only a few studies conducted on the fundamental colloidal stability in ionic liquids *(9)*. Surprisingly, certain colloidal particles can be dispersed in ionic liquids without any stabilisers such as surfactants and polymers. Such remarkable stabilisation is possibly a result of the electrostatic force and/or steric repulsive force produced by the coordination or adsorption of ions of ionic liquids on particle surfaces. Indeed, electrostatic and steric repulsive forces play a dominant role in kinetically stabilising the colloidal particles in several aqueous and organic dispersions. However, the high ionic atmosphere in ionic liquids may attenuate the electrostatic repulsion between the colloidal particles. In the case of reactions between low molecular species having the same charge *(10)*, the reaction rate is enhanced, because the electrostatic repulsion between the charged species is suppressed in ionic liquids. It should also be considered that charged colloidal particles can easily approach each other because of the charge screening effect if other repulsive forces are absent. Thus, the stabilisation mechanism of colloidal particles in ionic liquids is still unclear.

In this study, we investigate the colloidal stability of bare and polymer-grafted silica particles in 1-alkyl-3-methylimidazolium ([C$_n$mim])-based ionic liquids from both experimental and theoretical perspectives *(11)*. For studying the stabilisation mechanism, colloidal silica appears to be suitable because of its availability, and detailed studies have been conducted by using colloidal silica in aqueous and organic media. The primary objective of this study is to understand the colloidal behaviour of charged silica particles in ionic liquids by paying special attention to electrostatic stabilisation. Secondly, in order to evaluate the effect of steric repulsion between the silica particles, polymer chains compatible with ionic liquids are grafted on to the surface of the silica particles. Finally, on the basis of the colloidal stability of the silica nanoparticles in ionic liquids,

Downloaded by DUKE UNIV on June 29, 2012 | http://pubs.acs.org
Publication Date (Web): December 18, 2009 | doi: 10.1021/bk-2009-1030.ch014

nanocomposite gels consisting of silica nanoparticles and an ionic liquid have been prepared *(12)*.

## Results and Discussion

### Electrostatic repulsion in ionic liquids

It is well known that bare silica particles are negatively charged as a result of the dissociation of surface silanol groups in aqueous and organic media. These ionic groups leave their counterions near the surface and form an electrical double layer (EDL). The EDL causes the electrostatic repulsion between the particles *(13)*.

The colloidal interaction between the charged silica particles in various ionic liquids was determined by taking into account van der Waals attraction, electrostatic repulsion, and their mutual balance. The interaction potential between two charged colloidal particles can be determined using the well-known Derjaguin-Landau-Verwey-Overbeek (DLVO) theory that qualitatively describes the colloidal stability in dispersed media *(14)*. According to the DLVO theory, the total interparticle potential $V_{\text{total}}(d)$ can be expressed, Equation (1), as the sum of an attractive London-van der Waals potential $V_{\text{vdW}}(d)$ and a repulsive electrostatic potential $V_{\text{ele}}(d)$ owing to the EDL of the particles, where $d$ is the distance between the particle surfaces.

$$V_{\text{total}}(d) = V_{\text{vdW}}(d) + V_{\text{ele}}(d) \qquad (1)$$

$V_{\text{vdW}}(d)$ between two spherical particles of radius $R$ and Hamaker constant $A_{\text{p}}$ in a medium with Hamaker constant $A_{\text{m}}$ is given by Equation (2).

$$V_{\text{vdW}}(d) = -\frac{R}{12d}\left[\left(\sqrt{A_{\text{m}}} - \sqrt{A_{\text{p}}}\right)^2\right] \qquad (2)$$

The Hamaker constant can be calculated from the dielectric constant $\varepsilon$ and refractive index $n$ of compounds by using Equation (3):

$$A = \frac{3}{4}kT\frac{(\varepsilon-1)^2}{(\varepsilon+1)^2} + \frac{3h\nu_e}{16\sqrt{2}}\frac{(n^2-1)^2}{(n^2+1)^{3/2}} \qquad (3)$$

where $k$ is the Boltzmann constant; $T$, the absolute temperature; $h$, the Planck constant; and $\nu_{\text{e}}$, the frequency of the main electronic absorption for the dielectric permittivity, which can be assumed to be $3\times10^{15}$ $\text{s}^{-1}$ for the ionic liquids *(15)*. To evaluate the van der Waals attraction, the Hamaker constants of various compounds used in the study were calculated using Equation (3), the reported values of the dielectric constants *(16)*, and refractive indices of ionic

Downloaded by DUKE UNIV on June 29, 2012 | http://pubs.acs.org
Publication Date (Web): December 18, 2009 | doi: 10.1021/bk-2009-1030.ch014

liquids. The values of the Hamaker constant for the ionic liquids are almost independent of the structure of ionic liquids (typically $A_m = 5.2–5.6 \times 10^{-20}$ J).

On the other hand, the approximate expression for repulsive $V_{ele}(d)$ appropriate for this study ($\kappa R >> 1$) is given by Equation (4).

$$V_{ele}(d) = 2\pi R \varepsilon_0 \varepsilon \psi_0^2 \ln[1 + \exp(-\kappa d)] \qquad (4)$$

where $\kappa$ is the Debye reciprocal length parameter; $\varepsilon_0$, the permittivity of free space; and $\psi_0$, the surface potential. For ionic liquid dispersions, $\kappa$, Equation (5), is defined using the effective ionic charge concentration of the ionic liquids ($C_{eff}$), electronic charge ($e$), and Avogadro's number ($N_A$).

$$\kappa = \left( \frac{2 \times 10^3 N_A e^2 C_{eff}}{\varepsilon_0 \varepsilon k T} \right)^{1/2} \qquad (5)$$

The degree of self-dissociation, the so-called "ionicity", of common ionic liquids has been estimated by calculating the molar conductivity ratio ($\Lambda_{imp}/\Lambda_{NMR}$), where $\Lambda_{imp}$ is the molar conductivity calculated from the impedance measurements by using conductometry, and $\Lambda_{NMR,}$ is the molar conductivity calculated from the pulsed-gradient spin-echo NMR measurements by using ionic diffusion coefficients *(17)*. The $\Lambda_{imp}/\Lambda_{NMR}$ values of the ionic liquids are less than unity, indicating that the ions are partially associated with each other. Thus, the effective concentration of charged species $C_{eff}$ in the ionic liquids was determined by simply multiplying the molar concentration ($C$) with $\Lambda_{imp}/\Lambda_{NMR}$ ($C_{eff} = C \times \Lambda_{imp}/\Lambda_{NMR}$). The estimated values of $C_{eff}$ are very high (> 1.5 mol $l^{-1}$). Therefore, the Debye length ($\kappa^{-1}$) associated with the thickness of the double layer is very small in ionic liquids. It should be noted that the electrostatic terms, Equation (4) and Equation (5), are based on the classical Debye-Hückel theory that is applicable to diluted systems. As the first approximation, for the sake of simplicity, the classical theory has been adopted for the electrostatic interaction between the colloidal particles in the ionic liquids. However, the structure of the EDL in ionic liquids is very complicated *(18)*. Recent studies on this topic have revealed charge-density oscillations in the EDL of ionic liquids *(19)*. The extended Gouy-Chapmann theory that considers the ion size of ionic liquids has also been proposed *(20)*. However, since the thicknesss of the EDL is considerably less than that which is formed in molecular solvents, the interparticle electrostatic repulsion in ionic liquids may be weakened, especially in cases of long interparticle distances. Under a high ionic strength, the surface potential $\psi_0$ is presumably equal to the zeta potential. The approximate values of the zeta potential in the ionic liquids on the basis of the reported dependency of the surface zeta potential for silica nanoparticles on the donor number (DN) of an organic dispersion medium *(13)* and the DNs for the ionic liquids *(17)* have been estimated. The resulting zeta potentials for silica in the ionic liquids ranged from –52 to –38 mV. Recently, electrokinetic measurements were successfully obtained by employing an electroacoustic

Downloaded by DUKE UNIV on June 29, 2012 | http://pubs.acs.org
Publication Date (Web): December 18, 2009 | doi: 10.1021/bk-2009-1030.ch014

method *(21)*. A similar value was obtained for the zeta-potential (*ca.* –55 mV) for anatase $TiO_2$ in [$C_4$mim][$BF_4$].

Figure 1 shows the total pair potential profiles ($V_{\text{total}}(d)/kT$) of bare silica particles as a function of the distance ($d$) between the different surfaces of the silica particles in a common aqueous system and in different ionic liquids. For the aqueous system, the repulsion is very strong at a large $d$ and provides a significant potential barrier, rendering the suspension stable against aggregation. For the ionic liquid systems, the potential curves lie below the potential axis of zero over the entire range of $d$, indicating that the particles are attracted to each other at all degrees of separation. Except for [$C_4$mim][$PF_6$], the local minimum and small energy barrier can be observed in the vicinity of the distance of the adhesive contact ($d$ = 0). However, under ambient conditions, the particles appear to overcome such small barriers because of the particle thermal energy ($kT$). These results, which are based on the DLVO theory, suggest that colloidal particles cannot be electrostatically stabilised in the ionic liquids, and therefore they coagulate easily even if the particles are highly charged.

To confirm these calculations, the colloidal stability of bare silica particles with a diameter of 120 nm in the ionic liquids was experimentally examined. Figure 2 shows the size-distribution curves of silica colloidal particles in deionised water and the ionic liquids obtained from the dynamic light scattering (DLS) measurements. The aqueous dispersion remained stable on account of the electrostatic stabilisation. On the other hand, in all the ionic liquids, wider

Downloaded by DUKE UNIV on June 29, 2012 | http://pubs.acs.org
Publication Date (Web): December 18, 2009 | doi: 10.1021/bk-2009-1030.ch014

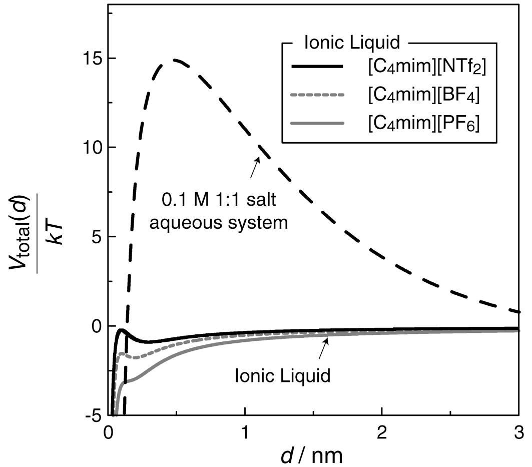

*Figure 1. DLVO interparticle interaction profiles (T = 25 °C) of bare silica particles with a diameter of 120 nm in 0.1 M 1:1 salt aqueous system ($\psi_0$ = -28 mV) and the ionic liquids, [$C_4$mim][$NTf_2$] ($\psi_0$ = –38 mV), [$C_4$mim][$PF_6$] ($\psi_0$ = –52 mV), and [$C_4$mim][$BF_4$] ($\psi_0$ = –45 mV).*

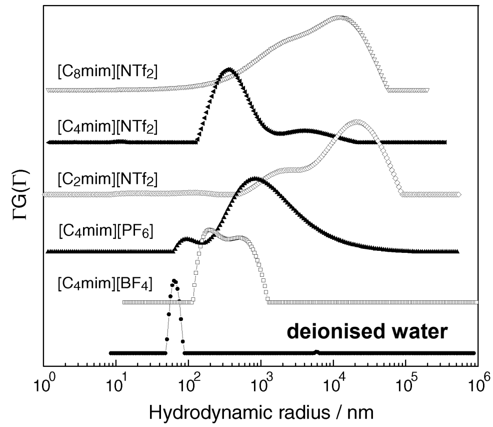

*Figure 2. Size distribution curves of bare silica particles (0.01 wt%) with a diameter of 120 nm in deionised water and the ionic liquids measured by DLS at 25 °C.*

distributions were observed, indicating aggregation of the particles. Moreover, direct transmission electron microscope (TEM) observations were carried out to observe the microscopic dispersibility in the ionic liquids. Despite the high vacuum condition and electron beam irradiation, ionic liquids can be observed by an electron microscope such as a scanning electron microscope (SEM) and TEM in the absence of evaporation and accumulation of electron charges (*22*). As shown in Figure 3, most particles adhered to each other and formed large aggregates in 1-ethyl-3-methylimidazolium bis{(trifluoromethyl)sulfonyl}amide ($[C_2mim][NTf_2]$).

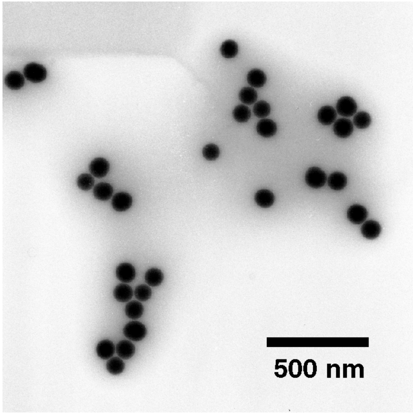

*Figure 3. Direct TEM image of a dilute suspension (1 wt %) of bare silica particles in $[C_2mim][NTf_2]$. The black spots correspond to silica particles, and the gray portion shows the image of $[C_2mim][NTf_2]$.*

Downloaded by DUKE UNIV on June 29, 2012 | http://pubs.acs.org
Publication Date (Web): December 18, 2009 | doi: 10.1021/bk-2009-1030.ch014

Downloaded by DUKE UNIV on June 29, 2012 | http://pubs.acs.org
Publication Date (Web): December 18, 2009 | doi: 10.1021/bk-2009-1030.ch014

### Steric repulsion in ionic liquids

In contrast to electrostatic stabilisation, the adsorption and grafting of a polymer onto a colloid surface leads to either steric stabilisation or bridging flocculation of the particles. The low surface concentration and high molecular weight of the grafted polymer increase the possibility of interparticle bridging by the polymers. Therefore, PMMA-grafted silica particles (PMMA = poly(methyl methacrylate)) were prepared by surface-initiated atom transfer radical polymerisation *(23)*, which results in a high graft density and controllability of the molecular weight. The particles that consisted of a silica core with a diameter of 120 nm and grafted PMMA with an average molecular weight of 53000 and graft density of 0.21 chains $nm^{-2}$ were used in this study.

The colloidal stability of sterically stabilised particles also depends on the affinity of the grafted polymer to the dispersion medium. In a good solvent, the grafted PMMA generates a strong repulsive force as a result of the excluded volume effect to avoid the interpolymer penetration of the PMMA-grafted particles. Meanwhile, the attraction is effective in a poor solvent because of the insolubility of the grafted PMMA. Among the ionic liquids used in the study, PMMA is soluble in $[C_4mim][PF_6]$ and $[C_nmim][NTf_2]$, whereas it is insoluble in $[C_4mim][BF_4]$. The colloidal stability was clearly dependent on the solubility of PMMA in the ionic liquids. In the $[C_4mim][BF_4]$ dispersion, the PMMA-grafted particles were phase-separated even during sample preparation, indicating the aggregation of the PMMA-grafted particles in the ionic liquid. However, a narrow size-distribution was observed in the case of the dispersions in $[C_nmim][NTf_2]$ and $[C_4mim][PF_6]$ (Figure 4). The excellent dispersibility was also confirmed by direct TEM observations of a dilute $[C_2mim][NTf_2]$ dispersion of the PMMA-grafted silica particles (Figure 5).

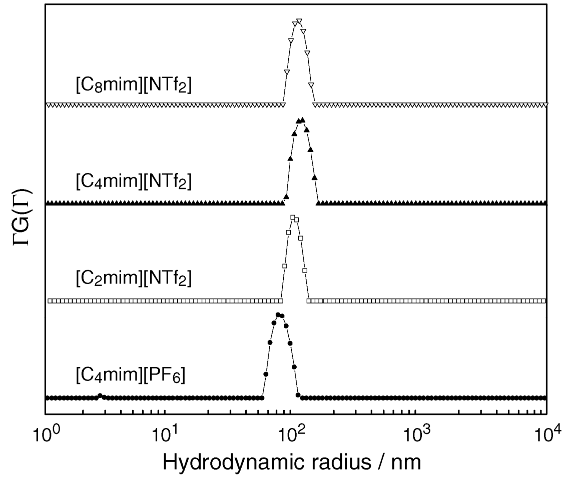

*Figure 4. Size distribution curves of PMMA-grafted silica particles (0.01 wt%) in the ionic liquids measured by DLS at 25 °C.*

Downloaded by DUKE UNIV on June 29, 2012 | http://pubs.acs.org
Publication Date (Web): December 18, 2009 | doi: 10.1021/bk-2009-1030.ch014

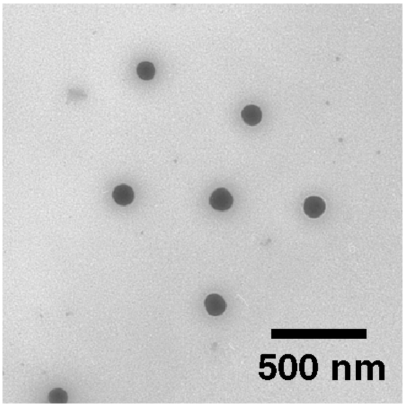

*Figure 5. Direct TEM image of a dilute suspension (1 wt %) of PMMA-grafted silica particles in [$C_2$mim][$NTf_2$].*

## Nanocomposite Ion Gels

Since typical ionic liquids have almost no vapour pressure, if they are treated as solids, they can be used to produce ionic liquid-based solid electrolytes that exhibit high ionic conductivity. The gelation of ionic liquids using polymer networks has been proposed *(24)* as a method for the production of solid electrolytes, and the combination of ionic liquids and polymers is expected to widen the scope of application of such materials *(25)*. Because bare silica particles aggregate in [$C_2$mim][$NTf_2$], nanocomposite ion gels were formed as a result of the flocculation of silica nanoparticles in the ionic liquid, thus, constituting a facile methodology affording highly ion-conductive solid electrolytes as well as functionalised soft materials *(12)*. In this section, ionic transport and viscoelastic properties of the nanocomposite ion gel are explained.

The gelation of [$C_2$mim][$NTf_2$] was accomplished, despite the addition of 3 wt% nanoparticles when smaller silica nanoparticles of 12 nm diameter were used. Due to poor colloidal stability, the silica particles formed interconnected aggregates with a loosely outspread fractal structure, facilitating the percolation of the aggregated clusters throughout the ionic liquid solution. This led to the gelation of the ionic liquid despite the addition of a small amount of silica particles.

Although they had a solid-like appearance, the nanocomposite ion gels exhibited a high ionic conductivity of *ca.* $10^{-2}$ S $cm^{-1}$ at 30 °C, which is comparable to that of pure [$C_2$mim][$NTf_2$]. The addition of silica particles has a small influence on ionic conductivity (Figure 6). These values are higher than those of the PMMA-based ion gels reported previously *(24)*. The high ionic conductivity was attributed to the high ionic mobility and concentration of the

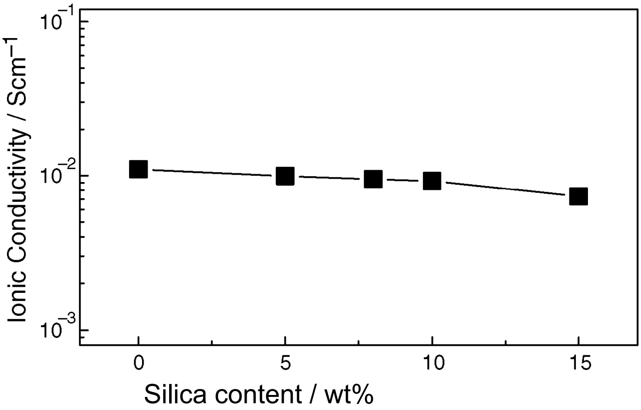

*Figure 6. Concentration dependence of ionic conductivity of nanocomposite ion gels at 30 °C.*

nanocomposite ion gels. The silica-based ion gels can be characterised as phase-separated binary systems wherein ionic transport is considered to be affected only by the obstruction of the interconnecting silica network. A large open structure of the particulate silica networks minimises the obstruction of ionic migration. On account of the gelation with a small amount of silica particles, the reduction in the total ionic carrier concentration was minimised. Thus, the higher ionic conductivity of the nanocomposite ion gels is brought about.

In contrast to ionic conductivity, mechanical properties such as the plateau elastic modulus ($G_p$) and yield stress ($\tau_y$) strongly depend on the silica concentration (Figure 7). $G_p$ and $\tau_y$ can be precisely controlled over more than three orders of magnitude by adjusting the amount of silica particles added to the ionic liquid. Furthermore, the nanocomposite ion gels exhibit reversible gel-sol transition in response to the strain amplitude (Figure 8). The transition from a solid-like ($G' > G''$) to a liquid-like ($G' < G''$) behaviour is detected at a certain strain amplitude corresponding to $\tau_y$: the nanocomposite ion gels behave like *pseudo*-plastic fluids. It can be recognised that sufficient shear disrupts the physical bonds of the silica particulate network and causes the system to flow. The shear-induced gel-sol transition is beneficial to the processing of nanocomposite ion gels and contributes to the fabrication of solid-state electrochemical devices using the gels *(8)*.

Downloaded by DUKE UNIV on June 29, 2012 | http://pubs.acs.org
Publication Date (Web): December 18, 2009 | doi: 10.1021/bk-2009-1030.ch014

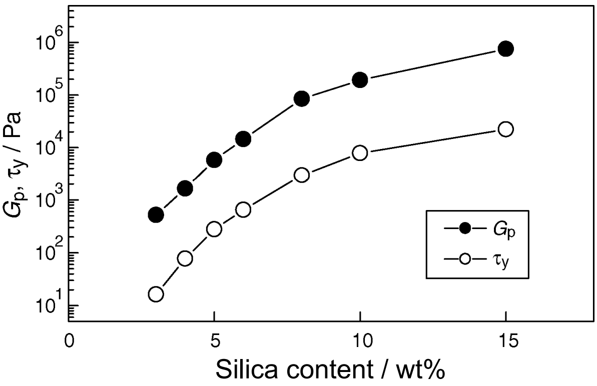

*Figure 7. Concentration dependence of plateau elastic modulus ($G_p$) and yield stress ($\tau_y$) of nanocomposite ion gels at 25 °C.*

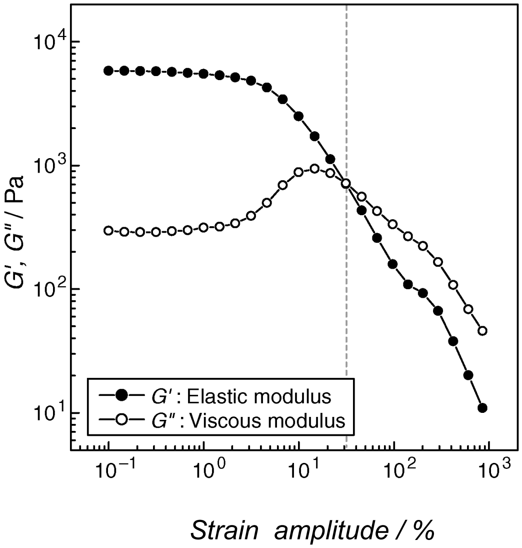

*Figure 8. Dynamic strain sweep of 5 wt% nanocomposite ion gel obtained by rheological measurement at 25 °C.*

# Conclusions

In this paper, we report the colloidal stability of bare and PMMA-grafted silica particles in imidazolium-based ionic liquids with different anions. The DLVO theory using macroscopic physicochemical properties of the ionic liquid-colloid systems suggests that the electrostatic repulsive force hardly stabilises the bare silica particles in the ionic liquids because of the high ionic strength of the ionic liquids, even though the particles are assumed to be highly charged. This hypothesis is consistent with the experimental results. The PMMA-grafted

Downloaded by DUKE UNIV on June 29, 2012 | http://pubs.acs.org
Publication Date (Web): December 18, 2009 | doi: 10.1021/bk-2009-1030.ch014

silica particles exhibit good colloidal stability in $[C_4mim][PF_6]$ and $[C_nmim][NTf_2]$, wherein the ionic liquids act as a good solvent for the grafted PMMA, indicating that steric repulsion is effective in the ionic liquids. Consequently, in order to obtain stable colloidal particles in ionic liquids, it is more important to induce steric repulsion rather than electrostatic repulsion into the colloidal particles.

Nanocomposite ion gels consisting of interconnected networks of silica nanoparticles and an ionic liquid, $[C_2mim][NTf_2]$, were studied. We demonstrated a facile route to the preparation of ion gels that exhibit high ionic conductivity comparable to that of a pure ionic liquid at room temperature and a shear-responsive sol-gel transition. The intriguing viscoelastic properties (*e.g.*, *pseudo*-plastic fluidity, and dependence of $G_p$ and $\tau_y$ on silica concentration) offer advantages for the fabrication of high-performance solid electrolytes and new functional soft materials based on ionic liquids, with regard to easy processability and the precise controllability of mechanical strength.

Downloaded by DUKE UNIV on June 29, 2012 | http://pubs.acs.org
Publication Date (Web): December 18, 2009 | doi: 10.1021/bk-2009-1030.ch014

## Acknowledgements

This research has been supported by a Grant-in-Aid for Scientific Research from the Ministry of Education, Culture, Sports, Science and Technology (MEXT), Japan (#452-17073009 and #B-20350104). K. Ueno acknowledges the financial support provided by JSPS.

## References

1. (a) Antonietti, M.; Kuang, D.; Smarsly, B.; Zhou, Y. *Angew. Chem. Int. Ed.* **2004**, *43*, 4988-4992. (b) Gelesky, M. A.; Umpierre, A. P.; Machado, G.; Correia, R. R. B.; Magno, W. C.; Morais, J.; Ebeling, G.; Dupont, J. *J. Am. Chem. Soc.* **2005**, *127*, 4588-4589. (c) Torimoto, T.; Okazaki, K.; Kiyama, T.; Hirahara, K.; Tanaka, N.; Kuwabata, S. *Appl. Phys. Lett.* **2006**, *89*, 243117 1-243117 3.
2. (a) Itoh, H.; Naka, K.; Chujo, Y. *J. Am. Chem. Soc.* **2004**, *126*, 3026-3027. (b) Tatumi, R.; Fujihara, H. *Chem. Commun.* **2005**, 83-85.
3. Wei, G.-T.; Yang, Z.; Lee, C.-Y.; Yang, H.-Y.; Wang, C. R. C. *J. Am. Chem. Soc.* **2004**, *126*, 5036-5037.
4. (a) Wojtków, W.; Trzeciak, A. M.; Choukroun, R.; Pellegatta, J. L. *J. Mol. Catal. A: Chemical.* **2004**, *224*, 81-86. (b) Fonseca, G. S.; Machado, G.; Teixeira, S. R.; Fecher, G. H.; Morais, J.; Alves, M. C. M.; Dupont, J. *J. Colloid Interface Sci.* **2006**, *301*, 193-204.
5. Fukushima, T.; Asaka, K.; Kosaka, A.; Aida, T. *Angew. Chem. Int. Ed.* **2005**, *44*, 2410-2413.
6. Nakashima, T.; Kawai, T. *Chem. Commun.* **2005**, 1643-1645.
7. Guerrero-Sanchez, C.; Lara-Ceniceros, T.; Jimenez-Regalado, E.; Raşa, M.; Schubert, U. S. *Adv. Mater.* **2007**, *19*, 1740-1747.

Downloaded by DUKE UNIV on June 29, 2012 | http://pubs.acs.org
Publication Date (Web): December 18, 2009 | doi: 10.1021/bk-2009-1030.ch014

8. (a) Wang, P.; Zakeeruddin, S. M.; Comte, P.; Exnar, I.; Grätzel, M. *J. Am. Chem. Soc.* **2003**, *125*, 1166-1167. (b) Katakabe, T.; Kawano, R.; Watanabe, M. *Electrochem. Solid-State Lett.* **2007**, *10*, F23-F25.
9. (a) Ott, L. S.; Cline, M. L.; Deetlefs, M.; Seddon, K. R.; Finke, R. G. *J. Am. Chem. Soc.* **2005**, *127*, 5758-5759. (b) Schrekker, H. S.; Gelesky, M. A.; Stracke, M. P.; Schrekker, C. M. L.; Machado, G.; Teixeira, S. R.; Rubim, J. C.; Dupont, J. *J. Colloid Interface Sci.* **2007**, *316*, 189-195.
10. (a) Kawano, R.; Watanabe, M. *Chem. Commun.* **2005**, 2107-2109. (b) Takahashi, K.; Sakai, S.; Tezuka, H.; Hiejima, Y.; Katsumura, Y.; Watanabe, M. *J. Phys. Chem. B.* **2007**, *111*, 4807-4811.
11. Ueno, K.; Inaba, A.; Kondoh, M.; Watanabe, M. *Langmuir.* **2008**, *24*, 5253-5259.
12. Ueno, K.; Hata, K.; Katakabe, T.; Kondoh, M.; Watanabe, M. *J. Phys. Chem. B.* **2008**, *112*, 9013-9019.
13. Spange, S.; Simon, F.; Heublein, G.; Jacobasch, H.-J.; Börner, M. *Colloid Polym. Sci.* **1991**, *269*, 173-178.
14. Israelachvili, J. *Intermolecular and Surface Forces* 2nd. edition; Academic Press: San Diego, 1991.
15. Matsuda, T.; Mishima, Y.; Azizian, S.; Matsubara, H.; Takiue, T.; Aratono, M. *Colloid Polym. Sci.* **2007**, *285*, 1601-1605.
16. (a) Wakai, C.; Oleinikova, A.; Ott, M.; Weingärtner, H. *J. Phys. Chem. B.* **2005**, *109*, 17028-17030. (b) Daguenet, C.; Dyson, P. J.; Krossing, I.; Oleinikova, A.; Slattery, J.; Wakai, C.; Weingärtner, H. *J. Phys. Chem. B.* **2006**, *110*, 12682-12688.
17. Tokuda, H.; Tsuzuki, S.; Susan, M. A. B. H.; Hayamizu, K.; Watanabe, M. *J. Phys. Chem. B.* **2006**, *110*, 19593-19600.
18. Kornyshev, A. A. *J. Phys. Chem. B.* **2007**, *111*, 5545-5557.
19. Fedorov, M. V.; Kornyshev, A. A. *Electrochim. Acta.* **2008**, *53*, 6835-6840.
20. Rollins, J. B.; Fitchett, B. D.; Conboy, J. C. *J. Phys. Chem. B.* **2007**, *111*, 4990-4999..
21. Kosmulski, M.; Rosenholm, J. B.; Saneluta, C.; Marczewska-Boczkowska, K, W. *Colloid and Surf. A.* **2005**, *267*, 16-18.
22. (a) Scheeren, C. W.; Machado, G.; Dupont, J.; Fichtner, P. F. P.; Texeira, S. R. *Inorg. Chem.* **2003**, *42*, 4738-4742. (b) Kuwabata, S.; Kongkanand, S.; Oyamatsu, D.; Torimoto, T. *Chem. Lett.* **2006**, *35*, 600-601.
23. von Werne, T.; Pattten, T. E. J. Am. Chem. Soc. 2001, 123, 7497-7505.
24. Susan, M. A. B. H.; Kaneko, T.; Noda, A.; Watanabe, M. *J. Am. Chem. Soc.* **2005**, *127*, 4976-4983.
25. (a) Ueki, T.; Watanabe, M. *Macromolecules.* **2008**, *41*, 3739-3749. (b) Lodge, T. P. *Science.* **2008**, *321*, 50-51. (c) Cho, J. H.; Lee J.; Xia, Y.; Kim, B.; He, Y.; Renn, M. J., Lodge, T. P.; Frisbie, C. D. *Nature Mater.* **2008**, *7*, 900-906.

Downloaded by COLUMBIA UNIV on June 28, 2012 | http://pubs.acs.org
Publication Date (Web): December 18, 2009 | doi: 10.1021/bk-2009-1030.ch015

## Chapter 15

# Facile Preparation of Hybrid Fluids from Ionic Liquid-Inorganic Nanoparticles:

## Focus on Surface Modification of the Nanoparticles

**Asako Narita,[a,c] Eisuke Miyoshi,[a] Kensuke Naka,[b] and Yoshiki Chujo[a]**

**[a]Department of Polymer Chemistry, Graduate School of Engineering, Kyoto University, Katsura, Nishikyo-ku, Kyoto, 615-8510, Japan**
**[b]Department of Chemistry and Materials Technology, Kyoto Institute of Technology, Matsugasaki, Sakyo-ku, Kyoto 606-8585, Japan**
**[c]Advanced Software Technology & Mechatronics Research Institute of Kyoto (ASTEM)**

Hybrid fluids formed from inorganic nanoparticles and ionic liquids have been prepared. Although nanoparticles covalently modified with 1-methylimidazolium chloride were uniformly dispersed in water containing 1-butyl-3-methylimidazolium chloride at first, they formed hydrophobic dispersions after potassium bis{(trifluoromethyl)sulfonyl}amide was added, due to anion exchange at the surface of the nanoparticles. The concentration method needs no evaporation, centrifuging, filtration, or dialysis techniques, even if the nanoparticles were dispersed at a low level in ionic liquids.

In Ionic Liquids: From Knowledge to Application; Plechkova, N., et al.;
ACS Symposium Series; American Chemical Society: Washington, DC, 2010.

## Background

Preparation of inorganic nanoparticles is one of the recent key technologies of nanoscience. In most cases, nanoparticles are prepared in liquid media, and frequently nanoparticles are used as dispersion in liquids. Thus, dispersion techniques are quite important for a nano-sized material chemistry. Usually, inorganic nanoparticles need surface stabilisers to keep their size and shape, because the crystal surfaces have high potential energy compared to the body of the crystal. Specifically, nanoparticles have a large surface area compared to their inner volume. For example, the surface area of a 1 cm cube is 6 $cm^2$. In contrast, the total surface area of nanoparticles (10 nm diameter) with a total volume of 1 $cm^3$ is approximately 600 $m^2$. The large surface area of the nanoparticles is explains the importance of the use of surface stabilisers compared to bulk materials. The surface stabiliser also affects the dispersibility of nanoparticles in liquid media. For example, nanoparticles stabilised by lipophilic molecules show a high dispersibility in hydrophobic oils. In contrast, nanoparticles coated by molecules having hydrophilic moieties are easy to disperse in aqueous media.

Ionic liquids are of interest as dispersion media for nanoparticles. If the dispersibility of nanoparticles in ionic liquids can be well controlled, the application could be expanded to more extreme environments, such as under reduced pressure, or at high temperature. The methodology for the concentration of inorganic nanoparticles into ionic liquids is an important subject, especially the relationship between dispersant and stabiliser on the surface of nanoparticles.

Recently, methods for the direct synthesis of nanoparticles in ionic liquids have been developed *(1)*. Such nanoparticles do not need any surface stabiliser. However, such methods are specific to each class of nanoparticles. On the other hand, focusing on the surface stabiliser has advantages, because the knowledge about surface properties can be generically applied to any components of the nanoparticles. Furthermore, classical synthetic methods for nanoparticles in aqueous or organic media can be applied. If there is simple method to disperse nanoparticles into ionic liquids, such hybrid fluids are promising materials for various fields.

Downloaded by COLUMBIA UNIV on June 28, 2012 | http://pubs.acs.org
Publication Date (Web): December 18, 2009 | doi: 10.1021/bk-2009-1030.ch015

## Objective

The objective of this study is the facile preparation of inorganic nanoparticles-ionic liquid hybrid fluids. The nanoparticles were prepared in aqueous solution; they were covalently modified with ionic liquid-derived organic salts as surface stabilisers. These nanoparticles are concentrated in a simple procedure without any centrifuging, filtration or evaporation, utilising the surface properties of the surface stabiliser.

# Experimental

## Materials

Dry 1-methylimidazole and 1-chlorobutane were purchased from Aldrich Chemical Co. Dry pyridine, tetrachloroauric(III) acid, sodium tetrahydroborate, sodium hydroxide and iron(III) chloride hexahydrate were purchased from Wako Pure Chemical Industries, Ltd. Oleic acid, (3-chloropropyl)trimethoxysilane and octyltrimethoxysilane were purchased from Tokyo Kasei Co. Ltd. Iron(II) chloride tetrahydrate, potassium bis{(trifluoromethyl)sulfonyl}amide ($K[NTf_2]$), and lithium bis{(trifluoromethyl)sulfonyl}amide ($Li[NTf_2]$) were purchased from Kanto Chemical Co. Ltd.

1-Butyl-3-methylimidazolium chloride ($[C_4mim]Cl$) was prepared by heating under reflux an equimolar mixture of 1-methylimidazole and 1-chlorobutane at 90 °C for three days *(2)*. The mixture was washed with dry ethyl ethanoate three times, and dried under reduced pressure. 1-Butylpyridinium chloride ($[C_4py]Cl$) was prepared similarly *(2)*.

## Preparation of organic salts-modified iron oxide nanoparticles

1-Methylimidazolium-modified iron(II,III) oxide nanoparticles ($[Rmim]Cl$-$Fe_3O_4$-NPs) were prepared by the method described in our earlier report *(3)*. Initially, a silane coupling agent was prepared by mixing 1-methylimidazole and (3-chloropropyl)trimethoxysilane at 90 °C for three days. The resulting viscous liquid was washed with dry ethyl ethanoate three times, and then dried under reduced pressure. Iron(II,III) oxide ($Fe_3O_4$) nanoparticles were prepared by hydrolysis of mixed aqueous solutions of iron(II) and iron(III) chloride (respectively 2 mmol and 4 mmol in 120 $cm^3$) using 15 $cm^3$ of 28 % aqueous ammonium hydroxide solution with vigorous mechanical stirring. After dispersant water was replaced by ethanol, the iron(II,III) oxide nanoparticles and silane coupling agent were mechanically stirred in ethanol containing a small amount of water at 70 °C. After six hours, the nanoparticles were washed three times with ethanol by centrifuge (9000 rpm; 1 h), and then ethanol was removed by pipette. The dispersant was replaced by water, and the nanoparticles were well dispersed with an ultrasonic wave bath.

Pyridinium chloride modified iron oxide nanoparticles ($[Rpy]Cl$-$Fe_3O_4$-NPs) were prepared by similar procedures, replacing 1-methylimidazole with pyridine (*vide supra*).

The structures of the silane coupling agents were confirmed by $^1H$ NMR spectroscopy. $^1H$ NMR (dmso) spectrum of coupling agent [Rmim]Cl, which is a yellow viscous liquid: $\delta$/p.p.m.: d 9.29 (s, 1H), 7.81 (s, 1H), 7.75 (s, 1H), 4.15 (t, 2H), 3.88 (s 3H), 3.46 (s, 9H), 1.83 (m, 2H), 0.54 (t, 2H). Yield: 95%. $^1H$ NMR spectrum (dmso) of coupling agent [Rpy]Cl, which is a brown viscous liquid: $\delta$/p.p.m.: d 9.17 (d, 2H), 8.62 (t, 1H), 8.17 (t, 2H), 4.61 (t, 2H), 3.47 (m 9H), 1.96 (m, 2H), 0.59 (t, 2H). Yield: 98%.

Downloaded by COLUMBIA UNIV on June 28, 2012 | http://pubs.acs.org
Publication Date (Web): December 18, 2009 | doi: 10.1021/bk-2009-1030.ch015

## Preparation of alkyl chain-modified iron oxide nanoparticles

Octyl chain-modified iron(II,III) oxide nanoparticles ($C_8$-$Fe_3O_4$-NPs) were prepared by stirring of prepared iron(II,III) oxide nanoparticles and octyltrimethoxysilane in ethanol in the same procedures as [Rmim]Cl-$Fe_3O_4$-NPs. Surface modification was confirmed by FT-IR spectroscopy, TGA weight loss, and the observation of totally insolubility in water.

Oleic acid coated iron(II,III) oxide nanoparticles (OA-$Fe_3O_4$-NPs), modified *via* hydrogen bonding, were prepared according to earlier reports *(4,5)*. Oleic acid (0.2 $cm^3$) was added to mixed aqueous solutions of iron(II) and iron(III) chloride (respectively 2 mmol and 4 mmol in 120 $cm^3$) with vigorous stirring. After addition of 28 % aqueous ammonium hydroxide solution (15 $cm^3$), the mixture was stirred for 30 min at 80 °C. Oleic acid (0.2 $cm^3$) was then added to the stirring mixture (four times at 5 min intervals). The resulting aqueous dispersion was used for experiments without washing. This modification by hydrogen bonding is weaker than that by covalent bonding using silane coupling agents, hence washing using a centrifuge tended to cause breakdown of the modified layer and high aggregation.

## Preparation of imidazolium cation-modified gold nanoparticles

Preparation of 1-methylimidazolium chloride-modified gold nanoparticles ([Rmim]Cl-Au-NPs) was reported elsewhere *(6,7)*. Gold nanoparticles were prepared by reduction of $H[AuCl_4]$ using sodium tetrahydroborate or sodium hydride in water in the presence of 3,3′-[disulfanylbis(hexane-1,6-diyl)]-bis(1-methyl-imidazol-3-ium) dichloride. The dispersant was replaced with pure distilled water by dialysis several times. The presence of the imidazolium salt on the surface was obtained by $^1H$ NMR spectroscopy.

## Preparation of nanoparticle-ionic liquid hybrid fluids

Hybrid mixtures of nanoparticles and ionic liquid were prepared by the same procedure for both iron(II,III) oxide and gold nanoparticles. At first, $[C_4mim]Cl$ or $[C_4py]Cl$ were dissolved in an aqueous dispersion of surface modified nanoparticles in a screw-capped vial. An aqueous solution of $K[NTf_2]$ was added to the mixture, which was then shaken until phase separation occurred. Then, the upper aqueous phase was removed by pipette, and the remaining hydrophobic ionic liquid phase was washed three times with distilled water. Details about volumes are shown in each Figure.

## Measurements

$^1H$ NMR spectra were obtained with a JOEL EX-400 spectrometer (400 MHz). Transmission electron microscopy (TEM) measurements were performed using a JOEL JEM-100SX instrument, operated at 100 kV electron

Downloaded by COLUMBIA UNIV on June 28, 2012 | http://pubs.acs.org
Publication Date (Web): December 18, 2009 | doi: 10.1021/bk-2009-1030.ch015

beam accelerating voltage. One drop of the sample solution was deposited onto a copper grid and the excess of the droplet was dried under ambient conditions. The TEM images (shown in the following section) are of a methanol dispersion of [Rmim]Cl-$Fe_3O_4$-NPs and an aqueous dispersion of [Rmim]Cl-Au-NPs, respectively. FT-IR spectra were recorded on a Perkin Elmer 1600 infrared spectrophotometer using a KBr disc dispersed with the powdered sample. Dynamic light scattering (DLS) was measured with a FPAR-1000 (Otsuka Electronics Co., Ltd.) instrument. Thermogravimetric analysis (TGA) was carried out using an Exster-6000 system (Seiko Instruments Inc.).

## Results & Discussion

### Characterisation of surface modified $Fe_3O_4$-NPs and Au-NPs

The diameter of [Rmim]Cl-$Fe_3O_4$-NPs was found to average at *ca.* 8 nm (Figure 1, left). The diameter measured by DLS was slightly larger (around 11 nm) *(3)*. The diameter measured by DLS is normally found to be larger than measured by TEM *(3,5)*. The difference could be due to organic salts and an electric bilayer around the particles *(5)*. Organic components were around 5 wt % according to the TGA curve, in both the cases of [Rmim]Cl-$Fe_3O_4$-NPs and [Rpy]Cl-$Fe_3O_4$-NPs. The number of attached 1-methylimidazolium chloride units was calculated as around 440 based on the nitrogen:carbon ratio measured by elemental analysis.

The average diameter of the gold nanoparticles was found to be 4.8 nm in a TEM image (Figure 1, right). The diameter measured by DLS was 5.4 nm.

### Facile preparation of ionic liquid based magnetic fluids

Preparation of ionic liquid based hydrophobic magnetic iron(II,III) oxide fluids is demonstrated in Figure 2. As reported previously, anion exchange occurred at the surface of the nanoparticles *(3,5,6)*. The anion exchange

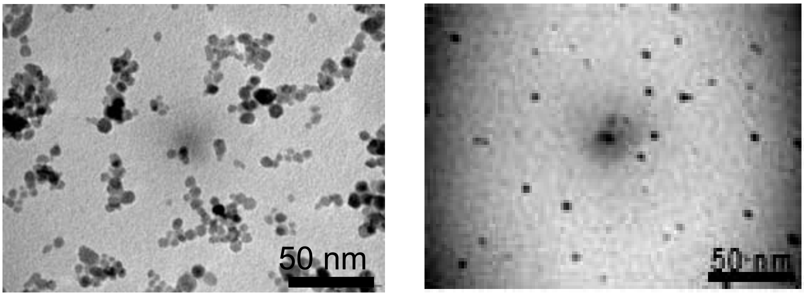

*Figure 1. TEM images of [Rmim]Cl-$Fe_3O_4$-NPs (left) and [Rmim]Cl-Au-NPs (right).*

Downloaded by COLUMBIA UNIV on June 28, 2012 | http://pubs.acs.org
Publication Date (Web): December 18, 2009 | doi: 10.1021/bk-2009-1030.ch015

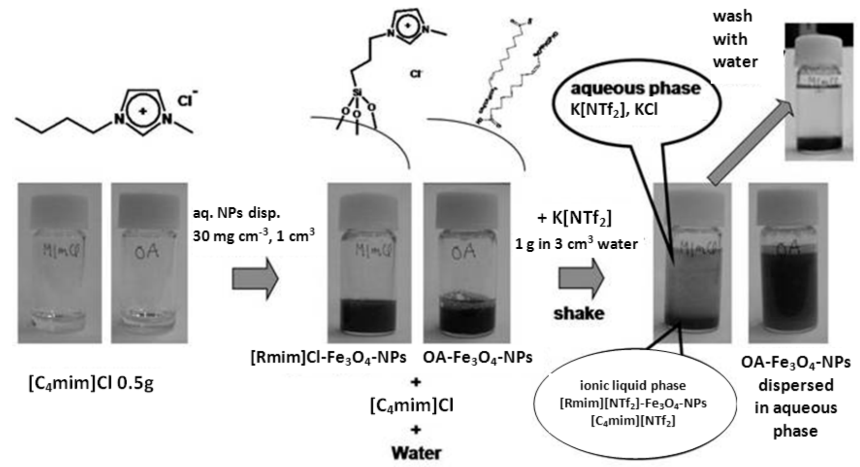

*Figure 2. Preparation of ionic liquid based hydrophobic magnetic fluids and the importance of imidazolium salt layers on the surface.*

easily turned the hydrophilic iron(II,III) oxide nanoparticles hydrophobic *(3,5)*, and caused concentration of iron(II,III) oxide nanoparticles in the hydrophobic ionic liquid phase. In our previous report about [Rmim]Cl-Au-NPs, phase transfer of the [Rmim]Cl-Au-NPs from the aqueous phase to the hydrophobic [C$_4$mim][PF$_6$] phase was observed when hexafluorophosphoric acid was added to an aqueous phase containing [Rmim]Cl-Au-NPs *(6)*. The phase transfer indicated that this is an easy method to concentrate nanoparticles modified with organic salts having the same structure as the ionic liquid dispersant. Similar concentration to the hydrophobic ionic liquid [C$_4$mim][NTf$_2$] was reported using ammonium salt modified quantum dots *(8)*. Also, in this system, the anion on the surface was exchanged, and the change of surface properties improved the miscibility with the [C$_4$mim][NTf$_2$] as dispersant. However, removal of generated small ion pairs and using the same structure for both surface stabiliser and dispersant should be important for making high purity systems.

As a reference experiment, OA-Fe$_3$O$_4$-NPs was also used with the same procedure. OA-Fe$_3$O$_4$-NPs did not concentrate to the [C$_4$mim][NTf$_2$] phase, mainly remaining in the aqueous phase. The result indicates that concentration of the [Rmim]Cl-Fe$_3$O$_4$-NPs was due to anion exchange of the surface modified organic salt moiety.

Figure 3 shows the comparison of the miscibility of [Rmim]Cl-Fe$_3$O$_4$-NPs and C$_8$-Fe$_3$O$_4$-NPs in aqueous and hydrophobic phases. Although both of these nanoparticles were hydrophobic, neither of them could be dispersed in a hexane phase. This result implies the key factor to dominate the dispersibility is not only hydrophobicity, but also good compatibility between the surface stabiliser and dispersant. Additionally, insufficient dispersibility of C$_8$-Fe$_3$O$_4$-NPs in hexane may suggest that the low density and viscosity of hexane make it difficult to keep a high dispersibility of large volumes of iron oxide nanoparticles with a high density comparing to dispersant.

Downloaded by COLUMBIA UNIV on June 28, 2012 | http://pubs.acs.org
Publication Date (Web): December 18, 2009 | doi: 10.1021/bk-2009-1030.ch015

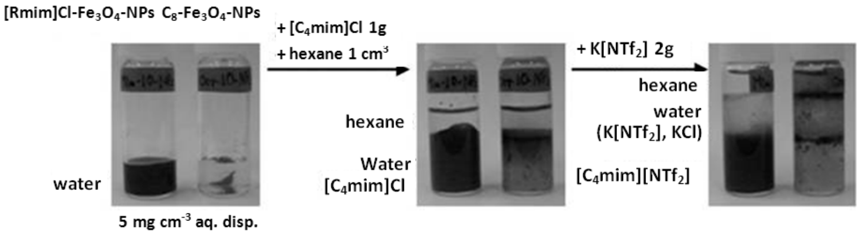

*Figure 3. Comparison of [Rmim]Cl-$Fe_3O_4$-NPs and $C_8$-$Fe_3O_4$-NPs preparations of ionic liquid based hydrophobic magnetic fluids, illustrating the importance of imidazolium salt layers on the surface.*

Downloaded by COLUMBIA UNIV on June 28, 2012 | http://pubs.acs.org
Publication Date (Web): December 18, 2009 | doi: 10.1021/bk-2009-1030.ch015

## Suitable combination of modified organic salts and ionic liquid dispersant

The importance of our method to concentrate nanoparticles relies on the similarity of the molecular structure of the surface stabiliser and ionic liquid as dispersant. If the combination is a mismatch, what will occur?

Figure 4 shows the results of concentration using mismatched structures between the modified organic salt and the dispersant. Interestingly, in a case that [Rpy]Cl-$Fe_3O_4$-NPs was concentrated in [$C_4$mim][$NTf_2$], good dispersibility was observed (Figure 4, upper). In contrast, when [Rmim]Cl-$Fe_3O_4$-NPs were concentrated in [$C_4$py][$NTf_2$], nanoparticles were not transferred to the hydrophobic phase, as shown in the lower pictures of Figure 4. Such experiments with "false" combinations were reported also in a case of gold nanoparticles *(9)*. However, in our result, the difference of miscibility, even if the combination has the same surface and dispersant, merits further discussion focusing on the different amounts of each. The amount of surface modified organic salt is only around 5 wt% of the total components of the nanoparticles. The organic salt layer would be nearly monolayer, meaning quite a low volume compared to that of the dispersant. The miscibility of [$C_4$mim][$NTf_2$] and [$C_4$py][$NTf_2$] should depend on this ratio *(10-12)*. In the upper part of Figure 4, the amount of pyridinium salt is approximately 0.2 mg (supposing 5 wt% of 4 mg is equal to the amount of organic salt), meaning a quite small quantity of [$C_4$py][$NTf_2$] was dissolved in [$C_4$mim][$NTf_2$]. In contrast, in the lower part of Figure 4, [$C_4$py][$NTf_2$] could not displace [$C_4$mim][$NTf_2$] even in low concentration. The fact suggests that dispersibility of ionic liquid-like organic salt-modified nanoparticles in ionic liquids should be strongly dominated by the miscibility of two-phase ionic liquids. In other words, knowledge about the miscibility of ionic liquids is useful to control the dispersibility of nanoparticles. We can choose ionic liquid as dispersants for nanoparticles without studying the dispersibility of the target nanoparticles.

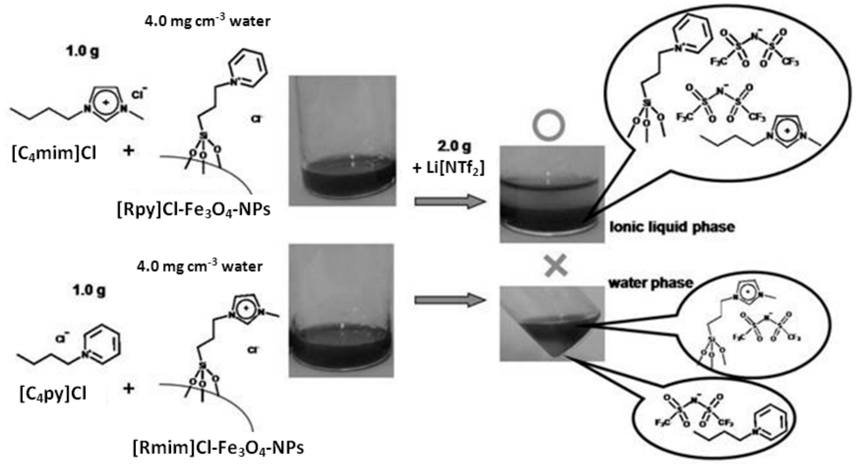

*Figure 4. Mismatch of molecular structure between surface modified salts and ionic liquids as dispersant.*

## Easy preparation of gold nanoparticle-ionic liquid hybrid fluids

One advantage of our method is the easy control of the nanoparticle concentration. Figure 5 illustrates concentration control of the gold nanoparticles. If the concentration of the starting aqueous dispersion is known, the final concentration of ionic liquid based fluid can be controlled by changing the amount of [C$_4$mim]Cl. Generally, although dilution of the dispersion is easy, concentration needs evaporation, centrifuging, filtration, or dialysis. However, the concentration method described here needs none of these procedures, saving a lot of time, manpower, energy and materials. Moreover, it is quite hard to concentrate ionic liquid based dispersions because many of ionic liquids have remarkably low vapour pressure. Indeed, gold nanoparticles synthesised by simply reduction in an aqueous solution are generally too small to concentrate by centrifuging. Actually, the gold nanoparticles in this study could not be concentrated by centrifuging, even at the maximum speed of our machine (20000 rpm). Our concentration method solves the difficulties of concentration, both in ionic liquids and with very small nanoparticles.

Downloaded by COLUMBIA UNIV on June 28, 2012 | http://pubs.acs.org
Publication Date (Web): December 18, 2009 | doi: 10.1021/bk-2009-1030.ch015

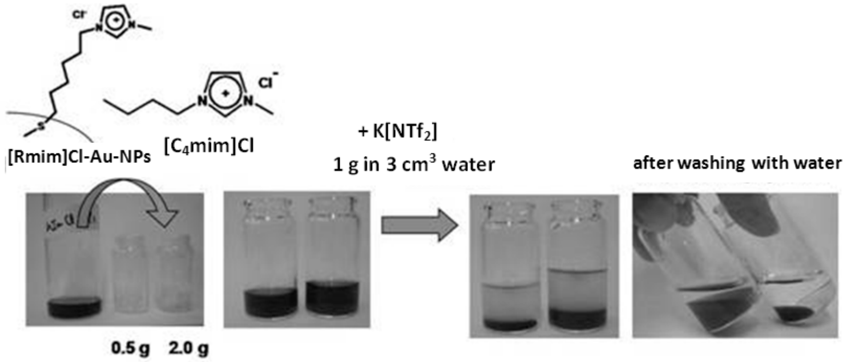

*Figure 5. Concentration of [Rmim]Cl-Au-NPs in to [$C_4$mim][$NTf_2$] in different concentrations, depending on the volume of [$C_4$mim]Cl .*

## Conclusions

In summary, we have reported a facile procedure to prepare inorganic fluids based on ionic liquids using inorganic nanoparticles covalently modified with ionic liquid-like organic salts on the surface. At first, nanoparticles modified with chloride salts of organic cations are dispersed in water containing the same salt. Then, after addition of a salt containing a hydrophobic anion such as bis{(trifluoromethyl)sulfonyl}amide or hexafluorophosphate, hydrophobic ionic liquid phases containing inorganic nanoparticles were formed. This is due to anion exchange between the dispersant and the surface of the nanoparticles. This method requires no evaporation, centrifuging, filtration, or dialysis to regulate the concentration, even if the nanoparticles are very small (being impossible to collect by centrifuging), and is based on ionic liquids with vanishingly small vapour pressures.

## Acknowledgement

This study is a part of a joint research programme, focussed on the development of basic technology for establishing the COE of nano-medicine, carried out through Kyoto City Collaboration of Regional Entities for Advancing Technology Excellence (CREATE), assigned by the Japan Science and Technology Agency (JST).

Downloaded by COLUMBIA UNIV on June 28, 2012 | http://pubs.acs.org
Publication Date (Web): December 18, 2009 | doi: 10.1021/bk-2009-1030.ch015

# References

1. Kiyama, T.; Hirahara, K.; Tanaka, N.; Kuwabata, S., *Appl. Phys. Lett.*, **2006**, *89*, 243117-1-3; Okazaki, K.; Kiyama, T.; Hirahara, K.; Tanaka, N.; Kuwabata, S.; Torimoto, T., *Chem. Commun.*, **2008**, 691-693.
2. Wilkes, J. S.; Levisky, J. A.; Wilson, R. A.; Hussey, C. L. *Inorg. Chem.* **1982**, *21*, 1263-1264; Bowlas, C. J.; Bruce, D. W.; Seddon, K. R. *Chem. Commun.* **1996**, 1625-1626.
3. Naka, K.; Narita, A.; Tanaka, H.; Chujo, Y.; Morita, M.; Inubushi, T.; Nishimura, I.; Hiruta, J.; Shibayama, H.; Koga, H.; Ishibashi, S.; Seki, J.; Kizaka-Kondoh, S.; Hiraoka, M., *Polym. Adv. Mater.,* **2008**, *19*, 1421-1429.
4. Maity, D.; Agrawal, D. C., *J. Magn. Magn. Mater.*, **2007**, *308*, 46-55.
5. Narita, A.; Naka, K.; Chujo, Y., *Colloids and Surface A*, 336, **2009**, 46-56.
6. Itoh, H.; Naka, K.; Chujo, Y., *J. Am. Chem. Soc.*, **2004**, *126*, 3026-3027.
7. Naka, K.; Tanaka, H.; Chujo, Y. *Polym. J.*, **2007**, *11*, 1122-1127.
8. Nakashima, T.; Kawai, T., *Chem. Commun.*, **2005**, 1643-1645.
9. Zhao, D.; Fei, Z.; Ang, W.-H.; Dyson, P. J., *Small*, **2006**, *2*, 879-883.
10. Arce, A.; Earle, M. J.; Katdare, S. P.; Rodríguez, H.; Seddon, K. R., *Chem. Commn.,* **2006**, 2548-2550.
11. Arce, A.; Earle, M. J.; Katdare, S. P.; Rodríguez, H.; Seddon, K. R., *Fluid Phase Equilibria,* **2007**, *261*, 427-433.
12. Arce, A.; Earle, M. J.; Katdare, S. P.; Rodríguez, H.; Seddon, K. R., *Phys. Chem. Chem. Phys.,* **2008**, *10*, 2538-2542.

Downloaded by COLUMBIA UNIV on June 28, 2012 | http://pubs.acs.org
Publication Date (Web): December 18, 2009 | doi: 10.1021/bk-2009-1030.ch015

Downloaded by PENNSYLVANIA STATE UNIV on June 29, 2012 | http://pubs.acs.org
Publication Date (Web): December 18, 2009 | doi: 10.1021/bk-2009-1030.ch016

## Chapter 16

# Ionic Liquids: Promising Media for Gas Separations

**Margarida F. Costa Gomes and Pascale Husson**

**Laboratoire Thermodynamique et Interactions Moléculaires,
CNRS/Université Blaise Pascal, Clermont-Ferrand, 63177 Aubière, France.**

Gas separations are difficult to achieve because differences in density or particle size cannot be used, separation being based on differences in vapour pressure, solubility or diffusivity. The most thoroughly developed process for gas separation is cryogenic distillation, which is an energy intensive process. There is an increasing interest to find more sustainable gas-separation processes, probably based on selective gas adsorption or absorption. Ionic liquids seem a promising alternative to more conventional liquids for gas separations. Their unique properties, and the possibility of synthesising particular ionic liquids for a given use, make them promising gas absorbents. Herein, we review the existing data on solubility, selectivity and diffusivity of different gases in ionic liquids. We compare the regeneration energies of different solvents and discuss the pertinence of continuing a research effort on the solvation properties of gases in ionic liquids.

In Ionic Liquids: From Knowledge to Application; Plechkova, N., et al.;
ACS Symposium Series; American Chemical Society: Washington, DC, 2010.

# Introduction

Separation may be defined as a process that transforms a mixture of substances into two or more components that differ from each other in composition *(1)*. Separation may be viewed as the opposite process to mixing, and so it is difficult to achieve since it is not favoured by the second law of thermodynamics. Separations can be achieved mechanically, by making use of the differences in density or particle size of the components, or by transferring material from one homogeneous phase to another. In this latter case, separation is based on differences in vapour pressure, solubility or diffusivity, the driving force being a concentration or an activity difference. These separations, normally designated as mass-transfer separations *(2)*, include such techniques as distillation, gas absorption, adsorption and membrane separations; they are normally used to separate the components of a gaseous flue.

The earliest and most thoroughly developed process for gas separations is cryogenic distillation *(3),* which involves a partial liquefaction of the gaseous mixture followed by conventional fractional distillation. Economy of scale is a major factor for the industrial use of cryogenic distillation, as there is a drastic reduction in the unit cost of the products when the capacity increases.

More recently, adsorbent-bed processes have been developed making use of the preferential attachment of gas molecules to the surface of a solid. This surface constitutes a discontinuity on the structure of the solid, characterised by the unsaturation of the intermolecular forces that are then available to form bonds with the gas molecules. Direct exploitation of the adsorption phenomenon for use in industry was limited, until the development of zeolites as new adsorbents and until the invention of a new process cycle (pressure-swing adsorption) made it a key process for gas separation in the chemical and petrochemical industries *(1)*. These developments have been accompanied by significant advances in the theories permitting the interpretation of the dynamics and equilibrium of the adsorption process and so adequately describing the performance of separations.

Gas separations through absorption are based in a physical or chemical process by which the gas selectively enters some bulk liquid phase. The solute is subsequently recovered from the liquid by distillation, and the absorbing liquid can be either discarded or reused. The major drawbacks of the traditional gas absorption processes are mainly caused by the nature of the solvent, and by the type of interactions between the solute and the solvent. In an industrial gas absorption process, it is desirable to achieve fast absorption rates and high solute capacities into a solvent that is easily regenerated and for which volume make-up is minimised *(4)*.

In membrane-based gas separations, one component of the gaseous mixture passes through a selective membrane more readily than the other components. The fundamental driving force is the difference in thermodynamic activity that can often be expressed as a difference in concentration or partial pressure. The key parameters to model membrane-based gas separation are the membrane permeability, defined as a product of a diffusivity, a solubility coefficient of the gas species, and the membrane selectivity, defined as the ratio of individual gas permeabilities *(5)*. Membrane gas separations are becoming increasingly

Downloaded by PENNSYLVANIA STATE UNIV on June 29, 2012 | http://pubs.acs.org
Publication Date (Web): December 18, 2009 | doi: 10.1021/bk-2009-1030.ch016

popular due to low capital and operating costs, lower energy requirements, and general ease of operation.

Ionic liquids have been used as reaction media for separations in gas and liquid phases, and for extraction processes. They also seem suitable solvents for gas absorption as they are capable of dissolving preferentially certain families of gases and, due mainly to their negligible vapour pressure and high thermal stability, are easily recycled. The following constraints are necessary before an efficient and economically viable separation process can be implemented: the durability of the ionic liquids in real process conditions must be demonstrated; ionic liquids must be, for certain processes, immobilised in robust, high-flux supports; ionic liquids with more favourable combinations of solubility and transport properties must be developed; and potential environmental impacts must be considered *(6)*.

In this paper, we review the existing data on gas solubility and diffusivity of gases in ionic liquids, and we assess the viability of this family of solvents as promising media for gas absorption and separation.

Downloaded by PENNSYLVANIA STATE UNIV on June 29, 2012 | http://pubs.acs.org
Publication Date (Web): December 18, 2009 | doi: 10.1021/bk-2009-1030.ch016

## Ionic Liquids for Gas Absorption

The solubility of gases in ionic liquids has been the subject of many experimental investigations. More than one hundred papers have been published in the last ten years concerning gas solubility data, both at pressures close to atmospheric and at higher pressures, generally as a function of temperature. The experimental techniques used are adapted from those previously used to measure the solubility of gases in liquids or of gases in solids. Those include pressure, volume and temperature measurements *(7,8)*, gravimetric methods *(9,10)*, electrochemical techniques *(11)* and NMR spectroscopy *(12)*.

The variation of the solubility with temperature allows assessment of the thermodynamic quantities of dissolution, in particular the enthalpy and entropy of solvation. These quantities provide valuable information both about the solute-solvent interactions and about the molecular structure of the solutions: the enthalpy of solution is closely related with the gas-ionic liquid molecular interactions, whereas the entropy of solution gives indications about the structure of the solvent molecules surrounding the solute *(13)*. For the large majority of the systems studied in the literature, an increase of the gas solubility is observed when decreasing the temperature, which corresponds to an exothermic solvation process. Gas solubility is directly proportional to the pressure of the gas above the liquid, provided that the partial pressure of the gas is not large, as stated by Henry's law *(14)*. The proportionality constant is called the Henry's law constant, $K_H$, which is not a function of the composition, which depends on the temperature, and which depends to a lesser extent on pressure. The variation of $K_H$ with pressure is related to the partial volume of the gaseous solute in the liquid phase.

Most of the ionic liquids studied as solvents for gases are based on the 1,3-dialkylimidazolium cation associated to different anions. It is observed that, for the same anion, the increase of the alkyl side-chain length on the imidazolium cation increases the gas solubility, while it is marginally decreased with the addition of a third alkyl substitution on the cation *(15-17)*. Ionic liquids based on different cations, like pyridinium, ammonium, pyrrolidinium and phosphonium associated with different anions, have also been investigated. Kilaru *et al.* *(18)* observed an increase of the gas solubility (carbon dioxide and light hydrocarbons) with the increase of the alkyl chain of the cation in ionic liquids based on the quaternary ammonium cation, and Ohlin *et al.* *(29)* made the same observation for carbon monoxide in pyridinium-based ionic liquids. Gas solubilities of the same order of magnitude were measured for ionic liquids including all these cations, as shown in Figure 1 for the solubility of carbon dioxide in different ionic liquids based on the anion bis{(trifluoromethyl)sulfonyl}amide, $[NTf_2]^-$.

It is the anion that seems to have a larger influence on the gas solubility in ionic liquids, as is illustrated in Figure 2 for the solubility of carbon dioxide in different ionic liquids based on the 1-butyl-3-methylimidazolium cation. The most studied anions are tetrafluoroborate, $[BF_4]^-$, hexafluorophosphate, $[PF_6]^-$, and bis{(trifluoromethyl)sulfonyl}amide, $[NTf_2]^-$. Ionic liquids based on this last anion are capable of dissolving much larger quantities of gases and have physicochemical properties (low viscosity, high thermal and chemical stability, for example) that make them promising new solvents. Trifluoromethanesulfonate (triflate, $[OTf]^-$), nitrate $[NO_3]^-$ , dicyanamide, chloride, alkylsulfate (methylsulfate, $[C_1SO_4]^-$; ethylsulfate, $[C_2SO_4]^-$ and octylsulfate $[C_8SO_4]^-$) and alkyl sulfonate anions are also commonly studied.

The solubilities of gases in ionic liquids are generally higher (lower Henry's law constants) than those measured in common organic solvents, as illustrated in Figure 3 for carbon dioxide. For example, this gas is five times less soluble in ethanol than in 1-butyl-3-methylimidazolium bis{(trifluoromethyl)sulfonyl}amide.

As observed for other gas-liquid systems, the solvation of the different gases depends strongly on the structure of the liquid solvent, and on how the liquid solvent interacts with the gaseous solutes *(13,17,19,20)*. Ionic liquids are considered as designer solvents in the sense that new ionic liquids can be created, either by appropriately combining different anions and cations or by chemically modifying their structure, and so modifying their properties as gas absorbents. These new ionic liquids, often designated as task-specific ionic liquids, conserve the properties of ionic liquids in terms of their low melting point, negligible vapour pressure, high thermal stability or capacity of dissolving different classes of substances, but are capable of fulfilling a particular objective *(21)*. New ionic liquids have recently been proposed to increase the capacity of selective gas absorption, most particularly of carbon dioxide, by physical solubility, by reversibly reacting with the absorbed gas, or by both *(22,23)*.

Downloaded by PENNSYLVANIA STATE UNIV on June 29, 2012 | http://pubs.acs.org
Publication Date (Web): December 18, 2009 | doi: 10.1021/bk-2009-1030.ch016

Downloaded by PENNSYLVANIA STATE UNIV on June 29, 2012 | http://pubs.acs.org
Publication Date (Web): December 18, 2009 | doi: 10.1021/bk-2009-1030.ch016

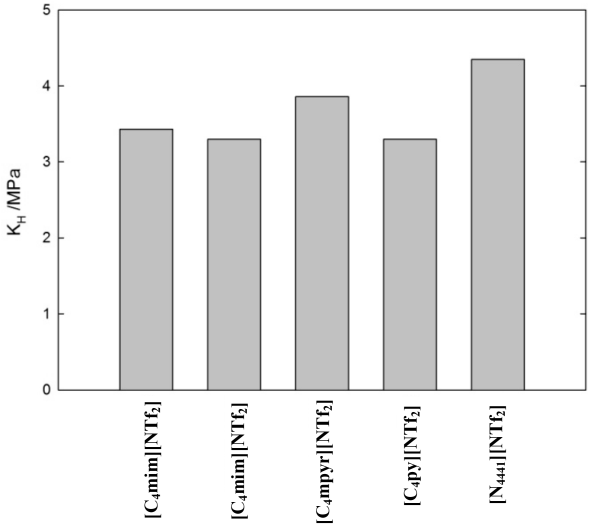

*Figure 1. Henry's law constants, $K_H$, for carbon dioxide at 298 K in left to right $[C_4mim][NTf_2]$ (1-butyl-3-methylimidazolium bis{(trifluoromethyl)sulfonyl}-amide) (24,37); $[C_4mpyr][NTf_2]$ (1-butyl-1-methylpyrrolidinium bis{(trifluoromethyl)sulfonyl}amide) (37); $[C_4py][NTf_2]$ (1-butyl-3-methyl-pyridinium bis{(trifluoromethyl)sulfonyl}amide) (23); and $[N_{441}][NTf_2]$ (tributymethylammonium bis{(trifluoromethyl)sulfonyl}amide) (37).*

Interesting examples include the fluorination of the alkyl-side chain of 1,3-dialkylimidazolium cations, which increases the solubility of carbon dioxide *(22,24,25)* as it makes use of the known affinity of perfluorinated alkyl chains for carbon dioxide *(26)*. The same success could not be achieved with the introduction of carboxyl groups in the alkyl-side chain of imidazolium cations, since a decrease of the solubility was observed for carbon dioxide *(27)*. As expected, changing the anion also influences gas solubility and, although this effect was extensively studied for carbon dioxide *(27)* and for fluorinated gases *(10)*, the mechanisms involved in the solvation are not yet fully understood *(9,28,29)*.

Downloaded by PENNSYLVANIA STATE UNIV on June 29, 2012 | http://pubs.acs.org
Publication Date (Web): December 18, 2009 | doi: 10.1021/bk-2009-1030.ch016

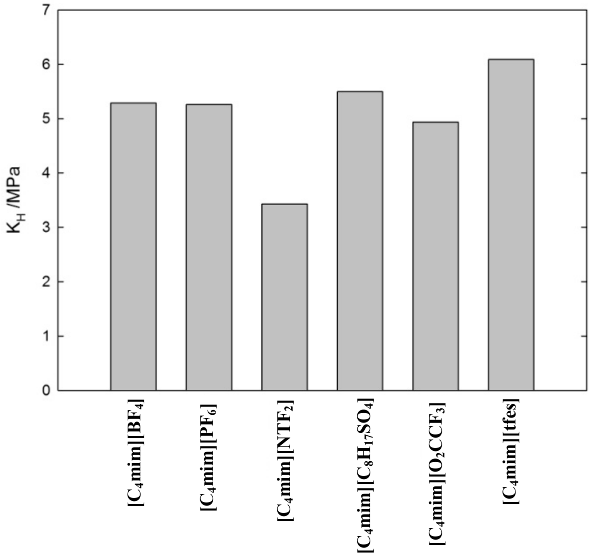

*Figure 2. Henry's law constants, $K_H$, for carbon dioxide at 298 K in $[C_4mim][BF_4]$ (1-butyl-3-methylimidazolium tetrafluoroborate) (28); $[C_4mim][PF_6]$ (1-butyl-3-methylimidazolium hexafluorophosphate) (28); $[C_4mim][NTf_2]$ (1-butyl-3-methylimidazolium bis{(trifluoromethyl)sulfonyl}-amide) (24); (1-butyl-3-methylimidazolium octylsulfate) (38); $[C_4mim][O_2CCF_3]$ (1-butyl-3-methylimidazolium trifluoroethanoate) (28); $[C_4mim][tfes]$ (1-butyl-3-methylimidazolium tetrafluoroethanesulfonate) (28).*

Spectacular increases in the solubility of different gases in ionic liquids have been accomplished by functionalising the ionic liquid, in the cation *(21)* or in the anion *(30)*, and so making the gas react reversibly with the ionic liquids. The absorption can then become selective to one gas, as in the case of the addition of a primary amine function to the alkyl-side chain of an 1,3-dialkylimidazolium cation, that leads to a highly specific carbon dioxide chemical absorption through the probable formation of an ammonium carbamate *(4,21)*. This chemical absorption results in a significant increase in the viscosity of the solution, thus implying mass transfer limitations.

Downloaded by PENNSYLVANIA STATE UNIV on June 29, 2012 | http://pubs.acs.org
Publication Date (Web): December 18, 2009 | doi: 10.1021/bk-2009-1030.ch016

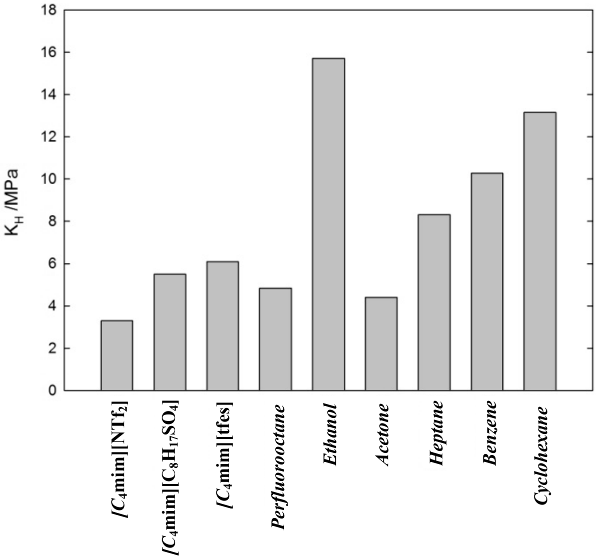

*Figure 3. Henry's law constants, $K_H$, for carbon dioxide at 298 K in [$C_4$mim][$NTf_2$] (1-butyl-3-methylimidazolium bis{(trifluoromethyl)sulfonyl}-amide) (24); [$C_4$mim][$C_8H_{17}SO_4$] (1-butyl-3-methylimidazolium octylsulfate) (38); [$C_4$mim][tfes] (1-butyl-3-methylimidazolium tetrafluoroethanesulfonate) (28); perfluorooctane (56); ethanol (60); propanone (60); heptane (60); benzene (60) and cyclohexane (60).*

The reasons that lead to an increase in gas solubility are not always clear and certainly joint efforts of experimentalists from different disciplines, as well as the contribution of theory and modelling, are desirable in order to clarify the mechanisms that govern the solution processes. For example, for the selective absorption of sulfur dioxide, several specific ionic liquids have been developed: hydroxylammonium-based ionic liquids *(31)*, tetramethylguanidinium-based ionic liquids *(32)* and functionalised ionic liquids *(33)*. Different authors interpret distinctively the mechanism of gas absorption and sometimes conclude that the absorption is chemical, or alternatively physical, even for the same or very similar ionic liquids.

The properties of different ionic liquids for gas absorption can also be modified by mixing them with different molecular compounds *(34)*. By analysing the drawbacks of the most used process for the carbon dioxide capture from flue gas, chemical absorption by aqueous amine solutions, Camper *et al. (35)* have combined the desirable properties of ionic liquids (low vapour pressure, thermal stability) with the performance of amines for carbon dioxide chemical absorption. For that, they have mixed ionic liquids with commercially available amines, carbon dioxide being captured as a carbamate species.

Mixing two ionic liquids can also increase the efficiency of gas separations and an enhancement of the selectivity of carbon dioxide (when mixed with dinitrogen or methane) was found *(36)* by mixing two imidazolium-based ionic liquids: 1-ethyl-3-methylimidazolium bis{(trifluoromethyl)sulfonyl}amide with 1-ethyl-3-methylimidazolium tetrafluoroborate.

The use of membranes containing ionic liquids has been attempted to separate gases. Supported ionic liquid membranes utilising porous supports impregnated with ionic liquids *(39),* and more recently polymers made of ionic liquid monomers *(40),* were found to increase the sorption, the rates of sorption and desorption, and the selectivity for carbon dioxide. Promising results were obtained with poly(ionic liquids)-ionic liquids solid composites as gas-separating membranes *(41)*.

Downloaded by PENNSYLVANIA STATE UNIV on June 29, 2012 | http://pubs.acs.org
Publication Date (Web): December 18, 2009 | doi: 10.1021/bk-2009-1030.ch016

## Selectivity of Gas Absorption in Ionic Liquids

The solubility of different gases in an ionic liquid can differ for more than one order of magnitude, depending on the molecular characteristics of the solute. These differences in solubility are related with the selectivity of gas absorption in ionic liquids and are represented in Figure 4 for different gases in $[C_4mim][BF_4]$.

Carbon dioxide, $CO_2$, sulfur oxide, $SO_2$, light hydrocarbons (*e.g.* methane, $CH_4$, ethane, $C_2H_6$ or ethylene, $C_2H_4$), dioxygen, $O_2$, dinitrogen, $N_2$, dihydrogen, $H_2$, argon, Ar, and carbon monoxide, CO are among the most studied gases in ionic liquids. The first two gases are the most soluble, light hydrocarbons present medium solubilities, while the other gases are one order of magnitude less soluble in ionic liquids. The relative solubility of different solutes in ionic liquids depends on the structure of the pure solvent and on the interactions between solute and solvent. The intrinsic complexity of ionic liquids – their nature as nanosegregated fluids *(42)* – must always be taken into account when dealing with their ability to dissolve different gases *(43)*, even when these are similar in molecular terms *(44)*.

Carbon dioxide is by far the most studied gas in ionic liquids. It is also one of the most soluble, with typical mole fraction solubilities of $10^{-2}$ and Henry's law constants below 100 bar. It has been suggested by molecular simulation that the electrostatic interactions between carbon dioxide and the ionic liquid are responsible for the high solubility of this gas *(19)*. The amount of carbon dioxide absorbed by an ionic liquid can be dramatically increased by using new functionalised ionic liquids specially designed to reversibly react with carbon dioxide and so sequestrate the gas *(21,28)*.

Downloaded by PENNSYLVANIA STATE UNIV on June 29, 2012 | http://pubs.acs.org
Publication Date (Web): December 18, 2009 | doi: 10.1021/bk-2009-1030.ch016

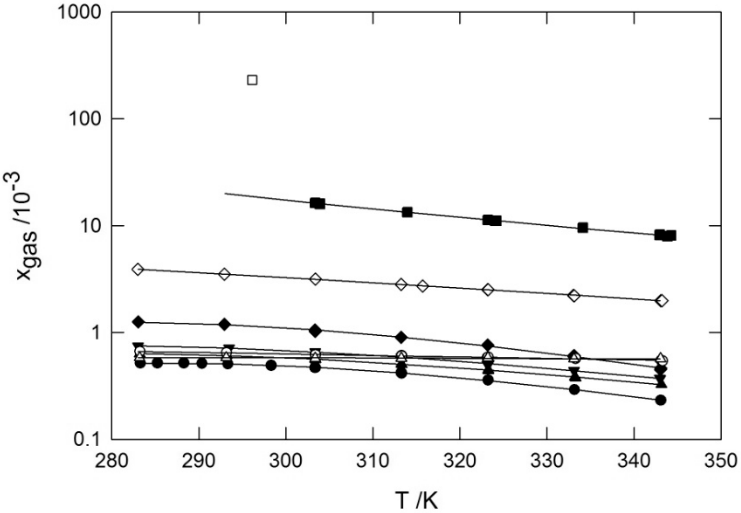

*Figure 4. Gas solubilities in [$C_4$mim][$BF_4$] expressed as gas mole fraction and as a function of temperature: □, $SO_2$(11); ■, $CO_2$(46); ◆, $CH_4$(46); ◇, $C_2H_6$(46); ○, $O_2$(46); ▲, $N_2$(46); ▼, Ar(46); ●, $H_2$(46); △, CO(46).*

The solubility of $SO_2$ in ionic liquids is extremely high, this gas being over one order of magnitude more soluble than carbon dioxide. For example, in [$C_6$mim][$NTf_2$], its mole fraction approaches 0.9 near the $SO_2$ saturation pressure at ambient temperature *(45)*. The reasons for such high solubilities are still not clear: in some cases, like in hydroxyammonium- *(31)* or guanidinium-based ionic liquids *(32)*, they have been explained by chemical absorption; in other ionic liquids, like [$C_4$mim][$BF_4$] and also guanidinium-based ionic liquids, Huang *et al. (33)* found no evidence of the formation of new chemical bonds and explain the high solubility of $SO_2$ by physical absorption only. Similar conclusions were drawn by Anderson *et al. (45)* who used NMR analysis before and after exposure of the ionic liquid to $SO_2$ to verify that no new products were formed, since no change was observed in the solvent sample during the gas absorption or desorption.

The solubility of light hydrocarbons in ionic liquids is lower than that of carbon dioxide but often of the same order of magnitude, tending to increase with the number of carbon atoms and double bonds of the gas molecule. The less soluble gases are dioxygen, dinitrogen, dihydrogen, argon and carbon monoxide with Henry's law constants in [$C_4$mim][$BF_4$] varying from 1500 to 2200 bar at 303 K *(46)*.

High solubilities were also measured for hydrogen sulfide *(47)*, ammonia *(48)* and nitrous oxide *(37)* in several ionic liquids. The explanation evoked for these high solubilities is that they are governed by specific gas-ionic liquid interactions. No evidence of chemical absorption was found by the different research groups.

The presence of a molecular component – water *(23)*, an alcohol *(57)* or ethanenitrile *(34)* – affects the gas solubility. The way in which the gas solubility in the ionic liquid is affected by the presence of a molecular compound must be taken into account in the choice of an absorbent for gas separation. The mixture to be treated can contain several components that, even when present at very low concentrations, can affect significantly the absorption properties of the solvent.

## Diffusivity of Gases in Ionic Liquids

The diffusion coefficients of gases in ionic liquids have been determined experimentally by cyclic voltammetry *(11,50,51)*, diffusion through liquid films (lag-time technique *(58)* or transient thin liquid film method *(24)*), or using a gravimetric microbalance *(10,59)*. Some of these techniques allow the determination, in a single experiment, of the gas solubility and of the diffusivity.

An average uncertainty on the diffusion coefficient of 5% (maximum 10%) is generally obtained by cyclic voltammetry *(11,51)*. Diffusion through liquid films leads to higher uncertainties on the diffusion coefficient (average of 10%, maximum 18% *(58)*) which can be explained by several assumptions made in the interpretation of the experimental data (liquid film of uniform thickness, gas transport governed solely by molecular diffusion) *(24)*. Finally, the highest uncertainties were obtained with the gravimetric microbalance (overall uncertainty limit in the diffusivity of a factor of two), which are mainly explained by experimental uncertainties *(10)*.

The diffusion coefficients of several gases ($SO_2$, $NO_2$, $CO_2$, $O_2$ and $H_2$) in imidazolium-, phosphonium-, ammonium- and pyridinium-based ionic liquids have been determined to be of the order of $10^{-6}$ $cm^2$ $s^{-1}$. Gas diffusivities in ionic liquids are more than one order of magnitude smaller than in traditional organic solvents like water, short-chain alcohols or low-molecular-weight hydrocarbons. This is attributed to the higher viscosities of the ionic liquids and is confirmed by the lower diffusion coefficients in the more viscous phosphonium-based ionic liquids. Higher diffusivities are nevertheless measured for phosphonium-based ionic liquids than for imidazolium-based solvents with the same viscosity.

Further research is needed to fully understand the transport of gases in ionic liquid media. The correlations typically used in literature for liquid systems (Stokes-Einstein, Wilke-Chang, *etc.*) were found to be inadequate to correlate the diffusivity of gases in ionic liquid. The dependence of diffusivity on temperature and size of the solute gas is different from that found for other classes of solvents.

The diffusion coefficients for different gases in one ionic liquid, the [$C_2$mim][$NTf_2$] are shown in Figure 5.

Downloaded by PENNSYLVANIA STATE UNIV on June 29, 2012 | http://pubs.acs.org
Publication Date (Web): December 18, 2009 | doi: 10.1021/bk-2009-1030.ch016

Downloaded by PENNSYLVANIA STATE UNIV on June 29, 2012 | http://pubs.acs.org
Publication Date (Web): December 18, 2009 | doi: 10.1021/bk-2009-1030.ch016

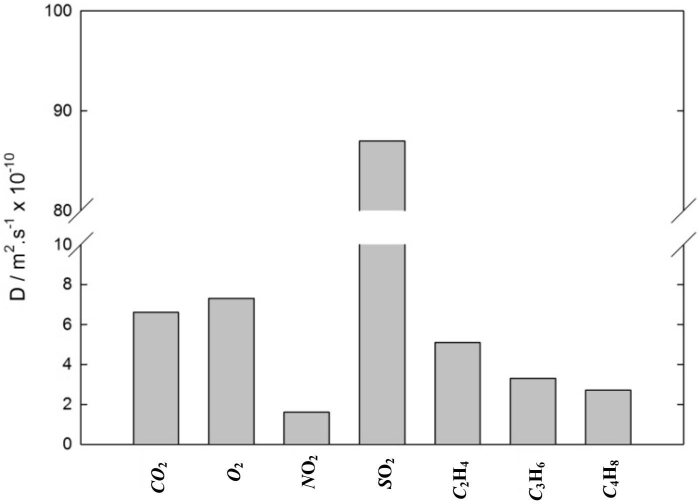

*Figure 5. Diffusion coefficients in 1-ethyl-3-methylimidazolium bis{(trifluoromethyl)sulfonyl}amide, [$C_2$mim][$NTf_2$] for $CO_2$, 30°C (49), $O_2$, 20°C (50), $NO_2$, 25°C (51), $SO_2$, 23°C (11), $C_2H_4$, 30°C (49), $C_3H_6$, 30°C (49), $C_4H_8$, 30°C (49).*

## Recycling of the Absorbent

A favourable characteristic of absorption as a way to separate or capture gases is that, with the choice of proper absorbents, the absorption can be reversed by sending the gas-rich absorbent to a desorber (or stripper) where the pressure is reduced and/or the temperature is raised. The regenerated absorbent is then returned (after pressurisation and/or cooling) to the absorption tower thereby creating a fully continuous process *(52)*. Significant amounts of energy are necessary for the recycling of the absorbent. The recycling energy depends on the heat of dissolution in the case of the physical absorption, and of the reaction stoicheiometry and heat of reaction in the case of chemical absorption of the gas or gases that are to be captured or separated. Furthermore, extensive equipment is required because unless specific technology is used (as in the case of liquid-membrane separations), large volumes of liquid absorbent are circulated and a heat exchange unit is necessary.

Gas-separation membranes are alternatives to more traditional absorption processes. They are normally constituted by solids and operate on the principle that their porous structure permits the preferential permeation of mixture components. The main design and operational parameters of membranes are their selectivity and permeability. Sometimes a two-stage system is needed to achieve good separation and the costs are still more important than those of more conventional separation processes. The principal cost component is compression energy since the recycling of the membrane can be done using current gas stripping techniques.

In Figure 6, the enthalpies of solution of carbon dioxide in different absorbents are compared. These values allow an assessment of the energy necessary to recover the solvents after gas absorption and show the advantage of using ionic liquids for physical gas absorption in terms of the recycling of the absorbent.

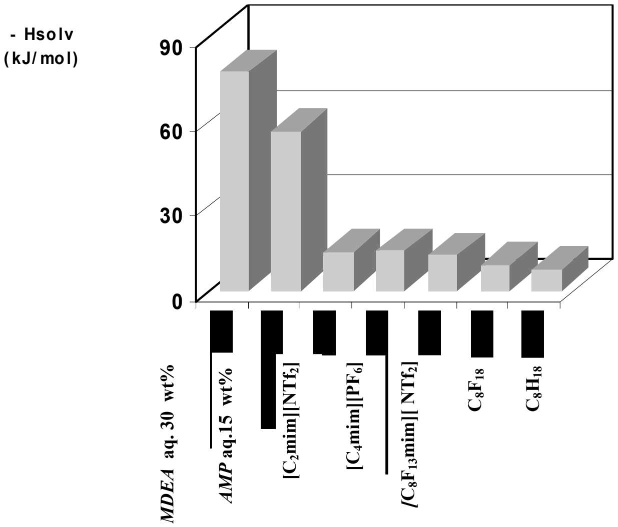

*Figure 6. Enthalpies of dissolution for carbon dioxide in different solvents: MDEA (methyldiethylamine), aq.30 wt% (53); AMP (2-amino-2-methyl-1-propanol), aq.15 wt% (54);* $[C_2mim][NTf_2]$ *(16);* $[C_4mim][PF_6]$ *(55);* $[C_8F_{13}mim][NTf_2]$ *(16);* $C_8F_{18}$ *(56);* $C_8H_{18}$ *(56).*

## Conclusions

Ionic liquids seem to present several advantages as new media for gas separations. Their unique properties can be useful to new separation processes, namely their negligible vapour pressure, thermal stability and the possibility of designing the appropriate ionic liquid for a given application. Even if the studies concerning gas absorption in ionic liquids have been quite numerous in recent years, as it has been demonstrated in this paper, there are still several issues that need to be addressed before large scale processes can be developed.

The first point concerns the quantity of a given gas that can be absorbed by an ionic liquid and how efficiently it is absorbed in terms of selectivity and mass transport. It has been shown that it is possible to modify the ionic liquid to increase the absorption of gases, by combining the appropriate anion and cation or by functionalising the ionic liquid, to favour a larger absorption that can be physical or chemical, the former leading to less quantities of absorbed gases but also to lower desorption energies. The enormous variety of possible ionic liquids makes a trial and error approach impossible and so there is a real need to

Downloaded by PENNSYLVANIA STATE UNIV on June 29, 2012 | http://pubs.acs.org
Publication Date (Web): December 18, 2009 | doi: 10.1021/bk-2009-1030.ch016

pursue fundamental research with the aim of understanding the mechanisms involved in the absorption processes.

Once the family of ionic liquid to be used is identified, several properties still need to be studied, like the chemical and physical stability of the liquid when exposed to the gas mixture to be treated (that can lead to the necessity of removing a certain number of reactive species prior to separation), the corrosion, fouling or foaming properties of the absorbent (that may impose the need of continuous or intermittent purification of partially contaminated absorbents), and biodegradability and toxicity (in order to determine the appropriate procedures to safely discard the ionic liquids after their use). If the absorption is mainly due to a chemical reaction, the characterisation of the chemical equilibria and kinetics are also necessary.

Ionic liquids show important potential in the development of absorption-based gas separations either in conventional designs, like columns or agitated vessels, or in gas absorption membranes that hold considerable promise provided their physical and chemical stability can be assured.

Downloaded by PENNSYLVANIA STATE UNIV on June 29, 2012 | http://pubs.acs.org
Publication Date (Web): December 18, 2009 | doi: 10.1021/bk-2009-1030.ch016

## References

1. Yang, R.T. *Gas Separation by Adsorption Processes*; Imperial College Press: London, 1997.
2. McCabe, W.L.; Smith, J.C.; Harriott, P. *Unit Operations of Chemical Engineering*; McGrawHill Professional: New York, 2005.
3. Gunardson, H. *Industrial Gases in Petrochemical Processing*; Marcel Dekker: New York, 1998.
4. Galan Sanchez, L.M.; Meindersma, G.W.; de Haan, A.B. *Chem. Eng. Res. Des.* **2007**, *85(A1)*, 31-39.
5. Javaid, A. *Chem. Eng. J.* **2005**, *112*, 219-226.
6. Baltus, R.E.; Counce, R.M.; Culbertson, B.; Luo, H.; DePaoli, D.W.; Dai, S.; Duckworth, D.C. *Separ. Sci. Technol.* **2005**, *40*, 525-541.
7. Costa Gomes, M.F. *J. Chem. Eng. Data* **2007**, *52*, 472-475.
8. Kumelan, J.; Kamps, A. P. S.; Tuma, D.; Yokozeki, A.; Shiflett, M. B.; Maurer, G. *J Phys Chem B* **2008**, *112*, 3040-3047.
9. Anderson, J. L.; Dixon, J. K.; Brennecke, J. F. *Accounts Chem. Res.* **2007**, 40, 1208-1216.
10. Shiflett, M.; Harmer, M.A.; Junk, C.P.; Yokozeki, A. *J. Chem. Eng. Data* **2006**, *51*, 483-495.
11. Barrosse-Antle, L. E.; Silvester, D. S.; Aldous, L.; Hardacre, C.; Compton, R. G. *J. Phys. Chem. C* **2008**, 112, 3398-3404.
12. Dyson, P. J.; Laurenczy, G.; Ohlin, C. A.; Vallance, J.; Welton, T. *Chem. Commun.* **2003**, 2418-2419.
13. Costa Gomes, M.F.; Padua, A.A.H. *Pure Appl. Chem.* **2005**, *77*, 653-665.
14. Prausnitz, J.M.; Lichtenthaler, R.N.; Gomes de Azevedo, E. *Molecular Thermodynamics of Fluid-Phase Equilibria*; Prentice-Hall: New Jersey, 1986.
15. Jacquemin, J.; Majer, V.; Husson, P.; Costa Gomes, M.F. *J. Solution Chem.* **2007**, *36*, 967-979.

16. Hong, G.; Jacquemin, J.; Deetlefs, M.; Hardacre, C.. Husson, P.; Costa Gomes, M.F. *Fluid Phase Equilib.* **2007**, *257*, 27-34.
17. Cadena, C.; Anthony, J. L.; Shah, J. K.; Morrow, T. I.; Brennecke, J. F.; Maginn, E. J. *J. Am. Chem. Soc.* **2004**, 126, 5300-5308.
18. Kilaru, P. K.; Condemarin, P. A.; Scovazzo, P. *Ind. Eng. Chem. Res.* **2008**, *47*, 900-909.
19. Deschamps, J.; Costa Gomes, M.F.; Padua, A.A.H. *ChemPhysChem* **2004**, *5*, 1049-1052.
20. Shi, W.; Maginn, E. J. *J. Phys. Chem. B* **2008**, *112*, 2045-2055.
21. Bates, E. D.; Mayton, R. D.; Ntai, I.; Davis, J. H. *J. Am. Chem. Soc.* **2002**, *124*, 926-927.
22. Muldoon, M.J. ; Aki, S. ; Anderson, J.L. ; Dixon, J.K. ; Brennecke, J.F. *J. Phys. Chem. B* **2007***, 111*, 9001-9009.
23. Fu, D. B.; Sun, X. W.; Pu, J. J.; Zhao, S. Q. *J. Chem. Eng. Data* **2006**, *51*, 371-375; Zhang, Z. F.; Wu, W. Z.; Gao, H. X.; Han, B. X.; Wang, B.; Huang, Y. *Phys. Chem. Chem. Phys.* **2004**, *6*, 5051-5055.
24. Hou, Y.; Baltus, R. E. *Ind. Eng. Chem. Res.* **2007**, *46*, 8166-8175.
25. Almantariotis, D.; Costa Gomes, M.F.; Coxam, J.-Y.; Gefflaut, T. *1st Congress of the Federation on Environmental Research*, Université Blaise Pascal, France (2008).
26. Costa Gomes, M.F. ; Padua, A.A.H. *J. Phys. Chem. B* **2003**, *107*, 14020-14024.
27. Bermejo, M.D. ; Montero, M. ; Daez, E. ; Florusse, L.J. ; Kotlewska, A.J. ; Cocero, M.J. ; van Rantwijk, F. ; Peters, C.J. *J. Phys. Chem. B* **2008**, *112*, 13532-13541.
28. Yokozeki, A.; Shiflett, M.B.; Junk, C.P.; Grieco, L.M.; Foo, T. *J. Phys. Chem. B* **2008**, 112 (51), 16654–16663.
29. Ohlin, C. A.; Dyson, P. J.; Laurenczy, G. *Chem. Commun.* **2004**, 1070-1071.
30. Shiflett, M.; Kasprzak, D.J.; Junk, C.P.; Yokozeki, A. *J. Chem. Thermodyn.* **2007**, *40*, 25-31.
31. Yuan, X.L.; Zhang, S.J.; Liu, J.; Lu, X.M. *Fluid Phase Equilib.* **2007**, *257*, 195-200; Yuan, X.L.; Zhang, S.J.; Lu, X.M. *J. Chem. Eng. Data* **2007**, *52*, 596-599.
32. Wu, W.Z.; Han, B.X.; Gao, H.X.; Liu, Z.M.; Jiang, T.; Huang, J. *Angew. Chem. Int. Edit.* **2004**, *43*, 2415-2417.
33. Huang, J.; Riisager, A.; Wasserscheid, P.; Fehrmann, R. *Chem. Commun.* **2006**, 4027-4029.
34. Hong, G.; Jacquemin, J.; Husson, P.; Costa Gomes, M.F.; Deetlefs, M.; Nieuwenhuyzen, M.; Sheppard, O.; Hardacre, C. *Ind. Eng. Chem. Res.* **2006**, *45*, 8180-8188.
35. Camper, D.; Bara, J.E.; Gin, D.L.; Noble, R.D. *Ind. Eng. Chem. Res.* **2008**, *47*, 8496-8498.
36. Finotello, A.; Bara, J.E.; Narayan, S.; Camper, D.; Noble, R.D. *J. Phys. Chem. B* **2008**, *112*, 2335-2339.
37. Anthony, J. L.; Anderson, J. L.; Maginn, E. J.; Brennecke, J. F. *J Phys. Chem. B* **2005**, *109*, 6366-6374.

Downloaded by PENNSYLVANIA STATE UNIV on June 29, 2012 | http://pubs.acs.org
Publication Date (Web): December 18, 2009 | doi: 10.1021/bk-2009-1030.ch016

38. Jacquemin, J.; Husson, P.; Majer, V.; Padua, A. A. H.; Costa Gomes, M. F. *Green Chem.* **2008**, *10*, 944-950.
39. Hu, X. D.; Tang, J. B.; Blasig, A.; Shen, Y. Q.; Radosz, M. *J. Membrane Sci.* **2006**, *281*, 130-138 ; Scovazzo, P.; Kieft, J.; Finna, D.A.; Koval, C.; DuBois, D.; Noble, R. *J. Membrane Sci.* **2004**, *238*, 57–63.
40. Tang, J. B.; Tang, H. D.; Sun, W. L.; Plancher, H.; Radosz, M.; Shen, Y. Q. *Chem. Commun.* **2005**, 3325-3327; Blasig, A.; Tang, J. B.; Hu, X. D.; Tan, S. P.; Shen, Y. Q.; Radosz, M. *Ind. Eng. Chem. Res.* **2007**, *46*, 5542-5547.
41. Bara, J. E.; Hatakeyama, E. S.; Gin, D. L.; Noble, R. D. *Polym. Advan. Technol.* **2008**, *19*, 1415-1420.
42. Padua, A.A.H.; Canongia Lopes, J.N. *J. Phys. Chem. B* **2006**, *110*, 3330.
43. Canongia Lopes, J.N.; Costa Gomes, M.F.; Padua, A.A.H. *J. Phys. Chem. B* **2006**, *110*, 16816-16818.
44. Pison, L.; Canongia Lopes, J.N.; Rebelo, L.P.N.; Padua, A.A.H.; Costa Gomes, M.F. *J. Phys. Chem. B* **2008**, *112*, 12394-12400.
45. Anderson, J.L.; Dixon, J.K.; Maginn, E.J.; Brennecke, J.F. *J. Phys. Chem. B* **2006**, *110*, 15059-15062.
46. Jacquemin, J.; Costa Gomes, M.F.; Husson, P.; Majer, V. *J. Chem. Thermodyn.* **2006**, *38*, 490-502.
47. Jou, F.Y.; Mather, A.E. *Int. J. Thermophys.* **2007**, *28*, 409-495; Pomelli, C.S.; Chiappe, C.; Vidis, A.; Laurenczy, G. Dyson, P. *J. Phys. Chem. B* **2007**, *111*, 13014-13019.
48. Yokozeki, A.; Shiflett, M. B. *Appl. Energ.* **2007**, *84*, 1258-1273. Yokozeki, A.; Shiflett, M. B. *Ind. Eng. Chem. Res.* **2007**, *46*, 1605-1610.
49. Morgan, D.; Ferguson, L.; Scovazzo, P. *Ind. Eng. Chem. Res.* **2005**, *44*, 4815-4823.
50. Buzzeo, M. C.; Klymenko, O. V.; Wadhawan, J. D.; Hardacre, C.; Seddon, K. R.; Compton, R. G. *J. Phys. Chem. A* **2003**, *107*, 8872-8878.
51. Broder, T. L.; Silvester, D. S.; Aldous, L.; Hardacre, C.; Compton, R. G. *J. Phys. Chem. B* **2007**, *111*, 7778-7785.
52. Meisen, A.; Shuai, X. *Energy Convers. Mgmt.* **1997**, *38*, S37-S42.
53. Kierszowska-Pawlak, H. *Separ. Sci. Technol.* **2007**, *42*, 2723-2737.
54. Arcis, H.; Rodier, L.; Coxam, J. Y. *J. Chem. Thermodyn.* **2007**, *39*, 878-887.
55. Jacquemin, J.; Husson, P.; Majer, V.; Costa Gomes, M.F. *Fluid Phase Equilibr.* **2006**, *240*, 87-95.
56. Deschamps, J.; Menz, D.-H.; Padua, A.A.H.; Costa Gomes, M.F. *J. Chem. Thermodyn.* **2007**, *39*, 847-854.
57. Kuhne, E.; Calvo, E. S.; Witkamp, G. J.; Peters, C. J. *J. Supercrit. Fluids* **2008**, *45*, 293-297; Liu, Z. M.; Wu, W. Z.; Han, B. X.; Dong, Z. X.; Zhao, G. Y.; Wang, J. Q.; Jiang, T.; Yang, G. Y. *Chem. – Eur. J.* **2003**, *9*, 3897-3903.
58. Ferguson, L.; Scovazzo, P. *Ind. Eng. Chem. Res.* **2007**, *46*, 1369-1374.
59. Shiflett, M.; Yokozeki, A. *AIChE J.* **2006**, *52*, 1205 ; Shiflett, M.; Harmer, M. A.; Junk, C. P.; Yokozeki, A. *Fluid Phase Equilib.* **2006**, *242*, 220.

60 Wilhelm, E.; Battino, R., *Chem. Rev.* **1973,** *73*, 1.

Downloaded by PENNSYLVANIA STATE UNIV on June 29, 2012 | http://pubs.acs.org
Publication Date (Web): December 18, 2009 | doi: 10.1021/bk-2009-1030.ch016

Downloaded by OHIO STATE UNIV LIBRARIES on June 28, 2012 | http://pubs.acs.org
Publication Date (Web): December 18, 2009 | doi: 10.1021/bk-2009-1030.ch017

## Chapter 17

# Ionic Liquid Complexes for Metal Extractions and Biphasic Catalysis

**Prashant U. Naik, Carrie Lee Trider, Jeff Farrell, and Robert. D. Singer***

**Department of Chemistry, Saint Mary's University, Halifax, Nova Scotia, Canada B3H 3C3**

Over the last few years, we have been engaged in the synthesis of ionic liquids bearing ethylamine diacetic acid ligands, $-(CH_2)_2N(CH_2COOH)_2$, for extraction of different metal ions from aqueous solutions. These ionic liquids form stable complexes with metal ions such as copper(II), nickel(II), cobalt(II), and zinc(II). In an extension to the above approach, we have designed and synthesised an imidazolium based ionic liquid containing a salicylaldoxime ligand that has demonstrated promising results in the formation of a stable complex with copper (II). The complex was characterised by single crystal X-ray crystallography and ESI-MS. Yet another related strategy pertaining to complexes of transition metals involves the preparation of an imidazolium ion containing a salen ligand. We are currently studying the ability of the ionic liquid-salen-metal complexes to act as catalysts in organic reactions.

## Introduction

As demonstrated throughout this symposium, ionic liquids are now well established as viable alternative solvents and have proven to be useful in a very interesting array of applications. Among these applications is the use of ionic liquids in analytical applications such as materials for MALDI-TOF-MS *(1)*, as lubricants *(2)*, and as thermal fluids *(3)* useful in heat transport and storage. Ionic liquids have also been applied in a variety of electrochemical scenarios

In Ionic Liquids: From Knowledge to Application; Plechkova, N., et al.;
ACS Symposium Series; American Chemical Society: Washington, DC, 2010.

Downloaded by OHIO STATE UNIV LIBRARIES on June 28, 2012 | http://pubs.acs.org
Publication Date (Web): December 18, 2009 | doi: 10.1021/bk-2009-1030.ch017

such as electrolytes in batteries and fuel cells *(4)*. Of course, ionic liquids are well known to be useful in synthetic and catalytic applications where organometallic catalysts can be readily immobilised in an ionic liquid phase *(5)*. This has been extended to the use of ionic liquids in enzymatic reactions as well *(6)*. Many, if not all, of these applications have arisen due to the recognition of ionic liquids for a number of their useful physical properties, from both a green chemistry point of view and a purely chemical point of view. Such properties include their polar, non-coordinating nature, generally low flammability due primarily to low volatility, and their ability to dissolve a range of organic and inorganic compounds *(7)*. More recently, exploitation of these properties has resulted in an increased use of ionic liquids in separations, while their reported applications in catalysis continue to increase. Of particular interest here is the fact that ionic liquids have proven to have great potential for the extraction of metal ions from aqueous waste streams. Furthermore, ionic liquids capable of forming complexes with transition metals may also be of use in biphasic catalysis where the complex is immobilised in an ionic liquid phase.

The design and synthesis of task specific ionic liquids has garnered considerable attention over the last few years. This terminology, coined by Davis and coworkers, refers to ionic liquids that have been intentionally functionalised with the intent of enabling the modified ionic liquid to perform a designated function, or specific task *(8)*. More recently, this term has been dropped in favour of the term funtionalised ionic liquids. One of the first functionalised ionic liquids, reported by Davis and coworkers, contained an amine moiety at the end of the alkyl substituent of a 1,3-disubstituted imidazolium salt (Figure 1) *(9)*. This functionalised ionic liquid was capable of reversibly forming a carbamate with $CO_2$ and has potential use in the scrubbing of $CO_2$ from gas streams. During the same year, this same group reported the preparation of Brönsted acidic functionalised ionic liquids containing sulfonic acid moieties *(10)*. Other Brönsted acidic functionalised ionic liquids containing hydrogensulfate anions were also reported *(11)*. These protic functionalised ionic liquids, as well as that reported by MacFarlane and coworkers containing the dicyanamide anion *(12)*, have use in acid (or base) catalysed reactions such as esterifications reactions. In this sense these functionalised ionic liquids could also be regarded as designer solvents (Figure 1).

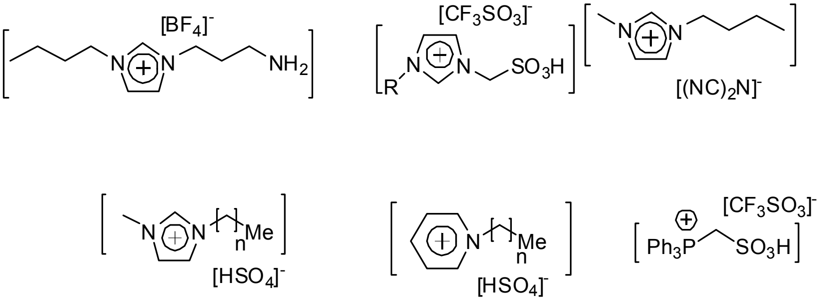

*Figure 1. Prototypical functionalised ionic liquids.*

A number of other research groups have been successful in preparing functionalised ionic liquids that contain ligands capable of coordinating transition metals. Among these is an imidazolium derived ligand (Figure 2) that forms a ruthenium complex in the presence of a chiral diamine *(13)*. Dyson and coworkers *(13)* have shown that this functionalised ionic liquid - ruthenium complex was useful in chiral hydrogenation reactions. Yet another ruthenium complex, prepared by Yao and Zhang, contains a ruthenium-carbene moiety that is useful in olefin metathesis *(14)*. It is noteworthy here that the strategy employed by these researchers relied on the adage "like dissolves like", in that they immobilised their functionalised ionic liquid in a common ionic liquid such as [$C_4$mim][$PF_6$], and as a result their catalytic complex could be recycled and reused without loss of activity and without appreciable leaching into the extracted organic solvent / product phase.

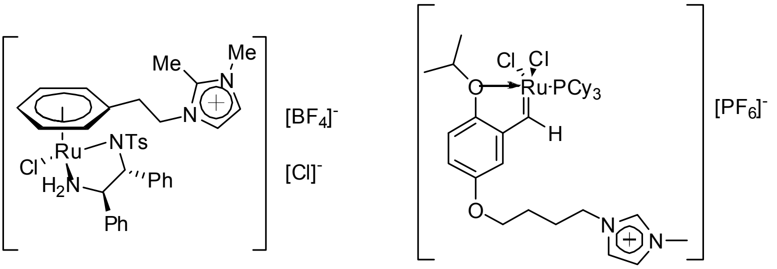

*Figure 2. Functionalised ionic liquid–metal complexes.*

As alluded to earlier, both common ionic liquids and functionalised ionic liquids have been used for the extraction of metal ions from solution, typically aqueous solution. For example, Rogers and coworkers dissolved crown ethers in [$C_4$mim][$PF_6$] and other room temperature ionic liquids *(15)*. These solutions could remove sodium, caesium, or strontium from aqueous solutions. When calixarenes were dissolved in these ionic liquids, transition metals such as copper(II), zinc(II), and cobalt(II) could successfully be removed from solution *(16)*. The use of functionalised ionic liquids then took the evolutionary step of tethering the metal coordinating ligand to the cation. Rogers and coworkers accomplished this by functionalising the cations with sulfide, thiourea, or crown ether moieties (Figure 3) *(8b,17)*. When these imidazolium base-functionalised ionic liquids were dissolved in other ionic liquids such as [$C_4$mim][$PF_6$], they rather efficiently removed metal ions such as cadmium(II) and mercury(II) from aqueous solution.

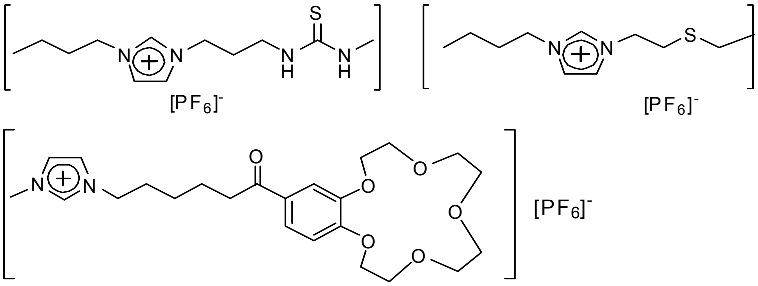

*Figure 3. Coordinating groups tethered to the cations of ionic liquids.*

Downloaded by OHIO STATE UNIV LIBRARIES on June 28, 2012 | http://pubs.acs.org
Publication Date (Web): December 18, 2009 | doi: 10.1021/bk-2009-1030.ch017

The metal-ion-extracting functionalised ionic liquids discussed thus far clearly demonstrate that they have substantial potential for this particular application. As is becoming evident from the various sessions held during this symposium, the use of ionic liquids in separations, in fact, represents one of the main areas of interest that is likely to show large advances in the coming years. The use of ionic liquids in catalytic and/or materials applications is also likely to be at the forefront of ionic liquid research in the near future. The adoption of ionic liquids as everyday green solvents has been contested by some; however, ionic liquids are certain to become popular "designer solvents" that will improve select chemical processes from both an economical and green chemistry point of view.

Inspired by the studies reported previously in this area, we endeavoured to prepare functionalised ionic liquids that could readily, selectively, and reversibly extract metals from aqueous and other solutions. During our design process, we sought to prepare functionalised ionic liquids that were easily isolated and characterised *via* a variety of means, so that rational design modifications could be conducted that would result in improved performance of our functionalised ionic liquids. To accomplish this, we also wished to prepare our functionalised ionic liquids from inexpensive and readily available starting materials. Ideally, these starting materials would be in the inventories of potential industrial users of the functionalised ionic liquids so that, if they were adopted for use in these industries, the users would have ready access to the raw materials from which the functionalised ionic liquids could be made cheaply and in large quantities. We ultimately adopted a modular synthetic approach to our functionalised ionic liquid design so that the various components could be modified as deemed necessary. For example, as will be discussed below, our appoach allows the cationic core, the anion, the spacer/tether groups, and the coordinating/chelating ligand all to be easily varied and interchanged. This allows us to "tune the properties" of our functionalised ionic liquids in an appropriate fashion – an acknowledged, attractive feature of ionic liquids and indeed the essence of the philosophy behind functionalised ionic liquids. Lastly, our modular design approach allows us to judiciously choose ligands that will reversibly form complexes with metals through chemical or perhaps physical means.

## Results and Discussion

Our initial foray into the preparation of functionalised ionic liquids capable of coordinating metal ions involved the incorporation of a well known chelating group; namely, one-half of an ethylene diamine tetraacetic acid, $H_4$edta, molecule was tethered to a 1-alkylimidazolium cation (Figure 4) *(18)*. We opted for this particular chelating group for a few reasons. Firstly, this chelating group is very well known to chelate a broad array of different metal ions. Metal complexes of this ligand are thermodynamically stable and have formation constants that are pH dependent. This not only improves the possibility of isolating any formed complexes, but also bodes well for selective and reversible metal complex formation simply by careful control of the pH. Additionally,

Downloaded by OHIO STATE UNIV LIBRARIES on June 28, 2012 | http://pubs.acs.org
Publication Date (Web): December 18, 2009 | doi: 10.1021/bk-2009-1030.ch017

since we are always conscious of the principles of green chemistry, some metal complexes containing this ligand are biodegradable.

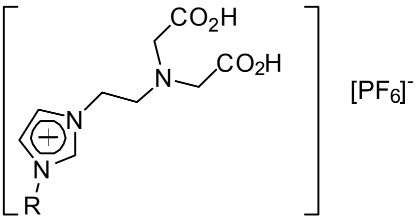

*Figure 4. A functionalised ionic liquid containing a tethered ethylamine diacetic acid moiety.*

The synthesis of the di-*t*-butyl ester protected functionalised ionic liquid, [$^t$Bu$_2$edamim][PF$_6$], **5**, began with a relatively straight forward synthesis of the amine, **4** (Scheme 1). The α,ω-haloamine equivalent, **1**, required for the synthetic route was protected as an *N*-(2-bromoethyl)phthalimide prepared by a one-pot, two-step procedure using the condensation between 2-aminoethanol and phthalic anhydride, followed by bromination with $PBr_3$ *(19).* 1-Methylimidazole was then quarternised with *N*-(2-bromoethyl)phthalimide, resulting in the formation of the quaternary bromide salt, **2**, in 40% yield. The water soluble quaternary bromide was subjected to an anion exchange reaction (metathesis) with an aqueous solution of $HPF_6$, resulting in the formation of an imidazolium salt, **3**, with a phthaloyl group on the side chain and $[PF_6]^-$ as the counter anion in a 98% yield *(20).* Use of the hexafluorophosphate salt enabled much easier isolation of the intermediate and final products of this synthetic sequence than did other common salts such as tetrafluoroborate or halide salts. This has been attributed to the decreased water solubility of the hexafluorophosphate salts.

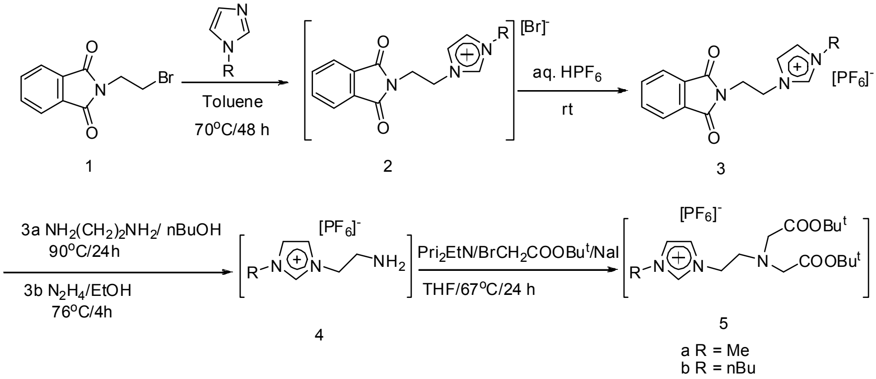

*Scheme 1. Synthesis of [$^t$Bu$_2$edamim][PF$_6$], **5**.*

Downloaded by OHIO STATE UNIV LIBRARIES on June 28, 2012 | http://pubs.acs.org
Publication Date (Web): December 18, 2009 | doi: 10.1021/bk-2009-1030.ch017

Downloaded by OHIO STATE UNIV LIBRARIES on June 28, 2012 | http://pubs.acs.org
Publication Date (Web): December 18, 2009 | doi: 10.1021/bk-2009-1030.ch017

This hexafluorophosphate salt was then subjected to the deprotection of the phthaloyl group with 1,2-daminoethane in 1-butanol at 90 °C for 24 h, to result in the formation of the imidazolium salt carrying an amino group in the side chain, *viz.* 1-(2'-aminoethyl)-3-methylimidazolium hexafluorophosphate, **4** *(21).* In the case of the analogous 1-(2'-aminoethyl)-3-butylimidazolium hexafluorophosphate, the use of hydrazine in ethanol to remove the phthaloyl group gave a better yield of the amine. The amino functionalised imidazolium salt was then subjected to base promoted *N,N*-dialkylation using two equivalents of *tert*-butyl bromoacetate, so as to afford the aminediacetic acid in the form of a diester derivative, **5**, in a 13 % overall yield (based on *N*-(2-bromoethyl)phthalimide).

The functionalised ionic liquid containing the ethylamine diacetic acid chelating ligand was liberated through deprotection of the di-t-butylester using trifluoroacetic acid. The formation of the copper(II), cobalt(II), and nickel(II) complexes, **6**, was accomplished through the addition of aqueous solutions containing the appropriate metal ion, followed by pH adjustment using aqueous ammonium hydroxide (Scheme 2).

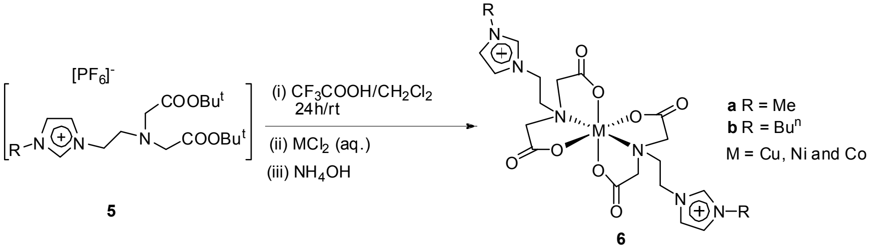

*Scheme 2. Formation of metal complexes, **6**, using [$^t$Bu$_2$edamim][PF$_6$].*

The X-ray crystal structures of the all three complexes are all structurally similar (Figure 5). These complexes, M(edamim)$_2$·2H$_2$O, M = Cu(II), Ni(II), and Co(II), are all *pseudo*-octahedral, with water molecules linking the two-dimensional network *via* hydrogen bonding. As expected there are only minor differences in their structures, mainly in terms of the bond lengths. They are all neutral complexes and hence no counter ions are found.

Based on the crystal structures of these three complexes – namely the position of the methyl groups protruding away from the centre of the complexes - we surmised that if longer more hydrophobic alkyl chains were incorporated into the ligands that more useful properties for metal extraction might result. A longer alkyl chain was expected to improve fluid properties of the resulting complexes owing to increased inability to close pack and crystallise. Increased hydrophobicity was also expected to improve partitioning of these complexes into an organic phase, while decreasing their solubility in an aqueous phase.

Downloaded by OHIO STATE UNIV LIBRARIES on June 28, 2012 | http://pubs.acs.org
Publication Date (Web): December 18, 2009 | doi: 10.1021/bk-2009-1030.ch017

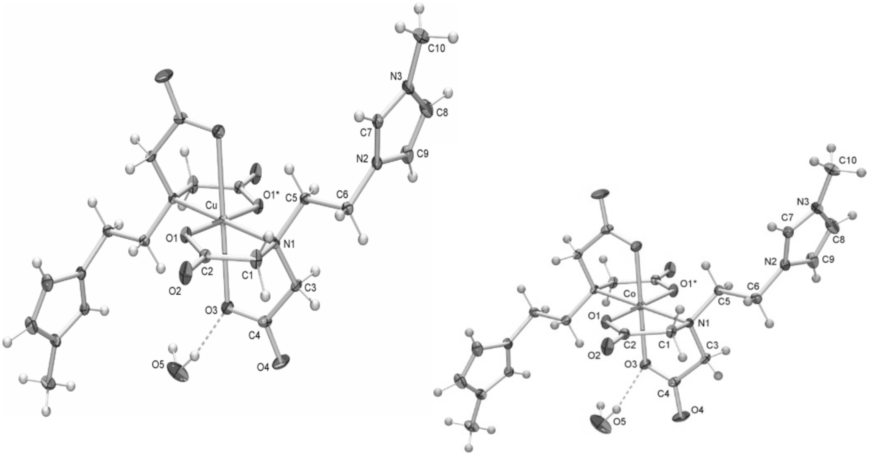
C10
N3
C8
C7
N2
C9
Cu
O1*
C5
C6
O1
N1
C2
C1
C3
O2
O3
C4
O5
O4
C10
N3
C7
C8
N2
C9
C6
Co
O1*
C5
O1
N1
C2
C1
C3
O2
O3
C4
O5
O4

**Cu(edamim)$_2$$^{\cdot}$2H$_2$O**

**Co(edamim)$_2$$^{\cdot}$2H$_2$O**

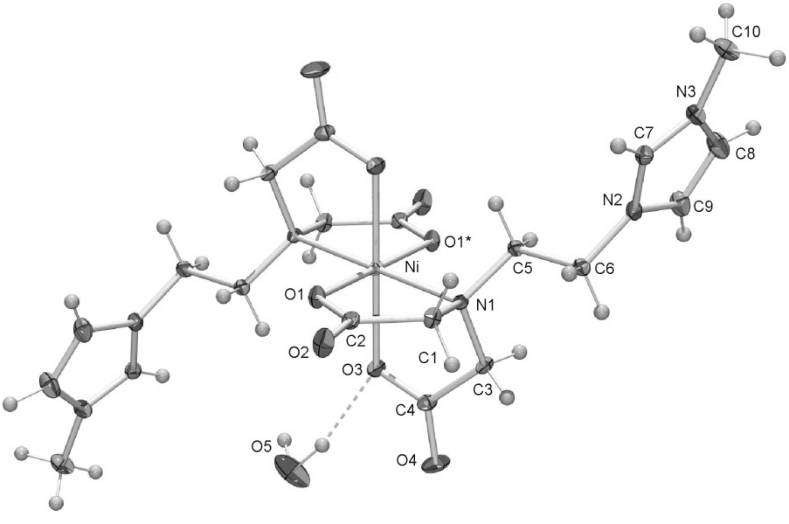
C10
N3
C7
C8
N2
C9
O1*
Ni
C5
C6
O1
N1
C2
O2
C1
O3
C3
C4
O5
O4

**Ni(edamim)$_2$$^{\cdot}$2H$_2$O**

*Figure 5. X-ray crystal structures of [M(edamim)$_2$] , M = Cu(II), Co(II), Ni(II)*

To synthesise a series of homologous functionalised ionic liquids bearing linear alkyl chains varied to hexyl, octyl, and decyl, a slightly different synthetic route had to be adopted (Scheme 3). Specifically, the tether group linking the ligating moiety to the imidazolium core had to be lengthened to three carbon atoms before the alkyl groups could be installed. This sequence was adopted primarily because 1-hexylimidazole, 1-octylimidazole, and 1-decylimidazole are not readily available from a commercial source. Hence, the alkylation step had to be conducted after the amine nitrogen containing moiety was added (*i.e.* in a reverse order compared to Scheme 1).

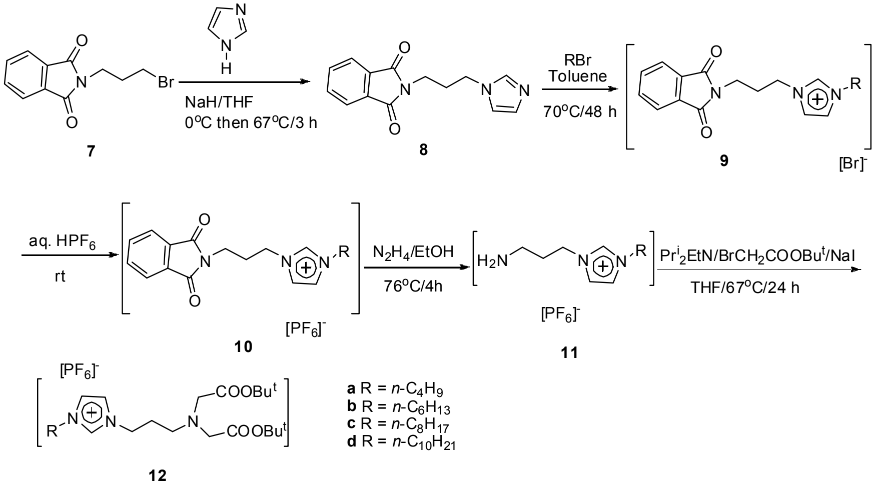
7
NaH/THF
0°C then 67°C/3 h
8
RBr
Toluene
70°C/48 h
9
[Br]⁻
aq. HPF6
rt
10
[PF6]⁻
N2H4/EtOH
76°C/4h
11
[PF6]⁻
Pr^i2EtN/BrCH2COOBu^t/NaI
THF/67°C/24 h
[PF6]⁻
COOBu^t
COOBu^t
12
a R = n-C4H9
b R = n-C6H13
c R = n-C8H17
d R = n-C10H21

*Scheme 3. Synthesis of $R = C_4 – C_{10}$ functionalised ionic liquids.*

As can be seen in Figure 6, only when the alkyl group contains ten carbon atoms is the resulting complex hydrophobic enough to spontaneously separate from aqueous solution. Using only a slight excess of this homologous functionalised ionic liquid, we were successful in removing *ca.* 93% of copper(II) from an aqueous solution (Table 1).

We are continuing our investigations into metal recovery from aqueous soutions and functionalised ionic liquid recycling using this series of functionalised ionic liquids and are interested in other metal ions than those noted here (*i.e.* Ag(I), Au(I) and Pd(II)).

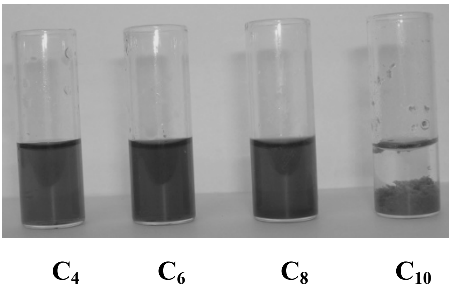

*Figure 6. Removal of aqueous copper(II) using functionalised ionic liquids derived from* ***12a-12d***

Downloaded by OHIO STATE UNIV LIBRARIES on June 28, 2012 | http://pubs.acs.org
Publication Date (Web): December 18, 2009 | doi: 10.1021/bk-2009-1030.ch017

**Table 1. Ratio of Cu(II) remaining in sample solution with respect to control.**

| Copper complex derived from | $C_n$ | $K_n$ |
|---|---|---|
| **12a** | $C_4$ | **0.986** |
| **12b** | $C_6$ | **0.652** |
| **12c** | $C_8$ | **0.194** |
| **12d** | $C_{10}$ | **0.071** |

Downloaded by OHIO STATE UNIV LIBRARIES on June 28, 2012 | http://pubs.acs.org
Publication Date (Web): December 18, 2009 | doi: 10.1021/bk-2009-1030.ch017

As noted above, our modular approach to functionalised ionic liquid design has enabled us to easily modify many components of the functionalised ionic liquids we are preparing. With this in mind, we sought to vary the coordinating group in these imidazolium based functionalised ionic liquids. Through our discussions with an industrial collaborator, we learned that the salicylaldoxime ligand is widely used for the hydrometallurgical purification of copper. This ligand could very easily be incorporated into our functionalised ionic liquids, as shown in Scheme 4, from inexpensive, readily available starting materials *(22)*. The reaction of salicylaldehyde with formaldehyde in the presence of hydrochloric acid at room temperature over one day afforded the product containing a chloromethyl group, **13** *(23)*. The quarternisation reaction of 1-methylimidazole with 2-hydroxy-5-chloromethylbenzaldehyde, **13**, afforded the imidazolium chloride salt. This salt was then readily metathesised into the hexafluorophosphate salt, **14**, *via* reaction with aqueous hexafluorophosphoric acid. Preparation of the chelating salt containing a salicylaldoxime ligand, **15**, involved the formation of an oxime through the reaction of this compound with hydroxylamine hydrochloride in the presence of sodium hydroxide.

Subsequent formation of a copper(II) complex, **16**, was easily accomplished by reacting a solution of the functionalised ionic liquid containing the sailicyl aldoxime moiety with copper(II) acetate monohydrate in methanol. Recrystallisation of the resulting precipitate in a methanol-water mixture afforded a dark brown crystalline solid in 70% yield (Figure 7).

Downloaded by OHIO STATE UNIV LIBRARIES on June 28, 2012 | http://pubs.acs.org
Publication Date (Web): December 18, 2009 | doi: 10.1021/bk-2009-1030.ch017

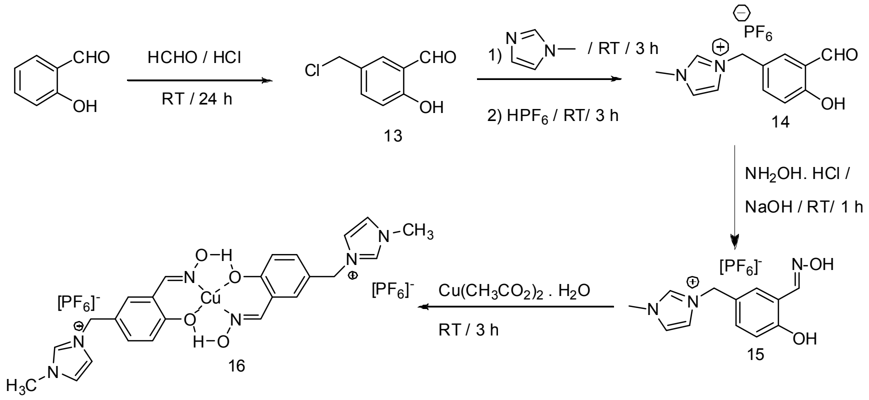
CHO
OH
HCHO / HCl
RT / 24 h
Cl
13
1) / RT / 3 h
2) HPF6 / RT/ 3 h
PF6
14
NH2OH. HCl /
NaOH / RT/ 1 h
[PF6]-
N-OH
15
Cu(CH3CO2)2 . H2O
RT / 3 h
[PF6]-
N-CH3
O-H
Cu
H-O
H3C
16

*Scheme 4. Synthesis of a copper(II) chelate complex, **16**, based on an oxime.*

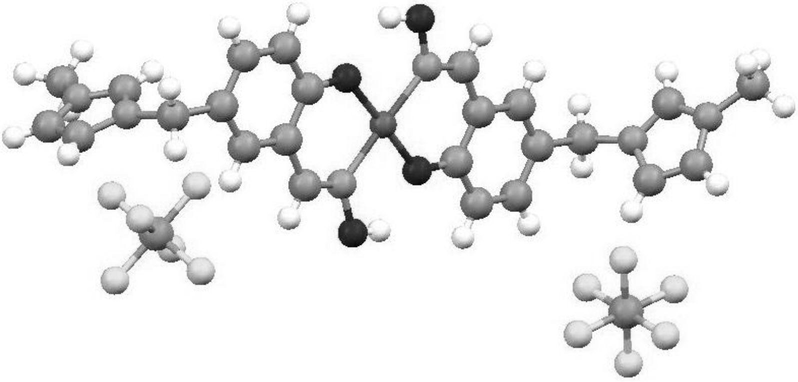

*Figure 7. X-ray crystal structure of a copper(II) chelate complex, **16**, based on an oxime.*

To further demonstrate the utility of our modular approach, we again varied the coordinating moiety in the functionalised ionic liquid. Using the same hexafluorophosphate salt, **14**, as was used to prepare the aldoxime functionality, we easily prepared the salen-containing functionalised ionic liquid. This functionalised ionic liquid readily formed a copper(II) complex, **17**, when the functionalised ionic liquid was formed in the presence of copper(II) acetate monohydrate in boiling methanol (Scheme 5).

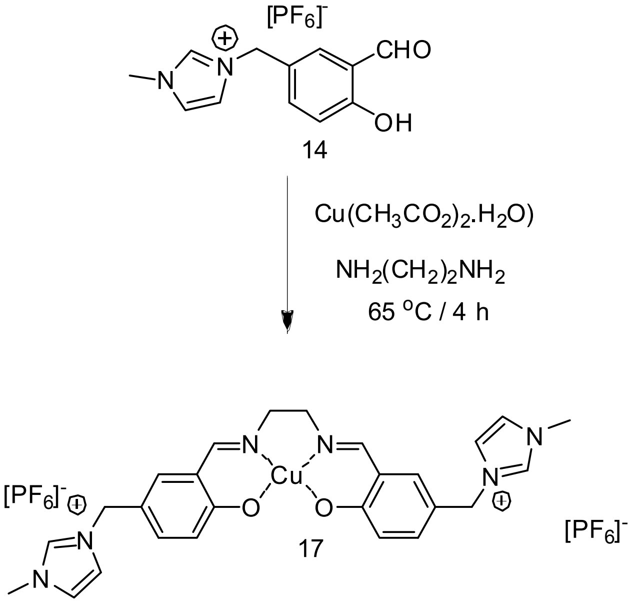

*Scheme 5. Synthesis of a copper(II) chelate complex, **17**, [Cu(salenmim)][$PF_6$]$_2$, based on salen*

This reaction afforded a 78 % yield that produced crystals appropriate for X-ray diffraction upon recrystallisation in a methanol-water mixture (Figure 8). The structure displays essentially square planar geometry around the copper(II) centre. In contrast with the oxime complex, **16**, the chelating phenolic oxygen atoms in this complex are in a *cis* arrangement, as are the two chelating nitrogen atoms. The two imidazolium cationic centres are directed away from the centre of the complex. This feature bodes well for the potential application of this type of complex in catalysis in other ionic liquids, as it enhances the solubility of the complex in ionic liquids.

Downloaded by OHIO STATE UNIV LIBRARIES on June 28, 2012 | http://pubs.acs.org
Publication Date (Web): December 18, 2009 | doi: 10.1021/bk-2009-1030.ch017

Downloaded by OHIO STATE UNIV LIBRARIES on June 28, 2012 | http://pubs.acs.org
Publication Date (Web): December 18, 2009 | doi: 10.1021/bk-2009-1030.ch017

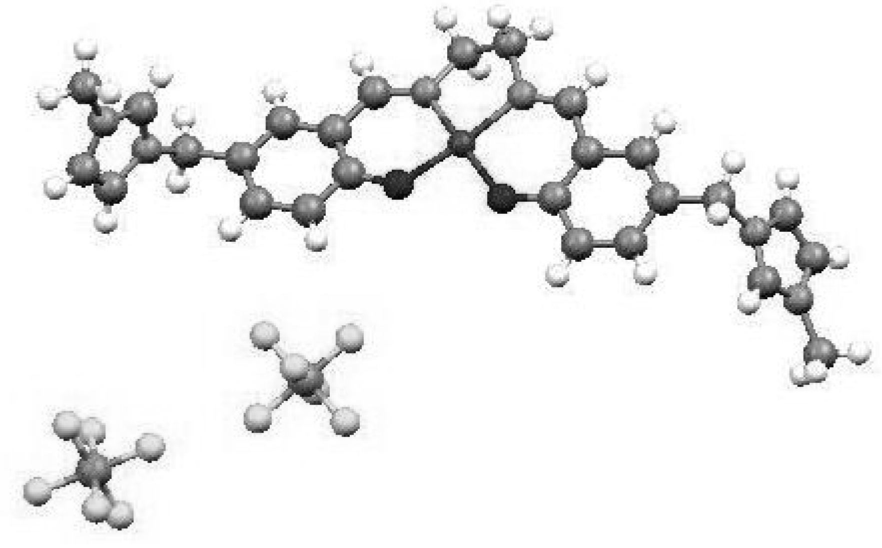

*Figure 8. X-ray crystal structure of a copper(II) chelate complex, **17**, [Cu(salenmim)][PF$_6$]$_2$, based on salen*

We then prepared the analogous manganese(III) chloride complex, [Mn$^{III}$Cl(salenmim)][PF$_6$]$_2$, to demonstrate the ability to use such functionalised ionic liquid-metal complexes in biphasic catalysis. [Mn$^{III}$Cl(salenmim)][PF$_6$]$_2$ readily dissolved and immobilised in [C$_4$mim][PF$_6$], and was used to catalyse the epoxidation of alkenes. As shown in Table 2, very good to excellent yields of oxirane products could be obtained when 10 mol % of the catalyst was used relative to the alkene substrate, and iodosobenzene was used as the oxidant. Styrene was quantitatively epoxidised in 1 h using a 5 mol excess of iodosobenzene relative to alkene (Table 2, Entry 1), while 6-cyano-2,2-dimethylchromene took 3 h to react completely (Table 2, Entry 2). *Trans*-stilbene underwent a 74 % conversion to the epoxide after 3 h, 90 % after 6 h, and was only completely reacted after 24 h (Table 2, Entries 3, 4, and 5).

**Table 2. Epoxidations using $[Mn^{III}Cl(salenmim)][PF_6]_2$ in $[C_4mim][PF_6]$.**

| Entry | Substrate | Time / h | Yield / % [a] |
|---|---|---|---|
| 1 | 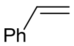 | 1 | 100 |
| 2 | 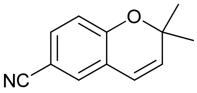 | 3 | 100 |
| 3 | 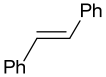 | 3 | 74 |
| 4 | 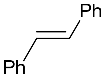 | 6 | 90 |
| 5 | 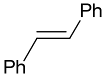 | 24 | 100 |

a Yield determined by GC analysis.

In conclusion, we have demonstrated that functionalised ionic liquids are viable options for the complexation of various metal ions, and that the three classes of functionalised ionic liquids discussed here can be used in metal extractions and in biphasic catalysis. The extension of this chemistry to the extraction of a broader array of metals, and the use of some of the resulting complexes in catalysis (*i.e.* homogeneous, asymmetric catalysis), is promising. We are continuing our investigations into the reversible formation of these complexes, as well as the use of related transition metal complexes in catalytic applications.

Downloaded by OHIO STATE UNIV LIBRARIES on June 28, 2012 | http://pubs.acs.org
Publication Date (Web): December 18, 2009 | doi: 10.1021/bk-2009-1030.ch017

Downloaded by OHIO STATE UNIV LIBRARIES on June 28, 2012 | http://pubs.acs.org
Publication Date (Web): December 18, 2009 | doi: 10.1021/bk-2009-1030.ch017

# References

1. (a) Laremore, T. N., Zhang, F. M., Linhardt, R. J. *Anal. Chem.* **2007**, 1604 - 1610; (b) Li, Y. L., Gross, M. L., Hsu, F. F. *J. Am. Soc. Mass Spec.* **2005**, 679 - 682; (c) Li, Y. L., Gross, M. L. *J. Am. Soc. Mass Spec.* **2004**, 1833 - 1837.
2. (a) Jiménez, A. –E., Bermúdez, M.-D. *Tribol. Lett.*, **2007**, 26, 53 - 69; (b) Mu, Z., Liu, W., Zang, S. and Zhou, F. *Chem. Lett.* **2004**, 33, 524 - 525.
3. Van Valkenburg, M. E., Vaughn, R. L., Williams, M., Wilkes, J. S. *Thermochimica Acta* **2005**, 425 181 - 188.
4. (a) Caja, J., Dunstan, T. D. J., Ryan, D. M., Katovic, V. in *Molten Salts XII*, P. C. Trulove, H. C. De Long, G. R. Stafford and S. Deki, Editors, **1999**, PV 99-41, P.150, *The Electrochemical Society Proceedings Series*, Pennington, NJ; (b) Matsumoto, H., Sakaebe, H., Tatsumi, K., Kikuta, M., Ishiko, E., and Kono, M. *J. Power Sources*, **2006**, 160, 1308 - 1313; (c) Ishikawa, M., Sugimoto, T., Kikuta, M., Ishiko, E., and Kono, M. *J. Power Sources*, **2006**, 162, 658 - 662; (d) Garcia, B., Lavallée, S., Perron, G., Michot, C. and Armand, M. *Electrochim. Acta*, **2004**, 49, 4583 - 4588.
5. Welton, T. *Coord. Chem. Rev.* **2004**, 248, 2459 - 2477.
6. van Rantwijk, F., Lau, R. M., Sheldon, R. A. *Trends in Biotech.* **2003**, 21, 131 – 138.
7. (a) Pârvulescu, V. I. and Hardacre, C. *Chem. Rev.*, **2007**, 107, 2615 - 2665; (b) Welton, T. *Chem. Rev.* **1999**, 99, 2071 - 2084; (c) Wasserscheid, P. and Keim, W. *Angew. Chem.* **2000**, 39, 3772 - 2789; (d) Earle, M. J. and Seddon, K. R. *Pure Appl. Chem.* **2000**, 72, 1391 - 1398; (e) Sheldon, R. *Chem. Commun.* **2001**, 2399 - 2407; (f) Wilkes, J. S. *Green Chem.* **2002**, 4, 73 - 80; (g) Hemeon, I. and Singer, R. D. *J. Mol. Cat. A* **2004**, 214, 33 - 44; (h) Hemeon, I. and Singer, R. D. *Chem. Commun.*, **2002**, 1884 - 1885.
8. (a) Davis, J. H. *Chem. Lett.* **2004**, 33, 1072 - 1077; (b) Visser, A. E., Swatloski, R. P., Reichert, W. M., Mayton, R., Sheff, S., Wierzbicki, A., Davis Jr., J. H. and Rogers, R. D. *Chem. Commun.* **2001**, 135 - 136.
9. Bates, E. D.; Eleanor D.; Mayton, R. D.; Ntai, I.; Davis, J. H., Jr. *J. Am. Chem. Soc.* **2002**, *124*, 926 - 927.
10. Cole, A.C.; Jensen, J. L.; Ntai, I.; Tran, K. L. T.; Weaver, K. J.; Forbes, D.C., Davis, J. H., Jr. *J. Am. Chem. Soc.* **2002**, *124*, 5962 - 5963.
11. Arfan, A.; Bazureau, J. P. *Org. Process Res. Dev.* **2005**, *9*, 743 - 748.
12. Forsyth, S. A.; MacFarlane, D. R.; Thomson R. J.; von Itzstein M. *Chem. Commun.* **2002**, 714 - 715.
13. Geldbach, T. J.; Dyson, P. J. *J. Am. Chem. Soc.* **2004**, *126*, 8114 - 8115.
14. Yao, Q.; Zhang, Y. *Angew. Chem. Int. Ed.* **2003**, *42*, 3395 - 3398.
15. Visser, A. E.; Swatloski, R. P.; Reichert, W. M.; Griffin, S. T., Rogers, R. D. *Ind. Eng. Chem. Res.* **2000**, *39*, 3596 - 3604.
16. Shimojo, K.; Goto, M. *Anal. Chem.* **2004**, *76*, 5039-5044.

17. (a) Visser, A. E.; Swatloski, R. P.; Reichert, W. M.; Mayton, R.; Sheff, S.; Wierzbicki, A.; Davis, J. H., Jr.; Rogers, R. D. *Environ. Sci. Technol.* **2002**, *36*, 2523-2529; (b) Liu, H.; Wang, H.-z.; Tao, G.-h.; Kou, Y. *Chemistry Letters* **2005**, *34*, 1184-1185.
18. (a) Jitendra R. Harjani, Prashant Naik, Tomislav Friščić,, Leonard R MacGillivray, and Robert D. Singer *Dalton Trans.* **2008**, 4595 – 4601; (b) Jitendra R. Harjani, Tomislav Friščić,, Leonard R. MacGillivray and Robert D. Singer *Inorg. Chem.* **2006**; 45(25); 10025-10027.
19. Soine, T. O., Buchdahl, M. R. *Organic Syntheses* Coll. Vol. 4, P. 106.
20. (a) Wilkes, J. S., Zaworotko, M. J. *Chem. Commun.* **1992**, 965-967; (b) Huddleston, J. G., Willauer, H. D., Swatloski, R. P., Visser, A. E., Rogers, R. D. *Chem. Commun.* **1998**, 1765-1766; (c) Chun, S. V., Dzyuba, S., Bartsch, R. A. *Anal. Chem.* **2001**, *73*, 3737-3741.
21. Kanie, O., Crawley, S. C., Palcic, M. M., Hindsgaul, O. *Carbohydr. Res.* **1993**, *243*, 139-164.
22. Naik, P. U., McManus, G., Zaworotko. M. J., Singer, R. D. *Dalton Trans.* **2008**, 4834-4836.
23. Dalla Cort, A., Mandolini, L., Pasquini, C., Schiaffino, L. *Org. Biomol. Chem.*, **2006**, 4, 4543-4546.

Downloaded by OHIO STATE UNIV LIBRARIES on June 28, 2012 | http://pubs.acs.org
Publication Date (Web): December 18, 2009 | doi: 10.1021/bk-2009-1030.ch017

Downloaded by OHIO STATE UNIV LIBRARIES on June 29, 2012 | http://pubs.acs.org
Publication Date (Web): December 18, 2009 | doi: 10.1021/bk-2009-1030.ch018

## Chapter 18

# Separation of Aromatic and Aliphatic Hydrocarbons with Ionic Liquids:

## A Conceptual Process Design

**G.Wytze Meindersma and A.B. de Haan**

**Department of Chemical Engineering and Chemistry/SPS, Eindhoven University of Technology, Eindhoven, The Netherlands**

Presently, there are no processes available to separate low concentration (< 20%) aromatic hydrocarbons from mixed aromatic aliphatic hydrocarbon streams, such as a feed stream to naphtha crackers, which may contain 10 to 25% of aromatic components, depending on the source of the feed (naphtha or gas condensate). Present practice is removal of the aromatic hydrocarbons from the $C_5^+$-stream in the naphtha cracker by extractive or azeotropic distillation. If a major part of the aromatic compounds present in the feed to the crackers could be separated upstream of the furnaces, it would offer several advantages: higher capacity, higher thermal efficiency and less fouling. The improved margin will be around €20/ton of feed or €48 million per year for a naphtha cracker with a feed capacity of 300 ton $h^{-1}$, due to lower operational costs. Extraction with sulfolane will result in a negative margin of M€10 per year. Therefore, a conceptual process for the extraction of aromatic hydrocarbons with the ionic liquid 1-butyl-4-methylpyridinium tetrafluoroborate was developed using ASPEN. The investment costs are estimated at M€56 and the annual costs about M€28 per year, resulting in a positive margin of about M€20 per year.

In Ionic Liquids: From Knowledge to Application; Plechkova, N., et al.;
ACS Symposium Series; American Chemical Society: Washington, DC, 2010.

## Introduction

Most ethylene cracker feeds contain 10 to 25% of aromatic components, depending on the source of the feed (naphtha or gas condensate). In Figure 1, a simplified flow scheme of a naphtha cracker is depicted and a typical naphtha feed composition is given in Table 1. The aromatic compounds present are not converted into olefins and even small amounts are formed during the cracking process in the cracker furnaces *(1)*. Therefore, they occupy a large part of the capacity of the furnaces and they put an extra load on the separation section of the $C_5^+$-aliphatic compounds. This is illustrated by the bold line in the process scheme in Figure 1, which the aromatic hydrocarbons follow. Moreover, the presence of aromatic compounds in the feed to the cracker also has a negative influence on the thermal efficiency. Aromatic compounds present in the feed tend to foul the radiation sections (coking of the coils) and the Transfer Line Exchangers.

Downloaded by OHIO STATE UNIV LIBRARIES on June 29, 2012 | http://pubs.acs.org
Publication Date (Web): December 18, 2009 | doi: 10.1021/bk-2009-1030.ch018

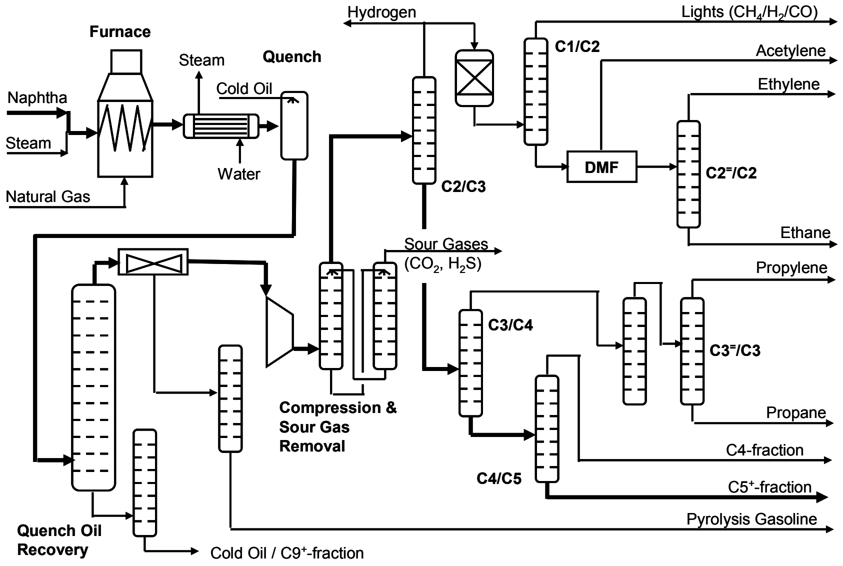
Hydrogen
Lights (CH4/H2/CO)
Furnace
Steam
Quench
Cold Oil
Naphtha
Steam
Water
Natural Gas
C1/C2
Acetylene
Ethylene
DMF
C2=/C2
C2/C3
Ethane
Sour Gases (CO2, H2S)
Propylene
C3/C4
C3=/C3
Compression & Sour Gas Removal
Propane
C4-fraction
C4/C5
C5+-fraction
Pyrolysis Gasoline
Quench Oil Recovery
Cold Oil / C9+-fraction

*Figure 1. Simplified flow scheme of a naphtha cracker*

If a major part of the aromatic compounds present in the feed to the crackers could be separated upstream of the furnaces, it would offer several advantages: higher capacity, higher thermal efficiency and less fouling. The improved margin for the removal of 10% aromatic hydrocarbons from the feed to the naphtha cracker will be around €20/ton of feed or €48 million per year for a cracker with a feed capacity of 300 ton $h^{-1}$, due to the lower operational costs. However, although separation of aromatic and aliphatic hydrocarbons after the furnace section is industrial practice, no suitable technology is currently available for the separation of aromatic compounds from the feed to cracker plants. Given this tremendous economic potential, the objective of this project is the development of a separation technology for the selective upstream recovery and purification of aromatic compounds benzene, toluene, ethylbenzene and xylenes (BTEX) from liquid ethylene cracker feeds.

**Table 1. Typical composition of a naphtha feed containing 10 wt% aromatics [Sabic]**

| *Component* | *wt%* | *Component* | *wt%* | *Component* | *wt%* |
|---|---|---|---|---|---|
| *n*-Butane | 1.5 | Cyclohexane | 2.8 | 2,6-Dimethyl-heptane | 1.9 |
| *i*-Pentane | 4.2 | 2-Methyl-hexane | 2.8 | Ethylbenzene | 2.0 |
| *n*-Pentane | 10.3 | 3-Methyl-hexane | 3.8 | *p*-Xylene | 1.9 |
| Cyclopentane | 1.5 | *n*-Heptane | 4.4 | 3-Methyloctane | 2.7 |
| 2,3-Dimethyl-butane | 0.8 | Methyl-cyclohexane | 4.8 | *o*-Xylene | 1.0 |
| 2-Methylpentane | 6.0 | Toluene | 3.0 | *n*-Nonane | 2.6 |
| 3-Methylpentane | 4.0 | 2-Methyl-heptane | 2.4 | *n*-Decane | 3.0 |
| *n*-Hexane | 8.6 | 1,3-Di-mecyclohexane | 7.0 | *i*-Decanes | 4.0 |
| Methyl-cyclopentane | 4.1 | *n*-Octane | 5.4 | | |
| Benzene | 1.8 | Ethyl-cyclohexane | 2.0 | Total | 100.3 |

The separation of aromatic hydrocarbons (benzene, toluene, ethylbenzene and xylenes) from $C_4$ - $C_{10}$ aliphatic hydrocarbon mixtures is challenging since these hydrocarbons have boiling points in a close range and several combinations form azeotropes. The conventional processes for the separation of these aromatic and aliphatic hydrocarbon mixtures are liquid extraction, suitable for the range of 20-65 wt% aromatic content, extractive distillation for the range of 65-90 wt% aromatics and azeotropic distillation for high aromatic content, >90 wt% (*2*). Typical solvents used are polar components such as sulfolane *(3-7)*, *N*-methyl- pyrrolidone (NMP) *(6)* *N*-formylmorpholine (NFM), ethylene glycols *(7-9)* or propylene carbonate *(10)*. Overviews of the use of extraction and extractive distillation for the separation of aromatic hydrocarbons from aliphatic hydrocarbons can be found elsewhere *(11-14)*.

Preliminary calculations, with confidential information from UOP, showed that extraction with conventional solvents, such as sulfolane, is not an option since additional separation steps are required to purify the raffinate, extract and solvent streams, which would induce high investment and energy costs. The costs of regeneration of sulfolane are high, since the sulfolane, which has a boiling point of 287.3 °C, is in the current process taken overhead from the regenerator and returned to the bottom of the aromatics stripper as a vapour *(15)*.

The application of ionic liquids for extraction processes is promising because of their non-volatile nature *(16)*. This facilitates solvent recovery using

Downloaded by OHIO STATE UNIV LIBRARIES on June 29, 2012 | http://pubs.acs.org
Publication Date (Web): December 18, 2009 | doi: 10.1021/bk-2009-1030.ch018

techniques as simple as flash distillation or stripping. The extraction of toluene from mixtures of toluene and heptane is used as a model for the aromatic/aliphatic separation. A conceptual process using the ionic liquid 1-butyl-4-methylpyridinium tetrafluoroborate ($[C_4m^4py][BF_4]$) as extractant was developed for this separation and with this process design, the optimal requirements for ionic liquids for extraction of aromatic hydrocarbons from mixed aromatic-aliphatic process streams can then be determined.

## Methods and Materials

Downloaded by OHIO STATE UNIV LIBRARIES on June 29, 2012 | http://pubs.acs.org
Publication Date (Web): December 18, 2009 | doi: 10.1021/bk-2009-1030.ch018

### Extraction with ionic liquids

Ionic liquids are organic salts that are liquid at low temperature (<100 °C) and they consist of organic cations based on 1-alkyl-3-methylimidazolium ($[Rmim]^+$), 1-butylpyridinium ($[C_4py]^+$), and others, with organic or inorganic anions.

A large number of ionic liquids with different cations and anions were tested with a mixture of 10 (v/v)% toluene in heptane as a reference for the selection of ionic liquids for the aromatic/aliphatic separation *(17-19)*. The solvent sulfolane is used as a benchmark for this separation ($S_{tol/hept} = 30.9$, $D_{tol} = 0.31$ mole/mole at 40 °C), because it is one of the most common solvents for extraction of aromatic hydrocarbons from mixtures of aromatic and aliphatic hydrocarbons used in industry. Therefore, suitable ionic liquids for this separation must show $S_{tol/hep} \geq 30$ and/or $D_{toluene} \geq 0.3$ mole/mole at 40 °C.

Liquid-liquid equilibrium data were collected for mixtures of 10 (v/v)% toluene in heptane at 40 °C with the selected ionic liquids *(20,21)*. The distribution coefficient, $D_i$, is directly calculated from the ratio of the mole fractions in the extract and raffinate phases at equilibrium. The distribution coefficients of toluene and heptane are defined by the ratio of the mole fractions of the solute in the extract (IL) phase and in the raffinate (organic) phase, according to Equation (1).

$$D_{\mathrm{tol}} = C^{\mathrm{IL}}{}_{\mathrm{tol}}/C^{\mathrm{org}}{}_{\mathrm{tol}} \text{ and } D_{\mathrm{hept}} = C^{\mathrm{IL}}{}_{\mathrm{hept}}/C^{\mathrm{org}}{}_{\mathrm{hept}} \tag{1}$$

The selectivity, $S_{tol/hept}$, of toluene/heptane is defined as the ratio of the distribution coefficients of toluene and heptanes, Equation (2).

$$S_{\mathrm{tol/hept}} = D_{\mathrm{tol}}/D_{\mathrm{hept}} = (C^{\mathrm{IL}}{}_{\mathrm{tol}}/C^{\mathrm{org}}{}_{\mathrm{tol}})/(C^{\mathrm{IL}}{}_{\mathrm{hept}}/C^{\mathrm{org}}{}_{\mathrm{hept}}) \tag{2}$$

Figure 2 shows the toluene/heptane selectivity as function of the distribution coefficient of toluene at 40 °C. It is apparent that the ionic liquids $[C_4m^4py][BF_4]$, $[C_4mim][BF_4]$ and $[C_4mpy][CH_3SO_4]$ show both a higher toluene distribution coefficient and a higher toluene/heptane selectivity than sulfolane.

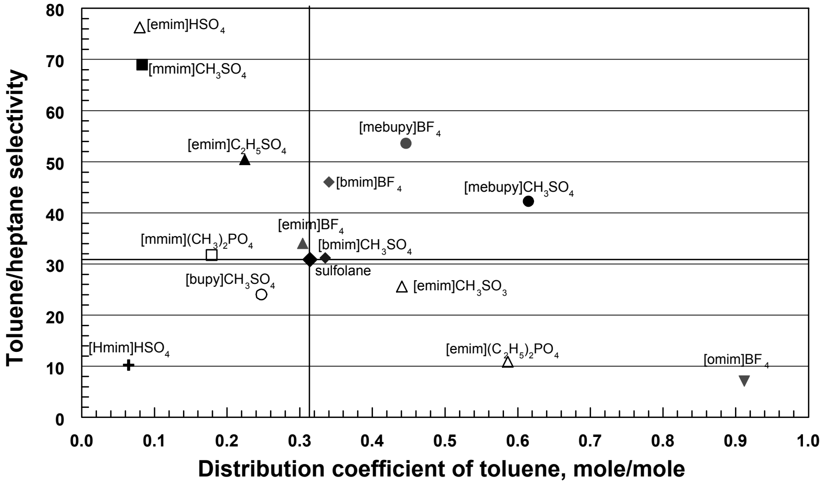

*Figure 2. Toluene/heptane separation with ionic liquids, 10 (v/v)% toluene, T = 40 °C. Ionic liquids abbreviations used in this Figure are defined in (18).*

The ionic liquid 1-butyl-4-methylpyridinium tetrafluoroborate, $[C_4m^4py][BF_4]$, exhibited the best combination of a high toluene distribution coefficient ($D_{tol}$ = 0.44 mole/mole) and a high toluene/heptane selectivity ($S_{tol/hep}$ = 53) at 10 (v/v)% toluene and 40 °C *(17-19)*. Therefore, further extraction experiments were carried out with benzene/*n*-hexane, ethylbenzene/*n*-octane and *m*-xylene/*n*-octane with this ionic liquid. Figures 3(a) and (b) show the aromatic distribution coefficients and the aromatic/aliphatic selectivities with this ionic liquid at 40 °C. In addition, the toluene distribution coefficient and the toluene/heptane selectivity with sulfolane is shown. From these Figures, it is apparent that the aromatic distribution coefficients and the aromatic/aliphatic selectivities increase with decreasing toluene concentration in the raffinate phase with the ionic liquid as extractant. However, the toluene distribution coefficient with sulfolane decreases with decreasing toluene concentration in the raffinate. Below a mole fraction of 0.5 of toluene in the raffinate, the toluene distribution coefficient with $[C_4mpy][BF_4]$ is higher than that with sulfolane, as can be seen in Figure 3(a). The toluene/heptane selectivity is higher for the ionic liquid than for sulfolane over the whole concentration range, as is shown in Figure 3(b).

Downloaded by OHIO STATE UNIV LIBRARIES on June 29, 2012 | http://pubs.acs.org
Publication Date (Web): December 18, 2009 | doi: 10.1021/bk-2009-1030.ch018

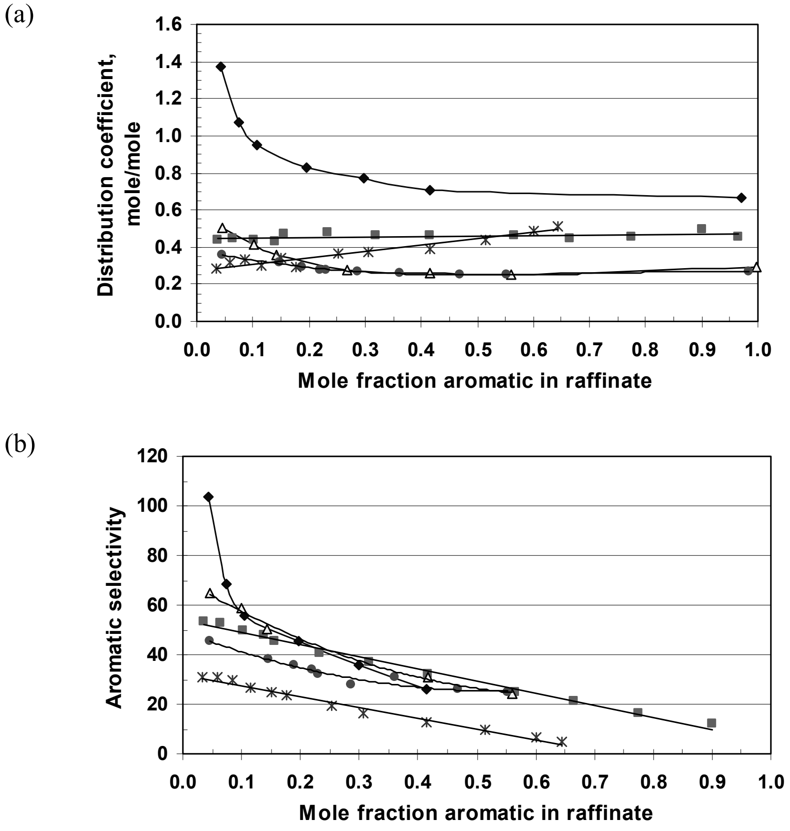

*Figure 3. (a) Distribution coefficients and (b)aromatic/aliphatic selectivities for aliphatic hydrocarbons with [$C_4$mpy][$BF_4$], ◆Benzene/hexane , ■Toluene/heptane, △Ethylbenzene/octane, ●m-Xylene/octane, *Toluene/heptane with sulfolane , T = 40 °C*

Considering the optimal combination of a high distribution coefficient and a high toluene/heptane selectivity, [$C_4$mpy][$BF_4$] was selected for the extractive removal of toluene from a toluene/heptane mixture in a pilot scale Rotating Disc Contactor (RDC) (Figure 4) *(22)*.

## Rotating Disc Contactor

Until this date, no pilot plant scale experiments with extraction with ionic liquids have been carried out. The RDC was chosen because it is the most commonly used extractor in petrochemical processing.

Downloaded by OHIO STATE UNIV LIBRARIES on June 29, 2012 | http://pubs.acs.org
Publication Date (Web): December 18, 2009 | doi: 10.1021/bk-2009-1030.ch018

Downloaded by OHIO STATE UNIV LIBRARIES on June 29, 2012 | http://pubs.acs.org
Publication Date (Web): December 18, 2009 | doi: 10.1021/bk-2009-1030.ch018

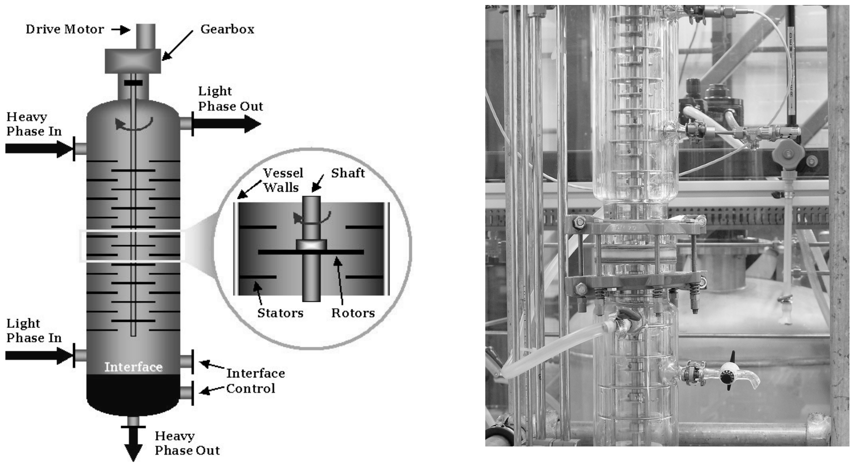

*Figure 4. Scheme of a Rotating Disc Column (www.liquid-extraction.com/rdc-column.htm) and the actual pilot plant column.*

Both a schematic representation and the actual RDC extraction column are shown in Figure 4. The column consisted of five jacketed glass segments of each 360 mm in length and an inside diameter 60 mm, with each eight stirred compartments. Settlers of 240 mm (bottom) and 210 mm (top) with an internal diameter of 90 mm enclosed the stirred segments. The internals of the stirred segments consist of alternating discs and doughnuts. The outside diameter of the doughnuts is 60 mm, the inner 22 mm and the thickness is 1.5 mm. The discs have a diameter of 40 mm and a thickness of 1.5 mm. The distance between two doughnuts is 32 mm, just as the distance between two discs. The internals were made of stainless steel.

The solvent was fed to the top of the column and the extract phase was collected from the bottom settler. The heptane/toluene phase was fed from the bottom and the raffinate phase was collected from the top settler. The concentration profiles of toluene and heptane in both phases along the column were determined by taking samples at different column heights through sample ports.

The solvents were regenerated in the extraction column at 80 $^{o}$C by bubbling nitrogen through the column for 16 to 22 hours. Total removal of heptane was possible, but total removal of toluene was not: 0.78 mole% was left in the sulfolane and 0.88 mole% in $[C_4m^4py][BF_4]$. The regenerated ionic liquid was reused in the extraction experiments during six months without any noticeable degradation.

### Economic Evaluation

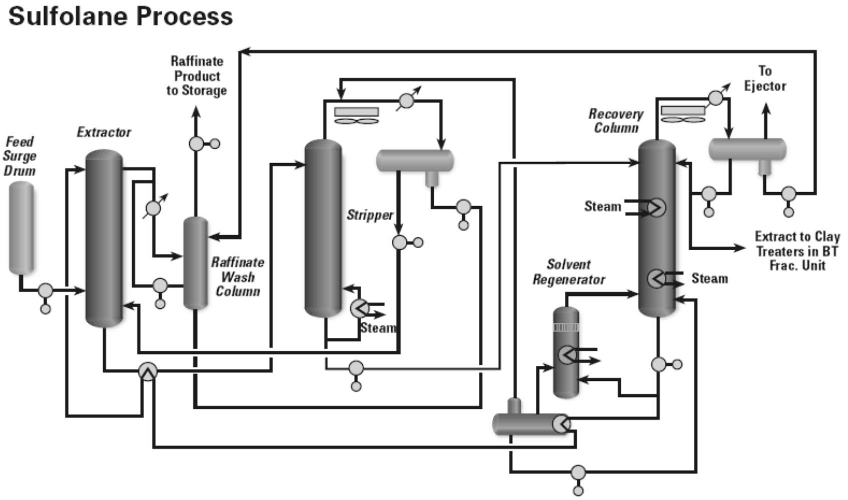

*Figure 5. UOP Sulfolane process (http://www.uop.com/aromatics/3030.html)*

The sulfolane process is one of the most used processes for the separation of aromatic and aliphatic hydrocarbons. Therefore, the potential cost of an extraction with an ionic liquid is evaluated by comparing the sulfolane process with an ionic liquid process. According to the supplier of this process, UOP, the extraction of aromatics from naphtha cracker feed is feasible with Sulfolane (Figure 5) or Carom processes. Normally, these processes are used for feed streams containing 68% aromatics or more (reformed petroleum naphtha, pyrolysis gasoline or coke oven light oil). UOP provided us with a rough estimate for the Sulfolane process for a feed stream of 300 ton $h^{-1}$ with 10% aromatics in the feed.

In the calculations, an ionic liquid price of €20 $kg^{-1}$ was used and BASF, a major producer of imidazole, one of the primary products for ionic liquids, has indicated that it is indeed possible to reach a level of €10–30 $kg^{-1}$ with production on a large scale *(23-25)*.

From a confidential process scheme for an extraction of aromatic hydrocarbons from a reformate feed, containing about 82 wt% aromatics, with Sulfolane (Figure 5), the sizes of the major equipment, the heat load of the heaters, coolers, heat exchangers, reboilers, condensers, etc., the investment costs and the scale-up/scale down capacity exponents were obtained. From these data, it is apparent that the most expensive equipment in the sulfolane process is not the columns, vessels *etc.*, but the heat exchangers, reboilers and coolers, which make up almost 65% of the total investment. The investment in the columns is about 28% of the total investment costs. The high share of the heat equipment for the sulfolane process is caused by the following reasons: the extraction is carried out at 100 °C, the extractive stripper and the recovery column operate at 190 °C and sulfolane, which has a boiling point of 287.3 °C, is taken from the top of the solvent regenerator column. These high temperatures

Downloaded by OHIO STATE UNIV LIBRARIES on June 29, 2012 | http://pubs.acs.org
Publication Date (Web): December 18, 2009 | doi: 10.1021/bk-2009-1030.ch018

require the use of high-pressure steam at several places, as can be seen in Figure 5. The high temperature has also another adverse effect: sulfolane decomposes at high temperatures and the decomposition products cause unacceptably high corrosion in the paraffin stripper and aromatics stripper if oxygen intrusion occurs *(15)*.

With the NRTL interaction parameters determined for the combinations of aromatic and aliphatic hydrocarbons with the ionic liquid [$C_4m^4$py][$BF_4$], a process model could be developed using the flow sheeting program of ASPEN Plus 12.1 *(20,21)*. Several process simulations were carried out with the ionic liquid [$C_4m^4$py][$BF_4$] as the solvent, with the objective to establish the minimum solvent-to-feed ratio and the number of stages for a toluene recovery of at least 98% and a heptane purity in the raffinate of at least 98%. The input data for all simulations were:

- $T = 40$ °C
- $P = 1.013$ bar
- Toluene concentration in the feed: 10 wt%
- Toluene content in the ionic liquid: 0 wt%

## Results and Discussion

### Column Experiments

The pilot RDC provided good results for the toluene/heptane separation with the ionic liquid [$C_4m^4$py][$BF_4$]: small droplets, in the range of 1 to 2 mm, depending on the rotation speed, were formed, resulting in high mass transfer rates and the column capacity was high. With sulfolane as the solvent the total flux (volumetric throughput) was 9.7 $m^3/m^2$ h and with [$C_4m^4$py][$BF_4$] as the solvent a 10% higher flux, 10.8 $m^3/m^2$ h, was obtained. Lower solvent to feed ratios (mole basis) were required with the ionic liquid than with sulfolane to extract the same amount of toluene and similar mass transfer efficiency were obtained.

Downloaded by OHIO STATE UNIV LIBRARIES on June 29, 2012 | http://pubs.acs.org
Publication Date (Web): December 18, 2009 | doi: 10.1021/bk-2009-1030.ch018

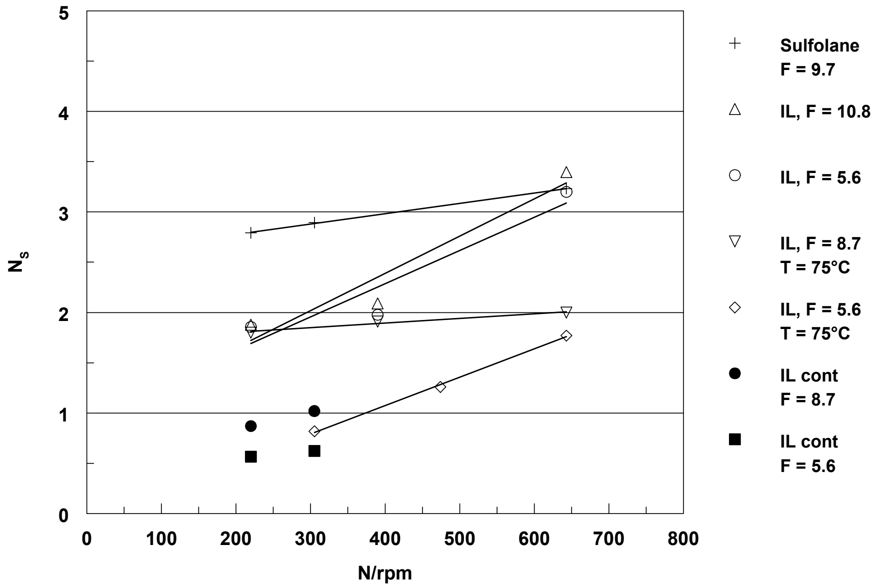

*Figure 6. Number of equilibrium stages with sulfolane and [$C_4$mpy][$BF_4$] in the RDC, T = 40°C, ~ 10% toluene, F: flux in $m^3/m^2.h$*

In Figure 6, the number of equilibrium stages, $N_S$, as function of the rotating speed is depicted. The best performance proved to be at the highest rotation speed used (643 rpm). At this rotation speed, about three equilibrium stages were contained in the 1.80 m high active section of the column for both the sulfolane and the ionic liquid. This means that the extraction with sulfolane and the ionic liquid [$C_4$mpy][$BF_4$] in this column are comparable and that the process evaluation concerning the extraction of toluene is valid in comparing both solvents.

## Extraction of toluene from toluene/heptane with [$C_4$mpy][$BF_4$]

In Table 2, the experimental and calculated data of the extraction in the pilot plant with the ionic liquid [$C_4$mpy][$BF_4$] are shown. The number of stages in the pilot plant for this extraction is about three with the highest rotation speed and the highest flux. Therefore, this number of stages was also used in a process simulation with ASPEN Plus 12.1.

The ionic liquid used for the extraction of toluene contains a small amount of toluene, because regenerated ionic liquid was used. Comparing the experimental and calculated data in Table 2, it can be concluded that the measured and calculated data are in reasonable agreement with each other. The largest differences are the concentration of the ionic liquid in the raffinate and the concentrations of toluene and heptane in the extract phase.

Downloaded by OHIO STATE UNIV LIBRARIES on June 29, 2012 | http://pubs.acs.org
Publication Date (Web): December 18, 2009 | doi: 10.1021/bk-2009-1030.ch018

**Table 2. Experimental and calculated data for the extraction of toluene with $[C_4mpy][BF_4]$ in three stages in the pilot plant RDC.**

| *Parameters* | *Feed* | *$[C_4mpy][BF_4]$* | *Raffinate* | *Extract* |
|---|---|---|---|---|
| Pilot plant | | | | |
| T, °C | 40 | 40 | 40 | 40 |
| P, atm | 1 | 1 | 1 | 1 |
| Flow, kg/h | 10 | 20 | n.a. | n.a. |
| Toluene, wt% | 7.55 | 0.58 | 5.91 | 1.38 |
| Heptane, wt% | 92.45 | - | 93.83 | 0.14 |
| $[mebupy]BF_4$, wt% | - | 99.42 | 0.26 | 98.48 |
| ASPEN | | | | |
| T, °C | 40 | 40 | 40 | 40 |
| P, atm | 1 | 1 | 1 | 1 |
| Flow, kg/h | 10 | 20 | 9.73 | 20.27 |
| Toluene, wt% | 7.55 | 0.58 | 5.71 | 1.56 |
| Heptane, wt% | 92.45 | - | 94.28 | 0.36 |
| $[mebupy]BF_4$, wt% | - | 99.42 | 0.01 | 98.08 |

The average concentration of the ionic liquid in the raffinate phase measured with equilibrium experiments was 0.24 wt% and this value compares very well with the one measured during the extraction in the column (0.26 wt%).

The experimental concentration of toluene in the extract phase is lower than expected. If the feed and raffinate phases in the pilot plant RDC were in equilibrium, a toluene concentration of 1.56 wt% in the extract phase was expected, instead of 1.38 wt%. The expected heptane concentration in the extract phase is 0.36 wt%, instead of 0.14 wt%. The expected concentrations of toluene and heptane in the raffinate phase are quite similar to the ones calculated with the flow-sheeting program. Therefore, the ASPEN Plus flow-sheeting program can be used to generate reasonably accurate data for conceptual process evaluation.

In order to achieve a toluene recovery of at least 98%, the number of stages must be higher than six. A higher number of stages than about fifteen hardly gave better results than twelve stages. For a purity of heptane in the raffinate of at least 98%, the S/F ratio on mass basis must be above 5.6 with three stages, 4.3 with six stages and 3.9 with ten or twelve stages. The minimum S/F ratio for the complete recovery of toluene with the ionic liquid $[C_4mpy][BF_4]$ is 4.7. In order to achieve a toluene recovery of at least 98%, the S/F ratio will be in the range of 5.8 with ten stages or 5.5 with twelve stages. Therefore, the obtained heptane purity will always be higher than 99.5%. In the simulations, an extraction column of twelve stages was chosen, because the toluene purity on a solvent free basis was higher than with ten stages, 82.6 wt% vs. 81.7wt%, due to the lower S/F ratio at twelve stages.

The results of the simulations for extraction with the ionic liquid $[C_4mpy][BF_4]$ of toluene from a 10% toluene in heptane feed were, that for a toluene recovery of at least 98% and a heptane purity of more than 98%, 12 stages and an S/F ratio of 5.5 were required. In Table 3, the results of the simulation of the extraction with $[C_4mpy][BF_4]$ in 12 stages is given.

Downloaded by OHIO STATE UNIV LIBRARIES on June 29, 2012 | http://pubs.acs.org
Publication Date (Web): December 18, 2009 | doi: 10.1021/bk-2009-1030.ch018

**Table 3. Results of the ASPEN simulation of the extraction of toluene and n-heptane with [$C_4$mpy][$BF_4$] in 12 stages.**

| | *Feed* | *IL* | *Raffinate* | *Extract* | *Split ratio, %* | |
|---|---|---|---|---|---|---|
| | | | | | *Raff.* | *Extr.* |
| Mass flow, t/h | 300 | 1654 | 265 | 1689 | | |
| Volum. flow, $m^3$/h | 439 | 1489 | 397 | 1534 | | |
| Mass flow, t/h | | | | | | |
| Toluene | 30 | - | 0.6 | 29 | 1.96 | 98.04 |
| N-heptane | 270 | - | 264 | 6 | 97.70 | 2.30 |
| [$C_4$mpy][$BF_4$] | - | 1654 | 0.018 | 1654 | 0.00 | 100.00 |

Since the recovery of the ionic liquid is much simpler than for sulfolane, due to the negligible vapour pressure of the ionic liquid, the process consists of an extractor, a small wash column to recover the ionic liquid from the aliphatic raffinate stream, an extractive stripper for the removal of aliphatics from the extract stream and an evaporator for the separation of the aromatics and recovery of the ionic liquid, which is then recycled to the extractor. A process flowsheet of the extraction process with an ionic liquid is depicted in Figure 7.

The loss of ionic liquid to the raffinate phase is minimal, estimated to be 0.006%, mostly due to entrainment of the ionic liquid. This seems a very small amount, but for a cracker with a capacity of 300 t/h, this will be around 140 ton of ionic liquid per year. With the cost price of € 20/kg, this amounts to a loss of M€ 2.8/year. Furthermore, it is unknown what will happen in the cracker with the ionic liquid and where the ionic liquid or its decomposition products will end up. However, the ionic liquid can be recovered from the raffinate with a one stage extraction with water in a mixer-settler or another simple extraction column.

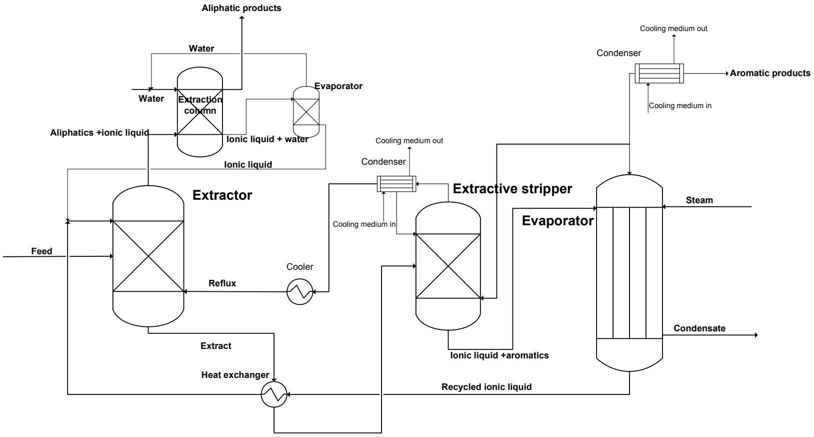
Aliphatic products
Water
Water
Extraction column
Evaporator
Aliphatics +ionic liquid
Ionic liquid + water
Ionic liquid
Extractor
Feed
Reflux
Cooler
Extract
Heat exchanger
Cooling medium out
Condenser
Cooling medium in
Extractive stripper
Evaporator
Ionic liquid +aromatics
Recycled ionic liquid
Cooling medium out
Condenser
Aromatic products
Cooling medium in
Steam
Condensate

*Figure 7. Conceptual flow scheme for the separation of aromatic and aliphatic hydrocarbons*

Downloaded by OHIO STATE UNIV LIBRARIES on June 29, 2012 | http://pubs.acs.org
Publication Date (Web): December 18, 2009 | doi: 10.1021/bk-2009-1030.ch018

## Economic Evaluation

### *1. Equipment and variable costs*

The solvent to feed ratio on mole basis is lower with the ionic liquid than for sulfolane, but the molecular weight of the ionic liquid is almost twice as high as that of sulfolane and, therefore, the about same amount of solvent will be used on a weight basis. This means that the extraction column will have comparable dimensions in both cases.

In the ionic liquid process, the recovery column and the solvent regenerator are replaced by one flash column and, therefore, the investment in the extractive stripper and the flash column for the ionic liquid process will be lower than the investment in the extractive stripper, sulfolane regenerator column and recovery columns of the sulfolane process. The investments in the other equipment will be in the same range, because the flows will also be in the same range. The sizes of the equipment were calculated by means of the flows and the investments in the equipment were calculated with the scale-up/scale-down capacity exponents for the individual components.

The total investment, without the solvent, in the ionic liquid process is then estimated to be about 45% of that of sulfolane. Including the solvent in both processes, the investment in the ionic liquid process will then be 65% of that of the sulfolane process, because the ionic liquid will cost more than sulfolane.

Since the total heat load for the sulfolane process is estimated at 160 MW and for the ionic liquid process at 32 MW, the investment in heat equipment in the ionic liquid process will then be about 20% of that of the sulfolane process, assuming that the investments in the heat exchangers, reboilers and coolers is proportional to the duty.

The annual capital costs (depreciation, 10%; ROI, 20% and other investment related costs, such as maintenance, 10%) are estimated to be 40% of the investment costs. The energy costs for the sulfolane process are estimated by UOP to be € 10/ton feed, which will amount to M€ 24/year.

### *2. Comparison of both extraction processes*

In Table 4, extraction with sulfolane and with the ionic liquid [$C_4$mpy][$BF_4$] is compared. The regeneration of this solvent is much simpler than that of sulfolane and low pressure steam can be used, because an ionic liquid has no vapour pressure. The improved margin for removing the aromatic hydrocarbons from the feed to the naphtha cracker is € 20/ton feed, which amounts to M€ 48/year, resulting in a loss of around M€ 10/year for the sulfolane process and a profit of M€ 20/year for the ionic liquid process with [$C_4$mpy][$BF_4$].

Therefore, it is obvious that the sulfolane extraction process is not in operation anywhere for removing aromatic compounds from streams containing relatively low concentrations of aromatic compounds. Although the calculations for the investment and energy costs for the ionic liquid process are very crude, the margin between the sulfolane and the ionic liquid process is large enough to recommend further research in this process.

Downloaded by OHIO STATE UNIV LIBRARIES on June 29, 2012 | http://pubs.acs.org
Publication Date (Web): December 18, 2009 | doi: 10.1021/bk-2009-1030.ch018

**Table 4. Estimated investment and variable costs in M€**

| | *Sulfolane (UOP)* | *[$C_4$mpy][$BF_4$]* |
|---|---|---|
| Materials and labour | 46 | 21 |
| Engineering | 15 | 6 |
| Inside battery limits | 61 | 27 |
| Outside battery limits | 20 | 9 |
| Solvent inventory | 5 | 20 |
| Total investment costs | 86 | 56 |
| Annual costs, 40% of total I | 34.4 | 22.4 |
| Energy costs | 24 | 5 |
| Total annual costs | 58.4 | 27.4 |

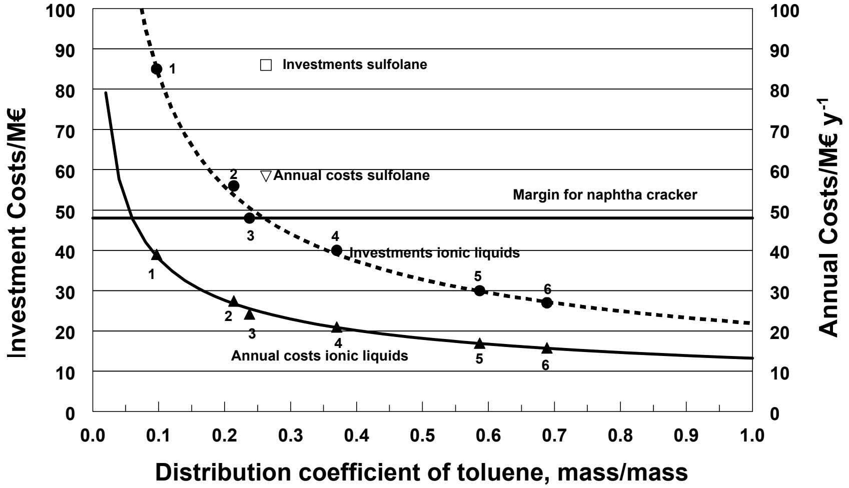

*Figure 8. Investment and annual costs for extraction with ionic liquids. 1: [$C_2$mim]$C_2H_5SO_4$, 2: [$C_4$mpy][$BF_4$], 3: [$C_4$mpy]$CH_3SO_4$, 4: [C3-mebupy][$N(CN)_2$], 5:[$C_4$mim][$AlCl_4$], 6: [$C_2$mim][$AlCl_4$].*

In Figure 8, the investment and annual costs for the separation of 10% aromatics from a cracker feed with sulfolane and several ionic liquids are shown. Even with a lower distribution coefficient than for sulfolane, a process with an ionic liquid can still be profitable, as can be seen in Figure 7 for the ionic liquid 1-ethyl-3-methylimidazolium ethylsulfate ([$C_2$mim][$C_2H_5SO_4$], IL1). The investment costs are in the same range as those for the sulfolane process, but the annual costs are much lower, due to the lower regeneration costs of the ionic liquid.

From the data in Figure 8, it is obvious that, with an ionic liquid with a high toluene distribution coefficient, in the order of 0.6 to 0.7 on mass basis, both the investment costs as the annual costs are very much lower than those for the sulfolane process. A large aromatic distribution coefficient means a lower S/F ratio with, consequently, a smaller extraction unit with lower investment costs

Downloaded by OHIO STATE UNIV LIBRARIES on June 29, 2012 | http://pubs.acs.org
Publication Date (Web): December 18, 2009 | doi: 10.1021/bk-2009-1030.ch018

and lower energy costs. Higher distribution coefficients than 0.7 hardly lead to lower costs, as can be seen in Figure 8. The investment costs can then be reduced to about M€ 25 – 30 and the annual costs will be in the range of M€ 16 – 17/year.

However, the ionic liquids [$C_4$mim][$AlCl_4$] and [$C_2$mim][$AlCl_4$] are not suitable for this separation due to their reaction with water. Also, the ionic liquid [$C_4$mpy][$BF_4$] is unsuitable for this separation, because the price of this ionic liquid will be too high, as almost all fluor containing ionic liquids are expensive. Therefore, another suitable ionic liquid has been selected: [3-mebupy][$N(CN)_2$] (dicyanamide), which has a toluene distribution coefficient of 0.37 (mass based) and a toluene/heptane selectivity of 38.4. The main conclusion of the process evaluation is that ionic liquids that show a high aromatic distribution coefficient with a reasonable aromatic/aliphatic selectivity could reduce the investment costs of the aromatic/aliphatic separation by a factor of 2 compared to that of a process that utilises sulfolane.

Downloaded by OHIO STATE UNIV LIBRARIES on June 29, 2012 | http://pubs.acs.org
Publication Date (Web): December 18, 2009 | doi: 10.1021/bk-2009-1030.ch018

## Conclusions

A high aromatic distribution coefficient is the key factor for a feasible aromatics extraction process with ionic liquids, provided the aromatic/aliphatic selectivity is high enough, (30 or higher), because the price of the ionic liquids will probably always be higher than that of sulfolane. The economic evaluation leads to the identification of key process parameters for the ionic liquid process, in order to achieve lower investment and annual costs.

The toluene/*n*-heptane extraction can be simulated by the flow-sheeting program in ASPEN Plus 12.1. The results of this simulation and the actual results obtained in a pilot plant extraction column are in reasonable agreement with each other. The complete recovery of the ionic liquid from the raffinate stream is a prerequisite for an economically feasible aromatic/aliphatic separation. For water-soluble ionic liquids, washing with water is a possibility, but this must be experimentally proven.

The energy requirement for an extraction process with an ionic liquid as solvent is much lower than that with sulfolane, due to the lower process temperatures and the simpler recovery of the ionic liquid.

The investment costs are about 35% lower for the extraction with [$C_4$mpy][$BF_4$] than with sulfolane. If ionic liquids are used with higher aromatic distribution coefficients, the investment costs may even be reduced to 30% of the costs of the sulfolane process.

## Requirements for Future Research

In order to replace a conventional separation process by a process which utilises ionic liquids, this process must be more economic, meaning less energy, lower use of feedstock, less waste, etc. In general, it is difficult to change existing processes, except when the savings in the investments are substantially lower, or if the novel ionic liquid process can be carried out in existing equipment, with no or small changes. To apply a novel ionic liquid separation process is, in principle, easier, but the technology must be proven on a reasonable scale and during a prolonged period.

The main challenges for applying ionic liquids in separations, and other processes for that matter, are the stability of the ionic liquid in the end, especially at higher temperatures, regeneration or re-use of the ionic liquid in the process and reduction of the toxicity in the aquatic environment. In addition, the physical properties of ionic liquids must be determined in order to better predict their properties in different applications and for modelling of (separation) processes.

Since there are no industrial applications for separations using ionic liquids in industry yet, more applied research is required, especially on pilot plant scale to determine optimal process conditions. In our laboratory at the Eindhoven University of Technology, we are continuing our experiments with the RDC, which has now a length of 6 m (*26*), and with a pulsed disc-and-doughnut column.

Development of a complete separation process with ionic liquids, *i.e.* including the primary separation, recovery of the products and the regeneration of the ionic liquid for re-use, must be carried out, as it is an important issue: in industry only regenerated ionic liquids will be used.

Since the properties of an ionic liquid are defined by the combination of the cation and anion, so-called tailoring offers the possibility to create a special solvent for a specific task. Because of the large number of combinations ($>10^{14}$), it is impossible to synthesise all ionic liquids and measure their properties. Thus, to determine suitable ionic liquids for a certain problem, simulation tools will be very useful. A dielectric continuum model (COSMO-RS), which is a quantum chemical approach, is chosen by a large number of authors for the a priori prediction of activity coefficients and other thermophysical data using only structural information of the molecules. This method enables to screen ionic liquids based on the surface charge, the polarity. In addition, it is possible to calculate activity coefficients at infinite dilution.

Activity coefficients at infinite dilution of ionic liquids are useful for screening purposes, but for separations with ionic liquids, real distribution coefficients and selectivities at finite dilutions will have to be obtained, as these are concentration dependent, as can be seen in Figure 3.

Ionic liquids are not always better than conventional solvents, but in a large number of publications, no benchmarks with conventional solvents are mentioned. Sulfolane is possibly a better extraction solvent for the separation of aromatic hydrocarbons in the concentration range of 0.4 to 0.6 aromatic mole fraction, since the toluene distribution coefficient is equal or higher than that of the ionic liquid [$C_4$mpy][$BF_4$]. However, at higher concentrations than 0.65 mole fraction, extraction with sulfolane is less feasible, because the aromatic/aliphatic selectivity is near 1 and the selectivity with the ionic liquid is still around 20, as is shown in Figure 3b.

Too much emphasis still exists on ionic liquids with $[PF_6]^-$ as anion, because these are versatile ionic liquids, but in industry, these ionic liquids will never be used, due to their instability in water and HF formation (*27*).

Downloaded by OHIO STATE UNIV LIBRARIES on June 29, 2012 | http://pubs.acs.org
Publication Date (Web): December 18, 2009 | doi: 10.1021/bk-2009-1030.ch018

Task-specific ionic liquids are generally more selective than standard ionic liquids and, therefore, more focus must be on the development of these ionic liquids.

## Acknowledgements

UOP is acknowledged for the supply of cost estimates. SenterNovem and DSM (now Sabic) are acknowledged for their financial support.

## References

1. Zimmermann, H.; Walzl, R., **2000**, Ethylene, 5. Production, 5.1.1 Cracking Conditions, in *Ullmann's Encyclopedia of Industrial Chemistry* (electronic version 2000).
2. Weissermel, K.; Arpe, H.-J., **2003** *Industrial Organic Chemistry*, 4th Completely Revised Edition, (Wiley-VCH, Weinheim, D.), pp 313–336.
3. Chen, J.; Duan, L.-P.; Mi, J.-G.; Feio, W.-Y.; Li, Z.-C., **2000**, Liquid-liquid equilibria of multi-component systems including n-hexane, n-octane, benzene, toluene, xylene and sulfolane at 298.15 K and atmospheric pressure, *Fluid Phase Equil.*, *173,* 109–119.
4. Chen, J.; Li, Z.; Duan, L., **2000**, Liquid-liquid equilibria of ternary and quaternary systems including cyclohexane, 1-heptane, benzene, toluene, and sulfolane at 298.15 K, *J. Chem. Eng. Data*, *45,* 689–692.
5. Choi, Y.J.; Cho, K.W.; Cho, B.W.; Yeo, Y.-K., **2002**, Optimization of the sulfolane extraction plant based on modeling and simulation**,** *Ind. Eng. Chem. Res.*, *41,* 5504–5509.
6. Krishna, R.; Goswami, A.N.; Nanoti, S.M.; Rawat, B.S.; Khana, M.K.; Dobhal. J. **1987**, Extraction of aromatics from 63–69°C naphtha fraction for food grade hexane production using sulpholane and NMP as solvents, *Ind. J. Techn*., *25,* 602–606.
7. Yorulmaz, Y.; Karpuzcu, F., **1985**, Sulpholane versus diethylene glycol in recovery of aromatics, *Chem. Eng. Res. Des.*, *63*, 184–190.
8. Al-Sahhaf, T.A.; Kapetanovic, E., **1996**, Measurement and prediction of phase equilibria in the extraction of aromatics from naphtha reformate by tetraethylene glycol, *Fluid Phase Equil.*, *118* (2), 271–285.
9. Wang, W.; Gou, Z.M.; Zhu, S.L., **1998**, Liquid-liquid equilibria for aromatics extraction systems with tetraethylene glycol, *J. Chem. Eng. Data*, *43* (1), 81–83.
10. Ali, S.H.; Lababidi, H.M.S.; Merchant, S.Q.; Fahim, M.A., **2003**, Extraction of aromatics from naphtha reformate using propylene carbonate, *Fluid Phase Equil.*, *214*, 25–38.
11. Firnhaber, B.; Emmerich, G.; Ennenbach, F.; Ranke, U., **2000**, Separation processes for the recovery of pure aromatics, *Erdöl Erdgas Kohle, 116* (5), 254–260.
12. Hamid, S.H.; Ali, M.A., **1996**, Comparative study of solvents for the extraction of aromatics from naphtha, *Energy Sources*, *18*, 65–84.
13. Hombourger, T.; Gouzien, L.; Mikitenko, P.; Bonfils, P., **2000**, Solvent extraction in the oil industry, in: *Petroleum Refining, 2. Separation*

Downloaded by OHIO STATE UNIV LIBRARIES on June 29, 2012 | http://pubs.acs.org
Publication Date (Web): December 18, 2009 | doi: 10.1021/bk-2009-1030.ch018

*Processes,* Wauquier, J.P. (Ed.) (Editions Technip, Paris), Ch 7. pp 359–456.

14. Rawat, B.S.; Gulati, I.B., **1976**, Liquid-liquid equilibrium studies for separation of aromatics, *J. Appl, Chem. Biotechnol.*, *26*, 425–435.
15. Schneider, D.F., **2004**, Avoid Sulfolane Regeneration Problems, *Chem. Eng. Progr.*, *100* (7), 34–29.
16. Huddleston, J.G.; Willauer, H.D.; Swatloski, R.P.; Visser, A.E.; Rogers, R.D., **1998**, Room temperature ionic liquids as novel media for 'clean' liquid-liquid extraction, *Chem. Commun.*, *16***,** 1765–1766.
17. Meindersma, G.W.; Podt, J.G.; Gutiérrez Meseguer, M.; de Haan, A.B., **2005**, Ionic liquids as alternatives to organic solvents in liquid-liquid extraction of aromatics, in: *ACS Symposium Series 902, Ionic Liquids IIIB, Fundamentals, Progress, Challenges, and Opportunities,* Rogers, Robin D. and Seddon, Kenneth R. (Eds.), (American Chemical Society, Washington, USA), Ch. 5, pp 57–71.
18. Meindersma, G.W.; Podt, J.G.; de Haan, A.B., **2005**, Selection of ionic liquids for the extraction of aromatic hydrocarbons from aromatic/aliphatic mixtures, *Fuel Process. Technol.*, *87* (1), 59–70.
19. Meindersma, G.W.; Podt, J.G.; Klaren, M.B.; de Haan, A.B., **2006**, Separation of aromatic and aliphatic hydrocarbons with ionic liquids, *Chem. Eng. Commun.*, *193* (11), 1384 – 1396.
20. Meindersma, G.W.; Podt, J.G.; de Haan, A.B., **2006**, Ternary liquid-liquid equilibria for mixtures of toluene+n-heptane+an ionic liquid, *Fluid Phase Equilib.*, *247* (1-2), 158–168.
21. Meindersma, G.W.; Podt, J.G.; de Haan, A.B., **2006**, Ternary liquid-liquid equilibria for mixtures of an aromatic+an aliphatic hydrocarbon+[mebupy]$BF_4$, *J. Chem. Eng. Data*, *51* (5), 1814–1819.
22. Meindersma, G.W.; Vos, G.S.; Klaren, M.B.; de Haan, A.B., **2005**, Evaluation of contactor performance for extraction with ionic liquids, in: *International Solvent Extraction Conference, ISEC 2005,* Beijing, 19 – 23 September 2005, paper B301, pp 735–741.
23. Maase, M., **2004**, Ionic liquids on a large scale,…how they can help to improve chemical processes, in: *Ionic Liquids – A Road-Map to Commercialisation*, London, UK, 22–04–2004.
24. Maase, M., **2005**, "Cosi fan tutte" ("They all do it") An improved way of "doing it", in: *Proceedings 1st International Congress on Ionic Liquids (COIL)*, Salzburg, A., 19 – 22 June 2005, (Dechema, Frankfurt am Main, D.), p 37.
25. Wasserscheid, P.; Welton, T., **2003**, Outlook, in: *Ionic Liquids in Synthesis*, Wasserscheid, P. and Welton, T. (Eds), (Wiley-VCH, Weinheim, D.), pp 348–355.
26. Onink, S.A.F.; Meindersma, G.W.; de Haan, A.B., **2008**, Ionic liquids in extraction operations: Comparison of Rotating Disc Contactor performance between [4-mebupy]$BF_4$ and sulfolane for aromatics extraction. *Proceedings ISEC 2008*, *Tucson, Az, USA*, pp 1337-1342.
27. Swatloski, R.P.; Holbrey, J.D.; Rogers, R.D., **2003**, Ionic liquids are not always green: hydrolysis of 1-butyl-3-methylimidazolium hexafluorophosphate. *Green Chem.* **5**(4): 361 - 363.

Downloaded by OHIO STATE UNIV LIBRARIES on June 29, 2012 | http://pubs.acs.org
Publication Date (Web): December 18, 2009 | doi: 10.1021/bk-2009-1030.ch018

Downloaded by CORNELL UNIV on June 28, 2012 | http://pubs.acs.org
Publication Date (Web): December 18, 2009 | doi: 10.1021/bk-2009-1030.ch019

## Chapter 19

# Investigation of Interfacial Properties of Supported [$C_4$mim][$NTf_2$] Thin Films by Atomic Force Microscopy

**Simone Bovio, Alessandro Podestà,* and Paolo Milani**

**C.I.Ma.I.Na. and Dipartimento di Fisica, Universita' degli Studi di Milano, via Celoria 16, 20133, Milano, Italy.**

We report the results of an atomic force microscopy investigation of the morphological and structural properties of thin films of [$C_4$mim][$NTf_2$] ionic liquid on mica, amorphous silica, oxidised Si(110), and highly-oriented pyrolytic graphite. We show that [$C_4$mim][$NTf_2$] forms solid-like ordered structures on these surfaces at room temperature, with a vertical structural periodicity of ~0.6 nm. Moreover, we analyse the contact angles of nano-scale [$C_4$mim][$NTf_2$] droplets on the different surfaces and show that they are sensitive to the chemical and morphological environment. Our findings highlight the potentialities of atomic force microscopy for the quantitative investigation of the interfacial properties of thin ionic liquid coatings. The results of this study suggest that at the liquid-solid interface, the structural properties of ionic liquids can be far more complex than those depicted so far, and indicate new fundamental investigations of the forces that drive supported ionic liquids through a liquid-to-solid-like transition.

## Introduction

The thermophysical bulk properties of room-temperature ionic liquids have been thoroughly investigated in the last two decades - see for example *(1-6)* - due to their promising application as more environment-friendly solvents, as an alternative to conventional organic solvents *(7,8)*. In several applications, however, the interfacial rather than the bulk properties of ionic liquids are determinant. Indeed, there is increasing evidence that the use of ionic liquids as replacements for conventional electrolytes can boost the performance of several photoelectrochemical devices used for energy storage and energy production, such as Grätzel cells *(9)* or supercapacitors *(10)*. Moreover, ionic liquids have been successfully employed as a new class of lubricants in miniaturised as well as in macroscopic mechanical systems *(11,12)*. In all these cases, the most relevant processes determining the operation of the device take place at the liquid-solid interface between the ionic liquid and some relevant surfaces. This is a region extending only a few nanometers into the bulk of the liquid, yet its properties can be dramatically different from those of the bulk. The investigation of the interfacial properties of ionic liquids is therefore of primary importance for their technological exploitation.

To date, the (bulk)liquid-vapour and solid-(bulk)liquid ionic liquid interfaces have been studied, mostly by sum-frequency generation spectroscopy *(13-17)*, by X-ray photoemission spectroscopy *(18,19)*, and by a combination of these and other surface science techniques *(20-24)*, including atomic force microscopy *(25,26)*. For imidazolium-based ionic liquids, ordering of the cations at the solid-liquid or liquid-vapour interface has been inferred from vibrational spectroscopic data. Sloutskin *et al. (21)* inferred from X-ray reflectivity data of imidazolium-based ionic liquids the existence of an ordered surface layer at the liquid-vapour interface, about 0.6-0.7 nm thick, composed of both cations and anions. Moreover, the existence of periodically ordered layers of ionic liquids, including imidazolium-based, at the (bulk)liquid-solid interface with mica and silica, has been recently reported by Atkin *et al. (26)*, and interpreted as solvation layers. Despite these interesting results, still the knowledge of the structural properties of ionic liquids at interfaces, in particular with solid surfaces, is very poor. For example, it is not known whether, and how far, the ordered layers extend into the bulk of the liquid, nor it is known how the cation-anion pairs are organised within each layer, and what is the phase (liquid, solid-like) of the ionic liquid in the ordered region. A better understanding of the behaviour of ionic liquids at interfaces can be achieved studying systems where the surface-to-volume ratio is very large, as in very thin supported films. To date, this is a largely unexplored field, since all the above-mentioned studies were conducted on systems where a bulk amount of ionic liquid was present right above, or below, the interface.

Despite their great potential, scanning probe microscopy techniques are still not widely used in the community of ionic liquid-related surface scientists. In particular, atomic force microscopy (AFM), when suitable characterisation and data analysis protocols are employed, can provide extremely valuable information about the interfacial properties of supported thin ionic liquid coatings. On one hand, thanks to the in-plane nanometer resolution and vertical sub-nanometer resolution, AFM can quantitatively and non-invasively

Downloaded by CORNELL UNIV on June 28, 2012 | http://pubs.acs.org
Publication Date (Web): December 18, 2009 | doi: 10.1021/bk-2009-1030.ch019

characterise the nano-scale structural and morphological properties of ionic liquids films; on the other hand, the AFM probe could be used to map several interfacial properties, simultaneously to topography, such as interfacial electric impedance *(27)*, friction, and adhesion *(28)*, with nanometer resolution. AFM can therefore valuably contribute, together with the other surface-sensitive techniques, like sum-frequency generation spectroscopy or X-ray photoemission spectroscopy, as well as numerical simulations, to the understanding of the basic mechanisms driving the reorganisation of ionic liquids on solid surfaces.

We report here on the application of atomic force microscopy to the study of nanoscale morphological and structural properties of very thin coatings of 1-butyl-3-methylimidazolium bis(trifluoromethylsulfonyl)amide, $[C_4mim][NTf_2]$, on different surfaces of technological interest.

Following the work of Liu *et al. (29)*, who recently reported about the layering at room-temperature of $[C_4mim][PF_6]$ on mica, we have visualised nanoscale structures of $[C_4mim][NTf_2]$ on a variety of surfaces: mica, amorphous silica, polished, oxidised *p*-doped Si(110), and highly oriented pyrolytic graphite (HOPG). Applying a rigorous protocol for the statistical analysis of AFM images, we have characterised the structural properties of ionic liquids films, validating a structural model according to which $[C_4mim][NTf_2]$ forms layered solid-like structures at room-temperature on mica and silica surfaces, with a basic periodicity in the perpendicular direction of ~0.6 nm. In contrast, on HOPG, $[C_4mim][NTf_2]$ segregates in nanometer-sized domains. Exploiting the capability of AFM of detecting and controlling nanoscale surface forces, we have qualitatively tested the mechanical properties of solid-like $[C_4mim][NTf_2]$ films, showing that the layered structures respond like lamellar solids to vertical and lateral stresses. Moreover, we have studied the local wettability of $[C_4mim][NTf_2]$ on different substrates, analysing the contact angles of nanoscale droplets in AFM topographies. The comparative study of morphology and wettability of these ionic liquid films provided some more hints on the surface organisation of liquid and solid-like phases.

Downloaded by CORNELL UNIV on June 28, 2012 | http://pubs.acs.org
Publication Date (Web): December 18, 2009 | doi: 10.1021/bk-2009-1030.ch019

## Material and methods

### Chemicals and substrates

Two samples of the ionic liquid $[C_4mim][NTf_2]$ from Sigma Aldrich and from the Queen's University Ionic Liquids Laboratories (QUILL) were used, both with purity grade greater than 98.0%.

Methanol, from Fluka, with 99.8% (HPLC) purity grade was further distilled two times and used for preparation of solutions with the ionic liquid.

Hydrochloric (HCl) and nitric ($HNO_3$) acids (Carlo Erba), with concentrations of 37% and 69.5%, respectively, and ratio 3:1 were used to prepare *aqua regia* solutions for cleaning silica substrates.

Ruby-muscovite mica and highly oriented pyrolytic graphite (HOPG) sheets were acquired from Ted Pella and Assing.

Standard 13mm-diameter discs of amorphous silica (glass coverslips) from Assing and squared, single-side polished specimens of oxidised Si(110) were used. In the text, the words ‘silica surfaces’ will be used to refer to amorphous and ordered silica surfaces together.

## Sample preparation

Samples suitable for the investigation by AFM of the solid-liquid-air interface of [C$_4$mim][NTf$_2$] have been obtained by drop-casting 20 μl of highly diluted solutions of [C$_4$mim][NTf$_2$] in methanol (concentrations lower than $10^{-2}$ - $10^{-3}$ mg cm$^{-3}$) on the substrates, allowing them to dry in ambient conditions. A comparative X-ray photoelectron spectroscopy analysis of pure and methanol-mixed [C$_4$mim][NTf$_2$] confirmed that the solvent used in the deposition process does not react with [C$_4$mim][NTf$_2$] (data not shown).

All substrates were freshly prepared immediately before deposition of the [C$_4$mim][NTf$_2$]-methanol solution. Mica and HOPG were typically freshly cleaved using an adhesive tape in order to obtain clean and atomically-smooth substrates. 13 mm-diameter discs of amorphous silica (glass coverslips) and squared specimens of polished, oxidised Si(110) were cured in *aqua regia* solution before deposition in order to remove organics and re-hydroxylise their surfaces.

Downloaded by CORNELL UNIV on June 28, 2012 | http://pubs.acs.org
Publication Date (Web): December 18, 2009 | doi: 10.1021/bk-2009-1030.ch019

## AFM measurements

A Bioscope II AFM from Veeco Instruments was used. The AFM was operated in tapping mode in ambient conditions with standard single-crystal silicon cantilevers (resonance frequency between 200 and 300 kHz, nominal radius of curvature of the tip 5-10 nm). Typically, image scan size was 5 μm x 5 μm and 15 μm x 15 μm, with scan rates in the range 0.5-1.5 Hz. Stable imaging conditions could be achieved and maintained for hours as if scanning on a solid surface. We did not observe significant changes in the imaging conditions when imaging in a dry dinitrogen atmosphere.

The AFM was also operated in force-spectroscopy mode, using force modulation tips with typical force constant $k = 4$ N m$^{-1}$. When force-spectroscopy is coupled to contact-mode imaging, several force-*vs.*-distance curves are acquired along a raster pattern spanning a finite area, and built on a previously-acquired AFM image. Each force curve is obtained recording the cantilever deflection (which is converted into a force, upon suitable calibration of the lever) as a function of the relative tip-surface distance *(30)*.

## Statistical analysis of AFM data

This analysis is based on the study of height histograms. This approach permits consideration in the analysis of a huge amount of topographic data (order of $10^6$-$10^7$ data points). Terraces, that are constant-height regions, produce sharp peaks in the histograms. Peak-to-peak distances represent terrace heights. A multi-Gaussian fit provides the peak positions, as well as the corresponding width. The error associated to the height of a terrace is calculated summing in quadrature the statistical error, related to the width of the histogram peaks, and an instrumental error that reflects the accuracy of the calibration of the vertical piezo (~2% of average terrace height).

Each terrace height $h_i$ is supposed to be an integer multiple of the same basic monolayer height $\delta$ (the latter being in principle different on different surfaces). In order to find the best divider of terrace heights, and the series of best integers, we minimise the following chi-squared function with respect to $\delta$ in the region 0.5 nm < $\delta$ < 0.9 nm:

$$\chi^2 = \sum w_i (h_i - \delta \cdot \mathrm{round}(h_i / \delta))^2$$

where $w_i = (\sigma_i^2 \delta^2)^{-1}$, $\sigma_i$ is the error associated with $h_i$, and $round(h_i/\delta)$ represents the closest integer $N_i$ such that $\delta N_i \sim h_i$. The extra weight $\delta^{-2}$ avoids weighting the small dividers, which systematically provide a smaller quadratic error ( $(h_i - \delta N_i)^2 < \delta^2$) and therefore would bias the chi-squared term.

Downloaded by CORNELL UNIV on June 28, 2012 | http://pubs.acs.org
Publication Date (Web): December 18, 2009 | doi: 10.1021/bk-2009-1030.ch019

### Contact angle measurements

A suitable analysis of three-dimensional AFM topographies allows a statistical evaluation of the morphological parameters of nanodroplets needed to calculate the contact angles (the droplet radius and height, see later). To calculate the morphological properties of each object (droplet) in an image, a filtering procedure was used. To analyse separately the contact angles of the droplets sitting on the substrate, and of those sitting on top of solid-like layers, the images were cropped in such a way that all the heights are calculated starting from the correct flat background. The droplets were separated from their backgrounds masking the data using manually-set height thresholds. Using the Image Processing Toolbox of Matlab (Mathworks) in conjunction with these masks, each object was labelled separately, and several morphological parameters were calculated, such as the area, the volume, the radius, the height, the eccentricity, *etc.* Then, automatic filters were applied, in order to select only the desired objects (the round droplets), discarding all the others (remnants of layers, elongated liquid-like patches, *etc.*). The first constraint applied is that the logarithm of the heights and the volumes must be linearly correlated (as for spherical-like objects): all those data were rejected that were more than one or two standard deviations from the best straight line fitting the data. Only those objects having a ratio between major and minor axes of the best-fitting ellipse smaller than 1.2 were then kept. The few non-droplet-like objects that survived the previous filtering procedures (actually a negligible fraction of the total) were eventually rejected manually. Of the remaining (good) objects, the contact angles were calculated, along with their average value for each substrate, with the associated standard deviation of the mean.

## Results and Discussion

### *Surface morphology of [$C_4$mim][$NTf_2$] films*

Figure 1 shows a collection of representative AFM topographies of thin coatings of [$C_4$mim][$NTf_2$] on polished oxidised Si(110), mica, amorphous silica, and HOPG. These AFM images have been acquired in tapping-mode, with the exception of Figure 1c, which has been acquired in contact-mode.

Downloaded by CORNELL UNIV on June 28, 2012 | http://pubs.acs.org
Publication Date (Web): December 18, 2009 | doi: 10.1021/bk-2009-1030.ch019

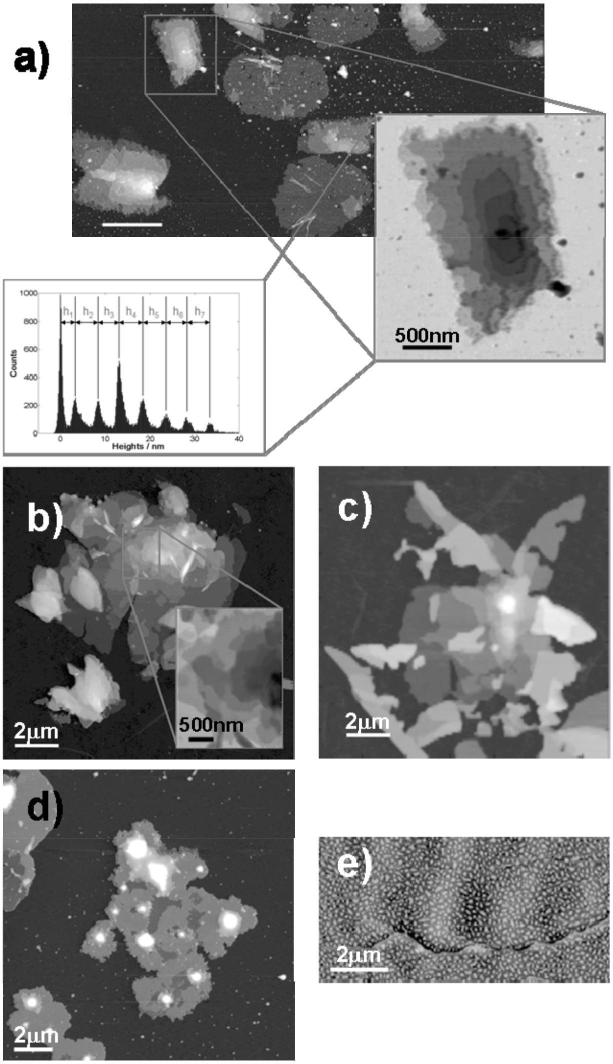
a)
500nm
1000
800
600
400
200
0
Counts
h1
h2
h3
h4
h5
h6
h7
0
10
20
30
40
Heights / nm
b)
2μm
500nm
c)
2μm
d)
2μm
e)
2μm

*Figure 1. AFM topographic maps of thin [$C_4$mim][$NTf_2$] films on a) Polished oxidised Si(110); b,c) Amorphous silica; d) Mica; e) HOPG. All images acquired in tapping-mode, except c), which has been acquired in contact-mode. In a) it is shown the histogram of heights of the layered structure in the inset. Peak-to-peak distances represent the heights $h_1$, $h_2$,… of single terraces. Vertical scales: a) 50 nm; b) 100 nm (inset 70 nm); c) 50 nm; d) 35 nm; e) 10 nm.*

Figures 1(a-d) show isolated layered structures, whose width is in the 1-20 μm range, and whose heights are well above 50 nm in some cases. Each layer has well defined edges, and height distributed typically between 2 nm and 6 nm. It is remarkable that also the layered structures that extend up to 50 nm away from the substrate behave like solid surfaces against the AFM probe. In particular, even during contact-mode imaging, no evidence of scratching or invasive tip/sample interaction was observed, Figure 1(c), despite the fact that the applied normal pressures and lateral forces are at least one order of magnitude larger than in tapping-mode. No changes in the shape of layered features were typically observed after repeated scanning of the same areas, if not occasionally, when working with high forces (see later). On silica substrates, a more pronounced tendency of $[C_4mim][NTf_2]$ to grow three-dimensionally than on mica was observed. No evidence of ordered extended structures could be found on HOPG substrates, Figure 1(e). On HOPG, only nanometre-sized, rounded domains (nanodroplets) of ionic liquid spontaneously form upon evaporation of methanol. Coexistence of sub-micrometer droplets and layers is observed occasionally on amorphous silica and mica, and very rarely on oxidised Si(110) surfaces. The observed structures were extremely stable, even in ambient (humid) conditions: layers have been imaged also after several months, and no changes in their average structure and morphology have been observed, demonstrating that such structures are extremely stable.

*Structural characterisation*

AFM three-dimensional topographies allow to extract quantitative information about the structure of $[C_4mim][NTf_2]$ films. In particular, AFM images suggest that the layered structures result from the regular vertical arrangement of a molecular layer with thickness $\delta$, Figure 2(a). Several basic layers arrange to form terraces, whose heights are typically in the range 1-6 nm. Terraces are typically observed growing on top of each other, each being delimited by a sharp step clearly observable in the AFM topographies. In order to characterise statistically and accurately the heights of the observed terraces, we considered the histograms of the heights in AFM topographies of layered structures. In the inset of Figure 1a is shown a typical height histogram of a layered structure. Such histograms consist in a series of peaks, each corresponding to a plateau in the AFM image. The peak-to-peak distances represent the average heights of piled-up terraces. These heights are supposed to be integer multiples of the height $\delta$ of the basic layer. We performed an optimisation procedure on terrace heights data in order to find the best value of $\delta$ for the different substrates. We found $\delta = 0.61 \pm 0.01$ nm, $0.56 \pm 0.02$ nm,

Downloaded by CORNELL UNIV on June 28, 2012 | http://pubs.acs.org
Publication Date (Web): December 18, 2009 | doi: 10.1021/bk-2009-1030.ch019

Downloaded by CORNELL UNIV on June 28, 2012 | http://pubs.acs.org
Publication Date (Web): December 18, 2009 | doi: 10.1021/bk-2009-1030.ch019

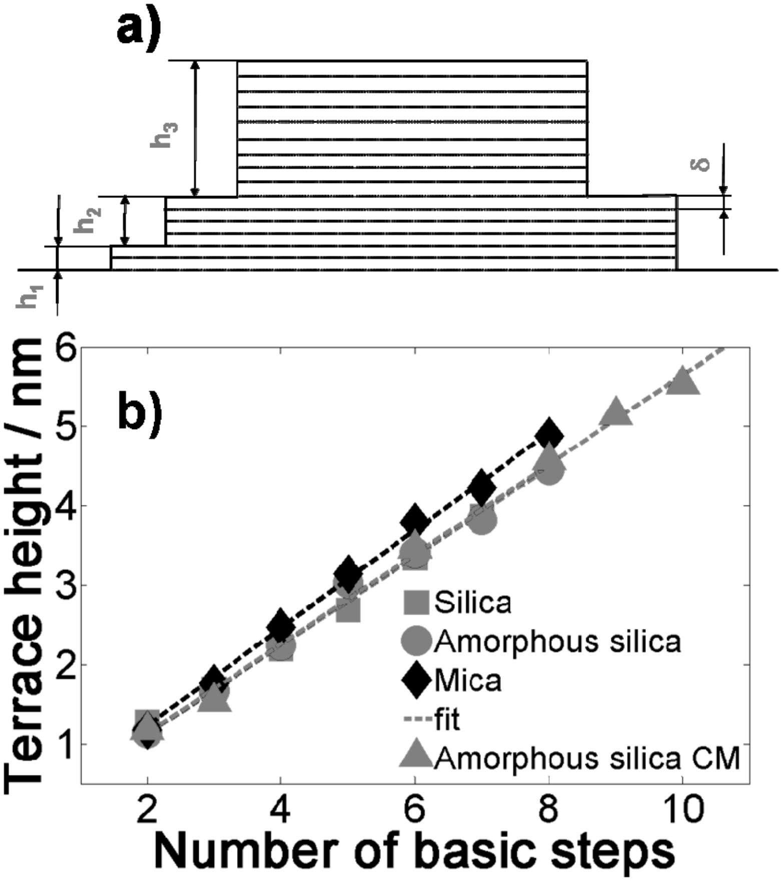

*Figure 2. a) Structural model of solid-like [$C_4$mim][$NTf_2$] films: a basic layer with thickness $\delta$ is stacked in terraces with different heights $h_1$, $h_2$,...b) Correlation between average terrace heights measured on different surfaces and the number of basic steps in each terrace, obtained by fitting structural data (error bars are comparable to marker size). In the case of amorphous silica, data from both tapping- and contact-mode AFM images are reported.*

0.56 ± 0.02 nm for mica, amorphous silica, and polished oxidised Si(110), accordingly. Figure 2(b) shows the curves obtained plotting the ratio of terrace heights to $\delta$, approximated to the closest integer $N_i$ (this ratio represents the number of basic layers stacked in a terrace) as abscissa, the average heights of the terraces with the same $N_i$ as ordinate. The good linear correlation of data reflects the good vertical structural order of [$C_4$mim][$NTf_2$] films on mica and silica substrates. Remarkably, the analysis of AFM images acquired in contact-mode on amorphous silica provided the same result as that of tapping-mode images: the average terrace heights measured on amorphous silica in contact-mode show the same correlation with the number of repeated layers than the heights measured in tapping-mode {Figure 2(b), circles and triangles}, with similar slope $\delta = 0.56$ nm. This is a further confirmation that these structures are solid-like. These results are in remarkably good agreement with the results of numerical simulations of thin [$C_4$mim][$NTf_2$] and [$C_4$mim][$PF_6$] films on silica *(31)*.

## *Test of the solid-like character of [$C_4$mim][$NTf_2$] films*

The force that the AFM probe exerts on the sample surface can be controlled. During imaging, the force is typically minimised, while in force-spectroscopy experiments it can be made large in order to test the mechanical resistance of the surface. Evidence has been collected that the layered structures oppose a strong mechanical resistance to the AFM tip. As already mentioned, there was no observation of any scratch or penetration of the tip into the structures, even after repeated scans, even when imaging in contact-mode (in contact-mode normal forces are typically 10-100 times larger than in tapping-mode, the contact pressure being of the order of 10-100 MPa). This proves that the layered structures are very compact, and in particular possess a strong mechanical resistance against vertical compression. The applied lateral force is expected to play a major role in disrupting the ordered [$C_4$mim][$NTf_2$] films. In fact, erosion of the terraces has been occasionally observed along the borders, in both tapping- and contact mode, as shown in Figure 3. In correspondence of the edges, the mechanical strength of the solid-like films is expected to be reduced, and therefore the lateral force exerted by the AFM tip can be enough to break the arrangement of the molecules. Noticeably, the applied lateral force is larger when the tip climbs the steep edges of the higher terraces, because the feedback loop of the AFM react with some delay to the quick changes of the topography. A stronger erosion is observed when imaging in contact-mode, Figure 3(a), because lateral force are greatly increased with respect to tapping-mode. Erosion observed in tapping-mode, Figure 3(b), is negligible. However, it is clear that erosion is localised only at the edges of the structures. When imaging in contact-mode at higher forces, delamination of a layered structure can also be observed. In Figures 4(a and b) AFM images of the same terrace before and after repeated scans in contact-mode at high force are shown. It can be seen by comparing Figure 4(a and b) that a complete stack of basic layers has been removed from the top of the terrace. Comparison of the height histograms before and after the scan, Figure 4(c), shows that the height of the removed layer is ten times the height $\delta$ of the basic layer. This layer has been delaminated by high lateral forces during the first two scans. In fact, the strong peak at $h \sim 15$ nm grows at the expense of the peak at $h \sim 20$ nm, corresponding to the topmost terrace that has been swept away. AFM images and height analysis suggest that this structure behaves like a lamellar solid, which can be cleaved along preferential directions.

Downloaded by CORNELL UNIV on June 28, 2012 | http://pubs.acs.org
Publication Date (Web): December 18, 2009 | doi: 10.1021/bk-2009-1030.ch019

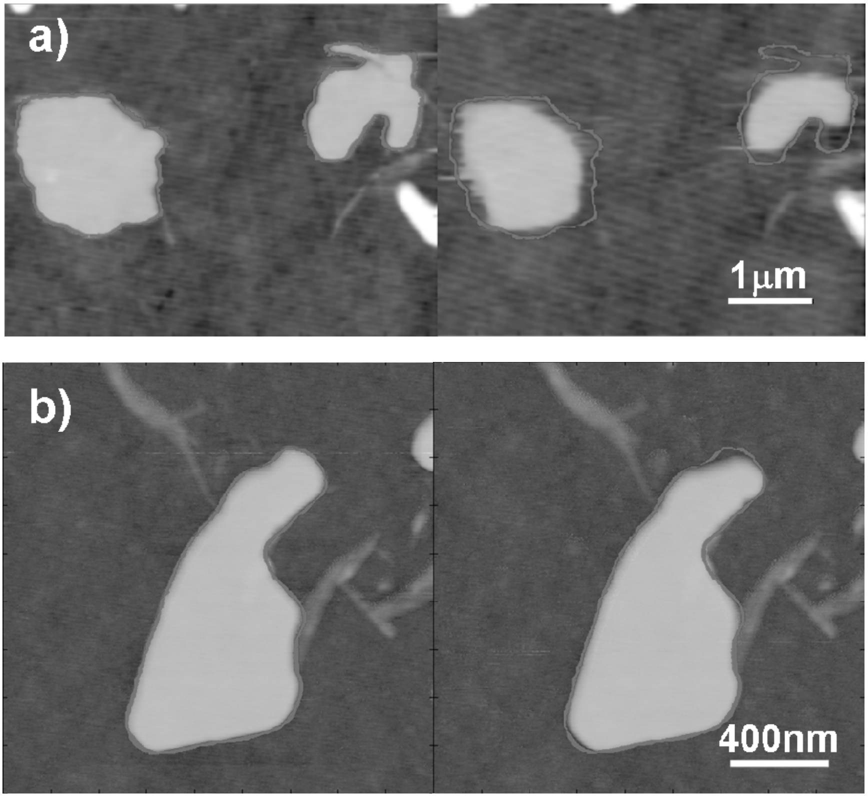

*Figure 3. Evidence of erosion at the edges of [$C_4$mim][$NTf_2$] terraces on amorphous silica after repeated scans in a) Contact-mode AFM, 4 scans; b) Tapping-mode AFM, 10 scans. The continuous line highlights the terrace border before erosion. Vertical scales: a) 10 nm; b) 20 nm.*

Downloaded by CORNELL UNIV on June 28, 2012 | http://pubs.acs.org
Publication Date (Web): December 18, 2009 | doi: 10.1021/bk-2009-1030.ch019

Downloaded by CORNELL UNIV on June 28, 2012 | http://pubs.acs.org
Publication Date (Web): December 18, 2009 | doi: 10.1021/bk-2009-1030.ch019

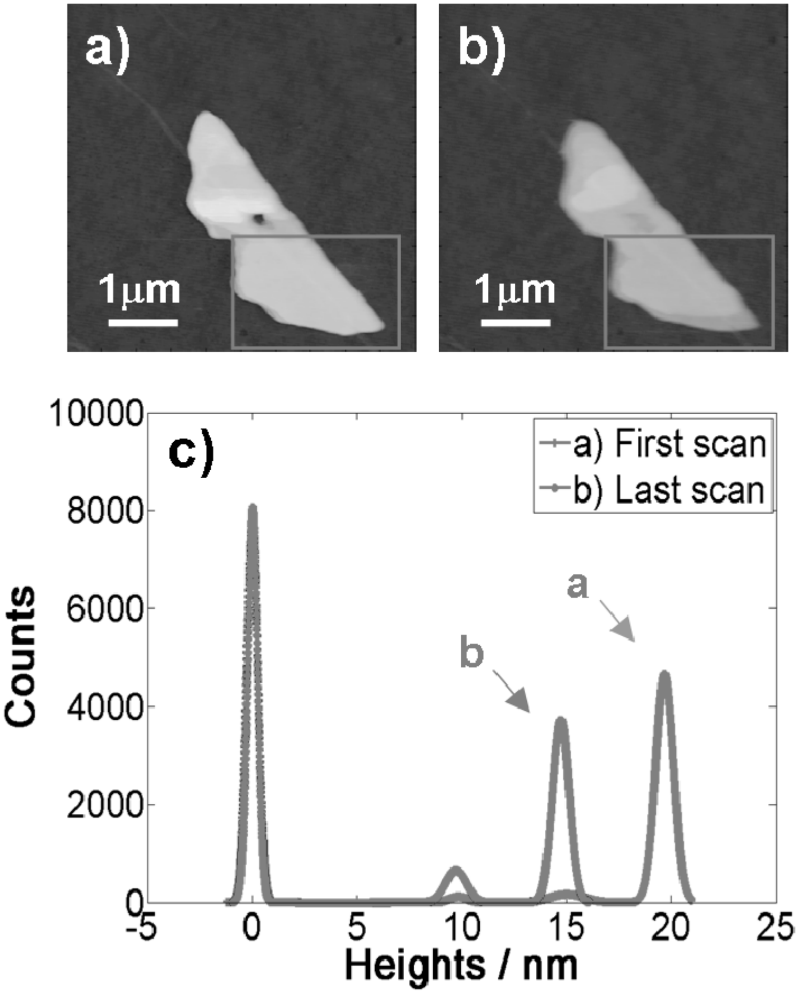

*Figure 4. Delamination of [$C_4$mim][$NTf_2$] layers on amorphous silica after three scans in contact-mode. a,b) AFM topographies before and after delamination (vertical scales: 35 nm); c) Multi-Gaussian -fitted height histograms of the boxed regions in a) and b), showing that a stack of basic layers is swept away from the top.*

Downloaded by CORNELL UNIV on June 28, 2012 | http://pubs.acs.org
Publication Date (Web): December 18, 2009 | doi: 10.1021/bk-2009-1030.ch019

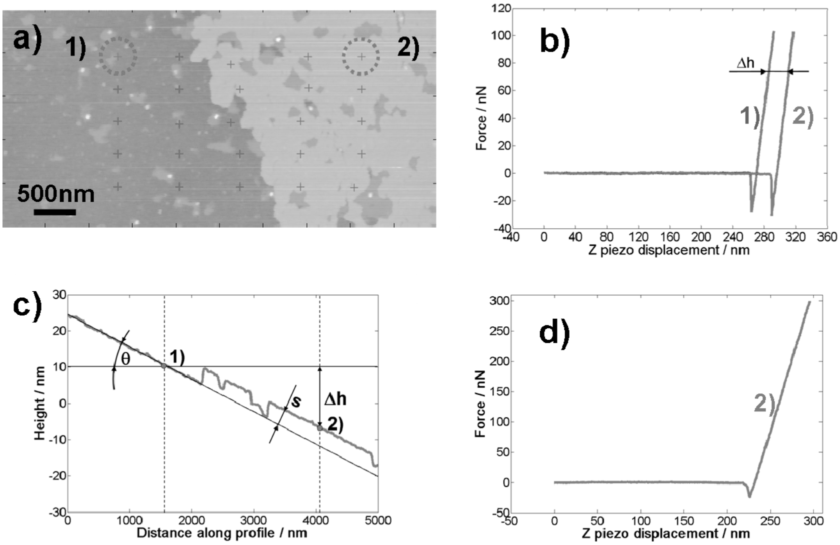

*Figure 5. Test of the normal hardness of solid-like [$C_4$mim][$NTf_2$] layers on oxidized Si(110). a) AFM contact-mode topography (Vertical scale: 15 nm). A force-distance curve has been acquired in each point marked by a cross; b)Two representative force curves acquired in the circled locations, on the bare substrate (1), and on top of the ionic liquid layer (2); c) The topographic profile from the non-flattened AFM image passing through points (1) and (2), highlighting the overall tilt of the sample; d) A force curve acquired in (2) with a higher normal force set point.*

The perpendicular hardness of [$C_4$mim][$NTf_2$] layered structures has been qualitatively tested by using the AFM in force-spectroscopy–mode. A topographic map of a terrace on polished oxidised Si(110) has been acquired, Figure 5(a), and several force-distance curves along a grid, on the substrate as well as on the film, have been collected. Figure 5(b) shows two approaching force curves, acquired on the silica substrate and on the film, in locations (1) and (2) (the circled spots). The slopes of these curves in the contact region are the same. This suggests that the film behaves upon loading exactly as the hard silica substrate, that is like an impenetrable, solid surface. If deformation of the [$C_4$mim][$NTf_2$] film occurred during contact, a different slope would be observed, together with discontinuities and irregularities in the first part of the linear region, witnessing the penetration of the film. The possibility that a sudden and traceless film penetration of [$C_4$mim][$NTf_2$] occurs right after contact could not be completely excluded. In this case the silica substrate, and not the film would be actually loaded, providing the same slopes in the two curves. The observation that the two curves are horizontally shifted by an amount $\Delta h$ corresponding to the thickness of the film {plus exactly the tilt of the sample! – see Figure 5(c)} allows elimination of this unlikely event. In the case of complete film penetration, only the displacement due to the tilt of the sample would be present. The surface of the film is actually loaded, not the substrate. Similar slopes and displacements were observed when much higher than normal pressures (up to 1 GPa) are applied to [$C_4$mim][$NTf_2$] films, Figure 5(d). These topography-related local force measurements provided a direct proof that the [$C_4$mim][$NTf_2$] layered structures are solid-like.

### *Analysis of the contact angles of [$C_4$mim][$NTf_2$] nanodroplets*

The coexistence of solid-like ordered layers and nanodroplets has been observed in samples deposited on mica and amorphous silica. On oxidised Si(110) only a very few droplets have been observed.

The contact angle of a droplet at equilibrium on a smooth surface is related to the surface energies by the Young equation:

$$\cos(\theta) = (\sigma_{sv} - \sigma_{sl})/\sigma_{lv}$$

where $\sigma_{sv}$, $\sigma_{sl}$, $\sigma_{lv}$ are the solid-vapour, solid-liquid, and liquid-vapour surface energies, accordingly. While $\sigma_{lv}$ of [$C_4$mim][$NTf_2$] is known, $\sigma_{sl}$ is not (as often is the case for $\sigma_{sv}$). Analysis of the contact angles of nanodroplets on the different substrates can therefore provide some insights into the chemistry of the interface, in particular on the effective surface energy $\Delta\sigma_{sl} = \sigma_{sv} - \sigma_{sl}$.

For droplets as small as those in our samples, gravity effect can be ignored, and it is possible to demonstrate that their shape is that of a spherical cap, with radius $r$, height $h$, Figure 6(c) *(32)*. The contact angle of a spherical cap can be expressed in terms of the droplet aspect ratio $A = 2r/h$ only:

$$\tan(\theta) = 4A^2/(A^2 - 4)$$

Figure 6(a) shows a region of [$C_4$mim][$NTf_2$] on amorphous silica where droplets and layers coexist. In particular, droplets have been observed sitting on the silica substrate and [$C_4$mim][$NTf_2$] layer. Figure 6(b) shows a three-dimensional view of a droplet sitting on a layer. Typical size of droplets is well below 1 μm, with the height typically between 20 nm and 50 nm.

Table 1 reports the values of the contact angles measured on mica, amorphous silica, and HOPG. On HOPG, the droplets are very small, typically 20-50 nm large and only a few nanometers tall, and this makes the calculation of

Downloaded by CORNELL UNIV on June 28, 2012 | http://pubs.acs.org
Publication Date (Web): December 18, 2009 | doi: 10.1021/bk-2009-1030.ch019

Downloaded by CORNELL UNIV on June 28, 2012 | http://pubs.acs.org
Publication Date (Web): December 18, 2009 | doi: 10.1021/bk-2009-1030.ch019

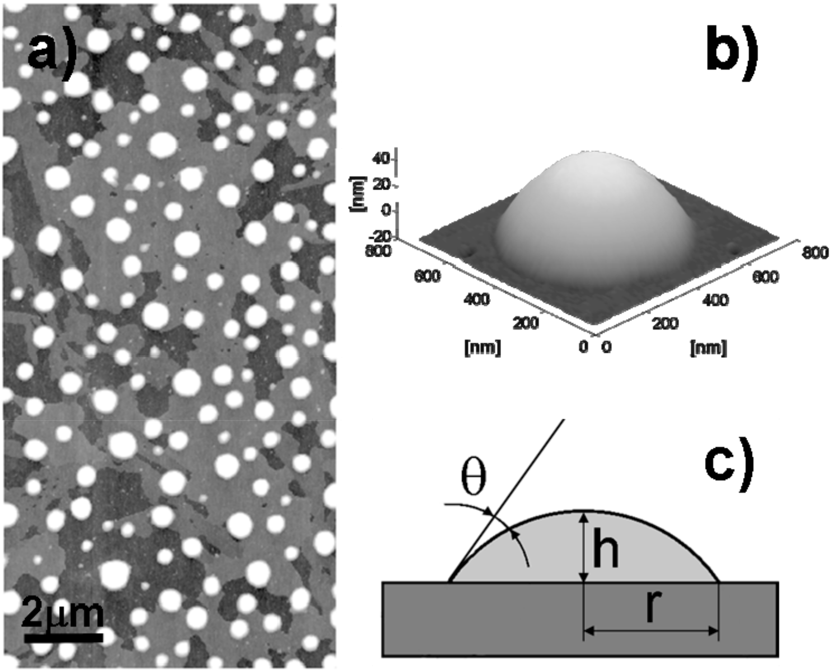

*Figure 6. a) AFM tapping-mode topography of a [$C_4$mim][$NTf_2$] film on amorphous silica, showing coexistence of layers and nanodroplets (Vertical scale 20 nm). b) A three-dimensional view of a nanodroplet sitting on top of a layer; c) The spherical cap model assumed for the droplets. $\theta$, h, and r are the contact angle, height, and radius of the droplet, accordingly.*

the contact angle less reliable, because convolution effects and tip-induced deformation of the droplets have a stronger impact on the imaging process.

**Table 1. Contact angles and effective surface energies of nano-droplets**

| *Substrate* | *Contact angle / °* | *$\Delta\sigma_{sl}$ / (mJ $m^{-2}$)* [a] |
|---|---|---|
| Mica | 41.7 ± 5.6 | 24.78 ± 2.16 |
| Terraces on mica | 45.7 ± 6.0 | 23.20 ± 2.48 |
| Amorphous silica | 12.2 ± 1.0 | 32.45 ± 0.28 |
| Terraces on am. silica | 27.0 ± 5.2 | 29.57 ± 1.38 |
| HOPG | 19.7 ± 2.2 | 31.25 ± 0.48 |

[a] $\sigma_{lv}$ = 33.20 ± 0.25 mJ $m^{-2}$ from *(4)*.

Downloaded by CORNELL UNIV on June 28, 2012 | http://pubs.acs.org
Publication Date (Web): December 18, 2009 | doi: 10.1021/bk-2009-1030.ch019

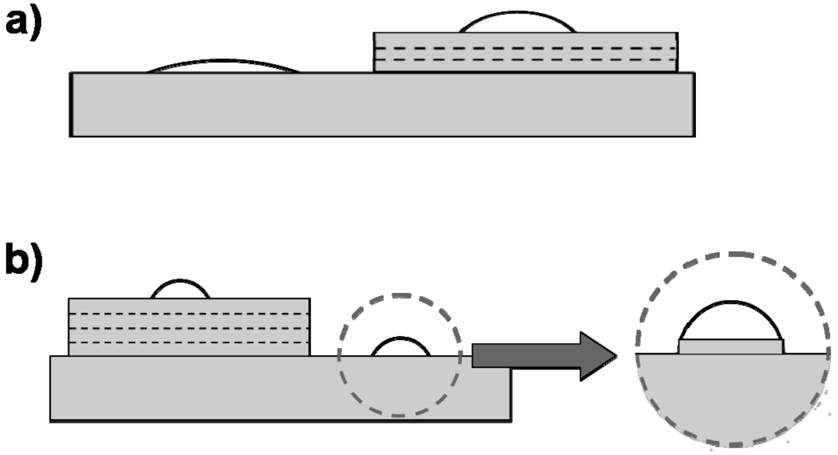

*Figure 7. Schematic view of [$C_4$mim][$NTf_2$] nanodroplets sitting on the substrate or on top of solid-like layers, in the case of a) Amorphous silica; b) Mica. A thin solid-like layer, not detectable by AFM, could be present below the droplets sitting on mica, explaining the similarity of contact angles found on the substrate and on top of layers.*

From Table 1, the measured contact angles show some variability, which deserves some consideration. The different situations have been summarised and represented in Figure 7. Firstly, the contact angles of [$C_4$mim][$NTf_2$] droplets on different surfaces are different, as expected. In particular, [$C_4$mim][$NTf_2$] wets better on amorphous silica, HOPG, and mica (in this order). On amorphous silica, Figure 7(b), the contact angle on the substrate is different from that on top of a solid-like layer, with the somewhat unexpected detail that the ionic liquid wets the silica substrate better than its solid-like phase. This represents a further confirmation that the phases of contacting [$C_4$mim][$NTf_2$] volumes are actually different. Other interesting observations can be made from Table 1 and Figure 7. [$C_4$mim][$NTf_2$] wets the solid-like layers that form on amorphous silica better than those on mica. This can suggest that, despite the strong structural similarity, some fine differences in the chemical surface properties of solid-like layers exist. Remarkably, a small (but still statistically significant) difference in the basic spacing of the solid-like phases which form on mica and silica was found. Eventually, it was noticed that, in the case of mica, there is no difference between the contact angles on the substrate and on the solid like layer (within statistical error). The intuitive explanation for this is sketched in Figure 7(b): a molecularly thin, solid-like layer, not detectable by the AFM, could be hidden below the droplet.

## Conclusions

When a few monolayers of [$C_4$mim][$NTf_2$] are deposited on a variety of surfaces, the whole ionic liquid rearranges in a solid-like phase, characterised by the stacking of a basic layer with thickness compatible to the size of the cation-anion pair ($\delta \sim 0.6$ nm). Structural order is maintained up to distances corresponding to much more than the single or the few molecular layers recently observed at the interface between a bulk amount of ionic liquid and a solid surface, or air. The solid-like character of these films has been qualitatively tested by exploiting the capability of the AFM of acting as a controlled local force transducer. Moreover, it has been shown that AFM allows characterising the contact angles of ionic liquids nanodroplets, providing information about the chemical heterogeneity of different interfaces, as well as quantitative data about the surface energies.

The potential of atomic force microscopy for the quantitative investigation of the interfacial properties of thin ionic liquids coatings was highlighted. The results of this study are directly relevant for those applications where ionic liquids are employed in form of thin films supported on solid surfaces, such as in micro-electromechanical or micro-electronic devices. More generally, they suggest that at the (bulk)liquid-solid interface the structural properties of ionic liquids can be far more complex than those depicted so far, and prompt new fundamental investigations of the forces that drive supported ionic liquids through a liquid-to-solid-like transition. Finally, it is concluded that the possibility of comparing the results of AFM investigations to those of numerical simulations will be extremely interesting.

Downloaded by CORNELL UNIV on June 28, 2012 | http://pubs.acs.org
Publication Date (Web): December 18, 2009 | doi: 10.1021/bk-2009-1030.ch019

## Acknowledgements

We thank P. Ballone and M. Del Pópolo for discussions and suggestions, K.R. Seddon and M. Deetlefs for providing the ionic liquid used in this study, and C. Lenardi and M. Perego for the XPS analysis of our samples. This project has been financially supported by Fondazione Cariplo under grant “Materiali e tecnologie abilitanti 2007”.

# References

1. Jin, H.; O'Hare, B.; Dong, J.; Arzhantsev, S.; Baker, G.A.; Wishart, J.F.; Benesi, A.J.; Maroncelli, M. *J. Phys. Chem. B* **2008**, *112*, 81–92.
2. Singh, T.; Kumar, A. *J. Phys. Chem. B* **2008**, *112*, 12968–12972.
3. Troncoso, J.; Cerdeirina, C.A.; Sanmamed, Y.A.; Romani, L.; Rebelo, L.P.N. *J. Chem. Eng. Data* **2006**, *51*, 1856–1859.
4. Deetlefs, M.; Seddon, K.R.; Shara, M. *Phys. Chem. Chem. Phys.* **2006**, *8*, 642-649.
5. de Azevedo, R.G.; Esperança, J.M.S.S.; Najdanovic-Visak, V.; Visak, Z.P.; Guedes, H.J.R.; da Ponte, M.N.; Rebelo, L.P.N. *J. Chem. Eng. Data* **2005**, *50*, 997.
6. de Azevedo, R.G.; Esperança, J.M.S.S.; Szydlowski, J.; Visak, Z.P.; Pires, P.F.; Guedes, H.J.R.; Rebelo, L.P.N. *J. Chem. Thermodyn.* **2005**, *37*, 888-899.
7. Welton, T. *Chem. Rev.* **1999**, *99*, 2071-2083.
8. Holbrey, J.D.; Seddon, K.R. *Clean Products and Processes* **1999**, *1*, 223-236.
9. Kuang, D.; Wang, P.; Ito, S.; Zakeeruddin, S.M.; Grätzel, M. *J. Am. Chem. Soc.* **2006**, *128*, 7732–7733.
10. Frackowiak, E.; Lota, G.; Pernak J. *Appl. Phys. Lett.* **2005**, *86*, 164104-1/3.
11. Qu, J.; Truhan, J. J.; Dai, S.; Luo, H.; Blau, P. J. *Tribology Letters* **2006**, *22*, 207-214.
12. Nainaparampil, J.J.; Eapen, K.C.; Sanders, J.H.; Voevodin, A.A. *J. Microelectromech. Syst.* **2007**., *16*, 836-843.
13. Fitchett, B.D.; Conboy, J.C. *J. Phys. Chem. B* **2004**, *108*, 20255-20262.
14. Romero, C; Baldelli, S. *J Phys Chem B* **2006**, *110*, 6213-6223.
15. Santos, C.S.; Baldelli, S. *J. Phys. Chem. B* **2007**, *111*, 4715-4723.
16. Romero C.; Moore, H.J.; Lee, T.R.; Baldelli, S. *J. Phys. Chem. C* **2007**, *111*, 240-247.
17. Rollins, J.B.; Fitchett, B.D.; Conboy, J.C. *J. Phys. Chem. B* **2007**, *111*, 4990–4999.
18. Caporali, S.; Bardi, U.; Lavacchi, A. *J. Electr. Spectr. Rel. Phen.* **2006**, *151*, 4–8.
19. Gottfried, J.M.; Maier, F.; Rossa, J.; Gerhard, D.; Schulz, P.S.; Wasserscheid, P.; Steinrück, H.-P. *Z. Phys. Chem.* **2006**, *220*, 1439-1453.
20. Iimori, T.;, Iwahashi, T.; Kanai, K.; Seki, K.;, Sung, J.; Kim, D.; Hamaguchi, H.-o; Ouchi, Y. *J. Phys. Chem. B* **2007**, *111*, 4860–4866.
21. Sloutskin, E.; Ocko, B.M.;Tamam, L.; Kuzmenko, I.; Gog, T.; Deutsch M. *J. Am. Chem. Soc.* **2005**, *127*, 7796−7804.
22. Hofft, O.; Bahr, S.; Himmerlich, M.; Krischok, S.; Schaefer, J.A.; Kempter, V. *Langmuir* **2006**, *22*, 7120-7123.
23. Krischok, S.; Eremtchenko, M.; Himmerlich, M.; Lorenz, P.; Uhlig, P.; Neumann, A. *J. Phys. Chem. B* **2007**, *111*, 4801-4806.
24. Smith, E.F.; Rutten, F.J.M.; Villar-Garcia, I.J.; Briggs, D.; Licence, P. *Langmuir* **2006**, *22*, 9386-9392.

Downloaded by CORNELL UNIV on June 28, 2012 | http://pubs.acs.org
Publication Date (Web): December 18, 2009 | doi: 10.1021/bk-2009-1030.ch019

25. Nainaparampil, J.J.; Phillips, B.S.; Eapen, K.C.; Zabinski, J.S. *Nanotechnology* **2005**, *16*, 2474–2481.
26. Atkin, R.; Warr, G.G. *J. Phys. Chem. C* **2007**, *111*, 5162-5168.
27. Gomila, G.; Toset, J.; Fumagalli, L. *J. Appl. Phys.* **2008**, *104*, 024315.
28. Dedkov, G.V.; *Phys. Status Solidi A* **2000**, *179*, 3-75.
29. Liu, Y.; Zhang, Y.; Wu, G.; Hu, J. *J. Am. Chem. Soc.* **2006**, *128*, 7456-7457.
30. Butt, H.-J.; Cappella, B.; Kappl, M. *Surf. Sci. Rep.* **2005**, *59*, 1–152.
31. M. Del Pópolo, P. Ballone, Queen's University, Belfast, private communication.
32. de Gennes, P. G. *Rev. Mod. Phys.* **1985**, *57*, 827-863.

Downloaded by CORNELL UNIV on June 28, 2012 | http://pubs.acs.org
Publication Date (Web): December 18, 2009 | doi: 10.1021/bk-2009-1030.ch019

Downloaded by CORNELL UNIV on June 29, 2012 | http://pubs.acs.org
Publication Date (Web): December 18, 2009 | doi: 10.1021/bk-2009-1030.ch020

## Chapter 20

# Sum Frequency Generation Spectroscopy and Electrochemical Analysis of the 1-Butyl-3-methylimidazolium Bis{(trifluoromethyl)sulfonyl}amide Double Layer Structure on the Platinum Electrode

**Selimar Rivera-Rubero and Steven Baldelli***

**Department of Chemistry, University of Houston, Houston, Texas 77204-5003**

Sum frequency generation vibrational spectroscopy (SFG), the vibrational Stark effect of CO on Pt, and electrochemical impedance spectroscopy (EIS) were used to determine the ionic arrangement of 1-butyl-3-methylimidazolium bis{(trifluoromethyl) sulfonyl}amide ionic liquid at a platinum electrode. A Stark shift of 24 $cm^{-1}$ $V^{-1}$ was found for CO adsorbed on Pt. From EIS, a capacitance of 0.15 F $m^{-2}$ was found at the potential of zero charge (~ -500 mV *vs* Ag(QRE)). Results indicate a double layer thickness of ~ 4 Å, suggesting that the ions are organised in a Helmholtz-type layer at the electrode surface. Analysis of the cation orientation as a function of the applied potential indicates a reorientation of the ions as the electrode surface charge changes.

## Introduction

For the past few years, there has been an increase in studies of ionic liquids in electrochemical systems *(1-8)*. Ionic liquids are salts with a melting point close to or below room temperature. Usually formed by an organic cation and a

In Ionic Liquids: From Knowledge to Application; Plechkova, N., et al.;
ACS Symposium Series; American Chemical Society: Washington, DC, 2010.

Downloaded by CORNELL UNIV on June 29, 2012 | http://pubs.acs.org
Publication Date (Web): December 18, 2009 | doi: 10.1021/bk-2009-1030.ch020

weakly coordinating anion, these salts offer a range of tuneable physical properties depending on the selected ionic combination. This tunability also applies to their electrochemical properties, such as conductivity and electrochemical window. Understanding the influence of the different ions on the electrochemical properties will facilitate the appropriate selection of ions for a specific application.

There is vast information on the molecular-level description of the liquid-electrode interface for aqueous electrolytes and molten salts *(9,10).* Surprisingly, molten salts were found to possess a potential of zero charge (PZC) similar to aqueous electrolytes *(9,10).* However, molten salts are usually formed by inorganic, spherically symmetric ions (*e.g.* NaCl) and these results cannot be related to non-spherical polarisable ionic liquids. In this report, a molecular-level description of the ionic arrangement at the metal/ionic liquid interface is provided for an imidazolium-based ionic liquid.

The first step in the description of the interfacial structure is the definition of the double-layer structure of the system and its PZC. The double layer is defined by the interface region at which the charge transfer occurs or at that range of potential decay at which the ions are influenced by the electrode potential. However, it is essential to know if the potential at the electrode is positive or negative with respect to the PZC. This will indicate if the electrode is positively or negatively charged, and provide a correlation to ions being repelled or attracted to the metal surface.

Even though the models for the double-layer structure are based on dilute aqueous systems, we recently reported a double layer structure for 1-butyl-3-methylimidazolium tetrafluoroborate ionic liquid as one-ion-layer thick, which is consistent with a Helmholtz model *(8).* This analysis was performed combining sum frequency generation (SFG) vibrational spectroscopy of the Stark effect of carbon monoxide on platinum in the ionic liquid, and electrochemical impedance spectroscopy (EIS).

In this report, the double layer structure of 1-butyl-3-methylimidazolium bis{(trifluoromethyl)sulfonyl}amide ($[C_4mim][NTf_2]$) is analysed. SFG as a function of potential, within the double layer region, will provide information on the cation orientation as the electrode surface goes from being negatively to positively charged. In addition, SFG analysis of the vibrational Stark effect of CO adsorbed to the Pt electrode in $[C_4mim][NTf_2]$ allows a correlation on the strength of the local fields to the double layer thickness. Using EIS, the capacitance ($C$) obtained as a function of potential provides the PZC for the system at which the capacitance is at its minimum. In addition, the capacitor thickness is equal to the double layer thickness allowing a direct correlation of the ionic liquid capacitance with the double layer thickness:

$$C \propto \frac{1}{d}$$

SFG is a second order nonlinear vibrational spectroscopic technique, sensitive to molecules in a non-centrosymmetric environment such as the liquid/electrode interface. For a detailed description of SFG, the reader is referred to several excellent reviews *(11-17).* In general, by overlapping a fixed frequency visible beam and a frequency tuneable infrared beam at the surface, a third beam is generated at the sum frequency of the incident beams. The intensity of the generated light is proportional to the square of the induced polarisation:

$$\mathrm{I_{SF}} \propto \left| \mathrm{P}^{(2)} = \chi^{(2)} : \mathrm{E_{vis}} \mathrm{E_{IR}} \right|^2 \tag{1}$$

$$\chi^{(2)} = \chi_{nr} + \sum \left[ \frac{N \langle \beta^{(2)} \rangle}{\omega_{IR} - \omega_q + i\Gamma_q} \right] \tag{2}$$

for which E refers to the electric field of the visible and infrared input beams and $\chi^{(2)}$ is the second order susceptibility tensor with $\chi_{nr}$ arising from the non-resonant component of the surface. The hyperpolarisability, $\beta^{(2)}$, contains the Raman polarisability and the infrared dipole transition averaged over the molecular orientation, indicated by the brackets $\langle\,\rangle$. $N$ is the number of modes contributing the SFG signal. The $\omega_{IR}$ and $\omega_q$ correspond to the frequency of the incoming IR radiation and the normal mode of vibration, respectively, with $\Gamma_q$ as the damping constant for the $q$th vibrational mode. With a polarisation analysis of the interface, the molecular orientation with respect to the surface normal is deduced *(18).*

Downloaded by CORNELL UNIV on June 29, 2012 | http://pubs.acs.org
Publication Date (Web): December 18, 2009 | doi: 10.1021/bk-2009-1030.ch020

## Experimental

The synthesis of [$C_4$mim][$NTf_2$] have been described previously *(19).* To determine the electrochemical window to be analysed, a PINE Instrument Potentiostat Model AFCBP1 was used. The same potentiostat was also used to control the electrochemical potential at which the SFG was acquired. EIS measurements were performed using an EG&G PAR Model 263A potentiostat/ galvanostat in combination with a PAR M5210 lock-in amplifier controlled by PowerSINE software. The frequency range used was from 100 kHz to 1 Hz with an applied sinusoidal signal of 5 mV. Impedance data were fitted to an equivalent circuit, R(QR), by ZSimpWin software.

The SFG spectroscopy system consisted of an Ekspla picosecond Nd:YAG laser which pumped (1064 nm) the optical parametric generation/amplification system, OPG/OPA (LaserVision). The OPG/OPA system generated the second harmonic 532 nm and the tuneable infrared beam (2000-4000 $\mathrm{cm^{-1}}$). The visible beam (532 nm) was at 56° from the surface normal and the infrared beam was at 63.7° at the ionic liquid/Pt interface. The SFG spectrum was collected while scanning over the desired infrared energy using a LabVIEW program. Each datum point was an average of 20 shots at 1 $\mathrm{cm^{-1}\ s^{-1}}$.

The laser beams passed through a quartz prism and a thin layer of ionic liquid (~10 μm thick), followed by the Pt electrode. The SFG signal was reflected out of the cell to the detection system, and the IR beam was reflected and directed towards the reference channel, which was collected concurrently with each SFG spectrum. The reference channel consisted of powdered KTP in glass at which the reflected IR signal was mixed with 532 nm light generating a sum frequency signal sensitive to the infrared fluctuations.

An important feature of these experiments is the custom-made vacuum-tight electrochemical cells used, which can hold vacuum to > $2\times10^{-5}$ Torr. For the cyclic voltammetry and impedance measurements, a glass cell with a flat Teflon stopcock was used, Figure 1. The working electrode was a polycrystalline Pt bead, with a contact area of 0.713 $cm^2$, along with a Pt counter electrode and a Ag wire reference electrode with a potential of ~ -200 mV *vs.* NHE (Normal Hydrogen Electrode).

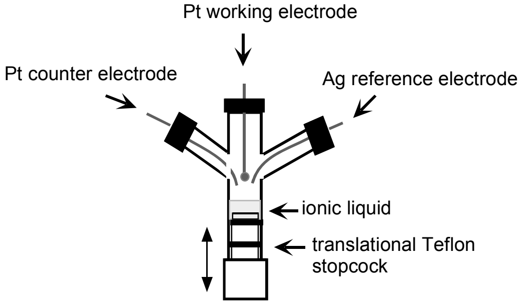

*Figure 1: Sketch of the electrochemical cell used for the cyclic voltammetry and impedance measurements*

All three electrodes were attached to the cell by a vacuum-tight thread seal. A translational Teflon stopcock with Kalrez O-rings controls the height of the ionic liquid inside the cell for the liquid-electrode contact, Figure 1. To prepare the sample, the ionic liquid was placed over the Teflon stopcock and pulled away from the level of the electrodes. The Ag electrode was cleaned with ammonium hydroxide and rinsed thoroughly before each experiment. The Pt working and counter electrodes were flame annealed in a hydrogen-air flame for one minute, and then cooled in the electrochemical cell under an argon flow. After the preparation of the electrodes, the cell was evacuated to > $2\times10^{-5}$ Torr. Once the ionic liquid was dried, the level of the liquid was raised to allow contact with the electrodes. Cyclic voltammetry was acquired at a scan rate of 100 mV $s^{-1}$. EIS was collected for a potential range of -1000 to +1000 mV.

For the potential controlled SFG spectroscopy, a glass cell with a Kel-F shaft and a quartz prism was used, Figure 2. An important feature of this cell is the way the Pt working electrode was attached to the Kel-F shaft. An O-ring around the electrode allowed a vacuum-seal when compressed between the threaded glass and the Kel-F cap, Figure 2B. The working electrode was a polycrystalline Pt rod with a diameter of 0.25 cm. The counter and reference electrodes were a Pt and Ag wire, respectively.

Downloaded by CORNELL UNIV on June 29, 2012 | http://pubs.acs.org
Publication Date (Web): December 18, 2009 | doi: 10.1021/bk-2009-1030.ch020

Prior each experiment, the Pt working electrode was flame annealed in a hydrogen-air flame and cooled in a glass tube with an argon flow for ~10 min

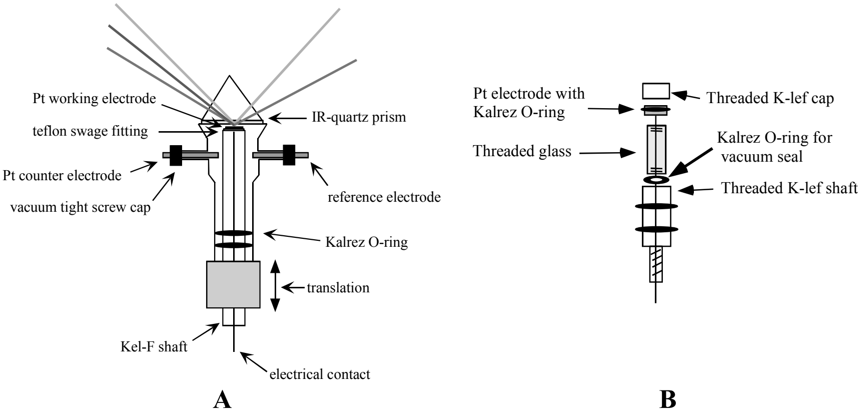
Pt working electrode
teflon swage fitting
Pt counter electrode
vacuum tight screw cap
IR-quartz prism
reference electrode
Kalrez O-ring
translation
Kel-F shaft
electrical contact
A
Pt electrode with Kalrez O-ring
Threaded glass
Threaded K-lef cap
Kalrez O-ring for vacuum seal
Threaded K-lef shaft
B

*Figure 2: (A) Sketch of the SFG-electrochemical cell. (B) Detailed description of the inside shaft design (B).*

*(20).* Immediately after removing the electrode from the glass tube, a drop of ionic liquid was placed on the surface of the Pt electrode and an O-ring was positioned over the electrode. A Kel-F cap, with a central hole for the Pt electrode, was used to attach the electrode to the translational shaft while making a vacuum tight seal by compressing the O-ring, Figure 2B. The shaft was then introduced into the SFG electrochemical cell. Subsequently, the SFG cell was evacuated with a vessel containing the dried [$C_4$mim][$NTf_2$] attached to it. Once the system was evacuated for approximately 4 h (at ~60 °C), the [$C_4$mim][$NTf_2$] flowed into the SFG cell without exposing the liquid to air. The Pt electrode was pressed against the quartz prism and the spectrum was acquired while controlling the potential applied to the system. SFG was acquired for a potential range of -1000 to +1500 mV at every 500 mV while scanning the infrared energy from 2750 to 3300 $cm^{-1}$. Each SFG spectrum corresponds to an average of 5 scans.

For the Stark shift analysis, the latter procedure was also followed except that the vessel containing the dried [$C_4$mim][$NTf_2$] was backfilled with CO instead of Ar. Furthermore, the potential of the system was hold at -200 mV for 1 h before the Pt electrode was pressed against the prism to allow the CO adsorption to the electrode surface. SFG was acquired for a potential range of -800 to +1600 mV at every 400 mV while scanning the infrared energy from 1950 to 2150 $cm^{-1}$. Each CO spectrum is an average of 3 scans.

Downloaded by CORNELL UNIV on June 29, 2012 | http://pubs.acs.org
Publication Date (Web): December 18, 2009 | doi: 10.1021/bk-2009-1030.ch020

## Results and discussion

From cyclic voltammetry of the [$C_4$mim][$NTf_2$], Figure 3, an electrochemical window of approximately 4 V is observed, from which a window of 2.5 V was selected for analysis (-1 to +1.5 V).

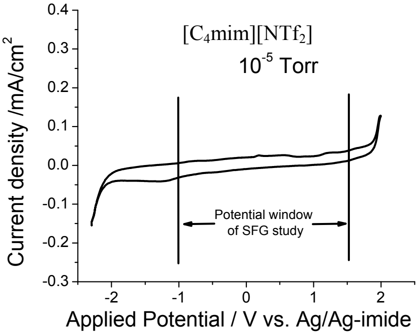

*Figure 3: Electrochemical window of [$C_4$mim][$NTf_2$] from cyclic voltammetry analysis scan rate =100 mV $s^{-1}$*

The SFG spectra obtained for [$C_4$mim][$NTf_2$], Figures 4 and 5, are similar to those previously reported by our group for [$C_4$mim][$PF_6$] and [$C_4$mim][$BF_4$] *(7)*. For the *ppp* spectra, there are three peaks at 2870, 2930 and 2970 cm$^{-1}$ assigned, respectively, to the symmetric, Fermi resonance and antisymmetric modes of $CH_3$ from the butyl chain. There are four peaks between 3000 and 3200 cm$^{-1}$ from the imidazolium ring. At 3027 cm$^{-1}$, a peak due to the interaction of the anion with the ring C-H bonds is observed, and at 3076 cm$^{-1}$ there is the ring C(2)-H peak. The peaks at 3160 and 3200 cm$^{-1}$ are the ring H-C(4)C(5)-H antisymmetric and symmetric peaks respectively.

Downloaded by CORNELL UNIV on June 29, 2012 | http://pubs.acs.org
Publication Date (Web): December 18, 2009 | doi: 10.1021/bk-2009-1030.ch020

Downloaded by CORNELL UNIV on June 29, 2012 | http://pubs.acs.org
Publication Date (Web): December 18, 2009 | doi: 10.1021/bk-2009-1030.ch020

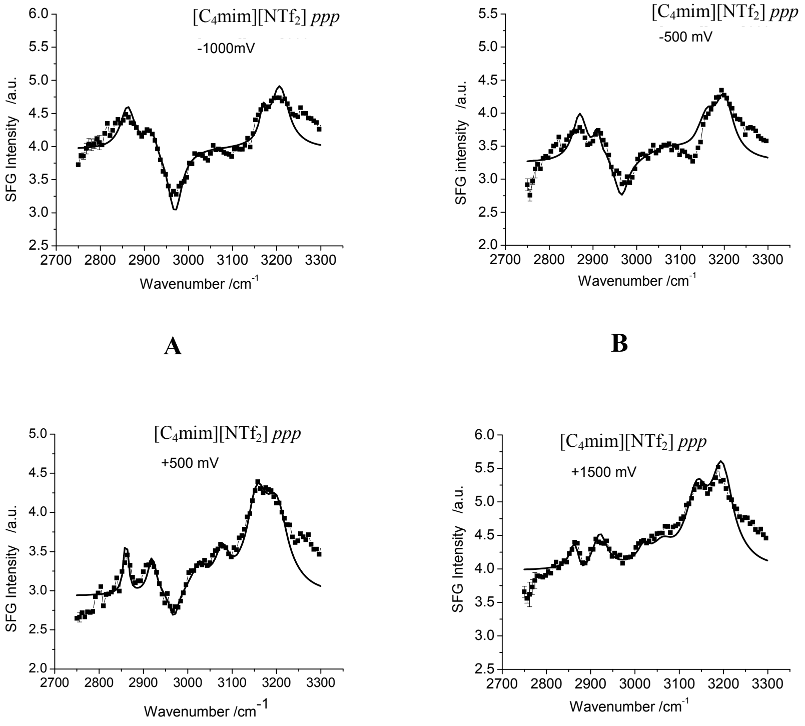

**A** **B**

**C** **D**

*Figure 4: SFG ppp polarised spectra of [C$_4$mim][NTf$_2$] at the Pt electrode for different applied potentials: A -1000 mV; B -500 mV; C +500 mV; D +1500 mV*

For the *ssp* spectra, five resonances are observed, Figure 5. At 2879 and 2940 cm$^{-1}$ are the butyl $CH_3$ symmetric and Fermi resonance in addition to the $CH_2$ antisymmetric mode observed at 2914 cm$^{-1}$. The imidazolium ring peaks are observed at 3170 and 3210 cm$^{-1}$ for the H-C(4)C(5)-H antisymmetric and symmetric modes.

Downloaded by CORNELL UNIV on June 29, 2012 | http://pubs.acs.org
Publication Date (Web): December 18, 2009 | doi: 10.1021/bk-2009-1030.ch020

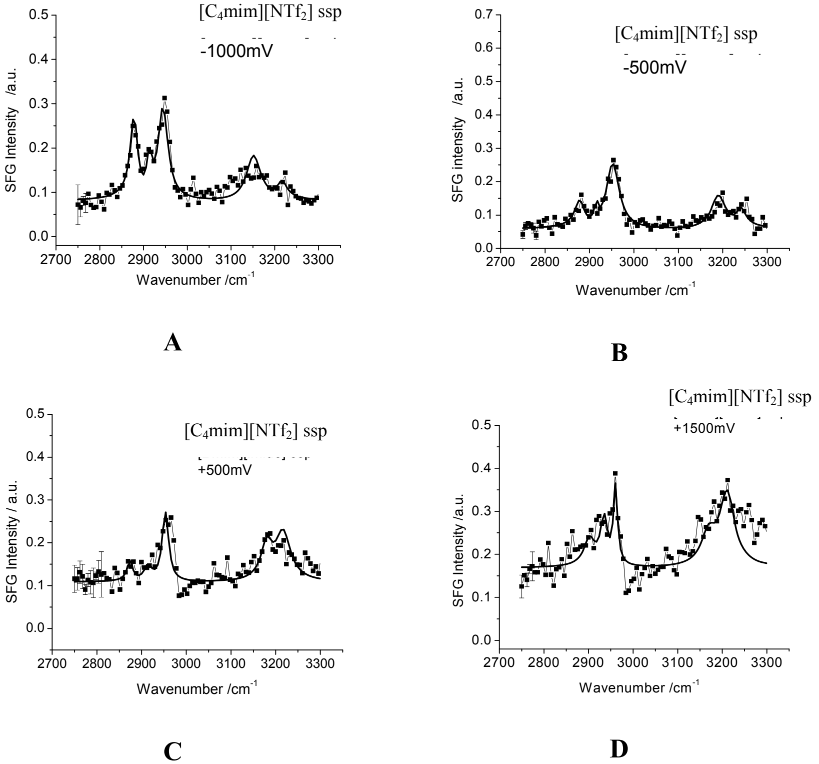

*Figure 5: SFG ssp polarised spectra of [$C_4$mim][$NTf_2$] at the Pt electrode for different applied potentials: A -1000 mV; B -500 mV; C+500 mV; D +1500 mV.*

The convolution given by the intense non-resonant background and the peaks interaction with the non-resonance, and within themselves, complicates the analysis of the spectra. When compared with previous results *(21),* different peaks are observed in the spectra, as well as the positions of the peaks being slightly different, possibly due to interaction of the molecule with the platinum electrode. Furthermore, the flexibility of the butyl chain does not allow correlating the butyl $CH_3$ orientation with the overall cation. Therefore, analysis of the imidazolium ring peaks as a function of the potential applied provides a more accurate relation to the overall cation orientation. Analysis of the spectra will be focussed over the changes observed for the H-C(4)C(5)-H peaks.

As the potential changes from -1000 to +1500 mV, changes in the H-C(4)C(5)-H peak intensities are observed for the *ppp* as well as the *ssp* spectra, Figures 4 and 5. At -1000 mV in the *ppp* spectra, the H-C(4)C(5)-H symmetric peak at 3200 $cm^{-1}$ is more intense than the antisymmetric peak at 3160 $cm^{-1}$, while the opposite is observed in the *ssp*, Figure 4A and 5A. As the potential becomes more positive, a difference on the intensity ratio of the two peaks is observed. For the potentials of -500 and +500 mV, this change is more pronounced in the *ssp* than the *ppp* polarised spectra. At -500 mV, Figure 5B, the intensity of the 3170 $cm^{-1}$ peak, in the *ssp* polarised spectra, is about twice the intensity of the peak at 3210 $cm^{-1}$, but when the potential varies to +500 mV, Figure 5C, the 3210 $cm^{-1}$ peak becomes more intense with an intensity similar to that observed for the 3170 $cm^{-1}$ peak. Furthermore, a change in potential to +1500 mV, Figure 5D, increases the intensity of the 3210 $cm^{-1}$ peak even more, the peak being now double the intensity of the 3170 $cm^{-1}$ peak, Figure 5. In the *ppp* polarised spectra, there is an increase in the peak's intensity, although a significant change is not observed. Only a clear definition of the H-C(4)C(5)-H antisymmetric and symmetric peaks is observed for the +1500 mV *ppp* spectra, which can be associated with the increase in intensity, Figure 4D.

For a determination of the cation orientation at the ionic liquid/Pt interface, the same coordinate definition used by Hirose was applied to relate the molecular coordinate (*a,b,c*) to the surface coordinate (*x,y,z*) *(15,16).* The orientation of the molecules is expressed by a tilt (θ) angle of the *c* axis with respect to the *z* axis and a twist (φ) along *c*, Figure 6. For the orientation analysis, a simulation of the intensity ratio as a function of the tilt and twist angles is compared with the experimental values using the *ssp* and *ppp* polarised spectra. Changing the electrode surface charge from negative to positive does not have an effect in the tilt of the cation ring as previously observed for $[BF_4]^-$ *(7).* Instead, the twist seems to be affected by the potential applied mimicking the behaviour previously observed for $[PF_6]^-$ *(21).* A wider range of twist angles are found when the electrode is negatively charged. For positive surface charge, the twist of the imidazolium ring is constrained, keeping the imidazolium charge away from the surface plane. For a negative surface charge, the cation is expected to dominate the surface, correlating to the wide range of possible tilt angles found. On the other side, positive surface charge repels the imidazolium ring from the surface giving surface access to the anion and limiting the possible orientations of the ring. The same analysis for $[C_4mim][PF_6]$ indicates a similar potential dependent orientation *(7).* For both ionic liquids, the tilt orientation is relatively constant from negative to positive potentials. The cation of $[C_4mim][PF_6]$ was oriented at about 12-26° at -500 mV and 23-34° at +1000 mV *(21).* For $[C_4mim][NTf_2]$, the orientation of the cation changes from 15-32° at -1000 mV to 35-60° at +1500 mV. However, the twist angle changes dramatically for both ionic liquids, from ~0-35° at negative potentials to about 65-90° at positive potentials, Figure 7. Further, the effect is different when compared to $[BF_4]^-$, most likely due to the size and/or charge density *(7).* The idea of the cation reorienting as the electrode surface potential becomes positive to allow the anion access to the surface was recently confirmed in an analysis of $[C_4mim][N(CN)_2]$, performed by Aliaga and Baldelli *(22).*

Downloaded by CORNELL UNIV on June 29, 2012 | http://pubs.acs.org
Publication Date (Web): December 18, 2009 | doi: 10.1021/bk-2009-1030.ch020

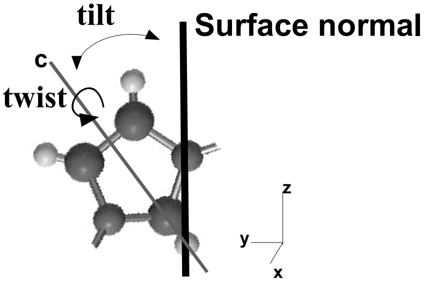

*Figure 6: Description of the imidazolium ring molecular coordinate axes (a,b,c) and surface coordinate axes (x,y,z).*

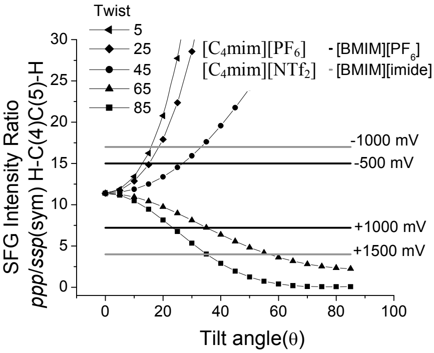

*Figure 7: Simulation curve for the ppp/ssp intensity ratio of the H-C(4)(C(5)-H of [$C_4$mim][$PF_6$] and [$C_4$mim][$NTf_2$].*

The structure and thickness of the double layer is an important aspect in the understanding of the electrolyte influence in the rate of the redox process at the electrode. Therefore, to establish a molecular model of [$C_4$mim][$NTf_2$] at the electrode surface, the thickness of the double layer structure must be determined.

To estimate the double layer thickness of the system, the same approach previously used for [$C_4$mim][$BF_4$] with the Stark effect of CO on Pt is followed *(8)*. From the SFG of CO on Pt as a function of the applied potential, the vibrational Stark effect is related to the double layer thickness of the system. The SFG spectra of CO on Pt in the [$C_4$mim][$NTf_2$], Figure 8, are found to have a change of 24 $cm^{-1}$ $V^{-1}$. To determine the double layer thickness, the local electric field Stark effect $\{\partial\nu_{CO}/\partial E_{loc} \sim 1 \times 10^{-6}\ cm^{-1}\ (V\ cm^{-1})^{-1}\}$ is related to the applied voltage:

Downloaded by CORNELL UNIV on June 29, 2012 | http://pubs.acs.org
Publication Date (Web): December 18, 2009 | doi: 10.1021/bk-2009-1030.ch020

$$\left(\frac{\partial \nu_{CO}}{\partial E_{loc}} / \frac{\partial \nu_{CO}}{\partial \phi}\right) = d = (5 \pm 1) \times 10^{-10}\ \mathrm{m} \qquad (3)$$

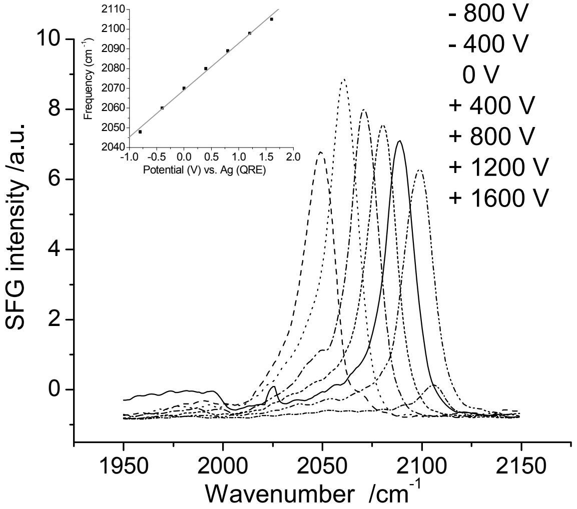

*Figure 8: SFG spectra of CO on a Pt electrode in [$C_4$mim][$NTf_2$] electrolyte. Insert: Plot of peak position as a function of electrode potential.*

A double layer thickness of 4.2 Å is found for [$C_4$mim][$NTf_2$], which is comparable to the 3.3 Å previously reported for [$C_4$mim][$BF_4$] and 3.8 Å also found for [$C_4$mim][$PF_6$] *(8).*

In addition, EIS measurements are acquired as a second technique used in the analysis of the double layer thickness, Figure 9A. An equivalent circuit R(QR) is used to fit the impedance data and obtained the capacitance as a function of potential, Figure 9B. From the capacitance curve a minimum is observed at ~ -500 mV *vs.* Ag(QRE) which is defined as the potential of zero charge for the system. The EIS capacitance, *C*, is related to the thickness of the double layer by:

$$d = \frac{\varepsilon \varepsilon_0}{C} \qquad (4)$$

where $\varepsilon$ and $\varepsilon_0$ are the relative and vacuum permittivity, respectively. Using the EIS capacitance of 0.15 F $m^{-2}$, a double layer thickness of 4 Å was determined in accord with the 4.2 Å found with the Stark effect analysis. Using the dimension of the imidazolium cation of (10 x 4 x 1) $Å^3$, a thickness of ~ 4 Å is an indication of a one-ion-thick double layer *(8).* These results support previous findings for [$C_4$mim][$BF_4$], for which a Helmholtz-type layer was also found *(8).*

Downloaded by CORNELL UNIV on June 29, 2012 | http://pubs.acs.org
Publication Date (Web): December 18, 2009 | doi: 10.1021/bk-2009-1030.ch020

Previous findings for [C$_4$mim][N(CN)$_2$] present a double layer thickness of 25 Å *(22)*. The difference in the results can be attributed to the strong interaction and adsorption of the dicyanamide anion to the platinum electrode.

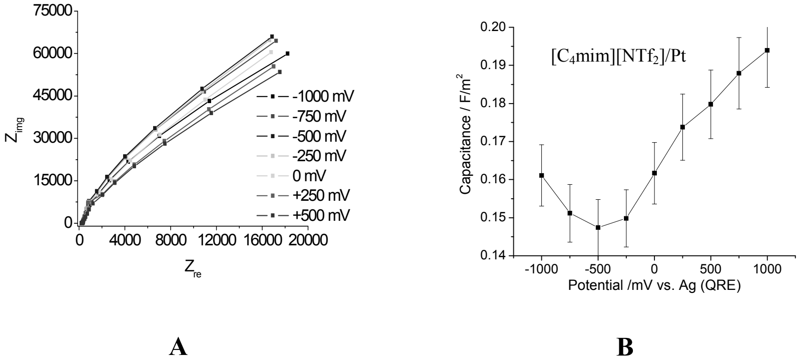

*Figure 9: Capacitance as a function of applied potential for a Pt electrode in [C$_4$mim][NTf$_2$]*

It is interesting to compare these results with recent theoretical analysis of the interfacial structure of ionic liquids near a charged electrochemical interface. Oldham used the Gouy, Chapman, and Sterns approach, where the dilute electrolyte is replaced by the pure ionic fluid *(23)*. Another approach was based on statistical mechanics and mean field theory simulations *(24-26)*. Both results reach conclusions that appear contradictory to the experimental observations, but their essential approach must be true. The theoretical work makes, as its primary link to experiment, the capacitance-voltage curve. The C-V plots usually give a “U” shape where the minimum corresponds to the PZC of the electrode interface *(10,27,28)*. This is the point where the double layer is the thinnest, and the ion concentration at the interface is the same as the bulk electrolyte, *i.e.* no surface excess. This is the situation for the dilute electrolyte solution, and is not expected to be a valid model for the ionic liquids. However, the recent experimental results do not indicate a maximum in the C-V curves for these ionic liquids *(8,22,29-37)* with one exception *(36)*. The results presented here using *in situ* spectroscopy (SFG and vibrational Stark effect) combined with electrical measurements (EIS) provide the view that the ‘double layer’ structure is very thin - approximately one ion layer thick. Since ionic liquids as a class of chemicals have widely variable physical and chemical properties depending on the ion type in the salt, many more experiments will be needed before a general conclusion can be reached.

## Conclusion

A double layer one-ion-thick, Helmholtz-type layer, was found for [C$_4$mim][NTf$_2$] at a Pt electrode. The structure at the electrode-liquid interface is dominated by the cation; at a negative surface charge (potential < -500 mV) the imidazolium cation is oriented over a wide range of possible twist angles.

Downloaded by CORNELL UNIV on June 29, 2012 | http://pubs.acs.org
Publication Date (Web): December 18, 2009 | doi: 10.1021/bk-2009-1030.ch020

This orientation is influenced by the interaction of the imidazolium ring positive charge with the negatively charged electrode. As the electrode becomes positive (potential > -500 mV), the charged ring twists away from the electrode surface, indicating the repulsion of the positive charges and allowing the anion to compensate for the electrode charge.

## Acknowledgements

This project was possible thanks to the support provided by the Welch Foundation (E-1531) and the Petroleum Research Fund.

Downloaded by CORNELL UNIV on June 29, 2012 | http://pubs.acs.org
Publication Date (Web): December 18, 2009 | doi: 10.1021/bk-2009-1030.ch020

## References

1. Suarez, P. A.; Selbach, V. M.; Dullius, J. E.; Einloft, S.; Pianicki, C. M.; Azambuja, D. S.; deSouza, R. F.; Dupont, J. *Electrochim. Acta* **1997**, *42*, 2533-2538.
2. Quinn, B. M.; Ding, Z.; Moulton, R.; Bard, A. J. *Langmuir* **2002**, *18*, 1734-1741.
3. Wang, P.; Zakeeruddin, S.; Moser, J.; Gratzel, M. *J. Phys. Chem. B* **2003**, *107*, 13280-13285.
4. Lu, W.; Fadeev, A. G.; Qi, B.; Smela, E.; Mattes, B. R.; Ding, J.; Spinks, G. M.; Mazurkiewicz, J.; Zhou, D.; Wallace, G. G.; MacFarlane, D. R.; Forsyth, M.; Forsyth, S. A. *Science* **2002**, *297*, 983-988.
5. Wang, P.; Zakeeruddin, S. M.; Comte, P.; Exnar, I.; Gratzel, M. *J. Am. Chem. Soc.* **2003**, *125*, 1166-1171.
6. Bonhote, P.; Dias, A.; Papageorgiou, N.; Kalyanasundaram, K.; Gratzel, M. *Inorg. Chem.* **1996**, *35*, 1168-1175.
7. Rivera-Rubero, S.; Baldelli, S. *J. Phys. Chem. B* **2004**, *108*, 15133-15140.
8. Baldelli, S. *J. Phys. Chem. B* **2005**, *109*, 13049-13503.
9. Inman, D.; Lovering, D. G. In *Comprehensive Treatise of Electrochemistry*; Conway, B. E., Bockris, J. O., Yeager, E., Khan, S. U., White, R. E., Eds.; Plenum: New York, **1983**; Vol. 7, p 593.
10. Bard, A. J.; Faulkner, L. R. *Electrochemical Methods*; 2nd Edit.; John Wiley and Sons: New York, **2001**.
11. Buck, M.; Himmelhaus, M. *J. Vac. Sci. Technol. A* **2001**, *19*, 2717-2723.
12. Shultz, M. J.; Schnitzer, C.; Simonelli, D.; Baldelli, S. *Int. Rev. Phys. Chem.* **2000**, *19*, 123-138.
13. Duffy, D. C.; Davies, P. B.; Bain, C. D. *J. Phys. Chem.* **1995**, *99*, 15241-15249.
14. Huang, J. Y.; Shen, Y. R. In *Laser Spectroscopy and Photochemistry on Metal Surfaces*; Dai, H. L., Ho, W., Eds.; World Scientific: Singapore, **1995**.

15. Hirose, C.; Akamatsu, N.; Domen, K. *Appl. Spectrosc.* **1992**, *46*, 1051-1095.
16. Hirose, C.; Akamatsu, N.; Domen, K. *J. Chem. Phys.* **1992**, *96*, 997-1007.
17. Wang, H. F.; Gan, W.; Lu, R.; Rao, Y.; Wu, B. H. *Int. Rev. Phys. Chem.* **2005**, *24*, 191-199.
18. Lu, R.; Gan, W.; Wu, B. H.; Chen, H.; Wang, H. F. *J. Phys. Chem. B* **2004**, *108*, 7297-7307.
19. Rivera-Rubero, S.; Baldelli, S. *J. Phys. Chem. B* **2006**, *110*, 4756-4766.
20. Clavilier, J.; Faure, R.; Guinet, G.; Durand, R. *J. Electroanal. Chem.* **1980**, *107*, 205-211.
21. Rivera-Rubero, S.; Baldelli, S. *J. Am. Chem. Soc.* **2004**, *126*, 11788-11795.
22. Aliaga, C.; Baldelli, S. *J. Phys. Chem. B* **2006**, *110*, 18481-18492.
23. Oldham, K. B. *J. Electrochem. Soc.* **2008**, *613*, 131-141.
24. Fedorov, M. V.; Kornyshev, A. A. *Electrochim. Acta* **2008**, *53*, 6835-6843.
25. Fedorov, M. V.; Kornyshev, A. A. *J. Phys. Chem. B* **2008**, *112*, 11868-11874.
26. Kornyshev, A. A. *J. Phys. Chem. B* **2007**, *111*, 5545-5555.
27. Bockris, J. O.; Reddy, A. K. N. *Modern Electrochemistry: Ionics*; 2nd edit.; Plenum Press: New York, **1998**; Vol. 1.
28. Sparnaay, M. J. *The Electrical Double Layer*; Pergamon: New York, **1972**.
29. Graves, A. D. *Electroanal. Chem.* **1970**, *25*, 349-357.
30. Graves, A. D.; Inman, D. *Electroanal. Chem.* **1970**, *25*, 357-371.
31. Horn, R. G.; Evans, D. F.; Ninham, B. W. *J. Phys . Chem.* **1988**, *92*, 3531-3539.
32. Alam, M. T.; Islam, M. M.; Okajima, T.; Ohsaka, T. *J. Phys. Chem. C* **2008**, *112*, 16600-16609.
33. Alam, M. T.; Islam, M. M.; Okajima, T.; Ohsaka, T. *J. Phys. Chem. C* **2008**, *112*, 16568-16599.
34. Kisza, A. *Electrochim. Acta* **2006**, 2315-2325.
35. Lockett, V.; Sedev, R.; Ralston, J.; Horne, M.; Rodopoulos, T. *J. Phys. Chem. C* 2008, *112*, 7486-7496.
36. Santos, C.; Rivera-Rubero, S.; Dibrov, S.; Baldelli, S. *J. Phys. Chem. B* 2007, *111*, 7682-7692.
37. Nanjundiah, C.; McDevitt, S. F.; Koch, V. R. *J. Electrochem. Soc.* 1997, *144*, 3392-3399.

Downloaded by CORNELL UNIV on June 29, 2012 | http://pubs.acs.org
Publication Date (Web): December 18, 2009 | doi: 10.1021/bk-2009-1030.ch020

Downloaded by CORNELL UNIV on June 28, 2012 | http://pubs.acs.org
Publication Date (Web): December 18, 2009 | doi: 10.1021/bk-2009-1030.ch021

## Chapter 21

# Interfacial Structure at Ionic-liquid/Molecular-liquid Interfaces Probed by Sum-Frequency Generation Vibrational Spectroscopy

**Takashi Iwahashi,[1] Takayuki Miyamae,[2] Kaname Kanai,[1]
Kazuhiko Seki,[1] Doseok Kim,[3] and Yukio Ouchi[1],***

**[1]Department of Chemistry, Graduate School of Science, Nagoya University, Nagoya, Japan**
**[2]Nanotechnology Research Institute, National Institute of Advanced Industrial Science and Technology (AIST), Ibaraki, Japan**
**[3]Department of Physics and Interdisciplinary Program of Integrated Biotechnology, Sogang University, Seoul, Korea**

IR-visible sum frequency generation (SFG) vibrational spectroscopy was employed to investigate the microscopic structures at interfaces between room temperature ionic liquids and various molecular liquids. The alkyl chain of the $[C_n\text{mim}]^+$ polar cation orients toward the hydrophobic ($CCl_4$) phase at the $CCl_4$/ionic liquid interface, while it orients randomly or points towards the ionic liquid phase at a $D_2O$/ionic liquid interface. An anomalous enhancement in the amplitude of the $CD_3$ asymmetric stretching mode is observed at a butanol/ionic liquid interface, suggesting the formation of a hydrophobic layer which consists of the alkyl chains of the butanol and the $[C_n\text{mim}]^+$ cation.

The interfaces of liquids, including the liquid/solid and liquid/liquid interfaces, are crucial to various applications such as batteries, capacitors, and phase separation catalysis because the properties of the interfaces are closely related to the performance of such applications *(1−8)*. The electrolyte/electrode interface is one of the typical examples, where liquid/solid interfaces play a key role in the electrochemical applications *(5−8)*. The liquid/liquid interfaces are

In Ionic Liquids: From Knowledge to Application; Plechkova, N., et al.;
ACS Symposium Series; American Chemical Society: Washington, DC, 2010.

also important not only for practical aspects, but also from a fundamental viewpoint. For example, characteristics of liquid/liquid interfaces directly affect the properties of lipid bilayers, a model biomembrane system *(9)*. Some ionic liquids, interestingly, can form an interface both with hydrophobic and hydrophilic molecular liquids having widely different ranges of polarity *(10)*, and hence the advent of ionic liquids has increased the possible combinations of the liquid/liquid interface extensively. The structural investigation of such totally new interfaces should lead to further understanding of the liquid/liquid interface, and advances in related application areas.

In spite of their importance, our understanding of the structures of liquid interfaces *(11−17)*, especially the liquid/liquid interface *(18−22)*, is very limited compared to the structures of the liquid surfaces (air/liquid interface), mainly due to the lack of suitable experimental tools to probe such an interface. In contrast, the computer simulation has recently been applied successfully to the structural study of the liquid/liquid interface *(23−27)*, and hence development of experimental techniques for the structural investigation of the liquid/liquid interface is in much demand for gaining an in-depth understanding of this system.

IR-visible sum frequency generation (SFG) vibrational spectroscopy is a surface- and interface-specific vibrational spectroscopic technique based on the second-order nonlinear optical process, and has proven to be a powerful tool for microscopic, structural investigation of various interfaces which the light beams can reach *(28)*. So far, SFG is mostly applied to the structural study of solid and liquid surfaces, and there are only a few studies on heterointerfaces.[29,30] For liquid/liquid interfaces, Richmond and coworkers have investigated the oil/water interfaces by passing light beams through the oil, which has no absorption band for the probing beams *(30)*. On the other hand, Bain and coworkers have developed a new SFG experimental method for structural investigation of the liquid/liquid interface, in which the thin liquid film is prepared on a transparent prism to minimise the light beam absorption by the solvent *(29)*. In this study, we have applied SFG for the structural investigation of the ionic liquid/molecular liquid interfaces by extending the experimental method developed by Bain and coworkers *(29)*, and report the first SFG observation of the ionic liquid/molecular liquid interfaces to discuss the microscopic structures of the interfaces. We chose 1-alkyl-3-methylimidazolium hexafluorophosphate ([$C_n$mim][$PF_6$] with $n = 4$ and 8; Figure 1) as representative ionic liquid samples, and investigated the alkyl chain-length dependence on the interfacial structure. For the molecular liquid samples, tetrachloromethane ($CCl_4$) and deuteriated water ($D_2O$) were chosen as nonpolar and polar molecular liquids, respectively. Butanol-$d_9$ was also chosen as a molecular liquid for which the polarity has been compared to that of [$C_n$mim][$PF_6$] *(10)*.

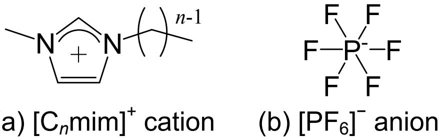

*Figure 1. Molecular structure of the ionic liquid components; (a) [$C_n$mim]$^+$ cation and (b) [$PF_6$]$^-$ anion.*

Downloaded by CORNELL UNIV on June 28, 2012 | http://pubs.acs.org
Publication Date (Web): December 18, 2009 | doi: 10.1021/bk-2009-1030.ch021

Downloaded by CORNELL UNIV on June 28, 2012 | http://pubs.acs.org
Publication Date (Web): December 18, 2009 | doi: 10.1021/bk-2009-1030.ch021

## SFG Spectroscopy: Theoretical and Experimental

The basic theory of surface SFG spectroscopy has been described elsewhere *(28,31).* SFG is based on the second-order nonlinear optical process where an IR beam at frequency $\omega_{\text{ir}}$ and a visible beam at frequency $\omega_{\text{vis}}$ overlap at the surface to generate a sum-frequency (SF) signal at a frequency $\omega_{\text{sf}} = \omega_{\text{ir}} + \omega_{\text{vis}}$. SFG signal intensity is proportional to the square modulus of an effective surface nonlinear susceptibility, $\chi_{\text{eff}}^{(2)}$, which depends on the incident beam geometry in the form:

$$\chi^{(2)}_{\text{eff}} = \left[\mathbf{L}(\omega_{\text{sf}})\cdot\hat{\mathbf{e}}(\omega_{\text{sf}})\right]\cdot\chi^{(2)} : \left[\mathbf{L}(\omega_{\text{vis}})\cdot\hat{\mathbf{e}}(\omega_{\text{vis}})\right]\left[\mathbf{L}(\omega_{\text{ir}})\cdot\hat{\mathbf{e}}(\omega_{\text{ir}})\right] \qquad (1)$$

where $\hat{\mathbf{e}}(\omega)$ and $\mathbf{L}(\omega)$ are the unit polarisation vector and the Fresnel factor of the field at frequency $\omega$, respectively. If we consider the interface between media 1 and 2 with the space-fixed coordinates chosen such that $Z$ is along the interface normal and $X$ in the incidence plane, and that the incident beams approach the interface by passing through medium 1, the components of $\mathbf{L}(\omega)$ are calculated by using the expressions:

$$L_{XX}(\omega) = \frac{2n_1(\omega)\cos\phi_2}{n_1(\omega)\cos\phi_2 + n_2(\omega)\cos\phi_1} \qquad (2a)$$

$$L_{YY}(\omega) = \frac{2n_1(\omega)\cos\phi_1}{n_1(\omega)\cos\phi_1 + n_2(\omega)\cos\phi_2} \qquad (2b)$$

$$L_{ZZ}(\omega) = \frac{2n_1^2(\omega)n_2(\omega)\cos\phi_1}{n_1(\omega)\cos\phi_2 + n_2(\omega)\cos\phi_1}\left(\frac{n_1(\omega)}{n'(\omega)}\right)^2 \qquad (2c)$$

where $n_1(\omega)$ and $n_2(\omega)$ are the refractive indices of media 1 and 2, respectively, $\phi_1$ and $\phi_2$ are incident and refracted angles of the light, respectively, and $n'(\omega)$ is the empirical refractive index of the interfacial layer *(31).* In case of an azimuthally isotropic interface, there are only four independent nonvanishing components of $\chi$s which are $\chi_{XXZ} = \chi_{YYZ}$, $\chi_{XZX} = \chi_{YZY}$, $\chi_{ZXX} = \chi_{ZYY}$, and $\chi_{ZZZ}$. The SF signal intensity $I_{\text{sf}}$ is given by

$$I_{\text{sf}}(\omega_{\text{ir}}) \propto \left|\chi_{\text{NR}} + \sum_q \frac{A_q}{\omega_q - \omega_{\text{ir}} - \mathrm{i}\,\Gamma_q}\right|^2 \qquad (3)$$

where $\chi_{\text{NR}}$ is the non-resonant contribution to the susceptibility, and $A_q$, $\omega_q$, and $\Gamma_q$ are the amplitude, frequency, and the damping constant of the $q$th vibrational mode, respectively.

Details of the experimental setup are described elsewhere *(32).* A mode-locked picosecond Nd:YAG laser (Ekspla, PL-2143B, 25 ps pulsewidth, 10 Hz) with a difference frequency generation (DFG) unit (Ekspla, DFG 401, mounting LBO and $AgGaS_2$ crystals) was used to generate a visible beam at 532 nm and a tuneable IR beam ranging from 2.5 to 10 μm. Typical input intensities were ~400 μJ/pulse for the visible beam and ~250 μJ/pulse for the IR beam, respectively. For the SFG measurements of the air/liquid interface, the visible and IR beams were overlapped at the surface of the liquid sample in a glass vessel with incidence angles of 70° and 50°, respectively. The sample setup for the SFG measurement of liquid/liquid interface is similar to that developed by Bain and coworkers *(29).* The ionic liquid thin film prepared on the $CaF_2$ prism was made to contact with the molecular liquid underneath. The film thickness is confirmed to be less than 20 μm. The visible and IR beams were overlapped at the liquid/liquid interface of the ionic liquids with incidence angles of 65° and 70°, respectively. The outgoing SFG beam was filtered, depolarised, and detected by a photomultiplier tube.

## Air/ionic liquid Interface: Reference Interface

Figure 2 shows the SFG spectra of air/[$C_n$mim][$PF_6$] interfaces ($n = 4$ or 8) taken in the CH stretching region with ssp (s-polarised SF, s-polarised visible, and p-polarised IR lights) polarisation. The solid lines in the SFG spectra show the fitting results using Equation (3). The peak at 2862 $cm^{-1}$ (prominent for SFG spectrum of air/[$C_8$mim][$PF_6$]) is assigned to the $CH_2$ symmetric stretching mode (designated as $d^+$); and the peak at 2883 $cm^{-1}$ is attributed to $CH_3$ symmetric stretching mode ($r^+$) *(11,12,32−37).* The small peak at 2921 $cm^{-1}$ should be the $CH_2$ symmetric stretching mode ($d^-$) *(11,12,32−37).* The peak at 2944 $cm^{-1}$ is assigned to the Fermi resonance ($r^+$FR) of the $CH_3$ symmetric stretching mode and the overtone of its bending mode *(11,12,32−37).*

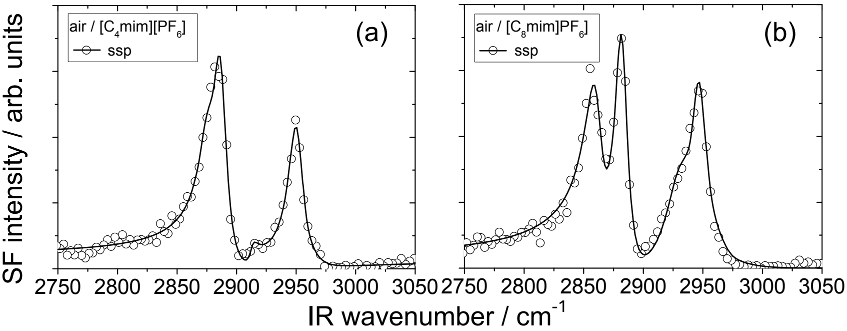

*Figure 2. SFG spectra of (a) the air/[$C_4$mim][$PF_6$] and (b) the air/[$C_8$mim][$PF_6$] interfaces taken in the CH stretching region with the ssp (circle) polarisation combination. The solid lines represent the fitting results.*

Our previous study using SFG and metastable atom electron spectroscopy (MAES) has clearly revealed that the [$C_n$mim]$^+$ cations tend to orient with the alkyl chain pointing away from the bulk into the air, and the anions exist under the alkyl chains at the air/[$C_n$mim]X interfaces (X = tetrafluoroborate,

Downloaded by CORNELL UNIV on June 28, 2012 | http://pubs.acs.org
Publication Date (Web): December 18, 2009 | doi: 10.1021/bk-2009-1030.ch021

trifluoromethane sulfonate, or bis{(trifluoromethane)sulfonyl}amide) *(38)*. The alkyl chain-length dependence on the spectral features of the SFG spectra of the air/[$C_n$mim][$PF_6$] interfaces are almost the same as our previous results *(32,38)*. Figure 3 shows the model structure for the air/liquid interface of [$C_n$mim][$PF_6$]. We will compare the SFG spectra of the air/ionic liquid interfaces with those of the ionic liquid/molecular liquid interfaces to find out the structural change induced by different liquids.

## $CCl_4$/ionic liquid Interface: Hydrophobic Interface

The SFG spectra of the $CCl_4$/[$C_n$mim][$PF_6$] interfaces are shown in Figure 4, and we can clearly see that the spectral features in the SFG spectra of the $CCl_4$/[$C_n$mim][$PF_6$] interfaces are almost identical to that of the air/[$C_n$mim][$PF_6$] interfaces in Figure 1. It clearly indicates that the alkyl chain of the [$C_n$mim]$^+$

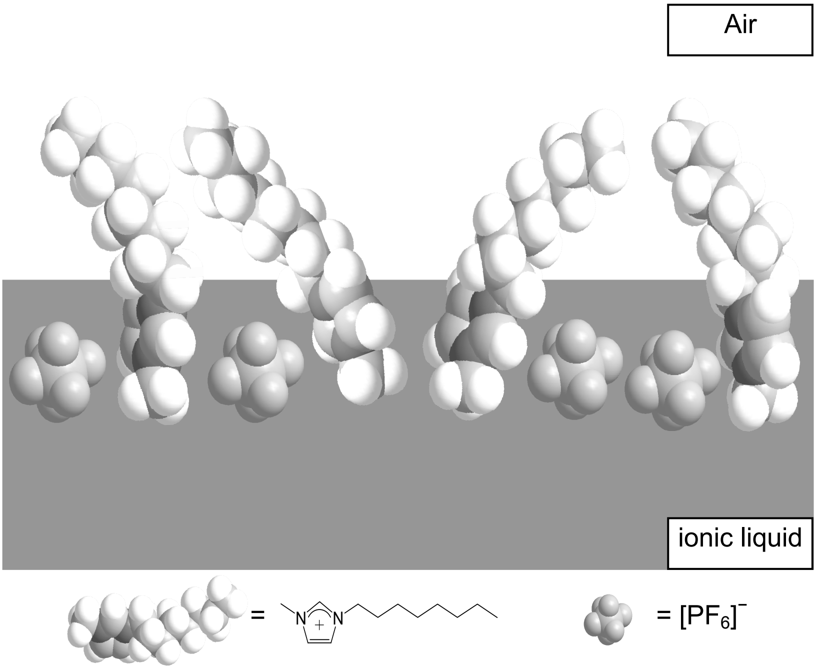

*Figure 3. Model structure of the air/[$C_8$mim][$PF_6$] interface*

Downloaded by CORNELL UNIV on June 28, 2012 | http://pubs.acs.org
Publication Date (Web): December 18, 2009 | doi: 10.1021/bk-2009-1030.ch021

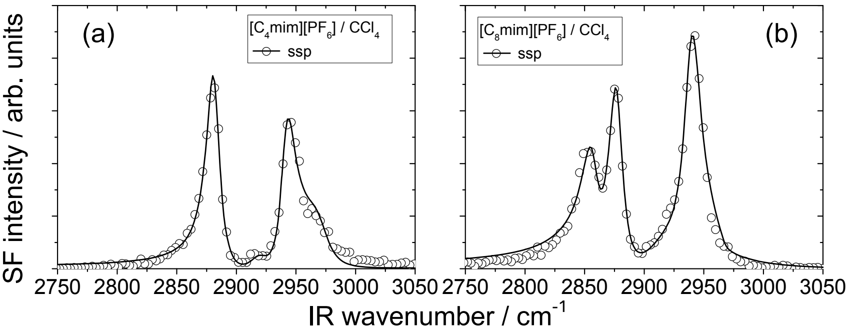

*Figure 4. SFG spectra of (a) the $CCl_4$/[$C_4$mim][$PF_6$] and (b) the $CCl_4$/[$C_8$mim][$PF_6$] interfaces taken in the CH stretching region with the ssp (circle) polarisation combinations. The solid lines represent the fitting results.*

cation preferentially points toward the $CCl_4$ phase, not toward the ionic liquid phase. This result seems to be reliable because the alkyl chain is a relatively hydrophobic functional group, and hence it is energetically stable for the [$C_n$mim]$^+$ cation configuration when alkyl chain points toward the hydrophobic $CCl_4$ phase at the interface.

## $D_2O$/ionic liquid Interface: Hydrophilic Interface

In contrast to the $CCl_4$/ionic liquid interfaces, the SFG spectra of the $D_2O$/[$C_n$mim][$PF_6$] interfaces have no characteristic peaks in the CH stretching region, as shown in Figure 5. The featureless SF signal is attributed to the shoulder of broad OD stretching mode centred at around 2600 cm$^{-1}$ *(39).* According to the selection principle of SF activity, it has been known that SFG is forbidden mainly for two cases; one case is that the molecules at the interface have no nett polar orientation *(40−42),* and the other is that the target functional group of the molecule preferentially points toward its bulk phase *(43).* The previous study of water/[$C_n$mim][$PF_6$] using the molecular dynamics (MD) simulation has predicted that the alkyl chain of the [$C_n$mim]$^+$ cation tends to orient randomly in the case of the short alkyl chain ($n = 4$), and point toward the ionic liquid phase in the case of the long alkyl chain ($n = 8$) *(24).* Therefore, our SFG results are in agreement with the computational study, although it is difficult to determine which of the two cases apply to our spectra in Figures 5a and 5b. Determination of the cation configuration at the water/ionic liquid interfaces will be addressed in our future studies.

Downloaded by CORNELL UNIV on June 28, 2012 | http://pubs.acs.org
Publication Date (Web): December 18, 2009 | doi: 10.1021/bk-2009-1030.ch021

Downloaded by CORNELL UNIV on June 28, 2012 | http://pubs.acs.org
Publication Date (Web): December 18, 2009 | doi: 10.1021/bk-2009-1030.ch021

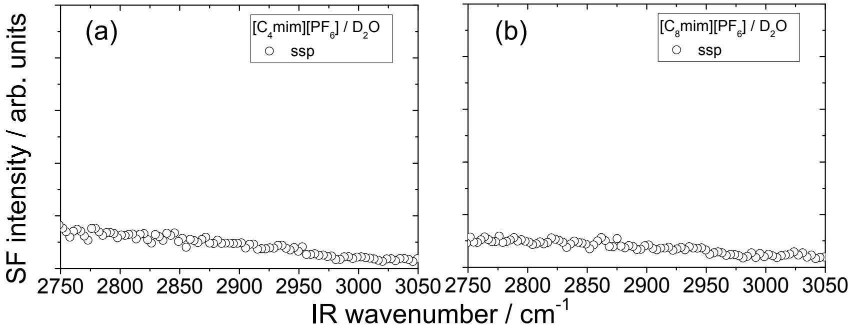

*Figure 5. SFG spectra of (a) the $D_2O/[C_4mim][PF_6]$ and (b) the $D_2O/[C_8mim][PF_6]$ interfaces taken in the CH stretching region with the ssp (circle) polarisation combinations. The solid lines represent the fitting results.*

## Butanol/ionic liquid Interface: Interface of Liquids with Similar Polarity

### Cation Configuration

Similar to the $CCl_4/[C_nmim][PF_6]$ interfaces, the SF signal from the alkyl chain of the $[C_nmim]^+$ cation is readily observable for the butanol-$d_9/[C_nmim][PF_6]$ interfaces, as shown in Figure 6. It clearly indicates that the alkyl chain of the $[C_nmim]^+$ cation is preferentially pointing toward the butanol phase *(43)*. On the other hand, the spectral peaks are much broader for the butanol-$d_9/[C_nmim][PF_6]$ interfaces relative to the air/ionic liquid and $CCl_4$/ionic liquid interfaces. The broad peak width could indicate the inhomogeneous environment of the alkyl chain of the $[C_nmim]^+$ cation at the butanol-$d_9/[C_nmim][PF_6]$ interface *(44)*.

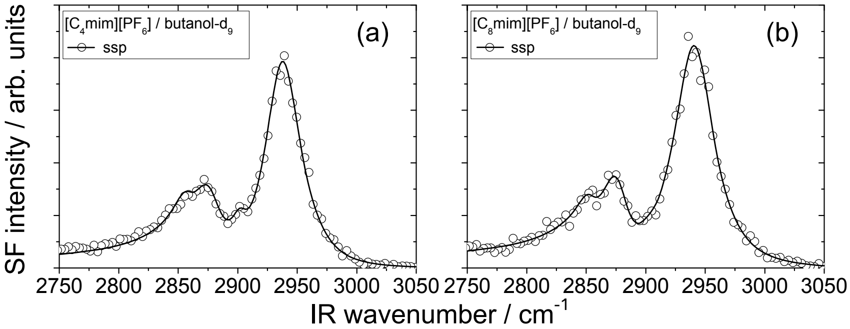

*Figure 6. SFG spectra of (a) the $[C_4mim][PF_6]$/butanol-$d_9$ and (b) the $[C_8mim][PF_6]$/butanol-$d_9$ interfaces taken in the CH stretching region with the ssp (circle) polarisation combinations. The solid lines represent fitting results.*

## Butanol Molecular Configuration

Figure 7 shows the SFG spectra of the air/butanol-$d_9$ and butanol-$d_9$/[$C_n$mim][$PF_6$] interfaces taken in the CD stretching region with ssp polarisation, noting that these spectra detect the vibrational modes of butanol-$d_9$, not the [$C_n$mim]$^+$ cation. The solid lines in the SFG spectra show the fitting results by using Equation (3). The peak at 2067 cm$^{-1}$, which in prominent in the spectrum of the air/butanol-$d_9$, is assigned to the $CD_3$ symmetric stretching mode ($r^+$) *(45−47)*. The peak at 2218 cm$^{-1}$, which is intense in the spectra of the butanol-$d_9$/[$C_n$mim][$PF_6$] interface, is attributed to the $CD_3$ asymmetric stretching mode ($r^-$) *(45−47)*.

Interestingly, there is only one distinct peak from the $r^-$ mode in the SFG spectra of the butanol-$d_9$/[$C_n$mim][$PF_6$] interfaces, while the same peak is almost negligible in the SFG spectrum of the air/butanol-$d_9$ interface. It seems that the amplitude of the $r^-$ mode peak is enhanced in the SFG spectra of the butanol-$d_9$/[$C_n$mim][$PF_6$] interfaces. So what is the origin of the enhancement of the $r^-$ mode peaks in the SFG spectrum? There is a previous report that observed such an enhancement of the $r^-$ mode *(48)*. In that study, the interfacial layer structure at the alcohol/silica interfaces have been investigated by SFG spectroscopy and the authors concluded that the enhancement of the $r^-$ mode peak was due to two oppositely oriented alcohol layers in which the two oppositely oriented methyl groups face each other with different orientational distributions for each species, as shown in Figure 7d (the $r^+$ mode peak should vanish if the orientational angles and distributions are identical). Accordingly, our result strongly suggests that the butanol molecules preferentially orient in such a way that their methyl groups face each other at the interface. The negligible peak intensity of the $r^+$ mode for the butanol-$d_9$/[$C_n$mim][$PF_6$] interfaces implies that the number density of molecules, orientational angle, and distribution are almost the same for the two species pointing toward the butanol and [$C_n$mim][$PF_6$] phases at the interface.

## Butanol/ionic liquid Interfacial Structure

Here we review the structural information for the butanol-$d_9$/[$C_n$mim][$PF_6$] interfaces obtained from the SFG results again. First, we found that the [$C_n$mim]$^+$ cation tends to orient its alkyl chain toward the butanol phase. Second, the butanol molecules tend to orient their methyl groups pointing toward each other at the interface. Third, the alkyl chains of the [$C_n$mim]$^+$ cation and the butanol molecule interact with each other, resulting in a quite inhomogeneous configuration at the interface. By putting all these structural conclusions at the butanol-$d_9$/[$C_n$mim][$PF_6$] interfaces together, we propose in Figure 8 a possible interfacial structure in which the alkyl chains of the butanol and [$C_n$mim][$PF_6$] converge to form the hydrophobic interfacial layer at the butanol-$d_9$/[$C_n$mim][$PF_6$] interface. The broad spectral peaks for both the [$C_n$mim]$^+$ cation and the butanol are likely due to the inhomogeneous hydrophobic interaction in the local layer. Such a formation of the local hydrophobic layer might allow the formation of a unique alcohol/ionic liquid interface composed of liquids with similar effective polarity.

Downloaded by CORNELL UNIV on June 28, 2012 | http://pubs.acs.org
Publication Date (Web): December 18, 2009 | doi: 10.1021/bk-2009-1030.ch021

Downloaded by CORNELL UNIV on June 28, 2012 | http://pubs.acs.org
Publication Date (Web): December 18, 2009 | doi: 10.1021/bk-2009-1030.ch021

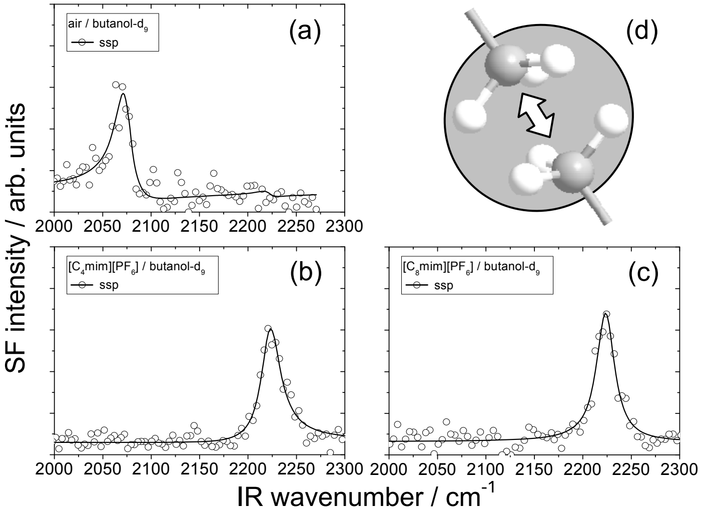

*Figure 7. SFG spectra of (a) the air/butanol-d$_9$, (b) the [C$_4$mim][PF$_6$]/butanol-d$_9$, and (c) the [C$_8$mim][PF$_6$]/butanol-d$_9$ interfaces taken in the CD stretching region with the ssp (circle) polarisation combinations. The solid lines represent the fitting results. (d) A schematic view of a unit of two oppositely oriented methyl groups.*

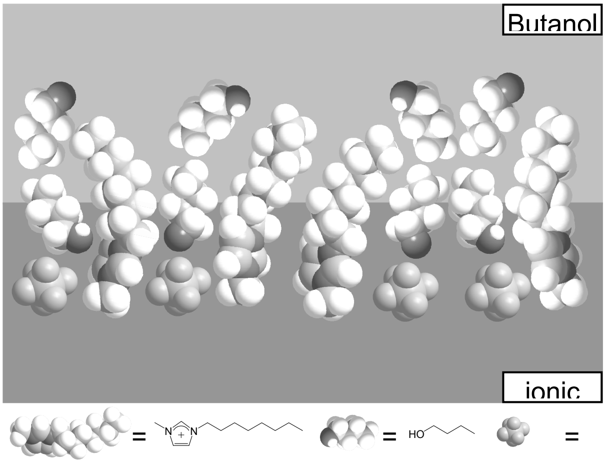

*Figure 8. Possible model structure for the alcohol/ionic liquid interface, with the butanol/[C$_8$mim][PF$_6$] system as a reference.*

## Conclusion

We have employed SFG vibrational spectroscopy to investigate the microscopic structure of ionic liquid/molecular liquid interfaces. Comparison of the SFG spectral features for the air/[$C_n$mim][$PF_6$] and $CCl_4$/[$C_n$mim][$PF_6$] interfaces reveals that the alkyl chain of the [$C_n$mim]$^+$ cation tends to point toward the $CCl_4$ phase. The SF signal from the [$C_n$mim]$^+$ cations is not observed from $D_2O$/[$C_n$mim][$PF_6$] interfaces, implying that the alkyl chain of the [$C_n$mim]$^+$ cation tends to point toward the [$C_n$mim][$PF_6$] phases, or is randomly oriented as predicted by a computational study. The SFG spectral peak widths are much broader for the butanol/[$C_n$mim][$PF_6$] interfaces relative to those for the air/liquid interfaces. It indicates the presence of an inhomogeneous intermolecular interaction among the alkyl chains of the [$C_n$mim]$^+$ cation and the butanol molecule. The enhancement of the $r^-$ mode peak is observed in the SFG spectra of the butanol taken with the ssp polarisation combination, and it could be due to the methyl groups of the butanol molecules facing each other at the butanol-$d_9$/[$C_n$mim][$PF_6$] interfaces, as in the case of the alcohol/$SiO_2$ interface. These observations strongly suggest the formation of a local hydrophobic layer, which consists of the alkyl chains of the butanol and [$C_n$mim]$^+$ cation at the butanol-$d_9$/[$C_n$mim][$PF_6$] interfaces. Such a local hydrophobic layer might allow the formation of a unique alcohol/ionic liquid interface.

Downloaded by CORNELL UNIV on June 28, 2012 | http://pubs.acs.org
Publication Date (Web): December 18, 2009 | doi: 10.1021/bk-2009-1030.ch021

## References

1. Chauvin, Y.; Mussmann, L.; Olivier, H. *Angew. Chem., Int. Ed. Engl.* **1996,** *34,* 2698−2700.
2. Blanchard, L. A.; Hancu, D.; Beckman, E. J.; Brennecke, J. F. *Nature,* **1999,** *399,* 28−29.
3. Visser, A. E.; Swatloski, R. P.; Reichert, W. M.; Mayton, R.; Sheff, S.; Wierzbicki, A.; Davis, J. H., Jr.; Rogers, R. D. *Environ. Sci. Technol.* **2002,** *36,* 2523−2529.
4. Cole-Hamilton, D. J. *Science* **2003,** *299,* 1702−1706.
5. Liu, F.; Abrams, M. B.; Baker, R. T.; Tumas, W. *Chem. Commun.* **2001,** 433−434.
6. Matsumoto, H.; Sakaebe, H.; Tatsumi, K. *J. Power Sources* **2005,** *146,* 45−50.
7. (a) Sakaebe, H.; Matsumoto, H. *Electrochem. Commun.* **2003,** *5,* 594−598. (b) Garcia, B.; Lavallée, S.; Perron, G.; Michot, C.; Armand, M. *Electrochim. Acta* **2004,** *49,* 4583−4588.
8. (a) Sato, T.; Masuda, G.; Takagi, K. *Electrochim. Acta* **2004,** *49,* 3603−3611. (b) de Souza, R. F.; Padilha, J. C.; Gonçalves, R. S.; Dupont, J. *Electrochem. Commun.* **2003,** *5,* 728−731.

9. (a) Wilson, M. A.; Pohorille, A. *J. Am. Chem, Soc.* **1996,** *118,* 6580−6587. (b) Rodgers. P. J.; Jing, P.; Kim, Y.; Amemiya, S. *J. Am. Chem, Soc.* **2008,** *130,* 7436−7442.
10. Carmichael, A. J.; Seddon, K. R. *J. Phys. Org. Chem.* **2000,** *13,* 591−595.
11. Fitchett, B. D.; Conboy, J. C. *J. Phys. Chem. B* **2004,** *108,* 20255−20262.
12. Romero, C.; Baldelli, S. *J. Phys. Chem. B* **2006,** *110,* 6213−6223.
13. Nanbu, N.; Sasaki, Y.; Kitamura, F. *Electrochem. Commun.* **2003,** *5,* 383−387.
14. Rivera-Rubero, S.; Baldelli, S. *J. Phys. Chem. B* **2004,** *108,* 15133−15140.
15. Aliaga, C.; Baldelli, S. *J. Phys. Chem. B* **2006,** *110,* 18481−18491.
16. Romero, C.; Moore, H. J. Lee, T. R.; Baldelli, S. *J. Phys. Chem. C* **2007,** *111,* 240−247.
17. Rollins, J. B.; Fitchett, B. D.; Conboy, J. C. *J. Phys. Chem. B* **2007,** *111,* 4990−4999.
18. Fitchett, B. D.; Rollins, J. B.; Conboy, J. C. *Langmuir,* **2005,** *21,* 12179−12186.
19. Kakiuchi, T.; Tsujioka, N.; Kurita, S.; Iwami, Y. *Electrochem. Commun.* **2003,** *5,* 159−164.
20. Kakiuchi, T.; Shigematsu, F.; Kasahara, T.; Nishi, N.; Yamamoto, M. *Phys. Chem. Chem. Phys.* **2004,** *6,* 4445−4449.
21. Kakiuchi, T.; Tsujioka, N. *J. Electroanal. Chem.* **2007,** *599,* 209−212.
22. Ishimatsu, R.; Shigematsu, F.; Hakuto, T.; Nishi, N.; Kakiuchi, T. *Langmuir,* **2007,** *23,* 925−929.
23. Lynden-Bell, R. M.; Kohanoff, J.; Del Popole, M. G. *Faraday Discuss.* **2005,** *129,* 57−67.
24. Chaumont, A.; Schurhammer, R.; Wipff, G. *J. Phys. Chem. B* **2005,** *109,* 18964−18973.
25. Sieffert, N.; Wipff, G. *J. Phys. Chem. B* **2006,** *110,* 13076−13085.
26. Sieffert, N.; Wipff, G. *J. Phys. Chem. B* **2006,** *110,* 19497−19506.
27. Sieffert, N.; Wipff, G. *J. Phys. Chem. B* **2007,** *111,* 4951−4962.
28. Shen, Y. R. *Surf. Sci.* **1994,** *299/300,* 551−562.
29. Knock, M. M.; Bell, G. R.; Hill, E. K.; Turner, H. J.; Bain, C. D. *J. Phys. Chem. B* **2003,** *107,* 10801−10814.
30. Walker, D. S.; Moore, F. G.; Richmond, G. L. *J. Phys. Chem. C* **2007,** *111,* 6103−6112.
31. Zhuang, X.; Miranda, P. B.; Kim, D.; Shen, Y. R. *Phys. Rev. B* **1999,** *59,* 12632−12640.
32. Iimori, T.; Iwahashi, T.; Kanai, K.; Seki, K.; Sung, J.; Kim, D.; Hamaguchi, H.; Ouchi, Y. *J. Phys. Chem. B* **2007,** *111,* 4860−4866.
33. Baldelli, S. *J. Phys. Chem. B* **2003,** *107,* 6148−6152.
34. Iimori, T.; Iwahashi, T.; Ishii, H.; Seki, K.; Ouchi, Y.; Ozawa, R.; Hamaguchi, H.; Kim, D, *Chem. Phys. Lett.* **2004,** *389,* 321−326.
35. Santos, C. S.; Rivera-Rubero, S.; Dibrov, S.; Baldelli, S. *J. Phys. Chem. C* **2007,** *111,* 7682−7691.
36. Aliaga, C.; Baldelli, S. *J. Phys. Chem. B* **2007,** *111,* 9733−9740.
37. Rivera-Rubero, S.; Baldelli, S. *J. Phys. Chem. B* **2006,** *110,* 4756−4765.
38. Iwahashi, T. et al. In preparation.
39. Venyaminov, S. Y.; Prendergast, F. G. *Anal. Biochem.* **1997,** *248,* 234−245.

Downloaded by CORNELL UNIV on June 28, 2012 | http://pubs.acs.org
Publication Date (Web): December 18, 2009 | doi: 10.1021/bk-2009-1030.ch021

40. Superfine, R.; Huang, J. Y.; Shen, Y. R. *Opt. Lett.* **1990,** *15,* 1276−1278.
41. Superfine, R.; Huang, J. Y.; Shen, Y. R. *Phys. Rev. Lett.* **1991,** *66,* 1066−1069.
42. Stanners, C. D.; Du, Q.; Chin, R. P.; Cremer, P.; Somorjai, G. A.; Shen, Y. R. *Chem. Phys. Lett.* **1995,** *232,* 407−413.
43. Sung, J.; Park, K.; Kim, D. *J. Phys. Chem. B.* **2005,** *109,* 18507−18514.
44. Herzberg, G. *Molecular Spectra and Molecular Structure II. Infrared and Raman Spectra of Polyatomic Molecules*; Academic Press: San Diego, 2001; Vol. 1.
45. Duncan, J. L.; Kelly, R. A.; Nivellini, G. D.; Tullini, F. *J. Mol. Spectrosc.* **1983,** *98,* 87−110.
46. Eng, J., Jr.; Raghavachari, K.; Struck, L. M.; Chabal, Y. J.; Bent, B. E.; Flynn, G. W.; Christman, S. B.; Chaban, E. E.; Williams, G. P.; Radermacher, K.; Mantl, S. *J. Chem. Phys.* **1997,** *106,* 9889−9898.
47. Haber, J. A.; Lewis, N. S. *J. Phys. Chem. B* **2002,** *106,* 3639−3656.
48. Liu, W.; Zhang, L.; Shen, Y. R. *Chem. Phys. Lett.* **2005,** *412,* 206−209.

Downloaded by CORNELL UNIV on June 28, 2012 | http://pubs.acs.org
Publication Date (Web): December 18, 2009 | doi: 10.1021/bk-2009-1030.ch021

Downloaded by UNIV OF DELAWARE MORRIS LIB on June 29, 2012 | http://pubs.acs.org
Publication Date (Web): December 18, 2009 | doi: 10.1021/bk-2009-1030.ch022

## Chapter 22

# Bulk and Interfacial Nanostructure in Protic Room Temperature Ionic Liquids

**Rob Atkin[1,*] and Gregory G. Warr[2]**

[1] School of Environmental and Life Sciences, The University of Newcastle, Callaghan, NSW 2308, Australia
[2] School of Chemistry, The University of Sydney, NSW, 2006, Australia

Until recently, protic ionic liquids were thought to be structurally homogenous. However, small angle neutron scattering experiments using selectively deuteriated ethylammonium nitrate ($[EtNH_3][NO_3]$) and propylammonium nitrate ($[PrNH_3][NO_3]$) conclusively show that these ionic liquids are nanostructured in the bulk. Electrostatic and solvophobic interactions within the liquid lead to the formation of alternating polar and apolar layers. In this chapter, these results are described in detail, and the relationship between bulk structure and interfacial structure, determined using atomic force microscopy, is elucidated.

## Introduction

Ionic liquids are currently attracting a great deal of research interest as solvents for a wide range of reactions and processes *(1,2)*. Much of this interest stems from the ability to predictably tune physical properties through the selection of appropriate cation and anion combinations. The cation structure, in particular, can be altered in a systematic fashion by varying the length or number of aliphatic chains covalently bound to a permanently charged group such an imidazolium or quaternary ammonium.

Ionic liquids may be broadly divided into two categories: protic and aprotic *(3)*. To date aprotic ionic liquids have received far greater attention but as new applications for protic ionic liquids are uncovered, this imbalance is beginning to be addressed *(3-7)*. Protic ionic liquids are formed when a proton is transferred from a Brønsted acid to a Brønsted base *(4)*, the method used to create the first reported ionic liquid of any type, ethanolammonium nitrate in 1888 *(8)*. A quarter of a century later, Walden reported the synthesis of ethylammonium nitrate *(9)*, which has become by far the most widely studied protic ionic liquid.

In the 1980s, Evans and co-workers demonstrated that many of the physical characteristics of $[EtNH_3][NO_3]$ were similar to water, most importantly the capacity to form a three-dimensional hydrogen-bond network, thought to be essentially for inducing solvophobic [The term solvophobic was first used by Ray to describe interactions akin to the hydrophobic effect in water, but in a non-aqueous solvent *(9)*.] interactions that drive amphiphilic self assembly *(10,11)*. The formation of small micelles was reported in $[EtNH_3][NO_3]$ a few years layer; the small size was attributed to relatively weak solvophobic interactions *(12,13)*. The formation and properties of lipid bilayer phases in $[EtNH_3][NO_3]$ were investigated around the same time, and many similarities with water-based structures were identified *(14)*. In 1991, hexagonal and cubic liquid crystal phases were first reported in $[EtNH_3][NO_3]$, again for cationic surfactants *(15)*.

In more recent studies, non-ionic surfactants in $[EtNH_3][NO_3]$ have been shown to: (i) have liquid crystalline phase behaviour similar to aqueous systems *(10)*; (ii) adsorb at the $[EtNH_3][NO_3]$-graphite interface in hemimicelle structures *(16)*; (iii) have micellar structure similar to aqueous systems by neutron scattering *(17)*; and (iv) form structured microemulsions when mixed with surfactant and oil *(18)*. It has also been demonstrated that many other protic ionic liquids support surfactant self-assembly *(3,19-22)*, recently reviewed in some detail *(5,6)*.

Despite these studies of surfactant aggregation in $[EtNH_3][NO_3]$, it was never suspected that the same solvophobic forces that drive surfactant self-assembly would induce structure within the ionic liquid itself. Most likely, researchers believed that the cation alkyl group, typically between $C_2$ and $C_4$, was too short to respond to the solvophobic effect (surfactant molecules typically have alkyl groups $C_8$ or longer). Nonetheless, small angle neutron scattering (SANS) experiments with selective deuteriation conclusively show that $[EtNH_3][NO_3]$ and $[PrNH_3][NO_3]$ possess nanoscale heterogeneity *(23)*. Atomic force microscopy (AFM) experiments reveal similar structure at the interface between these ionic liquids and solid surfaces *(24)*. In this chapter, the bulk and interfacial structures of $[EtNH_3][NO_3]$ and $[PrNH_3][NO_3]$ are reviewed in detail. We will also present data showing that disruption of the solvophobic interaction *via* the attachment of an alcohol moiety to the terminal carbon of the cation alkyl group decreases liquid nanostructure. Given the structural simplicity of these ionic liquids (*cf.* Table 1), these results are far reaching, and suggest many protic ionic liquids will exhibit such structural heterogeneity.

Downloaded by UNIV OF DELAWARE MORRIS LIB on June 29, 2012 | http://pubs.acs.org
Publication Date (Web): December 18, 2009 | doi: 10.1021/bk-2009-1030.ch022

**Table 1. Molecular structure, molecular weight (MW), density (*ρ*), ion pair diameter (*D*) and repeat spacing (D*) of the ionic liquids investigated.**

| *Ionic Liquid* | *Abbrev.* | *Structure* | *MW (g)* | *ρ* *(g.cm$^{-3}$)* | *D (nm)* | *D* (nm)* |
|---|---|---|---|---|---|---|
| Ethylammonium Nitrate | $[EtNH_3][NO_3]$ | 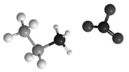 | 108 | 1.21 | 0.53 | 0.97 |
| Propylammonium Nitrate | $[PrNH_3][NO_3]$ | 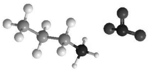 | 122 | 1.16 | 0.56 | 1.16 |
| Ethanolammonium Nitrate | $[HO(CH_2)_2NH_3][NO_3]$ | 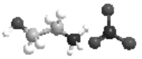 | 124 | 1.26 | 0.54 | - |
| Methylammonium Nitrate | $[MeNH_3][NO_3]$ | 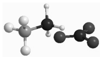 | 94 | 1.26 | 0.50 | 1.04 |

*D* is determined from (*ρ*) assuming a cubic packing geometry according to the method of by Horn *et. al. (26)*

## Preparation of Ionic Liquids

$[EtNH_3][NO_3]$ (m.p. 14 °C), $[PrNH_3][NO_3]$ (m.p. 3.5 °C) and ethanolammonium nitrate, $[HO(CH_2)_2NH_3][NO_3]$, used in AFM experiments were prepared by reacting equimolar amounts of the amine and conc. nitric acid to produce an aqueous solution *(12,25)*. Excess water was removed by rotary evaporation followed by purging the concentrated ionic liquid solutions with nitrogen, then heating at 110–120°C for several hours under a nitrogen atmosphere. This leads to water contents undetectable by Karl Fischer titration (<0.01 %) and prevents the formation of nitrous oxide impurities. The partially deuteriated $[PrNH_3][NO_3]$ ($d_n$-$[PrNH_3][NO_3]$) and $[EtNH_3][NO_3]$ ($d_n$-$[EtNH_3][NO_3]$) used in SANS experiments were prepared by performing the above reaction in $D_2O$ rather than water. NMR revealed that, on average, 2.5 of the three exchangeable amino hydrogens were replaced with deuterium. This generates a scattering contrast between the hydrogenous alkyl groups of the ammonium ion and the $ND_3^+$ and $NO_3^-$ polar groups that allows the detection of structural aggregation within the liquid.

Downloaded by UNIV OF DELAWARE MORRIS LIB on June 29, 2012 | http://pubs.acs.org
Publication Date (Web): December 18, 2009 | doi: 10.1021/bk-2009-1030.ch022

In Ionic Liquids: From Knowledge to Application; Plechkova, N., et al.;
ACS Symposium Series; American Chemical Society: Washington, DC, 2010.

Downloaded by UNIV OF DELAWARE MORRIS LIB on June 29, 2012 | http://pubs.acs.org
Publication Date (Web): December 18, 2009 | doi: 10.1021/bk-2009-1030.ch022

# Small Angle Neutron Scattering (SANS)

## Experiments

SANS measurements were performed on freshly prepared samples using the LOQ spectrometer on the ISIS pulsed neutron source at the Rutherford Appleton Laboratory, UK. The measurements determine the absolute scattering probability $I(q)$ (cm$^{-1}$) as a function of a momentum transfer $q = (4\pi/\lambda)\sin(\theta/2)$, where $\lambda$ is the incident neutron wavelength ($2.2 < \lambda < 10$ Å) and $\theta$ the scattering angle. SANS data were collected using both the main detector bank and the high-angle detector bank, thus covering a $q$ range from 0.008 to 1.4 Å$^{-1}$. Only the data from the high-angle detector bank are presented as the features of interest occur in this region. For further experimental details the reader is directed to our recent article *(23)*.

## SANS Results

SANS spectra at 45°C for pure $d_n$-[PrNH$_3$][NO$_3$] and $d_n$-[EtNH$_3$][NO$_3$] are presented in Figure 1. The striking feature is the peak at $q = 0.66$ Å$^{-1}$ for $d_n$-[EtNH$_3$][NO$_3$] and at $q = 0.54$ Å$^{-1}$ for $d_n$-[PrNH$_3$][NO$_3$], corresponding to Bragg spacings ($D^* = 2\pi/q_{\max}$) of 9.7 Å and 11.6 Å respectively. This result provides the first experimental evidence of nanoscale heterogeneity for ILs of any type with alkyl chains less than C$_4$. No similar structure peak could be detected in hydrogenous [EtNH$_3$][NO$_3$] and [PrNH$_3$][NO$_3$]. The calculated Bragg spacings are approximately twice the ion pair dimension of these ionic liquids (Table 1) which suggests that the ionic liquid is structured on the length scale of the ions, with the (hydrogenous) alkyl groups associated together and segregated from the H-bonded ionic moieties –ND$_3^+$ and NO$_3^-$.

Downloaded by UNIV OF DELAWARE MORRIS LIB on June 29, 2012 | http://pubs.acs.org
Publication Date (Web): December 18, 2009 | doi: 10.1021/bk-2009-1030.ch022

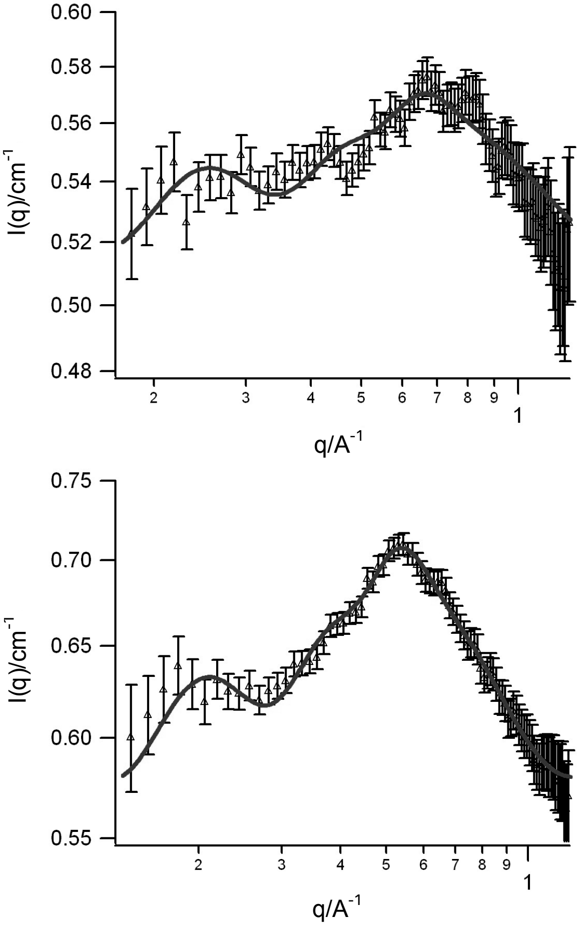

***Figure 1**. SANS spectra for pure* d$_n$*-[EtNH$_3$][NO$_3$] (top) and* d$_n$*-[PrNH$_3$][NO$_3$] (bottom) at 45°C on absolute scale.*

## SANS Interpretation and Data Fitting

Three factors could lead to nanosegregation in [PrNH$_3$][NO$_3$] and [EtNH$_3$][NO$_3$]. Electrostatic attractions between the ammonium cation and nitrate anion will favour the creation of ionic domains *(27)*, that may be enhanced by hydrogen bonding *(12,20)*. This will result in a solvophobic effect which promotes association of alkyl groups into non-polar domains. The substantially more pronounced structure peak for $d_n$-[PrNH$_3$][NO$_3$] than $d_n$-[EtNH$_3$][NO$_3$] is consistent with greater segregation and a stronger solvophobic effect.

Various geometries might be expected for this structure, reminiscent of amphiphilic self-assembly. Based on the volume ratio of the ionic and alkyl components near unity *(23)*, a locally lamellar structure is most probable. Indeed the data cannot be fit to spherical aggregates of either hydrogenous alkyl or charged groups using known scattering length densities and volume fractions. The data are better described by alternating polar–apolar layers, however the fact that these ionic liquids are not optically birefringent suggests that this layering is quite disordered. The solid lines show fits to a local smectic order using the model developed by Nallet *et al.* *(28)*, combining form and structure factor contributions to the scattering from stacks of flexible layers, including powder averaging. The broad scattering peak implies that correlations persist only over a small number of flexible layers, $N \sim 5$.

Such layering is also consistent with the known crystal structure of solid methylammonium nitrate *(29)*, which forms an intercalated bilayer of non-H-bonded methyl groups with H-bonded ammonium and nitrate ions. The unit cell dimension of 10.4Å along this axis is broadly consistent with the peak position for liquid $d_n$-[EtNH$_3$][NO$_3$] and $d_n$-[PrNH$_3$][NO$_3$].

## Mass Spectrometry Experiments

Kennedy and Drummond have recently found unusually large ion clusters in a variety of protic ionic liquids using electrospray ionisation mass spectrometry *(30)*. In the positive ion spectrum, the $C_8A_7^+$ cation (C = cation, A = Anion) was in by far the greatest abundance for both pure [EtNH$_3$][NO$_3$] and [PrNH$_3$][NO$_3$]. However, in negative ion mode, aggregates up to $A_{11}C_{10}^-$ were present in equal amounts. The authors inferred that pure [EtNH$_3$][NO$_3$] and [PrNH$_3$][NO$_3$] are composed of a polydisperse mixture of aggregated ions, with the exception of the $C_8A_7^+$ cation, which forms to an unusually high degree. While these results and the SANS data are consistent with some form of ionic liquid nanostructure, rationalizing the abundant $C_8A_7^+$ cation with the smectic model used to fit the SANS spectra is problematic. It is difficult to envisage the $C_8A_7^+$ cation forming anything other than a spherical or oblate spheroid aggregate, which is at odds with the SANS results. We will conduct neutron diffraction experiments in the near future which should help to resolve this disparity.

## Interfacial Structure

The same intermolecular forces that drive amphiphilic self-organization in bulk ionic liquids should also be evident at macroscopic interfaces. An improved understanding of the interfacial and near surface structure of ionic liquids is necessary for optimization of numerous, diverse applications including lubrication, electrodeposition *(31)*, mineral processing, and in dye-sensitised solar cells *(32,33)* as the mobility of confined ions plays a key role in determining electrical current *(34)*.

Adjacent to a smooth solid surface, many molecular liquids arrange into discrete layers *(35)*. This ordering leads to variation in the molecular density profile such that the measured force normal to the interface oscillates with a

Downloaded by UNIV OF DELAWARE MORRIS LIB on June 29, 2012 | http://pubs.acs.org
Publication Date (Web): December 18, 2009 | doi: 10.1021/bk-2009-1030.ch022

period approximately equal to the size of the molecule with an amplitude that decreases with increasing separation *(36,37)*. These forces are referred to as 'oscilliatory forces' or 'solvation forces', and are also exhibited by ionic liquids *(24, 26)*. Unlike molecular liquids, many such solvation layers are readily detected with a standard atomic force microscope (AFM). The ease with which such layering is observed suggests that the surface does not induce order, but merely orients and aligns the existing bulk structure.

## Oscillatory Forces

Oscillatory forces due to molecular layering in a liquid were first demonstrated between mica surfaces by Horn and Israelachvili *(26)*, for octamethylcyclotetrasiloxane (OMCTS) using the surface force apparatus (SFA). Subsequent experiments with other liquids revealed that the number of oscillations decreased with increasing molecular flexibility, as flexible molecules can pack (space fill) effectively without layering *(38)*. Surface roughness was also shown to disrupt layering in the liquid and the oscillatory forces are replaced by a purely monotonic force *(35)*.

The invention of the AFM allowed near surface molecular ordering to be studied on a wider variety of substrates. However, the contact area between the surface and the AFM tip is approximately $10^6$ times smaller and less well defined than for SFA, producing reduced signal to noise ratios, and in AFM the absolute separation between the tip and the substrate is not known. To compensate, AFM experiments have often been conducted in frequency modulation or tapping mode, which allows the deflection and tip-sample interaction stiffness to be monitored simultaneously *(39-45)*. However, the inherent nanostructure of $[EtNH_3][NO_3]$ and $[PrNH_3][NO_3]$ means that solvation layers are particularly well formed, and detectable using a standard AFM *(24)*.

## Surface Forces Apparatus Study of the EAN – Mica Interface

In 1988 Horn and co-workers used SFA to measure four to five oscillations for $[EtNH_3][NO_3]$ before the repulsion became so strong that it prevented closer approach *(26)*. On the basis of the absolute separations, the authors suggested that 8 or 9 surface layers were probably present, and that the similarity between the results obtained in $[EtNH_3][NO_3]$ and non-polar liquids suggested that neither ionic nature of $[EtNH_3][NO_3]$ or its ability to form a hydrogen bonding network significantly affected the force profile. The measured oscillation period of 0.5 – 0.6 nm agrees well with the dimensions of the $[EtNH_3][NO_3]$ molecule determined from the density, *c.f.* Table 1. This suggests that the cation and anion are present in approximately equal numbers in the layers.

Downloaded by UNIV OF DELAWARE MORRIS LIB on June 29, 2012 | http://pubs.acs.org
Publication Date (Web): December 18, 2009 | doi: 10.1021/bk-2009-1030.ch022

# Experiments

Force curves were collected using a Digital Instruments NanoScope IIIa Multimode AFM in contact mode. Scan sizes between 10 and 30 nm and a scan rate of 0.1 Hz was used in all experiments presented here. Cantilevers were standard $Si_3N_4$ with sharpened tips (Digital Instruments, CA).

Graphite (monochromators grade ZYH from Advanced Ceramics, OH.) and mica (Brown Co., Sydney) were prepared by using adhesive tape to cleave along the basal plane. Silicon wafers were baked at 1000 °C for 100 minutes in an oxygen atmosphere to produce an oxide layer ($SiO_2$). Hydroxylated silica was prepared by soaking pyrogenic silica in water for 48 hours, followed by treatment with 10wt% NaOH for 30 s, rinsing in water and then ethanol before drying under a nitrogen stream.

For further experimental details the reader is directed to our 2007 paper *(24)*.

# AFM Results and Analysis

## *EAN-Mica*

Force *versus* separation data for the EAN - mica system is shown in Figure 2 (top). A series of 'push-throughs' at discrete separations due to the AFM tip rupturing successive layers produces steps in the force profile. This data is different in form to the wave-like results obtained previously using SFA *(26)* due to differences in the experimental methods employed for SFA *(37)* and AFM *(46)*. However, the period of the near surface oscillations suggested by both studies is 0.5 nm, in good agreement with the diameter of EAN determined from the bulk density (Table 1). 0.5 nm is, as expected, half of the repeat spacing determined for the bulk liquid *(23)*. Steps due to the first six solvent layers at separations up to 3nm are clearly visible. Further steps at 3.5 and 4 nm are routinely observed, consistent with oscillations measured using the SFA *(26)*, but these are less distinct in individual runs due to the level of background noise. The magnitude of the force required to rupture each layer increases as the tip moves closer to the surface. This suggests that ordering into layers decays further from the substrate as the structure approaches that of bulk $[EtNH_3][NO_3]$.

The autophobic behaviour of $[EtNH_3][NO_3]$ on mica suggests that $EA^+$ ions are adsorbed onto the substrate with the ammonium groups associated with a surface charged site and the ethyl moiety facing the bulk liquid. This should give rise to a thinner layer, so it is surprising that the thickness of the step closest to the substrate is the same as all the other steps, 0.5 nm. Data presented below for silica shows that the most likely explanation is a layer of strongly adsorbed $EA^+$ ions electrostatically bound to the mica that cannot be displaced by the AFM tip. As $EA^+$ occupies an area greater than the that of the charged site on mica (one site per 0.48 $nm^2$),[47] the degree of surface charge neutralised cannot exceed 87%.[26] Thus, even at saturation coverage, there is always more

Downloaded by UNIV OF DELAWARE MORRIS LIB on June 29, 2012 | http://pubs.acs.org
Publication Date (Web): December 18, 2009 | doi: 10.1021/bk-2009-1030.ch022

than one surface charge site for each $EA^+$ ion. This could account for the strength of the adsorption of the first layer.

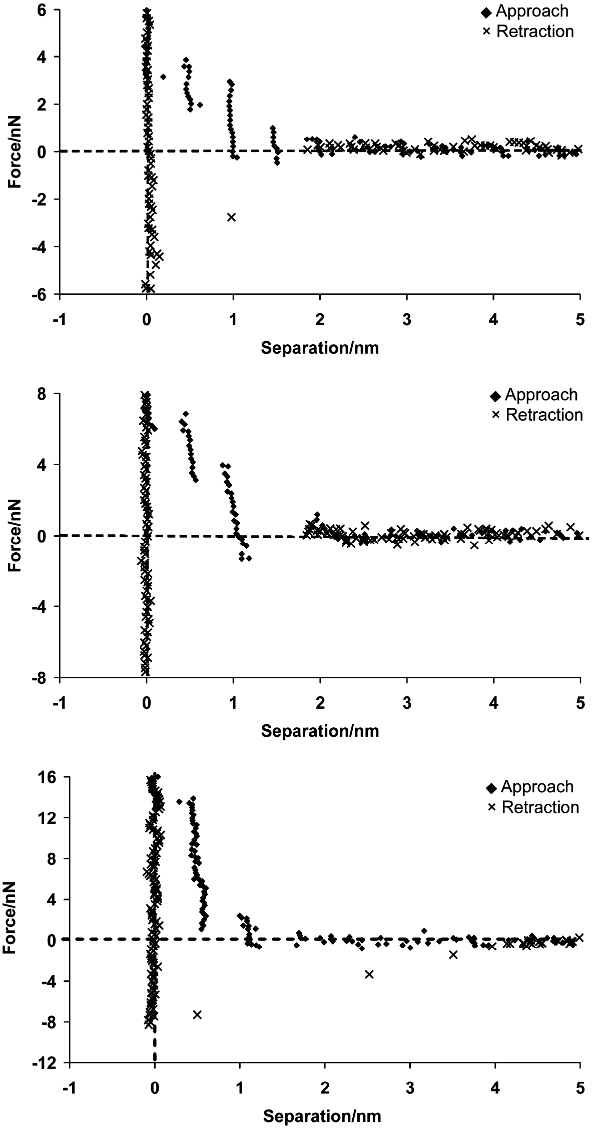

*Figure 2. Force versus distance profile between an AFM tip and a mica surface in $[EtNH_3][NO_3]$ (top), $[PrNH_3][NO_3]$ (middle), and $[HO(CH_2)_2NH_3][NO_3]$ (bottom).*

Downloaded by UNIV OF DELAWARE MORRIS LIB on June 29, 2012 | http://pubs.acs.org
Publication Date (Web): December 18, 2009 | doi: 10.1021/bk-2009-1030.ch022

Horn *et al.* *(26)* raised the possibility of alternating sublayers of positive and negative ions within solvation layers, and molecular modelling of molten KCl suggests that ionic sublayers form at high surface charge density, of the order of 32 μC cm$^{-2}$.[48] As the surface charge of fully ionised mica is comparable with this value, and SANS experiments suggests precisely this type of structure in bulk [EtNH$_3$][NO$_3$] *(23)*, it seems highly likely that alternating sublayers are present at the mica interface.

While there is no evidence of significant attraction between the tip and the substrate, there is a substantial adhesion (6 nN) as the tip is retracted. This is a consequence of attractions between EA$^+$ adsorbed layers on the tip and on mica. Zero force is reached at a separation of 2 nm, which corresponds to four solvent layers.

Downloaded by UNIV OF DELAWARE MORRIS LIB on June 29, 2012 | http://pubs.acs.org
Publication Date (Web): December 18, 2009 | doi: 10.1021/bk-2009-1030.ch022

### *[PrNH$_3$][NO$_3$]-Mica*

Increasing the size of the hydrocarbon moiety of the ionic liquid from C$_2$ in [EtNH$_3$][NO$_3$] to C$_3$ for [PrNH$_3$][NO$_3$] only slightly increases the molecular volume (Table 1) but does significantly alter the solvation layer data, *c.f.* Figure 2 (middle). Most notably, the steps are not vertical in [PrNH$_3$][NO$_3$] suggesting increased compressibility of the layers. Steps due to solvent layers are present at separations of 0.5, 1 nm and 2 nm consistent with the bulk [PrNH$_3$][NO$_3$] repeat spacing. It should be noted that the innermost layer at 0.5 nm was not always observed. Combined with the fact that the expected third step at 1.5 nm was never observed, this suggests that [PrNH$_3$][NO$_3$] also adopts a morphology where strongly and weakly formed molecular layers alternate, consistent with alternating sub – layers of propylammonium and nitrate as suggested by the model used to fit the SANS data. It is likely that the increased compressibility of [PrNH$_3$][NO$_3$] smears the sharpness of the features in the force profile. As the measured force beyond 2 nm is zero, the number of AFM detectable near surface layers is reduced to 4 in [PrNH$_3$][NO$_3$] compared to 6 or 7 in [EtNH$_3$][NO$_3$], even though the SANS experiments on the liquids show that bulk [PrNH$_3$][NO$_3$] is more highly ordered. Previous SFA experiments comparing the behaviour of cyclohexane and *n*-octane concluded that the more flexible n-octane molecules were able to pack more efficiently, resulting in fewer solvation layers *(49)*. The increased length of the alkyl length group of [PrNH$_3$][NO$_3$] compared to [EtNH$_3$][NO$_3$] produces a similar effect upon confinement. The adhesion observed on retraction is increased for [PrNH$_3$][NO$_3$] compared to [EtNH$_3$][NO$_3$], due to stronger interactions between [PrNH$_3$]$^+$ ions associated with mica and on the tip.

### *EtOAN – Mica*

Data for the approach and retraction of an AFM tip to mica in the presence of [HO(CH$_2$)$_2$NH$_3$][NO$_3$] is presented in Figure 2 (bottom). The retraction result is essentially the same as that obtained for [EtNH$_3$][NO$_3$], but the form of the approach is markedly different. While the data for the interfacial layer is similar to that obtained for $[EtNH_3][NO_3]$, there are a reduced number of subsequent steps, and the steps that are present are much more compressible *(50)*. This indicates that $[HO(CH_2)_2NH_3][NO_3]$ is much less ordered near the surface than $[EtNH_3][NO_3]$ and $[PrNH_3][NO_3]$, due to the alcohol moiety disrupting the solvophobic interactions between cation alkyl groups that produce nanostructure. Given the relationship between bulk and interfacial structure described above, it may reasonably be predicted that bulk $[HO(CH_2)_2NH_3][NO_3]$ is also less structured; recent electrospray ionisation mass spectrometry data is consistent with this suggestion *(30)*. The precise effect of the addition of the alcohol group on the arrangement of the ions in bulk will be elucidated by our forthcoming neutron diffraction experiments.

Downloaded by UNIV OF DELAWARE MORRIS LIB on June 29, 2012 | http://pubs.acs.org
Publication Date (Web): December 18, 2009 | doi: 10.1021/bk-2009-1030.ch022

## *EAN-Silica*

For the purposes of this work the primary differences between the silica and mica substrates are the lower surface charge density and greater roughness of silica. As the surface charge density of amorphous silica is due to hydrolysis of surface hydroxyl groups, which is determined by the relative population of charged species at the surface, the charge density of silica is expected to be significantly higher in ionic liquids than in water (typically one site per 20 nm$^2$ at neutral pH[51]), but still less than mica (one site per 0.48 nm$^2$),[47] The rms roughness of the silica used in this study was found to be by AFM imaging to be 1.3 nm for a 5 x 5 μm region and 0.2 nm for a 300 x 300 nm region, which is sufficient to broaden otherwise distinct solvation layers *(35)*. Roughness greater than the molecular size can eliminate solvation layers completely *(52)*.

Figure 3 (top) shows a typical force profile for the $[EtNH_3][NO_3]$ – silica system. The increased roughness of the silica substrate smears the repulsive peaks considerably, but clear steps in the data are still present. The fact that steps are observed at all may be due to the fact that bulk $[EtNH_3][NO_3]$ is nanostructured, and the small interaction area between the substrate and the AFM tip, which has a radius of ~20 nm. On this scale, the rms roughness is only 0.05 nm.

On approach, a repulsion begins at 2.7 nm. Clear steps in the data emerge at smaller separations, with a period approximately equal to the diameter of $[EtNH_3][NO_3]$, at 1.8, 1.3, 0.8 and 0.25 nm, as the repulsive force increases to 10 nN. The steps are not vertical like those on mica due to surface roughness.

Of critical importance is the fact that the layer nearest the surface has a thickness of only 0.25 nm. This suggests that this layer is comprised primarily of $[EtNH_3]^+$ ions with the ammonium group next to a surface charged site like that predicted (but never observed) for mica. That is, electrostatic attractions between the ammonium and the substrate results in a surface layer rich in the cation, as suggested by theory *(34)* and experiment *(53)*. The lower surface charge density of silica allows this layer to be displaced by the AFM tip at sufficiently high force, coming into direct contact with the substrate. On retraction, there is negligible adhesion of the AFM tip to the surface due to the reduced level of electrostatic adsorption of $[EtNH_3]^+$ to silica compared to mica. As a result, the force profile for the retraction is quite similar to that recorded for the approach.

## *PAN - Silica*

The force curve for the $[PrNH_3][NO_3]$ – silica system presented in Figure 3 (bottom) is quite similar to that for $[EtNH_3][NO_3]$. Jumps in the force curve from 1.65 to 1.1 nm and from 1.1 to 0.4 nm accompany an increase in the measured repulsive force. The separation then remains almost constant until the repulsive force reaches 6 nN, at which point the AFM moves into contact with the substrate. As for $[EtNH_3][NO_3]$, the layer next to the substrate is thinner than those further out, which suggests a layer of electrostatically adsorbed $[PrNH_3]^+$ next to the surface. The $[PrNH_3]^+$ layer can be penetrated using the AFM on

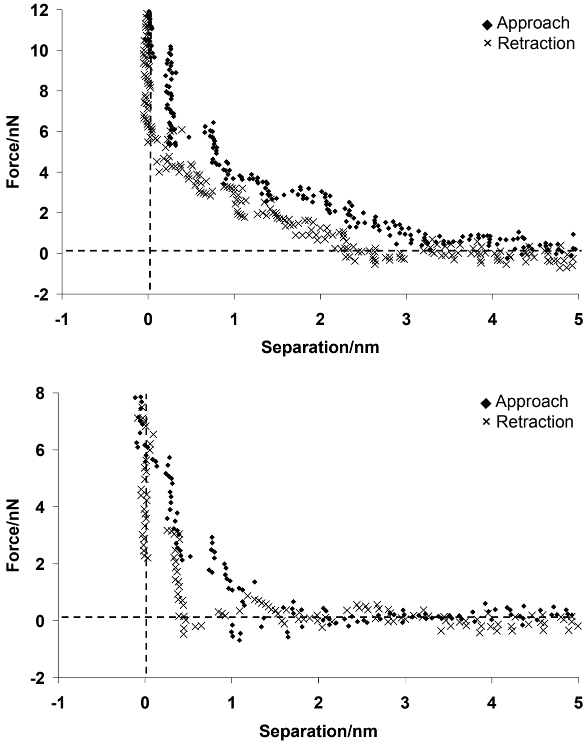

*Figure 3. Force versus distance profile between an AFM tip and a silica surface in $[EtNH_3][NO_3]$ (top) and $[PrNH_3][NO_3]$ (bottom).*

Downloaded by UNIV OF DELAWARE MORRIS LIB on June 29, 2012 | http://pubs.acs.org
Publication Date (Web): December 18, 2009 | doi: 10.1021/bk-2009-1030.ch022

silica due to the substrates low surface charge, but not on mica where the $[PrNH_3]^+$ layer is more strongly bound.

It is worth noting that the surface charge on $Si_3N_4$ AFM tips is lower than on pure silica, so electrostatic interactions between cations and the tip will be small. The roughness of the AFM tip *(54)* will also decrease the extent of layering, so the measured solvation surfaces are primarily due to interactions between the ionic liquid and the substrate.

## *$[EtNH_3][NO_3]$ – Graphite*

The force profile for $[EtNH_3][NO_3]$ on graphite (Figure 4 (top)) has very different form to that on mica and silica. On approach, the tip experiences an attraction towards the substrate, causing jumps from a separation of 1.7 nm to 1.1 nm to 0.4 nm while the force decreases from zero to -1.5 nN to -3 nN. [The jump distance ($D_j$) can be used to estimate the Hamaker constant (A) for this system using $D_j=(AR/3k)^{1/3}$, where k is the spring constant and R is the tip radius *(55)*. Using measured values for R (20 nm) and k (0.07 N $m^{-1}$), A = 2 x $10^{-20}$ J is found. This value is higher than for other liquids, but increasing R to 40 nm gives A with the expected order of magnitude. This increase in R is reasonable given the change in tip geometry due to wear that occurs over the course of an AFM experiment *(54)*.] This small jump in distance is consistent with an attraction between the tip and the substrate due to dispersion forces. A 0.4 nm separation is maintained as the force is increased from -3 nN to -2 nN, at which time the tip penetrates the layer and moves into contact with the substrate (no additional layer could be detected up to an applied force of 400 nN). Two adhesions are detected on retraction. The first is between the tip and the substrate to a force of -7 nN. The second is between the tip and the adsorbed $[EtNH_3]^+$ layer at a separation of 0.35 nm with a maximum adhesive force equal to -7.5 nN. The tip then jumps out of contact with the substrate, reaching zero force at a separation of 2.4 nm. Interactions between the ethyl group and graphite may produce a slight interfacial excess of this ion, similar to that observed for the squalene-OCMTS-graphite system *(53)*.

## *$[PrNH_3][NO_3]$ - Graphite*

The force curve for $[PrNH_3][NO_3]$ on graphite is presented in Figure 4 (bottom). A small repulsion occurs between 1.9 and 1.2 nm, followed by a jump from 1.2 to 0.75 nm on approach. Here there is a second, much steeper

Downloaded by UNIV OF DELAWARE MORRIS LIB on June 29, 2012 | http://pubs.acs.org
Publication Date (Web): December 18, 2009 | doi: 10.1021/bk-2009-1030.ch022

Downloaded by UNIV OF DELAWARE MORRIS LIB on June 29, 2012 | http://pubs.acs.org
Publication Date (Web): December 18, 2009 | doi: 10.1021/bk-2009-1030.ch022

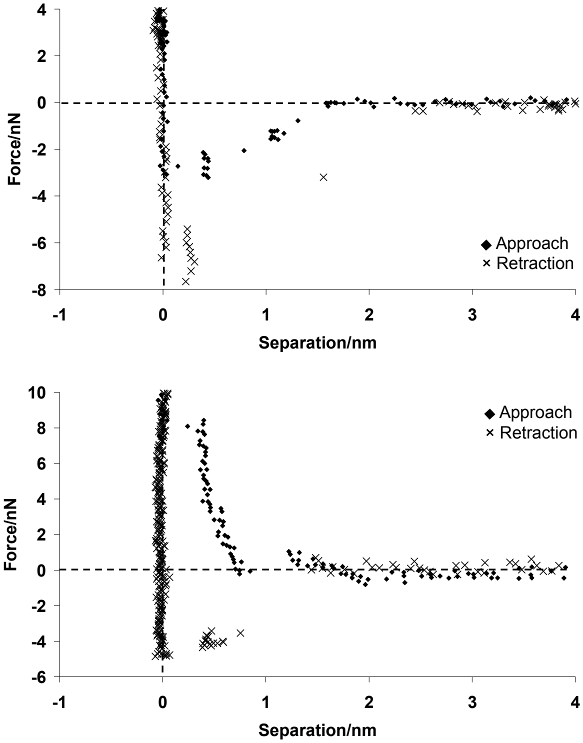

*Figure 4. Force versus distance profile between an AFM tip and a graphite surface in [$EtNH_3$][$NO_3$] (top) and [$PrNH_3$][$NO_3$] (bottom).*

repulsion, with the force increasing from zero to 8 nN as the separation decreases from 0.75 to 0.35 nm. The tip then pushes through the intervening layer into contact with the substrate.

The greater force required to rupture the interfacial layer for [$PrNH_3$][$NO_3$] compared to [$EtNH_3$][$NO_3$] is a consequence of the increased size of the hydrocarbon moiety of the propylammonium ion, which interacts more strongly with the substrate. This increased attraction is consistent with the higher intensity of the scattering peak for bulk [$PrNH_3$][$NO_3$]. Note that the final push through distance is somewhat lower than expected, which may due to [$PrNH_3$]$^+$ in the interfacial layer being, on average, orientated flat along the substrate, although greater layer compressibility may also contribute. On retraction a -4.5 nN adhesive force is measured, after which the tip jumps first to a separation of 0.4 nm at approximately the same force, then to 1.5 nm at zero force.

## General Comments

The SANS data for selectively $d_n$-[$EtNH_3$][$NO_3$] and $d_n$-[$PrNH_3$][$NO_3$] provides unequivocal evidence of structure in the bulk pure ionic liquids, and the peak position indicates a repeat spacing of twice the calculated molecular dimension of the ion pair. Models based on spherical morphologies and various structure factors are unable to fit the data, but excellent fits are obtained with a smectic model correlated over a small number of interfaces. This suggests a locally lamellar structure, consistent with the essentially equal volumes of the polar and apolar portions of the ionic liquid cation. Liquid nanostructure results from electrostatic and hydrogen bonding interactions between charged groups leading to the formation of ionic domains which repel the alkyl cation chains, creating a solvophobic effect that that induces aggregation. The overall picture for the bulk liquid, therefore, consists of alternating electrostatic and apolar regions on the length scale of the ions. Bulk $[PrNH_3][NO_3]$ is more structured than $[EtNH_3][NO_3]$ due to stronger solvophobic interactions on account of its longer alkyl group.

In molecular liquids an atomically smooth surface induces solvent layering. For these ionic liquids a different situation pertains in that the surface acts to align the pre-existing bulk solution structure. This leads to solvation layers that are particularly well formed, and may readily be detected using a standard AFM. However, surface effects still play an important role: on the basis of bulk structure one would predict more and clearer solvation layers for $[PrNH_3][NO_3]$ than $[EtNH_3][NO_3]$, but in fact the opposite occurs. Upon confinement, longer alkyl chain of $[PrNH_3][NO_3]$ imparts greater flexibility, disrupting layer formation as in traditional solvents. The layer thicknesses measured using AFM near solid surfaces are consistent with both the calculated molecular dimension and the SANS repeat spacing for the bulk liquids.

The results obtained for the $[EtNH_3][NO_3]$-mica system suggests that solvation layers in this system are well formed. The high surface charge of mica produces a strong interaction between surface and the interfacial layer and, combined with the inherent bulk structure, produces nitrate and ethylammonium sub-layers. The lower surface charge and increased roughness of silica decreases the number of detectable solvent layers. Graphite is also atomically smooth, but an attraction between the substrate and AFM tip occurs. Only two or three solvation layers are detected against an attractive background.

For all substrates, the steps in the force curves are less vertical for $[PrNH_3][NO_3]$ than $[EtNH_3][NO_3]$, showing that $[PrNH_3][NO_3]$ layers are more flexible. This is most likely due to the increased size of the alkyl group, which allows the hydrocarbon sublayers to become interdigitated. The larger alkyl group also increases attraction to graphite for $[PrNH_3][NO_3]$ compared to $[EtNH_3][NO_3]$, where the force required to rupture the interfacial solvent layer is greatly increased.

## Acknowledgments

This work was supported by an Australian Research Council (ARC) Discovery Project and the Access to Major Research Facilities program. RA wishes to acknowledge the ARC for the award of an Australian Postdoctoral Fellowship and the University of Newcastle for a Research Fellowship. We also acknowledge CCLRC for allocation of beam time at ISIS and Dr Richard Heenan for his assistance with LOQ.

Downloaded by UNIV OF DELAWARE MORRIS LIB on June 29, 2012 | http://pubs.acs.org
Publication Date (Web): December 18, 2009 | doi: 10.1021/bk-2009-1030.ch022

## References

1. Seddon, K. R.; Stark, A.; Torres, M. J., *Pure Appl. Chem.* **2000,** 72, 2275-2287.
2. Welton, T., *Chem. Rev.* **1999,** 99, 2071–2084.
3. Greaves, T. L.; Weerawardena, A.; Fong, C.; Krodkiewska, I.; Drummond, C. J., *J. Phys. Chem. B* **2006,** 110, (45), 22479-22487.
4. Belieres, J. P.; Angell, C. A., *J. Phys. Chem. B* **2007,** 111, (18), 4926-4937.
5. Greaves, T. L.; Drummond, C. J., *Chemical Society Reviews* **2008,** 37, (8), 1709-1726.
6. Greaves, T. L.; Drummond, C. J., *Chem. Rev.* **2008,** 108, (1), 206-237.
7. Byrne, N.; Wang, L.-M.; Belieres, J.-P.; Angell, C. A., *Chem. Commun.* **2007**, (26), 2714-2716.
8. Gabriel, S., *Berichte* **1888,** 21, 2664-2669.
9. Walden, P., *Bull. Acad. Imp. Sci.* **1914**, 1800.
10. Araos, M. U.; Warr, G. G., *J. Phys. Chem. B* **2005,** 109, (30), 14275-14277.
11. Evans, D. F., *Langmuir* **1988,** 4, (1), 3-12.
12. Evans, D. F.; Yamauchi, A.; Roman, R.; Casassa, E. Z., *J. Colloid Interface Sci.* **1982,** 88, 89-96.
13. Evans, D. F.; Yamauchi, A.; Wei, G. J.; Bloomfield, V. A., *J. Phys. Chem.* **1983,** 87, 3537-3542.
14. Evans, D. F.; Kaler, E. W.; Benton, W. J., *J. Phys. Chem.* **1983,** 87, (4), 533-535.
15. Bleasdale, T. A.; Tiddy, G. J. T.; Wyn-Jones, E., *J. Phys. Chem.* **1991,** 95, (14), 5385-5386.
16. Atkin, R.; Warr, G. G., *J. Am. Chem. Soc.* **2005,** 34, 11940-41.
17. Araos, M. U.; Warr, G. G., *Langmuir* **2008,** 24, (17), 9354-9360.
18. Atkin, R.; Warr, G. G., *J. Phys. Chem. B* **2007,** 111, (31), 9309-9316.
19. Bobillier, S. M. C. Self-assembly of non-ionic surfactants in some room-temperature ionic liquids. Honours, The University of Sydney, 2005.
20. Greaves, T. L.; Weerawardena, A.; Fong, C.; Drummond, C. J., *Langmuir* **2007,** 23, (2), 402-404.
21. Greaves, T. L.; Weerawardena, A.; Fong, C.; Drummond, C. J., *J. Phys. Chem. B* **2007,** 111, (16), 4082-4088.
22. Greaves, T. L.; Weerawardena, A.; Krodkiewska, I.; Drummond, C. J., *J. Phys. Chem. B* **2008,** 112, (3), 896-905.
23. Atkin, R.; Warr, G. G., *J. Phys. Chem. B* **2008,** 112, (14), 4164-4166.
24. Atkin, R.; Warr, G. G., *J. Phys. Chem. C.* **2007,** 111, 5162-5168.
25. Poole, C. F.; Kersten, B. R.; Ho, S. S. J.; Coddens, M. E.; Furton, K. G., *J. Chromatogr. A* **1986,** 352, 407-412.
26. Horn, R. G., Evans, D. F., Ninham, B. W.; *J. Phys. Chem.* **1988,** 92, 3531-3537.
27. Xiao, D.; Rajian, J. R.; Cady, A.; Li, S.; Bartsch, R. A.; Quitevis, E. L., *J. Phys. Chem. B* **2007,** 111, (18), 4669-4677.
28. Nallet, F.; Laversanne, R.; Roux, D. J., *Physique II France* **1993,** 3, 487-502.
29. Mylrajan, M.; Srinivasan, T. K. K.; Sreenivasamurthy, G., *J. Cryst. Spec. Res.* **1985,** 15, 493-500.

Downloaded by UNIV OF DELAWARE MORRIS LIB on June 29, 2012 | http://pubs.acs.org
Publication Date (Web): December 18, 2009 | doi: 10.1021/bk-2009-1030.ch022

30. Kennedy, D. F.; Drummond, C. J., *Chem Comms* **2008**, submitted.
31. Borisenko, N.; ZeinElAbedin, S.; Endres, F., *J. Phys. Chem. B* **2006,** 110, (12), 6250-6256.
32. Paulsson, H.; Hagfeldt, A.; Kloo, L., *J. Phys. Chem. B* **2003,** 107, (49), 13665-13670.
33. Gratzel, M., *Nature* **2001,** 414, (6861), 338-341.
34. Pinilla, C.; Del Popolo, M. G.; Lynden-Bell, R. M.; Kohanoff, J., *Journal Of Physical Chemistry B* **2005,** 109, (38), 17922-17927.
35. Israelachvili, J. N., *Intermolecular and Surface Forces*. Academic Press: London, 1992.
36. Christenson, H. K.; Horn, R. G., *J. Colloid Int. Sci.* **1985,** 103 50-60.
37. Horn, R. G.; Israelachvili, J. N., *J. Chem. Phys.* **1981,** 75, (3), 1400-1409.
38. Christenson, H. K., *J. Chem. Phys.* **1983,** 78, (11), 6906-6913.
39. Han, W.; Lindsay, S. M., *Appl. Phys. Lett.* **1998,** 72, 1656-1663.
40. Jeffery, S.; Hoffmann, P. M.; Pethica, J. B.; Ramanujan, C.; Ozer, H. O.; Oral, A., *Phys. Rev. B* **2004,** 70, (5), 054114-0541122.
41. Lim, R.; Li, S. F. Y.; O'Shea, S. J., *Langmuir* **2002,** 18, (16), 6116-6124.
42. Lim, R.; O'Shea, S. J., *Phys. Rev. Lett.* **2002,** 88, 246101-246101.
43. Lim, R. Y. H.; O'Shea, S. J., *Langmuir* **2004,** 20, (12), 4916-4919.
44. O'Shea, S. J.; Welland, M. E.; Pethica, J. B., *Chem. Phys. Lett.* **1994,** 223, (4), 336-340.
45. Uchihashi, T.; Higgins, M. J.; Yasuda, S.; Jarvis, S. P.; Akita, S.; Nakayama, Y.; Sader, J. E., *Appl. Phys. Lett.* **2004,** 85, (16), 3575-3582.
46. Senden, T. J., *Curr. Opin. Colloid Interface Sci.* **2001,** 6, (2), 95-99.
47. Patrick, H. N., Warr, G.G., Manne, S., Aksay, I.A., *Langmuir* **1997,** 13, 4349-4356.
48. Lanning, O. J.; Madden, P. A., *J. Phys. Chem. B* **2004,** 108, (30), 11069-11072.
49. Christenson, H. K.; Horn, R. G.; Israelachvili, J. N., *J. Colloid Interface Sci.* **1982,** 88, (1), 79-89.
50. Atkin, R.; Warr, G. G. In *The influence of Solvophobicity and Bulk Nanostructure on Solvation Layers of Room Temperature Ionic Liquids Confined Between Surfaces.*, 236th ACS National Meeting & Exposition, Philadelphia, August 17-21, 2008; Philadelphia, 2008.
51. Iler, R. K., *The Chemistry of Silica*. Wiley-Interscience Publishers: New York, 1979.
52. Horn, R., G.; Israelachvili, J., N. , *J. Chem. Phys.* **1981,** 75, (3), 1400-1411.
53. Lim, R. Y. H.; O’Shea, S. J., *Langmuir* **2004,** 20, 4916-4919.
54. O'Shea, S. J.; Welland, M. E., *Langmuir* **1998,** 14, (15), 4186-4197.

Downloaded by UNIV OF DELAWARE MORRIS LIB on June 29, 2012 | http://pubs.acs.org
Publication Date (Web): December 18, 2009 | doi: 10.1021/bk-2009-1030.ch022

Downloaded by PENNSYLVANIA STATE UNIV on June 28, 2012 | http://pubs.acs.org
Publication Date (Web): December 18, 2009 | doi: 10.1021/bk-2009-1030.ch023

## Chapter 23

# Ionic Liquids: Contained and Characterised

**Imee Su Martinez and Steven Baldelli**

**University of Houston, Houston, TX 77204-5003**

Three ionic liquids - [$C_4$mim][$BF_4$], [$C_4$mim][$N(CN)_2$] and [$C_4$mim][$MeOSO_3$] - were studied using three complementary surface techniques; SFG-polarisation mapping, surface tension measurement and surface potential measurement. Custom vacuum cells were designed for each technique to be able to perform measurements in a highly controlled environment, minimising the presence of water and other contaminants which may compromise measured values. SFG results depicted both anions and cations to be present on the surface with the butyl chain of the cation positioned toward the gas phase and the imidazolium ring parallel to the surface plane. Surface potential measurements showed an excess positive charge on the surface for all three ionic liquids. The surface tension of [$C_4$mim][$N(CN)_2$] was determined.

## Introduction and Rationale

Interest in ionic liquids has grown a great deal since the synthesis of the first ionic liquid called "red oil" in the mid-19th century *(1)*. At present, studies and papers regarding ionic liquids are being published at a rate corresponding to thousands per year. The special properties that these liquids possess, and their countless possible applications, are what attract the scientific community to study them.

Ionic liquids, in particular room-temperature ionic liquids, are pure liquid salts at temperatures below 100 °C *(2)*. The composition of these liquids is typically a combination of an organic cation and an inorganic anion *(1)*. Depending on the constituting ions, some ionic liquids have a wide liquidus range, wide electrochemical window, high conductivity, low vapour pressure,

In Ionic Liquids: From Knowledge to Application; Plechkova, N., et al.;
ACS Symposium Series; American Chemical Society: Washington, DC, 2010.

and thermal stability *(3-5)*. This group of liquids have tuneable properties, such that different combinations of the cation or anion can be made allowing for modifications in their properties such as hydrophobicity, viscosity, density and solvation. The properties mentioned are what led to the current most common applications of ionic liquids, specifically liquid-liquid extraction, biphasic catalysis, corrosion, lubrication and solar cells or electrochemical applications *(6-8)*.

The possible application of ionic liquids in the gas absorption of certain anthropogenic gas pollutants such as $CO_2$, $SO_2$, $NH_3$, and CFCs, can be used to address global issues concerning climate changes and ozone depletion *(9,10)*. Studies done on this particular application, however, were leaning towards the solvation properties of ionic liquids with respect to these gases *(11-13)*. Gas uptake, which is also a surface interaction, creates a need to study in detail gas-liquid interfaces of ionic liquids. Determining the molecular orientation, excess charge, ion size and geometry, or probing the interface at the molecular level in order to understand how these gases are absorbed into the liquid, becomes very significant. Parallel to this, the necessity of characterising these interfaces in a controlled and very clean environment becomes crucial in order to produce reliable results.

The presence of organic contaminants, chloride and water alters values of measured physical properties in ionic liquids. Seddon *et al.* investigated the effect of these contaminants on the viscosity, density and $^1$H NMR shifts in some ionic liquids *(14)*. Chloride, even in low concentrations of 0.01 mol kg$^{-1}$ in [$C_4$mim][$BF_4$] caused a dramatic decrease in viscosity, a nonlinear decrease in density and a downfield shift in the $^1$H NMR signals of the imidazolium ring of the cation. Co-solvents such as ethanenitrile, trimethylethanenitrile, 2-propenenitrile, 1-methylimidazole, toluene, 1,4-dimethylbenzene and 1,2-dimethoxyethane, when added incrementally to [$C_4$mim][$BF_4$] and [$C_4$mim][$PF_6$], caused the measured viscosity to decrease exponentially. A more pronounced decrease in viscosity was caused by water alongside ethanenitrile, and 2-propenenitrile. Density decreased rapidly as well, at excess mole fractions of water (> 0.5).

In an atmosphere filled with moisture, studying the effect of water on the physical properties of a substance is very important. Bowers and co-workers plotted surface tension and conductivity isotherms of imidazolium ionic liquids including [$C_4$mim][$BF_4$] in water *(15)*. The general trend was the surface tension and conductivity decreased with increasing ionic liquid concentration until a critical concentration is reached wherein the values plateau.

An experiment on the solubility of water vapour in ionic liquids including [$C_4$mim][$BF_4$] was performed by Anthony *et al.* using a gravimetric microbalance *(16)*. This provides an idea of how volatile components can actually dissolve into the ionic liquid and affect its properties. The determined enthalpies and entropies of water absorption into the ionic liquid were found to be similar to those of polar solvents, indicating a strong infinity of these ionic liquids with water.

The effect of water on the vapour-liquid interfaces of ionic liquids has been studied using Sum Frequency Generation (SFG). Previous work in our group on [$C_4$mim][$BF_4$] showed that water is only probed at ionic liquid concentrations of

Downloaded by PENNSYLVANIA STATE UNIV on June 28, 2012 | http://pubs.acs.org
Publication Date (Web): December 18, 2009 | doi: 10.1021/bk-2009-1030.ch023

Downloaded by PENNSYLVANIA STATE UNIV on June 28, 2012 | http://pubs.acs.org
Publication Date (Web): December 18, 2009 | doi: 10.1021/bk-2009-1030.ch023

$\leq$0.02 mole fractions, whereas at higher concentrations the surface showed SFG spectra similar to that of the pure ionic liquid *(17)*. Sung and co-workers studied the effects of water on the vapour-liquid interface of [$C_4$mim][$BF_4$] using surface tension and SFG *(18,19)*. A rapid decrease in surface tension was observed from 0 to 0.016 mole fraction of ionic liquid, which corresponds to the lowest value of the measured surface tension. A slight increase was observed at around 0.05 mole fraction, which evened out with the increase in ionic liquid concentration. The mole fraction which corresponds to a minimum in the measured surface tension exhibited an unusually intense signal in SFG at ssp and ppp polarisations compared to the pure ionic liquid. The group explained this phenomenon in terms of the surface being covered purely by cations at low concentrations up to 0.02 mole fraction where the anions start to appear on the surface. A mole fraction of 0.05 signalled that the surface is being equally populated by both cations and anions.

What makes ionic liquids interesting systems for research, in addition to the mentioned applications, is the fact that these liquids are composed of pure ions making them a relevant system for studying the surface structure of charged species minus solvent effects. The role of charge size, intermolecular interactions, and polarisability on surface conformation can be determined to test existing theories such as the Gouy-Chapman model of the double layer and to explore more likely models.

The goal of this study is to probe the gas-liquid interface of room temperature ionic liquids using sum frequency generation-polarisation mapping method, surface tension measurements using the ADSA (Axisymmetric Drop Shape Analysis) method, and surface potential measurements using the compensation/vibrating plate method. Special cells for these three different techniques were designed to be able to perform measurements in vacuum at $10^{-5}$-$10^{-6}$ Torr in order to perform measurements in a clean and controlled environment.

These three techniques combined will complement each other and will provide a better understanding on how the ions of these liquids are structured at the surface. SFG-polarisation mapping will give a better molecular level description of the interface. Surface potential measurements will be able to determine the excess charge on the surface and therefore determine which species prevail or are dominant over the other. Surface tension will determine excess surface energy and will correspond to the functional group as well as to the intermolecular forces prevalent on the surface. The results from these three techniques tied together will therefore determine the arrangement of these ions with respect to each other and how each ion whether cation or anion is oriented at the gas-liquid interface.

Three different ionic liquids were used for this study, with the same cation 1-butyl-3-methylimidazolium, [$C_4$mim]$^+$, and three different anions tetrafluoroborate [$BF_4$]$^-$, dicyanamide [$N(CN)_2$]$^-$ and methyl sulfate [$MeOSO_3$]$^-$, which have different sizes and geometries.

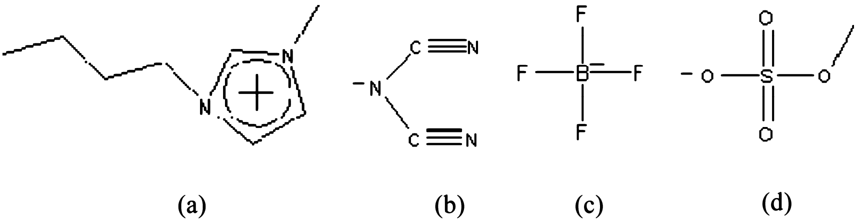

*Figure 1. Ionic liquids under study: (a) 1-butyl-3-methylimidazolium cation (b) dicyanamide anion (c) tetrafluoroborate anion (d) methyl sulfate anion*

# Background

## Sum Frequency Generation (SFG)-Polarisation Mapping Method

SFG is a nonlinear vibrational spectroscopic technique that involves two input laser beams; visible and tuneable IR that overlap in a medium to generate an output beam that has a frequency equal to the sum of the frequencies of the two incoming beams *(20)*. It is a highly surface specific technique, since it is forbidden in a medium with inversion symmetry *(20,21)*.

The intensity, $I(\omega_{SF})$, of the generated sum frequency beam is proportional to the square of the induced polarisation $P^{(2)}$ on the surface due to the coming together of the electric fields of the two incident beams ($E_{IR}$, $E_{vis}$) *(22)*. The term that relates the induced polarisation response to the electric fields is the second order nonlinear susceptibility tensor $\chi_{eff}^{(2)}$. This has two components, the $\chi_{nr}$ coming from the non-resonant background of the surface and the resonant term, which contains the vibrational spectroscopic information *(20)*. $\beta^{(2)}$ is the hyperpolarisability, which contains this information averaged over all molecular orientations composed of the Raman polarisability and the IR dipole transition. $\omega_{IR}$, $\omega_q$, and $\Gamma_q$ are the frequency of the IR beam, frequency of the normal mode and the damping constant of the $q^{th}$ vibrational mode, respectively *(23)*.

$$\mathrm{I}(\omega_s) \propto \left| \mathrm{P}^{(2)} = \chi^{(2)}_{\mathrm{eff}} : \mathrm{E_{vis}E_{IR}} \right|^2 \qquad (1)$$

$$\chi^{(2)} = \chi^{(2)}_{nr} + \sum\nolimits_q \left[ \frac{N\langle\beta^{(2)}\rangle}{(\omega_{IR} - \omega_q + i\Gamma_{\mathrm{q}})} \right] \qquad (2)$$

The polar orientation of a molecule on the surface is what dictates the magnitude of the $\chi_{eff}^{(2)}$. By varying the polarisations of the input and output beams, the Cartesian components of the susceptibility tensor can be determined, which allows for the determination of the molecular orientation relating to the surface normal *(20,21)*.

The structural orientation of the ionic liquids mentioned above has already been determined using SFG *(24-27)*. Results of previous authors in the group showed that both cation and anion are present on the surface. The ring of the

Downloaded by PENNSYLVANIA STATE UNIV on June 28, 2012 | http://pubs.acs.org
Publication Date (Web): December 18, 2009 | doi: 10.1021/bk-2009-1030.ch023

imidazolium cation lies flat at the gas-liquid interface, while the butyl chain is extended towards the gas phase at an angle from the surface normal. These previous SFG studies used the usual polarisation combinations in particular ssp, ppp, sps and pss to observe the surface.

Results from studies, both simulation and experimental, presented by other authors vary in relation to the results published by our group. Balasubramanian and Bhargava used atomistic molecular dynamic simulations to investigate [$C_4$mim][$PF_6$] *(28).* Both anions and cations enrich the surface with the anions contributing to the enhanced calculated electron density. The butyl chains are parallel to the surface normal protruding out of the liquid. The ring positioned closer to the vapour phase is parallel to the surface except at the densest part, where it is perpendicular.

X-ray reflectivity and surface tensiometry were performed by Sloutskin *et al.* to probe the surface of alkylimidazolium ionic liquids with anions $[PF_6]^-$ and $[BF_4]^-$ *(29).* Electron density results indicated that both anions and cations are present on the surface. Assuming that electroneutrality governs the surface, they have calculated a nett negative charge at the interface. The observed surface layer thickness was close to the length of a butyl chain, implying that the cations are standing up, although a stack of lying down molecules which are three layers in thickness cannot be discounted.

Capillary wave spectra and surface tension were measured by Halka and coworkers for [$C_4$mim][$PF_6$] *(30).* The calculated negative surface entropy from the surface tension values agreed with simulations which predicted anisotropic alignment of imidazolium cations on the surface. The resulting wave spectra gave surface dipole moment density described by the authors as a condensed liquid monolayer with the cations strongly aligned capable of sliding past each other.

Direct recoil spectrometry used to probe the surface structure of imidazolium ionic liquids showed atomic ratios implying the presence of both cations and anions without segregation occurring amongst them *(31).* According to this group, the cation is oriented perpendicular to the surface plane where the nitrogen atoms of the ring are positioned at the top. Increasing the alkyl chain length of the cations of [$C_4$mim][$PF_6$] and [$C_4$mim][$BF_4$] from four to twelve increased the rotation angular spread of the cations from 30° to 45°. Orientations however of certain ionic liquids such as [$C_8$mim]X (X = [$BF_4$], Cl or Br) cannot be clearly determined.

Jeon *et al.*, using X-ray reflectivity and SFG, postulated that the alkyl chains of the imidazolium cations are oriented toward the gas interface while the anions and the cation cores are in contact with the liquid *(32).* The SFG intensity for [$C_4$mim]I was double the intensities of [$C_4$mim][$BF_4$] and [$C_4$mim][$PF_6$], which made them conclude that the number densities for the cations of the last two ionic liquids are smaller than that for [$C_4$mim]I. These results are congruent to the X-ray results, which showed that the layer thickness for [$C_4$mim][$BF_4$] and [$C_4$mim][$PF_6$] are shorter than the extended chain length of the butyl chain, suggesting the chain is tilted at an angle. In contrast, that of the [$C_4$mim]I has a larger thickness compared to the length of the butyl chain suggesting otherwise. The electron density of [$C_4$mim]I is also higher, implying

Downloaded by PENNSYLVANIA STATE UNIV on June 28, 2012 | http://pubs.acs.org
Publication Date (Web): December 18, 2009 | doi: 10.1021/bk-2009-1030.ch023

that the anions are not coexisting with the imidazolium cations on one layer but are situated directly below the cations.

Recently, Iwahashi and co-workers performed SFG on 1-butyl-3-methylimidazolium trifluoromethanesulfonate, [$C_4$mim][OTf], and observed that polar ordering exists at the surface *(33).* The polar $SO_3$ groups are pointed toward the bulk and the non-polar $CH_3$ functional groups are directed towards the vapour phase. The SFG signal coming from the $SO_3$ suggests that the $SO_3$ on the surface is different from the bulk $SO_3$, even though both are in contact with the bulk. Also, blue shifting of the $SO_3$ peak implies that there is a strong interaction between the imidazolium cation and the $[OTf]^-$ anions, indicating that ions form an aggregated configuration on the surface. The narrow line width of the $SO_3$ peak implies a specific configuration of this so-called aggregation.

Polarisation mapping methods provide a better approach to analyse interfaces using SFG *(34).* This can improve fitting results by means of probing the interface using polarisation combinations other than the normal ssp, ppp, sps, and pss, obtaining more reliable spectral information if not a larger set of data with which to perform analysis.

$\chi_{eff}^{(2)}$ is a summation of its 27 Cartesian components, which reduces to four independent non-vanishing components considering an azimuthally isotropic interface *(20-23,35).* The contribution of these components to the intensity of the sum frequency beam or the $\chi_{eff}^{(2)}$ varies according to the polarisation of the incoming and outgoing beams *(20-22,34).* Setting the visible beam s-polarised and the IR beam p-polarised leads to $\chi_{yyz}$ contributing to the induced polarisation on the surface, producing an s-polarised emitted beam. When both incoming beams are p-polarised, the other four Cartesian components $\chi_{xxz}$, $\chi_{xzx}$, $\chi_{zxx}$ and $\chi_{zzz}$ contribute with their relative importance determined by the electric field on the surface to produce a p-polarised beam. Performing polarisation mapping, which is setting the polarisation of the IR p-polarised, the visible 45° from the s-polarisation direction and varying the angle ($\sigma_S$) of the polariser in front of the detector, the resulting contribution to the $\chi_{eff}^{(2)}$ is a combination or interference between the ssp and ppp $\chi_{eff}^{(2)}$ at half the intensity. The resulting series of spectra is therefore an interference of the ssp and ppp spectra. The intensity of the sum frequency beam at various polarisations is represented below:

$$I(\omega_s) \propto \left| \chi_{eff,ssp^{(2)}} \cos\sigma_S + \chi_{eff,ppp^{(2)}} \sin\sigma_S \right|^2 \qquad (3)$$

A 2D contour plot of wavenumber *versus* incrementing polarisation angles $\sigma_s$ can therefore be constructed to improve spectral analysis. This map will allow extraction of phase information since different vibrational modes will reach maximum peak intensity at different signal beam polarisation angles *(34).* It also means it can separate overlapping peaks according to phase difference, damping factor difference, and difference in intensity based on the fact that an SFG spectrum with very different spectral features can be collected by varying $\sigma_S$.

Downloaded by PENNSYLVANIA STATE UNIV on June 28, 2012 | http://pubs.acs.org
Publication Date (Web): December 18, 2009 | doi: 10.1021/bk-2009-1030.ch023

Increased fitting resolution because of SFG-polarisation mapping will enhance the usefulness of SFG in orientational analysis. Having seven different polarisation combinations compared to only four will probe the surface of ionic liquids at a more rigorous manner. Simultaneous fitting of spectra from these polarisation combinations will lessen bias, which is typical in fitting SFG spectra. Results from this mapping technique in terms of orientation of ions on the surface will be compared to previous studies performed on imidazolium ionic liquids.

Orientational analysis using the method of Wang and Hirose has been carried out on imidazolium ionic liquids previously in our group. In fact, the orientation of cation and anion of $[C_4mim][N(CN)_2]$ has been studied in detail *(26)*. The butyl chain of the cation based on the C-H stretching region of the terminal $CH_3$ functional group was determined to be 52°-80°, with a distribution of 0°-30° from the surface normal. The dicyanamide anion for the same ionic liquid was observed to have tilt angles of 52°-80° in a dipping configuration perpendicular to the length of the molecule and twisting angles along the length of the ion of 0°-30°. The tilt angles of the terminal carbon of the butyl chain from the cation of $[C_4mim][PF_6]$ and $[C_4mim]Br$ were also determined *(24)*. The tilt angles around the axis of the terminal methyl functional group were $(47 \pm 2)°$ and $(54 \pm 1)°$ for the $[C_4mim]Br$ and $[C_4mim][PF_6]$, respectively.

## Surface Potential Measurement Using Vibrating Plate Methods

At the interface, the distribution of ions, electrons, and electric field due to permanent or induced dipoles leads to a potential difference. This difference in potential in turn causes redistribution of charges in the interface forming the electric double layer *(36)*.

There are several models used to interpret the measured Volta potential, but the Gouy-Chapman Model of the electrical double layer is a simple approach to begin the discussion. This model looks at ions as point charges distributed in a solution according to the Boltzmann equation, where in at an infinite distance from the surface the electrical potential $\phi(x)$, must be equal to the inner potential, which changes as the surface is approached *(37,38)*.

## Boltzmann Equation

$$Ni(x) = Ni(\infty)exp\left[\left(-\frac{zie\phi(x)}{kT}\right)\right] \qquad (4)$$

where $N$ is the number of ions at distance $x$ and ∞ from the surface, $z_i$ the valency of the ion and $e$ the electronic charge.

**Poisson's Equation** relates electrical potential $\phi(x)$ to the nett charge density per unit volume $\rho(x)$ in a planar double layer such that:

Downloaded by PENNSYLVANIA STATE UNIV on June 28, 2012 | http://pubs.acs.org
Publication Date (Web): December 18, 2009 | doi: 10.1021/bk-2009-1030.ch023

$$\delta^2\phi(x)/\delta x^2 = -\rho(x)/\in_r\in_o \qquad (5)$$

$$\rho(x) = \textstyle\sum_i Z_i\, eN_i(x) \qquad (6)$$

Since the double layer, surface plus solution is electrically neutral, the charge per unit area of surface $\sigma$ is balanced by the charge in solution such that:

$$\sigma = -\int \rho\,(x)\,dx \qquad (7)$$

Combining these equations lead to an equation that relates surface charge density to the electrical potential at the surface.

$$\sigma = (8N(\infty))/\in_r\in_o kT)1/2\, sin\, h\,(ze\,\phi(0)/2kT \qquad (8)$$

Now, the reciprocal double layer thickness can be described as

$$\kappa^2 = e^2\textstyle\sum_i N_i\,(\infty)z_i^2/(\in_r\in_o kT) \qquad (9)$$

such that when $ze\phi(x) << kT$, Equation (8) simplifies to:

$$\sigma = -\in_r\in_o\kappa\,\phi(0) \qquad (10)$$

and

$$\phi(x) = \phi(0)exp(-\kappa x). \qquad (11)$$

The measured $\Delta V$ can therefore be equated to $\phi(0)$-$\phi(\infty)$ based on the premises above.

## Surface Tension Measurement using the Pendant Drop Method

Surface tension ($\gamma$) is defined as force per unit length (mN $m^{-1}$), which arises from the imbalance of forces on molecules at the interface (*i.e.* gas-liquid) *(21)*. Attraction of the molecules in the liquid by various intermolecular forces leads to this phenomenon *(38)*.

There are several ways to measure surface tension, the most common of these are the Dunuoy ring method, Wilhelmy plate method, the maximum bubble pressure method, capillary rise method, and the drop method *(38)*. Among these techniques, the drop method is selected since it requires minimum sample amount, gives accurate and precise results and is useful in monitoring surface ageing *(39)*. The pendant drop method will be used in this study since our concern is the gas-liquid interface. This method involves a drop of liquid suspended by a syringe needle.

Several algorithms have been derived to accurately calculate the surface tension of liquids from the shape of the drop. These algorithms all came from the Young-Laplace equation (Equation 12), which describes the mechanical equilibrium in a suspended drop *(40)*.

Downloaded by PENNSYLVANIA STATE UNIV on June 28, 2012 | http://pubs.acs.org
Publication Date (Web): December 18, 2009 | doi: 10.1021/bk-2009-1030.ch023

$$\gamma\left(\frac{1}{R_1}+\frac{1}{R_2}\right)=\Delta p \qquad (12)$$

where $\gamma$ is the surface tension, $R_1$ and $R_2$ are the two radii of curvature and $\Delta p$ is the change in pressure due to the change in surface area of the drop.

In 1882, Bashforth and Adams created an algorithm that relates drop profile to the interfacial tension using a nonlinear differential equation, Equations (13) and (14) *(41).* $1/R_1$ can be geometrically defined as $d\phi/ds$; where $s$ is the length of curvature of the meridional cross section and $\phi$ is the angle of curvature. $1/R_2$, on the other hand, which is the reciprocal of the other principal radius of curvature, can be expressed as $\sin\phi/x$, where $x$ is the distance along the $x$–axis.

$$d\phi/ds = 2 + \beta z - \sin\phi/x \qquad (13)$$

$$\gamma = \rho g R o^2/\beta \qquad (14)$$

$\beta$, is the term that represents the shape factor directly related to the surface tension, $\Delta\rho$ is the density of the liquid, $g$ is the gravitational constant, $R_0$ is the radius of curvature at the apex, and $z$ is the distance along the $z$-axis. Before the advent of computers, the difficulty in using this procedure was determining the value of the angle of inflection ($\phi$).

To do away with measuring the angle of inflection, other authors such as Andreas (1938), Roe (1966), and Juza (1996) thought of other ways to determine the shape of a drop, and used a parameter $S$ called the shape factor *(42-45).*

$$S = Ds/De; \qquad (15)$$

where $D_s$ is $D_e$ away from the apex and $D_e$ is the equatorial diameter.

Using liquids with known surface tension, a correction factor termed $H$ was determined from the equation:

$$\gamma = gDe2\Delta\rho/H \qquad (16)$$

and a table of $S$ *vs.* $1/H$ was derived.

Finally, in 1983, Rotenberg started the Axisymmetric Drop Shape Analysis (ADSA), which makes use of a more sophisticated optical and camera system *(46).* A computer performs a numerical fit between the shape of the experimental drops and the mathematical model of the Laplacian equation of capillarity. Since then, several improvements have been made to this technique, such as TIFA, or Theoretical Image Fitting Analysis *(47-50).* Commercially available instruments for determining the drop method are based on this algorithm.

The surface tension of ionic liquids has already been measured using the methods mentioned earlier, such as the pull method at various temperatures, but usually exposed to the atmosphere. Some authors performed their measurements in a more controlled environment, such as in a glove box or in an environment filled with inert gas. Measured surface tensions from the literature of the three ionic liquids are shown in Table 1.

Downloaded by PENNSYLVANIA STATE UNIV on June 28, 2012 | http://pubs.acs.org
Publication Date (Web): December 18, 2009 | doi: 10.1021/bk-2009-1030.ch023

**Table 1. Surface Tension Values of [$C_4$mim][$BF_4$], [$C_4$mim][$N(CN)_2$], and [$C_4$mim][$MeOSO_3$] from Literature.**

| IL | $\gamma$ / dynes $cm^{-1}$ | Technique | Temp/°C | Handling Condition |
|---|---|---|---|---|
| [$C_4$mim ][$BF_4$] | 38.4, ≈42 *(51)* (from graph) | Dunouy ring | 63, 25 | heating cell |
| | 46.6 *(3)* | tensiometer (Fisher model 20) | 25 | dry |
| | 42.8 *(52)* | Wilhelmy Plate Method with dynamic angle analyser | 25 | not stated |
| | ≈43.5,≈44.3 *(29)* | Dunouy ring | 25 | dry, wet |
| | 42.7 *(53)* | Dunouy ring | 25 | dry |
| [$C_4$mim][$N(CN)_2$] | 46.56 *(54,55)* | capillary rise | 25 | not stated |
| [$C_4$mim][$MeOSO_3$] | 41.8-45.9 *(56)* | hanging drop | 40-10 | Thermotank |

Downloaded by PENNSYLVANIA STATE UNIV on June 28, 2012 | http://pubs.acs.org
Publication Date (Web): December 18, 2009 | doi: 10.1021/bk-2009-1030.ch023

## Experimental Section

### Materials

All the materials used for synthesising the ionic liquids were ACS reagents purchased from Aldrich, except for the sodium dicyanamide, which was from Alfa-Aesar. The reagents used in the surface tension measurements are spectroscopic grade solvents and the water used was deionised using a Millipore A10 system, with a resistivity of 18 MΩ cm and TOC index of <3 ppb.

### Synthesis

The ionic liquids were synthesised according to the literature *(56-59)*. All the ionic liquids were heated in a roto-evaporator after extraction and dried in vacuum until a pressure of $5 \times 10^{-5}$ Torr was reached.

### SFG-Polarisation Mapping Technique

An average of five scans were performed per spectrum, and the polarisation angles for the polarisation mapping procedure were set at p polarisation for the IR beam, 45° from the s polarisation for the 532 nm beam, and increasing angles by 15° from 0-90° for the SFG beam *(34)*.

The sample holder is a specialised vacuum cell shown in Figure 2. This cell can hold approximately 50 $cm^3$ of liquid sample and it is made of Pyrex glass. The beams, IR and visible, enter the cell through quartz or $CaF_2$ windows. The liquid sample, which was sinter-glass filtered to keep it free of particulates, was then placed into the cell and vacuum dried to 5 x $10^{-5}$ Torr. The cell was then back filled with an inert gas.

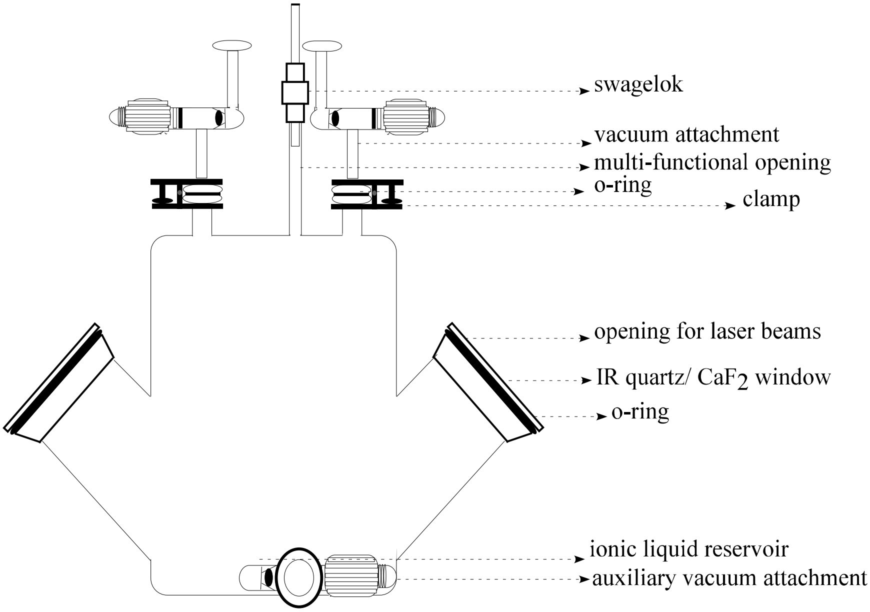

*Figure 2. SFG vacuum cell*

## Surface Potential

A customised cell (Figure 3) was designed to allow surface potential measurements in vacuum (5 x $10^{-5}$ Torr). The cell is made of Pyrex glass and has a vacuum valve, which can be attached to a vacuum line. The main opening of the cell holds the probe of an electrostatic voltmeter (TREK MODEL 323), which is kept vacuum-sealed by a valve that also allows translation of the probe. Inside the cell is a conductive gold-coated glass plate with five wells, each approximately 4 mm in diameter. This plate is attached to a thin silver wire that is connected to a potential source allowing the plate to be biased. The lower opening of the cell, which is a flat flange fitting, is closed with a glass plate that is sealed with a Viton 'O'-ring and a horseshoe clamp. A magnet embedded into the Teflon plate and another magnet outside of the cell allows the golden plate to be moved and controlled outside of the cell and still maintains a vacuum environment.

Downloaded by PENNSYLVANIA STATE UNIV on June 28, 2012 | http://pubs.acs.org
Publication Date (Web): December 18, 2009 | doi: 10.1021/bk-2009-1030.ch023

Downloaded by PENNSYLVANIA STATE UNIV on June 28, 2012 | http://pubs.acs.org
Publication Date (Web): December 18, 2009 | doi: 10.1021/bk-2009-1030.ch023

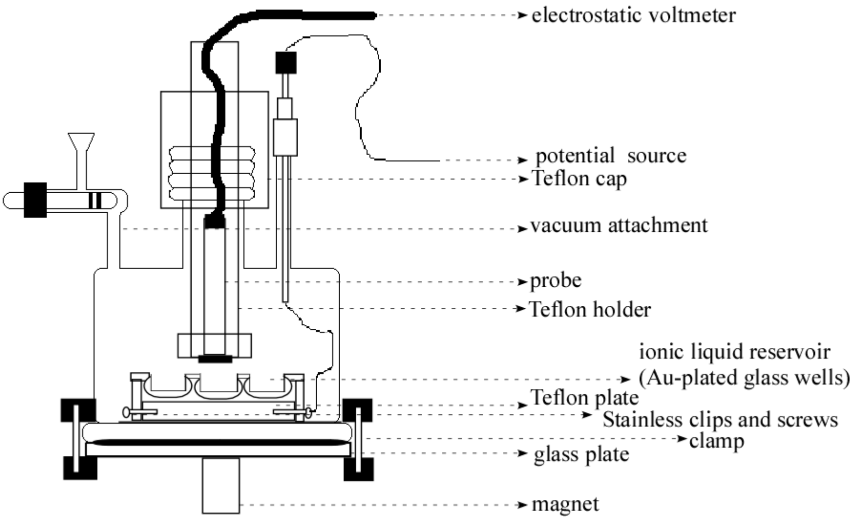

*Figure 3. Surface Potential Cell*

The apparatus was first tested on surfactants SDS and DTAB at ambient temperature and pressure to test the feasibility of the design as well as the polarity of the readings *(60-65).*

50 µl of each ionic liquid was placed in the wells for reading. These ionic liquids were previously pumped dry to 5 x $10^{-5}$ Torr prior to analysis. Once inside the cell, vacuum drying to the same pressure was once again done to maintain the integrity of the samples. Actual measurement of the surface potential involves zeroing the probe at a flat portion of the gold plate and moving the plate such that the probe is centred on the midpoint of the wells containing the ionic liquid.

## Surface Tension

A home-built drop method apparatus was used in this experiment. The set-up comprises a white light source, a pinhole and a diffuser to decrease the intensity of the light, filters to selectively transmit light, mirrors to direct light, a vacuum cell to hold the sample, a zoom and telecentric lens system, a WATEC high resolution WAT-902B CCD camera and a computer to process the collected images of the drop.

To process the images, such as determining the measurements of the dimension of the drop and the angle of curvature, Image J was used and an Image-J plug-in DROP SNAKE–ADSA *(66).* The surface tension was then calculated using the Bashforth–Adams algorithm, which is a direct application of the Young-Laplace Equation.

A vacuum cell was designed to allow measurement of surface tension in vacuum (5 x$10^{-5}$ Torr). Figure 4 shows a diagram of the parts of the cell. The cell is made of Pyrex, where the main body is composed of two ‘O’-ring joints fused together. This allows quartz window plates to be attached, where light passes through. The cell is equipped with a vacuum valve, which allows attachment to a vacuum line. The main opening of the cell has a thread fitting and it holds a modified 1 $cm^3$ 81301 Hamilton syringe. The plunger of the syringe was threaded and an aluminium holder was furnished to provide precision and control on drop formation. The bottom opening of the cell is occupied by the ionic liquid reservoir. This allows vertical translation and allows the ionic liquid to be drawn up into the syringe.

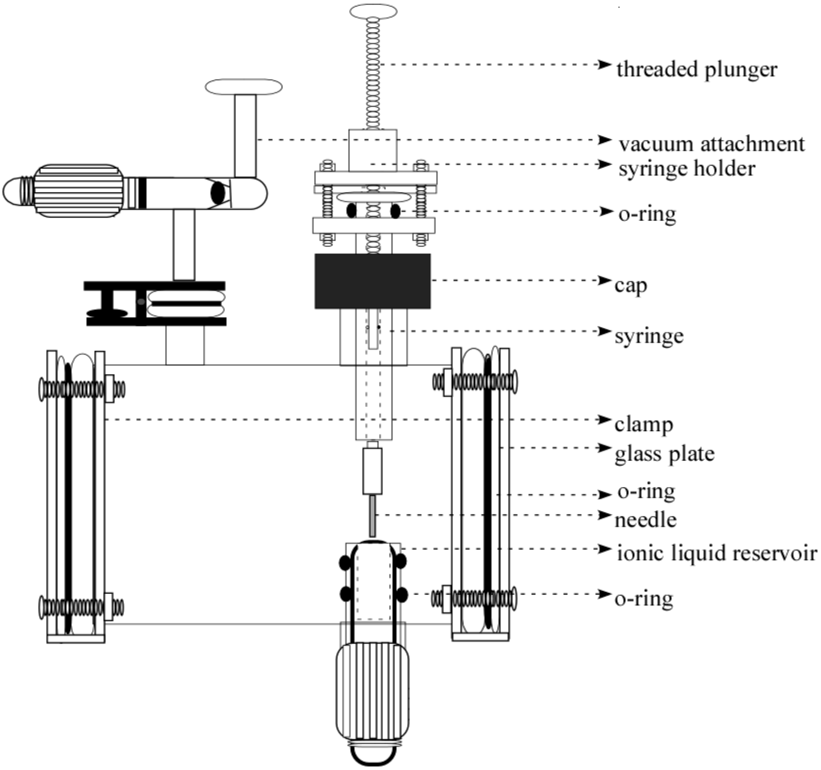

*Figure 4. Surface Tension Cell*

Common liquids with varying surface tension values were used to calibrate the optical set-up and to test the plausibility of the cell design. These liquids were water, glycerol, ethanol, and dimethylmethanamide.

## Sample-handling and Preparation

A vacuum line is used to degas the ionic liquid samples and evacuate the ionic liquid cells to at least 5 x $10^{-5}$ Torr. An ExTorr 3223 Quadropole Mass Spectrometer is attached to the vacuum line to monitor the presence and

Downloaded by PENNSYLVANIA STATE UNIV on June 28, 2012 | http://pubs.acs.org
Publication Date (Web): December 18, 2009 | doi: 10.1021/bk-2009-1030.ch023

amounts of volatile components prior to measurement, as well as the total pressure. Keeping track of these components in the vapour phase is significant because of the possibility of absorption into the ionic liquid altering measurable physical properties *(67-71)*. A typical mass spectrum is shown in Figure 5, indicating a clean cell and sample. Table 2 shows the amounts of each volatile component in the line and the cell as well as mole fractions of these volatile components in the ionic liquid calculated based on the determined Henry's constant for [$C_4$mim][$PF_6$] measured by Brennecke and co-workers *(70)*. Kumelan *et al.* determined the solubility of $H_2$ and CO in [$C_4$mim][$MeOSO_3$] and the calculated mole fractions of these gases from the measured partial pressures are 5.06 x $10^{-12}$ and 2.27 x $10^{-13}$ Torr, respectively *(68,72)*.

Once the cells are ready, an inert gas such as dinitrogen or argon is used to fill the cells. A pressure gauge is connected to the vacuum line to ensure 1 atm of gas pressure.

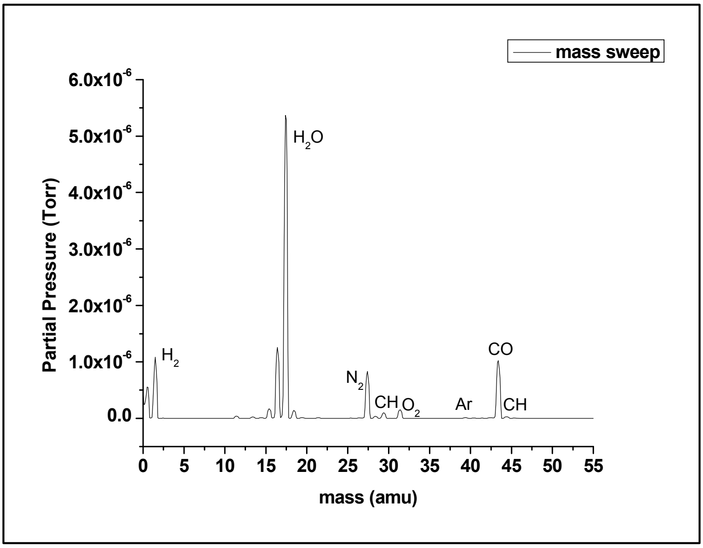

*Figure 5. Mass spectrum of vacuum cell.*

Downloaded by PENNSYLVANIA STATE UNIV on June 28, 2012 | http://pubs.acs.org
Publication Date (Web): December 18, 2009 | doi: 10.1021/bk-2009-1030.ch023

**Table 2. Amounts of Volatile Components**

| *Volatile Components* | *Partial Pressure / Torr* | *Mole Fraction* |
|---|---|---|
| $H_2$ | $1.93 \times 10^{-7}$ | $1.29 \times 10^{-14}$ |
| $H_2O$ | $3.96 \times 10^{-8}$ | $3.11 \times 10^{-10}$ |
| $N_2$ | $3.27 \times 10^{-6}$ | $7.26 \times 10^{-13}$ |
| $O_2$ | $7.41 \times 10^{-9}$ | $1.24 \times 10^{-15}$ |
| Ar | $3.30 \times 10^{-8}$ | $5.51 \times 10^{-15}$ |
| $CO_2$ | $1.10 \times 10^{-8}$ | $2.66 \times 10^{-13}$ |
| CO | $7.72 \times 10^{-9}$ | $2.06 \times 10^{-15}$ |
| $CH_2$ fragments | $1.65 \times 10^{-8}$ | $1.30 \times 10^{-14}$ |

# RESULTS AND DISCUSSION

## SFG Polarisation Mapping Method

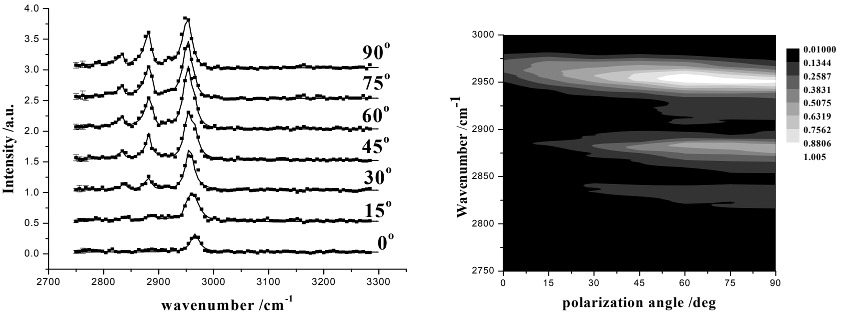

(a) (b)

*Figure 6. SFG-polarisation mapping results for [$C_4$mim][MeOSO3]. (a) SFG spectra at various polarisations (0.5 a.u. off-set for each succeeding polarisation). (b) Polarisation map.*

SFG polarisation mapping of [$C_4$mim][$MeOSO_3$] (see Figure 6) exhibits the $CH_3$ asymmetric stretch (2960-2970 cm$^{-1}$) belonging to the butyl chain of the cation at 0° polarisation. This peak becomes broader as the $CH_3$ Fermi resonance (2931-2942 cm$^{-1}$), still from the butyl chain, begins to contribute at 15° polarisation. At 30°, the Fermi resonance begins to dominate over the $CH_{3(as)}$ stretch and the peak shifts from 2966 cm$^{-1}$ to 2954 cm$^{-1}$. The $CH_3$ symmetric stretch from the butyl in the cation steadily gains intensity starting from 15° to 90°. The $OCH_3$ symmetric stretch (2828 cm$^{-1}$) and the Fermi resonance (~2915 cm$^{-1}$) from the anion also starts to become apparent at 15° and increases, subsequently. The 2D polarisation map shows that the vibrational

Downloaded by PENNSYLVANIA STATE UNIV on June 28, 2012 | http://pubs.acs.org
Publication Date (Web): December 18, 2009 | doi: 10.1021/bk-2009-1030.ch023

modes coming from the cation, which are the $CH_{3(as)}$, $CH_3$ Fermi resonance and the $CH_3$ symmetric reaches maximum at around 45°, 60°, and 70°, respectively. The $OCH_3$ symmetric stretch and $OCH_3$ Fermi resonance of the anion on the other hand are maximum at 90°. Vibrations coming from the $CH_2$ methylene stretches (symmetric stretch - 2845-2858 $cm^{-1}$, asymmetric stretch ~ 2900 $cm^{-1}$) should not be discounted, although their contributions are minimal.

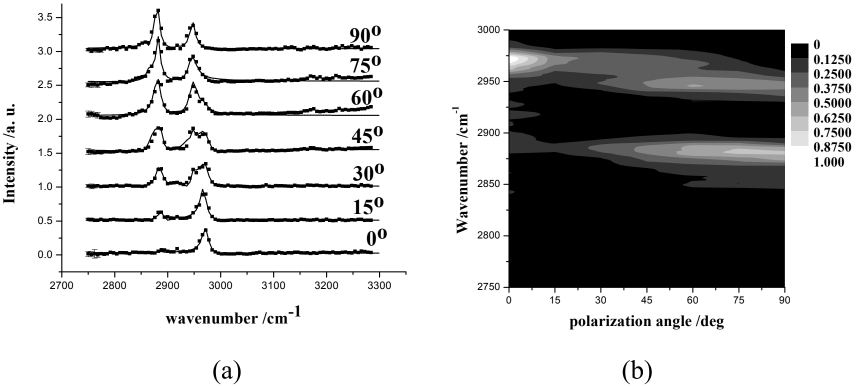

*Figure 7. SFG-polarisation mapping results for [$C_4$mim][$BF_4$]. (a) SFG spectra at various polarisations (0.5 a.u. off-set for each succeeding polarisation). (b) Polarisation map.*

For [$C_4$mim][$BF_4$], the set of spectra (Figure 7) shows a more dramatic transition from the $CH_3$ asymmetric to the $CH_3$ Fermi resonance as the polarisation is changed from 0° to 90°. The presence of these two well-resolved peaks at 45° is a good illustration that both modes are equally probed at this polarisation combination. The $CH_3$ symmetric mode can be seen to rise in intensity from 0° to 90° together with the $CH_3$ Fermi resonance peak. The 2D polarisation map shows that the methylene stretches contribute less in this set of spectra. The intensity of the $CH_3$ asymmetric stretch is maximum at 0°, the $CH_3$ Fermi resonance peaks at around 70°, and the $CH_3$ symmetric stretch reaches its highest intensity at around 80°.

[$C_4$mim][$N(CN)_2$] was analysed both in the CH and the CN region to observe both the vibrational modes of the cation and anion, respectively. Analogous to the other ionic liquids studied, the CH region (Figure 8) shows a

Downloaded by PENNSYLVANIA STATE UNIV on June 28, 2012 | http://pubs.acs.org
Publication Date (Web): December 18, 2009 | doi: 10.1021/bk-2009-1030.ch023

Downloaded by PENNSYLVANIA STATE UNIV on June 28, 2012 | http://pubs.acs.org
Publication Date (Web): December 18, 2009 | doi: 10.1021/bk-2009-1030.ch023

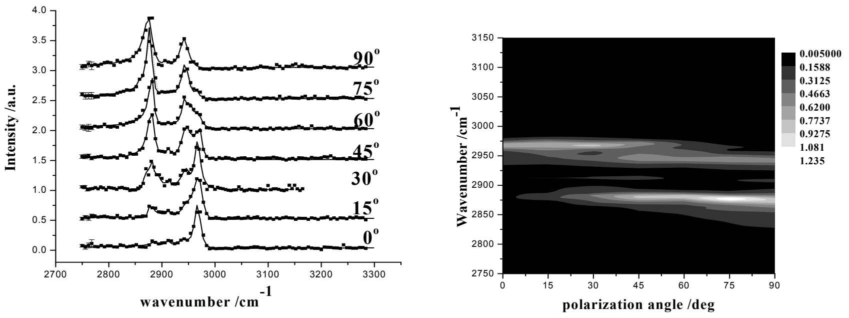

(a) (b)

*Figure 8. SFG-polarisation mapping results for [$C_4$mim][$N(CN)_2$] in the CH region. (a) SFG spectra at various polarisations (0.5 a.u. off-set for each succeeding polarisation). (b) Polarisation map.*

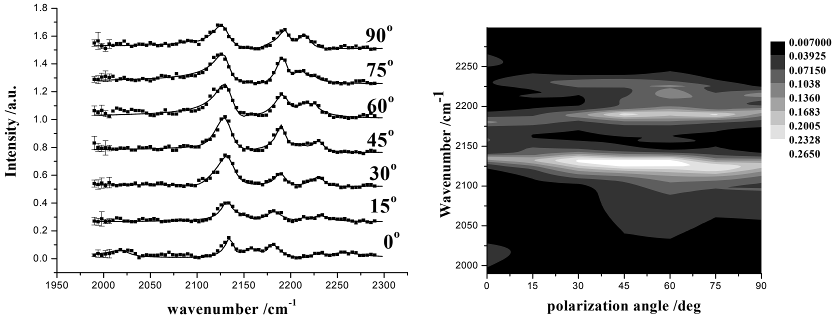

(a) (b)

*Figure 9. SFG-polarisation mapping results for [$C_4$mim][$N(CN)_2$] in the CN region. (a) SFG spectra at various polarisations (0.5 a.u. off-set for each succeeding polarisation). (b) Polarisation map.*

solitary $CH_3$ asymmetric stretch at 0° polarisation. This peak decreases in intensity as the polarisation angle is increased and the $CH_3$ Fermi resonance peak becomes more obvious. At 45°, it is important to take note that both peaks are present side by side with comparable intensity before the Fermi peak starts to become more intense at 60°. The $CH_3$ symmetric stretch, in contrast to the $CH_3$ asymmetric intensity, rises continuously with increasing angle of polarisation. For the CN region (Figure 9), the series showed the same vibrational mode, the CN symmetric stretch ( ~2130 $cm^{-1}$), the CN asymmetric stretch (~2180-2190 $cm^{-1}$) and the combination band (2225-2230 $cm^{-1}$) of these two modes. These peaks are best resolved at the polarisation angle set at 30°.

The CN stretches reach their maximum intensity at 45°, while the combination band at 60°.

For the three ionic liquids analysed, there were no ring modes observed, indicating that the imidazolium ring lies parallel to the surface. The presence of vibrational modes coming from both the cations and anions in $[C_4mim][MeOSO_3]$ and $[C_4mim][N(CN)_2]$ showed that both ions are present on the surface. The $CH_3$ vibrational modes and the very minimal contribution from the $CH_2$ modes illustrate that the alkyl chain is positioned towards the gas interface. The results in this study confirmed the previous studies performed on these ionic liquids.

## Surface Potential

The set-up was tested using surfactants sodium dodecyl sulfate (SDS) and dodecyltrimethyl ammonium bromide, $[N_{1\,1\,1\,12}]Br$. A negative surface potential was observed for SDS and a positive potential for $[N_{1\,1\,1\,12}]Br$, which are in agreement with results from the literature *(64,65,73).* Table 3 below shows these values.

**Table 3. Surface Potential Measurements of Surfactants**

| **Conc / $10^{-4}$ M** | **SDS (anionic)** | **$[N_{1\,1\,1\,12}]Br$ (cationic)** |
|---|---|---|
| Φ / V | **-0.12** | **0.17** |
| **Δ (std. dev.)** | **0.03** | **0.03** |

The positive values of the measured surface potentials of the ionic liquids (Table 4) agree with the simulation studies performed previously. Bresme *et al.* using hybrid molecular dynamics, canonical molecular dynamics, and Monte Carlo simulations investigated the liquid–vapour interface of size symmetric and size asymmetric ionic liquids *(74).* Results from their study showed that the electrostatic potential increases with size asymmetry due to a violation of the electroneutrality condition. The more asymmetric the size of the ion pairs, the bigger the measured potential difference. The difference in their sizes leads to a difference in the chemical potential, such that the bulkier ions tend to dominate the ion population at the surface. According to their calculations, a ratio of the ion sizes $\sigma_+/\sigma_- = 0.5$ gives an electrostatic potential of 0.1 V. The ionic liquids under study have asymmetrically large cations compared to their anions, which probably explains the positive values of the measured potential. The larger imidazolium cations predominate on the surface leading to a positive surface charge based on this proposition. It is important to mention, however, that for the surface potential measurements of surfactants, the dipole contribution of the headgroups and alkyl chains to the measured potential drop cannot be discounted *(65).*

Downloaded by PENNSYLVANIA STATE UNIV on June 28, 2012 | http://pubs.acs.org
Publication Date (Web): December 18, 2009 | doi: 10.1021/bk-2009-1030.ch023

**Table 4. Surface Potential of Ionic Liquids**

| *IL* | *(Φ ± Δ) / V* | | | |
|---|---|---|---|---|
| | *Trial* | | | |
| | *1* | *2* | *3* | *average* |
| $[C_4mim][BF_4]$ | 0.31±0.02 | 0.91±0.04 | 0.48±0.02 | 0.57±0.31 |
| $[C_4mim][N(CN)_2]$ | 0.43±0.02 | 0.63±0.03 | 0.31±0.02 | 0.46±0.16 |
| $[C_4mim][MeOSO_3]$ | 0.40±0.05 | 0.51±0.03 | 0.56±0.03 | 0.49±0.08 |

Simulation studies performed by Lynden-Bell *et al.* on $[C_4mim]Cl$, $[C_4mim][BF_4]$ and $[C_4mim][PF_6]$ used molecular dynamics and Monte Carlo simulations to determine the electrostatic potential on the gas-liquid interfaces of these ionic liquids *(75)*. In their study, the potential drop decreases as the size of the anion increases, which is very much in agreement with the asymmetric ion studies of Bresme *et al.* The larger anions tend to populate the surface so more negative ions on the surface mean less species in the bulk phase and a lower potential drop.

## Surface Tension

Four liquids of different known surface tensions were used to calibrate the pendant drop optical set–up and the mechanical aspect of the cell. Table 5 shows the average measured surface tension values and their corresponding theoretical values. The values that were collected are close to the known theoretical values.

**Table 5. Surface Tension of Various Liquids**

| ***Liquid*** | ***$\gamma$/ dynes cm$^{-1}$*** | ***Δ*** | ***Theoretical value*** | ***% error*** |
|---|---|---|---|---|
| Ethanol | 22.51 | 0.45 | 22.10 | 1.89 |
| Dimethylmethanamide | 38.71 | 0.88 | 37.10 | 4.34 |
| Glycerol | 64.00 | 0.62 | 64.00 | 0.01 |
| Water | 73.40 | 0.61 | 72.00 | 1.94 |

Measurement of the surface tensions of the ionic liquids samples is still in progress. So far the measured surface tension of $[C_4mim][N(CN)_2]$ is 44.93±1.28 dynes cm$^{-1}$. This value is lower than the measured surface tension value of $[C_4mim][N(CN)_2]$ from the literature, which is 46.56 dynes cm$^{-1}$ *(54,55)*. The lower measured value can be attributed to the minimal amount of moisture present in the sample.

As is the case for most imidazolium ionic liquids, the measured value is higher than the surface tension values of organic compounds, such as alkanes,

Downloaded by PENNSYLVANIA STATE UNIV on June 28, 2012 | http://pubs.acs.org
Publication Date (Web): December 18, 2009 | doi: 10.1021/bk-2009-1030.ch023

where dispersion forces predominate, but lower than the surface tension of water where hydrogen bonding is the dominant intermolecular force *(3)*. VDW forces must be present on the surface knowing that the alkyl chains are protruding towards the vapour phase, which is proven through SFG *(24,76)*. Since the dicyanamide anion has its C-N functional group extended towards the vapour phase, this can also mean that hydrogen bonding contributes to the tension on the surface, which also explains the lower value compared to water *(26)*. The presence of both ions on the surface can also add some ionic interaction or ion-dipole interactions, although not as dominant judging from the measured surface tension value. This can also prove that the charged portion of the ions is oriented towards the liquid phase, leading to a lower value. Forces aside from dispersion forces, which are mentioned here, must have contributed to the higher measured surface tension compared to organic compounds, where dispersion forces are more prevalent.

Downloaded by PENNSYLVANIA STATE UNIV on June 28, 2012 | http://pubs.acs.org
Publication Date (Web): December 18, 2009 | doi: 10.1021/bk-2009-1030.ch023

## Conclusion and Future Work

This study shows novel methods of characterising ionic liquids in a highly clean, controlled and contaminant-free environment. Since surface techniques are highly sensitive to impurities, including the techniques used here, these methods will provide substantially reliable measurement results.

The results from the SFG polarisation mapping method concur with the results from previous studies, which used only the four usual polarisation parameters ssp, ppp, sps and pss. This verified the previous results and showed that for simple molecules with minimal vibrational modes, like the ionic liquids studied, the previous method is acceptable. In this regard, simultaneous fitting will be done on the seven polarisations to get better fitting parameters for orientation analysis.

The results from the surface potential measurements were suitably elucidated by the simulation studies performed previously. In addition, the results from the surfactants agree with literature, which shows the feasibility of the technique. Future work will include more trials to measure the surface potential of these ionic liquids, measuring the potential of ionic liquids with a bigger anion compared to its cation, and looking at ionic liquids with increasing alkyl chain length.

The surface tension values of the other two ionic liquids are still to be measured. The measured surface tensions of common liquids agree with known values, verifying the calibration of the set-up.

Based on previous studies and results from this study at this point, the gas-liquid interface of the three imidazolium ionic liquids comprises both cations and anions on the surface. Positive surface potential readings may mean the presence of more cations than anions on the surface as well as the prevalence of dipole and dispersion interactions on the surface. Concurrently, the butyl chain of the cation is extended to the vapour phase at a certain angle while the charge constituent of the ions lie on the liquid phase, positioning the imidazolium ring parallel to the surface as established by SFG results, orientational analysis using SFG, as well as surface tension measurements.

## Acknowledgment

We are grateful to the R. A. Welch Foundation (E-1531) for the financial support for this study.

## References:

(1) Wilkes, J. S. In *Ionic Liquids in Synthesis* Wasserscheid, P., Welton, T., Eds.; Wiley-VCH: Weinheim, 2003, p 1-6.

(2) Anthony, J. L.; Brennecke, J. F.; Holbrey, J. D.; Maginn, E. J.; Mantz, R. A.; Rogers, R. D.; Trulove, P. C.; Visser, A. E.; Welton, T. In *Ionic Liquids in Synthesis*; Wasserscheid, P., Welton, T., Eds. Weinheim, 2003, p 41.

(3) Huddleston, J. G.; Visser, A. E.; Reichert, W. M.; Willauer, H. D.; Broker, G. A.; Rogers, R. D. *Green Chemistry* **2001**, *3*, 156-164.

(4) Grätzel, M.; Bônhote, P.; Dias, A.; Papageorgiou, N.; Kalayanasundram, K. *Inorg. Chem.* **1996**, *35*, 1168.

(5) Trulove, P. C.; Mantz, R. A. In *Ionic liquids in Synthesis*; Wasserscheid, P., Welton, T., Eds.; Wiley-VCH: Weinheim, 2003, p 103-121.

(6) Meindersma, G. W.; Podt, J. G.; Meseguer, M. G.; de Haan, A. B. S. In *Ionic Liquids IIIB: Fundamentals Progress, Challenges and Opportunities*; Rogers, R. D., Seddon, K. R., Eds.; American Chemical Society Washington, 2005, p 57-79.

(7) Dietz, M. L.; Dzielawa, J. A.; Jensen, M. P.; Bietz, J. V.; Borkowski, M. In *Ionic Liquids IIIB: Fundamentals, Progress, Challenges and Opportunities*; Rogers, R. D., Seddon K. R., Ed.; American Chemical Society: Washington, 2005; Vol. 902.

(8) Gaillard, C.; Moutiers, G.; Mariet, C.; Antoun, T.; Gadenne, B.; Hesemann, P.; Moreau, J. J. E.; Ouadi, A.; Labet, A.; Billard, I. In *Ionic Liquids IIIB: Fundamentals, Progress, Challenges and Opportunities*; Rogers, R. D., Seddon, K. R., Eds.; American Chemical Society: Washington, 2005.

(9) Farman, J. C.; Gardiner, B. G; Shanklin, J. D. *Nature* **1985**, *315*, 207-210.

(10) Pazmino, A. F.; Godin-Beekmann, S.; Luccini, E. A.; Piacentini, R. D.; Quel, E. J.; Hauchecorne, A. *Atmos. Chem. Phys.* **2008**, *8*, 5339–5352.

(11) Huang, J.; Riisager, A.; Wasserscheid, P.; Fehrmann, R. *Chem. Commun.* **2006**, 4027-4029.

(12) Blanchard, L. A.; Hancu, D.; Beckman, E. J; Brennecke, J. F. *Nature* **1999**, *399*, 28-29.

(13) Huang, J.; Riisager, A.; Berg, R. W.; Fehrmann, R. *J. Mol. Catal. A: Chem.* **2008**, *279*, 170-176.

(14) Seddon, K. R.; Stark, A.; Torres, M.-J. *Pure Appl. Chem.* **2000**, *72*, 2275-2287.

Downloaded by PENNSYLVANIA STATE UNIV on June 28, 2012 | http://pubs.acs.org
Publication Date (Web): December 18, 2009 | doi: 10.1021/bk-2009-1030.ch023

(15) Bowers, J.; Butts, C. P.; Martin, P. J.; Vergara-Gutierrez, M. C.; Heenan, R. K. *Langmuir* **2004**, *20*, 2191-2198.

(16) Anthony, J. L.; Maginn, E. J.; Brennecke, J. F. *J. Phys. Chem. B* **2001**, *105*, 10942-10949.

(17) Rivera-Rubero, S.; Baldelli, S. *J. Phys. Chem. B* **2006**, *110*, 15499-15505.

(18) Sung, J.; Jeon, Y.; Kim, D.; Iwahashi, T.; Iimori, T.; Seki, K.; Ouchi, Y. *Chem. Phys. Lett.* **2005**, *406*, 495-500.

(19) Sung, J.; Jeon, Y.; Kim, D.; Iwahashi, T.; Seki, K.; Iimori, T.; Ouchi, Y. *Colloids Surf., A* **2006**, *284*, 84-88.

(20) Shen, Y. R.; Miranda, P. B. *J. Phys. Chem. B* **1999**, *103*, 3292-3307.

(21) Buck, M.; Himmelhaus, M. *J. Vac. Sci. Technol. A* **2001**, *19*, 2717-2733.

(22) Bain, C. D. *Chem. Soc. Faraday Trans.* **1995**, *91*, 1281-1296.

(23) Wang, H. F.; Gan, W.; Lu, R.; Rao, Y.; Wu, B. H. *Int. Rev. Phys. Chem.* **2005**, *24*, 191-256.

(24) Rivera-Rubero, S.; Baldelli, S. *J. Phys. Chem B* **2006**, *110*, 4756-4765.

(25) Romero, C.; Baldelli, S. *J. Phys. Chem B* **2006**, 10.

(26) Aliaga, C.; Baldelli, S. *J. Phys. Chem B* **2007**, *111*, 9733-9740.

(27) Santos, C.; Baldelli, S. *J. Phys. Chem B* **2007**, *111*, 4715-4723.

(28) Bhargava, B. L.; Balasubramanian, S. *J. A. Chem. Soc.* **2006**, *128*, 10073-10078.

(29) Sloutskin, E.; Ocko, B. M.; Tamam, L.; Kuzmenko, I.; Gog, T.; Deutsch, M. *J. Am. Chem. Soc.* **2005**, *127*, 7796-7804.

(30) Halka, V.; Tsekov, R.; Freyland, W. *Phys. Chem. Chem. Phys.* **2005**, *7*, 2038-2043.

(31) Law, G.; Watson, P. R.; Carmichael, A. J.; Seddon, K. R. *Phys. Chem. Chem. Phys.* **2001**, *3*, 2879-2885.

(32) Jeon, Y.; Sung, J.; Bu, W.; Vaknin, D.; Ouchi, Y.; Kim, D. *J. Phys. Chem. C* **2008**, *112*, 19649-19654.

(33) Iwahashi; T.; Miyamae, T.; Kanai, K.; Seki, K.; Kim, D.; Ouchi, Y. *J. Phys. Chem . B* **2008**, *112*, 11936-11941.

(34) Chen, Z.; Wang, J.; Clarke, M. *Anal. Chem.* **2004**, *76*, 2159-2167.

(35) Wang, H. F. *Chin. J. Chem. Phys.* **2004**, *17*, 362-368.

(36) Jaycock, M. J.; Parfitt, G. D. *Chemistry Of Interfaces*; Ellis Horwood Limited: Sussex, 1981.

(37) Bockris, J. O. M.; Khan, S. U. M. *Surface Electrochemistry*; Plenum Press: New York, 1993.

(38) Adamson, A. *Physical Chemistry of Surfaces*; 3rd ed.; John Wiley and Sons: Toronto, 1976.

(39) Morita, A.; Carastan, D. J.; Demarquette, N. R. *Colloid Polym Sci* **2002**, *280*, 857-864.

(40) Hartland, S.; Hartley, R. *Axisymmetric Fluid-Liquid Interafaces*; Elsevier Scientific Publishing Company Amsterdam, 1976.

(41) Bashforth, F.; Adams, J. C. *An Attempt to test the Theory of capillary Action*; Cambride Univeristy Press and Deighton Bel Co.: Cambridge, 1892.

(42) Andreas, J. M.; Hauser, E. A.; Tucker, W. B. *J. Phys. Chem.* **1938**, *42*, 1001.

Downloaded by PENNSYLVANIA STATE UNIV on June 28, 2012 | http://pubs.acs.org
Publication Date (Web): December 18, 2009 | doi: 10.1021/bk-2009-1030.ch023

(43) Stauffer, C. E. *The Journal of Physical Chemistry* **1965**, *69*, 1933-1938.

(44) Roe, R. J.; Baccheta, V. L.; Wong, P. M. G. *J. of Phys. Chem.* **1967**, *71*, 4190-4193.

(45) Juza, J. *Czech. J. Phys.* **1997**, *47*, 351-355.

(46) Rotenberg, Y.; Boruvka, L.; Neumann, A. W. *J. Colloid Interface Sci.* **1983**, *93*, 169-183.

(47) Bateni, A.; Susnar, S. S.; Amirfazli, A.; Neumann, A. W. *Langmuir* **2004**, *20*, 7589-7597.

(48) Cabezas, M. G.; Bateni, A.; Montanero, J. M.; Neumann, A. W. *Appl. Surf. Sci.* **2004**, *238*, 480-484.

(49) Cabezas, M. G.; Bateni, A.; Montanero, J. M.; Neumann, A. W. *Colloids Surf., A* **2005**, *255*, 193-200.

(50) Zuo, Y. Y.; Do; C.; Neumann, A. W. *Colloids Surf., A* **2007**, *299*, 109-116.

(51) Law, G.; Watson, P. R. *Langmuir* **2001**, *17*, 6138-6142.

(52) Kim, K. S.; Demberelnyamba, D.; Shin, B. K.; Yeon, S.; H.; Choi, S.; Cha, J. H.; Lee, H.; Lee, C. S.; Shim, J. J. *Korean J. Chem. Eng.* **2006**, *23*, 113-116.

(53) Santos, C. S.; Baldelli, S. *J. Phys. Chem. C* **2008**, *112*, 11459-11467.

(54) Yoshida, Y.; Baba, O.; Larriba, C.; Saito, G. *J. Phys. Chem. B* **2007**, *111*, 12204-12210.

(55) Larriba, C.; Yoshida, Y.; de la Mora, J. F. *J. Phys. Chem. B* **2008,** *112,* 12401-12407.

(56) Pereiro, A. B.; Verdía, P.; Tojo, E.; Rodriguez, A. *J. Chem. Eng. Data* **2007**, *52*, 377-380.

(57) Goodchild, I.; Collier, L.; Millar, S. L.; Prokeš, I.; Lord, J. C. D.; Butts, C. P.; Bowers, J.; Webster, J. R. P.; Heenan, R. K. *J. Colloid Interface Sci.* **2007**, *307*, 455-469.

(58) Macfarlane, D. R.; Forsyth, S. A.; Golding, J.; Deacon, G. B. *Green Chem.* **2002**, *4*, 444-448.

(59) Holbrey, J. D.; Reichert, W. M.; Swatloski, R. P; Broker, G. A.; Pitner, W. R.; Seddon, K. R.; Rogers, R. D. *Green Chem.* **2002**, *4*, 407-413.

(60) Borwankar, R. P.; Wasan, D. T. *Chem. Eng. Sci.* **1986**, *41*, 199-201.

(61) Dukhin, S. S.; Miller, R.; Kretzschmar, G. *Colloid. Polym. Sci.* **1983**, *261*, 335-339.

(62) Miller, R.; Dukhin, S. S.; Kretzschmar, G. *Colloid. Polym. Sci.* **1985**, *263*, 420-423.

(63) Miller, R.; Kretzschmar, G.; Dukhin, S. S. *Colloid. Polym. Sci.* **1994**, *272*, 548-553.

(64) Pethica, B. A.; Few, A. V. *Discuss. Faraday Soc.* **1954**, *18*, 258-267.

(65) Warzynski, P.; Barzyk, W.; Lunkenheimer, K.; Fruhner, H. *J. Phys. Chem B* **1998**, *102*, 10948-10957.

(66) Stalder, A.; 2.1 ed. 2006, http://bigwww.epfl.ch/demo/dropanalysis.

(67) Anthony, J. L.; Anderson, J. L.; Maginn, E. J.; Brennecke, J. F. *J. Phys. Chem. B* **2005**, *109*, 6366-6374.

(68) Kumelan, J.; Kamps, Á. P. S.; Tuma, D.; Maurer, G. *J. Chem Eng. Data* **2007**, *52*, 2319-2324.

Downloaded by PENNSYLVANIA STATE UNIV on June 28, 2012 | http://pubs.acs.org
Publication Date (Web): December 18, 2009 | doi: 10.1021/bk-2009-1030.ch023

(69) Anthony, J. L.; Maginn, E. J.; Brennecke, J. F. *J. Phys. Chem. B* **2002**, *106*, 7315-7320.

(70) Brennecke, J. F.; Anthony, J. L.; Maginn, E. J. In *Ionic Liquids in Synthesis*; Wasserscheid, P. W., T., Ed.; Wiley-VCH Verlag GmbH and Co. KGaa: Weinheim, 2003, p 81-93.

(71) Cadena, C.; Anthony, J. L.; Shah, J. K.; Morrow, T. I.; Brennecke, J. F.; Maginn, E. J. *J. Am. Chem. Soc.* **2004**, *126*, 5300-5308.

(72) Kumelan, J.; Kamps, Á. P. S.; Tuma, D.; Maurer, G. *Fluid Phase Equilib.* **2007**, *260*, 3-8.

(73) Levine, S.; Mingins, J.; Bell, G. M. *J. Phys. Chem.* **1963**, *67*, 2095.

(74) Bresme, F. *Journal of Physics: Condensed Matter* **2005**, *17*, 3301-3307.

(75) Lynden-Bell, R. M.; Pópolo, M. D. *Phys. Chem. Chem. Phys.* **2006**, *8*, 949-955.

(76) Santos, C. S.; Rivera-Rubero, S.; Dibrov, S.; Baldelli, S. *J. Phys. Chem. C* **2007**, *111*, 7682-7691.

Downloaded by PENNSYLVANIA STATE UNIV on June 28, 2012 | http://pubs.acs.org
Publication Date (Web): December 18, 2009 | doi: 10.1021/bk-2009-1030.ch023

Downloaded by UNIV OF DELAWARE MORRIS LIB on June 28, 2012 | http://pubs.acs.org
Publication Date (Web): December 18, 2009 | doi: 10.1021/bk-2009-1030.ch024

## Chapter 24

# Prediction of Gas Solubility using COSMOthermX

**Christopher Hardacre,[1] Johan Jacquemin,[2] Norfaizah Ab Manan,[1] David W. Rooney,[1,*] and Tristan G. A. Youngs[1]**

**[1]The QUILL Research Centre, School of Chemistry and Chemical Engineering, Queen's University of Belfast, Stranmillis Road, Belfast BT9 5AG, United Kingdom**
**[2]Université François Rabelais, Laboratoire PCMB (E.A. 4244), Equipe CIME, Faculté des Sciences et Techniques, parc de Grandmont, 37200 Tours, France.**

Recent interest in the measurement of gas solubility in ionic liquids has led to a rapid increase in available data. Using this information, several attempts have been made to predict and estimate these values at different temperatures and pressures which can generally be categorised into four main families: Equation of State, Molecular Simulation, Group Contribution Models, and Correlation Models. Herein, we explore and evaluate the extent to which COSMOthermX may be used to predict the solubility of different gases in a range of ionic liquids, and show that this tool can be used to estimate solubilities and predict correct trends in most cases.

## Introduction

Ionic liquids (ILs) are commonly classed as a subset of the family of molten salts which have melting points below 373 K. These novel materials have considerable potential as "green" solvents due to their negligible vapour pressures *(1)*. One of the most appealing features is the ability to custom design

In Ionic Liquids: From Knowledge to Application; Plechkova, N., et al.;
ACS Symposium Series; American Chemical Society: Washington, DC, 2010.

Downloaded by UNIV OF DELAWARE MORRIS LIB on June 28, 2012 | http://pubs.acs.org
Publication Date (Web): December 18, 2009 | doi: 10.1021/bk-2009-1030.ch024

the ionic liquid with pre-selected characteristics by varying the constituents of the cation and anion. This unique property has allowed ionic liquids to be studied as reaction media *(2-9)*, catalysts *(10-16)*, novel solvents *(17-22)* in several potential applications such as liquids separations *(23,24)*, media for cleaning operations *(25)*, electrolytes/fuel cells *(26-28)* and heat-transfer fluids *(29-31)*.

Increasingly applications which take advantage of their properties for gas separations *(32,33)* or in multi-phase reactions (*i.e.* including a gaseous reactant) are being studied. However, in order to design ionic liquid processes which involve such phases, methods by which one could estimate the relevant physical properties are highly useful, particularly given the large number of possible combinations *(34,35)*. This is especially true when considering the huge range of possibilities if binary or ternary mixtures are considered. Recently, several attempts have been made to develop correlations which can be used to predict key properties, such as gas solubility, required for such applications. These can generally be categorised into one of the following methods:

- Equation of States (EOS) *(36-44)*
- Molecular Simulation *(45-53)*
- Group Contribution Models (GCM) *(54-56)*
- Correlation Models *(57,58)*.

Some examples of the EOS methods include those proposed by Camper *et al. (36)*, using a Regular Solution Theory (RTS) model for low pressure conditions or that of Ally *et al. (41)*, which uses an Irregular Ionic Lattice model to predict $CO_2$ solubility at temperatures ranging from 298.15 K to 333.15 K. However, this EOS model is unable to accurately predict the solubility for systems at high concentrations of $CO_2$. Molecular simulations, which require the determination of the pair potential parameters between each molecule, have shown reasonable agreement with experimental values *(53)*. Furthermore, group contribution models, which have been reported by Kim *et al. (54)* for the calculation of $CO_2$ solubility in 1-alkyl-3-methylimidazolium based ionic liquids as a function of temperature and pressure, predict solubilities with an average absolute deviation of approximately 0.23 to 5.11 %. However, in this study, no anion dependence was determined, therefore limiting the general applicability of the model. In addition to the above-mentioned estimation methods, Qin and Prausnitz *(59)* used perturbed-hard-sphere theory adapted from molecular physics where the solution is considered as "electrolyte-like" to predict the solubility of a number of gases in several ionic liquids. Nevertheless, this method estimated solubility values within ±70 % of experimental values. It is also worthy to note the work of Freire *et al. (60)* on the prediction of liquid-liquid equilibria and vapour-liquid equilibria of alcohols and ionic liquids. Therein, activity models such as Wilson *(61)*, UNIQUAC (UNIversal QUAsi-Chemical) *(62-65)*, original and modified UNIFAC (UNIversal quasi-chemical Functional group Activity Coefficients) *(66-68)*, and NRTL (Non-Random, Two-Liquids) *(69)* which have been applied previously were compared together with a discussion of their limitations *(60)*. These limitations were mainly due to a lack of ionic liquid group parameters available for the contribution methods which are necessary to predict properties for the wide range of ionic liquid combinations of cation and anion. Furthermore, the equation of state (EOS) prediction requires prior data such as critical properties and vapour pressures which are not directly measurable, and most of the time estimated due to lack of experimental measurements *(60)*.

The focus of this paper is to explore and evaluate the extent to which COSMOthermX (version 2.1, release 01.06) *(70)*, an advanced software tool based on Electron Density Functional Theory (DFT), may be used to calculate and predict gas solubilities of different gases in ionic liquids. The underlying theory of COSMOthermX software is a COSMO-RS (Conductor-like Screening Model for Real Solvents) method which describes the interactions in a fluid as local contact interactions of molecular surfaces, with the interaction energies being quantified using values of the two screening charge densities σ and σ' which form a molecular contact *(71,72)*. To date, a number of studies have examined the use of the COSMO-RS methodology as a descriptor of the Henry Law coefficients for the gas solubility of several gases in traditional solvents *(73)* (or, very recently, for the determination of this property for the $CO_2$ solubility in several ionic liquids *(74)*).

Downloaded by UNIV OF DELAWARE MORRIS LIB on June 28, 2012 | http://pubs.acs.org
Publication Date (Web): December 18, 2009 | doi: 10.1021/bk-2009-1030.ch024

## COSMOthermX Calculations of Gas Solubility in Ionic Liquids

As proposed by Klamt *et al.* *(75)*, COSMO-RS (Conductor-like Screening Model-Real Solvents) combines the electrostatic theory of locally interacting molecular surface descriptors, which are calculated using quantum chemistry methods, with a statistical thermodynamics methodology. This combination corresponds to the two steps required in COSMO-RS. Further explanation of COSMO-RS methodology and fundamental principle can be found in the COSMOlogic User's Manual. This work will discuss and evaluate the methodology for the prediction of gas solubility in ionic liquids using the COSMOthermX package.

The standard procedure for estimating gas solubility, when either the gas or ionic liquid is not contained within the supplied database, is that initially the ideal gas phase structure of the species should be optimised. Herein this was performed using DFT within Gaussian Version 3.0 *(76)* by means of the B3LYP method using the DGTZVP basis set, as recommended by COSMOThermX. The resultant optimised structure for each molecule is subsequently imported into the Turbomole programme *(77)* for the generation of the COSMO file, in this case using the BP-DFT method and the Ahlrichs-TZVP basis set *(78)*. These COSMO files can be finally imported into the COSMOThermX package and the gas solubility estimated using the procedures outlined within the manual.

When estimating solubilities in ionic liquids, the ionic liquid may be treated as either an ion pair or as discrete cations and anions. While the use of separate ions has the advantage of reducing the number of overall calculations necessary to describe a range of ionic liquids, the ion-pair description may, depending upon the system, be more realistic in describing the local potential. For systems of gas and ionic liquid using separated ions, COSMOthermX treats the system as a ternary mixture: cation, anion and gas. As the cation and anion are equimolar ($n_{\mathrm{ion}} = n_{\mathrm{anion}} = n_{\mathrm{cation}}$) the mole fraction of the gas is thus calculated as:

$$x^{T}{}_{gas} = \frac{n_{gas}}{n_{gas} + 2n_{ion}} \tag{1}$$

where $n_{gas}$ is the number of moles of solute dissolved. Experimentally, the determination of ionic liquid thermodynamic properties assumes a binary system, and thus the corrected mole fraction ($x^B$) from the COSMOthermX ($x^T$ value) calculation may be determined, as follows:

$$x^{B}{}_{gas} = \frac{2x^{T}{}_{gas}}{1 + x^{T}{}_{gas}} \tag{2}$$

The uncertainties in the gas solubility estimated using COSMOthermX were determined by calculating using the relative absolute deviation (RAD), as defined by Equation (3):

$$RAD = \frac{1}{N}\sum \left| \frac{X_{cal.} - X_{exp.}}{X_{exp.}} \right| \tag{3}$$

where $N$ is the total number of data used, $X_{cal.}$ is the desired property calculated using COSMOthermX for a given ionic liquid at a given temperature, and $X_{exp}$ is the corresponding value obtained from experimental work available within the literature. For comparison, a wide range of experimental values of gas solubility in ionic liquids is available and has been collated within the IUPAC database *(79)*. Herein solubilities were estimated and compared to literature data for $N_2O$, $CH_4$, $C_2H_6$, $C_3H_8$, $C_4H_{10}$, $C_2H_4$, $C_3H_6$, $C_4H_8$, $SO_2$ and $CO_2$ *(43,46,50,54,55,80-112)*. In addition, recent data reported by Jiang *et al. (113)* for $SO_2$ solubility in ionic liquids has also been included. The list and the abbreviations for each ionic liquid used in this manuscript are reported in Table 1.

Downloaded by UNIV OF DELAWARE MORRIS LIB on June 28, 2012 | http://pubs.acs.org
Publication Date (Web): December 18, 2009 | doi: 10.1021/bk-2009-1030.ch024

**Table 1. Ionic liquid abbreviations list**

| *Cation* | *Abbreviation* |
|---|---|
| 1-Alkyl-3-methylimidazolium | $[C_n\text{mim}]^+$ |
| 1-Alkyl-2,3-methylimidazolium | $[C_n\text{dmim}]^+$ |
| 1-Butyl-3-methylpyrrolidinium | $[C_4\text{mpyr}]^+$ |
| Methyltributylammonium | $[N_{1444}]^+$ |
| *Anion* | *Abbreviation* |
| Bis{(trifluoromethylsulfonyl)amide} | $[NTf_2]^-$ |
| Trifluoromethanesulfonate (triflate) | $[OTf]^-$ |
| Hexafluorophosphate | $[PF_6]^-$ |
| Tetrafluoroborate | $[BF_4]^-$ |
| Nitrate | $[NO_3]^-$ |

## Results and Discussion

Figure 1 shows the literature values for the solubility of both butane and ethane in $[C_4\text{mim}][NTf_2]$ as well as the prediction obtained using COSMOThermX over a wider temperature range. As reported in the literature, the solubility for butane is higher than that for ethane (by *ca.* 10 times), and this trend was estimated. Interestingly, a break can be observed in the ethane curve which occurs at a temperature of 305 K and corresponds to the critical temperature ($T_c$) of this gas.

Downloaded by UNIV OF DELAWARE MORRIS LIB on June 28, 2012 | http://pubs.acs.org
Publication Date (Web): December 18, 2009 | doi: 10.1021/bk-2009-1030.ch024

Downloaded by UNIV OF DELAWARE MORRIS LIB on June 28, 2012 | http://pubs.acs.org
Publication Date (Web): December 18, 2009 | doi: 10.1021/bk-2009-1030.ch024

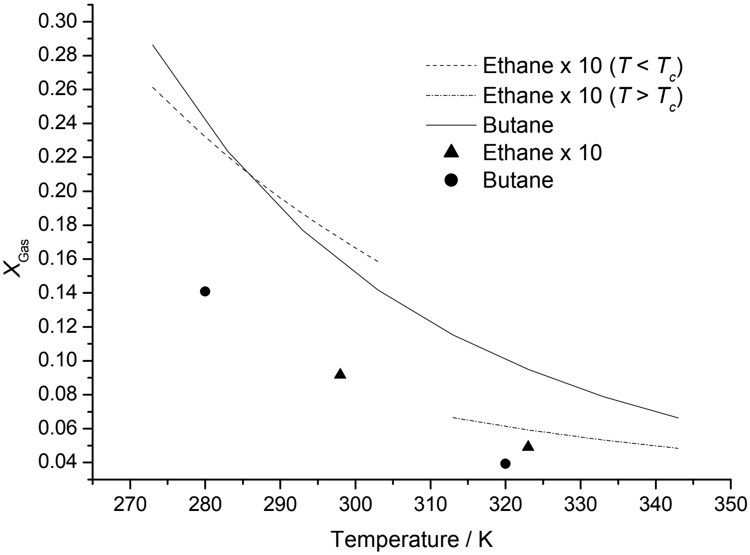

*Figure 1. Prediction of butane and ethane solubility in [C$_4$mim][NTf$_2$] at 298 K. Lines are COSMOThermX calculations, points are literature data.*

The reason why this occurs is due to the method by which COSMOThermX calculates the gas solubility. Within the program, the partial vapour pressure, and thus gas solubility, is estimated using the following equation:

$$p_{(i)} = p_o^{vap}{}_{(i)} x_{(i)} \gamma_{(i)} \qquad (4)$$

where $p_{(i)}$, $p_o^{vap}{}_{(i)}$, $x_{(i)}$, $\gamma_{(i)}$ are the partial and pure vapour pressure, mole fraction and activity coefficient of a selected gaseous species $i$ in a particular solvent. This equation shows that for such predictions, two components are necessary: namely the pure species vapour pressure and the activity coefficient. It is the former of these two which is responsible for this effect. COSMOThermX has two main options for estimation/evaluation of the vapour pressure; the first method uses Equation (5) for the gas phase chemical potential which is related to the vapour pressure.

$$\mu_{Gas}^{X_i} = E_{Gas}^{X_i} + E_{COSMO}^{X_i} - E_{vDw}^{X_i} + \omega_{Ring} n_{Ring}^{X_i} + \eta_{Gas} RT \qquad (5)$$

Here, $E_{Gas}^{X_i}$, $E_{COSMO}^{X_i}$ and $E_{vDw}^{X_i}$ are the quantum chemical total energies of the molecule in the gas phase, the COSMO conductor, and the van der Waals energy of species $X_i$ respectively. The other terms relate to a correction term for ring-shaped molecules with $n_{Ring}^{X_i}$ being the number of ring atoms in the molecule, $\omega_{Ring}$ being an adjustable parameter, and finally $\eta_{Gas}$ being a link between the reference states of the system's free energy in the gas and liquid phase *(71)*.

The value for $E_{Gas}^{X_i}$ can be determined using a program such as Turbomole, and referenced from an external energy file (herein referred to as the 'energy value') or calculated internally. The second method is to employ experimental data or the constants for standard correlations derived from such data. Here experimental $p_o^{vap}{}_{(i)}$ values of the gases were calculated using empirical correlations, such as the Antoine *(114)* and Wagner *(115)* equations *(116)*. The constants for these equations were taken from the NIST *(117)* and Korean KDB *(118)* database websites. These correlations should only be used for temperatures defined within the specified temperature range, and in particular below the critical temperature for each gas. However, many gases have a significantly lower critical temperature, for example 33 K, 151 K, 155 K for hydrogen, oxygen and argon, respectively. By removing temperature limits, the Antoine equation may be extrapolated in order to compare the calculated gas solubilities using both methods, although extrapolation over large temperature ranges is not advised, due to the exponential nature of the equation used. When the critical temperature is available to the programme, as in the case of ethane, COSMOThermX will switch from using vapour pressure correlations to the energy value when this temperature is exceeded. The result of this switch is an over prediction of the vapour pressure and hence a decrease in the solubility for the same activity coefficient. As recommended by COSMOLogic, experimental values or correlations for $p_o^{vap}{}_{(i)}$ are in general preferred to estimated values when available.

Figure 1 also clearly demonstrates that any evaluation of COSMOThermX for gas solubility measurements must consider the two components of pure vapour pressure and activity coefficient. Figure 2 shows the result for the estimated vapour pressure of butane, ethane and ethene over a 70 K temperature range.

Downloaded by UNIV OF DELAWARE MORRIS LIB on June 28, 2012 | http://pubs.acs.org
Publication Date (Web): December 18, 2009 | doi: 10.1021/bk-2009-1030.ch024

Downloaded by UNIV OF DELAWARE MORRIS LIB on June 28, 2012 | http://pubs.acs.org
Publication Date (Web): December 18, 2009 | doi: 10.1021/bk-2009-1030.ch024

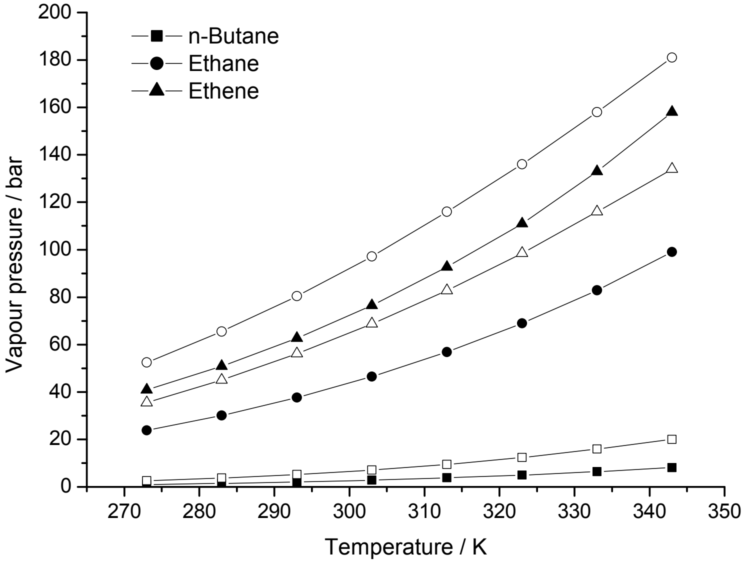

*Figure 2: Calculation of gas vapour pressures using both the extended Antoine correlation and energy value in COSMOThermX. Open symbols = energy value, closed symbols = Antoine equation.*

As can be observed from Figure 2, there is no consistent trend in the estimation of vapour pressure relative to the calculated values using available correlations. For both butane and ethane, the vapour pressure was overestimated, significantly in the case of ethane, whereas for ethene the vapour pressure was underestimated. Table 2 summarises this by calculating the vapour pressures for the nine gases which have critical temperatures greater than the used value of 273 K. In this table, the constants for the extended Antoine vapour pressure correlation, Equation (6), are also included.

$$\ln(p_0^{vap}) = A\ln(T) + \frac{B}{T} + C + DT^2 \qquad (6)$$

where $T$ is the temperature in Kelvin and the resultant vapour pressure is in kPa. From Table 2, it can be observed that the vapour pressure is in general overestimated, with olefins tending to give better results when compared to other gases.

Downloaded by UNIV OF DELAWARE MORRIS LIB on June 28, 2012 | http://pubs.acs.org
Publication Date (Web): December 18, 2009 | doi: 10.1021/bk-2009-1030.ch024

**Table 2: Constants for the calculation of vapour pressure, and summary of results at 273 K.**

| | *Constants for Equation (6)* | | | |
|---|---|---|---|---|
| *Name* | *A* | *B* | *C* | *D* |
| | | $/10^3K$ | | $/10^{-6}K^{-2}$ |
| Ethene | −4.90 | −2.36 | 43.20 | 16.41 |
| Ethane | −5.38 | −2.63 | 46.39 | 16.02 |
| Propene | −6.06 | −3.42 | 52.06 | 11.39 |
| Propane | −5.40 | −3.38 | 48.14 | 9.13 |
| 1-Butene | −7.79 | −4.51 | 64.35 | 9.82 |
| Butane | −6.92 | −4.35 | 58.70 | 9.15 |
| Sulfur dioxide | −11.52 | −5.41 | 88.03 | 19.41 |
| Carbon dioxide | −24.04 | −7.06 | 166.39 | 33.69 |
| Nitrogen dioxide | −1.33 | −2.26 | 23.69 | 1.08 |

| | *Critical Temp /K* | $p_{0_{Antoine}}^{vap}$ */bar* | $p_{0_{Energy}}^{vap}$ */bar* | *RAD* |
|---|---|---|---|---|
| Ethene | 282 | 40.87 | 35.50 | 13% |
| Ethane | 305 | 23.82 | 52.94 | 122% |
| Propene | 365 | 5.83 | 7.50 | 29% |
| Propane | 370 | 4.74 | 11.27 | 138% |
| 1-Butene | 419 | 1.29 | 1.85 | 43% |
| Butane | 425 | 1.03 | 2.56 | 149% |
| Sulfur dioxide | 430 | 1.54 | 0.13 | 92% |
| Carbon dioxide | 304 | 36.00 | 69.99 | 94% |
| Nitrogen dioxide | 309 | 31.45 | 115.93 | 269% |

According to Equation (5), the vapour pressure can be altered by modifying the original energy value. The recommend method for the evaluation of this term is to utilise the Ahlrichs-TZVP basis set within Turbomole; however, there are numerous others available. Within Gaussian 03, for example, several DFT methods exist each of which generates slightly different energies. These in turn can be used to replace the original energy value and hence determine a new vapour pressure curve. Using this approach, Figure 3 demonstrates how much the vapour pressure curve for propene can be altered by slight changes in this energy value.

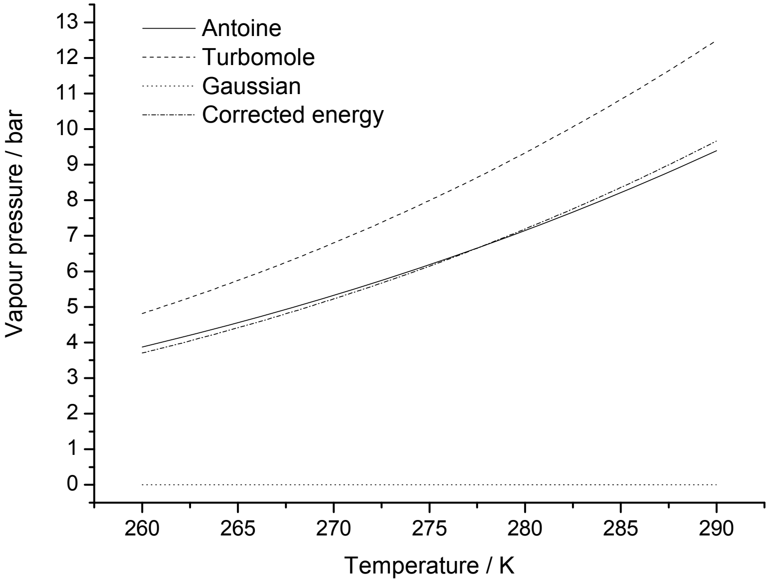

*Figure 3. Variation in estimated propene vapour pressure as a function of the energy value. Gaussian value calculated using B3LYP and DGTZVP method.*

In this case, the energy as calculated from Turbomole is −117.94919 au, which over predicts the vapour pressure by approximately 30% on average. Using the Gaussian 03 value of −117.91906 au, corresponding to a relative change of only 2.56 × $10^{-4}$ %, gives a vapour pressure of effectively zero over the studied temperature range. Further changing the energy to −117.94804 au gives a good correlation with that determined from the extended Antoine equation. Table 3 summarises these results by calculating the change in the energy value (where $\Delta E = E_{Gas}^{X_i}\,(\text{corrected}) - E_{Gas}^{X_i}\,(\text{Turbomole})$), as calculated by Turbomole, necessary to minimise the error between vapour pressures calculated using both Equations 5 and 6. As can be observed in Table 3, the RAD between the energy values calculated using both Gaussian 03 and Turbomole is only 0.29 × $10^{-3}$ % and like in the case of propene only very slight adjustments are required in order to produce a good correlation between the two methods.

Downloaded by UNIV OF DELAWARE MORRIS LIB on June 28, 2012 | http://pubs.acs.org
Publication Date (Web): December 18, 2009 | doi: 10.1021/bk-2009-1030.ch024

**Table 3. Calculated energies (au) for each gas and change in energy (*ΔE*) necessary minimise error with extended Antoine equation.**

| *Gas* | *TZVP-Gaussian* | *Turbomole* | *RAD /$10^{-6}$* | *ΔE /$10^{-3}$* |
|---|---|---|---|---|
| Ethene | − 78.596 | − 78.617 | 262 | -0.127 |
| Ethane | − 79.839 | − 79.856 | 223 | 0.869 |
| Propene | − 117.919 | − 117.949 | 256 | 0.250 |
| Propane | − 119.156 | − 119.183 | 227 | 0.750 |
| 1-Butene | − 157.236 | − 157.275 | 248 | 0.300 |
| Butane | − 158.473 | − 158.509 | 229 | 0.554 |
| Sulfur dioxide | − 548.596 | − 548.731 | 246 | 2.100 |
| Carbon dioxide | − 188.616 | − 188.677 | 324 | 0.472 |
| Nitrogen dioxide | − 184.688 | − 184.763 | 406 | 1.100 |

This is further summarised in the resulting parity plot of vapour pressures calculated using the adjusted energy value and Equation (6) for the nine gases, Figure 4. Some outliers are identified, which are associated with $CO_2$, suggesting that Equation 5 may not be a suitable model for this gas. These studies, however, clearly demonstrate the sensitivity of the vapour pressure calculations to the energy value used, and thus this poses a potential problem when evaluating solubilities for those gases were no literature vapour pressure data exist.

However, by using the experimental vapour pressures determined from the Antoine/Wagner correlations, the group of $C_2H_4$, $C_2H_6$, $C_3H_6$, $C_3H_8$, $C_4H_8$, $C_4H_{10}$, $N_2O$, $SO_2$ and $CO_2$ gases can serve to determine the accuracy of the activity calculation.

Downloaded by UNIV OF DELAWARE MORRIS LIB on June 28, 2012 | http://pubs.acs.org
Publication Date (Web): December 18, 2009 | doi: 10.1021/bk-2009-1030.ch024

Downloaded by UNIV OF DELAWARE MORRIS LIB on June 28, 2012 | http://pubs.acs.org
Publication Date (Web): December 18, 2009 | doi: 10.1021/bk-2009-1030.ch024

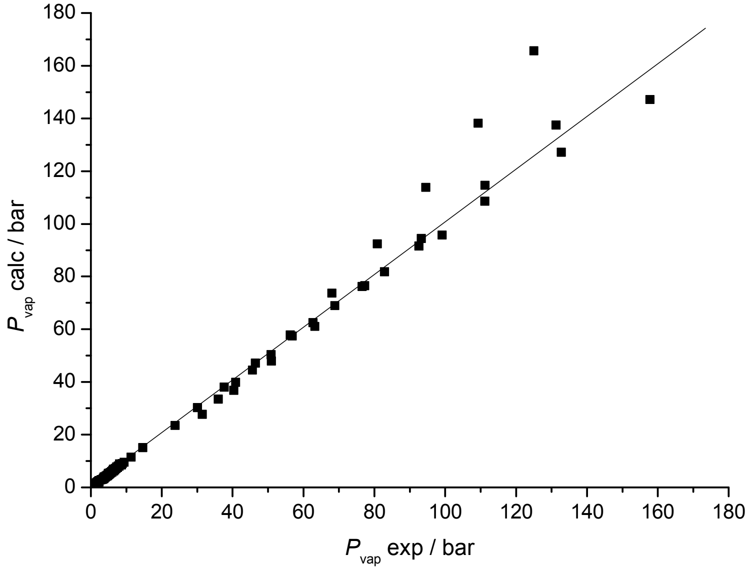

*Figure 4. Correlation plot of estimated vapour pressures using both the adjusted Turbomole energy value and the extended Antoine equation.*

Here, [$C_4$mim][$NTf_2$] was selected as the ionic liquid and the results of this study are shown in Figure 5. From this it can be observed that each gas gives a good correlation between the experimental and calculated values - however very few gases have a slope approximating a value of unity. The closest to unity is obtained with butane, however the overall linear fit for this gas has a higher error associated with it than the other alkanes. The largest deviation is attributed to $CO_2$, with a slope of 1.64 indicating a significant over prediction of the gas solubility in this ionic liquid. Of the groups studied, the olefins have the smallest deviation in the slope, although again the solubilities are overestimated (average slope = 1.56). Overall, given the linear nature of each plot, this suggests that COSMOThermX is able to show the correct trend in a particular gas's solubility as a function of both temperature and pressure.

The over prediction of $CO_2$ solubility is not specific to [$C_4$mim][$NTf_2$] - similar results are also observed for other ionic liquids. Figure 6 shows the estimated $CO_2$ solubility at a temperature of 298 K and 4 bar in a range of different ionic liquids which varying cations and anions.

Downloaded by UNIV OF DELAWARE MORRIS LIB on June 28, 2012 | http://pubs.acs.org
Publication Date (Web): December 18, 2009 | doi: 10.1021/bk-2009-1030.ch024

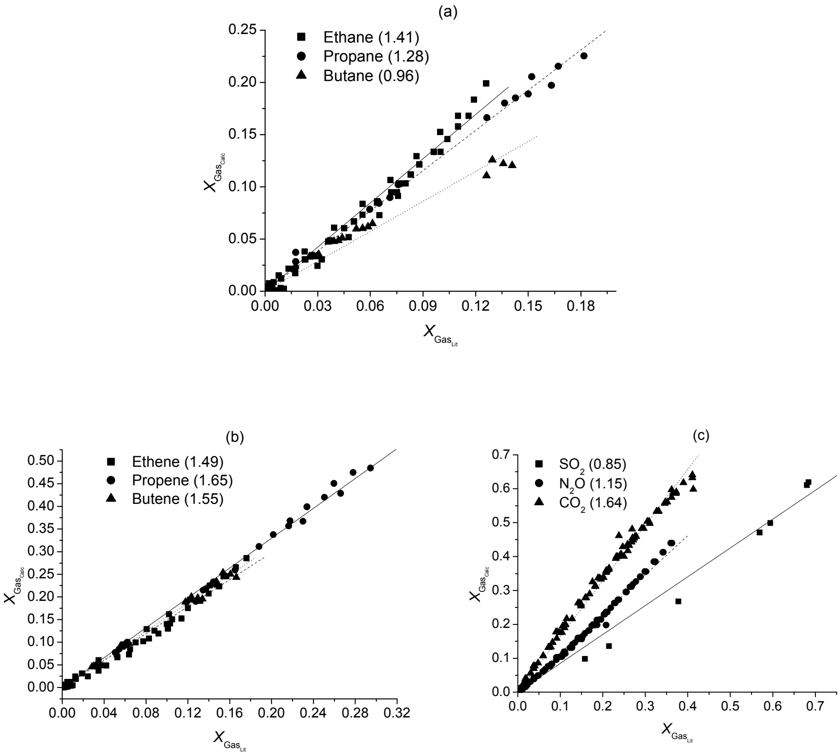

*Figure 5. Correlation plots for the calculation of gas solubilities in [$C_4$mim][$NTf_2$]. Slopes of the lines are in brackets.*

From this, it would appear that methyl substitution at the C(2) position has a negligible effect on the solubility, whereas this has been shown in the literature to reduce the solubility of this gas. The effect of changing the anion can also be observed for the 1-butyl-3-methylimidazolium based ionic liquids. Here, the calculations indicate that gases dissolving in $[NTf_2]^-$ ionic liquids have a higher solubility than in the analogous $[PF_6]^-$ ionic liquids, which is in agreement with the literature data. A further extension of this to five different anions predicted the following order for $CO_2$ solubility:

$$[NO_3]^- < [BF_4]^- < [OTf]^- < [PF_6]^- < [NTf_2]^-.$$

A similar trend is found in the experimental data, with the exception that $[PF_6]^- < [OTf]^-$ *(94)*. Similarly, $CO_2$ solubility in [$C_n$mim][$NTf_2$], with $n = 2$, 4 or 6 at 298 K, were compared using calculated values from COSMOthermX as a function of pressure, with the trend with regard to increasing alkyl chain length correctly predicted.

Downloaded by UNIV OF DELAWARE MORRIS LIB on June 28, 2012 | http://pubs.acs.org
Publication Date (Web): December 18, 2009 | doi: 10.1021/bk-2009-1030.ch024

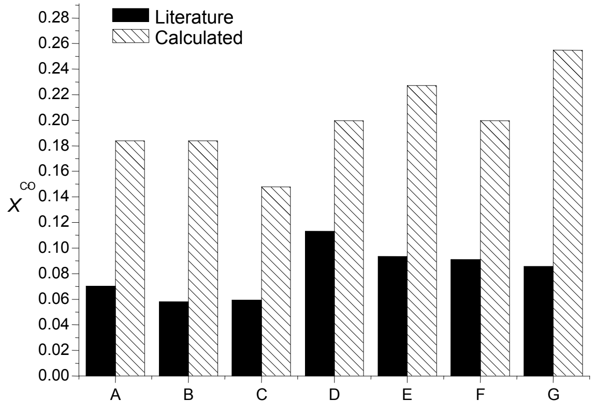

A = $[C_4mim][PF_6]$

B = $[C_4dmim][PF_6]$

C = $[C_4dmim][BF_4]$

D = $[C_4mim][NTF_2]$

E = $[C_4mpyr][NTf_2]$

F = $[C_2dmim][NTf_2]$

G = $[N_{1444}][NTf_2]$

*Figure 6. Estimated $CO_2$ solubility at 298 K and 4 bar in various ionic liquids.*

Observations by Freire *et al. (60)* for VLE and LLE using ionic liquids with alcohols indicated that conformers with the lowest state of energy gave the best prediction. These molecular conformers represent different energy states of the molecule which result from torsional rotations of the atoms within it. Therefore, conformers ultimately generate different charge distribution profiles, and hence each conformer will result in a different solubility. To examine the effect of these conformers on gas solubility, the example of $[C_4mim][NTf_2]$ will be again used. For this ionic liquid, there are three main ‘gas-phase’ conformers for the cation and two for anion, respectively. However, while the gas phase may indicate a relatively small number of conformers, the liquid phase structure is likely to contain a much broader range. Figure 7 shows a possible ‘snap-shot’ of the $[C_4mim][NTf_2]$ liquid phase, as determined using molecular dynamics methods. From this, it is possible to generate a number of different conformers of both the cation and anion and use these within the COSMOThermX program. Furthermore, it is possible to extract, for example, the central cation and its five closest anions and use these to create an approximation of the likely ion-pairs within the liquid. The effect of this on the gas solubility for $CO_2$ is shown in Figure 8(a). Here it can be observed that the use of the ‘liquid-phase’ individual ion conformers has an insignificant effect on the gas solubility relative to that of the ‘gas-phase’ conformers. It should be noted that to use a large number of conformers (in this case 20 of each of the cation and anion) increases the calculation time dramatically (over 200 times). Therefore, unlike the prediction of LLE, the effect of conformers on gas solubility is very small and, given the increase in computation time, it was considered unnecessary. Interestingly, the greatest effect of molecular conformers appears at the low concentrations of $CO_2$. Liquid phase ion-pair conformers do appear to lower the solubility and increase the accuracy of the prediction.

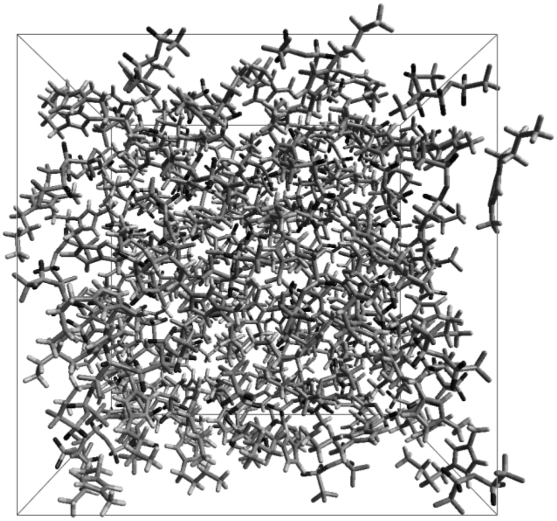

*Figure 7. Possible liquid phase structure for [$C_4$mim][$NTf_2$] showing the range of possible conformers.*

For $SO_2$, Figure 8(b), and ethene, Figure 8(c), it can be observed that the use of the individual ions for $SO_2$ is preferred, whereas for ethene the ion pairs generate a more accurate result. Such a result may be expected in the case of $SO_2$, which has a high solubility, if the dissolving gas helped to dissociate the ion pairs. However, for poorly soluble gases, the ionic liquid may tend to segregate itself from the dissolving gas and thus is better represented by ion-pairs. Assuming that $CO_2$ is an exception, these results suggest that COSMOThermX can provide some insight into the molecular interactions within the liquid phase.

Downloaded by UNIV OF DELAWARE MORRIS LIB on June 28, 2012 | http://pubs.acs.org
Publication Date (Web): December 18, 2009 | doi: 10.1021/bk-2009-1030.ch024

Downloaded by UNIV OF DELAWARE MORRIS LIB on June 28, 2012 | http://pubs.acs.org
Publication Date (Web): December 18, 2009 | doi: 10.1021/bk-2009-1030.ch024

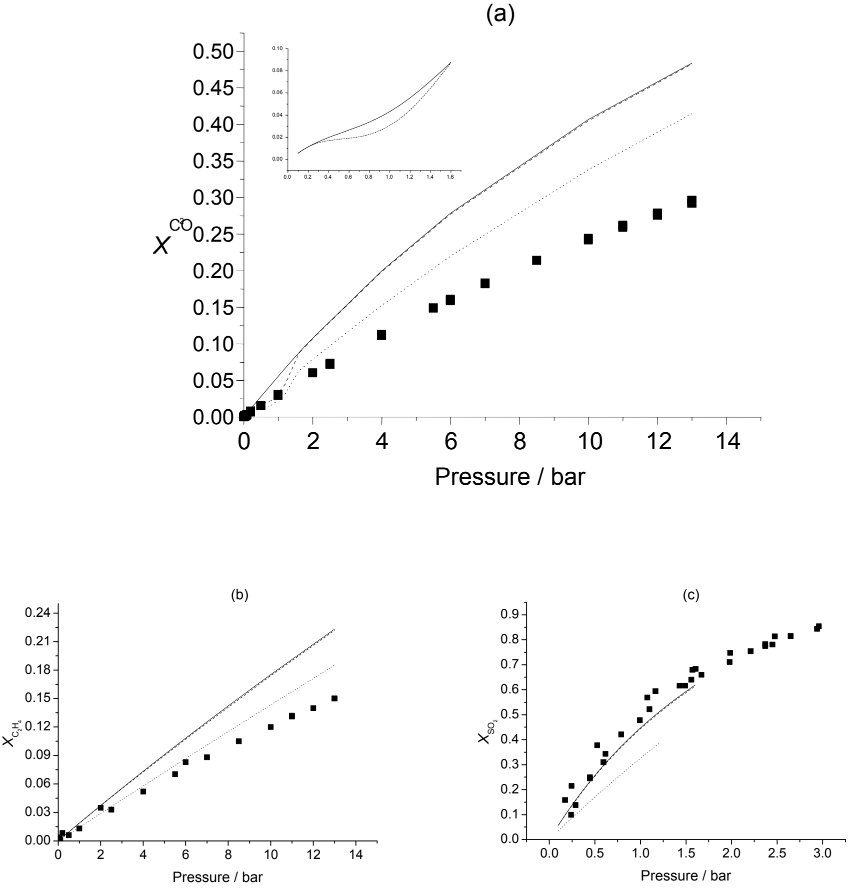

*Figure 8. Effect of conformers and ion pairs on the gas solubility in $[C_4mim][NTf_2]$. Points = Literature data, solid line = single gas conformer, dashed line = 20 liquid conformers (ions), dotted line = 5 liquid ion-pairs. (a) = $CO_2$, (b) = $SO_2$ and (c) = $C_2H_4$*

As a final note, it is worth mentioning that, like all software, COSMOthermX is undergoing continuing improvements to both its GUI and calculation engine. At the time of writing, the current release was COSMOthermX C2.1 Revision 1.08. While there are differences between the two revisions, these are small. For example, in the estimation of vapour pressure, the same trends were observed, in particular the sensitivity to the energy value. For ethane, the calculated vapour pressure was approximately 7% higher at a given temperature than release 1.06. Similar results were found for other gases such as $CO_2$. In terms of gas solubility, the increased vapour pressures resulted in a decrease in the gas solubility. Even when the vapour pressure data were used, the calculated gas solubilities were slightly lower than the earlier release. Due to this, the discussion of the trends noted above is still considered valid for this later release.

## Conclusions

Since ionic liquids have significant potential to be developed as “green” solvents for chemical processes, as well as being employed in gas separations, the need for the development of preliminary selection tools capable of assessing or scanning suitable ionic liquids for specific applications with minimal information available has increased. Using theoretical prediction capabilities of COSMOthermX, which are based on the COSMO-RS thermodynamic model, the solubilities of several gases in ionic liquids were evaluated and compared with experimentally reported data collected from the IUPAC database. Of the two components required for a gas solubility prediction (vapour pressure and activity), accurate vapour pressure determination would appear to be the most difficult to obtain. While the above studies have focused on gases where vapour pressure correlations exist, the techniques can be also extended to those gases where the temperature is significantly greater than the critical temperature of the gas. These results will only be summarised here, as this paper was aimed at highlighting the vapour pressure problem and investigating the activity component of the gas solubility prediction, rather than the combination of activity and vapour pressure. In these studies it was observed, perhaps unsurprisingly, that for those gases with vapour pressures outside the range of the correlations used, or which only required slight extrapolation, the gas solubility predictions are in general better when using the energy value. Therefore, when the system temperature ($T$) is below the critical temperature ($T_c$), the general trend is that better predictions are obtained for gases when using experimental correlations such as the Antoine or Wagner, while the energy value is preferred when $T >> T_c$. Like all rules, there are exceptions such as in the case of $CO_2$, and for other gases new correlations were found to be necessary. However without accurate values for *pseudo*-vapour pressures at $T >> T_c$, it is impossible to state, at this stage, the accuracy of the activity model for any system, be it ionic liquid or not, for gas solubility predictions at temperatures much greater than $T_c$.

For the case of $T < T_c$, it has been demonstrated that COSMOthermX is able to qualitatively predict the gas solubility in ionic liquids by describing the correct gas solubility order of magnitude, when compared with the literature. Furthermore, for a specific combination of an ionic liquid and a gas, the correct trend is predicted for both the effect of temperature and pressure. With only the odd exception, the trends were also predicted for the effect of cation and anion. From a chemical engineering or applied chemistry point of view, this information is thus highly useful in terms of estimating gas solubility in ionic liquids as functions of anion and cation, as well as the choice of gases. Furthermore, the qualitative prediction of COSMOthermX may be used to reduce the range of preliminary experimental measurements necessary to

Downloaded by UNIV OF DELAWARE MORRIS LIB on June 28, 2012 | http://pubs.acs.org
Publication Date (Web): December 18, 2009 | doi: 10.1021/bk-2009-1030.ch024

examine suitable ionic liquids prior to making detailed experimental measurements on specific properties of ionic liquids.

## Acknowledgements

The authors would like to thank the UK EPSRC under a portfolio partnership for financially supporting this work. NAM acknowledges funding from Petronas for supporting her studentship. P. Nancarrow (QUB) and F. Eckert (COSMOlogic) are acknowledged for useful discussions.

Downloaded by UNIV OF DELAWARE MORRIS LIB on June 28, 2012 | http://pubs.acs.org
Publication Date (Web): December 18, 2009 | doi: 10.1021/bk-2009-1030.ch024

## References

1. Earle, M. J.; Esperanca, J. M. S. S.; Gilea, M. A.; Canongia, Lopes J. N.; Rebelo, L. P. N.; Magee, J. W.; Seddon, K. R.; Widegren, J. A. The distillation and volatility of ionic liquids. *Nature* **2006**, *439*, 831-834.
2. Rasmussen, S. B.; Huang, J.; Riisager, A.; Hamma, H.; Rogez, J.; Winnick, J.; Wasserscheid, P.; Fehrmann, R. Flue gas cleaning with alternative processes and reaction media. *ECS Transactions* **2007**, *3*, 49-59.
3. Polshettiwar, V; Varma, R. S. Microwave-Assisted Organic Synthesis and Transformations using Benign Reaction Media. *Acc. Chem. Res.* **2008**, *41*, 629-639.
4. Xu, Q.; Kennedy, J. F.; Liu, L. An ionic liquid as reaction media in the ring opening graft polymerization of ε-caprolactone onto starch granules. *Carbohydrate Polymers* **2008**, *72*, 113-121.
5. Kumar, A.; Pawar, S. S. Ionic Liquids as Powerful Solvent Media for Improving Catalytic Performance of Silyl Borate Catalyst to Promote Diels-Alder Reactions. *J. Org. Chem.* **2007**, *72*, 8111-8114.
6. Lombardo, M.; Pasi, F.; Trombini, C.; Seddon, K. R.; Pitner, W. R. Task-specific ionic liquids as reaction media for the cobalt-catalysed cyclotrimerisation reaction of arylethynes. *Green Chem.* **2007**, *9*, 321-322.
7. Riisager, A.; Fehrmann, R.; Haumann, M.; Wasserscheid, P. Supported ionic liquids: versatile reaction and separation media. *Topics in Catalysis* **2006**, *40*, 91-102.
8. Amigues, E.; Hardacre, C.; Keane, G.; Migaud, M.; O'Neill, M. Ionic liquids - media for unique phosphorus chemistry. *Chem. Commun.* **2006**, 72-74.
9. Sheldon, R. Catalytic reactions in ionic liquids. *Chem. Commun.* **2001**, 2399-2407.
10. Joni, J.; Wasserscheid, P. Kinetic studies of rapid alkylation reaction in liquid-liquid biphasic reaction using acidic ionic liquid catalyst. *Abstracts of Papers, 236th ACS National Meeting, Philadelphia, PA, United States,* August 17-21, 2008.
11. Li, H.; Yu, S.; Liu, F.; Xie, C.; Li, L. Synthesis of dioctylphthalate using acid functionalized ionic liquid as catalyst. *Catalysis Commun.* **2007**, *8*, 1759-1762.

12. Choi, D. S.; Kim, J. H.; Shin, U. S.; Deshmukh, R. R.; Song, C. E. Thermodynamically- and kinetically-controlled Friedel-Crafts alkenylation of arenes with alkynes using an acidic fluoroantimonate(v) ionic liquid as catalyst. *Chem. Commun. 2007*, 3482-3484.
13. Ranu, B. C.; Banerjee, S.; Jana, R. Ionic liquid as catalyst and solvent: the remarkable effect of a basic ionic liquid, [bmim][OH] on Michael addition and alkylation of active methylene compounds. *Tetrahedron* 2006, *63*, 776-782.
14. Gu, Y.; Ogawa, C.; Kobayashi, J.; Mori, Y.; Kobayashi, S. A heterogeneous silica-supported scandium/ ionic liquid catalyst system for organic reactions in water. *Angew. Chem. Int. Ed.* **2006**, *45*, 7217-7220.
15. Zheng, Z.; Wu, T.; Zheng, R.; Wu, Y.; Zhou, X. Study on the synthesis of quaternary ammonium salts using imidazolium ionic liquid as catalyst. *Catalysis Commun.* **2006**, *8*, 39-42.
16. Bica, K.; Gaertner, P. An iron-containing ionic liquid as recyclable catalyst for aryl Grignard cross-coupling of alkyl halides. *Org. Lett.* **2006**, *8*, 733-5.
17. Arce, A.; Earle, M. J.; Katdare, S. P.; Rodriguez, H.; Seddon, K. R. Mutually immiscible ionic liquids. *Chem. Commun.* **2006**, 2548-50
18. Canongia Lopes, J. N.; Costa Gomes, M. F.; Padua, A. A. H. Nonpolar, polar, and associating solutes in ionic liquids. *J. Phys. Chem. B*. **2006**, *110*, 16816-16818.
19. Hussey, C. L. Room temperature haloaluminate ionic liquids. Novel solvents for transition metal solution chemistry. *Pure Appl. Chem.* **1988**, *60*, 1763-72.
20. Cole, A. C.; Jensen, J. L.; Ntai, I.; Tran, K. L. T.; Weaver, K. J.; Forbes, D. C.; Davis, J. H., Jr. Novel Bronsted Acidic Ionic Liquids and Their Use as Dual Solvent-Catalysts. *J. Am. Chem. Soc.* **2002**, *124*, 5962-5963.
21. Xie, H.; Li, S.; Zhang, S. Ionic liquids as novel solvents for the dissolution and blending of wool keratin fibers. *Green Chem.* **2005**, *7*, 606-608.
22. Weng, J.; Wang, C.; Li, H.; Wang, Y. Novel quaternary ammonium ionic liquids and their use as dual solvent-catalysts in a hydrolytic reaction. *Green Chem.* **2006**, *8*, 96-99.
23. Meindersma, G. W.; de Haan, A. B. Conceptual process design for aromatic/aliphatic separation with ionic liquids. *Chem. Eng. Res. Design* **2008**, *86*, 745-752.
24. Davis, S. E.; Morton, S. A., III. Investigation of Ionic Liquids for the Separation of Butanol and Water. *Sep. Sci. Tech.* **2008**, *43*, 2460-2472.
25. Hecht, S. E.; Price, K. N.; Berger, P. S.; Foley, P. R.; Hutton, H. D.; Showell, M. S.; Gardner, R. R.; Niehoff, R. L.; Seddon, K. R.; Gunaratne, H. Q. N.; Earle, M. Multiphase cleaning compositions having ionic liquid phase, cleaning a surface, and forming multiphase composition. *U.S. Pat. Appl. Publ.* 2006090777, **2006**, 10 pp.
26. Hacker, V.; Wallnoefer, E.; Wieser, B.; Kalb, R. Application of ionic liquids for fuel cells. *Abstracts of Papers, 236th ACS National Meeting, Philadelphia, PA, United States*, August 17-21, **2008**.

Downloaded by UNIV OF DELAWARE MORRIS LIB on June 28, 2012 | http://pubs.acs.org
Publication Date (Web): December 18, 2009 | doi: 10.1021/bk-2009-1030.ch024

27. Brotherston, I. D.; Bancroft, J. L. Ionic liquid based on quaternary ammonium compound, and applications. *UK Pat. Appl. GB2007 001084,* **2007**, 36 pp.

28. Nakamoto, H.; Watanabe, M. Bronsted acid-base ionic liquids for fuel cell electrolytes. *Chem. Commun.* **2007**, 2539-2541.

29. Zhang, M.; Reddy, R. G. Application of [$C_4$min][$Tf_2N$] ionic liquid as thermal storage and heat transfer fluids. *ECS Transactions* **2007**, *2*, 27-34.

30. Gurin, M. H. Nano-ionic liquids and methods of use. *PCT Int. Appl.* **2006**, 21pp.

31. Zhao, H. Innovative applications of ionic liquids as "green" engineering liquids. *Chem. Eng. Commun.* **2006**, *193*, 1660-1677.

32. Han, X.; Armstrong, D. W. Ionic liquids in separations. *Acc. Chem. Res.* **2007**, *40*, 1079-86.

33. Berthod, A.; Ruiz-Angel, M. J.; Carda-Broch, S. Ionic liquids in separation techniques. *J. Chrom. A* **2008**, *1184*, 6-18.

34. Seddon, K. R. *The International George Papathedorou Symposium: Proceedings (Ed.:S.Boghosian), Institute of Chemical Engineering and High Temperature Chemical Processes, Patras, Greece* **1999**, 131-135

35. Katritzky, A. R.; Jain, R.; Lomaka, A.; Karelson, M.; Visser, A. E.; Rogers, R. D. Correlation of the melting points of potential ionic liquids (imidazolium bromides and benzimidazolium bromides) using the CODESSA program. *J. Chem. Inf. Comput. Sci.* **2002**, *42*, 225-231.

36. Camper, D.; Scovazzo, P.; Koval, C.; Noble, R. D. Gas Solubilities in Room-Temperature Ionic Liquids. *Ind. Eng. Chem. Res.* **2004**, *43*, 3049-3054.

37. Scovazzo, P.; Camper, D.; Kieft, J.; Poshusta, J.; Koval, C.; Noble R. Regular Solution Theory and $CO_2$ Gas Solubility in Room-Temperature Ionic Liquids. *Ind. Eng. Chem. Res.* **2004**, *43*, 6855-6860.

38. Camper, D.; Becker, C.; Koval, C.; Noble R. D. Low Pressure Hydrocarbon Solubility in Room Temperature Ionic Liquids Containing Imidazolium Rings Interpreted Using Regular Solution Theory. *Ind. Eng. Chem. Res.* **2005**, *44*, 1928-1933.

39. Finotello, A.; Bara, J. E.; Camper, D.; Noble, R. D. Room-Temperature Ionic Liquids: Temperature Dependence of Gas Solubility Selectivity. *Ind. Eng. Chem. Res.* **2008**, *47*, 3453-3459.

40. Finotello, A.; Bara, J. E.; Narayan, S.; Camper D.; Noble R. D. Ideal Gas Solubilities and Solubility Selectivities in a Binary Mixture of Room-Temperature Ionic Liquids. *J. Phys. Chem. B.* **2008**, *112*, 2335-2339.

41. Ally, M. R.; Braunstein, J.; Baltus, R. E.; Dai S. Irregular Ionic Lattice Model for Gas Solubilities in Ionic Liquids. *Ind. Eng. Chem. Res.* **2004**, *43*, 1296-1301.

42. Kroon, M. C.; Karakatsini, E. K.; Economou, I. G. Modeling of the Carbon Dioxide Solubility in Imidazolium-Based Ionic Liquids with the tPC-PSAFT Equation of State. *J. Phys. Chem. B* **2006**, *110*, 9262-9269.

43. Shiflett, M. B.; Yokozeki, A. Solubilities and Diffusivities of Carbon Dioxide in Ionic Liquids: [bmim][$PF_6$] and [bmim][$BF_4$]. *Ind. Eng. Chem. Res.* **2005**, *44*, 4453-4464.

Downloaded by UNIV OF DELAWARE MORRIS LIB on June 28, 2012 | http://pubs.acs.org
Publication Date (Web): December 18, 2009 | doi: 10.1021/bk-2009-1030.ch024

44. Shariati, A.; Peters, C. J. High-Pressure phase behaviour of systems with ionic liquids: measurement and modeling of the binary system fluoroform + 1-ethyl-3-methylimidazolium hexafluorophosphate. *J. Supercrit. Fluids* **2003**, *25*, 109-117.
45. Urukova, I.; Vorholz, J.; Maurer, G. Solubility of $CO_2$, CO, and $H_2$ in the Ionic Liquid [bmim][$PF_6$] from Monte Carlo Simulations. *J. Phys. Chem. B* **2005**, *109*, 12154-12159.
46. Kumelan, J.; Kamps, A. P.-S.; Urukova, I.; Tuma, D.; Maurer, G. Solubility of oxygen in the ionic liquid [bmim][$PF_6$]: Experimental and molecular simulation results. *J. Chem. Thermodyn.* **2005**, *37*, 595-602.
47. Shah, J. K.; Maginn, E. J. Monte Carlo Simulations of Gas Solubility in the Ionic Liquid 1-n-Butyl-3-methylimidazolium Hexafluorophosphate. *J. Phys. Chem. B* **2005**, *109*, 10395-10405.
48. Shah, J. K.; Maginn, E. J. A Monte Carlo simulation study of the ionic liquid 1-*n*-butyl-3-methylimidazolium hexafluorophosphate: liquid structure, volumetric properties and infinite dilution solution thermodynamics of $CO_2$. *Fluid Phase Equilib.* **2004**, *222-223*, 195-203.
49. Cadena, C.; Zhao, Q.; Snurr, R. Q.; Maginn, E. J. Molecular Modeling and Experimental Studies of the Thermodynamic and Transport Properties of Pyridinium-Based Ionic Liquids. *J. Phys. Chem. B* **2006**, *110*, 2821-2832.
50. Cadena, C.; Anthony, J. L.; Shah, J. K.; Morrow, T. I.; Brennecke, J. F.; Maginn, E. J. Why Is CO2 So Soluble in Imidazolium-Based Ionic Liquids? *J. Am. Chem. Soc.* **2004,** *126*, 5300-5308.
51. Morrow, T. I.; Maginn, E. J. Molecular Dynamic Study of the Ionic Liquid 1-n-Butyl-3-methylimidazolium Hexafluorophosphate. *J. Phys. Chem. B* **2002**, *106*, 12807-12813.
52. Shah, J. K.; Brennecke, J. F.; Maginn, E. J. Thermodynamic properties of the ionic liquid 1-n-butyl-3-methylimidazolium hexafluorophosphate from Monte Carlo simulations. *Green Chem.* **2002**, *4*, 112-118.
53. Costa Gomes, M. F.; Padua, A. A. H. Gas-liquid interactions in solution. *Pure Appl. Chem.* **2005**, *77*, 653-665.
54. Kim, Y. S.; Choi, W. Y.; Jang, J. H.; Lee, C. S. Solubility measurement and prediction of carbon dioxide in ionic liquids. *Fluid Phase Equilib.* **2005**, *228-229*, 439-445.
55. Kim, Y. S.; Jang, J. H.; Lim, B. D.; Kang, J. W.; Lee, C. S. Solubility of mixed gases containing carbon dioxide in ionic liquids: Measurements and predictions. *Fluid Phase Equilib.* **2007**, *256*, 70-74.
56. Katritzky, A. R.; Kuanar, M.; Stoyanova-Slavova, I. B.; Slavov, S. H.; Dobchev, D. A.; Karelson, M.; Acree, Jr. W. E. Quantitative Structure–Property Relationship Studies on Ostwald Solubility and Partition Coefficients of Organic Solutes in Ionic Liquids. *J. Chem. Eng. Data* **2008**, *53*, 1085-1092.
57. Kilaru, P. K.; Condemarin, R. A.; Scovazzo, P. Correlations of Low-Pressure Carbon Dioxide and Hydrocarbon Solubilities in Imidazolium-, Phosphonium-, and Ammonium-Based Room-Temperature Ionic Liquids. Part 1. Using Surface Tension. *Ind. Eng. Chem. Res.* **2008**, *47*, 900-909.

Downloaded by UNIV OF DELAWARE MORRIS LIB on June 28, 2012 | http://pubs.acs.org
Publication Date (Web): December 18, 2009 | doi: 10.1021/bk-2009-1030.ch024

58. Kilaru, P. K.; Scovazzo, P. Correlations of Low-Pressure Carbon Dioxide and Hydrocarbon Solubilities in Imidazolium-, Phosphonium-, and Ammonium-Based Room-Temperature Ionic Liquids. Part 2. Using Activation Energy of Viscosity. *Ind. Eng. Chem. Res.* **2008**, *47*, 910-919.
59. Qin, Y.; Prausnitz, J. M. Solubilities in Ionic Liquids and Molten Salts from a Simple Perturbed-Hard-Sphere Theory. *Ind. Eng. Chem. Res.* **2006**, *45*, 5518-5523.
60. Freire, M. G.; Santos, L. M. N. B. F.; Marrucho, I. M.; Coutinho, J. A. P. Evaluation of COSMO-RS for the prediction of LLE and VLE of alcohols + ionic liquids. *Fluid Phase Equilib.* **2007**, *255*, 167-178.
61. Wilson, G. M. Vapor-liquid equilibrium. XI. A new expression for the excess free energy of mixing. *J. Am. Chem. Soc.* **1964**, *86*, 127-130.
62. Abrams, D. S.; Prausnitz, J. M. Statistical thermodynamics of liquid mixtures. A new expression for the excess Gibbs energy of partly and completely miscible systems. *AIChE J.* **1975**, *21*, 116-128.
63. Smith, J. M.; van Ness, H. C.; Abbot, M. M. Introduction to chemical engineering thermodynamics, *5 Ed.*, McGraw-Hill, New York, **1996**.
64. Prausnitz, J. M.; Lichtenthaler, R.N.; de Azevedo, E.G. Molecular thermodynamics of fluid-phase equilibria, *2 ed.*, Prentice-Hall, Englewood Cliffs, New Jersey, **1986**.
65. Raal, J. D.; Muhlbauer, A.L. Phase equilibria : measurement and computation, Taylor and Francis, Washington, **1997**.
66. Fredenslund, A.; Jones, R. L.; Prausnitz, J. M. Group-contribution estimation of activity coefficients in nonideal liquid mixtures. *AlChE J.* **1975**, *21*, 1086-1099.
67. Weidlich, U.; Gmehling, J. A Modified UNIFAC Model. 1. Prediction of VLE, hE, and gamma Infinite. *Ind. Eng. Chem. Res.* **1987**, *26*, 1372-1381.
68. Larsen, B. L.; Rasmussen, P.; Fredenslund, A. A modified UNIFAC group contribution model for prediction of phase equilibria and heats of mixing. *Ind. Eng. Chem. Res.* **1987**, *26*, 2274-2286.
69. Renon, H.; Prausnitz, J. M. Local composition in thermodynamic excess functions for liquid mixtures. *AIChE J.* **1968**, *14*, 135-144.
70. COSMOtherm & COSMOthermX, Version C2.1 Revision 01.06, (C) **1999-2006** COSMOlogic GmbH & Co KG, Bursheider Str. 515, D-51381 Leverkusen, Germany.
71. Eckert, F.; Klamt, A. COSMO*therm*, Version C2.1, Release 01.06, **2006,** COSMO*logic* GmbH & Co. KG, Leverkusen, Germany.
72. Eckert, F.; Klamt A. Fast Solvent Screening via Quantum Chemistry: COSMO-RS approach. *AlChE J.* **2002**, *48*, 369-385.
73. Kolár, P.; Nakata, H.; Shen, J.-W.; Tsuboi, A.; Suzuki, H.; Ue, M. Prediction of gas solubility in battery formulations. *Fluid Phase Equilib.* **2005**, *228-229*, 59-66.
74. Xiaochun, Z.; Zhiping, L.; Wenchuan, W. Screening of ionic liquids to capture $CO_2$ by COSMO-RS and experiments. *AIChE J.* **2008**, *54*, 2717-2728.

Downloaded by UNIV OF DELAWARE MORRIS LIB on June 28, 2012 | http://pubs.acs.org
Publication Date (Web): December 18, 2009 | doi: 10.1021/bk-2009-1030.ch024

Downloaded by UNIV OF DELAWARE MORRIS LIB on June 28, 2012 | http://pubs.acs.org
Publication Date (Web): December 18, 2009 | doi: 10.1021/bk-2009-1030.ch024

75. Eckert, F.; Klamt, A. COSMOtherm User's Manual: Version C2.1, Release 01.06 **2006**, COSMO*logic* GmbH & Co. KG, Leverkusen, Germany.
76. Gaussian View 3.0 **2000-2003**, Gaussian, Inc.; Semichem, Inc.; Pittsburgh, USA.
77. Ahlrichs, R. TURBOMOLE User's Manual: Version 5.7 **2004**, COSMO*logic* GmbH & Co. KG, Leverkusen, Germany.
78. Schäfer, A.; Huber, C.; Ahlrichs, R. Fully Optimized Contracted Gaussian-Basis Sets of Triple Zeta Valence Quality for Atoms Li to Kr. *J Chem. Phys.* **1994**, *100*, 5829-5835.
79. Dong, Q.; Muzny, C. D.; Kazakov, A.; Diky, V.; Magee, J. W.; Widegren, J. A.; Chirico, R. D.; Marsh, K. N.; Frenkel, M. ILThermo: A Free-Access Web Database for Thermodynamic Properties of Ionic Liquids. *J. Chem. Eng. Data* **2007**, *52*, 1151-1159 - updated in June 2008.
80. Husson-Borg, P.; Majer, V.; Costa Gomes, M. F. Solubilities of oxygen and carbon dioxide in butyl methyl imidazolium tetrafluoroborate as a function of temperature and at pressures close to atmospheric. *J. Chem. Eng. Data* **2003**, *48*, 480-485.
81. Jacquemin, J.; Costa Gomes, M. F.; Husson, P.; Majer, V. Solubility of carbon dioxide, ethane, methane, oxygen, nitrogen, hydrogen, argon and carbon monoxide in 1-butyl-3-methylimidazolium tetrafluoroborate between temperature 283K and 343 K and at pressures close to atmospheric. *J. Chem. Thermodyn.* **2006**, *38*, 490-502.
82. Jacquemin, J.; Husson, P.; Majer, V.; Costa Gomes, M. F. Low-pressure solubilities and thermodynamics of solvation of eight gases in 1-butyl-3-methylimidazolium hexafluorophosphate. *Fluid Phase Equilib.* **2006**, *240*, 87-95.
83. Anthony, J. L.; Maginn, E. J.; Brennecke, J. F. Solubilities and Thermodynamic Properties of Gases in the Ionic Liquid 1-n-Butyl-3-methylimidazolium Hexafluorophosphate. *J. Phys. Chem. B* **2002**, *106*, 7315-7320.
84. Anthony, J. L.; Anderson, J. L.; Maginn E. J.; Brennecke J. F. Anion Effects on Gas Solubility in Ionic Liquids. *J. Phys. Chem.* **2005**, *109*, 6366-6374.
85. Kumelan, J.; Kamps, A. P.-S.; Tuma, D.; Maurer, G. Solubility of $H_2$ in the Ionic Liquid [bmim][$PF_6$]. *J. Chem. Eng. Data* **2006**, *51*, 11-14.
86. Kumelan, J.; Kamps, A. P.-S.; Tuma, D.; Maurer, G. Solubility of $H_2$ in the Ionic Liquid [hmim][$Tf_2N$]. *J. Chem. Eng. Data* **2006**, *51*, 1364-1367.
87. Kumelan, J.; Kamps, A. P.-S.; Tuma, D.; Maurer, G. Solubility of CO in the ionic liquid [bmim][$PF_6$]. *Fluid Phase Equilib.* **2005**, *228-229*, 207-211.
88. Costa Gomes, M. F. Low-pressure Solubility and Thermodynamics of Solvation of Carbon Dioxide, Ethane, and Hydrogen in 1-Hexyl-3-methylimidazolium Bis(trifluoromethylsulfonyl)amide between Temperatures of 283 K and 343 K. *J. Chem. Eng. Data* **2007**, *52*, 472-475.

89. Shariati, A.; Peters, C. J. High-Pressure phase behaviour of systems with ionic liquids: II. The binary system carbon dioxide + 1-ethyl-3-methylimidazolium hexafluorophosphate. *J. Supercrit. Fluids* **2004**, *29*, 43-48.
90. Chen, Y.; Zhang, S.; Yuan, X.; Zhang, Y.; Zhang, X.; Dai, W.; Mori, R. Solubility of $CO_2$ in imidazolium-based tetrafluoroborate ionic liquids. *Thermochim. Acta* **2006**, *441*, 42-44.
91. Aki, S. N. V. K.; Mellein, B. R.; Saurer, E. M.; Brennecke, J. F. High-Pressure Phase Behaviour of Carbon Dioxide with Imidazolium-Based Ionic Liquids. *J. Phys. Chem. B* **2004**, *108*, 20355-20365.
92. Blanchard, L. A.; Gu, Z.; Brennecke, J. F. High-Pressure Phase Behaviour of Ionic Liquid/$CO_2$ Systems. *J. Phys. Chem. B* **2001**, *105*, 2437-2444.
93. Kamps, A. P.-S.; Tuma, D.; Xia, J.; Maurer, G. Solubility of $CO_2$ in the Ionic Liquid [bmim][$PF_6$]. *J. Chem. Eng. Data* **2003**, *48*, 746-749.
94. Zhang, S.; Yuan, X.; Chen, Y.; Zhang, X. Solubilities of $CO_2$ in 1-Butyl-3-methylimidazolium Hexafluorophosphate and 1,1,3,3-Tetramethylguanidium Lactate at Elevated Pressures. *J. Chem. Eng. Data* **2005**, *50*, 1582-1585.
95. Shiflett, M. B.; Yokozeki, A. Solubility and Diffusivity of Hydrofluorocarbons in Room-Temperature Ionic Liquids. *AIChE J.* **2006**, *52*, 1205-1219.
96. Lee, B.-C.; Outcalt, L. Solubilities of Gases in the Ionic Liquid 1-n-Butyl-3-methylimidazolium Bis(trifluoromethylsulfonyl)imide. *J. Chem. Eng. Data* **2006**, *51*, 892-897.
97. Kumelan, J.; Kamps, A. P.-S.; Tuma, D.; Maurer, G. Solubility of $CO_2$ in the Ionic Liquids [bmim][$CH_3SO_4$] and [bmim][$PF_6$]. *J. Chem. Eng. Data* **2006**, *51*, 1802-1807.
98. Constantini, M.; Toussaint, V. A.; Shariati, A.; Peters, C. J.; Kikic, I. High-Pressure Phase Behavior of Systems with Ionic Liquids: Part IV. Binary System Carbon Dioxide + 1-Hexyl-3-methylimidazolium Tetrafluoroborate. *J. Chem. Eng. Data* **2005**, *50* , 52-55.
99. Shariati, A.; Peters, C. J. High-Pressure phase behaviour of systems with ionic liquids Part III. The binary system carbon dioxide + 1-hexyl-3-methylimidazolium hexafluorophosphate. *J. Supercrit. Fluids* **2004**, *30*, 139-144.
100. Kumelan, J.; Kamps, A. P.-S.; Tuma, D.; Maurer, G. Solubility of $CO_2$ in the Ionic Liquids [hmim][$Tf_2N$]. *J. Chem. Eng. Data* **2006**, *38*, 1396-1401.
101. Anderson, J. L.; Dixon, J. K.; Maginn, E. J.; Brennecke, J. F. Measurement of $SO_2$ Solubility in Ionic Liquids. *J. Phys. Chem. B* **2006**, *110*, 15059-15062.
102. Jacquemin, J.; Husson, P.; Majer, V.; Costa Gomes, M. F. Influence of the Cation on the Solubility of $CO_2$ and $H_2$ in Ionic Liquids Based on the Bis(trifluoromethylsulfonyl)imide Anion. *J. Solution Chem.* **2007**, *36*, 967–979.
103. Hong, G.; Jacquemin, J.; Husson, P.; Costa Gomes, M. F.; Deetlefs, M.; Nieuwenhuyzen, M.; Sheppard, O.; Hardacre, C. Effect of Acetonitrile

Downloaded by UNIV OF DELAWARE MORRIS LIB on June 28, 2012 | http://pubs.acs.org
Publication Date (Web): December 18, 2009 | doi: 10.1021/bk-2009-1030.ch024

on the Solubility of Carbon Dioxide in 1-Ethyl-3-methylimidazolium Bis(trifluoromethylsulfonyl)amide. *Ind. Eng. Chem. Res.* **2006**, *45*, 8180-8188.

104. Hong, G.; Jacquemin, J.; Deetlefs, M.; Hardacre, C.; Husson, P.; Costa Gomes, M. F. Solubility of carbon dioxide and ethane in three ionic liquids based on the bis{(trifluoromethyl)sulfonyl}imide anion. *Fluid Phase Equilib.* **2007**, *257*, 27-34.
105. Kumelan, J.; Kamps, A.; Tuma, D.; Maurer, G. Solubility of the single gases $H_2$ and CO in the ionic liquid [bmim][$CH_3SO_4$]. *Fluid Phase Equilib.* **2007**, *260*, 3-8.
106. Kumelan, J.; Kamps, A. P.-S.; Tuma, D.; Maurer, G. Solubility of the Single Gases Methane and Xenon in the Ionic Liquid [bmim][$CH_3SO_4$]. *J. Chem. Eng. Data* **2007**, *52*, 2319-2324.
107. Kumelan, J.; Kamps, A. P.-S.; Tuma, D.; Maurer, G. Solubility of the Single Gases Methane and Xenon in the Ionic Liquid [hmim][$Tf_2N$]. *Ind. Eng. Chem. Res.* **2007**, *46*, 8236-8240.
108. Florusse, L. J.; Raeissi, S.; Peters, C. J. High pressure phase behaviour of ethane with 1-hexyl-3-methylimidazolium bis(trifluoromethylsulfonyl)imide. *J. Chem. Eng. Data* **2008**, *53*, 1283-1285.
109. Schilderman, A. M.; Raeissi, S.; Peters, C. J. Solubility of carbon dioxide in the ionic liquid l-ethyl-3-methylimidazolium bis(trifluoromethylsulfony1)imide. *Fluid Phase Equilib.* ***2007, 260***, 19-22.
110. Shin, E.-K.; Lee, B.-C.; Lim, J. S. High-pressure solubilities of carbon dioxide in ionic liquids: l-Alkyl-3-methylimidazolium bis(trifluoromethylsulfonyl)imide. *J. Supercrit. Fluids* **2008**, *45*, 282-292.
111. Muldoon, M. J.; Aki, S. N. V. K.; Anderson, J. L.; Dixon, J. K.; Brennecke, J. F. Improving Carbon Dioxide Solubility in Ionic Liquids. *J. Phys. Chem. B* **2007**, *111*, 9001-9009.
112. Shiflett, M. B.; Kasprzak, D. J.; Junk, C. P.; Yokozeki, A. Phase behavior of {carbon dioxide + [bmim][Ac]} mixtures. *J. Chem. Thermodyn.* **2008**, *40*, 25-31.
113. Jiang, Y.-Y.; Zhou, Z.; Jiao, Z.; Li, L.; Wu, Y-T.; Zhang, Z.-B. $SO_2$ Gas Separation Using Supported Ionic Liquids Membranes. *J. Phys. Chem. B* **2007**, *111*, 5058-5061.
114. Antoine, C. *Comptes Rendus* **1888**, *107*, 1143-45.
115. Wagner, W. A New Correlation Method for Thermodynamic Data applied to the Vapour-pressure Curve for Argon, Nitrogen and Water. *IUPAC Thermodynamic Tables Project Centre* **1977,** PC/T 15, London.
116. Poling, B.; Prausnitz, J. M.; O'Connell, J. P. The Properties of Gases and Liquids, *5th Ed., McGraw Hill*, New York, **2000**.
117. http://webbook.nist.gov/chemistry/
118. http://www.cheric.org/research/kdb/

Downloaded by UNIV OF DELAWARE MORRIS LIB on June 28, 2012 | http://pubs.acs.org
Publication Date (Web): December 18, 2009 | doi: 10.1021/bk-2009-1030.ch024

Downloaded by STANFORD UNIV GREEN LIBR on June 28, 2012 | http://pubs.acs.org
Publication Date (Web): December 18, 2009 | doi: 10.1021/bk-2009-1030.ch025

## Chapter 25

# Predictive Group Contribution Models for the Thermophysical Properties of Ionic Liquids

**João A. P. Coutinho[1,*] and Ramesh L. Gardas[1,2,*]**

**[1]CICECO, Departamento de Química, Universidade de Aveiro, 3810-193 Aveiro, Portugal**
**[2]Present address: The QUILL Research Centre, School of Chemistry and Chemical Engineering, Queen's University of Belfast, BT9 5AG, Northern Ireland, United Kingdom**
**e-mail:** jcoutinho@ua.pt**;** r.gardas@qub.ac.uk

Ionic liquids have been the object of intense interest from both academic and industrial research groups aiming at a wide range of applications in novel processes and products. The knowledge of their thermophysical properties, or the ability to estimate them, is often required for the design of these processes and products. However, experimental data for many properties are in short supply and often contradictory among various sources available. Based on experimental data collected from the literature, predictive group contribution models were developed after a critical analysis of the data for various thermophysical properties, *viz.* density, viscosity, surface tension, speed of sound, refractive index, heat capacity, electrical conductivity, thermal conductivity, isobaric expansivity, and isothermal compressibility, of various families of ionic liquids. The results of the proposed models show average absolute relative deviations generally of the same order as the experimental accuracy of the data itself. These rapid and facile predictive models are very easy to use, can provide predictions of property values for the new ionic liquids, and also allow them to be extended to new groups of cations and anions as further data become available.

In Ionic Liquids: From Knowledge to Application; Plechkova, N., et al.;
ACS Symposium Series; American Chemical Society: Washington, DC, 2010.

# Introduction

Ionic liquids, due to their unique properties, are expected to replace volatile organic compounds (VOCs) in several applications and to produce important developments in the chemical industry *(1).* They result from the combination of large organic cations with inorganic or organic anions; the possible number of ionic liquids is estimated to be more than a trillion. Changes in the cation, anion, or the moieties attached to each ion of ionic liquid, will allow the thermophysical properties to be modified to meet the design criteria for a given application.

The study of thermophysical and transport properties and structure-property relationships of ionic liquids is lagging behind when compared with the investigations of their potential applications. Thermophysical properties are required for the design of processes and products involving these compounds. Yet the experimental data available are currently scarce for most properties, and often data from various sources are contradictory.

Given the huge number of potential ionic liquids, the experimental measurement of the thermophysical and transport properties for all ionic liquids of interest is infeasible. The alternative is to develop predictive models, based on some experimental data, from which the required properties with the desired accuracy can be obtained. The development of group contribution methods for the properties of ionic liquids is particularly apt for this purpose as (i) from a restricted amount of data, it will be possible to expand the information available to a large number of compounds, and (ii) it will also allow for a critical evaluation of the accuracy of available data.

The possibility of tailoring the properties of an ionic liquid to meet the requirements of some specific application makes ionic liquids designer solvents par excellence. Given the large number of potential ionic liquids, designing an ionic liquid by experimental trial an error or based on some empirical heuristics is not the most promising approach *(2).* The design of ionic liquids will certainly require the development of methods for Computer Aided Molecular Design (CAMD) of these compounds. Besides their obvious interest for the prediction of thermophysical and transport properties, group contribution methods are also at the basis of the development of CAMD methods *(3,4).*

In this work, we present a number of group-contribution methods for the estimation of thermophysical and transport properties of ionic liquids. Our goal is to show that these methods can be used for fast and easy prediction of physical properties, with acceptable deviations, for a wide range of ionic liquids.

In a previous series of articles, a number of predictive methods for density *(5),* surface tension *(6),* viscosity *(7),* speed of sound *(8),* liquid heat capacity *(9),* electrical conductivity, thermal conductivity, refractive index, isobaric expansivity, and isothermal compressibility *(10)* of ionic liquids have been proposed. Moreover, a correlation for the self diffusion coefficients of ionic liquids based on the Stokes-Einstein relation will also be proposed. It will be shown that the proposed models allow a good description of the respective experimental data available, usually within the agreement of the experimental data of different authors, as described in the report of the IUPAC task group for the development of standard systems for the measurement of thermodynamic

Downloaded by STANFORD UNIV GREEN LIBR on June 28, 2012 | http://pubs.acs.org
Publication Date (Web): December 18, 2009 | doi: 10.1021/bk-2009-1030.ch025

properties of ionic liquids (http://www.iupac.org/web/ins/2002-005-1-100). The effect of the cation, anion and alkyl chain length on the studied properties is discussed briefly.

## Collection of Physical Properties of Ionic Liquids

The experimental density, surface tension, viscosity, speed of sound, liquid heat capacity, electrical conductivity, self-diffusion coefficients, thermal conductivity, refractive index, isobaric expansivity and isothermal compressibility data of ionic liquids, collected from open literature, measured in our laboratory, and from the International Union of Pure and Applied Chemistry (IUPAC) database *(11)* have been used to develop predictive methods for the estimation of the these properties of ionic liquids. The following ionic liquid ions were considered in this study: cations, 1,3-dialkylimidazolium, $[C_n\text{mim}]^+$; 1-alkylpyridinium, $[C_n\text{py}]^+$; 1,1-dialkylpyrrolidinium, $[C_n\text{mpyrr}]^+$; 1,1-dialkylpiperidinium, $[C_n\text{mpip}]^+$; tetraalkylphosphonium, $[P_{w\,x\,y\,z}]^+$; and tetraalkylammonium, $[N_{w\,x\,y\,z}]^+$: anions, hexafluorophosphate, $[PF_6]^-$; tetrafluoroborate, $[BF_4]^-$; bis{(trifluoromethyl)sulfonyl}amide, $[NTf_2]^-$; chloride, $Cl^-$; ethanoate, $[CH_3COO]^-$; methyl sulfate, $[MeSO_4]^-$; ethyl sulfate, $[EtSO_4]^-$; trifluoromethanesulfonate, $[CF_3SO_3]^-$; bis{(perfluoroethyl)sulfonyl}amide, $[NPf_2]^-$; trifluoroethanoate, $[CF_3COO]^-$; dimethylphosphate, $[(CH_3)_2PO_4]^-$; methoxyethyl sulfate, $[CH_3OC_2H_4SO_4]^-$; dicyanamide, $[N(CN)_2]^-$; tricyanomethanide, $[C(CN)_3]^-$; tetrachloroferrate(III), $[FeCl_4]^-$; tetrachloroaluminate(III), $[AlCl_4]^-$, tetrachlorogallate(III), $[GaCl_4]^-$; tetrachloroindate(III), $[InCl_4]^-$; and trichlorozincate(II), $[ZnCl_3]^-$.

After collection of physical property data, a critical analysis was carried out before using it for parameter estimation. Group contribution parameters were obtained using at least two different ionic liquids. Single available ionic liquids with a new cation and/or anion were discarded in this study with the exception of a cation with three methyl groups attached to the imidazolium ring that was used to estimate the methyl group.

## Group Contribution Parameters Calculation

For each property, initially, available data for each individual ionic liquid were fitted to the appropriate predictive equations to obtain parameters. Then, by comparison of the parameter values of ionic liquids containing similar cations and anions, it was possible to make an initial estimation for the values of parameters for each cation and anion. Then the cation was split into the parent cation (heterocyclic ring, or alkylammonium, or alkylphosphonium), methylene, and methyl group. Using these initial estimates, the objective function (square of the difference of experimental and predicted property data) is minimised for all the data points available, to obtain optimum values of the group parameter.

Downloaded by STANFORD UNIV GREEN LIBR on June 28, 2012 | http://pubs.acs.org
Publication Date (Web): December 18, 2009 | doi: 10.1021/bk-2009-1030.ch025

# Results and Discussion

## Density

We proposed a predictive method for the estimation of ionic liquids densities *(5)* over a wide range of temperatures (273.15-393.15) K and pressures (0.10-100) MPa, according to Equation (1).

$$\rho = \frac{Mw}{NV(a + bT + cP)} \tag{1}$$

where $\rho$ is the density in kg $m^{-3}$, $Mw$ is molecular weight in kg $mol^{-1}$, N is the Avogadro constant, $V$ is the molecular volume in $Å^3$, $T$ is the temperature in K and $P$ is the pressure in MPa. The coefficients $a$, $b$ and $c$ were estimated by fitting Equation (1) to our previously published experimental data *(12,13).* About 800 density data points were used. The values of coefficient $a$, $b$ and $c$ obtained were $8.005\times10^{-1} \pm 2.333\times10^{-4}$, $(6.652\times10^{-4} \pm 6.907\times10^{-7})$ $K^{-1}$ and $(-5.919\times10^{-4} \pm 2.410\times10^{-6})$ $MPa^{-1}$ respectively, at a 95% confidence level. The average percentage deviation of the calculated densities from the experimental densities is 0.29%. The experimental density ($\rho_{exp}$) for the ionic liquids used to derive coefficients $a$, $b$ and $c$ of Equation (1) are in very good agreement with the corresponding calculated density ($\rho_{cal}$): $\rho_{exp} = (0.9998 \pm 0.0003)\rho_{cal}$ (correlation coefficient: $R^2 = 0.9989$, at a 95% level of confidence). For the density calculation, volume parameters ($V$) of ions and groups were either directly taken from literature *(14)* or calculated following the Jenkins' procedure *(15).* Experimental densities available in the literature for imidazolium, pyridinium, pyrrolidinium and alkylphosphonium derived ionic liquids were predicted by using Equation (1). Predicted densities ($\rho_{cal}$) are in good agreement with experimental literature densities ($\rho_{exp}$) over a wide range of temperatures (273.15–393.15 K) and pressures (0.10–100 MPa) *(4);* $\rho_{exp} = (0.9968 \pm 0.0004)\rho_{cal}$ for imidazolium-based ionic liquids and $\rho_{exp} = (1.0133 \pm 0.0010)\rho_{cal}$ for phosphonium-based ionic liquids. The mean percent deviation (MPD) of 0.45% is observed for 1086 data points of imidazolium-based ionic liquids, while that is 1.49% for 404 data points of phosphonium-based ionic liquids. A low MPD ranging from 0.41% to 1.57% was also observed for 31 data points of pyridinium and pyrrolidinium-based ionic liquids. Recently *(16,17),* it was shown that Equation (1) can be applied with confidence to the ionic liquids from families other than those used in the development of the correlation *(5).*

## Isobaric Expansivity

Isobaric expansivity data of ionic liquids are required for their development as heat transfer fluids or for heat storage applications or, as recently suggested, for ionic liquid based liquid-in-glass thermometers *(18).* The isobaric expansivity ($\alpha_P$) is defined by Equation (2).

Downloaded by STANFORD UNIV GREEN LIBR on June 28, 2012 | http://pubs.acs.org
Publication Date (Web): December 18, 2009 | doi: 10.1021/bk-2009-1030.ch025

$$\alpha_P = \frac{1}{V_\mathrm{m}}\left(\frac{\partial V_\mathrm{m}}{\partial T}\right)_P = -\frac{1}{\rho}\left(\frac{\partial \rho}{\partial T}\right)_P = -\left(\frac{\partial \ln \rho}{\partial T}\right)_P \quad (2)$$

where $V_m$ is molar volume, $\rho$ is density, and $T$ is temperature at constant pressure $P$.

A total of 109 data points for experimental isobaric expansivity of 49 ionic liquids (based on imidazolium, pyridinium, pyrrolidinium, piperidinium, phosphonium, and ammonium cations with 19 different anions, at 298.15 K and 0.1 MPa) were collected from the literature or calculated using experimental density data using Equation (2). In spite of the wide range of ionic liquids investigated, the isobaric expansivities observed fall in a narrow range of values: $4.48\times10^{-4}$ to $7.44\times10^{-4}$ $K^{-1}$ at 298.15 K. As discussed previously *(5)*, the precision to which this property is currently known precludes any study of its temperature dependency, as this is inferior to the experimental uncertainty. For this reason the isobaric expansivity will be here correlated at the temperature of 298.15 K and atmospheric pressure by a group contribution approach:

$$\alpha_P = A_{\alpha_P} = \sum_{i=1}^{k} n_i a_{i,\alpha_P} \quad (3)$$

where $n_i$ is the number of groups of type $i$, and $k$ is the total number of different groups in the molecule, and the estimated parameters $a_{i,\alpha\mathrm{P}}$ are presented in reference *(10)*.

For the studied ionic liquids, the calculated isobaric expansivity values ($\alpha_{\mathrm{P,cal}}$), using Equation (3) and group contribution parameters $a_{i,\alpha\mathrm{P}}$ *(10)*, are in good agreement with the corresponding experimental isobaric expansivity ($\alpha_{\mathrm{P,exp}}$) data; where $\alpha_{\mathrm{P,cal}} = (1.0007 \pm 0.0027)\alpha_{\mathrm{P,exp}}$. For 109 data points of 49 ionic liquids available in literature, the overall MPD is 1.98 %, with a maximum deviation of the order of 7 %. It was noticed that the isobaric expansivity of the studied ionic liquids is weakly dependent on the anion and increases slightly with the alkyl chain length of the cation *(10)*.

## Isothermal Compressibility

Isothermal compressibility of ionic liquids is relevant for the design of industrial fluids to be used in pumps or compressors *(19)*. The isothermal compressibility ($\kappa_T$) can be expressed by Equation (4).

$$k_T = -\frac{1}{V_\mathrm{m}}\left(\frac{\partial V_\mathrm{m}}{\partial P}\right)_T = \frac{1}{\rho}\left(\frac{\partial \rho}{\partial P}\right)_T = \left(\frac{\partial \ln \rho}{\partial P}\right)_T \quad (4)$$

A total of 26 data points for experimental isothermal compressibility directly available in the literature, or calculated using experimental density data using Equation (4) for 22 ionic liquids based on imidazolium, pyridinium, pyrrolidinium, piperidinium, and phosphonium cations with different anions, at

Downloaded by STANFORD UNIV GREEN LIBR on June 28, 2012 | http://pubs.acs.org
Publication Date (Web): December 18, 2009 | doi: 10.1021/bk-2009-1030.ch025

298.15 K and 0.1 MPa, were collected. As discussed previously *(5,16)*, the precision to which this property is known precludes any study of its temperature or pressure dependency, as this is inferior to the experimental uncertainty. For this reason, the isothermal compressibility was correlated at 298.15 K and atmospheric pressure by a group contribution approach in the studied range 0.33 to 0.73 $\text{GPa}^{-1}$ of experimental isothermal compressibility data

$$\kappa_T = A_{\kappa_T} = \sum_{i=1}^{k} n_i a_{i,\kappa_T} \tag{5}$$

where $n_i$ is the number of groups of type $i$, and $k$ is the total number of different groups in the molecule, and the parameters $a_{i,\kappa T,}$ are reported in reference *(10).*

For the studied ionic liquids, the isothermal compressibility ($\kappa_{T,\text{cal}}$), calculated using Equation (5) and group contribution parameters $a_{\text{i},}\kappa_T$ *(10)*, are in good agreement with the corresponding experimental isothermal compressibility ($\kappa_{T,\text{exp}}$) data; where $\kappa_{T,\text{cal}} = (1.0055 \pm 0.0064)\kappa_{T,\text{exp}}$. For 26 data points of 22 ionic liquids available in literature, the overall MPD is 2.53 % with a maximum deviation of the order of 6.7 %, and from these about 46.2 % of the estimated isothermal compressibility data having less than 1 % relative deviation. However, with the limited amount of experimental data, it is not possible to provide any definitive conclusion on the effect of cation, anion and alkyl chain length on isothermal compressibility of ionic liquids.

## Surface tension

Experimental data for the surface tension of ionic liquids is very scarce and essentially restricted to imidazolium-based ionic liquids. Using surface tension data of ionic liquids measured in our laboratory along with a database obtained from the literature, a correlation was developed for the surface tensions of ionic liquids *(6)* showing that it is possible to use the parachor to obtain good predictions for surface tension.

The surface tensions of ionic liquids can be obtained using Equation (6),

$$\sigma = (P_{\text{ch}}\rho/Mw)^4 \tag{6}$$

where $P_{\text{ch}}$ is the parachor which is calculated from Knotts *et al. (20)* parachor QSPR correlation, using the parameter table estimated from the second training set containing experimental surface tension values with an uncertainty less than 1%, and $\rho$ is the density obtained using Equation (1). Predicted surface tensions ($\sigma_{\text{cal}}$), from Equation (6), of imidazolium-based ionic liquids display a good agreement with the corresponding experimental surface tensions ($\sigma_{\text{exp}}$): $\sigma_{\text{cal}} = (0.987 \pm 0.004)\sigma_{\text{exp}}$. For the 361 data points for 38 imidazolium based ionic liquids studied, the overall MPD is 5.75 %, and a maximum deviation inferior to 16% observed.

Downloaded by STANFORD UNIV GREEN LIBR on June 28, 2012 | http://pubs.acs.org
Publication Date (Web): December 18, 2009 | doi: 10.1021/bk-2009-1030.ch025

The predictive capability of Equation (6) for ionic liquid surface tension was further checked below through its potential to correlate the speed of sound of ionic liquids through Auerbach's relation, as discussed in the next Section.

## Speed of sound

Experimental data for speed of sound in ionic liquids is scarce and limited to imidazolium-based ionic liquids. The speed of sound ($u$) in units of m $s^{-1}$ can be estimated, using the surface tension (σ) in N $m^{-1}$ units and density (ρ) in kg $m^{-3}$ units, through the theoretical Auerbach's relation *(21)*

$$u = (\sigma / 6.33\times10^{-10}\rho)^{a} \qquad (7)$$

where $a = 2/3$.

To examine the functional dependence of $u$ and $\sigma/\rho$, a double logarithmic plot was drawn using speed of sound data from the literature and density and surface tension obtained using Equations (1) and (6) respectively, and the resulting linear correlation was:

$$\log_{10} u_{\text{exp}} = (0.6199 \pm 0.0092)\log_{10}(\sigma / \rho) + (5.9447 \pm 0.0414) \qquad (8)$$

with a correlation coefficient $R^2 = 0.9717$ at 95% confidence level.

Although Equation (7) directly (with $a$=2/3) is not capable of predicting sound velocities of ionic liquids, a modified version of it, following the approach of Oswal *et al. (22,23)*, could be used to correlate the speed of sound in ionic liquids *(8)*.

The experimental speed of sound ($u_{\text{exp}}$) of imidazolium-based ionic liquids displays a good agreement with the corresponding calculated speed of sound ($u_{\text{cal}}$) using Equation (8) where $u_{\text{exp}} = (0.9952 \pm 0.0022)\, u_{\text{cal}}$. For the 133 data points of 14 imidazolium-based ionic liquids, the overall MPD is 1.96 % with a maximum deviation inferior to 5 %.

## Viscosity

Experimental viscosity data for ionic liquids are still in short supply and restricted to a few families of well-studied ionic liquids. In a previous work *(7)*, the viscosity of ionic liquids was correlated using an Orrick–Erbar-type approach *(24)* by estimating parameters $A$ and $B$ in Equation (9):

$$\ln\frac{\eta}{\rho.Mw} = A + \frac{B}{T} \qquad (9)$$

where $\eta$ and ρ are the viscosity in cP and density in g $cm^{-3}$, respectively. $Mw$ is the molecular weight and $T$ is the absolute temperature. $A$ and $B$ can be obtained by a group contribution method and the group contribution parameters for them are presented in *(7)*. Equation (9) was used for about 500 data points for 29 ionic liquids, providing a relative average deviation of 8 % and a maximum deviation of 28 %.

Downloaded by STANFORD UNIV GREEN LIBR on June 28, 2012 | http://pubs.acs.org
Publication Date (Web): December 18, 2009 | doi: 10.1021/bk-2009-1030.ch025

The Orrick–Erbar method requires knowledge of the density for the prediction of viscosity. To overcome this limitation, and to attempt the development of an improved viscosity model with lower deviations in estimated viscosities, a new correlation based on the Vogel-Tammann-Fulcher (VTF) equation, Equation (10), was proposed *(10).*

$$\ln\eta = A_\eta + \frac{B_\eta}{(T - T_{0\eta})} \qquad (10)$$

where η is viscosity in Pa s, $T$ is temperature in K, and $A_\eta$, $B_\eta$, and $T_{0\eta}$ are adjustable parameters. The ratio of parameters $B_\eta$, and $T_{0\eta}$, $B_\eta/T_{0\eta}$, is also known as Angell strength parameter. It was found that the optimum value of $T_{0\eta}$ is 165.06 K. $A_\eta$ and $B_\eta$, can be obtained by a group contribution method according to Equations (11).

$$A_\eta = \sum_{i=1}^{k} n_i a_{i,\eta} \qquad B_\eta = \sum_{i=1}^{k} n_i b_{i,\eta} \qquad (11)$$

where $n_i$ is the number of groups of type $i$, and $k$ is the total number of different groups in the molecule, and the parameters $a_{i,\eta}$ and $b_{i,\eta}$ are presented in *(10).* Close to 500 data points for 25 ionic liquids based on imidazolium, pyridinium, and pyrrolidinium cations with different anions, covering wide ranges of temperature, 293.15-393.15 K and viscosity, 0.004-1.065 Pa s, were used in this study.

A remarkable agreement was observed between the calculated and the experimental viscosity data, using the Vogel-Tammann-Fulcher (VTF) equation with $T_{0\eta}$=165.06 K and the group contribution parameters $a_{i,\eta}$ and $b_{i,\eta}$ for imidazolium, pyridinium, and pyrrolidinium based ionic liquids containing $[PF_6]^-$, $[BF_4]^-$, $[NTf_2]^-$, $[CH_3COO]^-$, $[MeSO_4]^-$, $[EtSO_4]^-$, and $[CF_3SO_3]^-$ anions over a wide range of temperature and viscosity. Viscosities of ionic liquids having imidazolium-based cations increas according to the series: $[NTf_2]^- < [CF_3SO_3]^- < [BF_4]^- < [EtSO_4]^- < [MeSO_4]^- < [PF_6]^- < [CH_3COO]^-$ *(7).* For ionic liquids having a common anion and a similar alkyl chain length on the cation, the viscosity increases with cation following the order: $[C_n\text{mim}]^+ < [C_n\text{py}]^+ < [C_n\text{mpyrr}]^+$ *(7).*

The calculated viscosity ($\eta_{\text{cal}}$) of the ionic liquids studied displays a good agreement with the corresponding experimental viscosity ($\eta_{\text{exp}}$), where $\ln\eta_{\text{cal}} = (0.9647 \pm 0.0043)\ln\,\eta_{\text{exp}}$ ($R^2$=0.9907 at 95% level of confidence). For 482 data points for 25 ionic liquids available in literature, the overall MPD is 7.50 % with a maximum deviation inferior to 23 %. Rejection of doubtful experimental data was not possible due to the limited amount of experimental data currently available and the large discrepancies in experimental viscosity values reported in literature among authors, which may be due to impurities like water and halogen ions present in ionic liquid samples, or the experimental method adopted.

The predictive capability of the group contribution method here developed for ionic liquid viscosity was further checked by its potential to correlate with equivalent conductivity and the self-diffusion coefficient using fractional forms

Downloaded by STANFORD UNIV GREEN LIBR on June 28, 2012 | http://pubs.acs.org
Publication Date (Web): December 18, 2009 | doi: 10.1021/bk-2009-1030.ch025

of the Walden rule *(25)* and the Stokes-Einstein relation *(26)*, respectively, as discussed in subsequent Sections.

## Electrical Conductivity

A database of experimental electrical conductivity ($\lambda$) available from the open literature was collected. A global number of 300 data points for 15 ionic liquids based on imidazolium, pyridinium, pyrrolidinium, and tetraalkylammonium cations with $[PF_6]^-$, $[BF_4]^-$, $[NTf_2]^-$, $[EtSO_4]^-$, $[CF_3SO_3]^-$, $[NPf_2]^-$, or $[CF_3COO]^-$ as anions, covering wide ranges of temperature, 258.15-433.15 K and electrical conductivity, 0.01-12.68 S $m^{-1}$, were used in this study.

A Vogel-Tammann-Fulcher (VTF) type equation, Equation (12), similar to that used for viscosity, was used to correlate the electrical conductivity of ionic liquids.

$$\ln\lambda = \ln A_\lambda + \frac{B_\lambda}{(T - T_{0\lambda})} \qquad (12)$$

where $A_\lambda$, $B_\lambda$, and $T_{0\lambda}$ are adjustable parameters, from which $A_\lambda$ and $B_\lambda$ can be obtained with a group contribution method.

$$A_\lambda = \sum_{i=1}^{k} n_i a_{i,\lambda} \qquad B_\lambda = \sum_{i=1}^{k} n_i b_{i,\lambda} \qquad (13)$$

where $n_i$ is the number of groups of type $i$, and $k$ is the total number of different of groups in the molecule, and the parameters $a_{i,\lambda}$, and $b_{i,\lambda}$ estimated for the ionic liquids studied are presented in *(10)*. It was found that $T_{0\lambda}$ presents a value for all studied ionic liquids close to 165 K, surprisingly similar to $T_{0\eta}$, which clearly indicates that these values have a physical meaning. The $T_{0\lambda}$ value was thus fixed to a value identical to $T_{0\eta}$ ($T_{0\lambda} = T_{0\eta}$ = 165.06 K). About 300 experimental electrical conductivity data points for 15 ionic liquids available were then used to estimate the values of the group contribution parameters $a_{i,\lambda}$, and $b_{i,\lambda}$ .

The calculated electrical conductivity ($\lambda_{cal}$), using the Vogel-Tammann-Fulcher (VTF) equation, Equation (12), with $T_{0\lambda}$ =165.06 K and using group contribution parameters $a_{i,\lambda}$, and $b_{i,\lambda}$ for imidazolium, pyridinium, pyrrolidinium, and ammonium-based ionic liquids having $[PF_6]^-$, $[BF_4]^-$, $[NTf_2]^-$, $[EtSO_4]^-$, $[CF_3SO_3]^-$, $[NPf_2]^-$, or $[CF_3COO]^-$ as anions, are in good agreement with the corresponding experimental electrical conductivity ($\lambda_{exp}$), where $\lambda_{cal} = (0.9974 \pm 0.0022)\lambda_{exp}$ ($R^2$=0.9985 at 95% level of confidence). For 307 data points for 15 ionic liquids available in literature, the overall MPD is 4.57 % with a maximum deviation of the order of 16 %. Water content present in ionic liquid samples may increase its electrical conductivity significantly *(27)*, which may be a possible reason for some of the larger deviations observed in the calculated electrical conductivity.

For ionic liquids containing the $[C_4mim]^+$ (1-butyl-3-methylimidazolium) cation, electrical conductivity increases the anion following the order $[NPf_2]^- \leq [PF_6]^- < [CF_3SO_3]^- < [NTf_2]^- \leq [CH_3COO]^- < [BF_4]^-$ *(10)*. Electrical conductivity

Downloaded by STANFORD UNIV GREEN LIBR on June 28, 2012 | http://pubs.acs.org
Publication Date (Web): December 18, 2009 | doi: 10.1021/bk-2009-1030.ch025

decreases with the increase of alkyl chain length in the imidazolium cation, and this decrease is more pronounced at higher temperatures. For ionic liquids having a common anion and a similar alkyl chain length on the cation, the electrical conductivity, behaving in the opposite manner to viscosity, decreases with cation nature following the order: $[C_n\text{mim}]^+ > [C_n\text{py}]^+ > [C_n\text{mpyrr}]^+$. However, more experimental data and theoretical studies are required to fully understand the influence of cation and anion on the electrical conductivity of ionic liquids.

The relationship between viscosity and conductance in terms of the fractional Walden rule *(25)* can be written as:

$$\Lambda\eta^{\alpha} = \text{constant} \qquad (14)$$

where $\Lambda$ is equivalent conductivity and α is a constant between zero and unity. To evaluate if Equation (14) can provide an adequate relation between the electrical conductivities and viscosities of ionic liquids, experimental electrical conductivity data collected from the literature were converted into equivalent conductivity using density calculated from Equation (1), and fluidity is obtained as the reciprocal of viscosity from Equation (10). In a log-log plot; the slope (α) of the Walden line is obtained as 0.935 ± 0.008. This indicates that equivalent conductances ($\Lambda$) can be predicted from a correlation with viscosities ($\eta$), using the linear relation:

$$\log_{10}(\Lambda / \text{S cm}^2 \text{ mol}^{-1}) = (0.935 \pm 0.008)\log_{10}(\eta^{-1}/\text{Poise}^{-1}) - (0.226 \pm 0.005) \qquad (15)$$

and also indicates that the conductivity decreases with the increase in viscosity.

## Self-Diffusion Coefficient

The self-diffusion coefficient ($D$) is related to viscosity in terms of the fractional form of the Stokes-Einstein relation *(26)*, according to which the self-diffusion coefficient is proportional to the ratio of temperature and viscosity and can be written as:

$$D(\eta/T)^{\beta}=\text{constant} \qquad (16)$$

where β is a constant.

Experimental self-diffusion coefficient ($D$) data of ionic liquids available in the literature were collected to evaluate the relation between the self-diffusion coefficients ($D$) and the viscosities ($\eta$). For this purpose, the viscosity was calculated using Equation (10). For 45 data points for five ionic liquids based on the imidazolium cation with $[BF_4]^-$ or $[Tf_2N]^-$ as anion, covering wide ranges of temperature, 263.15-353.15 K and self-diffusion coefficient, $2.43\times10^{-12}$-$3.71\times10^{-10}$ $\text{m}^2\ \text{s}^{-1}$, a very good linear correlation is observed with $T/\eta$ *(10)*, where

$$10^{12} D / \text{m}^2\ \text{s}^{-1} = (6.995 \pm 0.061)(T/\eta) / \text{K mPa}^{-1}\ \text{s}^{-1} \qquad (17)$$

Downloaded by STANFORD UNIV GREEN LIBR on June 28, 2012 | http://pubs.acs.org
Publication Date (Web): December 18, 2009 | doi: 10.1021/bk-2009-1030.ch025

It would be interesting to correlate the ionic diffusivity with conductivity through the Nernst-Einstein equation, but the limited amount of experimental data available restricts such a development at this point. We are confident that such correlation for ionic liquids will be possible when an adequate amount of experimental data become available.

## Thermal Conductivity

The knowledge of thermal conductivity is important to obtain the heat transfer coefficient of fluids, which is essential for the design of heat transfer fluid and equipments. Among the different transport properties, thermal conductivity is one of the most difficult to estimate using predictive methods.

The data base of experimental thermal conductivity ($\kappa$) available in the literature contains 107 data points for sixteen ionic liquids based on imidazolium, pyrrolidinium, and phosphonium cations with $[PF_6]^-$, $[BF_4]^-$, $[NTf_2]^-$, $[EtSO_4]^-$, $[CF_3SO_3]^-$, or $Cl^-$ as anions, covering a wide range of temperatures, 293-390 K, and thermal conductivities, 0.124-0.199 W $m^{-1}$ $K^{-1}$. The experimental thermal conductivities suggest that they are weakly dependent on temperature, and could be fitted with a linear correlation of the form:

$$\kappa = A_\kappa - B_\kappa T \tag{18}$$

where $T$ is temperature in K, and $A_\kappa$ and $B_\kappa$ are fitting parameters that can be obtained from a group contribution approach as:

$$A_\kappa = \sum_{i=1}^{k} n_i a_{i,\kappa} \qquad B_\kappa = \sum_{i=1}^{k} n_i b_{i,\kappa} \tag{19}$$

where $n_i$ is the number of groups of type $i$, and $k$ is the total number of different groups in the molecule, and the parameters $a_{i,\kappa}$ and $b_{i,\kappa}$ are presented in *(10)*.

The calculated thermal conductivity ($\kappa_{cal}$) using the group contribution parameters $a_{i,\kappa}$ and $b_{i,\kappa}$ for imidazolium, pyrrolidinium, and phosphonium based ionic liquids having $[PF_6]^-$, $[BF_4]^-$, $[NTf_2]^-$, $[EtSO_4]^-$, $[CF_3SO_3]^-$, or $Cl^-$ as anions, are in very good agreement with the corresponding experimental thermal conductivity ($\kappa_{exp}$); where $\kappa_{cal} = (0.9991 \pm 0.0017)\kappa_{exp}$. For 107 data points for sixteen ionic liquids available in literature, the overall MPD is 1.06 % with a maximum deviation of 3.5 %. The thermal conductivity of the ionic liquids is similar to that observed for organic molecular liquids and much lower than that for pure water. Small amounts of impurities, such as water and chloride, in the ionic liquid sample do not seem to have a significant effect on the thermal conductivity; however, the thermal conductivity seems to increase with the amount of impurities *(28)*. For ionic liquids having an imidazolium based cation, the thermal conductivity increases with the anion following the trend: $[NTf_2]^- < [CF_3SO_3]^- \leq [PF_6]^- < [EtSO_4]^- < [BF_4]^-$ *(10)*. The thermal conductivity also increases somewhat with the increase of alkyl chain length on the imidazolium cation.

Downloaded by STANFORD UNIV GREEN LIBR on June 28, 2012 | http://pubs.acs.org
Publication Date (Web): December 18, 2009 | doi: 10.1021/bk-2009-1030.ch025

**Refractive Index**

Refractive index ($n_D$) is a fundamental physical property and it is used to test a material, confirm its purity, or for analytical purposes such as the assessment of the concentration of a mixture. It is also related to other properties such as dielectric constant, density, and surface tension through thermodynamic equations.

Experimental refractive index data available in the open literature, with 245 data points for 24 imidazolium-based ionic liquids having $[PF_6]^-$, $[BF_4]^-$, $[NTf_2]^-$, $[MeSO_4]^-$, $[EtSO_4]^-$, $[CF_3SO_3]^-$, or $Cl^-$ as anions, covering a wide range of temperature, 283.15-363.15 K, were used in the study. For the studied ionic liquids, in the temperature range available, it was observed that the experimental refractive index decreases linearly with temperature, and could be fitted with a linear correlation of the form:

$$n_D = A_n - B_n T \qquad (20)$$

where $A_n$ and $B_n$ can be obtained from a group contribution approach as:

$$A_{n_D} = \sum_{i=1}^{k} n_i a_{i,n_D} \quad B_{n_D} = \sum_{i=1}^{k} n_i b_{i,n_D} \qquad (21)$$

where $n_i$ is the number of groups of type $i$, and $k$ is the total number of different of groups in the molecule, and the parameters $a_{i,n}$, and $b_{i,n}$ here estimated are reported in *(10)*.

The calculated refractive indices ($n_{D,\text{cal}}$) were in excellent agreement with the corresponding experimental refractive index ($n_{D,\text{exp}}$); where $n_{D,\text{cal}} = (0.9999 \pm 0.0002) n_{D,\text{exp}}$. For 245 data points of 24 ionic liquids available in the literature, the overall MPD is 0.18 % with a maximum deviation of the order of 0.6 %. The results indicate that the refractive index of the studied ionic liquids is weakly dependent on temperature and slightly decreases with temperature. The refractive index of all studied ionic liquids is higher that observed for pure water. Water present in the ionic liquid sample as an impurity has little effect on the refractive index; however, from the refractive index data of aqueous solutions of ionic liquids *(21,29,30)*, it is clear that the refractive index decreases with increasing amount of water. For ionic liquids having imidazolium based cations, the refractive index increases with the anion following the trend: $[PF_6]^- < [BF_4]^- < [NTf_2]^- < [CF_3SO_3]^- < [MeSO_4]^- < [EtSO_4]^- < Cl^-$ *(10)*; and it increases slightly with the increase of alkyl chain length on the imidazolium cation. The low deviations observed in calculated refractive indices for a wide range of imidazolium based ionic liquids shows that the group contribution method here developed can predict refractive index of new ionic liquids over wide ranges of temperatures and, as data for new groups of cations and anions become available, can be easily extended to a larger range of ionic liquids.

Downloaded by STANFORD UNIV GREEN LIBR on June 28, 2012 | http://pubs.acs.org
Publication Date (Web): December 18, 2009 | doi: 10.1021/bk-2009-1030.ch025

## Heat Capacity

Heat capacity is one of the basic thermodynamic properties that characterises a compound. Variations in heat capacities provide information of phase transitions and are important for understanding changes in the structure of a compound. Experimental data for the heat capacity of ionic liquids are scarce and limited to a few classes of well-studied ionic liquids. A database of experimental liquid heat capacities ($C_{pL}$) of ionic liquids available in the open literature, a global number of 2396 data points for 19 ionic liquids based on imidazolium cations with $[PF_6]^-$, $[BF_4]^-$, $[NTf_2]^-$, $Br^-$, $[EtSO_4]^-$, or $[CF_3SO_3]^-$ as anions, and pyridinium and pyrrolidinium cations with $[NTf_2]^-$, covering wide ranges of temperature, 196.36-663.10 K and liquid heat capacity, 264.8-825.0 $J\ mol^{-1}\ K^{-1}$, were used in the study.

The approach proposed by Ruzicka and Domalski *(31,32)* was adopted and a second-order group additivity method used for the estimation of the liquid heat capacity of ($C_{pL}$) of ionic liquids. It employs a group contribution technique to estimate the $A_{Cp}$, $B_{Cp}$ and $D_{Cp}$ parameters in Equation (22):

$$C_{pL} = R \cdot \left[ A_{Cp} + B_{Cp} \cdot \left( \frac{T}{100} \right) + D_{Cp} \cdot \left( \frac{T}{100} \right)^2 \right] \qquad (22)$$

where R is the gas constant (8.314 $J\ mol^{-1}\ K^{-1}$) and $T$ is temperature in K. The group contributions to calculate $A_{Cp}$, $B_{Cp}$ and $D_{Cp}$ parameters are obtained from:

$$A_{Cp} = \sum_{i=1}^{k} n_i a_{iCp} \qquad B_{Cp} = \sum_{i=1}^{k} n_i b_{iCp} \qquad D_{Cp} = \sum_{i=1}^{k} n_i d_{iCp} \qquad (23)$$

where $n_i$ is the number of groups of type $i$, $k$ is the total number of different kinds of groups, and the parameters $a_{iCp}$, $b_{iCp}$, and $d_{iCp}$ are presented in *(9)*.

The method proposed here allows the estimation of heat capacities of ionic liquids as a function of temperature over wide ranges of temperature, 196.36-663.10 K, and can be extrapolated to temperatures outside the temperature range recommended. However, the predictive accuracy decreases with extrapolation and the user must also be aware of the possible degradation of the ionic liquids at high temperatures. Due to the low vapour pressures of ionic liquids, no distinction is made between the isobaric heat capacity and the saturation heat capacity.

The calculated heat capacity, $C_{pL}^{cal}$, of the ionic liquids studied displays a very good agreement with the corresponding experimental heat capacity, $C_{pL}^{exp}$, where $C_{pL}^{cal} = (0.9994 \pm 0.0002) C_{pL}^{exp}$. For 2396 data points for 19 ionic liquids available in literature, 90.2 % estimated heat capacities data present deviations of the experimental values smaller than 1 % and the overall MPD is 0.36 % with a maximum deviation smaller than 2.5 %. In almost all cases where the experimental uncertainty is provided in the original reference, the deviations in predicted heat capacities are inferior to the assigned experimental uncertainties. The proposed method for the estimation of the heat capacities of ionic liquids is not only a powerful and accurate tool for the estimation of heat capacities when

Downloaded by STANFORD UNIV GREEN LIBR on June 28, 2012 | http://pubs.acs.org
Publication Date (Web): December 18, 2009 | doi: 10.1021/bk-2009-1030.ch025

no experimental information is available, but also to evaluate the quality of the available or new data as it can check the coherence between the data from various data sets for different ionic liquids.

For ionic liquids containing the imidazolium cation, heat capacity increases with the anion mass in the order $Br^- < [BF_4]^- < [PF_6]^- < [EtSO_4]^- \approx [CF_3SO_3]^- < [NTf_2]^-$ *(9)*. For ionic liquids having a common anion and a similar alkyl chain length on the cation, it is observed that the heat capacity increases with cation following the order: $[C_n\text{py}]^+ < [C_n\text{mim}]^+ < [C_n\text{mpyrr}]^+$ *(9)*.

## Summary and Future Work

The total number of ionic liquids and data points used for the correlation of all studied thermophysical properties are summarised in Table 1, along with the mean percent deviation (MPD) and maximum deviation (MD) observed. By using the predictive models developed, we have started working for the Computer Aided Molecular Design (CAMD) of ionic liquids. As a part of that, a free online thermophysical property calculator, THERMOPHIL, which can be accessed at http://path.web.ua.pt/thermophil.asp, was developed for the estimation of thermophysical properties of ionic liquids.

**Table 1. Thermophysical Property Prediction for Ionic Liquids**

| *Property* | *MPD / %* | *Maximum deviation %* | *Number of data points* | *Number of Ils* |
|---|---|---|---|---|
| Density | 0.73 | 1.57 | 1521 | 21 |
| Isobaric Expansivity | 1.98 | 7.10 | 109 | 49 |
| Isothermal Compressibility | 2.53 | 6.67 | 26 | 22 |
| Surface Tension | 5.75 | 15.58 | 361 | 38 |
| Speed of Sound | 1.96 | 4.93 | 133 | 14 |
| Viscosity | 7.78 | 27.75 | 498 | 29 |
| Electrical Conductivity | 4.57 | 16.01 | 307 | 15 |
| Thermal Conductivity | 1.08 | 3.51 | 107 | 16 |
| Refractive Index | 0.18 | 0.61 | 221 | 24 |
| Heat Capacity | 0.36 | 2.43 | 2396 | 19 |

Downloaded by STANFORD UNIV GREEN LIBR on June 28, 2012 | http://pubs.acs.org
Publication Date (Web): December 18, 2009 | doi: 10.1021/bk-2009-1030.ch025

Downloaded by STANFORD UNIV GREEN LIBR on June 28, 2012 | http://pubs.acs.org
Publication Date (Web): December 18, 2009 | doi: 10.1021/bk-2009-1030.ch025

## Conclusions

Group contribution methods for the estimation of the thermophysical and transport properties of ionic liquids were developed for density, viscosity, surface tension, speed of sound, electrical conductivity, thermal conductivity, heat capacity, refractive index, isobaric expansivity, and isothermal compressibility. A further correlation for the self diffusion coefficients based on the Stokes Einstein relation is also proposed. The parameters of the group contribution methods were determined for imidazolium, pyridinium, pyrrolidinium, piperidinium, phosphonium, and ammonium based ionic liquids containing several different anions, and *ca.* 5680 experimental data points were used for this purpose. A comparison between the experimental and correlated values shows that the proposed models describe the experimental data available with absolute relative deviations generally of the same order as the agreement of experimental data between different authors as described in the report of the IUPAC task group for the development of standard systems for the measurement of thermodynamic properties of ionic liquids (http://www.iupac.org/web/ins/2002-005-1-100). Care is recommended when comparing or using physical properties of ionic liquids, as differences among the results of several authors may be important since the presence of small amounts of water or other impurities such as chloride seem to have a remarkable effect on most of the these properties.

The proposed methods can be useful for predicting the studied properties for the design of processes or products involving ionic liquids, as the procedures involved are rapid and facile. They can also be used for the development of Computer Aided Molecular Design (CAMD) methods for ionic liquids that could help identify a compound, or range of compounds to fit a set of requirements for a particular application.

The group contribution methods proposed here can, in the future, be extended to a larger range of ionic liquids, as data for these become available.

## References

1. Wasserscheid, P.; Welton T. *Ionic Liquids in Synthesis*; Wiley-VCH Verlag: Weinheim, 2003.
2. Smiglak M.; Metlen A.; Rogers R. D. The second evolution of ionic liquids: From solvents and separations to advanced materials - Energetic examples from the ionic liquid cookbook. *Accounts Chem. Res.* **2007,** *40,* 1182-1192.
3. Gani R.; Nielsen B.; Fredenslund A. Group contribution approach to computer-aided molecular design. *AIChE J.* **1991,** *37,* 1318-1332.
4. Harper P. M.; Gani R.; Kolar P.; Ishikawa T. Computer-aided molecular design with combined molecular modeling and group contribution. *Fluid Phase Equilib.* **1999,** *158-160,* 337-347.
5. Gardas R. L.; Coutinho J. A. P. Extension of the Ye and Shreeve group contribution method for density estimation of ionic liquids in a wide range of temperatures and pressures. *Fluid Phase Equilib.* **2008,** *263,* 26-32.

6. Gardas R. L.; Coutinho J. A. P. Applying a QSPR correlation to the prediction of surface tensions of ionic liquids. *Fluid Phase Equilib.* **2008,** *265,* 57-65.
7. Gardas R. L.; Coutinho J. A. P. A group contribution method for viscosity estimation of ionic liquids. *Fluid Phase Equilib.* **2008,** *266,* 195-201.
8. Gardas R. L.; Coutinho J. A. P. Estimation of speed of sound of ionic liquids using surface tensions and densities: A volume based approach. *Fluid Phase Equilib.* **2008,** *267,*182-186.
9. Gardas R. L.; Coutinho J. A. P. A Group Contribution Method for Heat capacity Estimation of Ionic Liquids. *Ind. Eng. Chem. Res.* 2008, 47, 5751-5757.
10. Gardas R. L.; Coutinho J. A. P. Group Contribution Methods for the Prediction of Thermophysical and Transport Properties of Ionic Liquids. *AIChE J.* **2009,** *55,* 1274-1290.
11. *NIST Ionic Liquids Database*, ILThermo. NIST Standard Reference Database 147. National Institute of Standards and Technology, Standard Reference Data Program: Gaithersburg, MD, 2006. http://ILThermo.boulder.nist.gov/ILThermo/.
12. Gardas R. L.; Freire M. G.; Carvalho P. J.; Marrucho I. M.; Fonseca I. M. A.; Ferreira A. G. M.; Coutinho J. A. P. High-Pressure Densities and Derived Thermodynamic Properties of Imidazolium-Based Ionic Liquids. *J. Chem. Eng. Data* **2007,** *52,* 80-88.
13. Gardas R. L.; Freire M. G.; Carvalho P. J.; Marrucho I. M.; Fonseca I. M. A.; Ferreira A. G. M.; Coutinho J. A. P. PρT measurements of imidazolium-based ionic liquids. *J. Chem. Eng. Data* **2007,** *52,* 1881-1888.
14. Ye, C.; Shreeve, J. M. Rapid and Accurate Estimation of Densities of Room-Temperature Ionic Liquids and Salts. *J. Phys. Chem. A* **2007**, *111*, 1456-1461.
15. Jenkins, H. D. B.; Roobottom, H. K.; Passmore, J.; Glasser, L. Relationships among Ionic Lattice Energies, Molecular (Formula Unit) Volumes, and Thermochemical Radii. *Inorg. Chem.* **1999**, *38*, 3609-3620.
16. Gardas, R. L.; Costa, H. F.; Freire, M. G.; Carvalho, P. J.; Marrucho, I. M.; Fonseca, I. M. A.; Ferreira, A. G. M.; Coutinho, J. A. P. Densities and Derived Thermodynamic Properties of Imidazolium-, Pyridinium-, Pyrrolidinium-, and Piperidinium-Based Ionic Liquids. *J. Chem. Eng. Data* **2008**, *53*, 805-811.
17. Tome, L. I. N.; Carvalho, P. J.; Freire, M. G.; Marrucho, I. M.; Fonseca, I. M. A.; Ferreira, A. G. M.; Coutinho, J. A. P.; Gardas, R. L. Measurements and Correlation of High-Pressure Densities of Imidazolium-Based Ionic Liquids. *J. Chem. Eng. Data* **2008**, *53*, 1914-1921.
18. Rodriguez H.; Williams M.; Wilkes J. S.; Rogers R. D. Ionic liquids for liquid-in-glass thermometers. *Green Chem.* **2008,** *10*, 501-507.
19. Predel T.; Schlucker E.; Wasserscheid P.; Gerhard D.; Arlt W. Ionic liquids as operating fluids in high pressure applications. *Chem. Eng. Tech.* **2007,** *30*, 1475-1480.
20. Knotts, T. A.; Wilding, W. V.; Oscarson, J. L.; Rowley, R. L. Use of the DIPPR Database for Development of QSPR Correlations: Surface Tension. *J. Chem. Eng. Data* **2001**, *46*, 1007-1012.

Downloaded by STANFORD UNIV GREEN LIBR on June 28, 2012 | http://pubs.acs.org
Publication Date (Web): December 18, 2009 | doi: 10.1021/bk-2009-1030.ch025

21. Auerbach, R. Oberflächenspannung und Schallgeschwindigkeit. *Experientia* **1948,** *4,* 473-474.
22. Oswal, S. L.; Oswal, P.; Modi, P. S.; Dave, J. P.; Gardas, R. L. Acoustic, volumetric, compressibility and refractivity properties and Flory's reduction parameters of some homologous series of alkyl alkanoates from 298.15 to 333.15 K. *Thermochim. Acta* **2004,** *410,* 1-14.
23. Oswal, S. L.; Oswal, P.; Gardas, R. L.; Patel, S. G.; Shinde, R. G. Acoustic, volumetric, compressibility and refractivity properties and reduction parameters for the ERAS and Flory models of some homologous series of amines from 298.15 to 328.15 K. *Fluid Phase Equilib.* **2004,** *216,* 33-45.
24. Reid, R. C.; Prausnitz, J. M.; Sherwood, T. K. *The Properties of Gases and Liquids*; 4th Edition; McGraw-Hill: New York, 1987.
25. Walden P. Organic solutions- and ionisation means. III. Chapter: Internal friction and its connection with conductivity. *Z. Phys. Chem.* **1906,** *55,* 207-249.
26. Bockris J. O. M.; Hooper G. W. Self-diffusion in molten alkali halides. *Discuss. Faraday Soc.* **1961**, *32*, 218-236.
27. Jarosik A.; Krajewski S. R.; Lewandowski A.; Radzimski P. Conductivity of ionic liquids in mixtures. *J. Mol. Liq.* **2006**, *123,* 43-50.
28. Ge R.; Hardacre C.; Nancarrow P.; Rooney D. W. Thermal conductivities of ionic liquids over the temperature range from 293 K to 353 K. *J. Chem. Eng. Data* **2007**, *52*, 1819-1823.
29. Gomez E.; Gonzalez B.; Calvar N.; Tojo E.; Dominguez A. Physical properties of pure 1-ethyl-3-methylimidazolium ethylsulfate and its binary mixtures with ethanol and water at several temperatures. *J. Chem. Eng. Data* **2006**, *51*, 2096-2102.
30. Liu W.; Cheng L.; Zhang Y.; Wang H.; Yu M. The physical properties of aqueous solution of room-temperature ionic liquids based on imidazolium: Database and evaluation. *J. Mol. Liq.* **2008**, *140*, 68-72.
31. Ruzicka, V.; Domalski, E. S. Estimation of the Heat-Capacities of Organic Liquids as a function of Temperature using Group Additivity. 1. Hydrocarbon Compounds. *J. Phys. Chem. Ref. Data* **1993**, *22*, 597-618.
32. Ruzicka, V.; Domalski, E. S. Estimation of the Heat-Capacities of Organic Liquids as a function of Temperature using Group Additivity. 2. Compounds of Carbon, Hydrogen, Halogens, Nitrogen, Oxygen, and Sulfur. *J. Phys. Chem. Ref. Data* **1993**, *22*, 619-657.

Downloaded by STANFORD UNIV GREEN LIBR on June 28, 2012 | http://pubs.acs.org
Publication Date (Web): December 18, 2009 | doi: 10.1021/bk-2009-1030.ch025

Downloaded by PENNSYLVANIA STATE UNIV on June 28, 2012 | http://pubs.acs.org
Publication Date (Web): December 18, 2009 | doi: 10.1021/bk-2009-1030.ch026

## Chapter 26

# Ion Association in 1-Butyl-3-methylimidazolium Hexafluorophosphate / Naphthalene Mixtures

**Mario G. Del Pópolo and Pietro Ballone**

**Atomistic Simulation Centre, The Queen's University of Belfast, Belfast BT7 1NN, UK**

Mixtures of the ionic liquid 1-butyl-3-methylimidazolium hexafluorophosphate ([$C_4$mim][$PF_6$]) and naphthalene have been investigated by molecular dynamics simulations based on an empirical potential model, covering the full range of concentrations from the pure ionic liquid to pure naphthalene. The composition dependence of thermodynamic functions and of dynamical properties highlights a continuous but relatively sharp transition taking place at 20% ionic liquid concentration. The analysis of the electric conductivity and of simulation snapshots reveals that the transition marks the transformation of the [$C_4$mim][$PF_6$] bonding from molecular-dipolar at low concentration to ionic at high concentration. The probability distribution for the microscopic electric fields acting on the naphthalene atoms broadens significantly in going from the molecular to the ionic state, suggesting that optical spectroscopy and core level spectroscopy could be used to probe the transition at the atomistic scale.

In Ionic Liquids: From Knowledge to Application; Plechkova, N., et al.;
ACS Symposium Series; American Chemical Society: Washington, DC, 2010.

## Introduction

As their name implies, the most characteristic feature of room temperature ionic liquids *(1)* is their dissociation into individual ions, able to diffuse independently from each other and thus to conduct electricity even at relatively mild temperature and pressure conditions. Electrical conductivity and Coulomb interactions, in turn, underlie the ionic liquid ability to screen external fields, greatly affecting their physical parameters and electrochemical activity, as well as their properties as solvents, surfactants and lubricants.

As explained even in elementary textbooks, ionicity arises from the energy gain of assembling particles of opposite charge overcoming the cost of producing ions out of neutral species. As a result, ionicity is primarily a collective property, favoured by solvation in a polar environment (such as water), that decreases the energy of the bare ions, and, even more, promoted by high density and increasing coordination, that enhance the attractive interaction of anions and cations *(2)*.

The validity and relevance of this picture is emphasised by the fact that the vapour phase of most ionic liquids (including the room temperature ones) is an electrical insulator, being made of highly polar but otherwise neutral contact ion pairs *(3,4)*. The ionic-to-polar crossover taking place with increasing temperature and/or decreasing density is one of the fundamental aspects of all Coulomb systems, and, as such, is still an open and very active subject of research. The current debate concerns even the very nature of the conductor-insulator transition in ionic systems, that can be seen either as a sudden phase change in the atomic and electronic structure, or as a continuous transformation of their ion dynamics that reduces the transport of charge, leaving nearly unaffected the diffusional motion of neutral mass currents.

The small ionic size and tight packing of traditional molten salts imply that the non-conducting to ionic transition takes place at very high temperature and pressure. Room temperature ionic liquids provide an appealing new path to investigate this phenomenon under easily accessible conditions. Moreover, several ionic liquids are soluble in organic solvents, thus providing a simple way to vary the ionic liquid density over a wide range without incurring into the complexity and chemical activity of ionic liquid/water solutions.

Recent measurements of the molar conductivity of ionic liquid solutions in neutral organic solvents *(5,6,7)* display a conductivity maximum at low but not negligible ionic liquid concentrations, that is highly suggestive of an underlying non-conducting to ionic transformation. The result of other studies *(8) do not* display such a maximum within the experimentally accessible range, but highlight deviations from the ideal Nernst-Einstein behaviour *(9)* that point again to an incipient change in the system bonding and dynamics as a function of ion density. Although these anomalies are generally attributed to ion association, the microscopic origin of the conductivity maximum in ionic liquid has not been investigated in detail before. The interpretation of molar conductivities as a measure of the effective concentration of charge carries requires, however, a careful analysis of the concentration dependence of the solution viscosity. This is particularly important in the case of ionic liquids,

Downloaded by PENNSYLVANIA STATE UNIV on June 28, 2012 | http://pubs.acs.org
Publication Date (Web): December 18, 2009 | doi: 10.1021/bk-2009-1030.ch026

which often show viscosities much higher than the most common organic solvents.

We have studied by atomistic simulation the transformation of [$C_4$mim][$PF_6$] (see Figure 1) in [$C_4$mim][$PF_6$]/naphthalene solutions from a prototypical ionic liquid to a fluid made of neutral contact ion pairs floating within liquid naphthalene. The transition takes place by decreasing the concentration of [$C_4$mim][$PF_6$], measured by the ionic liquid mole fraction $x$.

The computational analysis unambiguously confirms that the conductivity maximum seen in experiments marks the transition from the ionic to the non-conducting state.

Downloaded by PENNSYLVANIA STATE UNIV on June 28, 2012 | http://pubs.acs.org
Publication Date (Web): December 18, 2009 | doi: 10.1021/bk-2009-1030.ch026

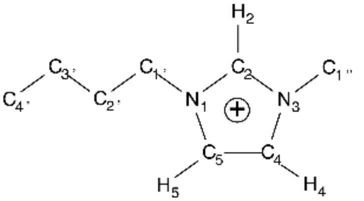

*Figure 1: Schematic drawing of the structure of the 1-butyl-3-methylimidazolium cation, [$C_4$mim]$^+$.*

## [$C_4$mim][$PF_6$]/Naphthalene Mixtures: The Experimental Picture

A quick scan of experimental data *(10)* for the solubility of ionic liquid in low dielectric constant organic solvents allows the identification of combinations to give rise to a homogeneous mixture over the widest possible composition range. The results point to [$C_4$mim][$PF_6$]/naphthalene mixtures as the most suitable system for our investigation.

Naphthalene and [$C_4$mim][$PF_6$] have similar densities, and the data for the mixtures join smoothly and monotonically the two extreme cases (See Fig. 2 ). The $\rho(x)$ curve *(5),* however, apparently deviates from the analytical expression valid for ideal mixtures.

Downloaded by PENNSYLVANIA STATE UNIV on June 28, 2012 | http://pubs.acs.org
Publication Date (Web): December 18, 2009 | doi: 10.1021/bk-2009-1030.ch026

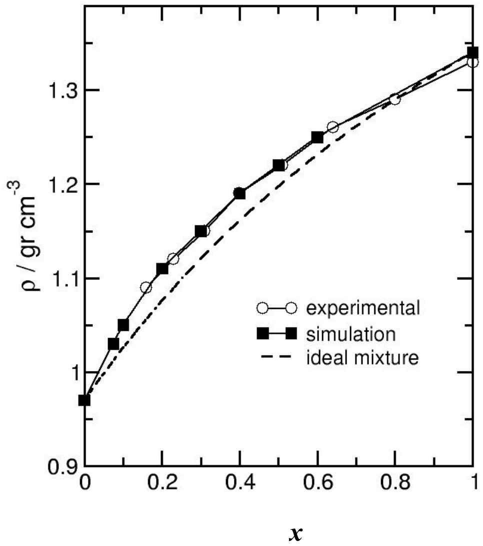

*Figure 2. Comparison of measured and computed density of [$C_4$mim][$PF_6$]/naphthalene mixtures as a function of composition (5).*

The experimental results for the viscosity coefficient *(5)* as a function of composition $x$ are reported in Figure 3. Close to their melting point, ionic liquids are usually fairly viscous fluids, and also in the present case the viscosity of the solvent (naphthalene) is much less than that of [$C_4$mim][$PF_6$]. Disregarding the slight anomaly at intermediate composition ($x \sim 0.4 - 0.5$), the measured viscosities display a nearly monotonic increase with increasing ionic liquid concentration from pure naphthalene to pure [$C_4$mim][$PF_6$].

The results for the conductivity $\sigma$ are collected in Figure 4. Starting from a fairly high value for pure [$C_4$mim][$PF_6$], conductivity increases slightly with decreasing ionic liquid content down to $x \sim 50$ %, apparently because the related decrease of viscosity overcompensates the reduction of the carrier's density. Further reduction of the ionic liquid concentration below $x = 50$ % brings about a rapid drop of $\sigma$, obviously vanishing in the $x \rightarrow 0$ limit. However, once the effect of the decreasing carrier concentration is factored out by plotting the conductivity *per ion* $\sigma/x$, the experimental data show a different picture (see Figure 4), and display a clear conductivity maximum at $0.10 \leq x \leq 0.15$.

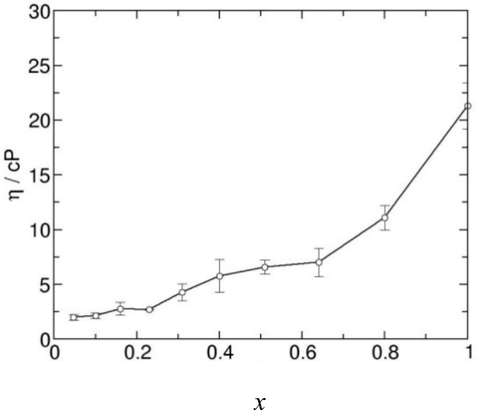

*Figure 3. The viscosity (η) of $[C_4mim][PF_6]$/naphthalene mixtures as a function of ionic liquid mole fraction x measured at T = 353 K, P = 1 atm (5).*

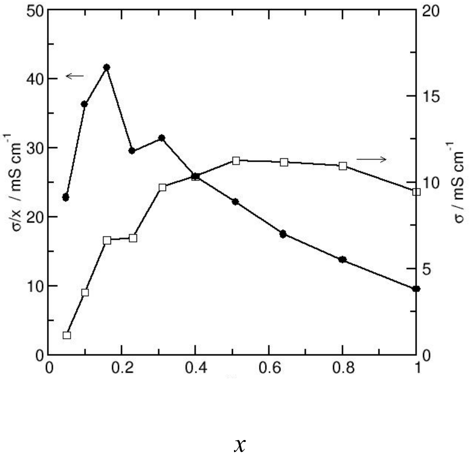

*Figure 4. Filled squares and right axis: ionic conductivity of $[C_4mim][PF_6]$/naphthalene mixtures as a function of ionic liquid mole fraction x measured at T =353 K, P =1 atm. Open circles and left axis: conductivity per ion σ(x)/x (5).*

Downloaded by PENNSYLVANIA STATE UNIV on June 28, 2012 | http://pubs.acs.org
Publication Date (Web): December 18, 2009 | doi: 10.1021/bk-2009-1030.ch026

## The Simulation Model

The relation between the macroscopic properties and the atomistic picture has been investigated using computer simulation. Simulations have been performed at 350 K, or 77 °C, closely matching the temperature of the experimental measurements (80 °C) (5). The system potential energy as a function of the atomic positions has been approximated by an empirical force field potential described in detail in *(5)* (see also *(11)*). Special care has been required by the definition of the ionic liquid-naphthalene cross interaction, that represents the least known ingredient of the model.

The model is able, in particular, to reproduce the equilibrium volume and crystal structure of $[C_4mim][PF_6]$, of naphthalene, as well as the complex clathrate structure of 1,3-dimethylimidazolium hexafluorophosphate/0.5 benzene crystals *(10)*, whose bonding pattern is apparently closely related to that of $[C_4mim][PF_6]$/naphthalene mixtures. Moreover, it reproduces remarkably well the concentration dependence of the density over the entire $0 \leq x \leq 1$ range (see Figure 2). Visual inspection of simulation samples equilibrated over long MD runs shows that $[C_4mim][PF_6]$/naphthalene mixtures are homogeneous.

In our simulations, neutral samples made of $N_{IL}$ $[C_4mim][PF_6]$ ion pairs and $N_{C10H8}$ naphthalene molecules at concentration $x = N_{IL}/(N_{IL}+N_{C10H8})$ were considered, enclosed in a cubic simulation box periodically repeated in space. Each sample has been equilibrated for at least 1 ns. Statistics have been accumulated over runs lasting at least 4 ns. Longer runs have been carried out at the lowest ionic liquid concentrations to compensate for the low number of ions and large fluctuations of these samples.

## Simulation Results

The first qualitative analysis of the mixture properties is obtained by inspecting snapshots of the simulated systems (see Figure 5 *(5)*). At fairly high ionic liquid concentration ($x > 0.2$) the simulated samples are apparently homogeneous. Ions, in particular, do not display any tendency to form closely associated neutral pairs, and are instead equally shared among several neighbours of opposite charge, consistently with the basic idea of ionic liquids.

Snapshots of the $x = 0.075$ (see Figure 5) and $x = 0.1$ samples, however, reveal a different picture. In these cases, the $[C_4mim]^+$ and $[PF_6]^-$ ions tend to aggregate into globular blobs of nanometric dimension, joined by elongated structures (filaments) also made of $[C_4mim]^+$ and $[PF_6]^-$ ions. Naphthalene molecules cluster in the voids left in between blobs and filaments. The elongated ionic liquid structures are very thin, consisting in fact of one-dimensional chains of alternating cations and anions. Blobs, instead, look like small droplets of the dense ionic liquid, and therefore appear to be ionic.

Downloaded by PENNSYLVANIA STATE UNIV on June 28, 2012 | http://pubs.acs.org
Publication Date (Web): December 18, 2009 | doi: 10.1021/bk-2009-1030.ch026

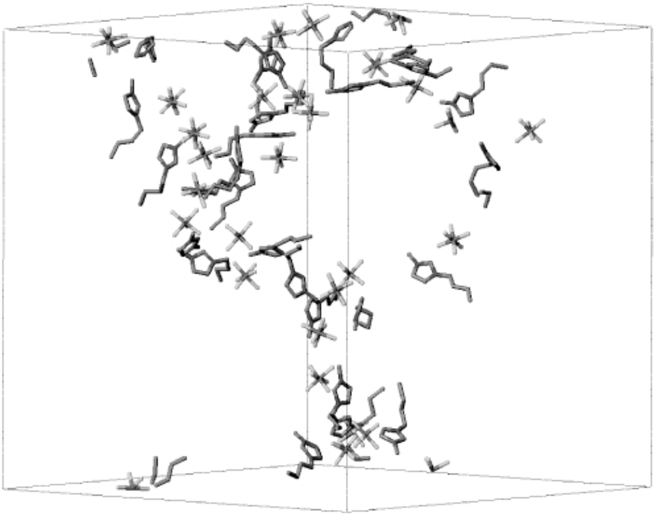

*Figure 5: Snapshot of a simulated sample at composition: x = 0.075. T = 350 K and P = 1 atm.*

In all the snapshots analysed (including the larger sample at $x = 0.075$), blobs and chains stretch across the entire simulation cell; there were no isolated chain segments or rings. The absence of open chains might be due to the high potential energy of the bare ionic terminations, while rings might be penalised by the high entropy cost of closing a chain on itself. Thus, the combination of blobs and filaments percolating across the entire system might indeed represent the most convenient configuration at low ionic liquid content in terms of free energy.

The strict alternation of cations and anions, and especially the formation of filaments, suggest that a sizable fraction of the ions in low-$x$ samples are associated into neutral pairs, that bind to each other *via* dipolar forces *(12)*. In other words, the simple visualisation of the simulated samples of [$C_4$mim][$PF_6$] mixtures already points to a simultaneous change of geometry and bonding taking place between $x = 0.1$ and $x = 0.2$. The sizeable fraction of ions that condense into dipolar chains especially at low ionic liquid concentrations motivates our (admittedly loose) usage of the term *transition* to characterise the shift of equilibrium between the ionic and ion-paired forms of [$C_4$mim][$PF_6$].

The most apparent experimental evidence that something remarkable is taking place in [$C_4$mim][$PF_6$]/naphthalene mixtures is provided by the peak in the conductivity per ion seen in Figure 4 at low ionic liquid concentrations. Therefore, the ionic conductivity of the simulated samples was computed, in order to verify that our model reproduces the experimental behaviour. As

Downloaded by PENNSYLVANIA STATE UNIV on June 28, 2012 | http://pubs.acs.org
Publication Date (Web): December 18, 2009 | doi: 10.1021/bk-2009-1030.ch026

expected, and as discussed in several papers *(13)*, the determination of the conductivity turns out to be challenging. Nevertheless, the simulation results shown in Figure 6 compare fairly well with the experimental data, and the agreement is particularly good at high ionic liquid concentrations. Sizeable deviations in the absolute value of the conductivity appear at $x \leq 0.5$, probably due to the approximations made by the force field model. However, the qualitative trends of the experimental data are reproduced by the simulation results, and the peak at low ionic liquid concentration is the most remarkable feature of the $\sigma(x)/x$ *versus* $x$ curve both in the experiments and in the simulation.

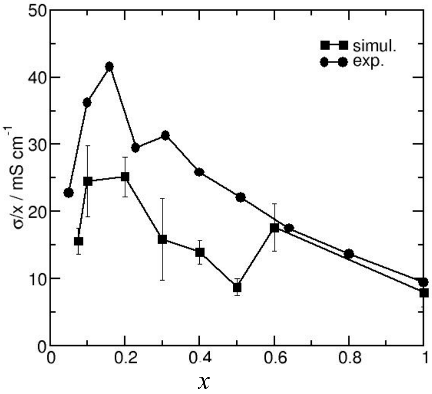

*Figure 6. Comparison of measured and computed conductivity per ion $\sigma(x)/x$ as a function of composition. Experimental measurements at 353 K, simulation results obtained for 350 K.*

A first link between the conductivity data and the microscopic dynamics is established by computing the diffusion coefficient for all the species in the mixture. The results are reported in Figure 7. First of all naphthalene is always the most mobile component, as could have been expected since the viscosity of liquid $C_{10}H_8$ is much less than that of $[C_4mim][PF_6]$. Despite the marked asymmetry of anions and cations, their diffusion coefficient is very similar, as is often the case for electrolyte species whose motion is highly correlated *(14)*. Starting from a relatively low value at $x = 1.0$, the diffusion coefficients of cations and anions ($D^+$ and $D^-$, respectively) increase slowly but monotonically with decreasing $x$ down to $x \sim 0.2$, probably because of the corresponding decrease of the system viscosity.

Downloaded by PENNSYLVANIA STATE UNIV on June 28, 2012 | http://pubs.acs.org
Publication Date (Web): December 18, 2009 | doi: 10.1021/bk-2009-1030.ch026

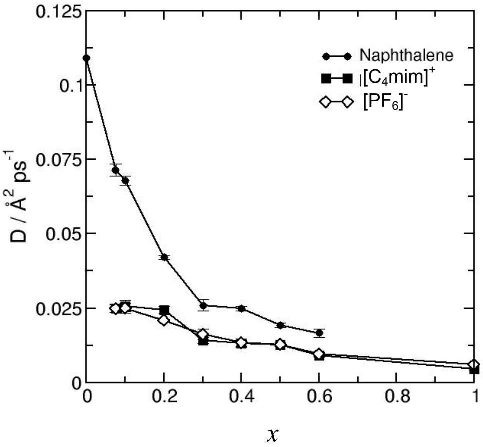

*Figure 7. Computed diffusion coefficients of [C$_4$mim]$^+$, [PF$_6$]$^-$ and naphthalene at 350 K and 1 atm.*

However, both $D^+$ and $D^-$ display a plateau for $0 \le x \le 0.2$, in sharp contrast with the remarkable rise of $D_{\mathrm{C10H8}}$ over the same concentration range, a behaviour that in electrolytic solutions is often attributed to the formation of molecular and ionic complexes. At the very least, these results confirm the relevance of the conductivity anomaly, and point to a change in the aggregation state of the ions in solutions of low ionic liquid content.

The characterisation of the local average structure of molecular liquids *via* their pair distribution functions is obviously far more challenging and less direct than in the case of atomic liquids. The simplicity of this analysis is to some extent restored by considering the radial distribution functions computed with respect to the geometric centre of each unit. In the case of [PF$_6$]$^-$ and naphthalene, this reference point coincides with their centre of mass, while in the case of [C$_4$mim]$^+$ it is the centre of the imidazolium ring. The results are collected in Figures 8 and 9 that show the cation-anion ($g_{+-}$) and the cation-cation and anion-anion ($g_{++}$, $g_{--}$) radial distribution functions. At first sight, these functions seem to provide little new information apart from displaying a remarkable alternation of anions and cations, emphasising once again the role of Coulomb interactions down to the lowest ionic liquid concentrations. A closer look, however, shows that the $x$-dependence of the $g_{+-}$ peak is fairly different at low and at high ionic liquid concentrations. Starting from the pure ionic liquid side, the height of the $g_{+-}$ peak changes only slightly with decreasing ionic liquid concentration down to $x = 0.4$. The rate of change of the $g_{+-}$ peak increases somewhat between $x = 0.4$ and $x = 0.2$, and finally displays a major enhancement below this concentration. The peak of $g_{+-}$ at $r = 5$ Å is an order of magnitude higher than in the case of simple ionic liquids (such as NaCl) near their triple point, and this observation alone already provides strong evidence for ion pairing.

Downloaded by PENNSYLVANIA STATE UNIV on June 28, 2012 | http://pubs.acs.org
Publication Date (Web): December 18, 2009 | doi: 10.1021/bk-2009-1030.ch026

Downloaded by PENNSYLVANIA STATE UNIV on June 28, 2012 | http://pubs.acs.org
Publication Date (Web): December 18, 2009 | doi: 10.1021/bk-2009-1030.ch026

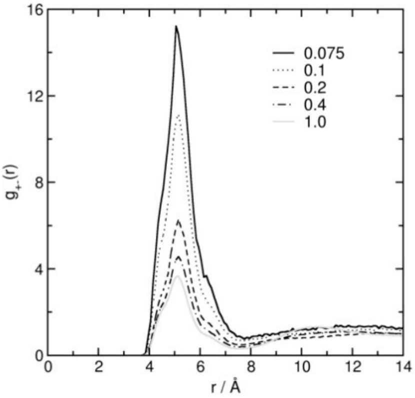

*Figure 8. Radial distribution function for the geometric centres of $[C_4mim]^+$ and $[PF_6]^-$ (see text) computed by simulation at 350 K and 1 atm for different ionic liquid concentrations x.*

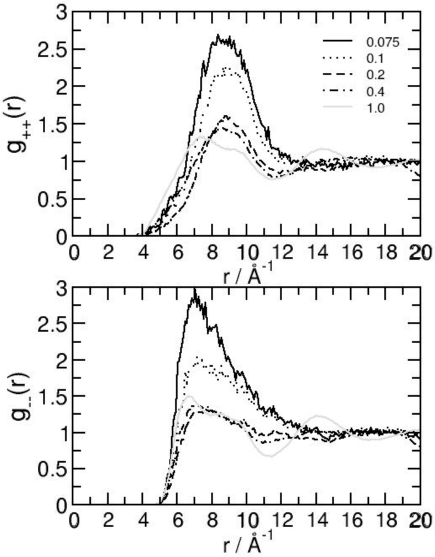

*Figure 9. Composition dependence of the radial distribution functions $g_{++}$ and $g_{--}$ for the geometric centres $[C_4mim]^+$ and $[PF_6]^-$ (see text) computed by simulation at 350 K and 1 atm.*

The previous conclusion is strengthened by the $x$ dependence of the cation-cation and anion-anion radial distribution functions. In this case, $g_{++}$ and $g_{--}$ are nearly independent of $x$ from $x = 1.0$ down to $x = 0.2$. The change of behaviour at lower concentration, revealed by a drastic growth of the first peak of $g_{++}$ and $g_{--}$ with decreasing $x$, is even more apparent than in the case of the $g_{+-}$ radial correlation function. Moreover, the enhancement of correlation between like charges in mixtures of progressively vanishing ionic concentration is an obvious sign of clustering.

The formation of neutral ion pairs at low ionic liquid concentration is confirmed by the computation of the coordination number <*n*> for the ions, defined as the average number of anions within a distance $R_c$ from a central cation. For a 1:1 electrolyte such as $[C_4mim][PF_6]$ the result is the same if the role of anions and cations is reversed in the definition given above.

As it is usually done, we set $R_c$ to the radius of the first minimum in $g_{+-}$, *i.e.*, $R_c = 8$ Å. The results are reported in Figure 10. The coordination of pure $[C_4mim][PF_6]$ turns out to be six, reminiscent of the six-fold coordination of spherical and unpolarisable anions and cations in the NaCl structure. The composition dependence of <*n*> is slightly sub-linear from $x = 0.3$ to $x = 1.0$ ($\langle n \rangle \sim 1{+}5x^{0.7}$, $0.3 \leq x \leq 1$). The coordination number remains nearly constant for $0 \leq x \leq 0.2$ at a value that is only slightly higher than two, consistent with the formation of linear chains of ions in equilibrium with nanometric ionic droplets.

Downloaded by PENNSYLVANIA STATE UNIV on June 28, 2012 | http://pubs.acs.org
Publication Date (Web): December 18, 2009 | doi: 10.1021/bk-2009-1030.ch026

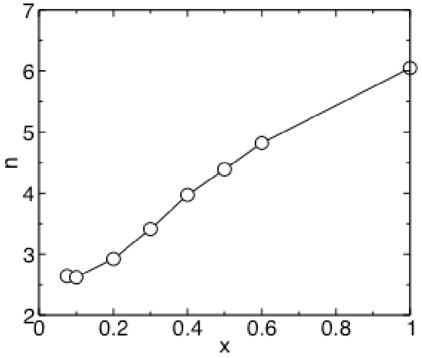

*Figure 10. Anion-anion coordination number n computed by MD simulation using a spherical cutoff radius $R_c$ =8 Å. Distances are computed with respect to the geometric centre of $[C_4mim]^+$ and $[PF_6]^-$.*

The analysis of the first coordination shell can be extended to the time domain by monitoring the rate at which ions interchange their closest partners. This is done by identifying all the neighbours within $R_c$ of each ion at time $t_0$=0, and computing the average number $\langle n(t) \rangle$ of ions still belonging to the same coordination shell at any later time *t*.

The results are shown on a logarithmic scale in Figure 11(a). The simulation data are well approximated by the exponential law $n(t) = n_0\exp[-t/\tau(x)]$ that identifies activated processes for $t \geq 200$ ps. The time constants $\tau(x)$ are reported in Figure 11(b) as a function of composition *x*. Starting from a remarkably high value ($\tau = 1.8$ ns) for $x = 1$, $\tau(x)$ decreases monotonically with decreasing *x* reaching the value $\tau = 0.9$ ns at $x = 0.2$. Then, it rises again rapidly at lower concentration, providing further evidence of the marked change of coordination and bonding taking place for $0 \leq x \leq 0.2$.

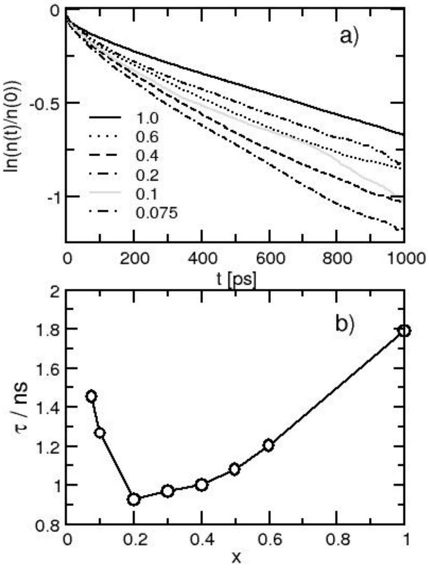

*Figure 11. (a) Persistence index n(t) as a function of t for [$C_4$mim][$PF_6$] mixtures at various concentrations. n(t) is the number of ion pairs (per ion) belonging to the first coordination shell ($R_c = 8$) at t =0 and at a generic time t. (b) Time constant of an exponential fit for n(t).*

It might be useful at this point to discuss the signature of the polar to ionic transition on quantities that can be measured by structure-sensitive experiments such as neutron or X-ray scattering *(15)*. The Fourier transform of the radial distribution functions of Figure 8 provides a new set of functions $S_{\alpha\beta}(k)$ ($\alpha,\beta =$ [$C_4$mim]$^+$, [$PF_6$]$^-$ or naphthalene) that can be identified with the structure factors of ions and molecules centres (see Figure 12).

The onset of the nanometric structures (chains, blobs and naphthalene clusters) described above are reflected in the growth of a prominent peak at $k \leq 0.5$ Å$^{-1}$ for ionic liquid concentrations $x \leq 0.2$. The height and shape of the peak and, even more, its dependence on the system size *(16)* provide the most precise information on the transformation taking place in the system and confirms that the transformation of the bonding character in [$C_4$mim][$PF_6$] is accompanied by the formation of nanometric patterns in the liquid structures (mesophase), without a macroscopic phase separation.

Downloaded by PENNSYLVANIA STATE UNIV on June 28, 2012 | http://pubs.acs.org
Publication Date (Web): December 18, 2009 | doi: 10.1021/bk-2009-1030.ch026

Downloaded by PENNSYLVANIA STATE UNIV on June 28, 2012 | http://pubs.acs.org
Publication Date (Web): December 18, 2009 | doi: 10.1021/bk-2009-1030.ch026

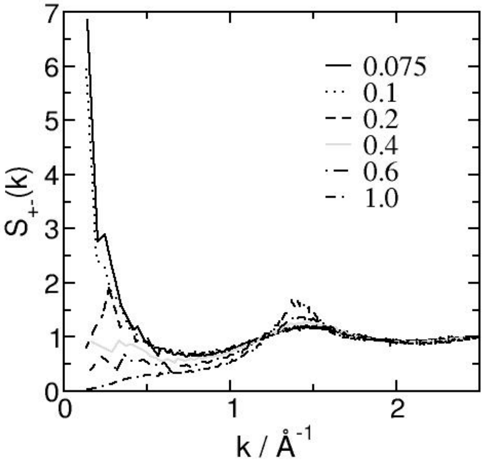

*Figure 12. Structure factor for the centres of the [$C_4$mim]$^+$ and [$PF_6$]$^-$ ion species. Apart from trivial shifts and scale factors, S(k) is the Fourier transform of the radial distribution functions in Figure 8.*

## The Probability Distribution of Microfields

Electric fields acting on atoms (microfields) affect the result of spectroscopic measurements by shifting the energy of core and valence electrons, and by increasing linewidths because of Stark broadening. These effects, although quantitatively fairly small, provide one of the major diagnostic tools in low- and high-density plasmas. To some extent, they must play a role also in low-temperature plasmas such as ionic liquids, thus opening the way to the application of optical spectroscopy and core-level photoemission (PE) to investigate structural and bonding transitions at the atomistic level.

Here, we focus mainly on Stark broadening (SB), since the energy shift of atomic levels is controversial in the first place *(17),* and the role of microfields in this case might be obscured by even minute amounts of charge transfer, which are not described by our model.

Statistical mechanics theories *(18)* developed for plasmas show that SB depends primarily on the low-order, even moments of the microfield probability distribution $P(E)$, defined as the probability for an atom to be acted upon by an electric field of intensity $E$ due to all the other charges in the system. Moreover, we restrict our attention to carbon atoms in naphthalene, because this molecule has rich and well characterised optical and PE spectra, and the baseline microfield distribution in pure naphthalene, a neutral and non-polar compound, is expected to be relatively narrow.

The simulation results for $P(E)$ for different concentrations of ionic liquid in the mixture are shown in Figure 13(a), while the composition dependence of the second moment of this probability distribution is reported in Figure 13(b). First of all, we observe that the probability distribution *P*(*E*) is remarkably Gaussian at all concentrations *x*. As expected, the magnitude of micro-fields increases, and thus *P*(*E*) broadens, with increasing ionic liquid concentration, reflecting the raise in charge density of the system. The increase of the low-order moments, however, saturates for $x > 0.2$, marking the rise of ionic-like screening in the system.

The statistical theories mentioned above do not tell us how big the SB is in absolute units, since broadening depends on the actual size of the atomic orbitals. Nevertheless, the results shown in Figures 13(a) and 13(b) already provide sufficient motivation to investigate in more detail how SB could be used to characterise the dipolar to ionic transition in ionic liquid/neutral-organic mixtures.

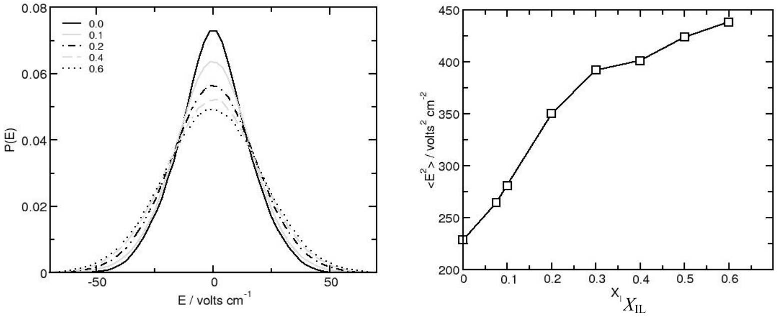

*Figure 13. (a) Microfield probability distribution P(E) on carbon atoms of naphthalene at different ionic liquid concentrations. (b) Second moment, <$E^2$>, of the microfield probability distribution P(E).*

Structural and dynamic properties of [$C_4$mim][$PF_6$]/naphthalene mixtures have been computed by MD simulations based on an empirical force field. The composition, density and temperature ($T$ = 350 K) of the simulations closely match those of experimental measurements *(5)*.

The conductivity per ion computed in our study exhibits a maximum at composition $x \sim 0.15$, closely matching a similar feature found in experimental data. The peak in $\sigma(x)/x$ contrasts markedly with the near monotonic increase of the viscosity with increasing ionic liquid concentration over the full composition range from pure naphthalene to pure [$C_4$mim][$PF_6$]. The composition dependence of conductivity and viscosity highlighted in our study closely correspond to those found in previous experimental studies *(6,8)*, and might represent a fairly general feature of ionic liquid/molecular organic mixtures.

The analysis of the configurations generated in our simulations shows that the conductivity maximum is due to a qualitative change in the bonding character of [$C_4$mim][$PF_6$] in solution, that transforms from ionic to non-conducting with decreasing ionic liquid concentration. As expected, the transformation in the bonding character is fairly sharp, but continuous. It arises from a gradual shift of the chemical equilibrium between ionic and ion-paired species, and is driven mainly by potential energy considerations.

Downloaded by PENNSYLVANIA STATE UNIV on June 28, 2012 | http://pubs.acs.org
Publication Date (Web): December 18, 2009 | doi: 10.1021/bk-2009-1030.ch026

Downloaded by PENNSYLVANIA STATE UNIV on June 28, 2012 | http://pubs.acs.org
Publication Date (Web): December 18, 2009 | doi: 10.1021/bk-2009-1030.ch026

In a fairly broad composition range around the conductivity maximum, the ionic and ion-paired phases appear to coexist, giving rise to a complex structure. We find, in particular, that the residual ionic fraction forms nanometric droplets, while the neutral ion pairs condense into molecular-thin chains that stretch between ionic droplets and sometimes fold into blobs also of nanometric dimension. All the ionic liquid domains found by simulation in samples of low ionic liquid concentration are connected and percolate throughout the simulated samples. This observation is consistent with the fact that $[C_4mim][PF_6]$/naphthalene mixtures have non-vanishing ionic conductivity down to the lowest concentration considered in our measurements and computations. No significant variation in the naphthalene structure is observed in the $0 \leq x \leq 0.5$ composition range, supporting the simplifying assumption that naphthalene provides the nearly inert filling that allows a wide variation of the ion density, without the additional complication of strong interactions with the ions.

In the last part of our study, we investigated how the changes in the ionic liquid bonding at $x = 0.2$ are reflected in the probability distribution $P(E)$ of microfields in the mixture, whose variations could be detected by optical and PE spectroscopy. Our results for the electric field acting upon the carbon atoms of naphthalene reveal a clear broadening of $P(E)$ in going from the dipolar to the ionic state. Further computations at the *ab initio* level are now required to quantify the changes in the Stark broadening due to the composition dependence of $P(E)$ measured in our simulations.

More in general, and beyond the (already broad) interest in ionic liquids, the results of our simulations provide a direct view of the transformation from ionic liquid to an ion-paired fluid that is expected to take place in a wide variety of Coulomb systems. Then, the vast number of ionic liquids and solvent combinations that are available provide an invaluable opportunity to investigate the transition at near ambient conditions and fairly high ionic liquid concentrations. Furthermore, the formation of nanometric patterns in the liquid structure of ionic liquid/organic-solvent mixtures, driven by the condensation of ion-pairs, complements the already complex structural organisation of certain ionic liquids, where alkyl-chains and ionic bodies segregate at a molecular level leading to the formation of mesophases *(19)*.

Ion aggregation, discussed here in the case of $[C_4mim][PF_6]$, is expected to play an important role also for applications involving ionic liquids and their mixtures with organic solvents of low dielectric constant. On the one hand, the transition marks the stability boundary of the ionic liquid phase, and might limit the composition range that can be considered for specific applications. On the other hand, the transition provides a further handle to monitor and to change the properties of ionic liquid samples. In this respect, the relative sharpness of the transition represents an additional advantage that might allow a precise control of the system state and behaviour.

## References

1. Freemantle, M. *Chem. Eng. News* 1**998**, *76*, 32-37; Seddon, K. R. *Nature Mater.* **2003**, *2*, 363 - 365; Welton, T.; *Chem. Rev.* **1999**, *99*, 2071-2084.
2. Weingärtner, H.; Schröer, W.; *Adv. Chem. Phys.* **2001**, *116*, 1-67.
3. Bjerrum, N.; *Kgl. Dan. Vidensk. Selsk. Mater.-Fys. Medd.* **1926**, 1, 1-48.
4. Marcus, Y.; Hefter, G. *Chem. Rev.* **2006**, *106*, 4585-4621.
5. Del Pópolo, M. G.; Mullan, C. L. ; Holbrey, J. D.; Hardacre, C.; Ballone, P. *J. Am. Chem. Soc.* **2008**, *130,* 7032-7041.
6. Jarosik, A.; Krajewski, S. R.; Lewandowski, A.; Radzimski, P. *J. Mol. Liq.* **2006**, *123*, 43-50.
7. Comminges, C.; Barhdadi, R.; Laurent, M.; Troupel, M. *J. Chem. Eng. Data* **2006**, *51*, 680-685.
8. Li, W.; Zhang, Z.; Han, B.; Hu, S.; Xie, Y.; Yang, G. *J. Phys. Chem. B* **2007**, *111*, 6452-6456; Fraser, K. J.; Izgorodina, E. I.; Forsyth, M.; Scott, J. L.; MacFarlane, D. R.; *Chem. Commun.* **2007**, 3817-3819.
9. Atkins, P.; de Paula, J.; *Physical Chemistry*, 7th Edit., W. H. Freeman & Company; New York, 2002; pp. 775.
10. Holbrey, J. D.; Reichert, W. M.; Nieuwenhuyzen, M.; Sheppard, O.; Hardacre, C.; Rogers, R. D. *Chem. Commun.* **2003**, 476-477.
11. Canongia-Lopes, J. N.; Dechamps, J.; Padua, A. A. H. *J. Phys. Chem. B* **2004**, *108*, 2038-2047.
12. de Gennes, P. G.; Pincus, P. A. *Phys. Kondens. Mater.* **1970**, *11*, 189; Weis, J. J.; Levesque, D. *Phys. Rev. Lett.* **1993**, *71*, 2729-2732.
13. See, for instance, Ciccotti, G.; Jacucci, G.; McDonald, I. R. *Phys. Rev. A* **1976**, *13*, 426-436.
14. For instance, simulation data for alkali halide salts show that the diffusion coefficient of anion and cation is similar even for ions whose size and mass are as different as those of $Na^+$ and $I^-$. See Table II in *(13)*.
15. Hansen, J. P.; McDonald, I. R. *Theory of Simple Liquids*; Academic Press, London, 1986, pp. 451.
16. Camp, P. J.; Patey, G. N. *Phys. Rev. E* **2000**, *62*, 5403-5408.
17. Iglesias, C. A. *Phys. Rev. A*, **1984**, *29*, 1366-1370.
18. Iglesias, C. A.; DeWitt, H. E.; Lebowitz, J. L.; MacGowan, D.; Hubbard, W. B. *Phys. Rev. A*, **1985**, *31*, 1698-1702. See also: Nersisyan, H. B.; Toepffer, C.; Zwicknagel, G. *Phys. Rev. E*, **2005**, *72*, 036403.
19. Canongia Lopes, J. N. A. and Pádua, A. A. H. *J. Phys. Chem. B*, **2006**, *110*, 3330–3335.

Downloaded by PENNSYLVANIA STATE UNIV on June 28, 2012 | http://pubs.acs.org
Publication Date (Web): December 18, 2009 | doi: 10.1021/bk-2009-1030.ch026

## Chapter 27

# Computational Comparison of Tethering Strategies for Amine Functionalised Ionic Liquids

**Elaine M. Mindrup[1] and William F. Schneider[1,2]**

**1Department of Chemical and Biomolecular Engineering, University of Notre Dame, Notre Dame, IN 45565**
**2Department of Chemistry and Biochemistry, University of Notre Dame, University of Notre Dame, Notre Dame, IN 46556**

Downloaded by COLUMBIA UNIV on June 28, 2012 | http://pubs.acs.org
Publication Date (Web): December 18, 2009 | doi: 10.1021/bk-2009-1030.ch027

Carbon dioxide capture and sequestration from flue gas is a promising strategy for mitigating global climate change, but success depends on the discovery of selective $CO_2$ adsorbents with optimal physical and chemical characteristics. Amine- functionalised ionic liquids are a promising alternative to the most commonly used aqueous monoethanolamine (MEA) because of their stability, low volatility, and chemical tunability. In this work, we use first principles computation to contrast the effects of cation and anion tethering on the chemistry of amine-functionalised ionic liquids, and show that anion tethering promotes a 1:1 amine:$CO_2$ stoicheiometry, while cation tethering promotes a 2:1 stoicheiometry similar to MEA. These differences arise from differing electrostatic charging effects in the anions and cations. Anion tethering has promise for increasing $CO_2$ carrying capacity over cation tethering.

In Ionic Liquids: From Knowledge to Application; Plechkova, N., et al.;
ACS Symposium Series; American Chemical Society: Washington, DC, 2010.

Downloaded by COLUMBIA UNIV on June 28, 2012 | http://pubs.acs.org
Publication Date (Web): December 18, 2009 | doi: 10.1021/bk-2009-1030.ch027

## Introduction

As concern over global climate change increases, so does the need to find ways to abate the emissions of carbon dioxide ($CO_2$) from major combustion sources. Energy consumption is expected to grow significantly in the coming years, and it is expected that coal will continue to be a major component of this energy equation. With more coal being burned, more $CO_2$ will be released into the atmosphere; therefore, the capture of $CO_2$ from flue gas is essential to diminish potentially harmful increases in atmospheric $CO_2$ concentration *(1-3)*.

Aqueous alkanolamines have been widely used to separate $CO_2$ from natural gas and combustion gas streams. The industry standard for $CO_2$ separations is aqueous monoethanolamine (MEA). MEA is a common and strong base that reacts readily and reversibly with $CO_2$. The equilibria and kinetics of reaction of MEA with $CO_2$ have been well studied *(4-9)*. While the reaction mechanism is still debated, the accepted overall stoicheiometry is two aqueous amine molecules reacting per $CO_2$ molecule to form a carbamate anion and an ammonium cation (2:1 stoicheiometry):

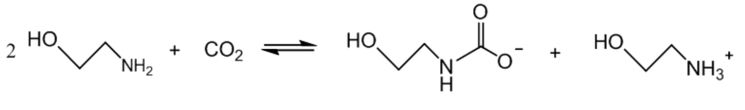

(1)

Several problems are associated with the use of aqueous amines. MEA reacts quite exothermically with $CO_2$, which makes it energetically costly to break the bond between the two and regenerate the unreacted MEA. The amines are volatile to the air, react irreversibly with $SO_2$, and are corrosive to equipment materials. These problems lead to high costs for replacement and regeneration; therefore, a material that captures $CO_2$ as effectively as aqueous amines but mitigates these problems would be an improvement.

Ionic liquids are salts of bulky cations and anions that have melting points below room temperature. Ionic liquids have extremely low vapour pressures which makes them well suited for gas separations. Many types of cation and anion pairs form ionic liquids. Examples include organic ammonium, phosphonium, imidazolium, or pyridinium cations, inorganic chloride, tetrafluoroborate, or hexafluorophosphate anions, and organic anions such as those of amino acids. By carefully selecting cations and anions, it is possible to chemically tune the ionic liquid to meet desired performance parameters.

Experiments have shown that ionic liquids have a high physical solubility of $CO_2$ *(10-19)*, but in general this solubility is too low to be used unmodified for $CO_2$ capture. "Task-specific" ionic liquids, preferable now known as functionalised ionic liquids, tether a functional group, such as an amine, to an ionic liquid to introduce chemical reactivity with $CO_2$. These functionalised ionic liquids can thus combine the advantages of both ionic liquids and amine absorbants. Davis and co-workers were among the first to study $CO_2$ absorption on amine-functionalised ionic liquids *(20)*, by incorporating a primary amine onto the side-chain of an imidazolium cation. This functionalised ionic liquid had a significantly higher uptake of $CO_2$ than physically absorbing ionic liquids, on the same order as the uptake by MEA. Most subsequent related research has focused on characterising and optimising cation-tethered amines. These materials are generally found to exhibit the same 2:1 amine:$CO_2$ reaction stoicheiometry as aqueous amines *(21)*.

One degree of freedom unique to ionic liquids is the choice to tether the amine functionality to the cation or anion. The tethering location may have a direct electronic effect on the energetics of the amine-$CO_2$ bond. Further, because the reactants are charged and, as shown in Equation 1, the 2:1 reaction potentially causes further charge separation, ion tethering may even affect the overall reaction stoicheiometry. In principle, proper selection of amine and tethering site could promote a 1:1 amine:$CO_2$ stoicheiometry that increases overall $CO_2$ capture capacity from 33% to 50%. Experimental reports *(22,23)* of anion-tethered amines do suggest different $CO_2$ uptake capacities compared to cation-tethered, although the origins of these differences have not been explained.

Electronic structure computations use quantum mechanics to describe the interactions between electrons and nuclei in an atom or molecule that determine physical and chemical properties *(24)*. These methods can be used to calculate molecular shape and structure (bond lengths and angles), electrostatic properties (charge and dipole moments), spectroscopic properties, like vibrational frequencies, and even reaction energies. These computations provide a potential route to understand and predict amine-$CO_2$ chemistry and even to design molecules *in silico*. Several groups have applied electronic structure methods to study carbamate formation and stability, as well as provide mechanistic insights into the reactions of neutral amines with $CO_2$ *(25-29)*. To date, the application of electronic structure calculations to functionalised ionic liquids for $CO_2$ capture has not be reported.

In this work, we use electronic structure simulations to contrast the reactant and product structures and energetics of $CO_2$ reactions with anion- and cation-tethered amines. We compare the energetics of 2:1 amine:$CO_2$ and 1:1 amine:$CO_2$ reactions as a function of amine charge and tethering site. We model the 1:1 reaction as the combination of an amine-containing molecule and $CO_2$ to form a carbamic acid:

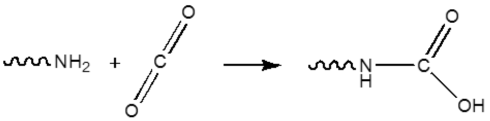

(2)

The 2:1 reaction stoicheiometry can be considered to arise from the transfer of the carbamic acid proton to a second, unreacted amine group, removing that second amine from the pool available to react with $CO_2$.

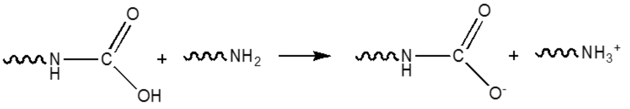

(3)

Because MEA is widely used today for $CO_2$ capture and its stoicheiometry has been well studied, it is taken here as a base case for comparison against two amine-functionalised cations (Figure 1, upper), 1-aminomethylpyridinium and

Downloaded by COLUMBIA UNIV on June 28, 2012 | http://pubs.acs.org
Publication Date (Web): December 18, 2009 | doi: 10.1021/bk-2009-1030.ch027

Downloaded by COLUMBIA UNIV on June 28, 2012 | http://pubs.acs.org
Publication Date (Web): December 18, 2009 | doi: 10.1021/bk-2009-1030.ch027

4-aminomethylpyridinium, and two amino-acid-based anions (Figure 1, lower), glycine and taurine.

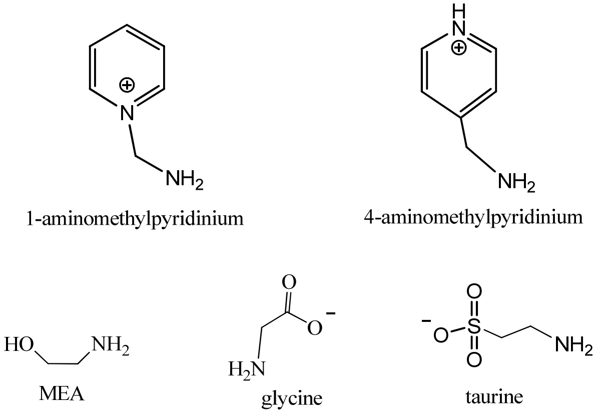
1-aminomethylpyridinium
4-aminomethylpyridinium
MEA
glycine
taurine

*Figure 1: Chemical structures of functionalised amines*

We report the conformation-averaged energies of reactions (2) and (3) for each of these functionalised amines, and find that reaction (2) is uniformly exothermic, and reaction energies vary only several kcal mol$^{-1}$ across the various amines studied. Because it involves a charge separation, reaction (3) as written in the gas-phase is uniformly endothermic. This background electrostatic contribution can be removed by referencing all energies to the MEA reaction (3) energy. As shown below, these results indicate that reaction (3) is promoted by cation-tethering but inhibited by anion-tethering. Thus, the choice of anion- or cation-tethering is expected to have a greater influence on the $CO_2$ capture reaction than the exact structure of the cation or anion.

## Methods

The molecular structures and energies of reactant amine and product carbamate species were calculated using the B3LYP hybrid density functional theory (DFT) functional *(30, 31)* and the 6-311++G(d,p) basis, as implemented in the Gaussian *(32)* program. Geometry optimisation *via* the Berny algorithm is used to locate stable molecular structures. Many of these species exhibit several conformations arising from rotations about internal bonds; the conformational space of each species was explored by systematically varying dihedral angles about all rotatable bonds, as shown in Figure 2, and performing geometry optimisations to locate all local energy minima.

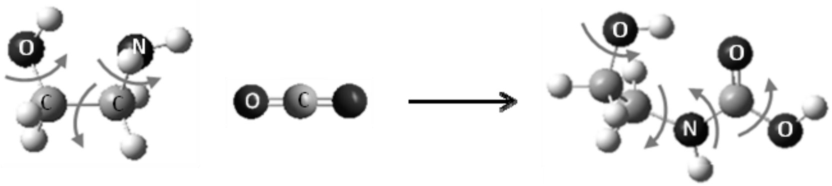

*Figure 2: Example of rotatable bonds explored to identify local energy minima.*

The total number of reactant and product conformations ranged from eight (4-aminomethylpyridinium) to forty-eight (MEA). The internal electronic energy $E_{DFT,i}$ of each conformer $i$ was calculated after geometry optimisation. Harmonic vibrational frequencies of each optimised conformer were obtained analytically. The zero-point vibrational energy (ZPVE) is determined by:

$$ZPVE = \frac{1}{2}h\sum_{j=1}^{3n-6} v_j \tag{4}$$

where $v_j$ are the $3n$-6 harmonic vibrational frequencies of an $n$ atom molecule, and $h$ is Planck's constant. The zero-point corrected internal energy is $E_{o,I} = E_{DFT,i} + ZPVE$. A Boltzmann distribution was used to average over these at 298 K; the Boltzmann-weighted internal energy of species $N$ is given by:

$$E_N = \sum_i w_i E_{o_i} \tag{5}$$

where $w_i$ is the Boltzmann weight defined by $\exp\{-E_{o,i}/(k_B T)\}$, where $k_B$ is Boltzmann's constant. Reaction energies are determined by the difference between the weighted total energies of products and reactant:

$$\Delta E_{rxn} = \sum_{N_{products}} E_N - \sum_{N_{reactants}} E_N \tag{6}$$

# Results

Table 1 shows the most stable conformers for the reactants and products of both the carbamic acid formation reaction (Equation 2) and the deprotonation reaction (Equation 3), as well as the Boltzmann-weighted, zero-point corrected energies for both reactions. Also included in the Table is the Mulliken charge on the amine nitrogen of each species, which indicates how the charge of the molecule is distributed with regards to the amine nitrogen, as well as the $CO_2$-nitrogen distance for each product.

## Carbamic Acid Reaction, Equation (2)

As can be seen in Table 1, the most stable unreacted MEA conformer has internal hydrogen bonding between the alcohol hydrogen and amine nitrogen. When MEA combines with $CO_2$ to form carbamic acid, one hydrogen atom (that was previously attached to the nitrogen) moves to one of the $CO_2$ oxygen atoms to form the carbamic acid group. A conjugated π bond is formed between the amine nitrogen and $CO_2$ carbon, as evidenced by the near planarity of the C(H)N=COOH fragment and the C–N bond distance of 1.35 Å, intermediate between that typical of C–N single (1.47 Å as calculated for $CH_3$-$NH_2$) and double (1.27 Å as calculated for $(CH_3)_2C$=$NCH_3$) bonds. The C–O bond distances lengthen from 1.16 Å in unreacted $CO_2$ to 1.22 and 1.36 Å, and the O-C-O-H group prefers to be *cis*, as is typical of carboxylic acid groups. In the lowest energy conformation, the MEA molecule is bent in such a way that hydrogen bonding occurs between the hydroxyl group and the carbamic acid

Downloaded by COLUMBIA UNIV on June 28, 2012 | http://pubs.acs.org
Publication Date (Web): December 18, 2009 | doi: 10.1021/bk-2009-1030.ch027

group. This internal hydrogen bonding provides 2.89 kcal $mol^{-1}$ of stabilisation relative to a conformation without this interaction. The lowest energy MEA zero-point-corrected reaction energy is 0.89 kcal $mol^{-1}$, while the conformation-averaged reaction energy is 1.06 kcal $mol^{-1}$.

We compared these results to two pyridinium cation-tethered amines that differ in the separation between the amine and ring pyridinium nitrogen. In the 1-aminomethylpyridinium case, the aminomethyl group is attached to the ring nitrogen while in 4-aminomethylpyridinium it is *para* to the ring nitrogen. Both cation reactants have similar structures and differ only slightly in the Mulliken charges on the amine nitrogen atoms. When the cation-tethered amines combine with $CO_2$, the products are similar to MEA, in that they all exhibit the same partial double bond character between nitrogen and carbon. All three prefer conformations in which the O-C-O-H dihedral angle is in the *cis* configuration. The calculated aminomethylpyridinium reaction energies are slightly less exothermic than the MEA reaction, by +5 and +3 kcal $mol^{-1}$ for the 1- and 4-substituted pyridiniums, respectively. Cation-tethering and amine positioning thus have modest destabilising effects on the 1:1 reaction energies.

These results can be contrasted with those for the anion-tethered amines glycine and taurine (Table 1). These are naturally occurring amino acids, differing in the acid functional groups (carboxylate *vs.* sulfonate) and in the distance between amine and anion groups. Similar to MEA, both glycine and taurine exhibit some internal hydrogen bonding. In the lowest energy conformations of both anions, the amine hydrogen atoms are directed towards the acid groups at the opposite end of the molecule, as shown in Table 1. Both anion-tethered amines have less negative Mulliken charges on the nitrogen atom than MEA. The nitrogen atom in glycine has a charge of -0.411 and that in taurine has a charge of -0.344, compared to -0.432 in MEA. When combined with $CO_2$, both anion-tethered amines form partial double bonds between the nitrogen atom of the compound and the carbon atom of the $CO_2$, just as for MEA and both cation-tethered amines. Similar to MEA and the two cation-tethered amines, the taurine-$CO_2$ complex has an O-C-O-H dihedral angle that is in the *cis* configuration. Taurine, compared to MEA, has a shorter nitrogen-$CO_2$ bond distance of 1.34 Å compared to 1.35 Å. The shorter bond distance indicates a stronger bond and a more stable product, which is consistent with a taurine reaction energy 8 kcal $mol^{-1}$ more exothermic than MEA.

The glycine-$CO_2$ complex differs from all others in preferring an O-C-O-H dihedral angle close to 180°. This unusual distortion is due to significant internal hydrogen bonding between carboxylate and carbamate groups on opposite ends of the molecule. As can be seen in Table 1, what was an amine hydrogen atom bridges the oxygen atoms, more closely approaching the carbamate, and imparting significant stabilisation to the product. Referenced to this product conformation, glycine has a reaction energy 15 kcal $mol^{-1}$ more exothermic than MEA due to this stabilising internal hydrogen bonding. Other product conformations do not have this same level of hydrogen bonding and as such are less exothermic by 8 kcal $mol^{-1}$ or more.

Downloaded by COLUMBIA UNIV on June 28, 2012 | http://pubs.acs.org
Publication Date (Web): December 18, 2009 | doi: 10.1021/bk-2009-1030.ch027

Downloaded by COLUMBIA UNIV on June 28, 2012 | http://pubs.acs.org
Publication Date (Web): December 18, 2009 | doi: 10.1021/bk-2009-1030.ch027

**Table 1: The lowest energy reactant and product conformations of the carbamate formation reaction (2) and the deprotonation reaction (3). Molecules from top to bottom are the 1-aminomethylpyridinium cation, the 4-aminomethylpyridinium cation, monoethanolamine, the glycine anion, and the taurine anion. Boltzmann-weighted carbamate formation energies normalised to MEA are shown between columns 1 and 2; deprotonation energies are similarly shown between columns 2 and 3.**

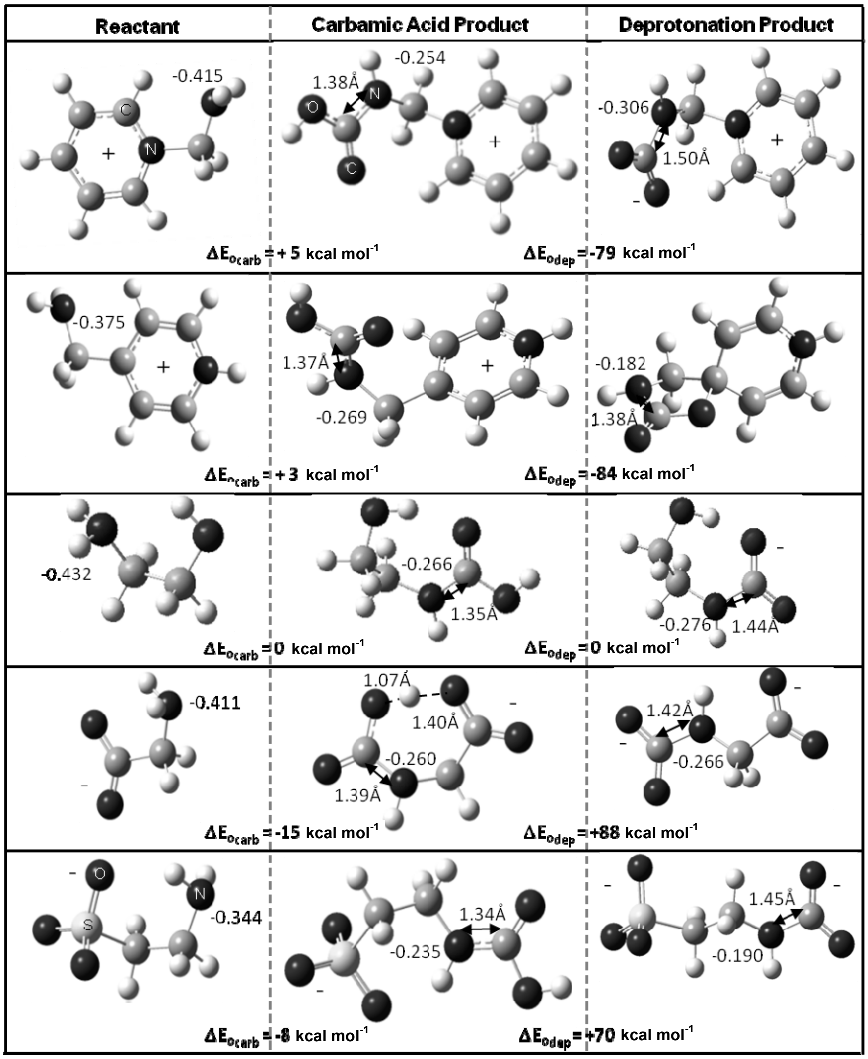
Reactant
Carbamic Acid Product
Deprotonation Product
-0.415
C
N
+
1.38Å
-0.254
O
N
C
+
-0.306
1.50Å
+
-
ΔE$_{0carb}$ = + 5 kcal mol$^{-1}$
ΔE$_{0dep}$ = -79 kcal mol$^{-1}$
-0.375
+
1.37Å
-0.269
+
-0.182
1.38Å
ΔE$_{0carb}$ = + 3 kcal mol$^{-1}$
ΔE$_{0dep}$ = -84 kcal mol$^{-1}$
-0.432
-0.266
1.35Å
-
-0.276
1.44Å
ΔE$_{0carb}$ = 0 kcal mol$^{-1}$
ΔE$_{0dep}$ = 0 kcal mol$^{-1}$
-0.411
-
1.07Å
1.40Å
-
-0.260
1.39Å
1.42Å
-
-
-0.266
ΔE$_{0carb}$ = -15 kcal mol$^{-1}$
ΔE$_{0dep}$ = +88 kcal mol$^{-1}$
- O
S
N
-0.344
1.34Å
-0.235
-
-
1.45Å
-
-0.190
ΔE$_{0carb}$ = -8 kcal mol$^{-1}$
ΔE$_{0dep}$ = +70 kcal mol$^{-1}$

In summary, the cation-tethered amines are calculated to react slightly less exothermically with $CO_2$ by reaction (2) than does MEA, while the anion-tethered react slightly more exothermically, consistent with the greater basicity expected for an anion. In these single ion models, internal hydrogen bonding can contribute significantly to overall reaction energies; in real environments, such hydrogen bonding is likely to take place *via* intermolecular hydrogen bonding *(33)*.

## Deprotonation Reaction, Equation (3)

All the carbamic acid products of reaction (2) have at least two potentially acidic protons, the amine and the carbamic acid hydrogen atoms. In all cases, the carbamic acid proton is the most acidic and most readily removed.

Table 1 shows the minimum energy conformation of the deprotonated carbamate of MEA, which is similar in structure to the carbamic acid and preserves the internal hydrogen bonding between carboxylate and alcohol groups. With deprotonation, the partial double bond between the nitrogen atom and $CO_2$ is lost, as the bond length between them increases from 1.35 Å in the carbamic acid to 1.44 Å in the carbamate and the carbamate fragment changes from being planar to pyramidal. The O-C-O angle of the carbamate group increases from 122° for the protonated form to 129° for the deprotonated form. Also with deprotonation, the C-O bonds of the carbamate change from 1.22 Å to 1.27 Å for the double bonded oxygen and from 1.36 Å to and 1.25 Å for the oxygen that was attached to the deprotonated hydrogen.

With deprotonation, both 1-aminomethylpyridinium and 4-aminomethylpyridinium form neutral zwitterions. Similar to MEA, with deprotonation, 1-aminomethylpyridinium loses the double bond characteristic between the nitrogen atom and carbon of the $CO_2$ as the bond distance lengthens from 1.38 to 1.50 Å. For the 4-aminomethylpyridinium, the double bond characteristic stays intact as the N-C bond distance only increases from 1.37 to 1.38 Å. With deprotonation, a new bond forms in 4-aminomethylpyridinium between one of the oxygen atoms of the carbamate group and a carbon of the ring as shown in Table I. Due to this intermolecular interaction, the Mulliken charge on the amine increases from -0.27 to -0.18. This differs from both MEA and 1-aminomethylpyridinium, where with deprotonation, the Mulliken charge on the nitrogen atom becomes more negative.

The averaged energies show that both cation-tethered amines are more easily deprotonated than MEA by -79 and -84 kcal $mol^{-1}$, respectively, when all three are referenced to the same proton acceptor. This large negative relative energy is due to the electrostatic stabilisation that arises between the opposite charges of these overall neutral zwitterions. While the magnitude of this electrostatic interaction is undoubtedly significantly overestimated due to the neglect of screening that would occur within an ionic liquid, the chemical tethering that ensures the proximity of these two will ensure that a significant amount of this interaction will be preserved.

Glycine and taurine both form dianions when deprotonated. Similar to MEA and both cation-tethered amines, both glycine and taurine no longer show double bond characteristics between the nitrogen and carbon atoms as the bonds between the two lengthen from 1.39 Å to 1.42 Å for glycine and from 1.34 Å to 1.45 Å for taurine. A single N-C bond is 1.47 Å, as calculated for $CH_3$-$NH_2$, while an N=C double bond is 1.27 Å, as calculated for $(CH_3)_2C{=}NCH_3$. As both anion-tethered amines form dianions, they prefer to adopt more linear conformations that move the anionic centres apart, as can be seen in Table 1.

Downloaded by COLUMBIA UNIV on June 28, 2012 | http://pubs.acs.org
Publication Date (Web): December 18, 2009 | doi: 10.1021/bk-2009-1030.ch027

The glycine and taurine deprotonation reaction energies are +88 and +70 kcal mol$^{-1}$ greater than MEA, respectively, due to this electrostatic repulsion between the two anionic ends of the products.

## Discussion

The $CO_2$ uptake capacity of amine-functionalised ionic liquids will be determined by the relative extents of reactions (2) and (3). If reaction terminates with the formation of carbamic acid product (that is, if amine hydrogen atoms remain associated with the carbamate functional groups), then every amine can react with a $CO_2$ and a 1:1 reaction stoicheiometry would be observed, which corresponds to a 50% mole fraction of $CO_2$ in the liquid phase. On the other hand, if deprotonation is favoured (that is, if carbamic acid protons prefer to transfer to unreacted amine groups to form ammonium), then each $CO_2$ reacted consumes two amines, and a 2:1 reaction stoicheiometry results, which corresponds to a 33% mole fraction of $CO_2$ in the liquid phase. This factor-of-two difference in capacity could have a significant impact on the viability of functionalised ionic liquids for $CO_2$ capture.

The carbamate formation energies for reaction (2) were calculated to vary over a window of about 13 kcal mol$^{-1}$, neglecting the likely artificially large stability of the glycine carbamic acid. As shown in Table 1, anion tethering generally leads to more exothermic reactions than MEA, and cation tethering to less exothermic. These energy differences are modest, but to the extent there is a trend, anion tethering favours reaction (2) to a greater extent than reaction (3).

The proton transfer energies for reaction (3) normalised to MEA vary over a large range, from > +70 kcal mol$^{-1}$ for cation-tethering to < –80 kcal mol$^{-1}$ for anion tethering. These energy differences arise from the very different electrostatics of the products: the dication products of cation-tethered amines are strongly disfavoured relative to the zwitterionic products of anion-tethered amines. Again, these energy differences are exaggerated by the neglect of any screening in these gas-phase calculations, but they do illustrate the potentially significant impact of electrostatics on product selectivity.

While definitive predictions cannot be made, these results indicate that anion tethering generally promotes the 1:1 stoicheiometry, while cation tethering promotes the more commonly assumed 2:1 stoicheiometry. Experimental observations support these predictions. Some experiments have been carried out to determine $CO_2$ isotherms both volumetrically and gravimetrically for amine-tethered imidazolium cations. These studies find a 33% maximum $CO_2$ uptake capacity *(20,21,34)*. Few experiments have been reported on anion-tethered amines. Zhang and coworkers determined $CO_2$ isotherms and IR spectra for $CO_2$ absorption by amino acid ionic liquids, which are essentially anion-tethered amines. The results from their experiments show a maximum capacity of 50% $CO_2$ uptake using the anion-tethered amines *(22)*. Davis and coworkers used gravimetric measurements to determine $CO_2$ absorption by amine containing anions, and found that some of them exhibited a 1:1 reaction stoicheiometry with $CO_2$ *(23)*.

Much of the emphasis in development of neutral amines for $CO_2$ capture

Downloaded by COLUMBIA UNIV on June 28, 2012 | http://pubs.acs.org
Publication Date (Web): December 18, 2009 | doi: 10.1021/bk-2009-1030.ch027

has centred on tuning the reaction thermodynamics and kinetics by varying amine substituents or using amine mixtures *(35,36)*. Amine-functionalised ionic liquids *(20)* introduce an additional optimisation parameter: the amine-tethering site. The results here indicate that this choice can impact not only reaction energies but even reaction stoicheiometry, with potentially significant impacts on $CO_2$ capture capacity.

## Conclusions

In this work, DFT-based atomistic computations were used to probe the potential importance of cation *vs.* anion tethering on the energy and stoicheiometry of $CO_2$ reactions with primary amines. Comparisons of reaction products and reaction energies normalised to a neutral amine indicate that anion-tethered amines tend to favour a 1:1 $CO_2$ reaction ratio or 50% $CO_2$ uptake capacity, while cation tethered amines tend to favour a 2:1 $CO_2$ reaction ratio or 33% $CO_2$ uptake capacity. Experimental reports support these conclusions, although detailed product analyses remain to be done to confirm the observations. The computations neglect the effects of ion-pairing and solvation on the overall reaction energies, and the inclusion of such effects is the topic of future work. Nonetheless, anion-tethered amines would appear to be a promising avenue for optimising $CO_2$-capture in functionalised ionic liquids, and atomistic computations can provide a useful screening tool for selecting these anions.

## Acknowledgments

The authors would like to acknowledge the Maginn and Brennecke groups at the University of Notre Dame for their input and help. For our computer resources, we would like to thank the University of Notre Dame Center for Research Computing. Funding for this project was provided by the DOE NETL grant number DE-FC26-07NT4309, and by the University of Notre Dame Lilly Fellowship.

## References

1. Schrag, D. P. *Science* **2007***, 315*, 812-813.
2. Kintisch, E. *Science* **2007***, 317*, 184-186.
3. Kintisch, E. *Science* **2007***, 315*, 1481-1481.
4. Astarita, G.; Marrucci, G.; Gioia, F. *Chem. Eng. Sci.* **1964***, 19*, 95-103.
5. Danckwerts, P. V.; McNeil, K. M. *Trans. Inst. Chem. Eng.* **1967***, 45*, T32-T49.
6. Lee, J. I.; Otto, F. D.; Mather, A. E. *J. Appl. Chem. Biotechnol.* **1976***, 26*, 541-549.
7. Hikita, H.; Asai, S.; Ishikawa, H.; Honda, M. *Chem. Eng. J.* **1977***, 13*, 7-12.
8. Crooks, J. E.; Donnellan, J. P. *J. Chem. Soc. Perkins Trans. 2* **1989**, 331-333.

Downloaded by COLUMBIA UNIV on June 28, 2012 | http://pubs.acs.org
Publication Date (Web): December 18, 2009 | doi: 10.1021/bk-2009-1030.ch027

9. Laddha, S. S.; Danckwerts, P. V. *Chem. Eng. Sci.* **1981**, *36*, 479-482.
10. Brennecke, J. F.; Maginn, E. J. *AIChE J.* **2001**, *47*, 2384-2389.
11. Anthony, J. L.; Maginn, E. J.; Brennecke, J. F. *J. Phys. Chem. B* **2002**, *106*, 7315-7320.
12. Baltus, R. E.; Culbertson, B. H.; Dai, S.; Luo, H.; DePaoli, D. W. *J. Phys. Chem. B* **2003**, *108*, 721-727.
13. Kamps, A. P.; Tuma, D.; Xia, J.; Maurer, G. *J. Chem. Eng. Data* **2003**, *48*, 746-749.
14. Camper, D.; Scovazzo, P.; Koval, C.; Noble, R. *Ind. Eng. Chem. Res.* **2004**, *43*, 3049-3054.
15. Cadena, C.; Anthony, J. L.; Shah, J. K.; Morrow, T. I.; Brennecke, J. F.; Maginn, E. J. *J. Am. Chem. Soc.* **2004**, *126*, 5300-5308.
16. Anthony, J. L.; Anderson, J. L.; Maginn, E. J.; Brennecke, J. F. *J. Phys. Chem. B* **2005**, *109*, 6366-6374.
17. Shiflett, M. B.; Yokozeki, A. *Ind. Eng. Chem. Res.* **2005**, *44*, 4453-4464.
18. Anderson, J. L.; Dixon, J. K.; Brennecke, J. F. *Acc. Chem. Res.* **2007**, *40*, 1208-1216.
19. Anderson, J. L.; Anthony, J. L.; Brennecke, J. F.; Maginn, E. J. In *Gas Solubilities in Ionic Liquids*; Wasserschneid, P.; Welton, T., Eds.; Ionic Liquids in Synthesis; Wiley-VCH: Weinheim, 2007; Vol. 1, pp 103-129.
20. Bates, E. D.; Mayton, R. D.; Ntai, I.; Davis, James H., Jr. *J. Am. Chem. Soc.* **2002**, *124*, 926-927.
21. Yuan, X.; Zhang, S.; Liu, J.; Lu, X. *Fluid Phase Equilibria* **2007**, *257*, 195-200.
22. Zhang, J.; Zhang, S.; Dong, K.; Zhang, Y.; Shen, Y.; Lv, X. *Chem. Eur. J.* **2006**, *12*, 4021-4026.
23. Soutullo, M. D.; Odom, C. I.; Wicker, B. F.; Henderson, C. N.; Stenson, A. C.; Davis, J. H. Jr., *Chem. Mater.* **2007**, *19*, 3581.
24. Cramer, C. J. In *Essentials of Computation Chemistry: Theories and Models*, 2nd Ed.*;* John Wiley & Sons: West Sussex, England, 2004; pp 596.
25. da Silva, Eirik F.; Svendsen, H. F. *Ind. Eng. Chem. Res.* **2004**, *43*, 3413-3418.
26. Arstad, B.; Blom, R.; Swang, O. *J. Phys. Chem. A* **2007**, *111*, 1222-1228.
27. Carpenter, B. K. *J. Phys. Chem. A* **2007**, *111*, 3719-3726.
28. da Silva, Eirik F. *J. Phys. Chem. A* **2005**, *109*, 1603-1607.
29. Jamroz, M. H.; Dobrowolski, J. C.; Borowiak, M. A. *J. Mol. Strut.* **1997**, *404*, 105-111.
30. Becke, A. D. *J. Chem. Phys.* **1993**, *98*, 5648-5652.
31. Lee, C.; Yang, W.; Parr, R. G. *Phys. Rev. B* **1988**, *37*, 785-789.
32. Frisch, M. J.; Trucks, G. W.; Schlegel, H. B.; Scuseria, G. E.; Robb, M. A.; Cheeseman, J. R.; Montgomery, Jr., J. A.; Vreven, T.; Kudin, K. N.; Burant, J. C.; Millam, J. M.; Iyengar, S. S.; Tomasi, J.; Barone, V.; Mennucci, B.; Cossi, M.; Scalmani, G.; Rega, N.; Petersson, G. A.; Nakatsuji, H.; Hada, M.; Ehara, M.; Toyota, K.; Fukuda, R.; Hasegawa, J.; Ishida, M.; Nakajima, T.; Honda, Y.; Kitao, O.; Nakai, H.; Klene, M.; Li, X.; Knox, J. E.; Hratchian, H. P.; Cross, J. B.; Bakken, V.; Adamo, C.; Jaramillo, J.; Gomperts, R.; Stratmann, R. E.; Yazyev, O.; Austin, A. J.; Cammi, R.; Pomelli, C.; Ochterski, J. W.; Ayala, P. Y.; Morokuma, K.; Voth, G. A.;

Downloaded by COLUMBIA UNIV on June 28, 2012 | http://pubs.acs.org
Publication Date (Web): December 18, 2009 | doi: 10.1021/bk-2009-1030.ch027

Salvador, P.; Dannenberg, J. J.; Zakrzewski, V. G.; Dapprich, S.; Daniels, A. D.; Strain, M. C.; Farkas, O.; Malick, D. K.; Rabuck, A. D.; Raghavachari, K.; Foresman, J. B.; Ortiz, J. V.; Cui, Q.; Baboul, A. G.; Clifford, S.; Cioslowski, J.; Stefanov, B. B.; Liu, G.; Liashenko, A.; Piskorz, P.; Komaromi, I.; Martin, R. L.; Fox, D. J.; Keith, T.; Al-Laham, M. A.; Peng, C. Y.; Nanayakkara, A.; Challacombe, M.; Gill, P. M. W.; Johnson, B.; Chen, W.; Wong, M. W.; Gonzalez, C.; and Pople, J. A. **2004***, Gaussian 03, Revision D01*.

33. Gutowski, K. E.; Maginn, E. J. *J. Am. Chem. Soc.* **2008**, *130*, 14690-14704.
34. Zhang, S.; Yuan, X.; Chen, Y.; Zhang, X. *J. Chem. Eng. Data* **2005**, 50, 1582-1585.
35. Dang, H.; Rochelle, G. T. *Sep. Sci. Tech.* **2003**, 38, 337-357.
36. Al-Juaied, M.; Rochelle, G. T. *Chem. Eng. Sci.* **2006**, 61, 3830-3837.

Downloaded by COLUMBIA UNIV on June 28, 2012 | http://pubs.acs.org
Publication Date (Web): December 18, 2009 | doi: 10.1021/bk-2009-1030.ch027

# Author Index

Alammar, T., 177–188
Anthony, J. L., 189–197
Atkin, R., 317–333

Bäcker, T., 177–188
Baldelli, S., 291–304, 335–358
Ballone, P., 403–418
Bovio, S., 273–290
Buchner, R., 61–74

Chujo, Y., 211–220
Constantinescu, D., 107–117
Costa Gomes, M. F., 223–237
Coutinho, J. A. P., 385–401

de Haan, A. B., 255–272
Del Pópolo, M. G., 403–418
Dyson, P. J., 135–146

Elliott, G. D., 95–105
Erdmenger, T., 147–155

Farrell, J., 239–253

Gardas, R. L., 385–401
Ge, R., 43–60
Guerrero-Sanchez, C., 147–155

Hardacre, C., 43–60, 359–383
Hefter, G., 61–74
Henderson, M. A., 135–146
Herrmann, C., 107–117
Hunger, J., 61–74
Husson, P., 223–237

Iwahashi, T., 305–316

Jacquemin, J., 43–60, 359–383
Jimenez-Regalado, E., 147–155

Kanai, K., 305–316
Kemp, R., 95–105
Kim, D., 305–316

Lara-Ceniceros, T., 147–155
Liu, Z., 75–91

MacFarlane, D. R., 95–105
McIndoe, J. S., 135–146
Manan, N. A., 359–383
Martinez, I. S., 335–358
Maurer, G., 1–20
Meindersma, G. W., 255–272
Milani, P., 273–290
Mindrup, E. M., 419–430
Miyamae, T., 305–316
Miyoshi, E., 211–220
Moyna, G., 75–91
Mudring, A.-V., 177–188

Naik, P. U., 239–253
Naka, K., 211–220
Narita, A., 211–220

O'Brien, B. B., 75–91
Ouchi, Y., 305–316

Petrik, I. D., 75–91
Podestà, A., 273–290

Remsing, R. C., 75–91
Richter, K., 177–188
Rivera-Rubero, S., 291–304
Rooney, D. W., 43–60, 359–383

Schneider, W. F., 419–430
Schubert, U. S., 147–155
Seki, K., 305–316
Shiflett, M. B., 21–42
Shkrob, I. A., 119–134
Singer, R. D., 239–253
Stoppa, A., 61–74
Sun, X., 189–197

Takayama, S., 157–173
Trider, C. L., 239–253
Tuma, D., 1–20
Tung, Y.–C., 157–173

Ueno, K., 199–210

Warr, G. G., 317–333
Watanabe, M., 199–210
Weingärtner, H., 107–117
Wishart, J. F., 119–134

Yokozeki, A., 21–42
Youngs, T. G. A., 359–383

Downloaded by 89.163.35.42 on June 28, 2012 | http://pubs.acs.org
Publication Date (Web): December 18, 2009 | doi: 10.1021/bk-2009-1030.ix001

# Subject Index

**A**

Absorption
  gas separations through, 224
  *See also* Gas separations
Acetone, Henry's law for $CO_2$ in, 229*f*
Activity models
  fluorocarbons, 27–28
  solubility, 360–361
Actuation
  droplet-based passive pumping, 159–160
  external magnetic field, 160–161
  ionic liquid for sustained stable, 169–170
  microfluidic schemes, 158–161
  multilayer soft lithography with pneumatic, 163
  *See also* Braille display microfluidics; Microfluidics
Advanced Fuel Cycle (AFC)
  nuclear fuel reprocessing, 120–121
  *See also* Nuclear fuel processing
Air/ionic liquid interface
  reference, 308–309
  *See also* Interfaces of ionic liquids
Alcohol dehydrogenase, differential scanning calorimetry, 115
1-Alkyl-3-methylimidazolium bromide $[C_n mim]Br$
  intermolecular forces vs. $SiO_2$ solubility, 194–195
  ionic liquids in study, 190, 191*t*
  melting points, 193
  silica saturation, 192*t*, 195
  solubility and side-chain length, 192
  *See also* Silica saturation
Amine functionalized ionic liquids
  anion and cation tethering, 427
  anion-tethered amines glycine and taurine, 424, 425*t*
  carbamate formation energies, 427
  carbamic acid reaction, 423–426
  chemical structures, 422*f*
  $CO_2$ capture, 420, 427–428
  $CO_2$ uptake capacity, 427
  comparing monoethanolamine (MEA) for $CO_2$ capture, 420, 421–422
  deprotonation reaction, 426–427
  development of neutral amines for $CO_2$ capture, 427–428
  electronic structure computations, 421
  lowest energy reactant and product conformations, 425*t*
  methods, 422–423
  proton transfer energies, 427
  pyridinium cation-tethered amines, 424
  task-specific ionic liquids, 420–421
  tethering choice for amine functionality, 421
Anions
  density of $[C_4mim]^+$ based ionic liquids, 46*f*
  nomenclature for ionic liquids, 54–55
Anti-microbial activity, protein or cellular formulations, 101–102
Antoine correlation
  calculated energies of gas and change of energy by, 369*t*
  calculation of gas vapor pressures, 366*f*
  correlation plot of estimated vapor pressures, 370*f*
  estimated propene vapor pressure vs. energy value, 368*f*
Apparatus
  measuring gas solubility in solvent, 3*f*
  measuring phase equilibria at elevated pressures, 14*f*, 15
Aromatic/aliphatic hydrocarbon separation
  ASPEN simulation of toluene extraction, 266*t*
  1-butyl-4-methylpyridinium tetrafluoroborate $[C_4m^4py][BF_4]$, 259
  column experiments, 263–264
  comparing extraction with sulfolane and ionic liquid $[C_4mpy][BF_4]$, 267–269
  cracker plants, 256–257

Downloaded by 89.163.35.42 on June 28, 2012 | http://pubs.acs.org
Publication Date (Web): December 18, 2009 | doi: 10.1021/bk-2009-1030.ix002

Downloaded by 89.163.35.42 on June 28, 2012 | http://pubs.acs.org
Publication Date (Web): December 18, 2009 | doi: 10.1021/bk-2009-1030.ix002

  - distribution coefficients for aliphatics with [$C_4m^4py$][$BF_4$], 260*f*
  - economic evaluation, 262–263, 267–269
  - equipment and variable costs, 267
  - estimated investment and variable costs, 268*t*
  - experimental and calculated data for toluene extraction with [$C_4mpy$][$BF_4$], 265*t*
  - extraction with ionic liquids, 258–260
  - flow scheme for, 266*f*
  - flow scheme of naphtha cracker, 256*f*
  - future research, 269–271
  - investment and annual costs for extraction with ionic liquids, 268*f*
  - methods and materials, 258–263
  - naphtha feed composition, 257*t*
  - pilot plant column, 261*f*
  - rotating disc contactor (RDC), 260–261
  - selectivities for aliphatics with [$C_4m^4py$][$BF_4$], 260*f*
  - sulfolane process, 262–263
  - toluene extraction from toluene/heptane with [$C_4mpy$][$BF_4$], 264–269
  - toluene/heptane separation with ionic liquids, 259*f*
- Atomic force microscopy (AFM)
  - AFM topographic maps of [$C_4mim$][$NTf_2$] thin films, 278*f*
  - measurement method, 276
  - statistical analysis, 276–277
  - *See also* Thin films of [$C_4mim$][$NTf_2$]

**B**

- Benzene, Henry's law for $CO_2$ in, 229*f*
- Biocompatibility, ionic liquids, 99
- Biomedical applications
  - anti-microbial activity, 101–102
  - biocompatibility of ionic liquids (ILs), 99
  - biological formulation, 98–103
  - clinical translation, 103–104
  - ionic liquids (ILs), 95–96
  - maximizing shelf-life, 97
  - osmolality of formulations, 102–103
  - shelf life, 100–101
  - solubility of proteins in ILs, 99–100
  - specialized packaging, 97, 98*f*
  - thermal stability, 100–101
- Boltzmann equation, surface potential, 341
- Bovine ribonuclease A (RNase A). *See* Ribonuclease A (RNase A)
- Braille display microfluidics
  - device design, 168–169
  - device fabrication and preparation, 170–171
  - fabrication process of device with ionic liquid filled, 171*f*
  - fluid flow control, 166–168
  - ionic liquid filled hydraulic valve, 168–171
  - ionic liquid for sustained stable actuation, 169–170
  - photographs, 167*f*
  - schematic of, systems, 167*f*
  - schematic of, with ionic liquid filled hydraulic valves, 169*f*
  - valve ability to stay closed on actuation, 170*f*
  - *See also* Microfluidics
- Butane
  - calculated energies by Antoine equation, 369*t*
  - calculation of gas vapor pressure, 366*f*
  - constants for calculation of vapor pressure, 367*t*
  - literature and predicted values for solubility in [$C_4mim$][$NTf_2$], 363, 364*f*
- Butanol/ionic liquid interface
  - butanol molecular configuration, 312, 313*f*
  - cation configuration, 311
  - interfacial structure, 312, 313*f*
  - liquids with similar polarity, 311–312, 313*f*
  - possible model structure, 313*f*
  - *See also* Interfaces of ionic liquids
- 1-Butene
  - calculated energies by Antoine equation, 369*t*
  - constants for calculation of vapor pressure, 367*t*
- 1-Butyl-1-methylpyrrolidinium bis(trifluoromethylsulfonyl)amide [$C_4mpyr$][$NTf_2$]

  gas solubility in, 4*t*
  heat capacity, 50*f*
  Henry's law for $CO_2$ in, 227*f*
1-Butyl-1-methylpyrrolidinium tris(perfluoroethyl)trifluorophosphate [$C_4$mpyr][FAP]
  heat capacity, 50*f*
  thermal conductivity, 53*f*
1-Butyl-3-methylimidazolium bis(trifluoromethylsulfonyl)amide [$C_4$mim][$NTf_2$]
  capacitance-potential plots for Pt electrode in, 302*f*
  correlation plots for calculating gas solubility in, 370, 371*f*
  cyclic voltammetry, 296
  density, 46*f*
  description of inside shaft design, 295*f*
  determining cation orientation at ionic liquid/Pt interface, 299
  double layer structure, 292
  double layer thickness, 300–301
  electrochemical cell for cyclic voltammetry and impedance measurements, 294*f*
  electrochemical impedance spectroscopy (EIS) for double layer thickness, 301–302
  experimental, 293–295
  heat capacity, 50*f*
  Henry's law for $CO_2$ in, 227*f*, 228*f*, 229*f*
  imidazolium ring molecular coordinate axes and surface coordinate axes, 300*f*
  literature values for butane and ethane solubility in, 363, 364*f*
  possible liquid phase structure for, 372, 373*f*
  potential changes in H-C(4)C(5)-H peak intensities for *ppp* and *ssp* spectra, 298–299
  prediction of butane and ethane solubility in, 363, 364*f*
  SFG (sum frequency generation vibrational spectroscopy) system, 292, 293, 293–295
  SFG *ppp* polarized spectra for, at Pt electrode, 296, 297*f*
  SFG spectra of CO on Pt electrode in, 301*f*
  SFG *ssp* polarized spectra for, at Pt electrode, 297, 298*f*
  simulation curve for *ppp/ssp* intensity ratio, 300*f*
  sketch of SFG-electrochemical cell, 295*f*
  Stark shift analysis, 295
  thermal conductivity, 53*f*
  transmission electron micrograph of copper evaporation into dispersion of ZnO nanorods in, 181*f*
  *See also* Thin films of [$C_4$mim][$NTf_2$]
1-Butyl-3-methylimidazolium chloride [$C_4$mim]Cl
  angular distribution functions (ADFs), 86*f*, 87*f*
  Arrhenius plots for ionic liquids and cellobiose solutions, 84, 85*f*
  $^{35/37}$Cl $T_1$ relaxation for chloride ion in, 82*f*
  correlation time ($\tau_c$) of nuclei in, 82–83, 84*f*
  $^{13}$C $T_1$ relaxation vs. cellobiose for C-2, C-4' and C-1" in, 81*f*
  $^{13}$C $T_1$ relaxation vs. temperature for C-2, C-4' and C-1" in, 80*f*
  ionic liquid, 76
  molecular dynamic simulation of [$C_4$mim]Cl/cellobiose, 85–86, 87*f*
  nuclear magnetic resonance (NMR) study of, with cellobiose, 79–85
  radial distribution functions (RDFs), 86*f*, 87*f*
  relaxation of chloride ion in solutions, 83
  solutions of cellobiose with, 77
  spatial distribution, 86, 87*f*
  structure and numbering, 77*f*
  temperature dependence of $^{35/37}$Cl $T_1$ relaxation of chloride ion, 81*f*
  *See also* Molecular dynamics (MD) simulation
1-Butyl-3-methylimidazolium dicyanamide [$C_4$mim][$N(CN)_2$]
  structure of ions, 338*f*
  sum frequency generation (SFG)-polarization mapping, 350–352
  surface potential, 353*t*
  surface tension, 353–354
  surface tension values from literature, 344*t*
  *See also* Ionic liquid characterization

Downloaded by 89.163.35.42 on June 28, 2012 | http://pubs.acs.org
Publication Date (Web): December 18, 2009 | doi: 10.1021/bk-2009-1030.ix002

Downloaded by 89.163.35.42 on June 28, 2012 | http://pubs.acs.org
Publication Date (Web): December 18, 2009 | doi: 10.1021/bk-2009-1030.ix002

- 1-Butyl-3-methylimidazolium hexafluorophosphate $[C_4mim][PF_6]$
  - binary azeotropic mixtures, 35–36
  - $[C_4mim]^+$ drawing, 405*f*
  - correlation of Henry's constants with $T_c$ for methane- and ethane-series HFCs in, 34*f*
  - $D_2O$/ionic liquid interface, 310, 311*f*
  - density, 46*f*
  - enthalpy of dissolution of $CO_2$ in, 234*f*
  - equation for Henry's law constants, 35
  - estimated $CO_2$ solubility in, 370, 372*f*
  - gas solubility in, 4*t*
  - Henry's law for $CO_2$ in, 228*f*
  - isothermal PTx phase diagrams for HFC–23 mixtures with, 32*f*
  - isothermal PTx phase diagrams for HFC–41 mixtures with, 33*f*
  - normalized fugacity vs. mole fraction refrigerant in, 31*f*
  - phase behavior of $CO_2$, methanol and, 16*f*
  - positive ion ESI–MS of [Ru(η6-4-isopropyltoluene)(η2-triphos)Cl]$[PF_6]$ in, 138, 139*f*
  - SFG spectra of butanol/$[C_8mim][PF_6]$ interface, 311–312, 313*f*
  - SFG spectra of $CCl_4$/ionic liquid interface, 309–310
  - simulation curve for *ppp/ssp* intensity ratio, 299, 300*f*
  - simulation for $CO_2$ solubility in, 11, 12*f*
  - sum frequency generation (SFG) spectra of air/ionic liquid interface, 308–309
  - three-phase liquid-liquid-vapor equilibrium, 16*f*
  - transmission electron micrograph of copper particles in $[C_4mim][PF_6]$, 181*f*
  - *See also* Electrospray ionization mass spectrometry (ESI–MS); Ionic liquid/naphthalene mixtures
- 1-Butyl-3-methylimidazolium methylsulfate $[C_4mim][CH_2SO_4]$
  - gas solubility in, 4*t*
  - simulation for $CO_2$ solubility in, 11, 12*f*
  - structure of ions, 338*f*
  - sum frequency generation (SFG) polarization mapping, 349–350
  - surface potential, 353*t*
  - surface tension values from literature, 344*t*
  - *See also* Ionic liquid characterization
- 1-Butyl-3-methylimidazolium octylsulfate $[C_4mim][C_8H_{17}SO_4]$, Henry's law for $CO_2$ in, 229*f*
- 1-Butyl-3-methylimidazolium tetrafluoroborate $[C_4mim][BF_4]$
  - density, 46*f*
  - dielectric relaxation (DR) spectrum, 64, 65*f*
  - gas solubilities as function of gas mole fraction and temperature, 231*f*
  - Henry's law for $CO_2$ in, 228*f*
  - positive-ion ESI–MS spectrum, 137*f*
  - structure of ions, 338*f*
  - sum frequency generation (SFG) polarization mapping, 350
  - surface potential, 353*t*
  - surface tension value from literature, 344*t*
  - *See also* Electrospray ionization mass spectrometry (ESI–MS); Ionic liquid characterization
- 1-Butyl-3-methylimidazolium trifluoromethanesulfonate $[C_4mim][OTf]$
  - density, 46*f*
  - heat capacity, 50*f*
  - thermal conductivity, 53*f*
- 1-Butyl-4-methylpyridinium tetrafluoroborate $[C_4m^4py][BF_4]$
  - aromatic/aliphatic selectivity, 260*f*
  - column experiments of toluene/heptane separation, 263–264
  - comparing, extraction with sulfolane process, 267–269
  - distribution coefficients, 260*f*
  - equipment and variable costs, 267
  - experimental and calculated extraction of toluene using, 265*t*
  - extraction simulations, 265, 266*t*
  - flow scheme for aromatic/aliphatic separation, 266*f*
  - future research, 270
  - investment and annual extraction costs, 268*t*

pilot plant column, 261*f*
rotating disc contactor (RDC), 260–261
toluene distribution coefficient, 259
toluene extraction from toluene/heptane, 264–269
toluene/heptane selectivity, 259*f*
*See also* Aromatic/aliphatic hydrocarbon separation

**C**

Capillary wave spectra, [$C_4$mim][$PF_6$], 339
Carbamic acid reaction
  amine functionalized ionic liquids, 423–426
  carbamate formation energies, 427
  lowest energy reactant and product conformations, 425*t*
Carbon dioxide ($CO_2$)
  calculated energies by Antoine equation, 369 *t*
  capture, 420, 427–428
  conformers and ion pairs on, solubility in [$C_4$mim][$NTf_2$], 373, 374*f*
  constants for calculation of vapor pressure, 367*t*
  efficiency of gas separations and ionic liquids, 229–230
  estimated solubility in ionic liquids, 370, 372*f*
  gas solubility in ionic liquid, 4, 5*f*
  Henry's law constants for, in various ionic liquids, 227*f*, 228*f*, 229*f*
  monoethanolamine (MEA) for industrial separation, 420, 421–422
  order of solubility, 371
  phase equilibria above critical temperature of, 15, 16*f*
  predicting solubility in ionic liquids, 10–11, 12*f*
Carbon-free energy, nuclear power, 119–120
Cations
  density of [$NTf_2$]$^-$ based ionic liquids, 46*f*
  nomenclature for ionic liquids, 55
Cavell equation, effective dipole moments, 70*f*, 72, 73*f*
$CCl_4$/ionic liquid interface
  hydrophobic, 309–310
  *See also* Interfaces of ionic liquids
Cellobiose. *See* Molecular dynamics (MD) simulation
Cellular therapies
  anti-microbial activity, 101–102
  ionic liquids, 96
  storage, 97
Chemical speciation
  diagram, 70, 71*f*
  dielectric relaxation (DR) spectroscopy, 62–63
Circular ferrofluidic pump, operating principle, 161
Clinical translation, protein stabilized formulations, 103–104
Cloud-point measurement, temperature, 27
Cobalt(II) chelate complex, ethylamine diacetic acid chelating ligand, 244, 245*f*
Coin metals, ionic liquids acting as metal reductant, 182, 183*f*
Cole–Cole process
  dielectric relaxation (DR), 67, 68*f*
  relaxation time for, 69, 71*f*
  *See also* Dielectric relaxation spectroscopy (DRS)
Colloidal dispersions
  applications, 199
  colloidal stability of silica particles in 1-alkyl-3-methylimidazolium ([$C_n$mim])-based ionic liquids, 200–201
  degree of self-dissociation, 202
  Derjaguin–Landau–Verwey–Overbeen (DLVO) theory, 201, 203
  direct TEM image of dilute suspension of bare silica particles in [$C_2$mim][$NTf_2$], 204*f*
  direct TEM image of dilute suspension of PMMA-grafted silica particles in [$C_2$mim][$NTf_2$], 206*f*
  DLVO interparticle interaction profile of bare silica particles, 203*f*
  dynamic strain sweep of nanocomposite ion gels, 207, 208*f*
  electrical double layer (EDL), 201, 202

Downloaded by 89.163.35.42 on June 28, 2012 | http://pubs.acs.org
Publication Date (Web): December 18, 2009 | doi: 10.1021/bk-2009-1030.ix002

Downloaded by 89.163.35.42 on June 28, 2012 | http://pubs.acs.org
Publication Date (Web): December 18, 2009 | doi: 10.1021/bk-2009-1030.ix002

- electrostatic repulsion in ionic liquids, 201–204
- ionic conductivity of nanocomposite ion gels, 207*f*
- ionicity, 202
- ionic liquids as, media for nanomaterials, 199–200
- nanocomposite ion gels, 206–207
- plateau elastic modulus of nanocomposite ion gels, 207, 208*f*
- size distribution curves of bare silica particles, 204*f*
- size distribution curves of PMMA-grafted silica particles, 205*f*
- steric repulsion in ionic liquids, 205, 206*f*
- yield stress of nanocomposite ion gels, 207, 208*f*

Computer Aided Molecular Design (CAMD)
- ionic liquid design, 386, 399
- *See also* Thermophysical properties of ionic liquids

Conductivity, $[C_4mim][PF_6]$/naphthalene mixture, 410*f*

Contact angles
- AFM tapping-mode topography of $[C_4mim][NTf_2]$ film, 286*f*
- $[C_4mim][NTf_2]$ nanodroplets, 285–287
- measurement method, 277
- schematic of $[C_4mim][NTf_2]$ nanodroplet, 287*f*
- spherical cap model, 286*f*
- three-dimensional view of nanodroplet on layer, 286*f*
- *See also* Thin films of $[C_4mim][NTf_2]$

Contaminants, organic, in ionic liquids, 336–337

Copper(II) chelate complex
- aqueous copper(II) removal using functionalized ionic liquids, 246*f*, 247*t*
- ethylamine diacetic acid chelating ligand, 244, 245*f*
- synthesis of, based on oxime, 247, 248
- synthesis of, based on salen, 248, 249
- X-ray crystal structures, 248*f*, 250*f*
- *See also* Functionalized ionic liquids

Copper salts, ionic liquids reducing to metal, 182, 183*f*

Copper/zinc oxide (Cu/ZnO), nanocomposites, 181

Corrected energy, estimated propene vapor pressure vs. energy value, 368*f*

Correlation models, gas solubility, 360

COSMO-RS (conductor-like screening model-real solvents), 361

COSMOthermX
- abbreviations list, 363*t*
- advanced software tool, 361
- calculated energies for gas and change in energy, 369*t*
- calculations of gas solubility in ionic liquids, 361–362
- conformers and gas solubility in $[C_4mim][NTf_2]$, 373, 374*f*
- constants for calculation of vapor pressure, 367*t*
- continuing improvements, 374–375
- correlation plot of estimated vapor pressures using adjusted Turbomole energy value and Antoine equation, 369, 370*f*
- correlation plots for calculating gas solubilities in $[C_4mim][NTf_2]$, 370, 371*f*
- electron density functional theory, 361
- estimated $CO_2$ solubility in various ionic liquids, 370, 372*f*
- gas phase chemical potential, 364–365
- ion pairs and gas solubility in $[C_4mim][NTf_2]$, 373, 374*f*
- literature values for butane and ethane in $[C_4mim][NTf_2]$, 363, 364*f*
- order of $CO_2$ solubility, 371
- partial vapor pressure estimation, 364
- possible snap-shot of $[C_4mim][NTf_2]$, 372, 373*f*
- predicting gas solubility, 375–376
- pure vapor pressure and activity coefficient, 365, 366*f*
- quantum chemical total energies, 365
- relative absolution deviation (RAD), 362

Downloaded by 89.163.35.42 on June 28, 2012 | http://pubs.acs.org
Publication Date (Web): December 18, 2009 | doi: 10.1021/bk-2009-1030.ix002

  Turbomole program, 365
  variation in estimated propene vapor pressure vs. energy, 368*f*
Cryogenic distillation, gas separation, 224
1-Cyanomethyl-1-methylpyrrolidinium $[(NCCH_2)mpyr]^+$, density of $[NTf_2]^-$ based ionic liquid, 46*f*
1-Cyanomethylpyridinium $[(NCCH_2)py]^+$, density of $[NTf_2]^-$ based ionic liquid, 46*f*
Cyclohexane, Henry's law for $CO_2$ in, 229*f*

**D**

$D_2O$/ionic liquid interface
  hydrophilic, 310, 311*f*
  *See also* Interfaces of ionic liquids
Debye (D) process
  dielectric relaxation (DR), 67, 68*f*
  parameters from DR spectra for, in mixture, 72*f*
  *See also* Dielectric relaxation spectroscopy (DRS)
1-Decyl-3-methylimidazolium bis(trifluoromethylsulfonyl)amide $[C_{10}mim][NTf_2]$
  density, 46*f*
  thermal conductivity, 53*f*
Degree of self-dissociation, ionicity, 202
Delamination, $[C_4mim][NTf_2]$ thin films on silica, 281, 283*f*
Density
  $[C_4mim]^+$ based ionic liquids, 46*f*
  $[C_4mim][PF_6]$/naphthalene mixture, 405, 406*f*
  function of temperature for ionic liquids, 45
  impurities in ionic liquids, 46–47
  models estimating, 47–48
  $[NTf_2]^-$ based ionic liquids, 46*f*
  prediction for ionic liquids, 398*t*
  predictive method for estimating, 388
  vibrating-tube densitometer, 45
Density functional theory (DFT)
  B3LYP hybrid, 422–423
  COSMOthermX software tool, 361
Deprotonation reaction
  amine functionalized ionic liquids, 426–427
  lowest energy reactant and product conformations, 425*t*
  proton transfer energies, 427
Derjaguin–Landau–Verwey–Overbeek (DLVO) theory
  charged colloidal particle interaction, 201, 203
  DLVO interparticle interaction profiles of bare silica particles in salt system and ionic liquids, 203*f*
Dielectric relaxation spectroscopy (DRS)
  chemical speciation model, 70, 71*f*
  dipole moment for Cole–Cole process in mixtures, 70*f*
  effective dipole moments from Cavell equation, 72, 73*f*
  features, 63, 64*f*
  frequency-dependent complex permittivity, 62
  ion pairs in electrolyte solutions, 63
  mixtures of ionic liquids with polar solvents, 67–72
  origin of relaxation, 62–63
  oscillating electric field, 63*f*
  parameters for ($[C_4mim][BF_4]$ + $CH_2Cl_2$) mixtures, 69*f*
  parameters from DR spectra for Debye mode, 72*f*
  relaxation time for Cole–Cole process and bulk viscosity for mixture, 71*f*
  spectra for ($[C_4mim][BF_4]$ + $CH_2Cl_2$) mixtures, 68*f*
  spectra of ionic liquids, 64–66
  spectrum of $[C_2mim][EtSO_4]$, 66*f*
  spectrum of $[C_4mim][BF_4]$, 64, 65*f*
  spectrum of $MgSO_4$ (aq), 63, 65*f*
  studying chemical speciation in ionic liquids, 61, 62
Differential scanning calorimetry (DSC). *See* Proteins
Diffusion coefficient, $[C_4mim][PF_6]$/naphthalene mixture, 410, 411*f*
Diffusivity, gases in ionic liquids, 232, 233*f*
Dilution, ionic liquid by molecular solvent, 67, 68*f*
Dimethylmethanamide, surface tension, 353*t*
Dipole moment

Downloaded by 89.163.35.42 on June 28, 2012 | http://pubs.acs.org
Publication Date (Web): December 18, 2009 | doi: 10.1021/bk-2009-1030.ix002

  - [$C_4$mim][$BF_4$] + (MeCN or $H_2O$) mixture, 72, 73*f*
  - [$C_4$mim][$BF_4$] + $CH_2Cl_2$ mixture, 70*f*
- Direct recoil spectrometry, surface structure, 339
- Dissolution, enthalpy of, of $CO_2$ in ionic liquids, 234*f*
- Double layer structure, 1-butyl-3-methylimidazolium bis{(trifluoromethyl)sulfonyl}amide [$C_4$mim][$NTf_2$], 292
- Droplet-based passive pumping, actuation scheme, 159–160
- Drug formulations, maximizing shelf-life, 97
- Dynamic strain sweep, nanocomposite ion gels, 207, 208*f*

**E**

- Electrical conductivity
  - ionic liquids, 393–394
  - prediction for ionic liquids, 398*t*
- Electrical double layer (EDL), electrostatic repulsion, 201–202
- Electrochemical impedance spectroscopy (EIS)
  - capacitance and thickness of double layer of ionic liquid, 301–302
  - capacitance-potential plot, 302*f*
  - double layer structure of ionic liquid, 292
  - *See also* 1-Butyl-3-methylimidazolium bis(trifluoromethylsulfonyl)amide [$C_4$mim][$NTf_2$]
- Electrolyte solutions
  - chemical speciation, 62
  - dielectric relaxation (DR) sensitivity, 63
  - magnesium sulfate solution, 63, 65*f*
- Electron paramagnetic resonance (EPR)
  - aliphatic cations, 128
  - consistency with pulse radiolysis data, 130–131
  - electron affinities, 129
  - ionic liquid ions, 129
  - ionization potentials, 129
  - irradiated ionic liquids, 125–129
  - radical generation, 126–127
  - radiolysis, 125–126
  - spreading spin density, 128
  - stability of excited states, 127
  - *See also* Radiation chemistry
- Electron reactivity, ionic liquids, 124–125
- Electrospray ionization mass spectrometry (ESI–MS)
  - characterization of ionic liquid solutes, 138–140
  - facilitation of ESI process in non-polar solvents, 144*f*
  - ion current vs. time for direct probe analysis, 141*f*
  - ionic liquids in, 136–137
  - method, 136
  - nanospray studies, 140, 142*f*
  - negative ion ESI–MS of [$HNEt_3$][$HFe_3(CO)_{11}$] in hexane, 145*f*
  - non-polar solvents, 142–144
  - [$P(C_6H_{13})_3(C_{14}H_{29})$][$NTf_2$] in toluene and in hexane, 143*f*
  - positive-ion ESI–MS of [Ru(η6-4-isopropyltoluene)(η2-triphos)Cl][$PF_6$] in [$C_4$mim][$PF_6$], 139*f*
  - positive-ion ESI–MS of benchmark [$C_4$mim][$BF_4$], 137*f*
  - positive-ion nanospray MA of [Ru(η6-*p*-cymene)-(η2-triphos)Cl][$PF_6$] in [$C_4$mim][$PF_6$], 140, 142*f*
  - suspension of ionic liquid in path of desolvation gas for direct probe analysis, 141*f*
- Electrostatic repulsion, ionic liquids, 201–204
- Enthalpy of dissolution, $CO_2$ in ionic liquids, 234*f*
- Enzymes. *See* Ribonuclease A (RNase A)
- Equation of state (EOS)
  - fluorocarbons, 28–31
  - gas solubility, 360, 361
  - solubility data of fluorocarbons in ionic liquids, 32–33
- Erosion, [$C_4$mim][$NTf_2$] thin films, 281, 282*f*
- Ethane
  - calculated energies by Antoine equation, 369*t*
  - calculation of gas vapor pressure, 366*f*

- constants for calculation of vapor pressure, 367*t*
- literature and predicted values for solubility in [$C_4$mim][$NTf_2$], 363, 364*f*

Ethanol
- Henry's law for $CO_2$ in, 229*f*
- surface tension, 353*t*

Ethanolammonium nitrate [HO($CH_2$)$_2$$NH_3$][$NO_3$] (EtOAN)
- atomic force microscopy (AFM) of EtOAH-mica, 326–327
- properties, 319*t*
- *See also* Protic ionic liquids

Ethene
- calculated energies by Antoine equation, 369*t*
- calculation of gas vapor pressure, 366*f*
- conformers and ion pairs on, solubility in [$C_4$mim][$NTf_2$], 373, 374*f*
- constants for calculation of vapor pressure, 367*t*

1-Ethyl-3-methylimidazolium bis{(trifluoromethyl)sulfonyl}-amide [$C_2$mim][$NTf_2$]
- chemical analysis, 25*t*
- density, 46*f*
- diffusion coefficients for $CO_2$ in, 232, 233*f*
- enthalpy of dissolution of $CO_2$ in, 234*f*
- gelation, 206
- heat capacity, 50*f*
- ionic liquid, 23
- nanocomposite ion gels in, 206–207
- thermal conductivity, 53*f*
- *See also* Colloidal dispersions

1-Ethyl-3-methylimidazolium ethanoate [$C_2$mim][$O_2$CMe]
- angular distribution functions (ADFs), 88*f*, 89*f*
- Arrhenius plots for ionic liquids and cellobiose solutions, 84, 85*f*
- correlation time ($\tau_c$) of nuclei in, 82–83, 84*f*
- $^{13}$C $T_1$ relaxation vs. cellobiose for C-2, C-2', and C-1" in, 81*f*
- $^{13}$C $T_1$ relaxation vs. cellobiose for carbonyl and methyl C's of anion in, 82*f*
- $^{13}$C $T_1$ relaxation vs. temperature for C-2, C-2' and C-1" in, 80*f*
- ionic liquid, 76
- molecular dynamics simulation of [$C_2$mim][$O_2$CMe]/cellobiose, 86–89
- nuclear magnetic resonance (NMR) study of, with cellobiose, 79–85
- radial distribution functions (RDFs), 88*f*, 89*f*
- spatial distribution, 88*f*
- structure and numbering, 77*f*
- temperature dependence of $^{13}$C $T_1$ for carbonyl and methyl Cs of anion in, 81*f*
- *See also* Molecular dynamics (MD) simulation

1-Ethyl-3-methylimidazolium ethylsulfate [$C_2$mim][$EtSO_4$]
- dielectric relaxation (DR) spectrum, 66*f*
- heat capacity, 50*f*
- thermal conductivity, 53*f*

Ethylamine diacetic acid
- tethered moiety on functionalized ionic liquid, 242–244
- *See also* Functionalized ionic liquids

Ethylammonium nitrate [$EtNH_3$][$NO_3$]
- AFM (atomic force microscopy) of EAN-graphite, 329
- AFM of EAN-mica, 324–326
- AFM of EAN-silica, 327–328
- force vs. distance profile between AFM tip and graphite surface in, 330*f*
- mass spectrometry, 322
- oscillatory forces, 323
- preparation, 319
- properties, 319*t*
- small angle neutron scattering (SANS), 320–322, 330–331
- surface forces apparatus study of EAN-mica interface, 323
- *See also* Protic ionic liquids

**F**

Ferroelectric plugs, microfluidic channels, 161

Ferrofluidic pump, operating principle for circular, 161

Films. *See* Thin films of [$C_4$mim][$NTf_2$]

Downloaded by 89.163.35.42 on June 28, 2012 | http://pubs.acs.org
Publication Date (Web): December 18, 2009 | doi: 10.1021/bk-2009-1030.ix002

Downloaded by 89.163.35.42 on June 28, 2012 | http://pubs.acs.org
Publication Date (Web): December 18, 2009 | doi: 10.1021/bk-2009-1030.ix002

Fissile materials, ionic liquids for nuclear separations, 121
Fluorocarbons
  activity model, 27–28
  classifications, 22
  cloud-point measurements, 27
  equation of state model, 28–31
  erythro- and threo-2,3-dihydrodecafluoropentanes (HFC-4310mee), 36*f*, 37*f*
  experimental, 23–27
  gas solubility measurements, 25–26
  Henry's law constants, 34–35
  HFC-4310mee as ozone-depleting solvent replacement, 37
  industrial compounds, 22
  isothermal PTx phase diagram for HFC-23 + [$C_4$mim][$PF_6$], 32*f*
  isothermal PTx phase diagram for HFC-41 + [$C_4$mim][$PF_6$], 33*f*
  liquid-liquid equilibria of HFC-4310mee diastereomers in ionic liquids, 37, 38*f*, 39*f*
  mass-volume measurements, 25–26
  mass-volume method, 33–34
  materials, 23, 25
  modeling, 27–31
  molecular structures of HFC-4310mee, 36*f*, 37*f*
  phase behavior of room temperature ionic liquids, 22
  properties, 24*t*
  room temperature ionic liquids, 35–36
  safety, 27
  solubility data (P,T,x) in ionic liquids, 31–33
  vapor-liquid equilibria, 25–26
  vapor-liquid-liquid equilibria, 25–26
Formulation
  biological, using ionic liquids, 98–99
  osmolality of, 102–103
  *See also* Biomedical applications
Fugacity
  calculation, 6
  normalized, vs. mole fraction of refrigerant in ionic liquid, 31*f*
Fugacity coefficient
  calculation, 6
  equation of state, 30
Functionalized ionic liquids
  coordinating groups tethered to cations of ionic liquids, 241*f*
  coordinating transition metals with, 240–241
  deprotection of di-*t*-butyl ester by trifluoroacetic acid, 244
  design and synthesis, 240
  epoxidations using manganese(III) chloride complex, 250, 251*t*
  imidazolium derived ligand with ruthenium complex, 241*f*
  incorporating tethered ethylamine diacetic acid moiety, 242, 243*f*
  metal complex formation using [$tBu_2$edamin][$PF_6$], 244
  metal-ion-extracting potential, 242
  metal ion extraction from solution, 241
  prototypical, 240*f*
  removal of aqueous copper(II) using, 246, 247*t*
  syntheses of copper(II) chelate complexes, 247, 248*f*, 249*f*
  synthesis of $C_4$-$C_{10}$, 246
  synthesis of di-*t*-butyl ester protected [$tBu_2$edamin][$PF_6$], 243
  synthesis of manganese(III) chloride complex, 250
  varying coordinating group in imidazolium based, 247
  X-ray crystal structure of copper(II) chelate complexes, 248*f*, 250*f*
  X-ray crystal structures of complexes, 244, 245*f*

**G**

Gas absorption
  Henry's law constants for $CO_2$ in various ionic liquids, 227*f*, 228*f*, 229*f*
  ionic liquids for, 225–230
  selectivity in ionic liquids, 230–232
Gas in ionic liquid, Henry's law, 5–6
Gas molality, sparsely soluble gases, 9–10
Gas separations
  application of ionic liquids, 360
  cryogenic distillation, 224
  diffusivity of gases in ionic liquids, 232, 233*f*

  enthalpies of dissolution for $CO_2$ in solvents, 234*f*
  gas solubilities in [$C_4$mim][$BF_4$] as function of mole fraction gas and temperature, 231*f*
  Henry's law constants for $CO_2$ in various ionic liquids, 227*f,* 228*f,* 229*f*
  ionic liquids for gas absorption, 225–230
  light hydrocarbon solubility in ionic liquids, 231
  membrane, 224–225
  mixing ionic liquids and, efficiency, 229–230
  recycling absorbent, 233–234
  selectivity of gas absorption in ionic liquids, 230–232
  $SO_2$ solubility in ionic liquids, 231
  solubility of gases in ionic liquids, 228
Gas solubility
  abbreviations list, 363*t*
  apparatus for measuring, 3*f*
  $CO_2$ and $H_2$ in ionic liquid, 4, 5*f*
  correlation plots for calculating, in [$C_4$mim][$NTf_2$], 370, 371*f*
  COSMOthermX calculations of, in ionic liquids, 361–362
  experimental vs. molecular simulation, in ionic liquids, 12*f*
  experimental work on, in ionic liquids, 4*t*
  ionic liquids, 1–2
  prediction by molecular simulation, 10–11, 12*f*
  technique to measure, in ionic liquid, 2–7
  vapor-liquid equilibria measurement, 25–26
  *See also* COSMOthermX
Gas vapor pressure, calculation using extended Antoine correlation and energy in COSMOthermX, 366*f*
Gaussian energy, estimated propene vapor pressure vs. energy value, 368*f*
Genomics, treating disease, 95–96
Gibbs Ensemble Monte Carlo simulations, solubility of $CO_2$ in ionic liquid, 11, 12*f*
Glycerol, surface tension, 353*t*
Gold nanoparticle-ionic liquids (Au-NP)
  characterization, 215
  miscibility, 216, 217*f*
  preparation of hybrid fluids, 214, 218, 219*f*
  *See also* Hybrid fluids
Gold salts, ionic liquids reducing to metal, 183, 184
Gouy–Chapmann theory
  double layer, 337
  size of ionic liquids, 202
Gravimetric method, measuring gas solubility in ionic liquid, 2
Green chemistry
  ionic liquids as potential green solvents, 359–360, 375
  nanoparticle synthesis in ionic liquids, 186
Group contribution models (GCM)
  gas solubility, 360
  heat capacity, 50–52
  parameter calculation, 387, 399
  process design, 45
  *See also* Thermophysical properties of ionic liquids

**H**

Hardness, [$C_4$mim][$NTf_2$] thin films, 284–285
Heat capacity
  energy and temperature relationship, 49
  group contribution equation, 51, 52
  group contribution model, 50–51
  ionic liquids, 49–50, 397–398
  ionic liquids as function of temperature, 50*f*
  molar, 50
  prediction for ionic liquids, 398*t*
Henry's constant
  $CO_2$ in various ionic liquids, 227*f,* 228*f,* 229*f*
  gases in [$C_6$mim][$NTf_2$], 7*f*
  higher pressures, 7
  low pressures, 6
  solubility data to obtain, 34–35
  zero pressure, 6
Henry's law
  gas in ionic liquid, 5–6
  molality scale, 4–5
Heptane, Henry's law for $CO_2$ in, 229*f*

Downloaded by 89.163.35.42 on June 28, 2012 | http://pubs.acs.org
Publication Date (Web): December 18, 2009 | doi: 10.1021/bk-2009-1030.ix002

- 1-Hexyl-3-methylimidazolium bis(trifluoromethylsulfonyl)amide $[C_6mim][NTf_2]$
  - density, 46*f*
  - gas solubility in, 4*t*
  - heat capacity, 50*f*
  - Henry's constant of gases in, 7*f*
  - thermal conductivity, 53*f*
  - volume expansion by pressurization of, with gas, 10*t*
  - volume to solvent mass ratio vs. solute molality for $CO_2$ in, 9*f*
- Hofmeister series, bimolecular solutes, 110–112
- Human diseases
  - treating, 95–96
  - *See also* Biomedical applications
- Hybrid fluids
  - Au-NP (gold nanoparticle)-ionic liquid, 218, 219*f*
  - characterization of surface modified $Fe_3O_4$-NPs and Au-NPs, 215
  - combination of modified organic salts and ionic liquid dispersant, 217, 218*f*
  - experimental, 213–215
  - facile preparation of ionic liquid based magnetic fluids, 215–216
  - measurements, 214–215
  - miscibility comparisons, 216, 217*f*
  - preparation of alkyl chain-modified $Fe_3O_4$-NPs, 214
  - preparation of imidazolium cation-modified Au-NPs, 214
  - preparation of nanoparticle-ionic liquid hybrid fuels, 214
  - preparation of organic salts-modified $Fe_3O_4$-NPs, 213
  - promise, 212
- Hydraulic valve actuation
  - device design, 168–169
  - ionic liquid filled, 168–171
  - ionic liquid for sustained stable actuation, 169–170
  - *See also* Microfluidics
- Hydrocarbons
  - solubility in ionic liquids, 231
- *See also* Aromatic/aliphatic hydrocarbon separation
- Hydrogen, gas solubility in ionic liquid, 4, 5*f*
- Hydrophobic interface
  - $CCl_4$/ionic liquid, 309–310
  - $D_2O$/ionic liquid, 310, 311*f*

**I**

- IL Thermo, IUPAC ionic liquid database, 44
- Impurities, density of ionic liquids, 46–47
- Inorganic nanoparticles
  - preparation, 212
  - *See also* Hybrid fluids
- Interfaces of ionic liquids
  - air/ionic liquid interface, 308–309
  - applications, 305–306
  - butanol/ionic liquid interface, 311–312, 313*f*
  - $CCl_4$/ionic liquid interface, 309–310
  - $D_2O$/ionic liquid interface, 310, 311*f*
  - hydrophilic interface, 310, 311*f*
  - hydrophobic interface, 309–310
  - liquids with similar polarity, 311–312, 313*f*
  - reference interface, 308–309
  - sum frequency generation (SFG) theory and experimental, 307–308
- Interfacial properties. *See* Thin films of $[C_4mim][NTf_2]$
- Ion association. *See* Ionic liquid/naphthalene mixtures
- Ion dissociation, room temperature ionic liquids, 404
- Ionic conductivity
  - $[C_4mim][PF_6]$/naphthalene mixture, 406, 407*f*
  - nanocomposite ion gels, 206, 207*f*
- Ionicity, degree of self-dissociation, 202
- Ionic liquid characterization
  - background for, 338–343
  - Boltzmann equation, 341
  - cation 1-butyl-3-methylimidazolium $[C_4mim]^+$ with three different anions, 337, 338*f*
  - complementary techniques, 337
  - composition, 335–336
  - experimental, 344–348
  - future work, 354
  - gas-liquid interface, 337
  - mass spectrum of vacuum cell, 348*f*
  - organic contaminants, 336
  - Poisson's equation, 341–342
  - sample-handling and preparation, 347–348

Downloaded by 89.163.35.42 on June 28, 2012 | http://pubs.acs.org
Publication Date (Web): December 18, 2009 | doi: 10.1021/bk-2009-1030.ix002

Downloaded by 89.163.35.42 on June 28, 2012 | http://pubs.acs.org
Publication Date (Web): December 18, 2009 | doi: 10.1021/bk-2009-1030.ix002

  - SFG (sum frequency generation)-polarization mapping method, 338–341
  - SFG polarization mapping of [$C_4$mim][$BF_4$], 350
  - SFG polarization mapping of [$C_4$mim][$MeOSO_3$], 349–350
  - SFG polarization mapping of [$C_4$mim][$N(CN)_2$], 350–352
  - SFG-polarization mapping technique, 344–345
  - SFG vacuum cell, 345*f*
  - surface potential measurement using vibrating plate methods, 341–342
  - surface potential of [$C_4$mim][$BF_4$], [$C_4$mim][$N(CN)_2$], and [$C_4$mim][$MeOSO_3$], 352–353
  - surface potential using customized cell, 345–346
  - surface tension by pendant drop method, 342–343
  - surface tension in home-built drop method, 346–347
  - surface tension of [$C_4$mim][$N(CN)_2$], 353–354
  - surface tension of various liquids, 353*t*
  - surface tension values of [$C_4$mim][$BF_4$], [$C_4$mim][$N(CN)_2$] and [$C_4$mim][$MeOSO_3$], 344*t*
  - volatile components, 349*t*
  - water and physical properties of ILs, 336
  - water and vapor-liquid interfaces, 336–337

- Ionic liquid-metal complexes
  - functionalized, 240–241
  - *See also* Functionalized ionic liquids
- Ionic liquid/naphthalene mixtures
  - anion-anion coordination number by MD simulation, 413*f*
  - 1-butyl-3-methylimidazolium [$C_4$mim]$^+$ drawing, 405*f*
  - composition dependence of radial distribution functions, 411, 412*f*
  - computed diffusion coefficients of [$C_4$mim]$^+$, [$PF_6$]$^-$ and naphthalene, 410, 411*f*
  - conductivity per ion as function of composition, 410*f*
  - density of [$C_4$mim][$PF_6$]/naphthalene vs. composition, 405, 406*f*
  - dissociation of ions, 404
  - experimental of [$C_4$mim][$PF_6$]/naphthalene, 405–407
  - formation of neutral ion pairs, 413
  - ionic conductivity of [C4mim][$PF_6$]/naphthalene vs. composition, 406, 407*f*
  - microfield probability distribution, 416*f*
  - pair distribution functions, 411, 412*f*
  - persistence index as function of time, 413, 414*f*
  - probability distribution of microfields, 415–417
  - radial distribution function, 411, 412*f*
  - simulation model, 408
  - simulation results, 408–414
  - snapshot of simulated sample, 408–409
  - structure factor for centers of [$C_4$mim]$^+$ and [$PF_6$]$^-$, 414, 415*f*
  - time constant of exponential fit, 413, 414*f*
  - viscosity of [$C_4$mim][$PF_6$]/naphthalene vs. composition, 406, 407*f*
- Ionic liquids (ILs)
  - abbreviations list, 363*t*
  - anion and densities of [$C_4$mim]$^+$ based, 46*f*
  - anion nomenclature, 54–55
  - biomedical applications, 95–96
  - cation and densities of [$NTf_2$]$^-$ based, 46*f*
  - cation nomenclature, 55
  - density, 45–48, 388
  - design for biological solutions, 96
  - diffusivity of gases, 232, 233*f*
  - effective molar volume, 48, 49*f*
  - electrostatic repulsion, 201–204
  - experimental work on gas solubility, 4*t*
  - extraction with, 258–260
  - gas solubility, 1
  - group contribution equation, 51, 52
  - group contribution method, 50–51
  - heat capacities as function of temperature, 50*f*
  - heat capacity, 49–50, 397–398

Downloaded by 89.163.35.42 on June 28, 2012 | http://pubs.acs.org
Publication Date (Web): December 18, 2009 | doi: 10.1021/bk-2009-1030.ix002

  influence of temperature on molar volume, 10*f*
  IUPAC database (IL Thermo), 44
  modeling thermal conductivity, 53–54
  models estimating density, 47–48
  molar heat capacity, 50
  molecular simulation predicting gas solubility, 10–11, 12*f*
  nanoparticles and, 178–179
  nomenclature, 54–55
  osmolality of formulations, 102–103
  potential applications, 44–45
  potential "green" solvents, 359–360, 375
  potential organic solvent replacement, 44
  predicted vs. experimental molar volume for, 49*f*
  properties, 44–45
  reducing agents for coinage metal salts, 183*f*
  solubility of proteins in, 99–100
  specific heat capacity, 49–52
  task-specific, 420–421
  thermal conductivity, 52–54
  thermophysical bulk properties, 274
  volume expansion by pressurization, 10 *t*
  water impurities and calculated molar volume of, 47*t*
  *See also* Electrospray ionization mass spectrometry (ESI–MS); Functionalized ionic liquids; Hybrid fluids; Interfaces of ionic liquids; Radiation chemistry; Thermophysical properties of ionic liquids; Thin films of [$C_4$mim][$NTf_2$]
Ionic liquid-solvent mixtures
  chemical speciation model for ([$C_4$mim][$BF_4$] + $CH_2Cl_2$), 70, 71*f*
  dilution scheme, 67, 68*f*
  effective dipole moments from Cavell equation, 70*f,* 72, 73*f*
  parameters for Debye mode in ([$C_4$mim][$BF_4$] + $CH_2Cl_2$), 72*f*
  parameters from DR spectra for [$C_4$mim][$BF_4$] + $CH_2Cl_2$ mixture, 69*f*
  relaxation time and viscosity for ([$C_4$mim][$BF_4$] + $CH_2Cl_2$), 71*f*
Ionizing radiation
  processes, 123*f*
  radiation-induced reactivity, 123–125
  *See also* Radiation chemistry
Irregular ionic lattice model, $CO_2$ solubility, 360
Isobaric expansivity
  definition, 388–389
  ionic liquids, 389
  prediction for ionic liquids, 398*t*
Isothermal compressibility
  ionic liquids, 389–390
  prediction for ionic liquids, 398*t*
IUPAC ionic liquid database, IL Thermo, 44

**L**

Lanthanide(III) oxides, nanostructured $Tb_2O_3$ nanospindles, 185–186
Liquid-liquid phase, ionic liquids, 2
Lithography, multilayer soft, with pneumatic actuation, 163
Lower critical endpoint (LCEP), phase equilibria, 15
Lyophilized medicine, specialized packaging, 97, 98*f*

**M**

Magnesium sulfate, dielectric relaxation (DR) spectrum, 65*f*
Magnetic actuation, peristaltic pumping by, 165
Magnetic field
  actuation by external, 160–161
  *See also* Magnetorheological fluids (MRFs); Smart materials
Magnetic fluids. *See* Hybrid fluids
Magnetorheological fluids (MRFs)
  conventional, in oil, water or glycols, 150
  ionic liquids as carriers of, 148–149, 150–151
  magnetic field application, 153
  magnetic particle interactions with and without magnetic field, 150*f*
  optical microscopy images, 151*f*
  preparation, 149
  rheological measurements of, based on [$C_2$mim][$Et_2PO_4$] with magnetic field, 153*f*

Downloaded by 89.163.35.42 on June 28, 2012 | http://pubs.acs.org
Publication Date (Web): December 18, 2009 | doi: 10.1021/bk-2009-1030.ix002

  rheological measurements without magnetic field, 152*f*
  temporary magnetization before demagnetization, 153–154
  *See also* Smart materials
Manganese(III) chloride complex
  epoxidations, 251*t*
  functionalized ionic liquid-metal complex, 250, 251*t*
  *See also* Functionalized ionic liquids
Mass-volume measurement
  fluorocarbon solubility in ionic liquids, 33–34
  vapor-liquid-liquid equilibria, 26–27
Melting temperature, ribonuclease A (RNase A) vs. added ionic liquid, 110, 111*f*
Membranes, gas separations, 224–225
Metabolomics, treating disease, 95–96
Metal extractions
  ionic liquids and functionalized ionic liquids, 241
  *See also* Functionalized ionic liquids
Methylammonium nitrate [$MeNH_3$][$NO_3$], properties, 319*t*
1-Methylimidazolium-modified iron(II,III) oxide nanoparticles
  characterization, 215
  miscibility, 216, 217*f*
  preparation, 213
  preparation of ionic liquid based magnetic fluids, 215–216
  *See also* Hybrid fluids
Microfields, probability distribution of, 415–417
Microfluidics
  actuation by external field, 160–161
  actuation of polydimethylsiloxane (PDMS) system, 161–165
  actuation schemes, 158–161
  array of 192 channels with access ports, 159*f*
  Braille display, 166–168
  Braille display with ionic liquid filled hydraulic valves, 169*f*
  characteristics, 158
  circular micro PCR device, 161*f*
  3D diagram of elastomeric peristaltic pump, 163*f*
  device design, 168–169
  device fabrication and preparation, 170–171
  droplet-based passive pumping, 159–160
  fabrication of device with ionic liquid filled channels for Braille display actuation, 171*f*
  integrated magnetic stir-bar driven device, 160*f*
  ionic fluid filled hydraulic valve, 168–171
  ionic liquid for sustained stable actuation, 169–170
  microfluidic flow cytometry system, 167*f*
  multilayer soft lithography with pneumatic actuation, 163
  operating principle for circular ferrofluidic pump, 161*f*
  PDMS device fabrication process, 162*f*
  peristaltic pumping by magnetic actuation, 165
  photographs of Braille display devices, 167*f*
  programmable cell stretching microwell array system, 167*f*
  rapid prototyping of microfluidic channels in PDMS, 162–163
  schematic of planar peristaltic pump with microfluidic device, 165*f*
  shape memory alloy (SMA) actuators, 164–165
  single micro stir-bar in, channel, 160*f*
  SMA valve design, 165*f*
  thermally actuated phase-change components, 164
  *See also* Braille display microfluidics
Microwave irradiation
  nanoparticle synthesis, 182–184
  silver and gold particles, 184*f*
  synthesis of colloidal copper solution, 183*f*
  *See also* Nanoparticles
Mixtures. *See* Ionic liquid-solvent mixtures
Modeling
  activity model, 27–28
  equation of state model, 28–31
  fluorocarbons, 27–31
  thermal conductivity of ionic liquids, 53–54

Downloaded by 89.163.35.42 on June 28, 2012 | http://pubs.acs.org
Publication Date (Web): December 18, 2009 | doi: 10.1021/bk-2009-1030.ix002

  - *See also* Molecular dynamics (MD) simulation
- Molality scale, Henry's law, 4–5
- Molar conductivity, ionic liquid solutions, 404
- Molar heat capacity
  - ionic liquid, 50
  - *See also* Heat capacity
- Molar volume
  - effective, of ionic liquids, 48
  - water impurities in ionic liquids, 47*t*
- Molecular dynamics (MD) simulation
  - [$C_2$mim][$O_2$CMe]-cellobiose system, 86–89
  - [$C_4$mim]Cl/cellobiose system, 85–86, 87*f*
  - details, 78–79
  - ionic liquid anions and cations, 76
  - O···$H_2$-$C_2$ angular distribution functions (ADFs), 86, 87*f,* 89*f*
  - O···$H_2$ radial distribution functions (RDFs), 86, 87*f,* 89*f*
  - OH···Cl ADFs, 85, 86*f*
  - OH···Cl RDFs and coordination numbers, 85, 86*f*
  - spatial distribution, 86, 87*f,* 88*f*
  - stoichiometry of interaction by coordination numbers, 86
- Molecular dynamic simulation, [$C_4$mim][$PF_6$], 339
- Molecular sieves
  - ionic liquids for synthesis of, 189–190
  - *See also* Silica saturation
- Molecular simulation
  - gas solubility, 360
  - prediction of gas solubility by, 10–11, 12*f*
  - *See also* Simulation
- Mole fraction, gas solubilities as function of, 231*f*
- Multilayer soft lithography, pneumatic actuation, 163

**N**

- Nanocomposite ion gels
  - dynamic strain sweep, 207, 208*f*
  - formation in ionic liquid, 206–207
  - ionic conductivity by silica content, 206, 207*f*
  - mechanical properties, 207, 208*f*
  - plateau elastic modulus, 207, 208*f*
  - yield stress, 207, 208*f*
  - *See also* Colloidal dispersions
- Nanoparticles
  - ionic liquids and, 178–179
  - ionic liquids as reducing agents for coinage metal salts, 183*f*
  - microwave synthesis, 182–184
  - photoluminescence spectrum of $Tb_2O_3$ nanospindles, 186*f*
  - selected area electron diffraction (SAED) pattern of particle, 184, 185*f*
  - setup for physical vapor deposition (PVD) of substrates into ionic liquids, 180*f*
  - silver and gold, by microwave synthesis, 184*f*
  - synthesis in ionic liquids, 186
  - synthesis of colloidal copper solution, 183*f*
  - synthesis via PVD, 179–182
  - TEM (transmission electron microscopy) image of copper evaporation into dispersion of ZnO nanorods in [$C_4$mim][$NTf_2$], 181*f*
  - TEM image of copper particles in [$C_4$mim][$PF_6$] via PVD, 181*f*
  - TEM image of $Tb_2O_3$ nanospindles, 185*f*
  - TEM images of ZnO power, 185*f*
  - ultrasound synthesis, 184–186
  - *See also* Hybrid fluids
- Naphtha cracker
  - ethylene cracker feeds, 256
  - separation of aromatic and aliphatic hydrocarbons, 257
  - simplified flow scheme, 256*f*
  - typical composition, 257*t*
  - *See also* Aromatic/aliphatic hydrocarbon separation
- Naphthalene. *See* Ionic liquid/naphthalene mixtures
- Near-critical gas in system, phase behavior, 13*f*
- Nickel(II) chelate complex, ethylamine diacetic acid chelating ligand, 244, 245*f*
- Nitrogen dioxide
  - calculated energies by Antoine equation, 369*t*
  - constants for calculation of vapor pressure, 367*t*

Downloaded by 89.163.35.42 on June 28, 2012 | http://pubs.acs.org
Publication Date (Web): December 18, 2009 | doi: 10.1021/bk-2009-1030.ix002

NMR spectroscopic method, measuring gas solubility in ionic liquid, 2
Nomenclature, ionic liquids, 54–55
Non-polar solvents, electrospray ionization mass spectrometry (ESI–MS), 142–144
Nuclear fuel processing
  Advanced Fuel Cycle (AFC), 121–122
  fissile materials, 121
  ionic liquid-based separations, 122–123
  ionic liquids for nuclear separations, 121–123
  *See also* Radiation chemistry
Nuclear magnetic resonance (NMR) spectroscopy
  analysis of $^{13}C$ and $^{35/37}Cl$ relaxation data, 82–84
  experiments, 77–78
  ionic liquid/cellobiose systems, 79–85
  longitudinal relaxation time vs. temperature, 79, 80*f*
  relaxation of NMR-active nuclei, 79
  translational mobility, 84
  *See also* 1-Butyl-3-methylimidazolium chloride [$C_4$mim]Cl; 1-Ethyl-3-methylimidazolium ethanoate [$C_2$mim][$O_2$CMe]
Nuclear power, carbon-free energy, 119–120
Nuclear separations, ionic liquids for, 121–123

**O**

1-Octyl-3-methylimidazolium bis(trifluoromethylsulfonyl)amide [$C_8$mim][$NTf_2$]
  density, 46*f*
  heat capacity, 50*f*
  thermal conductivity, 53*f*
1-Octyl-3-methylimidazolium hexafluorophosphate [$C_8$mim][$PF_6$]
  model structure of air/[ $C_8$mim][$PF_6$], 309*f*
  possible model structure for butanol/[ $C_8$mim][$PF_6$], 313*f*
  SFG (sum frequency generation) spectra of air/ionic liquid interface, 308–309
  SFG spectra of butanol/ionic liquid interface, 311–312, 313*f*
  SFG spectra of $CCl_4$/ionic liquid interface, 309–310
  SFG spectra of $D_2O$/ionic liquid interface, 310, 311*f*
Organic contaminants, ionic liquids, 336–337
Organic solvents, ionic liquids as potential replacement, 44
Orrick–Erbar method, predicting viscosity, 392
Oscillating electric field, dielectric relaxation (DR) spectroscopy, 63*f*
Osmolality, protein stabilized formulations, 102–103

**P**

Packaging, specialty, for drugs, 97, 98*f*
Pair distribution functions, [$C_4$mim][$PF_6$]/naphthalene mixture, 411, 412*f*
Passive pumping, droplet-based, 159–160
Pendant drop method
  surface tension, 342–343
  *See also* Surface tension
Perfluorooctane, Henry's law for $CO_2$ in, 229*f*
Peristaltic pumping, magnetic actuation, 165
Perpendicular hardness, [$C_4$mim][$NTf_2$] thin films, 284–285
Persistence index, [$C_4$mim][$PF_6$]/naphthalene mixture, 413, 414*f*
Phase-change microfluidics, thermal actuation, 164
Phase diagrams, liquid-liquid equilibria of fluorocarbon diastereomers in ionic liquids, 37, 38*f,* 39*f*
Phase equilibria
  above critical temperature of $CO_2$, 15, 16*f*
  apparatus for measuring, 14*f,* 15
  "near critical" gas + water + solvent, 13*f*
  qualitative behavior of $CO_2$ + water + ionic liquid, 17*f,* 18
Physical properties
  collection of, of ionic liquids, 387

- *See also* Thermophysical properties of ionic liquids

Physical vapor deposition (PVD)
- copper/ZnO nanocomposites, 181
- experimental setup, 180*f*
- nanoparticle synthesis via, 179–182
- TEM (transmission electron microscopy) of copper evaporated into ZnO nanorod dispersion in [$C_4$mim][$NTf_2$], 181*f*
- TEM of copper particles in [$C_4$mim][$PF_6$] via, 181*f*
- *See also* Nanoparticles

Plateau elastic modulus, nanocomposite ion gels, 207, 208*f*

Platinum electrode
- capacitance-potential plots for, in [$C_4$mim][$NTf_2$], 302*f*
- double layer thickness of [$C_4$mim][$NTf_2$], 300–302
- *See also* 1-Butyl-3-methylimidazolium bis(trifluoromethylsulfonyl)amide [$C_4$mim][$NTf_2$]

Pneumatic actuation
- multilayer soft lithography, 163
- *See also* Actuation

Poisson's equation, surface potential, 341–342

Polarization mapping method
- analyzing surfaces, 340
- *See also* Sum frequency generation (SFG) polarization mapping

Polar solvent
- ionic liquid mixtures with, 67–72
- *See also* Ionic liquid-solvent mixtures

Polydimethylsiloxane (PDMS)
- microfluidic channel for Braille displays, 166, 167*f*
- microfluidic system and actuation, 161–165
- multilayer soft lithography with pneumatic actuation, 163
- peristaltic pumping by magnetic actuation, 165
- rapid prototyping of microfluidic channels in, 162–163
- shape memory alloy (SMA) actuators, 164–165
- thermally actuated phase-change microfluidic components, 164
- *See also* Microfluidics

Polymerase chain reaction (PCR), phase-change microfluid component, 164

Prediction. *See* COSMOthermX; Thermophysical properties of ionic liquids

Probability distribution, microfields, 415–417

Propane
- calculated energies by Antoine equation, 369*t*
- constants for calculation of vapor pressure, 367*t*

Propene
- calculated energies by Antoine equation, 369*t*
- constants for calculation of vapor pressure, 367*t*
- estimated, vapor pressure vs. energy value, 368*f*

Propylammonium nitrate [$PrNH_3$][$NO_3$]
- AFM (atomic force microscopy) of [$PrNH_3$][$NO_3$]–graphite, 329–330
- AFM of [$PrNH_3$][$NO_3$]–mica, 326
- AFM of [$PrNH_3$][$NO_3$]–silica, 328–329
- force vs. distance profile between AFM tip and graphite surface in, 330*f*
- mass spectrometry, 322
- oscillatory forces, 323
- preparation, 319
- properties, 319*t*
- small angle neutron scattering (SANS), 320–322, 330–331
- *See also* Protic ionic liquids

Proteins
- differential scanning calorimetry (DSC) for thermal stability, 108
- DSC profile of fresh ribonuclease (RNase A) solution and with choline dihydrogen phosphate [chol][$H_2PO_4$], 108, 109*f*
- DSC profiles of initial scans and first rescans for RNase A, 113, 114*f*
- DSC profiles of third DSC cycle of RNase A, 113*f*
- DSC profiles of yeast alcohol dehydrogenase (ADH), 115*f*
- fraction of irreversible deactivated RNase A, 114, 115*f*

Downloaded by 89.163.35.42 on June 28, 2012 | http://pubs.acs.org
Publication Date (Web): December 18, 2009 | doi: 10.1021/bk-2009-1030.ix002

Downloaded by 89.163.35.42 on June 28, 2012 | http://pubs.acs.org
Publication Date (Web): December 18, 2009 | doi: 10.1021/bk-2009-1030.ix002

- Hofmeister series, 110–112
- ionic liquid and enzymatic function of, 107–108
- irreversible deactivation, 112–115
- melting temperature and [chol][ $H_2PO_4$] concentration, 109, 110*f*
- melting temperature of RNase vs. concentration of ionic liquids, 110, 111*f*
- organic chlorides as denaturating agents, 111
- osmolality for stability, 103
- shelf life of ionic liquid stabilized, 100–101
- solubility in ionic liquids, 99–100
- stabilizing effect of [chol][ $H_2PO_4$], 109
- thermal stability of ionic liquid stabilized, 100–101
- two-state approximation model, 109
- unfolding, 108–110
- unfolding/refolding equilibrium, 108

Protein therapies
  - anti-microbial activity, 101–102
  - ionic liquids, 96
  - maximizing shelf–life, 97

Protic ionic liquids
  - atomic force microscopy (AFM) results, 324–330
  - [$EtNH_3$][$NO_3$]–graphite, 329
  - [$EtNH_3$][$NO_3$]–mica, 324–326
  - [$EtNH_3$][$NO_3$]–silica, 327–328
  - force vs. distance profile between AFM tip and graphite surface in [$EtNH_3$][$NO_3$] and [$PrNH_3$][$NO_3$], 330*f*
  - formation, 318
  - [$HO(CH_2)_2NH_3$][$NO_3$]–mica, 326–327
  - interfacial structure, 322–330
  - mass spectrometry experiments, 322
  - molecular dimension of ion pairs, 330–331
  - oscillatory forces, 323
  - preparation, 319
  - [$PrNH_3$][$NO_3$]–mica, 326
  - [$PrNH_3$][$NO_3$]–graphite, 329–330
  - [$PrNH_3$][$NO_3$]–silica, 328–329
  - properties of various, 318, 319*t*
  - small angle neutron scattering (SANS), 320–322
  - solvation layers, 331
  - surface forces apparatus study of [$EtNH_3$][$NO_3$]–mica interface, 323

Prototyping, rapid, of microfluidic channels, 162

Pumping process, droplet-based passive, 159–160

**R**

Radial distribution functions
  - anion-anion, of
    - [$C_4$mim][$PF_6$]/naphthalene mixture, 412–413
  - [$C_4$mim][$PF_6$]/naphthalene mixture, 411, 412*f*

Radiation chemistry
  - aliphatic cations, 128
  - diffusion-controlled reaction rates of solvated electron, 124*f*, 125
  - electron affinities, 129
  - excited ionic liquid components after irradiation, 130*f*
  - ionic liquids with aliphatic cations, 129
  - ionic liquids with aromatic cations, 129
  - ionization potentials, 129
  - ionizing radiation, 123
  - irradiated ionic liquids by electron paramagnetic resonance (EPR), 125–129
  - neutralization of ions, 126
  - pre-solvated electron reactivity, 124
  - processes by ionizing radiation, 123*f*
  - pulse radiolysis and EPR consistency, 130
  - radiation damage of ionic liquids, 129–131
  - radiation-induced reactivity on early time scales, 123–125
  - radical generation, 126–127
  - radiolysis of ionic liquids, 124*f*
  - reaction paths of cations, 127
  - recombination of holes and electrons, 125
  - spreading of spin density, 128
  - stability of excited states of ions and radicals, 127
  - *See also* Nuclear fuel processing

Radiolysis, ionic liquids, 124*f*

Downloaded by 89.163.35.42 on June 28, 2012 | http://pubs.acs.org
Publication Date (Web): December 18, 2009 | doi: 10.1021/bk-2009-1030.ix002

Rapid prototyping, microfluidic channels, 162
Recycling, gas absorbents, 233–234
Redlich–Kwong (RK)
  equation of state, 28
  solubility data using RK model, 32
Refractive index
  ionic liquids, 396
  prediction for ionic liquids, 398*t*
Refrigerants
  fluorocarbons in modern society, 22
  *See also* Fluorocarbons
Regular Solution Theory, model, 360
Relaxation time
  Cole–Cole process, 69, 71*f*
  *See also* Dielectric relaxation spectroscopy (DRS)
Ribonuclease A (RNase A)
  differential scanning calorimetry (DSC), 108, 109*f*
  DSC profiles of, with choline dihydrogen phosphate [chol][$H_2PO_4$], 108, 109*f*
  DSC profiles of initial scans and first rescans for, 113, 114*f*
  DSC profiles of third DSC cycle of, 113*f*
  fraction of irreversible deactivated, 115*f*
  irreversible deactivation, 112–115
  melting temperature of, vs. added ionic liquid, 110, 111*f*
  protein experiments, 108
  *See also* Proteins
Room temperature ionic liquids (RTILs)
  binary azeotropic fluorocarbon mixtures, 35–36
  phase behavior, 22
  *See also* Fluorocarbons

**S**

Safety, fluorocarbons, 27
"Salting-out" by a near-critical gas (SONG)
  apparatus for measuring phase equilibria, 14*f,* 15
  coexisting liquid phases in ternary system, 16*f,* 17
  ionic liquids, 13–18
  lower critical endpoint (LCEP), 15
  phase behavior in system, 13*f*
  phase equilibria above critical temperature of $CO_2$, 15, 16*f*
  phenomenon, 1, 13, 15, 18
  qualitative phase behavior of $CO_2$ + water + ionic liquid, 17*f,* 18
  three-phase liquid-liquid-vapor equilibrium, 16*f,* 17
  upper critical endpoint (UCEP), 15
Selectivity, gas absorption in ionic liquids, 230–232
Self-diffusion coefficient, ionic liquids, 394–395
Self-dissociation degree, ionicity, 202
Separation
  definition, 224
  ionic liquids for nuclear, 122–123
  *See also* Aromatic/aliphatic hydrocarbon separation; Gas separations
Shape memory alloy (SMA), actuators, 164–165
Shelf-life
  ionic liquid solubilized protein, 100–101
  maximizing, of protein drugs, 97
Silica particles
  size-distribution curves of bare, 203, 204*f*
  size-distribution curves of PMMA-grafted, 204, 205*f*
Silica saturation
  1-alkyl-3-methylimidazolium bromide [$C_n$mim]Br ionic liquids, 190, 191*t,* 192*t,* 195
  determination of saturation point, 191
  experimental, 190–191
  influence of side-chain length, 192
  intermolecular forces driving $SiO_2$ solubility, 194–195
  ionic liquids in study, 191*t*
  melting points in [$C_n$mim]Br, 193*t*
  silica source, 191
  solubility, 190
  solubility vs. melting point trends, 193
  solution behavior, 191–192
Silica substrate. *See* Thin films of [$C_4$mim][$NTf_2$]
Silver salts, ionic liquids reducing to metal, 183, 184
Simulation
  [$C_4$mim][$PF_6$]/naphthalene mixture, 408–414

- prediction of gas solubility by molecular, 10–11, 12*f*
- *See also* COSMOthermX; Ionic liquid/naphthalene mixtures; Modeling; Molecular dynamics (MD) simulation

Size distribution
- bare silica particles, 203, 204*f*
- PMMA-grafted silica particles, 204, 205*f*

Smart materials
- characterization methods, 149
- experimental, 149
- fine-tuning properties, 148
- interactions between magnetic particles with and without magnetic field, 150
- magnetorheological fluids (MRFs), 148–149
- MRFs in oils, water or glycols, 150
- MRFs with ionic liquids as liquid carriers, 150–151
- MRFs with magnetic field application, 153
- optical microscopy images of dispersed magnetite particles in ionic liquids, 151*f*
- preparation of MRFs, 149
- random distribution of particles in ionic liquid, 151*f*
- responding to external stimuli, 147–148
- rheological measurements of MRFs in [$C_2$mim][$Et_2PO_4$] with magnetic field, 153*f*
- rheological measurements without magnetic field, 152
- self-assembly and parallel alignment with magnetic field, 151*f,* 152
- temporary magnetization before demagnetization, 153–154

Soft lithography, multilayer, with pneumatic actuation, 163

Software tool. *See* COSMOthermX

Solid character, [$C_4$mim][$NTf_2$] thin films, 281, 284–285

Solubility
- activity models, 360–361
- fluorination of alkyl-side chain of 1,3-dialkylimidazolium cations, 227
- fluorocarbon diastereomers, 36–37, 38*f,* 39*f*
- fluorocarbons in ionic liquids, 31–33
- proteins in ionic liquids, 99–100
- variation with temperature, 225
- water in ionic liquids, 336
- *See also* COSMOthermX; Fluorocarbons; Gas solubility; Silica saturation

Specialized packaging, lyophilized medicine, 97, 98*f*

Specific heat capacity
- ionic liquids, 49–52
- *See also* Heat capacity

Speed of sound
- experimental data for, in ionic liquids, 391
- prediction for ionic liquids, 398*t*

Steric repulsion, ionic liquids, 205, 206*f*

Stokes–Einstein relation, self-diffusion coefficient, 394

Structural characterization
- [$C_4$mim][$NTf_2$] thin films, 279–281
- orientation of ionic liquids, 338–339

Sulfolane extraction
- aromatic and aliphatic hydrocarbon separation, 262–263
- comparing economic evaluation with ionic liquid separation, 267–269
- estimated investment and variable costs, 268*t*
- process, 262*f*
- *See also* Aromatic/aliphatic hydrocarbon separation

Sulfur dioxide
- calculated energies by Antoine equation, 369*t*
- conformers and ion pairs on, solubility in [$C_4$mim][$NTf_2$], 373, 374*f*
- constants for calculation of vapor pressure, 367*t*

Sum frequency generation (SFG)
- polarization mapping
- background, 338–341
- [$C_4$mim]-based ionic liquids, 349–352
- technique, 344–345
- vacuum cell, 345*f*
- *See also* Ionic liquid characterization

Sum frequency generation spectroscopy (SFG)

Downloaded by 89.163.35.42 on June 28, 2012 | http://pubs.acs.org
Publication Date (Web): December 18, 2009 | doi: 10.1021/bk-2009-1030.ix002

Downloaded by 89.163.35.42 on June 28, 2012 | http://pubs.acs.org
Publication Date (Web): December 18, 2009 | doi: 10.1021/bk-2009-1030.ix002

- air/ionic liquid interface, 308–309
- butanol/ionic liquid interface, 311–312, 313*f*
- 1-butyl-3-methylimidazolium bis{(trifluoromethyl)sulfonyl}amide [$C_4$mim][$NTf_2$], 293–295
- $CCl_4$/ionic liquid interface, 309–310
- $D_2O$/ionic liquid interface, 310, 311*f*
- determining cation orientation at ionic liquid/Pt interface, 299
- H-C(4)C(5)-H peak intensities for *ppp* and *ssp* spectra, 298–299
- *ppp* polarized spectra of [$C_4$mim][$NTf_2$], 296, 297*f*
- SFG spectra of CO on Pt electrode in [$C_4$mim][$NTf_2$], 301*f*
- sketch of SFG electrochemical cell, 295*f*
- *ssp* polarized spectra of [$C_4$mim][$NTf_2$], 297, 298*f*
- surface- and interface-specific vibrational technique, 306
- theoretical and experimental, 307–308
- *See also* 1-Butyl-3-methylimidazolium bis(trifluoromethylsulfonyl)amide [$C_4$mim][$NTf_2$]; Interfaces of ionic liquids

Surface morphology
- AFM topographic maps of [$C_4$mim][$NTf_2$] thin films, 278*f*
- [$C_4$mim][$NTf_2$] films, 277, 279

Surface potential
- Boltzmann equation, 341
- [$C_4$mim]-based ionic liquids, 352–353
- experimental, 345–346
- measurement using vibrating plate methods, 341–342
- Poisson's equation, 341–342
- schematic of cell, 346*f*
- surfactants, 352, 352*t*
- *See also* Ionic liquid characterization

Surface tensiometry, alkylimidazolium ionic liquids, 339

Surface tension
- [$C_4$mim][$PF_6$], 339
- experimental, 346–347
- experimental data for, of ionic liquids, 390–391
- ionic liquid [$C_4$mim][$N(CN)_2$], 353–354
- literature values, 344*t*
- pendant drop method, 342–343
- prediction for ionic liquids, 398*t*
- schematic of cell, 347*f*
- various liquids, 353*t*
- *See also* Ionic liquid characterization

Synthetic method, measuring gas solubility in ionic liquid, 2–3

**T**

$Tb_2O_3$ nanospindles, nanostructures, 185–186

Temperature
- cloud-point measurement, 27
- gas solubilities as function of, 231*f*
- ionic liquid heat capacities, 50
- thermal conductivities of ionic liquids, 52, 53*f*
- variation of solubility with, 225
- volume expansion in ionic liquid, 10*f*

Temperature-x (Tx) phase diagrams, fluorocarbon diastereomers in ionic liquids, 36–37, 38*f,* 39*f*

Tethering strategies
- anion and cation, 424, 425*t,* 427
- *See also* Amine functionalized ionic liquids

Thermal actuation, phase-change microfluidic components, 164

Thermal conductivity
- ionic liquids, 52–54, 395
- prediction for ionic liquids, 398*t*

Thermal stability
- ionic liquid solubilized protein, 100–101
- *See also* Proteins

Thermophysical properties of ionic liquids
- collection of physical properties, 387
- density, 388
- electrical conductivity, 393–394
- future work, 398
- group contribution methods, 399
- group contribution parameters calculation, 387
- heat capacity, 397–398
- isobaric expansivity, 388–389
- isothermal compressibility, 389–390
- prediction, 398*t*

- refractive index, 396
- self-diffusion coefficient, 394–395
- speed of sound, 391
- surface tension, 390–391
- thermal conductivity, 395
- viscosity, 391–393

Thin films of [$C_4$mim][$NTf_2$]
- AFM (atomic force microscopy) for interfacial properties, 274–275
- AFM measurements, 276
- AFM tapping-mode topography of, on amorphous silica, 285, 286*f*
- AFM topographic maps of, on surfaces, 278*f*
- contact angle measurements, 277
- contact angles and surface energies of nanodroplets, 286*t*
- contact angles of, nanodroplets, 285–287
- contact-mode AFM, 281, 282*f*
- delamination of, on silica after scans in contact-mode, 281, 283*f*
- erosion at edges of, terraces on silica, 281, 282*f*
- materials and methods, 275–277
- perpendicular hardness, 284
- sample preparation, 276
- schematic of [$C_4$mim][$NTf_2$] droplets on substrate, 287*f*
- statistical analysis of AFM data, 276–277
- structural characterization, 279–281
- structural model of solid-like, 280*f*
- surface morphology of, 277, 279
- tapping-mode AFM, 281, 282*f*
- terrace height vs. number of steps in each terrace, 280*f*
- test of normal hardness of solid-like, on oxidized Si(110), 284*f*
- test of solid-like character of, 281, 284–285

Trihexyl(tetradecyl)phosphonium
- density of [$NTf_2$]-based ionic liquids, 46*f*
- thermal conductivity of, ionic liquids, 53

Trihexyl(tetradecyl)phosphonium bis(trifluoromethylsulfonyl)amide [$P_{66614}$][$NTf_2$], heat capacity, 50*f*

Turbomole
- correlation plot of estimated vapor pressures, 370*f*
- estimated propene vapor pressure vs. energy value, 368*f*
- program for calculating quantum chemical energy of molecules, 365
- *See also* COSMOthermX

**U**

Ultrasound, nanoparticle synthesis, 184–186

Upper critical endpoint (UCEP), phase equilibria, 15, 17*f*

**V**

Vapor-liquid equilibria, gas solubility measurement, 25–26

Vapor-liquid-liquid equilibria, mass-volume measurement, 26–27

Vapor pressure, constants for calculation, 367*t*

Vibrating plate methods, surface potential, 341–342

Vibrating-tube densitometer, density measurement, 45

Viscosity
- [$C_4$mim][$PF_6$]/naphthalene mixture, 406, 407*f*
- experimental, data for ionic liquids, 391–393
- prediction for ionic liquids, 398*t*

Vogel–Tammann–Fulcher (VTF) equation, electrical conductivity, 393

Volume expansion
- gas, 1–2
- liquid mixture, 8–10
- pressurization of ionic liquid, 10*t*

Volumetric method, measuring gas solubility in ionic liquid, 2

**W**

Walden rule, viscosity and conductance, 394

Water
- contaminant in ionic liquids, 336–337
- dielectric relaxation (DR) spectrum, 64*f*
- solubility in ionic liquids, 336
- surface tension, 353*t*

Downloaded by 89.163.35.42 on June 28, 2012 | http://pubs.acs.org
Publication Date (Web): December 18, 2009 | doi: 10.1021/bk-2009-1030.ix002

    vapor-liquid interfaces, 336–337
Water impurities, density of ionic liquids, 46–47

**X**

X-ray crystallography. *See* Functionalized ionic liquids
X-ray reflectivity, alkylimidazolium ionic liquids, 339

**Y**

Yeast alcohol dehydrogenase, differential scanning calorimetry, 115
Yield stress, nanocomposite ion gels, 207, 208*f*

**Z**

Zinc oxide (ZnO)
    formation of Cu/ZnO nanocomposites, 181
    selected area electron diffraction (SAED) of particle, 184, 185*f*
    transmission electron microscopy (TEM) of ZnO powder, 185*f*
    UV-vis absorption spectrum of ZnO nanorods, 185

Downloaded by 89.163.35.42 on June 28, 2012 | http://pubs.acs.org
Publication Date (Web): December 18, 2009 | doi: 10.1021/bk-2009-1030.ix002